

ORIGINAL PAGE IS
OF POOR QUALITY

211720
345

**CRACKING OF A LAYERED MEDIUM
ON AN ELASTIC FOUNDATION
UNDER THERMAL SHOCK**

by
Abd El-Fattah A. Rizk
and
Fazil Erdogan

Lehigh University
Bethlehem, Pennsylvania

August 1988

(NASA-CR-185316) CRACKING OF A LAYERED
MEDIUM ON AN ELASTIC FOUNDATION UNDER
THERMAL SHOCK (Lehigh Univ.) 345 pCSCL 20K

N89-23925

Unclas
G3/39 0211720

THE NATIONAL AERONAUTICS AND SPACE ADMINISTRATION
GRAND NAG-1-713

**CRACKING OF A LAYERED MEDIUM
ON AN ELASTIC FOUNDATION
UNDER THERMAL SHOCK**

by
Abd El-Fattah A. Rizk
and
Fazil Erdogan

Lehigh University
Bethlehem, Pennsylvania
August 1988

**THE NATIONAL AERONAUTICS AND SPACE ADMINISTRATION
GRAND NAG-1-713**

Table of Contents

ABSTRACT	1
1. INTRODUCTION	3
2. ANALYSIS OF THE PROBLEM	10
2.1 Model I- Semi-infinite elastic medium (base metal) bonded to a surface layer of different material (clad)	10
2.1.1 Temperature distribution	10
2.1.1.1 Unit step function at the boundary	10
2.1.1.2 Ramp function at the boundary	15
2.1.2 Thermal stresses in uncracked problem	18
2.1.3 Formulation of the crack problem (perturbation problem)	20
2.2 Model II - Layered Medium on an Elastic Foundation	32
2.2.1 Temperature distribution	32
2.2.1.1 Unit step function at the boundary	32
2.2.1.2 Ramp function at the boundary	36
2.2.2 Thermal stresses in uncracked problem	38
2.2.2.1 Stiffness of the elastic foundation	43
2.2.3 Formulation of the crack problem	46
3. THE SINGULARITY AT THE CRACK TIP	52
3.1 Embedded crack in both materials	52
3.2 Edge crack	56
3.2.1 Edge crack for Model I	56
3.2.2 Edge crack for Model II	59
3.3 Crack tip terminating at the interface from material (1)	61
3.4 Crack tip terminating at the interface from material (2)	65
3.5 Crack going through the interface	68
4. Numerical Procedure	76
4.1 Embedded Crack	81
4.2 Edge Crack	84
4.3 Crack Terminating at the Interface	85
4.4 Crack Going Through the Interface	87
4.5 Edge crack going through the interface	89
5. Stress Intensity Factors	91
5.1 Embedded Crack	91
5.2 Edge Crack	94
5.3 Crack Terminating at the Interface	96
5.4 Crack going through the interface	100
5.5 Edge crack going through the interface	108
6. RESULTS AND DISCUSSION	109
6.1 Model I	109
6.2 Model II	113
6.3 Conclusions	118
6.4 Suggestions for Future Research	120

References	287
Appendix (A)	291
Appendix (B)	293
Appendix (C)	295
Appendix (D)	299
Appendix (E)	302
Appendix (F)	304
Appendix (G)	318

Nomenclature

A_i	the cross section areas, $i=1,2$.
a_i, b_i	crack dimensions, $i=1,2$.
C_{ij}	constant functions of material properties, $i=1,2, j=1,2,3$.
D_i	coefficients of thermal diffusivity, $i=1,2$.
d_{ij}	constant functions of material properties, $i,j=1,2$.
E_i	Young's Modulus, $i=1,2$.
G_{ij}^∞	the asymptotic values of G_{ij} , as $\alpha \rightarrow \infty$, and t_i, x_i go to the end points, $i=1,2$.
h	thickness of the clad in Model I.
h_i	thickness of the materials in Model II, $i=1,2$.
$H(t)$	Heaviside step function.
k	stress intensity factor at the irregular points.
k_i	coefficients of thermal conductivity, $i=1,2$.
k_{ij}	the kernels of the singular integral equations.
k_{ij}^b	bounded terms of the kernels, $i,j=1,2$.
k_{ij}^s	singular terms of the kernels, $i=1,2, j=1,2,3,4$.
k_x, k_{xy}	the normal and shear components of the stress intensity factor at the interface.
L	total thickness, $(h_1 + h_2)$.
l	the total length of the crack, $(l_1 + l_2)$.
l_i	length of the cracks, $i=1,2$.
L_n	Laguerre polynomial.
m	$= \mu_1 / \mu_2$.
p	transform variable of Laplace Transform.

$P_n^{(-\beta, -\alpha)}$	Jacobi polynomial .
R	$=h_2/h_1$.
R_n	radius of neutral surface of the cylinder.
S_{1k}, S_{2l}	the collocation points .
T_i	temperatures , $i=1, 2$.
T_∞	initial temperature .
T_0	temperature at the boundary at any time.
t	time.
t_0	the actual duration time of the ramp function.
u_i, v_i	displacement components in x and y directions, $i=1, 2$.
w_i	fundamental functions of the singular integral equations , $i=1, 2$.
x	horizontal coordinate measured from the boundary.
x'	horizontal coordinate measured from the interface.
x^*	dimensionless distance, x/h in Model I and x/h_1 in Model II .
x_n	the distance from the neutral axis.
\bar{x}_{in}	the distance from the neutral axis to the center of the cross section , $i=1, 2$.
y	vertical coordinate.

Greek letters

$\Theta_i(x', t)$	$=T_i(x', t) - T_\infty$, $i=1, 2$.
Θ_0	$=T_0 - T_\infty$.
$\bar{\Theta}_i(x', p)$	Laplace Transform of $\Theta_i(x', t)$, $i=1, 2$.
η	$=\frac{k_2}{k_1} \sqrt{\frac{D_1}{D_2}}$.
δ	$=\sqrt{D_1/D_2}$.

τ	Fourier Number = tD_1/h^2 for Model I , tD_1/h_1^2 for Model II .
τ_0	= t_0D_1/h^2 for Model I , t_0D_1/h_1^2 for Model II .
α'_i	coefficients of thermal expansion , $i=1,2$.
ϵ_0	uniform strain over the shell thickness .
ϵ_{ij}	strain components , $i,j=x,y,z$.
σ_{ij}	stress components , $i,j=x,y,z$.
ν_i	Poisson's ratio , $i=1,2$.
σ_0^T	= $-\alpha'_1 E_1 \Theta_0 / (1 - \nu_1)$.
σ_i^T	thermal stresses , $i=1,2$.
ϕ_i	density functions = $\partial v_i(x,0)/\partial x$, $i=1,2$.
μ_i	shear modulus , $i=1,2$.
κ_i	= $(3 - 4\nu_i)$ for plane strain . = $(3 - \nu_i)/(1 + \nu_i)$ for generalized plane stress .
α, β	transform variables of Fourier Transform .
α_i, β_i	singularity at the crack tips , $i=1,2$.
λ_m	the m^{th} root of equation (2.81) .
χ	stiffness of the elastic foundation.
ρ	radius of curvature of the deflected composite beam .
ρ	= $\chi / 2\mu_2 \alpha$.
Γ	contour integral .

List of Figures

Figure 1-1: a-The geometry for Model I, b-The geometry for Model II, c-The temperature boundary condition at the inner wall.	6
Figure 1-2: The superposition	8
Figure 2-1: a-Geometry of the problem (Model I) b-Temperature boundary condition (unit step function)	10
Figure 2-2: Contour for evaluating the integrals in eqns. (2.13)	14
Figure 2-3: a-Geometry of the problem (Model I) b-Temperature boundary condition (ramp function)	15
Figure 2-4: Geometry of Model I (uncracked problem)	19
Figure 2-5: Crack geometry (Model I)	20
Figure 2-6: a-Geometry of the problem (Model II) b-Temperature boundary condition (unit step function)	32
Figure 2-7: The contour for evaluation of integrals in equations (2.72)	35
Figure 2-8: a-Geometry of the problem (Model II) b-Temperature boundary condition (ramp function)	36
Figure 2-9: Geometry of thin-wall hollow cylinder with cladding to calculate thermal stresses in uncracked problem	39
Figure 2-10: Geometry of thin-wall hollow cylinder with cladding to calculate stiffness of elastic foundation χ	43
Figure 2-11: Geometry of composite beam to calculate the radius of neutral axis R_n	45
Figure 2-12: Crack geometry Model II	47
Figure 3-1: Geometry of embedded crack in both materials	53
Figure 3-2: Geometry of edge crack (Model I)	56
Figure 3-3: Geometry of edge crack (Model II)	60
Figure 3-4: Geometry of the crack terminating at the interface from material (1)	61
Figure 3-5: Geometry of the crack terminating at the interface from material (2)	65
Figure 3-6: Geometry of crack going through the interface	68
Figure 4-1: Geometry of edge crack going through the interface	89
Figure 6-1: The normalized transient temperature distribution in Model I for $\tau_0=0.0$, $\tau_0=t_0 D_1/h^2$, (Material pair A)	137
Figure 6-2: The normalized transient stress distribution σ_{yy}/σ_0^T in Model I for $\tau_0=0.0$, $\tau_0=t_0 D_1/h^2$, $\sigma_0^T = -\alpha_1' E_1 \Theta_0/(1-\nu_1)$. (Material pair A)	138
Figure 6-3: The normalized transient temperature distribution in Model I for $\tau_0=10.0$, $\tau_0=t_0 D_1/h^2$, (Material pair A)	139
Figure 6-4: The normalized transient stress distribution σ_{yy}/σ_0^T in Model I for $\tau_0=10.0$, $\tau_0=t_0 D_1/h^2$, $\sigma_0^T = -\alpha_1' E_1 \Theta_0/(1-\nu_1)$ (Material pair A)	140
Figure 6-5: The normalized transient temperature distribution in Model I for $\tau_0=20.0$, $\tau_0=t_0 D_1/h^2$, (Material pair A)	141
Figure 6-6: The normalized transient stress distribution σ_{yy}/σ_0^T in	142

- Model I for $\tau_0=20.0$, $\tau_0=t_0 D_1/h^2$, $\sigma_0^T=-\alpha_1' E_1 \Theta_0/(1-\nu_1)$
(Material pair A)
- Figure 6-7:** The normalized transient temperature distribution in 143
Model I for $\tau_0=40.0$, $\tau_0=t_0 D_1/h^2$, (Material pair A)
- Figure 6-8:** The normalized transient stress distribution σ_{yy}/σ_0^T in 144
Model I for $\tau_0=40.0$, $\tau_0=t_0 D_1/h^2$, $\sigma_0^T=-\alpha_1' E_1 \Theta_0/(1-\nu_1)$
(Material pair A)
- Figure 6-9:** The normalized transient temperature distribution in 145
Model I for $\tau_0=60.0$, $\tau_0=t_0 D_1/h^2$, (Material pair A)
- Figure 6-10:** The normalized transient stress distribution σ_{yy}/σ_0^T in 146
Model I for $\tau_0=60.0$, $\tau_0=t_0 D_1/h^2$, $\sigma_0^T=-\alpha_1' E_1 \Theta_0/(1-\nu_1)$
(Material pair A)
- Figure 6-11:** The normalized stress intensity factor $k(b_1)$ as a function 147
of nondimensional time τ for an edge crack of various
lengths in Model I for $\tau_0=0.0$, $\tau_0=t_0 D_1/h^2$,
 $\sigma_0^T=-\alpha_1' E_1 \Theta_0/(1-\nu_1)$ (Material pair A)
- Figure 6-12:** The influence of τ_0 on the normalized stress intensity 148
factor $k(b_1)$ as a function of nondimensional time τ for an
edge crack of length $l_1/h=0.5$ in Model I , $\tau_0=t_0 D_1/h^2$,
 $\sigma_0^T=-\alpha_1' E_1 \Theta_0/(1-\nu_1)$ (Material pair A)
- Figure 6-13:** The influence of τ_0 on the normalized stress intensity 149
factor $k(b_1)$ as a function of nondimensional time τ for a
broken clad in Model I , $\tau_0=t_0 D_1/h^2$,
 $\sigma_0^T=-\alpha_1' E_1 \Theta_0/(1-\nu_1)$ (Material pair A)
- Figure 6-14:** The normalized stress intensity factor $k(a_2)$ as a function 150
of nondimensional time τ for an under-clad crack of
various lengths in Model I for $\tau_0=0.0$, $\tau_0=t_0 D_1/h^2$,
 $\sigma_0^T=-\alpha_1' E_1 \Theta_0/(1-\nu_1)$.(Material pair A)
- Figure 6-15:** The normalized stress intensity factor $k(b_2)$ as a function 151
of nondimensional time τ for an under-clad crack of
various lengths in Model I for $\tau_0=0.0$, $\tau_0=t_0 D_1/h^2$,
 $\sigma_0^T=-\alpha_1' E_1 \Theta_0/(1-\nu_1)$.(Material pair A)
- Figure 6-16:** The influence of τ_0 on the normalized stress intensity 152
factor $k(a_2)$ as a function of nondimensional time τ for an
under-clad crack of length $l_2/h=1.0$ in Model I ,
 $\tau_0=t_0 D_1/h^2$, $\sigma_0^T=-\alpha_1' E_1 \Theta_0/(1-\nu_1)$ (Material pair A)
- Figure 6-17:** The influence of τ_0 on the normalized stress intensity 153
factor $k(b_2)$ as a function of nondimensional time τ for an
under-clad crack of length $l_2/h=1.0$ in Model I ,
 $\tau_0=t_0 D_1/h^2$, $\sigma_0^T=-\alpha_1' E_1 \Theta_0/(1-\nu_1)$ (Material pair A)
- Figure 6-18:** The normalized stress intensity factor $k(b_2)$ as a function 154

- of nondimensional time τ for an edge crack of various lengths crossing the interface of in Model I for $\tau_0=0.0$,
 $\tau_0=t_0 D_1/h^2$, $\sigma_0^T = -\alpha'_1 E_1 \Theta_0/(1-\nu_1)$ (Material pair A)
- Figure 6-19:** The influence of τ_0 on the normalized stress intensity factor $k(b_2)$ as a function of nondimensional time τ for an edge crack crossing the interface in Model I for $l/h=4.0$,
 $\tau_0=t_0 D_1/h^2$, $\sigma_0^T = -\alpha'_1 E_1 \Theta_0/(1-\nu_1)$ (Material pair A) 155
- Figure 6-20:** The normalized stress intensity factor $k(a_1)$ as a function of nondimensional time τ for an embedded crack of various lengths crossing the interface in Model I for $b_2/h=2.0$, $\tau_0=0.0$, $\tau_0=t_0 D_1/h^2$,
 $\sigma_0^T = -\alpha'_1 E_1 \Theta_0/(1-\nu_1)$ (Material pair A) 156
- Figure 6-21:** The normalized stress intensity factor $k(b_2)$ as a function of nondimensional time τ for an embedded crack of various lengths crossing the interface in Model I for $b_2/h=2.0$, $\tau_0=0.0$, $\tau_0=t_0 D_1/h^2$, $\sigma_0^T = -\alpha'_1 E_1 \Theta_0/(1-\nu_1)$ (Material pair A) 157
- Figure 6-22:** The influence of τ_0 on the normalized stress intensity factor $k(a_1)$ as a function of nondimensional time τ for an embedded crack crossing the interface, $a_1/h=0.2$, $b_1/h=2.0$ in Model I , $\tau_0=t_0 D_1/h^2$, $\sigma_0^T = -\alpha'_1 E_1 \Theta_0/(1-\nu_1)$ (Material pair A) 158
- Figure 6-23:** The influence of τ_0 on the normalized stress intensity factor $k(b_2)$ as a function of nondimensional time τ for an embedded crack crossing the interface in Model I for $a_1/h=0.2$, $b_1/h=2.0$, $\tau_0=t_0 D_1/h^2$, $\sigma_0^T = -\alpha'_1 E_1 \Theta_0/(1-\nu_1)$ (Material pair A) 159
- Figure 6-24:** The normalized transient temperature distribution in Model I for $\tau_0=0.0$, $\tau_0=t_0 D_1/h^2$, (Material pair B) 160
- Figure 6-25:** The normalized transient stress distribution σ_{yy}/σ_0^T in Model I for $\tau_0=0.0$, $\tau_0=t_0 D_1/h^2$, $\sigma_0^T = -\alpha'_1 E_1 \Theta_0/(1-\nu_1)$ (Material pair B) 161
- Figure 6-26:** The normalized transient temperature distribution in Model I for $\tau_0=20.0$, $\tau_0=t_0 D_1/h^2$, (Material pair B) 162
- Figure 6-27:** The normalized transient stress distribution σ_{yy}/σ_0^T in Model I for $\tau_0=20.0$, $\tau_0=t_0 D_1/h^2$, $\sigma_0^T = -\alpha'_1 E_1 \Theta_0/(1-\nu_1)$ (Material pair B) 163
- Figure 6-28:** The normalized transient temperature distribution in Model I for $\tau_0=60.0$, $\tau_0=t_0 D_1/h^2$, (Material pair B) 164
- Figure 6-29:** The normalized transient stress distribution σ_{yy}/σ_0^T in Model I for $\tau_0=60.0$, $\tau_0=t_0 D_1/h^2$, $\sigma_0^T = -\alpha'_1 E_1 \Theta_0/(1-\nu_1)$ (Material pair B) 165

- Figure 6-30:** The normalized stress intensity factor $k(b_1)$ as a function of nondimensional time τ for an edge crack of various lengths in Model I for $\tau_0=0.0$, $\tau_0=t_0D_1/h^2$, $\sigma_0^T=-\alpha_1' E_1 \Theta_0/(1-\nu_1)$ (Material pair B) 166
- Figure 6-31:** The influence of τ_0 on the normalized stress intensity factor $k(b_1)$ as a function of nondimensional time τ for an edge crack of length $l_1/h=0.5$ in Model I , $\tau_0=t_0D_1/h^2$, $\sigma_0^T=-\alpha_1' E_1 \Theta_0/(1-\nu_1)$ (Material pair B) 167
- Figure 6-32:** The influence of τ_0 on the normalized stress intensity factor $k(b_1)$ as a function of nondimensional time τ for a broken clad in Model I , $\tau_0=t_0D_1/h^2$, $\sigma_0^T=-\alpha_1' E_1 \Theta_0/(1-\nu_1)$, $\beta_1=0.552538$. (Material pair B) 168
- Figure 6-33:** The normalized stress intensity factor k_x as a function of nondimensional time τ for an edge crack of various lengths crossing the interface in Model I for $\tau_0=0.0$, $\tau_0=t_0D_1/h^2$, $\sigma_0^T=-\alpha_1' E_1 \Theta_0/(1-\nu_1)$, $\beta_1=\alpha_2=0.01872238$. (Material pair B) 169
- Figure 6-34:** The normalized stress intensity factor k_{xy} as a function of nondimensional time τ for an edge crack for various lengths crossing the interface in Model I for $\tau_0=0.0$, $\tau_0=t_0D_1/h^2$, $\sigma_0^T=-\alpha_1' E_1 \Theta_0/(1-\nu_1)$, $\beta_1=\alpha_2=0.01872238$. (Material pair B) 170
- Figure 6-35:** The normalized stress intensity factor $k(b_2)$ as a function of nondimensional time τ for an edge crack of various lengths crossing the interface in Model I for $\tau_0=0.0$, $\tau_0=t_0D_1/h^2$, $\sigma_0^T=-\alpha_1' E_1 \Theta_0/(1-\nu_1)$, $\beta_1=\alpha_2=0.01872238$. (Material pair B) 171
- Figure 6-36:** The influence of τ_0 on the normalized stress intensity factor k_x as a function of nondimensional time τ for an edge crack crossing the interface $l/h=2.0$ in Model I , $\tau_0=t_0D_1/h^2$, $\sigma_0^T=-\alpha_1' E_1 \Theta_0/(1-\nu_1)$, $\beta_1=\alpha_2=0.01872238$. (Material pair B) 172
- Figure 6-37:** The influence of τ_0 on the normalized stress intensity factor k_{xy} as a function of nondimensional time τ for an edge crack crossing the interface $l/h=2.0$ in Model I , $\tau_0=t_0D_1/h^2$, $\sigma_0^T=-\alpha_1' E_1 \Theta_0/(1-\nu_1)$, $\beta_1=\alpha_2=0.01872238$. (Material pair B) 173
- Figure 6-38:** The influence of τ_0 on the normalized stress intensity factor $k(b_2)$ as a function of nondimensional time τ for an edge crack crossing the interface $l/h=2.0$ in Model I , $\tau_0=t_0D_1/h^2$, $\sigma_0^T=-\alpha_1' E_1 \Theta_0/(1-\nu_1)$, $\beta_1=\alpha_2=0.01872238$. (Material pair B) 174

Figure 6-39: The normalized transient temperature distribution in Model II for $\tau_0=0.0$, $h_2/h_1=3.0$, $\tau_0=t_0 D_1/h_1^2$, (Material pair A)	175
Figure 6-40: The normalized transient stress distribution σ_{yy}/σ_0^T in Model II for $\tau_0=0.0$, $h_2/h_1=3.0$, $\tau_0=t_0 D_1/h_1^2$, $\sigma_0^T=-\alpha_1' E_1 \Theta_0/(1-\nu_1)$. (Material pair A)	176
Figure 6-41: The normalized transient temperature distribution in Model II for $\tau_0=1.0$, $h_2/h_1=3.0$, $\tau_0=t_0 D_1/h_1^2$, (Material pair A)	178
Figure 6-42: The normalized transient stress distribution σ_{yy}/σ_0^T in Model II for $\tau_0=1.0$, $h_2/h_1=3.0$, $\tau_0=t_0 D_1/h_1^2$, $\sigma_0^T=-\alpha_1' E_1 \Theta_0/(1-\nu_1)$. (Material pair A)	179
Figure 6-43: The normalized transient temperature distribution in Model II for $\tau_0=6.0$, $h_2/h_1=3.0$, $\tau_0=t_0 D_1/h_1^2$, (Material pair A)	181
Figure 6-44: The normalized transient stress distribution σ_{yy}/σ_0^T in Model II for $\tau_0=6.0$, $h_2/h_1=3.0$, $\tau_0=t_0 D_1/h_1^2$, $\sigma_0^T=-\alpha_1' E_1 \Theta_0/(1-\nu_1)$. (Material pair A)	182
Figure 6-45: The normalized transient temperature distribution in Model II for $\tau_0=0.0$, $h_2/h_1=9.0$, $\tau_0=t_0 D_1/h_1^2$, (Material pair A)	184
Figure 6-46: The normalized transient stress distribution σ_{yy}/σ_0^T in Model II for $\tau_0=0.0$, $h_2/h_1=9.0$, $\tau_0=t_0 D_1/h_1^2$, $\sigma_0^T=-\alpha_1' E_1 \Theta_0/(1-\nu_1)$. (Material pair A)	185
Figure 6-47: The normalized transient temperature distribution in Model II for $\tau_0=6.0$, $h_2/h_1=9.0$, $\tau_0=t_0 D_1/h_1^2$, (Material pair A)	187
Figure 6-48: The normalized transient stress distribution σ_{yy}/σ_0^T in Model II for $\tau_0=6.0$, $h_2/h_1=9.0$, $\tau_0=t_0 D_1/h_1^2$, $\sigma_0^T=-\alpha_1' E_1 \Theta_0/(1-\nu_1)$. (Material pair A)	188
Figure 6-49: The normalized transient temperature distribution in Model II for $\tau_0=10.0$, $h_2/h_1=9.0$, $\tau_0=t_0 D_1/h_1^2$, (Material pair A)	190
Figure 6-50: The normalized transient stress distribution σ_{yy}/σ_0^T in Model II for $\tau_0=10.0$, $h_2/h_1=9.0$, $\tau_0=t_0 D_1/h_1^2$, $\sigma_0^T=-\alpha_1' E_1 \Theta_0/(1-\nu_1)$. (Material pair A)	191
Figure 6-51: The normalized transient temperature distribution in Model II for $\tau_0=20.0$, $h_2/h_1=9.0$, $\tau_0=t_0 D_1/h_1^2$, (Material pair A)	193
Figure 6-52: The normalized transient stress distribution σ_{yy}/σ_0^T in	194

- Model II for $\tau_0=20.0$, $h_2/h_1=9.0$, $\tau_0=t_0 D_1/h_1^2$,
 $\sigma_0^T = -\alpha'_1 E_1 \Theta_0 / (1-\nu_1)$. (Material pair A)
- Figure 6-53:** The normalized transient temperature distribution in 196
 Model II for $\tau_0=0.0$, $h_2/h_1=24.0$, $\tau_0=t_0 D_1/h_1^2$, (Material
 pair A)
- Figure 6-54:** The normalized transient stress distribution σ_{yy}/σ_0^T in 197
 Model II for $\tau_0=0.0$, $h_2/h_1=24.0$, $\tau_0=t_0 D_1/h_1^2$,
 $\sigma_0^T = -\alpha'_1 E_1 \Theta_0 / (1-\nu_1)$. (Material pair A)
- Figure 6-55:** The normalized transient temperature distribution in 199
 Model II for $\tau_0=6.0$, $h_2/h_1=24.0$, $\tau_0=t_0 D_1/h_1^2$, (Material
 pair A)
- Figure 6-56:** The normalized transient stress distribution σ_{yy}/σ_0^T in 200
 Model II for $\tau_0=6.0$, $h_2/h_1=24.0$, $\tau_0=t_0 D_1/h_1^2$,
 $\sigma_0^T = -\alpha'_1 E_1 \Theta_0 / (1-\nu_1)$. (Material pair A)
- Figure 6-57:** The normalized transient temperature distribution in 202
 Model II for $\tau_0=10.0$, $h_2/h_1=24.0$, $\tau_0=t_0 D_1/h_1^2$, (Material
 pair A)
- Figure 6-58:** The normalized transient stress distribution σ_{yy}/σ_0^T in 203
 Model II for $\tau_0=10.0$, $h_2/h_1=24.0$, $\tau_0=t_0 D_1/h_1^2$,
 $\sigma_0^T = -\alpha'_1 E_1 \Theta_0 / (1-\nu_1)$. (Material pair A)
- Figure 6-59:** The normalized transient temperature distribution in 205
 Model II for $\tau_0=20.0$, $h_2/h_1=24.0$, $\tau_0=t_0 D_1/h_1^2$, (Material
 pair A)
- Figure 6-60:** The normalized transient stress distribution σ_{yy}/σ_0^T in 206
 Model II for $\tau_0=20.0$, $h_2/h_1=24.0$, $\tau_0=t_0 D_1/h_1^2$,
 $\sigma_0^T = -\alpha'_1 E_1 \Theta_0 / (1-\nu_1)$. (Material pair A)
- Figure 6-61:** The normalized transient temperature distribution in 208
 Model II for $\tau_0=40.0$, $h_2/h_1=24.0$, $\tau_0=t_0 D_1/h_1^2$, (Material
 pair A)
- Figure 6-62:** The normalized transient stress distribution σ_{yy}/σ_0^T in 209
 Model II for $\tau_0=40.0$, $h_2/h_1=24.0$, $\tau_0=t_0 D_1/h_1^2$,
 $\sigma_0^T = -\alpha'_1 E_1 \Theta_0 / (1-\nu_1)$. (Material pair A)
- Figure 6-63:** The normalized stress intensity factor $k(b_1)$ as a 211
 function of nondimensional time τ for an edge crack in
 Model II for $\tau_0=0.0$, $h_2/h_1=3.0$, $R_i/L=9.0$ and
 $\chi L/E_2=0.01108$, $\tau_0=t_0 D_1/h_1^2$, $\sigma_0^T = -\alpha'_1 E_1 \Theta_0 / (1-\nu_1)$
 (material pair A)
- Figure 6-64:** The normalized stress intensity factor $k(b_1)$ as a 212
 function of nondimensional time τ for an edge crack in
 Model II for $\tau_0=6.0$, $h_2/h_1=3.0$, $R_i/L=9.0$ and

$\chi L/E_2=0.01108$, $\tau_0=t_0 D_1/h_1^2$, $\sigma_0^T=-\alpha'_1 E_1 \Theta_0/(1-\nu_1)$
(material pair A)

Figure 6-65: The influence of τ_0 on the normalized stress intensity 213

factor $k(b_1)$ as a function of nondimensional time τ for an
edge crack of length $l_1/h_1=0.2$ in Model II , $h_2/h_1=3.0$,
 $R_i/L=9.0$ and $\chi L/E_2=0.01108$, $\tau_0=t_0 D_1/h_1^2$,
 $\sigma_0^T=-\alpha'_1 E_1 \Theta_0/(1-\nu_1)$ (material pair A)

Figure 6-66: The influence of τ_0 on the normalized stress intensity 214

factor $k(b_1)$ as a function of nondimensional time τ for an
edge crack of length $l_1/h_1=0.9$ in Model II , $h_2/h_1=3.0$,
 $R_i/L=9.0$ and $\chi L/E_2=0.01108$, $\tau_0=t_0 D_1/h_1^2$,
 $\sigma_0^T=-\alpha'_1 E_1 \Theta_0/(1-\nu_1)$ (material pair A)

Figure 6-67: The normalized stress intensity factor $k(b_1)$ as a 215

function of nondimensional time τ for an edge crack in
Model II for $\tau_0=0.0$, $h_2/h_1=9.0$, $R_i/L=9.0$ and
 $\chi L/E_2=0.01108$, $\tau_0=t_0 D_1/h_1^2$, $\sigma_0^T=-\alpha'_1 E_1 \Theta_0/(1-\nu_1)$
(material pair A)

Figure 6-68: The normalized stress intensity factor $k(b_1)$ as a 216

function of nondimensional time τ for an edge crack in
Model II for $\tau_0=10.0$, $h_2/h_1=9.0$, $R_i/L=9.0$ and
 $\chi L/E_2=0.01108$, $\tau_0=t_0 D_1/h_1^2$, $\sigma_0^T=-\alpha'_1 E_1 \Theta_0/(1-\nu_1)$
(material pair A)

Figure 6-69: The influence of τ_0 on the normalized stress intensity 217

factor $k(b_1)$ as a function of nondimensional time τ for an
edge crack of length $l_1/h_1=0.2$ in Model II , $h_2/h_1=9.0$,
 $R_i/L=9.0$ and $\chi L/E_2=0.01108$, $\tau_0=t_0 D_1/h_1^2$,
 $\sigma_0^T=-\alpha'_1 E_1 \Theta_0/(1-\nu_1)$ (material pair A)

Figure 6-70: The influence of τ_0 on the normalized stress intensity 218

factor $k(b_1)$ as a function of nondimensional time τ for an
edge crack of length $l_1/h_1=0.9$ in Model II , $h_2/h_1=9.0$,
 $R_i/L=9.0$ and $\chi L/E_2=0.01108$, $\tau_0=t_0 D_1/h_1^2$,
 $\sigma_0^T=-\alpha'_1 E_1 \Theta_0/(1-\nu_1)$ (material pair A)

Figure 6-71: The normalized stress intensity factor $k(b_1)$ as a function 219

of nondimensional time τ for an edge crack in Model II
for $\tau_0=0.0$, $h_2/h_1=24.0$, $R_i/L=9.0$ and $\chi L/E_2=0.01108$,
 $\tau_0=t_0 D_1/h_1^2$, $\sigma_0^T=-\alpha'_1 E_1 \Theta_0/(1-\nu_1)$ (material pair A)

Figure 6-72: The normalized stress intensity factor $k(b_1)$ as a 220

function of nondimensional time τ for an edge crack in
Model II for $\tau_0=20.0$, $h_2/h_1=24.0$, $R_i/L=9.0$ and
 $\chi L/E_2=0.01108$, $\tau_0=t_0 D_1/h_1^2$, $\sigma_0^T=-\alpha'_1 E_1 \Theta_0/(1-\nu_1)$

- (material pair A)
- Figure 6-73:** The influence of τ_0 on the normalized stress intensity factor $k(b_1)$ as a function of nondimensional time τ for an edge crack of length $l_1/h_1=0.2$ in Model II , $h_2/h_1=24.0$, $R_i/L=9.0$ and $\chi L/E_2=0.01108$, $\tau_0=t_0 D_1/h_1^2$, $\sigma_0^T=-\alpha'_1 E_1 \Theta_0/(1-\nu_1)$ (material pair A) 221
- Figure 6-74:** The influence of τ_0 on the normalized stress intensity factor $k(b_1)$ as a function of nondimensional time τ for an edge crack of length $l_1/h_1=0.9$ in Model II , $h_2/h_1=24.0$, $R_i/L=9.0$ and $\chi L/E_2=0.01108$, $\tau_0=t_0 D_1/h_1^2$, $\sigma_0^T=-\alpha'_1 E_1 \Theta_0/(1-\nu_1)$ (material pair A) 222
- Figure 6-75:** The influence of τ_0 on the normalized stress intensity factor $k(b_1)$ as a function of nondimensional time τ for a broken clad in Model II $h_2/h_1=3.0$, $R_i/L=9.0$ and $\chi L/E_2=0.01108$, $\tau_0=t_0 D_1/h_1^2$, $\sigma_0^T=-\alpha'_1 E_1 \Theta_0/(1-\nu_1)$ (material pair A) 223
- Figure 6-76:** The influence of τ_0 on the normalized stress intensity factor $k(b_1)$ as a function of nondimensional time τ for a broken clad in Model II $h_2/h_1=9.0$, $R_i/L=9.0$ and $\chi L/E_2=0.01108$, $\tau_0=t_0 D_1/h_1^2$, $\sigma_0^T=-\alpha'_1 E_1 \Theta_0/(1-\nu_1)$ (material pair A) 224
- Figure 6-77:** The influence of τ_0 on the normalized stress intensity factor $k(b_1)$ as a function of nondimensional time τ for a broken clad in Model II $h_2/h_1=24.0$, $R_i/L=9.0$ and $\chi L/E_2=0.01108$, $\tau_0=t_0 D_1/h_1^2$, $\sigma_0^T=-\alpha'_1 E_1 \Theta_0/(1-\nu_1)$ (material pair A) 225
- Figure 6-78:** The influence of τ_0 on the normalized stress intensity factor $k(a_2)$ as a function of nondimensional time τ for an under-clad crack of length $l_2/h_1=0.004$ in Model II $h_2/h_1=3.0$, $R_i/L=9.0$ and $\chi L/E_2=0.01108$, $\tau_0=t_0 D_1/h_1^2$, $\sigma_0^T=-\alpha'_1 E_1 \Theta_0/(1-\nu_1)$ (material pair A) 226
- Figure 6-79:** The influence of τ_0 on the normalized stress intensity factor $k(b_2)$ as a function of nondimensional time τ for a fixed under-clad crack length $l_2/h_1=0.004$ in Model II $h_2/h_1=3.0$, $R_i/L=9.0$ and $\chi L/E_2=0.01108$, $\tau_0=t_0 D_1/h_1^2$, $\sigma_0^T=-\alpha'_1 E_1 \Theta_0/(1-\nu_1)$ (material pair A) 227
- Figure 6-80:** The normalized stress intensity factor $k(a_2)$ as a function of nondimensional time τ for an under-clad crack in Model II for $\tau_0=0.0$, $h_2/h_1=9.0$, $R_i/L=9.0$ and $\chi L/E_2=0.01108$, $\tau_0=t_0 D_1/h_1^2$, $\sigma_0^T=-\alpha'_1 E_1 \Theta_0/(1-\nu_1)$ 228

- .(material pair A)
- Figure 6-81:** The normalized stress intensity factor $k(b_2)$ as a function 229
of nondimensional time τ for an under-clad crack in
Model II for $\tau_0=0.0$, $h_2/h_1=9.0$, $R_i/L=9.0$ and
 $\chi L/E_2=0.01108$, $\tau_0=t_0 D_1/h_1^2$, $\sigma_0^T=-\alpha_1' E_1 \Theta_0/(1-\nu_1)$
.(material pair A)
- Figure 6-82:** The normalized stress intensity factor $k(a_2)$ as a 230
function of nondimensional time τ for an under-clad
crack in Model II for $\tau_0=10.0$, $h_2/h_1=9.0$, $R_i/L=9.0$ and
 $\chi L/E_2=0.01108$, $\tau_0=t_0 D_1/h_1^2$, $\sigma_0^T=-\alpha_1' E_1 \Theta_0/(1-\nu_1)$
.(material pair A)
- Figure 6-83:** The normalized stress intensity factor $k(b_2)$ as a 231
function of nondimensional time τ for an under-clad
crack in Model II for $\tau_0=10.0$, $h_2/h_1=9.0$, $R_i/L=9.0$ and
 $\chi L/E_2=0.01108$, $\tau_0=t_0 D_1/h_1^2$, $\sigma_0^T=-\alpha_1' E_1 \Theta_0/(1-\nu_1)$
.(material pair A)
- Figure 6-84:** The influence of τ_0 on the normalized stress intensity 232
factor $k(a_2)$ as a function of nondimensional time τ for an
under-clad crack of length $l_2/h_1=1.0$ in Model II
 $h_2/h_1=9.0$, $R_i/L=9.0$ and $\chi L/E_2=0.01108$, $\tau_0=t_0 D_1/h_1^2$,
 $\sigma_0^T=-\alpha_1' E_1 \Theta_0/(1-\nu_1)$ (material pair A)
- Figure 6-85:** The influence of τ_0 on the normalized stress intensity 233
factor $k(b_2)$ as a function of nondimensional time τ for an
under-clad crack of length $l_2/h_1=1.0$ in Model II
 $h_2/h_1=9.0$, $R_i/L=9.0$ and $\chi L/E_2=0.01108$, $\tau_0=t_0 D_1/h_1^2$,
 $\sigma_0^T=-\alpha_1' E_1 \Theta_0/(1-\nu_1)$ (material pair A)
- Figure 6-86:** The influence of τ_0 on the normalized stress intensity 234
factor $k(a_2)$ as a function of nondimensional time τ for an
under-clad crack of length $l_2/h_1=3.0$ in Model II
 $h_2/h_1=9.0$, $R_i/L=9.0$ and $\chi L/E_2=0.01108$, $\tau_0=t_0 D_1/h_1^2$,
 $\sigma_0^T=-\alpha_1' E_1 \Theta_0/(1-\nu_1)$ (material pair A)
- Figure 6-87:** The influence of τ_0 on the normalized stress intensity 235
factor $k(b_2)$ as a function of nondimensional time τ for an
under-clad crack of length $l_2/h_1=3.0$ in Model II
 $h_2/h_1=9.0$, $R_i/L=9.0$ and $\chi L/E_2=0.01108$, $\tau_0=t_0 D_1/h_1^2$,
 $\sigma_0^T=-\alpha_1' E_1 \Theta_0/(1-\nu_1)$ (material pair A)
- Figure 6-88:** The normalized stress intensity factor $k(a_2)$, $k(b_2)$ as a 236
function of nondimensional time τ for under-clad crack
in Model II for $l_2/h_1=9.0$, $\tau_0=0.0$, $h_2/h_1=24.0$, $R_i/L=9.0$
and $\chi L/E_2=0.01108$, $\tau_0=t_0 D_1/h_1^2$, $\sigma_0^T=-\alpha_1' E_1 \Theta_0/(1-\nu_1)$
.(material pair A)

- Figure 6-89:** The normalized stress intensity factor $k(b_2)$ as a function of nondimensional time τ for an under-clad crack in Model II for $\tau_0=0.0$, $h_2/h_1=24.0$, $R_i/L=9.0$ and $\chi L/E_2=0.01108$, $\tau_0=t_0 D_1/h_1^2$, $\sigma_0^T=-\alpha'_1 E_1 \Theta_0/(1-\nu_1)$ (material pair A) 237
- Figure 6-90:** The normalized stress intensity factor $k(a_2)$, $k(b_2)$ as a function of nondimensional time τ for an under-clad crack in Model II for $l_2/h_1=9.0$, $\tau_0=20.0$, $h_2/h_1=24.0$, $R_i/L=9.0$ and $\chi L/E_2=0.01108$, $\tau_0=t_0 D_1/h_1^2$, $\sigma_0^T=-\alpha'_1 E_1 \Theta_0/(1-\nu_1)$ (material pair A) 238
- Figure 6-91:** The normalized stress intensity factor $k(b_2)$ as a function of nondimensional time τ for an under-clad crack in Model II for $\tau_0=20.0$, $h_2/h_1=24.0$, $R_i/L=9.0$ and $\chi L/E_2=0.01108$, $\tau_0=t_0 D_1/h_1^2$, $\sigma_0^T=-\alpha'_1 E_1 \Theta_0/(1-\nu_1)$ (material pair A) 239
- Figure 6-92:** The influence of τ_0 on the normalized stress intensity factor $k(a_2)$ as a function of nondimensional time τ for an under-clad crack of length $l_2/h_1=0.5$ in Model II, $h_2/h_1=24.0$, $R_i/L=9.0$ and $\chi L/E_2=0.01108$, $\tau_0=t_0 D_1/h_1^2$, $\sigma_0^T=-\alpha'_1 E_1 \Theta_0/(1-\nu_1)$ (material pair A) 240
- Figure 6-93:** The influence of τ_0 on the normalized stress intensity factor $k(b_2)$ as a function of nondimensional time τ for an under-clad crack of length $l_2/h_1=0.5$ in Model II, $h_2/h_1=24.0$, $R_i/L=9.0$ and $\chi L/E_2=0.01108$, $\tau_0=t_0 D_1/h_1^2$, $\sigma_0^T=-\alpha'_1 E_1 \Theta_0/(1-\nu_1)$ (material pair A) 241
- Figure 6-94:** The influence of τ_0 on the normalized stress intensity factor $k(a_2)$ as a function of nondimensional time τ for an under-clad crack of length $l_2/h_1=4.0$ in Model II, $h_2/h_1=24.0$, $R_i/L=9.0$ and $\chi L/E_2=0.01108$, $\tau_0=t_0 D_1/h_1^2$, $\sigma_0^T=-\alpha'_1 E_1 \Theta_0/(1-\nu_1)$ (material pair A) 242
- Figure 6-95:** The influence of τ_0 on the normalized stress intensity factor $k(b_2)$ as a function of nondimensional time τ for an under-clad crack of length $l_2/h_1=4.0$ in Model II, $h_2/h_1=24.0$, $R_i/L=9.0$ and $\chi L/E_2=0.01108$, $\tau_0=t_0 D_1/h_1^2$, $\sigma_0^T=-\alpha'_1 E_1 \Theta_0/(1-\nu_1)$ (material pair A) 243
- Figure 6-96:** The normalized stress intensity factor $k(b_2)$ as a function of nondimensional time τ for an edge crack crossing the interface in Model II for $\tau_0=0.0$, $h_2/h_1=3.0$, $R_i/L=9.0$ and $\chi L/E_2=0.01108$, $\tau_0=t_0 D_1/h_1^2$, $\sigma_0^T=-\alpha'_1 E_1 \Theta_0/(1-\nu_1)$ (material pair A) 244

- Figure 6-97:** The normalized stress intensity factor $k(b_2)$ as a function of nondimensional time τ for an edge crack crossing the interface in Model II for $\tau_0=6.0$, $h_2/h_1=3.0$, $R_i/L=9.0$ and $\chi L/E_2=0.01108$, $\tau_0=t_0 D_1/h_1^2$, $\sigma_0^T=-\alpha'_1 E_1 \Theta_0/(1-\nu_1)$ (material pair A) 245
- Figure 6-98:** The influence of τ_0 on the normalized stress intensity factor $k(b_2)$ as a function of nondimensional time τ for an edge crack of length $l/h_1=1.2$ crossing the interface in Model II, $h_2/h_1=3.0$, $R_i/L=9.0$ and $\chi L/E_2=0.01108$, $\tau_0=t_0 D_1/h_1^2$, $\sigma_0^T=-\alpha'_1 E_1 \Theta_0/(1-\nu_1)$ (material pair A) 246
- Figure 6-99:** The influence of τ_0 on the normalized stress intensity factor $k(b_2)$ as a function of nondimensional time τ for an edge crack of length $l/h_1=2.0$ crossing the interface in Model II, $h_2/h_1=3.0$, $R_i/L=9.0$ and $\chi L/E_2=0.01108$, $\tau_0=t_0 D_1/h_1^2$, $\sigma_0^T=-\alpha'_1 E_1 \Theta_0/(1-\nu_1)$ (material pair A) 247
- Figure 6-100:** The normalized stress intensity factor $k(b_2)$ as a function of nondimensional time τ for an edge crack crossing the interface in Model II for $\tau_0=0.0$, $h_2/h_1=9.0$, $R_i/L=9.0$ and $\chi L/E_2=0.01108$, $\tau_0=t_0 D_1/h_1^2$, $\sigma_0^T=-\alpha'_1 E_1 \Theta_0/(1-\nu_1)$ (material pair A) 248
- Figure 6-101:** The normalized stress intensity factor $k(b_2)$ as a function of nondimensional time τ for an edge crack crossing the interface in Model II for $\tau_0=10.0$, $h_2/h_1=9.0$, $R_i/L=9.0$ and $\chi L/E_2=0.01108$, $\tau_0=t_0 D_1/h_1^2$, $\sigma_0^T=-\alpha'_1 E_1 \Theta_0/(1-\nu_1)$ (material pair A) 249
- Figure 6-102:** The influence of τ_0 on the normalized stress intensity factor $k(b_2)$ as a function of nondimensional time τ for an edge crack of length $l/h_1=1.5$ crossing the interface in Model II, $h_2/h_1=9.0$, $R_i/L=9.0$ and $\chi L/E_2=0.01108$, $\tau_0=t_0 D_1/h_1^2$, $\sigma_0^T=-\alpha'_1 E_1 \Theta_0/(1-\nu_1)$ (material pair A) 250
- Figure 6-103:** The influence of τ_0 on the normalized stress intensity factor $k(b_2)$ as a function of nondimensional time τ for an edge crack of length $l/h_1=4.0$ crossing the interface in Model II, $h_2/h_1=9.0$, $R_i/L=9.0$ and $\chi L/E_2=0.01108$, $\tau_0=t_0 D_1/h_1^2$, $\sigma_0^T=-\alpha'_1 E_1 \Theta_0/(1-\nu_1)$ (material pair A) 251
- Figure 6-104:** The normalized stress intensity factor $k(b_2)$ as a function of nondimensional time τ for an edge crack crossing the interface in Model II for $\tau_0=0.0$, $h_2/h_1=24.0$, $R_i/L=9.0$ and $\chi L/E_2=0.01108$, $\tau_0=t_0 D_1/h_1^2$, $\sigma_0^T=-\alpha'_1 E_1 \Theta_0/(1-\nu_1)$ (material pair A) 252

Figure 6-105: The normalized stress intensity factor $k(b_2)$ as a function of nondimensional time τ for an edge crack crossing the interface in Model II for $\tau_0=20.0$, $h_2/h_1=24.0$, $R_i/L=9.0$ and $\chi L/E_2=0.01108$, $\tau_0=t_0 D_1/h_1^2$, $\sigma_0^T=-\alpha'_1 E_1 \Theta_0/(1-\nu_1)$ (material pair A)	253
Figure 6-106: The influence of τ_0 on the normalized stress intensity factor $k(b_2)$ as a function of nondimensional time τ for an edge crack of length $l/h_1=1.5$ crossing the interface in Model II , $h_2/h_1=24.0$, $R_i/L=9.0$ and $\chi L/E_2=0.01108$, $\tau_0=t_0 D_1/h_1^2$, $\sigma_0^T=-\alpha'_1 E_1 \Theta_0/(1-\nu_1)$ (material pair A)	254
Figure 6-107: The influence of τ_0 on the normalized stress intensity factor $k(b_2)$ as a function of nondimensional time τ for an edge crack of length $l/h_1=5.0$ crossing the interface in Model II , $h_2/h_1=24.0$, $R_i/L=9.0$ and $\chi L/E_2=0.01108$, $\tau_0=t_0 D_1/h_1^2$, $\sigma_0^T=-\alpha'_1 E_1 \Theta_0/(1-\nu_1)$ (material pair A)	255
Figure 6-108: The normalized transient temperature distribution in Model II for $\tau_0=0.0$, $h_2/h_1=9.0$, $\tau_0=t_0 D_1/h_1^2$, (material pair B)	256
Figure 6-109: The normalized transient stress distribution σ_{yy}/σ_0^T in Model II for $\tau_0=0.0$, $h_2/h_1=9.0$, $\tau_0=t_0 D_1/h_1^2$, $\sigma_0^T=-\alpha'_1 E_1 \Theta_0/(1-\nu_1)$. (material pair B)	257
Figure 6-110: The normalized transient temperature distribution in Model II for $\tau_0=6.0$, $h_2/h_1=9.0$, $\tau_0=t_0 D_1/h_1^2$, (material pair B)	259
Figure 6-111: The normalized transient stress distribution σ_{yy}/σ_0^T in Model II for $\tau_0=6.0$, $h_2/h_1=9.0$, $\tau_0=t_0 D_1/h_1^2$, $\sigma_0^T=-\alpha'_1 E_1 \Theta_0/(1-\nu_1)$. (material pair B)	260
Figure 6-112: The normalized transient temperature distribution in Model II for $\tau_0=10.0$, $h_2/h_1=9.0$, $\tau_0=t_0 D_1/h_1^2$, (material pair B)	262
Figure 6-113: The normalized transient stress distribution σ_{yy}/σ_0^T in Model II for $\tau_0=10.0$, $h_2/h_1=9.0$, $\tau_0=t_0 D_1/h_1^2$, $\sigma_0^T=-\alpha'_1 E_1 \Theta_0/(1-\nu_1)$. (material pair B)	263
Figure 6-114: The normalized transient temperature distribution in Model II for $\tau_0=20.0$, $h_2/h_1=9.0$, $\tau_0=t_0 D_1/h_1^2$, (material pair B)	265
Figure 6-115: The normalized transient stress distribution σ_{yy}/σ_0^T in Model II for $\tau_0=20.0$, $h_2/h_1=9.0$, $\tau_0=t_0 D_1/h_1^2$, $\sigma_0^T=-\alpha'_1 E_1 \Theta_0/(1-\nu_1)$. (material pair B)	266
Figure 6-116: The normalized stress intensity factor $k(b_1)$ as a	268

function of nondimensional time τ for an edge crack in Model II for $\tau_0=0.0$, $h_2/h_1=9.0$, $R_i/L=9.0$ and $\chi L/E_2=0.01185$, $\tau_0=t_0 D_1/h_1^2$, $\sigma_0^T=-\alpha'_1 E_1 \Theta_0/(1-\nu_1)$ (material pair B)

Figure 6-117: The normalized stress intensity factor $k(b_1)$ as a 269

function of nondimensional time τ for an edge crack in Model II for $\tau_0=10.0$, $h_2/h_1=9.0$, $R_i/L=9.0$ and $\chi L/E_2=0.01185$, $\tau_0=t_0 D_1/h_1^2$, $\sigma_0^T=-\alpha'_1 E_1 \Theta_0/(1-\nu_1)$ (material pair B)

Figure 6-118: The influence of τ_0 on the normalized stress intensity 270

factor $k(b_1)$ as a function of nondimensional time τ for an edge crack of length $l_1/h_1=0.2$ in Model II , $h_2/h_1=9.0$, $R_i/L=9.0$ and $\chi L/E_2=0.01185$, $\tau_0=t_0 D_1/h_1^2$, $\sigma_0^T=-\alpha'_1 E_1 \Theta_0/(1-\nu_1)$ (material pair B)

Figure 6-119: The influence of τ_0 on the normalized stress intensity 271

factor $k(b_1)$ as a function of nondimensional time τ for a broken clad in Model II for $\beta_1=0.552538$, $h_2/h_1=9.0$, $R_i/L=9.0$ and $\chi L/E_2=0.01185$, $\tau_0=t_0 D_1/h_1^2$, $\sigma_0^T=-\alpha'_1 E_1 \Theta_0/(1-\nu_1)$ (material pair B)

Figure 6-120: The normalized stress intensity factor $k(a_2)$ as a 272

function of nondimensional time τ for an under-clad crack in Model II for $\alpha_2=0.4512416$, $\tau_0=0.0$, $h_2/h_1=9.0$, $R_i/L=9.0$ and $\chi L/E_2=0.01185$, $\tau_0=t_0 D_1/h_1^2$, $\sigma_0^T=-\alpha'_1 E_1 \Theta_0/(1-\nu_1)$.(material pair B)

Figure 6-121: The normalized stress intensity factor $k(b_2)$ as a 273

function of nondimensional time τ for an under-clad crack in Model II for $\alpha_2=0.4512416$, $\tau_0=0.0$, $h_2/h_1=9.0$, $R_i/L=9.0$ and $\chi L/E_2=0.01185$, $\tau_0=t_0 D_1/h_1^2$, $\sigma_0^T=-\alpha'_1 E_1 \Theta_0/(1-\nu_1)$.(material pair B)

Figure 6-122: The normalized stress intensity factor $k(a_2)$ as a 274

function of nondimensional time τ for an under-clad crack in Model II for $\alpha_2=0.4512416$, $\tau_0=10.0$, $h_2/h_1=9.0$, $R_i/L=9.0$ and $\chi L/E_2=0.01185$, $\tau_0=t_0 D_1/h_1^2$, $\sigma_0^T=-\alpha'_1 E_1 \Theta_0/(1-\nu_1)$.(material pair B)

Figure 6-123: The normalized stress intensity factor $k(b_2)$ as a 275

function of nondimensional time τ for an under-clad crack in Model II for $\alpha_2=0.4512416$, $\tau_0=10.0$, $h_2/h_1=9.0$, $R_i/L=9.0$ and $\chi L/E_2=0.01185$, $\tau_0=t_0 D_1/h_1^2$, $\sigma_0^T=-\alpha'_1 E_1 \Theta_0/(1-\nu_1)$.(material pair B)

Figure 6-124: The influence of τ_0 on the normalized stress intensity 276

- factor $k(a_2)$ as a function of nondimensional time τ for an under-clad crack of length $l_2/h_1=1.0$ in Model II, $\alpha_2=0.4512416$ $h_2/h_1=9.0$, $R_i/L=9.0$ and $\chi L/E_2=0.01185$, $\tau_0=t_0 D_1/h_1^2$, $\sigma_0^T=-\alpha_1' E_1 \Theta_0/(1-\nu_1)$ (material pair B)
- Figure 6-125:** The influence of τ_0 on the normalized stress intensity factor $k(b_2)$ as a function of nondimensional time τ for an under-clad crack of length $l_2/h_1=1.0$ in Model II $\alpha_2=0.4512416$ $h_2/h_1=9.0$, $R_i/L=9.0$ and $\chi L/E_2=0.01185$, $\tau_0=t_0 D_1/h_1^2$, $\sigma_0^T=-\alpha_1' E_1 \Theta_0/(1-\nu_1)$ (material pair B) 277
- Figure 6-126:** The normalized stress intensity factor k_x as a function of nondimensional time τ for an edge crack crossing the interface in Model II for $\beta_1=\alpha_2=0.0187223$, $\tau_0=0.0$, $h_2/h_1=9.0$, $R_i/L=9.0$ and $\chi L/E_2=0.01185$, $\tau_0=t_0 D_1/h_1^2$, $\sigma_0^T=-\alpha_1' E_1 \Theta_0/(1-\nu_1)$. (material pair B) 278
- Figure 6-127:** The normalized stress intensity factor k_{xy} as a function of nondimensional time τ for an edge crack crossing the interface in Model II for $\beta_1=\alpha_2=0.0187223$, $\tau_0=0.0$, $h_2/h_1=9.0$, $R_i/L=9.0$ and $\chi L/E_2=0.01185$, $\tau_0=t_0 D_1/h_1^2$, $\sigma_0^T=-\alpha_1' E_1 \Theta_0/(1-\nu_1)$. (material pair B) 279
- Figure 6-128:** The normalized stress intensity factor $k(b_2)$ as a function of nondimensional time τ for an edge crack crossing the interface in Model II for $\beta_1=\alpha_2=0.0187223$, $\tau_0=0.0$, $h_2/h_1=9.0$, $R_i/L=9.0$ and $\chi L/E_2=0.01185$, $\tau_0=t_0 D_1/h_1^2$, $\sigma_0^T=-\alpha_1' E_1 \Theta_0/(1-\nu_1)$. (material pair B) 280
- Figure 6-129:** The normalized stress intensity factor k_x as a function of nondimensional time τ for an edge crack crossing the interface in Model II for $\beta_1=\alpha_2=0.0187223$, $\tau_0=10.0$, $h_2/h_1=9.0$, $R_i/L=9.0$ and $\chi L/E_2=0.01185$, $\tau_0=t_0 D_1/h_1^2$, $\sigma_0^T=-\alpha_1' E_1 \Theta_0/(1-\nu_1)$. (material pair B) 281
- Figure 6-130:** The normalized stress intensity factor k_{xy} as a function of nondimensional time τ for an edge crack crossing the interface in Model II for $\beta_1=\alpha_2=0.0187223$, $\tau_0=10.0$, $h_2/h_1=9.0$, $R_i/L=9.0$ and $\chi L/E_2=0.01185$, $\tau_0=t_0 D_1/h_1^2$, $\sigma_0^T=-\alpha_1' E_1 \Theta_0/(1-\nu_1)$. (material pair B) 282
- Figure 6-131:** The normalized stress intensity factor $k(b_2)$ as a function of nondimensional time τ for an edge crack crossing the interface in Model II for $\beta_1=\alpha_2=0.0187223$, $\tau_0=10.0$, $h_2/h_1=9.0$, $R_i/L=9.0$ and $\chi L/E_2=0.01185$, $\tau_0=t_0 D_1/h_1^2$, $\sigma_0^T=-\alpha_1' E_1 \Theta_0/(1-\nu_1)$. (material pair B) 283
- Figure 6-132:** The influence of τ_0 on the normalized stress intensity 284

factor k_x as a function of nondimensional time τ for an edge crack of length $l/h_1=1.5$ crossing the interface, in Model II for $\beta_1=\alpha_2=0.01872238$, $h_2/h_1=9.0$, $R_i/L=9.0$ and $\chi L/E_2=0.01185$, $\tau_0=t_0 D_1/h_1^2$, $\sigma_0^T=-\alpha_1' E_1 \Theta_0/(1-\nu_1)$. (material pair B)

Figure 6-133: The influence of τ_0 on the normalized stress intensity factor k_{xy} as a function of nondimensional time τ for an edge crack of length $l/h_1=1.5$ crossing the interface, in Model II for $\beta_1=\alpha_2=0.01872238$, $h_2/h_1=9.0$, $R_i/L=9.0$ and $\chi L/E_2=0.01185$, $\tau_0=t_0 D_1/h_1^2$, $\sigma_0^T=-\alpha_1' E_1 \Theta_0/(1-\nu_1)$. (material pair B) 285

Figure 6-134: The influence of τ_0 on the normalized stress intensity factor $k(b_2)$ as a function of nondimensional time τ for an edge crack of length $l/h_1=1.5$ crossing the interface, in Model II for $\beta_1=\alpha_2=0.01872238$, $h_2/h_1=9.0$, $R_i/L=9.0$ and $\chi L/E_2=0.01185$, $\tau_0=t_0 D_1/h_1^2$, $\sigma_0^T=-\alpha_1' E_1 \Theta_0/(1-\nu_1)$. (material pair B) 286

List of Tables

Table 6-1: Properties of materials pairs used in this work	122
Table 6-2: Normalized stress intensity factor for an embedded crack (equation (6.6)), obtained from the plastic strip model, $\tau_0=0.0$, $\sigma_0^T=-\alpha_1' E_1 \Theta_0/(1-\nu_1)$, for Model I. (Material pair A)	122
Table 6-3: Comparison of the normalized stress intensity factors obtained from a yielded clad and an elastic clad for various values of the crack length, $\tau_0=0.0$, $\sigma_0^T=-\alpha_1' E_1 \Theta_0/(1-\nu_1)$, for Model I.(Material pair A)	122
Table 6-4: Normalized stress intensity factors for an edge crack in a homogeneous strip of thickness L under uniform load σ_0 (without elastic foundation, $\chi=0.0$ and with elastic foundation $R_i/L=9.0$ and $\chi L/E=0.01108$)	123
Table 6-5: Normalized stress intensity factors for a crack terminating at the interface under uniform load σ_0 , ($l_2/h_1=0.1$ in the present work).	123
Table 6-6: Normalized stress intensity factors for an embedded crack going through the interface under loading $P_1/P_2=(E_1/E_2)(1-\nu_2^2/1-\nu_1^2)$, $\nu_1=0.3$, $\nu_2=0.35$, $\mu_1/\mu_2=23.077$, $\beta=\beta_1=\alpha_2=0.273692$, $l_1/h_1=0.1$, $l_2/h_1=0.05, 0.025$.	124
Table 6-7: Normalized stress intensity factors for an edge crack in a homogeneous strip of thickness L under uniform stress σ_0 and for fixed crack length $b_1/L=0.5$, various values of χ (stiffness of the elastic foundation)	124
Table 6-8: Comparison between normalized stress intensity factors for an edge crack under uniform loading σ_0 in a homogeneous strip on an elastic foundation χ , and a homogeneous cylinder $R_i/L=9.0$.	125
Table 6-9: Comparison between transient temperature distribution Θ/Θ_0 for a hollow cylinder and a homogeneous strip on an elastic foundation χ due to a unit step temperature change on the inner wall, $R_i/L=9.0$ and $\chi L/E=0.01108$, $\tau=tD/L^2$.	126
Table 6-10: Comparison between Stress distribution σ_{yy}/σ_0 for a hollow cylinder and a homogeneous strip on an elastic foundation χ due to a unit step temperature change on the inner wall, $R_i/L=9.0$ and $\chi L/E=0.01108$, $\tau=tD/L^2$.	128
Table 6-11: Comparison between normalized stress intensity factors for an edge crack subjected to transient thermal stresses in a hollow cylinder and a homogeneous strip on an elastic foundation χ , $R_i/L=9.0$ and $\chi L/E=0.01108$, $\tau=tD/L^2$, $\sigma_0^T=-\alpha E \Theta_0/(1-\nu)$.	130
Table 6-12: The maximum of normalized stress intensity factors for an under-clad crack subjected to transient thermal stresses, $h_2/h_1=3.0$, $R_i/L=9.0$ and $\chi L/E=0.01108$.	131

	(material pair A).	
Table 6-13:	The maximum of normalized stress intensity factors for an under-clad crack subjected to transient thermal stresses, $h_2/h_1=9.0$, $R_i/L=9.0$ and $\chi L/E_2=0.01108$. (material pair A).	132
Table 6-14:	The maximum of normalized stress intensity factors for an under-clad crack subjected to transient thermal stresses, $h_2/h_1=24.0$, $R_i/L=9.0$ and $\chi L/E_2=0.01108$. (material pair A).	133
Table 6-15:	The maximum of normalized stress intensity factors for an edge crack subjected to transient thermal stresses, $h_2/h_1=3.0$, $R_i/L=9.0$ and $\chi L/E_2=0.01108$. (material pair A).	134
Table 6-16:	The maximum of normalized stress intensity factors for an edge crack subjected to transient thermal stresses, $h_2/h_1=9.0$, $R_i/L=9.0$ and $\chi L/E_2=0.01108$. (material pair A).	135
Table 6-17:	The maximum of normalized stress intensity factors for an edge crack subjected to transient thermal stresses, $h_2/h_1=24.0$, $R_i/L=9.0$ and $\chi L/E_2=0.01108$. (material pair A).	136

ABSTRACT

In many applications, such as nuclear pressure vessels, micro-electronics, and the chemical industry, the study of transient thermal stresses in layered cylinders and plates in the presence of a crack is required. In this study first the cladded pressure vessel under thermal shock conditions which is simulated by using two simpler models. The first model (Model I) assumes that, if the crack size is very small compared to the vessel thickness, the problem can be treated as a semi-infinite elastic medium bonded to a very thin layer of different material. However, if the crack size is of the same order as the vessel thickness, the curvature effects may not be negligible. In this case it is assumed that the relatively thin walled hollow cylinder with cladding can be treated as a composite beam on an elastic foundation (Model II). In both models, the effect of surface cooling rate is studied by assuming the temperature boundary condition to be a ramp function. Among the crack geometries considered are: the edge crack in the clad, the broken clad, the edge crack going through the interface, the under-clad crack in the base material, and an internal crack crossing the interface.

The calculated results include the transient temperature, thermal stresses in the uncracked medium and stress intensity factors which are presented as a function of time, and the duration of cooling ramp. The stress intensity factors are also presented as a function of the size and the location of the crack. The problem is solved for two bonded materials of different thermal and mechanical properties. The mathematical formulation results in two singular integral equations which are solved numerically. The results are given for two material pairs, namely an austenitic steel layer welded on a ferritic steel substrate, and a ceramic coating on ferritic steel. In the case of the yielded clad, the stress

intensity factors for a crack under the clad are determined by using a plastic strip model and are compared with elastic clad results. When the results obtained are compared with the corresponding elasticity solution for the thick-walled cylinder, the agreement was found to be quite satisfactory.

In the composite plate with finite thickness the calculated results indicate that the peak values of the stress intensity factors decrease with decreasing cooling rate of the surface. On the other hand, in the case of semi-infinite medium (Model I), since the medium is fully constrained at infinity, the maximum values of the stress intensity factors are attained at steady state.

The technique developed and the dimensionless results given in this study are , of course, applicable to any composite plate that is locally subjected to thermal shock.

Chapter 1

INTRODUCTION

It is known that the cladding, when bonded to the inner wall of pressure vessels or pipes, can be very effective in protecting the base metal from severe corrosion. In the nuclear pressure vessels the cladding serves the additional purpose of protecting the base metal from radiation damage. In some other applications, as in micro-electronics and the chemical industry where coating is used very widely, the study of residual stresses and transient thermal stresses in layered cylinders and plates is required.

Our aim in this work is to study the structural integrity of clad materials under severe thermal transient stresses in the presence of pre-existing flaws. These flaws may be due to imperfections such as voids, inclusions, or weld defects, which are generally treated as cracks. In case of pressure vessels with cladding, the cracks have been observed underneath the clad oriented in a plane perpendicular to the cylinder axis and terminating at the interface.

In analyzing the subcritical crack growth in homogeneous materials, it is generally accepted that the stress intensity factor can be used quite effectively as a correlation parameter. The objective of this study is therefore to investigate the effect of the clad on the stress intensity factors in the case of a crack perpendicular to the interface under transient thermal stresses. Once we know the stress intensity factor, we could also determine whether catastrophic failure will occur in brittle materials due to unstable crack propagation.

The thermal shock problem for a circumferentially cracked hollow cylinder with cladding was considered by Nied [1] for two special crack configurations. First, the circumferential crack embedded in the base metal, where the crack tip

is located just underneath the clad. Second, the edge crack which completely passes through the clad. His basic assumptions were

1. The problem is axisymmetric for both crack geometry and temperature boundary conditions.
2. The change in surface temperature is a unit step function.
3. The transient thermal stress is quasi-static, i.e, the inertia effects are negligible.
4. The materials are assumed to be isotropic, homogeneous, and linearly elastic such that the clad and the base material have the same elastic modulus and Poisson's ratio. i.e, $E_1 = E_2$, $\nu_1 = \nu_2$, but non-homogeneous in thermal properties.
5. If the cladding is sufficiently ductile, during a thermal transient, the cladding may yield. In this case the clad is examined by using a plastic strip model, which assumes that the clad is perfectly plastic.

Now, by assuming an extremely severe temperature change at the inner wall of the cylinder, i.e., a step change in the inner wall temperature, he obtained a peak value of thermal stresses. These stresses should be lower if one assumes a more realistic temperature boundary condition. Erdogan [2] compared two sets of data to show the effect of the temperature boundary condition at the inner wall of a vessel without cladding, first set for a homogeneous vessel which contains a circumferential edge crack on the inner wall obtained from [3] where a step change in temperature is used as the boundary condition, and the second set for the same problem where a smoother temperature boundary condition obtained from [4] was used. He showed a significant difference between the two sets. Hence, a reduction in the stress intensity factors in Nied's results would occur if we repeat his work with more realistic temperature boundary condition.

The main objective of this work is to solve the crack problem under transient thermal stresses with temperature boundary conditions at the inner wall of the cylinder that are somewhat more realistic than the step function

temperature used in previous studies as shown in Figure 1.1.c , and provided that the clad and the base materials have different thermal and mechanical properties.

The actual problem is a very complicated three-dimensional problem and seems to be analytically intractable. So, we are going to simulate the problem by using two simpler models depending on the crack size.

Model I

Since the clad has a relatively small thickness, the base material has a large bulk, and the radius of the cylinder is large, the total strains in axial and circumferential directions would be nearly zero during transient heating or cooling. Also, since the surfaces of the cylinder are stress free, the radial stresses would also be negligible small. Thus, in case of a crack that is very small in size compared to the other dimensions, the problem can be treated as a semi-infinite elastic medium (base) bonded to a surface layer of different material (clad) of thickness h , shown in Figure 1.1.a (see for example [2]). In some other applications, this model can also be applied to certain micro-electronic devices and ceramic coated metal parts consisting of a relatively thin coating bonded to an elastic substrate and subjected to rapidly changing thermal environments.

Model II

In the case of a relatively large crack size, the more realistic model for thin walled hollow cylinders with cladding would be a composite beam on an elastic foundation in which the modulus of the foundation χ is a function of the thickness of the cylinder wall, the radius of the cylinder, and the modulus of elasticity, see [5]. The problem of interest is depicted in Figure 1.1.b. This model can also be used in other cases such as, for example, a fully or partially constrained composite plate in which the effect of the constraints can be

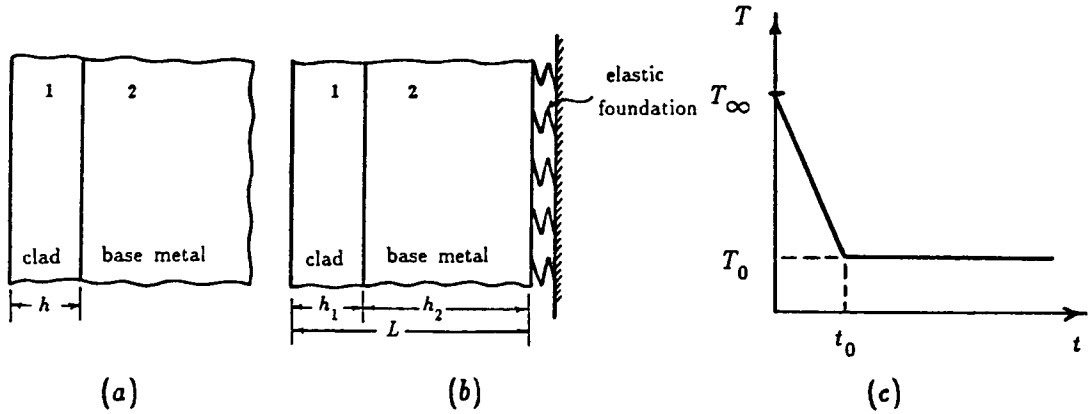


Figure 1-1: a-The geometry for Model I, b-The geometry for Model II, c-The temperature boundary condition at the inner wall.

represented by an elastic foundation.

In recent years the results of various studies on the fracture mechanics of layered composites appeared in literature. These studies were concerned with interface cracks, cracks perpendicular to the interface, cracks terminating at the interface, and cracks crossing the interface. The singular behavior of stresses around a crack at the interface of two elastic half-planes of dissimilar material are examined by Williams [6]. Rice and Sih [7] considered a finite crack at an interface of two joined materials subjected to both symmetric and skew-symmetric in-plane loading. Also, the interface crack problem under "bending" was reported by Sih and Rice [8]. Stress distribution of two half-planes bonded to each other containing cracks along the bond was considered by England [9] and Erdogan [10]. The interface crack problem in multi-layered material has also been studied by Erdogan and Gupta [11]. Stress distribution in case of penny-shaped cracks lying between two bonded half-spaces are reported by Lowengrub and Sneddon [12], Lowengrub [13], and Willes [14]. A more generalized situation corresponds to the case of interface cracks lying on a

circular arc was considered by Perlman and Sih [15,16].

Khrapkov [17], and Cook and Erdogan [18] have considered the problem of a crack normal to a bimaterial interface. The case of a laminated composite containing a broken lamina was investigated by Ashbaugh [19] and Gupta [20]. Erdogan [21] has investigated the singular nature of the crack tip stress field in a non-homogeneous medium having a shear modulus with a discontinuous derivative for the antiplane shear loading of two bonded half spaces in which the crack is perpendicular to the interface. The fracture problem of a single layer of dissimilar material with a crack normal to the interface between two other layers of infinite height was considered by Hilton and Sih [22], Bogy [23], and Arin [24], while a crack parallel to the interface was considered by Hilton and Sih [25]. The anti-plane shear case was treated by Chen and Sih [26]. The same problem with penny-shaped crack under normal extension was solved by Arin and Erdogan [27] and torsion by Sih and Chen [28].

A crack going through the interface in two bonded half planes was investigated by Erdogan and Biricikoglu [29]. Erdogan and Cook [30] considered antiplane shear cracks terminating at and going through the interface. The fracture problem of a composite plate which consists of a bonded parallel load carrying laminates and buffer strips, and its limiting case of the collinear cracks joining and forming a stress-free end have been considered by Erdogan and Bakioglu [31, 32]. Also, Delale and Erdogan [33] considered the same problem but for orthotropic materials. Goree and Venezia [34] have investigated the bonded elastic half-planes with an interface crack and a crack perpendicular to the interface. The problem of two bonded semi-infinite elastic media with a crack in one of the half-planes lying parallel to, and at an arbitrary distance from the interface has been investigated by Erdogan [34]. A summary and discussion of the various modes of cracks in composite material has been

reported by Erdogan [36].

The problem considered can be solved by the superposition technique as shown in Figure 1.2. Once the temperature distribution is known, the thermal stresses for uncracked problem can be obtained. The perturbation problem (mixed boundary value problem) can then be formulated by using the thermal stresses from uncracked problem, but with opposite sign, as the crack surface traction along the line of the crack.

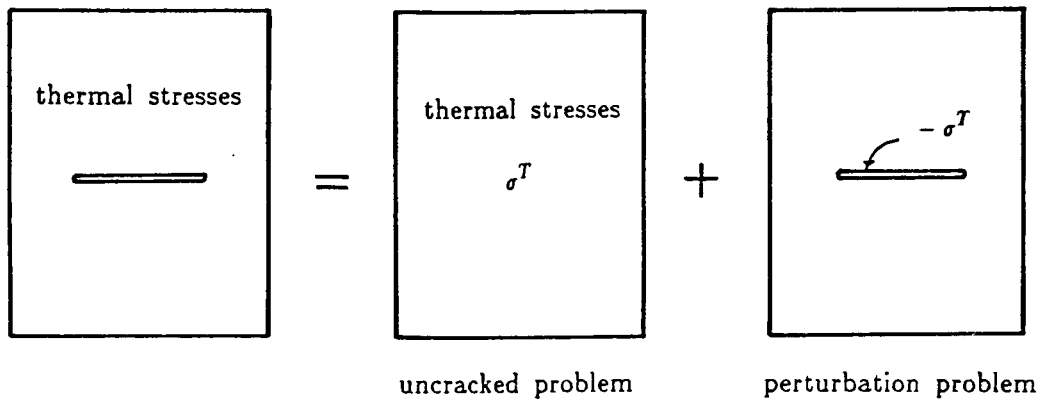


Figure 1-2: The superposition

First, the problem of cracks fully embedded into the homogeneous strips, perpendicular to the interface is considered. A general formulation of the perturbation problem is given for plane strain and generalized plane stress cases by the use of Fourier Integral Transform. The singular behavior of the stresses for different crack geometries is studied in some detail by using the Muskhelishvili Technique [37]. In cases where the crack terminates at the interface, or goes through the interface, the stress singularity is a function of material constants as well as the intersection angle.

The resulting system of singular integral equations is solved numerically by using the technique described in [38 , 39]. The stress intensity factors are calculated as functions of time and dimensions concerning the size and location

of the crack for various crack geometries and for two materials combinations described in Table 6-1. Also, in order to study the influence of the thermal boundary conditions on the stress intensity factor, the increase in time of the surface temperature is assumed to be an additional variable.

Chapter 2

ANALYSIS OF THE PROBLEM

2.1 Model I- Semi-infinite elastic medium (base metal) bonded to a surface layer of different material (clad)

2.1.1 Temperature distribution

2.1.1.1 Unit step function at the boundary

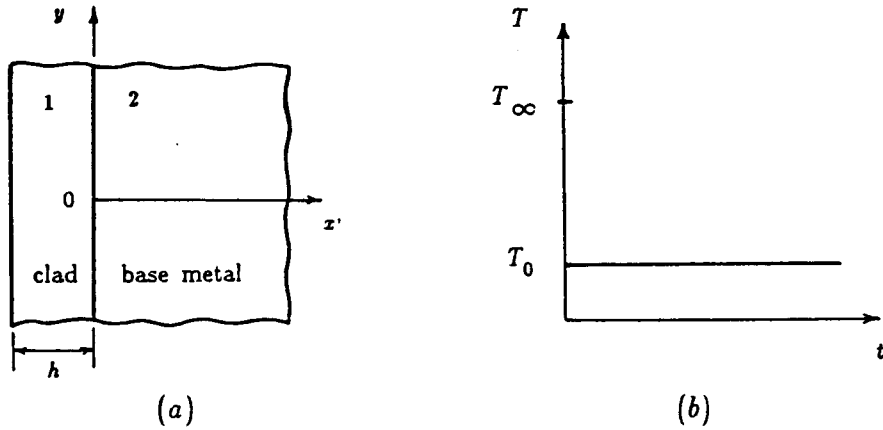


Figure 2-1: a-Geometry of the problem (Model I) b-Temperature boundary condition (unit step function)

Figure 2-1(a) represents the problem of interest, where x' is measured from the interface of the two materials, and Figure 2-1(b) represents the temperature change at the boundary. Let D_1 , k'_1 and D_2 , k'_2 are the thermal diffusivity and thermal conductivity for the clad (1) and base (2), respectively.

So, the differential equations for materials 1, 2 are :

$$\frac{\partial^2 T_1(x,t)}{\partial x'^2} = \frac{1}{D_1} \frac{\partial T_1(x,t)}{\partial t} ; \quad -h < x' < 0, t > 0, \quad (a)$$

$$\frac{\partial^2 T_2(x,t)}{\partial x'^2} = \frac{1}{D_2} \frac{\partial T_2(x,t)}{\partial t} ; \quad 0 < x' < \infty, t > 0. \quad (b)$$

(2.1)

where T_1 and T_2 are the temperatures in materials 1, 2 respectively. The initial and boundary conditions are

$$T_1(x,0) = T_2(x,0) = T_\infty, \quad (a)$$

$$T_1(0,t) = T_2(0,t), \quad (b)$$

$$k_1 \frac{\partial T_1(0,t)}{\partial x} = k_2 \frac{\partial T_2(0,t)}{\partial x}, \quad (c) \quad (2.2)$$

$$\lim_{x \rightarrow \infty} T_2(x,t) = T_\infty, \quad (d)$$

$$T_1(-h,t) = T_\infty + (T_0 - T_\infty)H(t). \quad (e)$$

where T_∞ is the initial temperature for both materials 1, 2, and T_0 is the temperature at the boundary at any time $t > 0$, and $H(t)$ is the Heaviside step function. Condition (2.2)(c) implies perfect heat transfer at the interface ($x=0$).

Let,

$$\Theta_1(x,t) = T_1(x,t) - T_\infty, \quad (a)$$

$$\Theta_2(x,t) = T_2(x,t) - T_\infty, \quad (b) \quad (2.3)$$

$$\Theta_0 = T_0 - T_\infty. \quad (c)$$

Then, the two differential equations (2.1) can be written as

$$\frac{\partial^2 \Theta_1(x,t)}{\partial x^2} = \frac{1}{D_1} \frac{\partial \Theta_1(x,t)}{\partial t}, \quad -h < x < 0, t > 0, \quad (a)$$

$$\frac{\partial^2 \Theta_2(x,t)}{\partial x^2} = \frac{1}{D_2} \frac{\partial \Theta_2(x,t)}{\partial t}, \quad 0 < x < \infty, t > 0. \quad (b) \quad (2.4)$$

Also, the initial and boundary conditions (2.2) become

$$\Theta_1(x,0) = \Theta_2(x,0) = 0, \quad (\text{a})$$

$$\Theta_1(0,t) = \Theta_2(0,t), \quad (\text{b})$$

$$k_1 \frac{\partial \Theta_1(0,t)}{\partial x} = k_2 \frac{\partial \Theta_2(0,t)}{\partial x}, \quad (\text{c}) \quad (2.5)$$

$$\lim_{x \rightarrow \infty} \Theta_2(x,t) = 0, \quad (\text{d})$$

$$\Theta_1(-h,t) = \Theta_0 H(t). \quad (\text{e})$$

By applying Laplace Transform to the partial differential equations (2.4) with respect to t , and by using condition (2.5)(a), they may be reduced to two ordinary differential equations of the form

$$\frac{d^2 \bar{\Theta}_1(x,p)}{dx^2} = q_1^2 \bar{\Theta}_1(x,p), \quad (\text{a})$$

(2.6)

$$\frac{d^2 \bar{\Theta}_2(x,p)}{dx^2} = q_2^2 \bar{\Theta}_2(x,p). \quad (\text{b})$$

where

$$q_1 = \sqrt{\frac{p}{D_1}}, \quad q_2 = \sqrt{\frac{p}{D_2}}. \quad (2.7)$$

The integral transform is defined by

$$\bar{\Theta}(x,p) = \int_0^\infty \Theta(x,t) e^{-pt} dt. \quad (2.8)$$

The general solutions of (2.6) are

$$\bar{\Theta}_1(x,p) = A_1(p) \cosh q_1 x + B_1(p) \sinh q_1 x, \quad (\text{a})$$

(2.9)

$$\bar{\Theta}_2(x,p) = A_2(p) e^{q_2 x} + B_2(p) e^{-q_2 x}. \quad (\text{b})$$

where, $A_1(p)$, $B_1(p)$, $A_2(p)$, $B_2(p)$ are unknown functions to be determined from conditions (2.5)(b-e). By applying Laplace Transform to the conditions (2.5)(b-e) we obtain

$$\bar{\Theta}_1(0,p) = \bar{\Theta}_2(0,p), \quad (b)$$

$$k_1 \frac{d\bar{\Theta}_1(0,p)}{dx} = k_2 \frac{d\bar{\Theta}_2(0,p)}{dx}, \quad (c)$$

$$\lim_{x \rightarrow \infty} \bar{\Theta}_2(x,p) = 0, \quad (d) \quad (2.10)$$

$$\bar{\Theta}_1(-h,p) = \frac{\Theta_0}{p}. \quad (e)$$

After substitution of the conditions (2.10)(b-e), and determination of the constants $A_1(p)$, $B_1(p)$, $A_2(p)$, $B_2(p)$, the equations (2.9) become

$$\bar{\Theta}_1(x,p) = \frac{\Theta_0 [\cosh q_1 x - \eta \sinh q_1 x]}{p [\cosh q_1 h + \eta \sinh q_1 h]}, \quad (a)$$

(2.11)

$$\bar{\Theta}_2(x,p) = \frac{\Theta_0 e^{-q_2 x}}{p [\cosh q_1 h + \eta \sinh q_1 h]}. \quad (b)$$

where

$$\eta = \frac{k_2}{k_1} \sqrt{\frac{D_1}{D_2}}. \quad (2.12)$$

The temperature distribution $\Theta_1(x,t)$, $\Theta_2(x,t)$ can be obtained by applying the Inversion Theorem of Laplace Transform on equations (2.11), i.e,

$$\Theta_1(x,t) = \frac{1}{2\pi i} \int_{\gamma-i\infty}^{\gamma+i\infty} \frac{\Theta_0 [\cosh \zeta_1 x - \eta \sinh \zeta_1 x]}{z [\cosh \zeta_1 h + \eta \sinh \zeta_1 h]} e^{tz} dz, \quad (a)$$

(2.13)

$$\Theta_2(x,t) = \frac{1}{2\pi i} \int_{\gamma-i\infty}^{\gamma+i\infty} \frac{\Theta_0 e^{-\zeta_2 x}}{z [\cosh \zeta_1 h + \eta \sinh \zeta_1 h]} e^{tz} dz. \quad (b)$$

where

$$\zeta_1 = \sqrt{z/D_1}, \quad \zeta_2 = \sqrt{z/D_2}. \quad (2.14)$$

Since, the functions $(e^{-\sqrt{z/D_2}x})$ and $(\sinh \sqrt{z/D_1}h)$ are double-valued

functions when the angle in the complex domain is changed from 0 to 2π , the integrands in (2.13) have a branch point at $z = 0$, and the integration contour should be as shown in Figure 2-2.

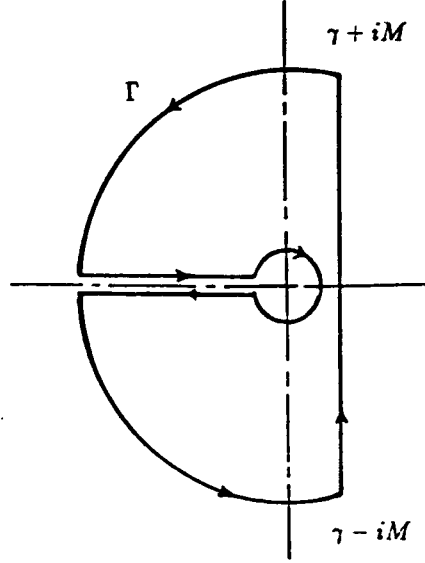


Figure 2-2: Contour for evaluating the integrals in eqns. (2.13)

So, applying the Residue Theorem in equations (2.13), and using the contour integral Γ shown in Figure 2-2, we obtain the following closed form solutions for $\Theta_1(x, t)$, $\Theta_2(x, t)$

$$\frac{\Theta_1(x, t)}{\Theta_0} = 1 - \frac{2\eta}{\pi} \int_0^\infty \frac{e^{-tD_1\xi^2} \sin \xi(x+h)}{[\cos^2 \xi h + \eta^2 \sin^2 \xi h]} \frac{d\xi}{\xi}, \quad (a)$$

$$\frac{\Theta_2(x, t)}{\Theta_0} = 1 - \frac{2}{\pi} \int_0^\infty \frac{e^{-tD_1\xi^2} [\cos \xi h \sin \xi \delta x + \eta \sin \xi h \cos \xi \delta x]}{[\cos^2 \xi h + \eta^2 \sin^2 \xi h]} \frac{d\xi}{\xi}, \quad (b) \quad (2.15)$$

$$\delta = \sqrt{D_1/D_2}. \quad (c)$$

Defining now the Fourier Number τ and the dimensionless parameters by

$$\tau = tD_1/h^2, \quad \xi_* = h\xi, \quad x^* = (x+h)/h. \quad (2.16)$$

equations (2.15) become

$$\frac{\Theta_1(x^*, \tau)}{\Theta_0} = 1 - \frac{2\eta}{\pi} \int_0^\infty \frac{e^{-\tau \xi^2} \sin \xi \cdot x^*}{[\cos^2 \xi + \eta^2 \sin^2 \xi]} \frac{d\xi}{\xi}; \quad 0 \leq x^* \leq 1, \quad (a)$$

(2.17)

$$\frac{\Theta_2(x^*, \tau)}{\Theta_0} = 1 - \frac{2}{\pi} \int_0^\infty \frac{e^{-\tau \xi^2} [\cos \xi \cdot \sin \xi \cdot \delta(x^* - 1) + \eta \sin \xi \cdot \cos \xi \cdot \delta(x^* - 1)] d\xi}{[\cos^2 \xi + \eta^2 \sin^2 \xi]} \frac{d\xi}{\xi},$$

$$; \quad 1 \leq x^* \leq \infty. \quad (b)$$

2.1.1.2 Ramp function at the boundary

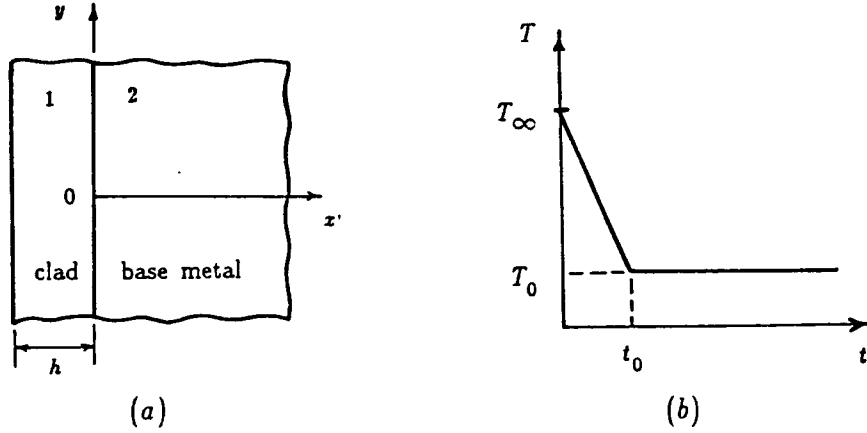


Figure 2-3: a-Geometry of the problem (Model I) b-Temperature boundary condition (ramp function)

Figure 2-3(a) represents the problem of interest, and Figure 2-3(b) represents the temperature change at the boundary. The differential equations for 1, 2 are:

$$\frac{\partial^2 \Theta_1(x, t)}{\partial x^2} = \frac{1}{D_1} \frac{\partial \Theta_1(x, t)}{\partial t}; \quad -h < x < 0, t > 0, \quad (a)$$

(2.18)

$$\frac{\partial^2 \Theta_2(x, t)}{\partial x^2} = \frac{1}{D_2} \frac{\partial \Theta_2(x, t)}{\partial t}; \quad 0 < x < \infty, t > 0. \quad (b)$$

The initial and the boundary conditions are:

$$\Theta_1(x,0) = \Theta_2(x,0) = 0, \quad (a)$$

$$\Theta_1(0,t) = \Theta_2(0,t), \quad (b)$$

$$k_1 \frac{\partial \Theta_1(0,t)}{\partial x} = k_2 \frac{\partial \Theta_2(0,t)}{\partial x}, \quad (c) \quad (2.19)$$

$$\lim_{x \rightarrow \infty} \Theta_2(x,t) = 0, \quad (d)$$

$$\Theta_1(-h,t) = \frac{\Theta_0}{t_0} t H(t) - \frac{\Theta_0}{t_0} (t-t_0) H(t-t_0). \quad (e)$$

As before, by applying Laplace Transform to equations (2.18), and using the condition (2.19)(a), we will obtain two ordinary differential equations having the general solution of the form

$$\bar{\Theta}_1(x,p) = A_1(p) \cosh q_1 x + B_1(p) \sinh q_1 x, \quad (a) \quad (2.20)$$

$$\bar{\Theta}_2(x,p) = A_2(p) e^{q_2 x} + B_2(p) e^{-q_2 x}. \quad (b)$$

where $A_1(p)$, $B_1(p)$, $A_2(p)$, $B_2(p)$, are unknown functions to be determined from the conditions (2.19)(b-e).

Now, applying Laplace Transform to the boundary conditions, we may have

$$\bar{\Theta}_1(0,p) = \bar{\Theta}_2(0,p), \quad (b)$$

$$k_1 \frac{d\bar{\Theta}_1(0,p)}{dx} = k_2 \frac{d\bar{\Theta}_2(0,p)}{dx}, \quad (c)$$

$$\lim_{x \rightarrow \infty} \bar{\Theta}_2(x,p) = 0, \quad (d) \quad (2.21)$$

$$\bar{\Theta}_1(-h,p) = \frac{\Theta_0}{t_0} \frac{1}{p^2} - \frac{\Theta_0}{t_0} \frac{1}{p^2} e^{-pt_0}. \quad (e)$$

Then, by substituting from equation (2.20) into equation (2.21), and

solving for the constants $A_1(p), B_1(p), A_2(p), B_2(p)$, we find

$$\bar{\Theta}_1(x, p) = F_{11}(p) \cdot B_{11}(p), \quad (a) \quad (2.22)$$

$$\bar{\Theta}_2(x, p) = F_{12}(p) \cdot B_{12}(p). \quad (b)$$

where

$$F_{11}(p) = \frac{\Theta_0 [\cosh q_1 x - \eta \sinh q_1 x]}{p [\cosh q_1 h + \eta \sinh q_1 h]}, \quad (a)$$

$$F_{12}(p) = \frac{\Theta_0 e^{-q_2 x}}{p [\cosh q_1 h + \eta \sinh q_1 h]}, \quad (b) \quad (2.23)$$

$$B_{11}(p) = B_{12}(p) = \frac{1}{t_0} \left(\frac{1}{p} - \frac{e^{-pt_0}}{p} \right). \quad (c)$$

It is clear that, F_{11}, F_{12} , are the same as equations (2.11).

By applying the convolution theorem to equations (2.22), we find

$$\Theta_j(x, t) = \int_0^t b_{1j}(\tau) f_{1j}(t - \tau) d\tau, \quad ; \quad (j = 1, 2). \quad (2.24)$$

where,

$$\begin{aligned} f_{11}(t) &= L^{-1} [F_{11}(p)] \\ &= \Theta_0 \left[1 - \frac{2\eta}{\pi} \int_0^\infty \frac{e^{-tD_1 \xi^2} \sin \xi(x+h)}{[\cos^2 \xi h + \eta^2 \sin^2 \xi h]} \frac{d\xi}{\xi} \right], \end{aligned} \quad (a)$$

$$\begin{aligned} f_{12}(t) &= L^{-1} [F_{12}(p)] \\ &= \Theta_0 \left[1 - \frac{2}{\pi} \int_0^\infty \frac{e^{-tD_1 \xi^2} [\cos \xi h \sin \xi \delta x + \eta \sin \xi h \cos \xi \delta x]}{[\cos^2 \xi h + \eta^2 \sin^2 \xi h]} \frac{d\xi}{\xi} \right], \end{aligned} \quad (b) \quad (2.25)$$

$$b_{11}(t) = b_{12}(t) = L^{-1} [G_{11}(p)] = \frac{1}{t_0} [1 - H(t - t_0)]. \quad (c)$$

From (2.16), (2.24) and (2.25) it then follows that

$$\begin{aligned} \frac{\Theta_1(x^*, \tau)}{\Theta_0} &= \frac{\tau}{\tau_0} + \frac{2\eta}{\pi} \int_0^\infty \frac{(e^{-\tau \xi^2} - 1)}{\tau_0} * \\ &\quad \frac{\sin \xi x^*}{[\cos^2 \xi h + \eta^2 \sin^2 \xi h]} \frac{d\xi}{\xi^3} \quad ; \quad 0 \leq x^* \leq 1, \tau \leq \tau_0, \end{aligned} \quad (a)$$

$$\frac{\Theta_1(x^*, \tau)}{\Theta_0} = 1 - \frac{2\eta}{\pi} \int_0^\infty \frac{e^{-\tau\xi^2} (e^{\tau_0\xi^2} - 1)}{\tau_0} * \frac{\sin \xi x^*}{[\cos^2 \xi + \eta^2 \sin^2 \xi]} \frac{d\xi}{\xi^3} ; 0 \leq x^* \leq 1, \tau > \tau_0, (b)$$

$$\frac{\Theta_2(x^*, \tau)}{\Theta_0} = \frac{\tau}{\tau_0} + \frac{2}{\pi} \int_0^\infty \frac{e^{-\tau\xi^2} - 1}{\tau_0} *$$

$$\frac{(\cos \xi \sin \xi \delta(x^* - 1) + \eta \sin \xi \cos \xi \delta(x^* - 1))}{[\cos^2 \xi + \eta^2 \sin^2 \xi]} \frac{d\xi}{\xi^3},$$

$$1 \leq x^* \leq \infty, \tau \leq \tau_0, (c)$$

$$\frac{\Theta_2(x^*, \tau)}{\Theta_0} = 1 - \frac{2}{\pi} \int_0^\infty \frac{e^{-\tau\xi^2} (e^{\tau_0\xi^2} - 1)}{\tau_0} *$$

$$\frac{(\cos \xi \sin \xi \delta(x^* - 1) + \eta \sin \xi \cos \xi \delta(x^* - 1))}{[\cos^2 \xi + \eta^2 \sin^2 \xi]} \frac{d\xi}{\xi^3},$$

$$1 \leq x^* \leq \infty, \tau > \tau_0. (d)$$

where

$$\tau_0 = \frac{t_0 D_1}{h^2}, \eta = \frac{k_2}{k_1} \sqrt{\frac{D_1}{D_2}}, \delta = \sqrt{\frac{D_1}{D_2}}. (2.27)$$

2.1.2 Thermal stresses in uncracked problem

Consider the plane strain problem in y and z directions as shown in Figure 2-4, i.e.,

$$\varepsilon_{ixy} = \varepsilon_{iyz} = \varepsilon_{izx} = \varepsilon_{iyy} = \varepsilon_{izz} = 0, (i = 1, 2). (2.28)$$

Since the temperatures Θ_j , ($j = 1, 2$) are functions of (x, t) , then the stresses are functions of (x, t) only. It is obvious that all the shear stresses are zero. Then, the equilibrium equation for each medium (ignoring the inertia effects) is :

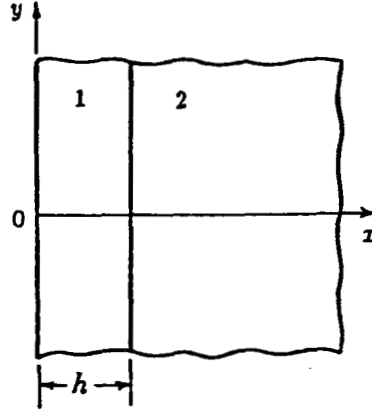


Figure 2-4: Geometry of Model I (uncracked problem)

$$\frac{d\sigma_{xx}(x,t)}{dx} = 0. \quad (2.29)$$

Since, we have a stress-free boundary, i.e, $\sigma_{xx}(0, t) = 0$, then,

$$\sigma_{xx}(x,t) = 0. \quad (2.30)$$

So, the Hooke's Law becomes

$$-\alpha \cdot \Theta = \frac{1}{E} [\sigma_{yy} - \nu \sigma_{zz}], \quad (a) \quad (2.31)$$

$$-\alpha \cdot \Theta = \frac{1}{E} [\sigma_{zz} - \nu \sigma_{yy}]. \quad (b)$$

where α is the coefficient of thermal expansion, E is the Young's modulus, and ν is the Poisson's ratio of the material. From equations (2.31) we may have

$$\sigma_{yy} = \sigma_{zz} = -\frac{\alpha \cdot E \Theta}{(1-\nu)}. \quad (2.32)$$

Then, the thermal stresses in materials 1, 2 are:

$$\sigma_{1yy}(x,t) = \sigma_{1zz}(x,t) = -\frac{\alpha'_1 E_1 \Theta_1(x,t)}{(1-\nu_1)} ; 0 \leq x \leq h, \quad (a) \quad (2.33)$$

$$\sigma_{2yy}(x,t) = \sigma_{2zz}(x,t) = -\frac{\alpha'_2 E_2 \Theta_2(x,t)}{(1-\nu_2)} ; h \leq x \leq \infty. \quad (b)$$

Let,

$$\sigma_0^T = -\frac{\alpha_1' E_1 \Theta_0}{(1-\nu_1)}, \quad x^* = \frac{x}{h}, \quad \tau = \frac{tD_1}{h^2}. \quad (2.34)$$

Then, equations (2.33) become

$$\frac{\sigma_{1yy}(x^*, \tau)}{\sigma_0^T} = \frac{\Theta_1(x^*, \tau)}{\Theta_0}; \quad 0 \leq x^* \leq 1, \quad (a)$$

(2.35)

$$\frac{\sigma_{2yy}(x^*, \tau)}{\sigma_0^T} = \frac{\alpha_2'}{\alpha_1'} \frac{E_2}{E_1} \frac{(1-\nu_1)}{(1-\nu_2)} \frac{\Theta_2(x^*, \tau)}{\Theta_0}; \quad 1 \leq x^* \leq \infty. \quad (b)$$

2.1.3 Formulation of the crack problem (perturbation problem)

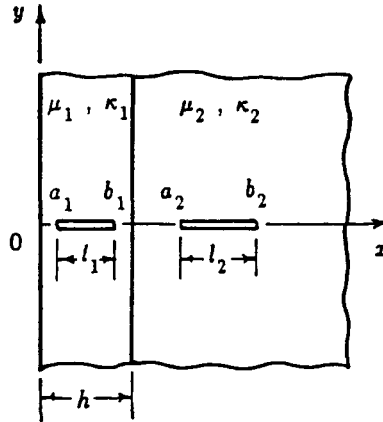


Figure 2-5: Crack geometry (Model I)

Consider the two-dimensional composite medium shown in Figure 2-5, where each material contains a finite crack perpendicular to the interface. Because of symmetry, the problem will be considered for, $0 \leq y < \infty$. It can be shown that, the governing differential equations for the displacements in each medium are (Appendix A)

$$\begin{aligned}
(\kappa-1)\nabla^2 u + 2\left(\frac{\partial^2 u}{\partial x^2} + \frac{\partial^2 v}{\partial x \partial y}\right) &= 0, & (a) \\
(\kappa-1)\nabla^2 v + 2\left(\frac{\partial^2 u}{\partial x \partial y} + \frac{\partial^2 v}{\partial y^2}\right) &= 0. & (b)
\end{aligned}
\tag{2.36}$$

where u and v are x and y components of the displacement vector, respectively. $\kappa=(3-4\nu)$ for plain strain, and $\kappa=(3-\nu)/(1+\nu)$ for generalized plane stress, ν is Poisson's ratio.

Assume that the solution of equations (2.36) may be expressed in terms of the following Fourier Integral, i.e,

$$\begin{aligned}
u(x,y) &= \frac{2}{\pi} \int_0^\infty f(x,\alpha) \cos y\alpha \, d\alpha + \frac{1}{2\pi} \int_{-\infty}^\infty h(y,\beta) e^{ix\beta} \, d\beta, & (a) \\
v(x,y) &= \frac{2}{\pi} \int_0^\infty g(x,\alpha) \sin y\alpha \, d\alpha + \frac{1}{2\pi} \int_{-\infty}^\infty k(y,\beta) e^{ix\beta} \, d\beta. & (b)
\end{aligned}
\tag{2.37}$$

Because u , v , are symmetric and antisymmetric with respect to y , respectively, the first term of u is a Cosine transform, and the first term of v is a Sine transform. The second terms in equations (2.37) represent the general Fourier transform. Substituting equations (2.37) into equations (2.36) we obtain a system of ordinary differential equations for the unknown functions f , h , g , k .

$$\begin{aligned}
\frac{d^4}{dx^4} f(x,\alpha) - 2\alpha^2 \frac{d^2}{dx^2} f(x,\alpha) + \alpha^4 f(x,\alpha) &= 0, & (a) \\
\frac{d^4}{dy^4} h(y,\beta) - 2\beta^2 \frac{d^2}{dy^2} h(y,\beta) + \beta^4 h(y,\beta) &= 0, & (b) \\
\frac{d^4}{dx^4} g(x,\alpha) - 2\alpha^2 \frac{d^2}{dx^2} g(x,\alpha) + \alpha^4 g(x,\alpha) &= 0, & (c) \\
\frac{d^4}{dy^4} k(y,\beta) - 2\beta^2 \frac{d^2}{dy^2} k(y,\beta) + \beta^4 k(y,\beta) &= 0. & (d)
\end{aligned}
\tag{2.38}$$

The general solution of these four differential equations are:

$$\begin{aligned}
f(x, \alpha) &= (C_1 + C_2 x) e^{x\alpha} + (C_3 + C_4 x) e^{-x\alpha}, & (a) \\
g(x, \alpha) &= (C'_1 + C'_2 x) e^{x\alpha} + (C'_3 + C'_4 x) e^{-x\alpha}, & (b) \\
k(y, \beta) &= (D_1 + D_2 y) e^{y|\beta|} + (D_3 + D_4 y) e^{-y|\beta|}, & (c) \\
h(y, \beta) &= (D'_1 + D'_2 y) e^{y|\beta|} + (D'_3 + D'_4 y) e^{-y|\beta|}. & (d)
\end{aligned} \tag{2.39}$$

where $0 < \alpha < \infty$, $-\infty < \beta < \infty$, $y \geq 0$. C_i and C'_i , ($i=1, \dots, 4$) are functions of the transform variable α and are linearly dependent. Similarly, D_i and D'_i , ($i=1, \dots, 4$) are functions of the transform variable β and are not independent.

Since, u, v are bounded as $y \rightarrow \infty$, from (2.39) it follows that D_1, D_2, D'_1, D'_2 must be zero. Thus, after eliminating C'_i and D'_j ($i=1, \dots, 4; j=3, 4$) by using coupling relations, equations (2.39) may be written as

$$\begin{aligned}
f(x, \alpha) &= (C_1 + C_2 x) e^{x\alpha} + (C_3 + C_4 x) e^{-x\alpha}, & (a) \\
g(x, \alpha) &= (-C_1 - \frac{\kappa}{\alpha} C_2 - C_2 x) e^{x\alpha} + (C_3 - \frac{\kappa}{\alpha} C_4 + C_4 x) e^{-x\alpha}, & (b) \\
k(y, \beta) &= (D_3 + D_4 y) e^{-y|\beta|}, & (c) \\
h(y, \beta) &= \frac{-i|\beta|}{\beta} (D_3 - \frac{\kappa}{|\beta|} D_4 + D_4 y) e^{-y|\beta|}. & (d)
\end{aligned} \tag{2.40}$$

Defining, $D_4(\beta) = A(\beta)$, the equations (2.40) (c,d) can be written in the form

$$\begin{aligned}
k(y, \beta) &= \frac{A(\beta)}{|\beta|} \left(\frac{D_3}{A(\beta)} |\beta| + |\beta| y \right) e^{-y|\beta|}, & (c) \\
h(y, \beta) &= \frac{-i|\beta|}{\beta} \frac{A(\beta)}{|\beta|} \left(\frac{D_3}{A(\beta)} |\beta| - \kappa + |\beta| y \right) e^{-y|\beta|}. & (d)
\end{aligned} \tag{2.41}$$

Hence the displacements u, v are in the form

$$\begin{aligned}
u(x, y) &= \frac{2}{\pi} \int_0^\infty [(C_1 + C_2 x) e^{x\alpha} + (C_3 + C_4 x) e^{-x\alpha}] \cos y\alpha \, d\alpha \\
&+ \frac{1}{2\pi} \int_{-\infty}^\infty \frac{-i|\beta|}{\beta} \frac{A(\beta)}{|\beta|} \left[\frac{D_3}{A(\beta)} |\beta| - \kappa + |\beta| y \right] e^{-y|\beta|} e^{ix\beta} \, d\beta, & (a)
\end{aligned}$$

(2.42)

$$v(x,y) = \frac{2}{\pi} \int_0^\infty [(-C_1 - C_2 \{ \frac{\kappa}{\alpha} + x \}) e^{x\alpha} + (C_3 - C_4 \{ \frac{\kappa}{\alpha} - x \}) e^{-x\alpha}] \sin y\alpha d\alpha + \frac{1}{2\pi} \int_{-\infty}^\infty \frac{A(\beta)}{|\beta|} \left(\frac{D_3}{A(\beta)} |\beta| + |\beta| y \right) e^{-y|\beta|} e^{ix\beta} d\beta. \quad (b)$$

The stress-strain relations for plane-strain problem are

$$\sigma_{xx} = \mu \frac{2(1-\nu)}{(1-2\nu)} (\epsilon_{xx} + \frac{\nu}{1-\nu} \epsilon_{yy}), \quad (a)$$

$$\sigma_{yy} = \mu \frac{2(1-\nu)}{(1-2\nu)} (\epsilon_{yy} + \frac{\nu}{1-\nu} \epsilon_{xx}), \quad (b) \quad (2.43)$$

$$\sigma_{xy} = \mu \gamma_{xy}. \quad (c)$$

where $\mu = E/2(1+\nu)$ is the shear modulus.

Also, the strain-displacement relations are

$$\epsilon_{xx} = \frac{\partial u}{\partial x}, \quad (a)$$

$$\epsilon_{yy} = \frac{\partial v}{\partial y}, \quad (b) \quad (2.44)$$

$$\gamma_{xy} = \frac{\partial u}{\partial y} + \frac{\partial v}{\partial x}. \quad (c)$$

By substituting equations (2.42) into equations (2.43) and (2.44), and observing that at the plane of symmetry $y = 0$ the shear stress σ_{xy} is zero, we find

$$\frac{D_3}{A(\beta)} |\beta| = \frac{\kappa+1}{2}. \quad (2.45)$$

Equations (2.42), (2.43), (2.44), and (2.45) are valid for both materials. Therefore, the stresses and the displacement fields in terms of the Fourier Integral for each material may be expressed as

Material (1) $0 \leq x \leq h, 0 \leq y < \infty$

$$\begin{aligned}\frac{1}{2\mu_1}\sigma_{1xx}(x,y) &= \frac{2}{\pi}\int_0^\infty [(C_1\alpha + C_2\{\frac{\kappa_1-1}{2} + \alpha x\})e^{x\alpha} \\ &\quad + (-C_3\alpha + C_4\{\frac{\kappa_1-1}{2} - \alpha x\})e^{-x\alpha}] \cos y\alpha d\alpha \\ &\quad + \frac{1}{2\pi}\int_{-\infty}^\infty A_1(-1+|\beta|y)e^{-y|\beta|}e^{ix\beta}d\beta,\end{aligned}\quad (a)$$

$$\begin{aligned}\frac{1}{2\mu_1}\sigma_{1yy}(x,y) &= \frac{2}{\pi}\int_0^\infty [(-C_1\alpha - C_2\{\frac{\kappa_1+3}{2} + \alpha x\})e^{x\alpha} \\ &\quad + (C_3\alpha - C_4\{\frac{\kappa_1+3}{2} - \alpha x\})e^{-x\alpha}] \cos y\alpha d\alpha \\ &\quad + \frac{1}{2\pi}\int_{-\infty}^\infty A_1(-1-|\beta|y)e^{-y|\beta|}e^{ix\beta}d\beta,\end{aligned}\quad (b)$$

$$\frac{1}{2\mu_1}\sigma_{1xy}(x,y) = \frac{2}{\pi}\int_0^\infty [(-C_1\alpha - C_2\{\frac{\kappa_1+1}{2} + \alpha x\})e^{x\alpha} \quad (2.46)$$

$$\begin{aligned}&\quad + (-C_3\alpha + C_4\{\frac{\kappa_1+1}{2} - \alpha x\})e^{-x\alpha}] \sin y\alpha d\alpha \\ &\quad + \frac{1}{2\pi}\int_{-\infty}^\infty iA_1\beta ye^{-y|\beta|}e^{ix\beta}d\beta,\end{aligned}\quad (c)$$

$$\begin{aligned}u_1(x,y) &= \frac{2}{\pi}\int_0^\infty [(C_1 + C_2x)e^{x\alpha} + (C_3 + C_4x)e^{-x\alpha}] \cos y\alpha d\alpha \\ &\quad + \frac{1}{2\pi}\int_{-\infty}^\infty \frac{iA_1}{|\beta|}(\frac{|\beta|}{\beta}\frac{\kappa_1-1}{2} - \beta y)e^{-y|\beta|}e^{ix\beta}d\beta,\end{aligned}\quad (d)$$

$$\begin{aligned}v_1(x,y) &= \frac{2}{\pi}\int_0^\infty [(-C_1 - C_2\{\frac{\kappa_1}{\alpha} + x\})e^{x\alpha} \\ &\quad + (C_3 - C_4\{\frac{\kappa_1}{\alpha} - x\})e^{-x\alpha}] \sin y\alpha d\alpha \\ &\quad + \frac{1}{2\pi}\int_{-\infty}^\infty \frac{A_1}{|\beta|}(\frac{\kappa_1+1}{2} + |\beta|y)e^{-y|\beta|}e^{ix\beta}d\beta.\end{aligned}\quad (e)$$

Material (2) $h \leq x \leq \infty, 0 \leq y < \infty$

As $x \rightarrow \infty$, $u, v, \sigma_{xx}, \sigma_{yy}, \sigma_{xy}$ are bounded. Then

$$\begin{aligned}\frac{1}{2\mu_2}\sigma_{2xx}(x,y) &= \frac{2}{\pi}\int_0^\infty [-C_5\alpha + C_6\{\frac{\kappa_2-1}{2}-\alpha x\}]e^{-x\alpha}\cos y\alpha d\alpha \\ &+ \frac{1}{2\pi}\int_{-\infty}^\infty A_2(-1+|\beta|y)e^{-y|\beta|}e^{ix\beta}d\beta,\end{aligned}\quad (a)$$

$$\begin{aligned}\frac{1}{2\mu_2}\sigma_{2yy}(x,y) &= \frac{2}{\pi}\int_0^\infty [C_5\alpha - C_6\{\frac{\kappa_2+3}{2}-\alpha x\}]e^{-x\alpha}\cos y\alpha d\alpha \\ &+ \frac{1}{2\pi}\int_{-\infty}^\infty A_2(-1-|\beta|y)e^{-y|\beta|}e^{ix\beta}d\beta,\end{aligned}\quad (b)$$

$$\frac{1}{2\mu_2}\sigma_{2xy}(x,y) = \frac{2}{\pi}\int_0^\infty [-C_5\alpha + C_6\{\frac{\kappa_2+1}{2}-\alpha x\}]e^{-x\alpha}\sin y\alpha d\alpha \quad (2.47)$$

$$+ \frac{1}{2\pi}\int_{-\infty}^\infty iA_2\beta ye^{-y|\beta|}e^{ix\beta}d\beta, \quad (c)$$

$$\begin{aligned}u_2(x,y) &= \frac{2}{\pi}\int_0^\infty [C_5 + C_6x]e^{-x\alpha}\cos y\alpha d\alpha \\ &+ \frac{1}{2\pi}\int_{-\infty}^\infty \frac{iA_2}{|\beta|}(\frac{|\beta|}{\beta}\frac{\kappa_2-1}{2}-\beta y)e^{-y|\beta|}e^{ix\beta}d\beta,\end{aligned}\quad (d)$$

$$\begin{aligned}v_2(x,y) &= \frac{2}{\pi}\int_0^\infty [C_5 - C_6\{\frac{\kappa_2}{\alpha}-x\}]e^{-x\alpha}\sin y\alpha d\alpha \\ &+ \frac{1}{2\pi}\int_{-\infty}^\infty \frac{A_2}{|\beta|}(\frac{\kappa_2+1}{2}+|\beta|y)e^{-y|\beta|}e^{ix\beta}d\beta.\end{aligned}\quad (e)$$

where the unknowns $C_i, (i=1, \dots, 6)$ are functions of α , and $A_j, (j=1, 2)$ are functions of β , and are to be determined from the boundary and continuity conditions.

The homogeneous boundary and continuity conditions of the problem described in Figure 2-5 are

$$\sigma_{1xx}(0,y) = 0 \quad ; \quad 0 \leq y < \infty, \quad (a)$$

$$\sigma_{1xy}(0,y) = 0 \quad ; \quad 0 \leq y < \infty, \quad (b)$$

$$\sigma_{1xx}(h,y) = \sigma_{2xx}(h,y) \quad ; \quad 0 \leq y < \infty, \quad (c)$$

$$\sigma_{1xy}(h,y) = \sigma_{2xy}(h,y) \quad ; \quad 0 \leq y < \infty, \quad (d) \quad (2.48)$$

$$u_1(h,y) = u_2(h,y) \quad ; \quad 0 \leq y < \infty, \quad (e)$$

$$v_1(h,y) = v_2(h,y) \quad ; \quad 0 \leq y < \infty. \quad (f)$$

The mixed boundary conditions are

$$\begin{aligned} v_1(x,0) &= 0 \quad ; \quad 0 \leq x \leq a_1, \quad b_1 \leq x \leq h \\ v_2(x,0) &= 0 \quad ; \quad h \leq x \leq a_2, \quad b_2 \leq x \leq \infty \end{aligned} \quad (a)$$

$$\begin{aligned} \sigma_{1yy}(x,0) &= -\sigma_1^T(x) \quad ; \quad a_1 < x < b_1 \\ \sigma_{2yy}(x,0) &= -\sigma_2^T(x) \quad ; \quad a_2 < x < b_2 \end{aligned} \quad (b) \quad (2.49)$$

where, σ_1^T , σ_2^T are the thermal stresses which can be determined from the uncracked problem.

First, let us define the following density functions

$$\phi_1(x) = \frac{\partial}{\partial x} v_1(x,0) \quad ; \quad 0 < x < h, \quad (a)$$

$$\phi_2(x) = \frac{\partial}{\partial x} v_2(x,0) \quad ; \quad h < x < \infty. \quad (b) \quad (2.50)$$

If we substitute equations (2.50) into equations (2.46)(e) and (2.47)(e) we obtain

$$\lim_{y \rightarrow 0} \frac{1}{2\pi} \int_{-\infty}^{\infty} \frac{i\beta A_1}{|\beta|} \left(\frac{\kappa_1 + 1}{2} + |\beta|y \right) e^{-y|\beta|} e^{ix\beta} d\beta = \phi_1(x), \quad (a)$$

$$\lim_{y \rightarrow 0} \frac{1}{2\pi} \int_{-\infty}^{\infty} \frac{i\beta A_2}{|\beta|} \left(\frac{\kappa_2 + 1}{2} + |\beta|y \right) e^{-y|\beta|} e^{ix\beta} d\beta = \phi_2(x). \quad (b) \quad (2.51)$$

By applying Fourier inverse Transform, we have

$$\frac{i\beta A_1}{|\beta|} \frac{\kappa_1 + 1}{2} = \int_{-\infty}^{\infty} \phi_1(t) e^{-i\beta t} dt, \quad (a)$$

$$\frac{i\beta A_2}{|\beta|} \frac{\kappa_2 + 1}{2} = \int_{-\infty}^{\infty} \phi_2(t) e^{-i\beta t} dt. \quad (b)$$

(2.52)

From condition (2.49)(a), it may be seen that

$$\phi_1(x) = 0 \quad ; \quad 0 < x < a_1, \quad b_1 < x < h, \quad (a)$$

$$\phi_2(x) = 0 \quad ; \quad h < x < a_2, \quad b_2 < x < \infty. \quad (b)$$

(2.53)

Then, A_1, A_2 can be put in the form

$$A_1 = \frac{-2i}{\kappa_1 + 1} \frac{|\beta|}{\beta} \int_{a_1}^{b_1} \phi_1(t_1) e^{-i\beta t_1} dt_1, \quad (a)$$

(2.54)

$$A_2 = \frac{-2i}{\kappa_2 + 1} \frac{|\beta|}{\beta} \int_{a_2}^{b_2} \phi_2(t_2) e^{-i\beta t_2} dt_2. \quad (b)$$

By applying the boundary conditions (2.48), and using Fourier Inverse Transforms and equations (2.54), with the help of the integration formulas given in Appendix (B), we find

$$-B_1 - e_1 C_2 - B_3 + e_1 C_4 = \frac{1}{\kappa_1 + 1} \int_{a_1}^{b_1} M_1 \phi_1(t_1) dt_1, \quad (a)$$

$$B_1 + e_2 C_2 - B_3 + e_2 C_4 = \frac{1}{\kappa_1 + 1} \int_{a_1}^{b_1} M_2 \phi_1(t_1) dt_1, \quad (b)$$

$$\begin{aligned} & e_4 B_1 + e_3 C_2 - m B_3 + e_5 C_4 + B_5 + e_6 C_6 \\ & = \frac{1}{\kappa_1 + 1} \int_{a_1}^{b_1} M_3 \phi_1(t_1) dt_1 + \frac{1}{\kappa_2 + 1} \int_{a_2}^{b_2} M_4 \phi_2(t_2) dt_2, \end{aligned} \quad (c)$$

(2.55)

$$\begin{aligned}
& -e_4 B_1 + e_7 C_2 - m B_3 + e_8 C_4 + B_5 + e_9 C_6 \\
& = \frac{1}{\kappa_1 + 1} \int_{a_1}^{b_1} M_5 \phi_1(t_1) dt_1 + \frac{1}{\kappa_2 + 1} \int_{a_2}^{b_2} M_6 \phi_2(t_2) dt_2,
\end{aligned} \tag{d}$$

$$\begin{aligned}
& e_{10} B_1 + e_{11} C_2 + B_3 + e_{12} C_4 - B_5 - e_{12} C_6 \\
& = \frac{1}{\kappa_1 + 1} \int_{a_1}^{b_1} M_7 \phi_1(t_1) dt_1 + \frac{1}{\kappa_1 + 1} \int_{a_2}^{b_2} M_8 \phi_2(t_2) dt_2,
\end{aligned} \tag{e}$$

$$\begin{aligned}
& -e_{10} B_1 + e_{13} C_2 + B_3 + e_{14} C_4 - B_5 + e_{15} C_6 \\
& = \frac{1}{\kappa_1 + 1} \int_{a_1}^{b_1} M_9 \phi_1(t_1) dt_1 + \frac{1}{\kappa_2 + 1} \int_{a_2}^{b_2} M_{10} \phi_2(t_2) dt_2.
\end{aligned} \tag{f}$$

where, $B_1 = C_1 \alpha$, $B_3 = C_3 \alpha$, $B_5 = C_5 \alpha$, $m = \mu_1 / \mu_2$ and e 's and M 's are given in Appendix (C).

Equations (2.55) form a system of six equations in eight unknowns C_i , ($i=1, \dots, 6$), ϕ_j , ($j=1, 2$). After lengthly calculations, we can solve the first six unknowns in terms of ϕ_j , ($j=1, 2$). The results are presented in Appendix (C).

The two unknowns ϕ_j , ($j=1, 2$) can then be obtained by using the mixed boundary conditions (2.49)(b). Noting that

$$\sigma_{1yy}(x, 0) = -\sigma_1^T(x) \quad ; \quad a_1 < x < b_1. \tag{2.56}$$

By substituting from equation (2.46)(b) and taking the limits $y \rightarrow 0^+$ we have

$$\begin{aligned}
& \lim_{y \rightarrow 0} 2\mu_1 \frac{2}{\pi} \int_0^\infty [(-C_1 \alpha - C_2 \{\frac{\kappa_1 + 3}{2} + \alpha x\}) e^{x\alpha} \\
& + (C_3 \alpha - C_4 \{\frac{\kappa_1 + 3}{2} - \alpha x\}) e^{-x\alpha}] \cos y \alpha d\alpha \\
& + 2\mu_1 \frac{1}{2\pi} \int_{-\infty}^\infty A_1 (-1 - |\beta| y) e^{-y|\beta|} e^{ix\beta} d\beta = -\sigma_1^T(x).
\end{aligned} \tag{2.57}$$

Or

$$\begin{aligned}
& 2\mu_1 \frac{2}{\pi} \int_0^\infty [(-C_1\alpha - C_2\{\frac{\kappa_1+3}{2} + \alpha x\}) e^{x\alpha} \\
& + (C_3\alpha - C_4\{\frac{\kappa_1+3}{2} - \alpha x\}) e^{-x\alpha}] d\alpha \\
& + \lim_{y \rightarrow 0} 2\mu_1 \frac{1}{2\pi} \int_{-\infty}^\infty A_1(-1 - |\beta|y) e^{-y|\beta|} e^{ix\beta} d\beta = -\sigma_1^T(x). \tag{2.58}
\end{aligned}$$

By using equation (2.54)(a) and taking the limit, the last integral of equation (2.58) will be equal to

$$\frac{2}{\pi} \frac{1}{\kappa_1 + 1} \int_{a_1}^{b_1} \frac{\phi_1(t_1)}{t_1 - x} dt_1. \tag{2.59}$$

Substituting into equation (2.58), and dividing by $\pi(\kappa_1 + 1)/4\mu_1$, we may have

$$\begin{aligned}
& (\kappa_1 + 1) \int_0^\infty [(-C_1\alpha - C_2\{\frac{\kappa_1+3}{2} + \alpha x\}) e^{x\alpha} \\
& + (C_3\alpha - C_4\{\frac{\kappa_1+3}{2} - \alpha x\}) e^{-x\alpha}] d\alpha \\
& + \int_{a_1}^{b_1} \frac{\phi_1(t_1)}{t_1 - x} dt_1 = -\frac{\pi(\kappa_1 + 1)}{4\mu_1} \sigma_1^T(x) ; a_1 < t_1 < b_1, a_1 < x < b_1. \tag{2.60}
\end{aligned}$$

Similarly for the second condition (2.49)(b) we find

$$\begin{aligned}
& (\kappa_2 + 1) \int_0^\infty (C_5\alpha - C_6\{\frac{\kappa_2+3}{2} - \alpha x\}) e^{-x\alpha} d\alpha \\
& + \int_{a_2}^{b_2} \frac{\phi_2(t_2)}{t_2 - x} dt_2 = -\frac{\pi(\kappa_2 + 1)}{4\mu_2} \sigma_2^T(x) ; a_2 < t_2 < b_2, a_2 < x < b_2. \tag{2.61}
\end{aligned}$$

Substituting for $C_i, (i=1, \dots, 6)$, from Appendix (C), we obtain the following singular integral equations for the unknowns $\phi_j, (j=1, 2)$:

$$\int_{a_1}^{b_1} \left[\frac{1}{t_1 - x_1} + k_{11}(x_1, t_1) \right] \phi_1(t_1) dt_1 + \int_{a_2}^{b_2} k_{12}(x_1, t_2) \phi_2(t_2) dt_2$$

$$= -\frac{\pi(\kappa_1 + 1)}{4\mu_1} \sigma_1^T(x_1) ; a_1 < x_1 < b_1 . \quad (2.62)$$

$$\int_{a_1}^{b_1} k_{21}(x_2, t_1) \phi_1(t_1) dt_1 + \int_{a_2}^{b_2} \left[\frac{1}{t_2 - x_2} + k_{22}(x_2, t_2) \right] \phi_2(t_2) dt_2$$

$$= -\frac{\pi(\kappa_2 + 3)}{4\mu_2} \sigma_2^T(x_2) ; a_2 < x_2 < b_2 . \quad (2.63)$$

where

$$k_{11}(x_1, t_1) = \int_0^\infty G_{11}(x_1, t_1, \alpha) d\alpha , \quad (a)$$

$$k_{12}(x_1, t_2) = \int_0^\infty G_{12}(x_1, t_2, \alpha) d\alpha , \quad (b)$$

(2.64)

$$k_{21}(x_2, t_1) = \int_0^\infty G_{21}(x_2, t_1, \alpha) d\alpha , \quad (c)$$

$$k_{22}(x_2, t_2) = \int_0^\infty G_{22}(x_2, t_2, \alpha) d\alpha . \quad (d)$$

and

$$G_{11}(x_1, t_1, \alpha) = \left[-H_1 - \left(\frac{\kappa_1 + 3}{2} + \alpha x_1 \right) \frac{1}{D} H_3 \right] e^{x_1 \alpha}$$

$$+ \left[H_5 - \left(\frac{\kappa_1 + 3}{2} - \alpha x_1 \right) \frac{1}{D} H_7 \right] e^{-x_1 \alpha} , \quad (a)$$

$$G_{12}(x_1, t_2, \alpha) = \left(\frac{\kappa_1 + 1}{\kappa_2 + 1} \right) \left\{ \left[-H_2 - \left(\frac{\kappa_1 + 3}{2} + \alpha x_1 \right) \frac{1}{D} H_4 \right] e^{x_1 \alpha} \right.$$

$$\left. + \left[H_6 - \left(\frac{\kappa_2 + 3}{2} - \alpha x_1 \right) \frac{1}{D} H_8 \right] e^{-x_1 \alpha} \right\} , \quad (b)$$

(2.65)

$$G_{21}(x_2, t_1, \alpha) = \left(\frac{\kappa_2 + 1}{\kappa_1 + 1} \right) \left\{ \left[H_9 - \left(\frac{\kappa_2 + 3}{2} - \alpha x_1 \right) H_{11} \right] e^{-x_2 \alpha} \right\} , \quad (c)$$

$$G_{22}(x_2, t_2, \alpha) = \left[H_{10} - \left(\frac{\kappa_2 + 3}{2} - \alpha x_2 \right) H_{12} \right] e^{-x_2 \alpha} . \quad (d)$$

where H_j , ($j = 1, 2, \dots, 11, 12$), D , can be found in Appendix (C).

For internal cracks, i.e, $a_1 > 0$, $b_1 < h$, $a_2 > h$, $b_2 < \infty$ it can be shown that the kernels $k_{ij}, (i, j=1, 2)$, are bounded for any combination of the variables $x_j, t_j, \alpha, (j=1, 2)$. So, the two singular integral equations (2.62) and (2.63) are of the Cauchy-type.

2.2 Model II - Layered Medium on an Elastic Foundation

2.2.1 Temperature distribution

2.2.1.1 Unit step function at the boundary

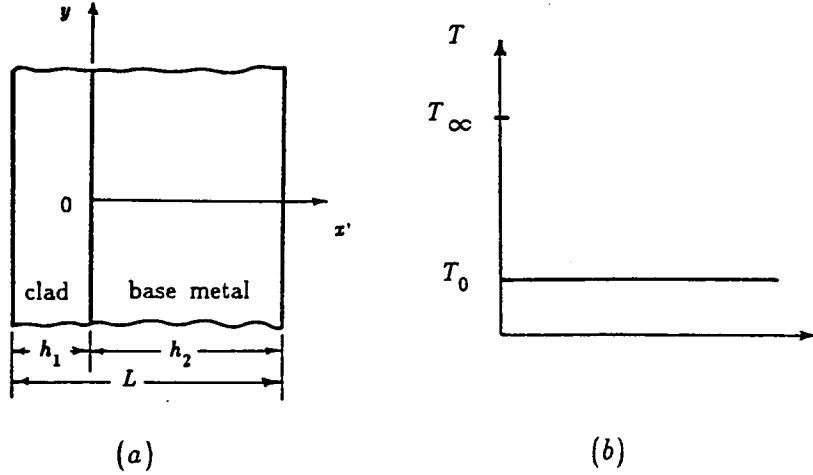


Figure 2-6: a-Geometry of the problem (Model II) b-Temperature boundary condition (unit step function)

Consider two dissimilar infinite layers having thicknesses h_1 (coating) and h_2 (base material) as shown in Figure 2-6(a). Figure 2-6(b) shows the temperature change at the boundary. Let D_1 , k'_1 , D_2 , k'_2 be the thermal diffusivity and thermal conductivity for the coating and base, respectively.

Then, the differential equations for 1, 2 are

$$\frac{\partial^2 \Theta_1(x,t)}{\partial x^2} = \frac{1}{D_1} \frac{\partial \Theta_1(x,t)}{\partial t} ; \quad -h_1 < x' < 0, t > 0, \quad (a)$$

$$\frac{\partial^2 \Theta_2(x,t)}{\partial x^2} = \frac{1}{D_2} \frac{\partial \Theta_2(x,t)}{\partial t} ; \quad 0 < x' < h_2, t > 0. \quad (b)$$

The initial and boundary conditions for the heat conduction problem are

$$\Theta_1(x,0) = \Theta_2(x,0) = 0, \quad (a)$$

$$\Theta_1(0,t) = \Theta_2(0,t), \quad (b)$$

$$k_1 \frac{\partial \Theta_1(0,t)}{\partial x} = k_2 \frac{\partial \Theta_2(0,t)}{\partial x}, \quad (c) \quad (2.67)$$

$$\frac{\partial \Theta_2(h_2,t)}{\partial x} = 0, \quad (d)$$

$$\Theta_1(-h_1,t) = \Theta_0 H(t). \quad (e)$$

where

$$\Theta_1(x,t) = T_1(x,t) - T_\infty, \quad (a)$$

$$\Theta_2(x,t) = T_2(x,t) - T_\infty, \quad (b) \quad (2.68)$$

$$\Theta_0 = T_0 - T_\infty. \quad (c)$$

T_∞ is the initial temperature for both materials, and T_0 is the temperature at the boundary at any time, $t > 0$. Condition (2.67)(c) implies no resistance at the interface, and condition (2.67)(d) implies insulated outer boundary.

Again, if we apply Laplace Transform to equations (2.66), and use condition (2.67)(a), we will end up with two ordinary differential equations that have the general solutions in the form

$$\bar{\Theta}_1(x,p) = A_1(p) \cosh q_1 x + B_1(p) \sinh q_1 x, \quad (a) \quad (2.69)$$

$$\bar{\Theta}_2(x,p) = A_2(p) \cosh q_2 x + B_2(p) \sinh q_2 x. \quad (b)$$

where $A_1(p)$, $B_1(p)$, $A_2(p)$, $B_2(p)$ are four constants that can be determined from the conditions (2.67)(b-e). So, after some manipulations equations (2.69) will become

$$\bar{\Theta}_1(x,p) = \frac{\Theta_0 [\cosh q_2 h_2 \cosh q_1 x - \eta \sinh q_2 h_2 \sinh q_1 x]}{p [\cosh q_1 h_1 \cosh q_2 h_2 + \eta \sinh q_1 h_1 \sinh q_2 h_2]}, \quad (a) \quad (2.70)$$

$$\bar{\Theta}_2(x,p) = \frac{\Theta_0 [\cosh q_2 h_2 \cosh q_2 x - \sinh q_2 h_2 \sinh q_2 x]}{p [\cosh q_1 h_1 \cosh q_2 h_2 + \eta \sinh q_1 h_1 \sinh q_2 h_2]}. \quad (b)$$

where

$$q_1 = \sqrt{\frac{p}{D_1}}, \quad q_2 = \sqrt{\frac{p}{D_2}}, \quad \eta = \frac{k_2}{k_1} \sqrt{\frac{D_1}{D_2}}. \quad (2.71)$$

Applying the Inversion Theorem the temperatures $\Theta_1(x,t)$, $\Theta_2(x,t)$, are found to be

$$\Theta_1(x,t) = \frac{1}{2\pi i} \int_{\gamma-i\infty}^{\gamma+i\infty} \frac{\Theta_0 [\cosh \zeta_2 h_2 \cosh \zeta_1 x - \eta \sinh \zeta_2 h_2 \sinh \zeta_1 x] e^{tz}}{z [\cosh \zeta_1 h_1 \cosh \zeta_2 h_2 + \eta \sinh \zeta_1 h_1 \sinh \zeta_2 h_2]} dz, \quad (a) \quad (2.72)$$

$$\Theta_2(x,t) = \frac{1}{2\pi i} \int_{\gamma-i\infty}^{\gamma+i\infty} \frac{\Theta_0 \cosh \zeta_2 (x-h_2) e^{tz}}{z [\cosh \zeta_1 h_1 \cosh \zeta_2 h_2 + \eta \sinh \zeta_1 h_1 \sinh \zeta_2 h_2]} dz. \quad (b)$$

where

$$\zeta_1 = \sqrt{z/D_1}, \quad \zeta_2 = \sqrt{z/D_2}. \quad (2.73)$$

It is clear that the integrands in equations (2.72) are single-valued functions of z , with simple poles at $z = 0$, and at the roots of the equation

$$\cosh \zeta_1 h_1 \cosh \zeta_2 h_2 + \eta \sinh \zeta_1 h_1 \sinh \zeta_2 h_2 = 0. \quad (2.74)$$

Let,

$$\zeta_1 = \sqrt{z/D_1} = i\omega, z = -D_1 \omega^2. \quad (2.75)$$

Then equation (2.74) becomes

$$\cos \omega h_1 \cos \delta \omega h_2 - \eta \sin \omega h_1 \sin \delta \omega h_2 = 0. \quad (2.76)$$

where

$$\delta = \sqrt{\frac{D_1}{D_2}}. \quad (2.77)$$

It can be seen that the roots of equation (2.76) are real and symmetrically placed with respect to $\omega = 0$. The roots ω_j are obtained from the intersection of the two families of curves $y = \cot \omega h_1$, $y = \eta \tan \delta \omega h_2$. The simple poles of

equation (2.76) are distributed along the real axis in the negative direction, and are equal to

$$z_m = -D_1 \omega_m^2, \quad m=1,2,3, \dots \quad (2.78)$$

The residue at these poles ($z = 0, z = -D_1 \omega_m^2$) can be found in Appendix (D). Then, by using the Residue Theorem, the contour Γ shown in Figure 2-7, and letting

$$\frac{x^*}{h_1} = (x^* - 1), \quad R = \frac{h_2}{h_1}, \quad \lambda_m = h_1 \omega_m, \quad \tau = \frac{tD_1}{h_1^2}, \quad (2.79)$$

the closed form solutions for Θ_1, Θ_2 are found to be

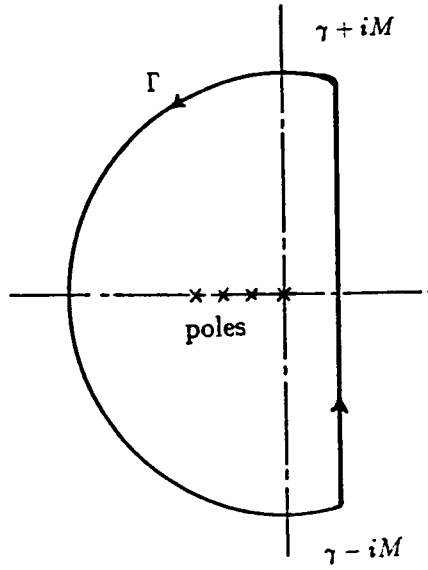


Figure 2-7: The contour for evaluation of integrals in equations (2.72)

$$\frac{\Theta_1(x^*, \tau)}{\Theta_0} = 1 - 2 \sum_{m=1}^{\infty} \frac{e^{-\tau \lambda_m^2}}{\lambda_m} \frac{[\cos \lambda_m (x^* - 1) \cos \lambda_m \delta R + \eta \sin \lambda_m (x^* - 1) \sin \lambda_m \delta R]}{[(1 + \eta \delta R) \sin \lambda_m \cos \lambda_m \delta R + (\delta R + \eta) \cos \lambda_m \sin \lambda_m \delta R]} ; 0 \leq x^* \leq 1, \quad (a)$$

(2.80)

$$\frac{\Theta_2(x^*, \tau)}{\Theta_0} = 1 - 2 \sum_{m=1}^{\infty} \frac{e^{-\tau \lambda_m^2}}{\lambda_m} \frac{\cos \lambda_m \delta (x^* - 1 - R)}{[(1 + \eta \delta R) \sin \lambda_m \cos \lambda_m \delta R + (\delta R + \eta) \cos \lambda_m \sin \lambda_m \delta R]} ; \quad 1 \leq x^* \leq (R+1). \quad (b)$$

where $\lambda_m, (m = 1, 2, 3, \dots)$ are the roots of the equation

$$\cos \lambda_m \cos \lambda_m \delta R - \eta \sin \lambda_m \sin \lambda_m \delta R = 0. \quad (2.81)$$

2.2.1.2 Ramp function at the boundary

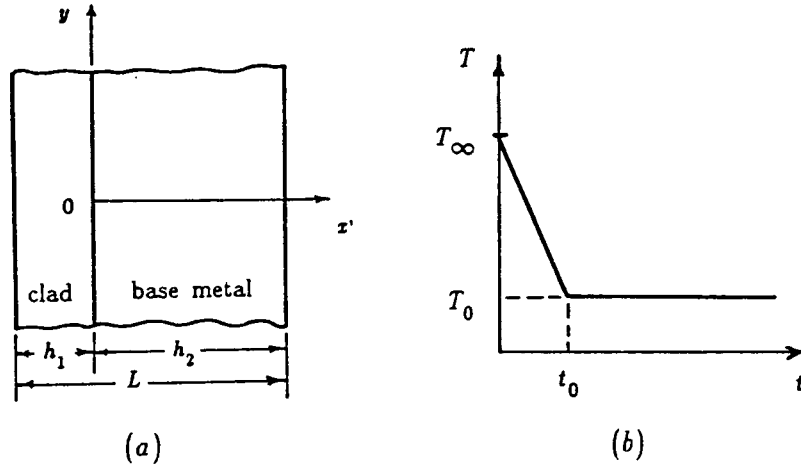


Figure 2-8: a-Geometry of the problem (Model II) b-Temperature boundary condition (ramp function)

If we apply a ramp function at the boundary, Figure 2-8(b), the differential equations for the materials 1, 2, and the initial and the boundary conditions are the same as equations (2.66), (2.67), except that, condition (2.67)(e) should be changed to

$$\Theta_1(-h, t) = \frac{\Theta_0}{t_0} t H(t) - \frac{\Theta_0}{t_0} (t - t_0) H(t - t_0). \quad (2.82)$$

Again, by applying Laplace Transform, we obtain equations

$$\bar{\Theta}_1(x,p) = F_{21}(p) \cdot B_{21}(p), \quad (a) \quad (2.83)$$

$$\bar{\Theta}_2(x,p) = F_{22}(p) \cdot B_{22}(p). \quad (b)$$

where

$$F_{21}(p) = \frac{\Theta_0[\cosh q_2 h_2 \cosh q_1 x' - \eta \sinh q_2 h_2 \sinh q_1 x']}{p[\cosh q_1 h_1 \cosh q_2 h_2 + \eta \sinh q_1 h_1 \sinh q_2 h_2]}, \quad (a)$$

$$F_{22}(p) = \frac{\Theta_0[\cosh q_2 h_2 \cosh q_2 x' - \sinh q_2 h_2 \sinh q_2 x']}{p[\cosh q_1 h_1 \cosh q_2 h_2 + \eta \sinh q_1 h_1 \sinh q_2 h_2]}, \quad (b) \quad (2.84)$$

$$B_{21}(p) = B_{22}(p) = \frac{1}{t_0} \left(\frac{1}{p} - \frac{e^{-pt_0}}{p} \right). \quad (c)$$

By applying the Convolution Theorem to equations (2.83), and observing that F_{21}, F_{22} are the same as equations (2.70), and letting

$$\frac{x'}{h_1} = (x^* - 1), \quad R = \frac{h_2}{h_1}, \quad \lambda_m = h_1 \omega_m, \quad \tau = \frac{tD_1}{h_1^2}, \quad \tau_0 = \frac{t_0 D_1}{h_1^2}. \quad (2.85)$$

the temperature distribution for strips 1, 2 become

$$\frac{\Theta_1(x^*, \tau)}{\Theta_0} = \frac{\tau}{\tau_0} + 2 \sum_{m=1}^{\infty} (e^{-\tau \lambda_m^2} - 1) \frac{[\cos \lambda_m (x^* - 1) \cos \lambda_m \delta R + \eta \sin \lambda_m (x^* - 1) \sin \lambda_m \delta R]}{\tau_0 \lambda_m^3 [(1 + \eta \delta R) \sin \lambda_m \cos \lambda_m \delta R + (\delta R + \eta) \cos \lambda_m \sin \lambda_m \delta R]} ; \quad 0 \leq x^* \leq 1, \quad \tau \leq \tau_0, \quad (a)$$

$$\frac{\Theta_1(x^*, \tau)}{\Theta_0} = 1 - 2 \sum_{m=1}^{\infty} e^{-\tau \lambda_m^2} (e^{\tau_0 \lambda_m^2} - 1) \frac{[\cos \lambda_m (x^* - 1) \cos \lambda_m \delta R + \eta \sin \lambda_m (x^* - 1) \sin \lambda_m \delta R]}{\tau_0 \lambda_m^3 [(1 + \eta \delta R) \sin \lambda_m \cos \lambda_m \delta R + (\delta R + \eta) \cos \lambda_m \sin \lambda_m \delta R]} ; \quad 0 \leq x^* \leq 1, \quad \tau > \tau_0, \quad (b)$$

$$\frac{\Theta_2(x^*, \tau)}{\Theta_0} = \frac{\tau}{\tau_0} + 2 \sum_{m=1}^{\infty} (e^{-\tau \lambda_m^2} - 1) \quad (2.86)$$

$$\frac{\cos \lambda_m \delta (x^* - 1 - R)}{\tau_0 \lambda_m^3 [(1 + \eta \delta R) \sin \lambda_m \cos \lambda_m \delta R + (\delta R + \eta) \cos \lambda_m \sin \lambda_m \delta R]}$$

; $1 \leq x^* \leq (R+1)$, $\tau \leq \tau_0$, (c)

$$\frac{\Theta_2(x^*, \tau)}{\Theta_0} = 1 - 2 \sum_{m=1}^{\infty} e^{-\tau \lambda_m^2} (e^{\tau \lambda_m^2} - 1)$$

$$\frac{\cos \lambda_m \delta (x^* - 1 - R)}{\tau_0 \lambda_m^3 [(1 + \eta \delta R) \sin \lambda_m \cos \lambda_m \delta R + (\delta R + \eta) \cos \lambda_m \sin \lambda_m \delta R]}$$

; $1 \leq x^* \leq (R+1)$ $\tau > \tau_0$. (d)

where $\delta = \sqrt{D_1/D_2}$, and λ_m are the roots of equation (2.81)

2.2.2 Thermal stresses in uncracked problem

Consider a thin-walled hollow cylinder with cladding of thickness h_1 , and base metal of thickness h_2 , shown in figure 2-9(a).

Let us take an element from the composite shell of unit length and a very small angle $d\phi$, as shown in Figure 2-9(b). Assume a uniform strain over the shell thickness ε_{0y} , ε_{0t} , then from the Hooke's Law we have

$$\varepsilon_{0y} = \frac{1}{E_1} (\sigma_{1y} - \nu_1 \sigma_{1t}) + \alpha'_1 \Theta_1 = \frac{1}{E_2} (\sigma_{2y} - \nu_2 \sigma_{2t}) + \alpha'_2 \Theta_2, \quad (a)$$

$$\varepsilon_{0t} = \frac{1}{E_1} (\sigma_{1t} - \nu_1 \sigma_{1y}) + \alpha'_1 \Theta_1 = \frac{1}{E_2} (\sigma_{2t} - \nu_2 \sigma_{2y}) + \alpha'_2 \Theta_2. \quad (b)$$

(2.87)

where σ_{1y} , σ_{1t} , σ_{2y} , σ_{2t} , are the stresses in axial and tangential directions for 1, 2, respectively, ν_1 , E_1 , α'_1 , ν_2 , E_2 , α'_2 are the Poisson's ratio, Young's modulus and thermal expansion coefficients, respectively. By integrating equations (2.87) over the shell thickness we obtain

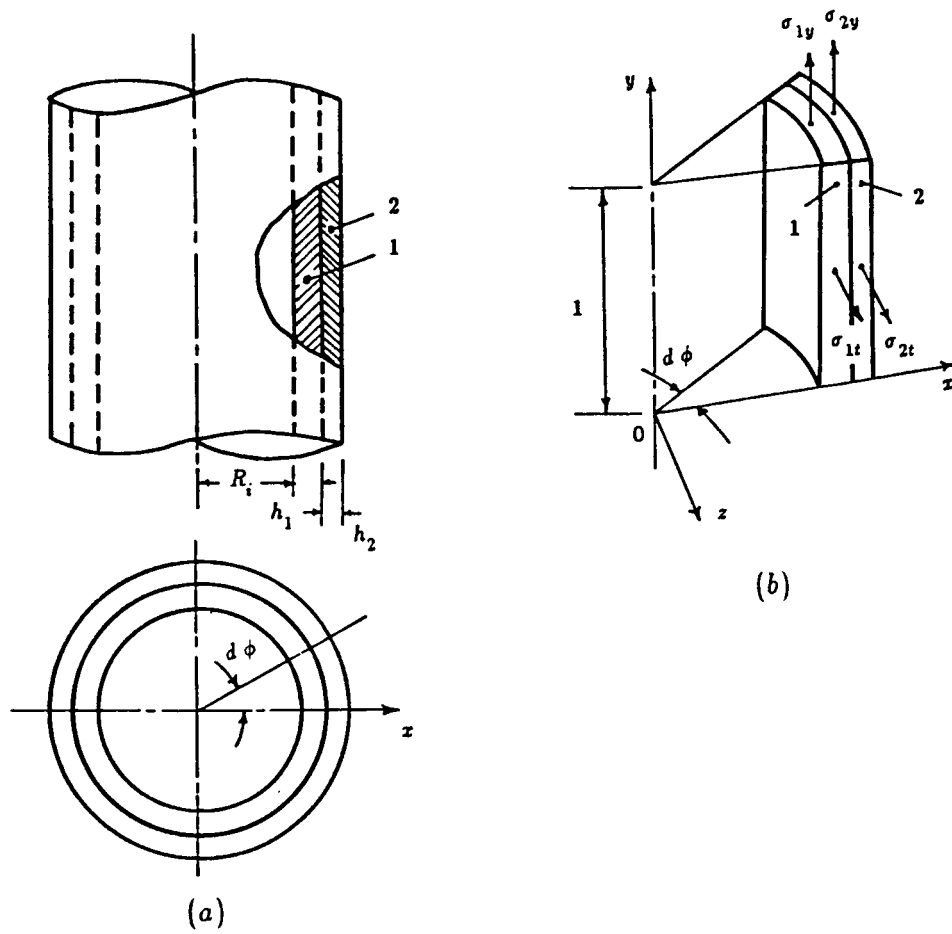


Figure 2-9: Geometry of thin-wall hollow cylinder with cladding to calculate thermal stresses in uncracked problem

$$\epsilon_{0y} = \frac{1}{E_1} (\bar{\sigma}_{1y} - \nu_1 \bar{\sigma}_{1t}) + \alpha'_1 \Theta_{1av} = \frac{1}{E_2} (\bar{\sigma}_{2y} - \nu_2 \bar{\sigma}_{2t}) + \alpha'_2 \Theta_{2av}, \quad (a)$$

(2.88)

$$\alpha_{0t} = \frac{1}{E_1} (\bar{\sigma}_{1t} - \nu_1 \bar{\sigma}_{1y}) + \alpha'_1 \Theta_{1av} = \frac{1}{E_2} (\bar{\sigma}_{2t} - \nu_2 \bar{\sigma}_{2y}) + \alpha'_2 \Theta_{2av}. \quad (b)$$

where

$$\begin{aligned}
\bar{\sigma}_{1y} &= \frac{1}{h_1} \int_0^{h_1} \sigma_{1y} dx, & \bar{\sigma}_{1t} &= \frac{1}{h_1} \int_0^{h_1} \sigma_{1t} dx \\
\bar{\sigma}_{2y} &= \frac{1}{h_2} \int_{h_1}^{h_1+h_2} \sigma_{2y} dx, & \bar{\sigma}_{2t} &= \frac{1}{h_2} \int_{h_1}^{h_1+h_2} \sigma_{2t} dx \\
\Theta_{1av} &= \frac{1}{h_1} \int_0^{h_1} \Theta_1(x,t) dx, & \Theta_{2av} &= \frac{1}{h_2} \int_{h_1}^{h_1+h_2} \Theta_2(x,t) dx
\end{aligned} \tag{2.89}$$

The resultant force in radial and axial directions must vanish giving

$$\begin{aligned}
\int_0^{h_1} \sigma_{1t} dx + \int_{h_1}^{h_1+h_2} \sigma_{2t} dx &= 0, & (a) \\
\int_0^{h_1} \sigma_{1y} dx + \int_{h_1}^{h_1+h_2} \sigma_{2y} dx &= 0. & (b)
\end{aligned} \tag{2.90}$$

Equations (2.90) can be put in the form

$$\begin{aligned}
\bar{\sigma}_{1t} h_1 + \bar{\sigma}_{2t} h_2 &= 0, & (a) \\
\bar{\sigma}_{1y} h_1 + \bar{\sigma}_{2y} h_2 &= 0. & (b)
\end{aligned} \tag{2.91}$$

Equations (2.88) and (2.91) are six equations with six unknowns (ϵ_{0y} , ϵ_{0t} , $\bar{\sigma}_{1y}$, $\bar{\sigma}_{1t}$, $\bar{\sigma}_{2y}$, $\bar{\sigma}_{2t}$). By examining these equations we can see that they would be unaltered if the subscripts y and t were changed. Therefore,

$$\begin{aligned}
\bar{\sigma}_{1y} &= \bar{\sigma}_{1t} = \bar{\sigma}_1, & (a) \\
\bar{\sigma}_{2y} &= \bar{\sigma}_{2t} = \bar{\sigma}_2, & (b) \\
\epsilon_{0y} &= \epsilon_{0t} = \epsilon_0. & (c)
\end{aligned} \tag{2.92}$$

Then, equations (2.88) and (2.91) are reduced to

$$\varepsilon_0 = \frac{1}{E_1}(\bar{\sigma}_1 - \nu_1 \bar{\sigma}_1) + \alpha'_1 \Theta_{1av}, \quad (a)$$

$$\varepsilon_0 = \frac{1}{E_2}(\bar{\sigma}_2 - \nu_2 \bar{\sigma}_2) + \alpha'_2 \Theta_{2av}, \quad (b) \quad (2.93)$$

$$\bar{\sigma}_1 h_1 + \bar{\sigma}_2 h_2 = 0. \quad (c)$$

By solving equations (2.93) together we can get

$$\varepsilon_0 = \frac{\frac{E_1 \alpha'_1 \Theta_{1av}}{1 - \nu_1} h_1 + \frac{E_2 \alpha'_2 \Theta_{2av}}{1 - \nu_2} h_2}{\frac{E_1}{1 - \nu_1} h_1 + \frac{E_2}{1 - \nu_2} h_2}. \quad (2.94)$$

Also, from equations (2.87) we can see that

$$\sigma_{1y} = \sigma_{1t} = \sigma_1, \quad \sigma_{2y} = \sigma_{2t} = \sigma_2. \quad (2.95)$$

Then equations (2.87) become

$$\varepsilon_0 = \frac{1 - \nu_1}{E_1} \sigma_1(x, t) + \alpha'_1 \Theta_1(x, t), \quad (a)$$

$$\varepsilon_0 = \frac{1 - \nu_2}{E_2} \sigma_2(x, t) + \alpha'_2 \Theta_2(x, t). \quad (b) \quad (2.96)$$

Substituting equation (2.94) into equations (2.96), the thermal stresses in materials 1, 2 can be written as

$$\sigma_1(x, t) = \frac{E_1}{1 - \nu_1} [\varepsilon_0 - \alpha'_1 \Theta_1(x, t)], \quad (a)$$

$$\sigma_2(x, t) = \frac{E_2}{1 - \nu_2} [\varepsilon_0 - \alpha'_2 \Theta_2(x, t)]. \quad (b) \quad (2.97)$$

Thus, in the concentric cylindrical shells having a radial temperature variation, the axial and tangential stresses are given by equations (2.97) at all points except at the ends of the cylinder. The end surface tractions produce thermal end moments at the rim of the cylinder, and these generate axial bending stresses which disappear rapidly with the increase of distance from the

end. Let

$$x^* = \frac{x}{h_1}, \quad R = \frac{h_2}{h_1}, \quad \tau = \frac{tD_1}{h_1^2}. \quad (2.98)$$

Then, equation (2.94) becomes

$$\varepsilon_0 = \alpha'_1 \Theta_0 \left[\frac{\int_0^1 \frac{\Theta_1(x^*, \tau)}{\Theta_0} dx^* + \frac{E_2 \alpha'_2 (1-\nu_1)}{E_1 \alpha'_1 (1-\nu_2)} \int_1^{1+R} \frac{\Theta_2(x^*, \tau)}{\Theta_0} dx^*}{1 + \frac{E_2 (1-\nu_1)}{E_1 (1-\nu_2)} R} \right] \quad (2.99)$$

By letting $\sigma_0^T = -\frac{E_1 \alpha'_1 \Theta_0}{1-\nu_1}$, from (2.97) and (2.99) the thermal stresses in materials 1, 2 are found to be

$$\frac{\sigma_1(x^*, \tau)}{\sigma_0^T} = \frac{\Theta_1(x^*, \tau)}{\Theta_0} - \frac{\int_0^1 \frac{\Theta_1(x^*, \tau)}{\Theta_0} dx^* + \frac{E_2 \alpha'_2 (1-\nu_1)}{E_1 \alpha'_1 (1-\nu_2)} \int_1^{1+R} \frac{\Theta_2(x^*, \tau)}{\Theta_0} dx^*}{1 + \frac{E_2 (1-\nu_1)}{E_1 (1-\nu_2)} R} \quad ; 0 \leq x^* \leq 1, \quad (a) \quad (2.100)$$

$$\frac{\sigma_2(x^*, \tau)}{\sigma_0^T} = \frac{E_2 (1-\nu_1)}{E_1 (1-\nu_2)} \left\{ \frac{\alpha'_2 \Theta_2(x^*, \tau)}{\alpha'_1 \Theta_0} - \frac{\int_0^1 \frac{\Theta_1(x^*, \tau)}{\Theta_0} dx^* + \frac{E_2 \alpha'_2 (1-\nu_1)}{E_1 \alpha'_1 (1-\nu_2)} \int_1^{1+R} \frac{\Theta_2(x^*, \tau)}{\Theta_0} dx^*}{1 + \frac{E_2 (1-\nu_1)}{E_1 (1-\nu_2)} R} \right\} \quad ; 1 \leq x^* \leq R+1. \quad (b)$$

where the integrals

$$\int_0^1 \frac{\Theta_1(x^*, \tau)}{\Theta_0} dx^* , \int_1^{1+R} \frac{\Theta_2(x^*, \tau)}{\Theta_0} dx^* \quad (2.101)$$

are given in Appendix (E). Equation (2.100) give, essentially, the thermal stresses in a composite plate constrained to remain in its own plane.

2.2.2.1 Stiffness of the elastic foundation

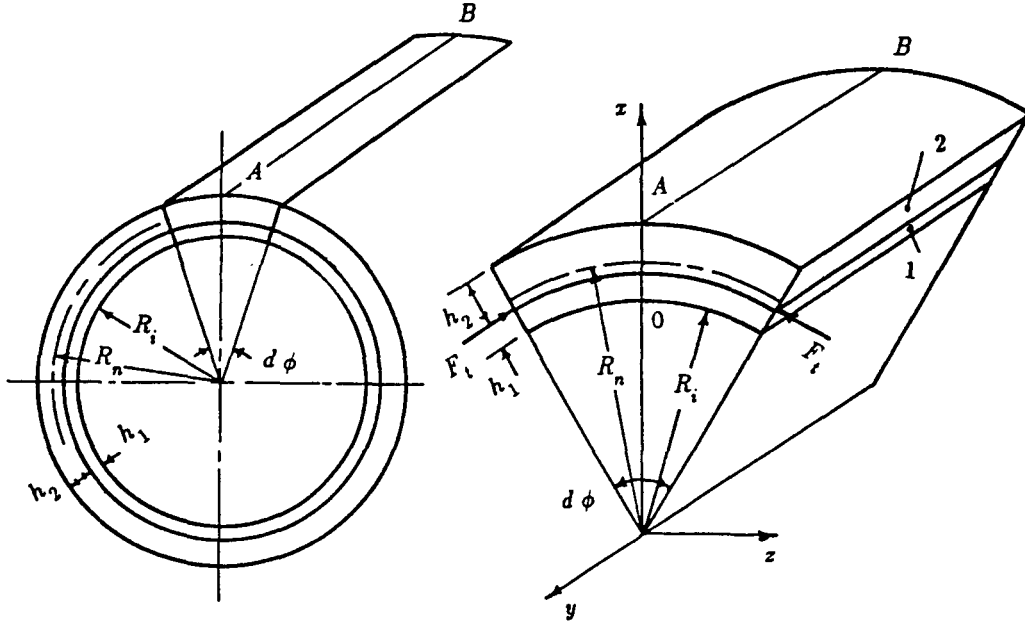


Figure 2-10: Geometry of thin-wall hollow cylinder with cladding to calculate stiffness of elastic foundation χ

It is well known that the thin-wall hollow cylinder can be simulated as a beam on an elastic foundation of stiffness related to the radius of the neutral surface of the cylinder, the thickness of the cylinder, and the Young's modulus, [5].

In case of thin-walled hollow cylinder with cladding, Figure 2-10, the stiffness of the elastic foundation χ can be determined by taking a strip AB of unit width cut from the composite cylinder. Assume that x_n denote the change of the radius R_n (radius of the neutral surface, $\varepsilon = 0$), i.e, $x_n = \Delta R_n$, which is the

deflection of the strip at any section measured from neutral surface. The strain over the cross section ϵ_t , would then be

$$\epsilon_t = \frac{\Delta R_n}{R_n} = \frac{x_n}{R_n}. \quad (2.102)$$

Now, the corresponding stresses are

$$\sigma_{1t} = \frac{E_1 x_n}{R_n}, \quad (a) \quad (2.103)$$

$$\sigma_{2t} = \frac{E_2 x_n}{R_n}. \quad (b)$$

Then, the force per unit length on the strip AB is

$$F_t = \frac{E_1 x_n}{R_n} h_1 + \frac{E_2 x_n}{R_n} h_2. \quad (2.104)$$

The radial component of this force is

$$F_t d\phi = \left[\frac{E_1 x_n}{R_n} h_1 + \frac{E_2 x_n}{R_n} h_2 \right] d\phi = \left[\frac{E_1 h_1 + E_2 h_2}{R_n^2} \right] x_n. \quad (2.105)$$

where $d\phi = 1/R_n$.

That is, radial force is proportional to the deflection x_n . So, we conclude that a longitudinal element of a cylindrical tube loaded symmetrically with respect to its axis can be regarded as a beam on an elastic foundation, having the stiffness

$$\chi = \frac{E_1 h_1 + E_2 h_2}{R_n^2}. \quad (2.106)$$

where R_n is the radius of neutral surface of the cylinder. To obtain R_n , let us consider the composite beam shown in Figure 2-11.

Let ρ' is the radius of curvature of deflected beam and x_n is the distance from the neutral axis, then

$$\epsilon_y = \frac{x_n}{\rho'}. \quad (2.107)$$

So, the stresses in 1, 2 become

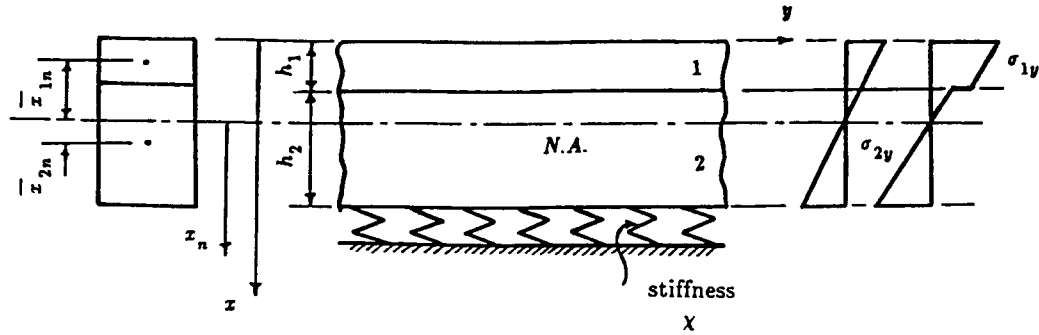


Figure 2-11: Geometry of composite beam to calculate the radius of neutral axis R_n

$$\sigma_{1y} = \frac{E_1 x_n}{\rho'}, \quad (a) \quad (2.108)$$

$$\sigma_{2y} = \frac{E_2 x_n}{\rho'}. \quad (b)$$

The total force in y-direction must vanish, then

$$\int \sigma_{1y} dA_1 + \int \sigma_{2y} dA_2 = 0. \quad (2.109)$$

where A_1 , A_2 are the cross section areas of 1, 2, respectively. Substituting equations (2.108) into equation (2.109) we may have

$$\frac{E_1}{\rho'} \int x_n dA_1 + \frac{E_2}{\rho'} \int x_n dA_2 = 0. \quad (2.110)$$

Since

$$\int x_n dA_1 = -\bar{x}_{1n} A_1, \quad (a)$$

$$(2.111)$$

$$\int x_n dA_2 = \bar{x}_{2n} A_2. \quad (b)$$

where \bar{x}_{1n} , \bar{x}_{2n} are the distance from the neutral axis to the center of the cross sectional area for strips 1 and 2 respectively. Then equation (2.110) can be

written as

$$-E_1 \bar{x}_{1n} A_1 + E_2 \bar{x}_{2n} A_2 = 0. \quad (2.112)$$

Also

$$\bar{x}_{1n} + \bar{x}_{2n} = \frac{1}{2}(h_1 + h_2). \quad (2.113)$$

Solving equations (2.112) and (2.113) for \bar{x}_{1n} , \bar{x}_{2n} , we have

$$\bar{x}_{1n} = \frac{1}{2}(h_1 + h_2) \frac{E_2 A_2}{E_1 A_1 + E_2 A_2}. \quad (2.114)$$

Since, the beam has a unit width, i.e., $A_1 = h_1 \cdot 1$, $A_2 = h_2 \cdot 1$, then equation (2.114) becomes

$$\bar{x}_{1n} = \frac{1}{2}(h_1 + h_2) \frac{E_2 h_2}{E_1 h_1 + E_2 h_2}. \quad (2.115)$$

So, the natural axis radius R_n is

$$R_n = R_i + \frac{h_1}{2} + \bar{x}_{1n}, \quad (2.116)$$

where R_i is the inner radius of the cylinder.

2.2.3 Formulation of the crack problem

Consider the problem that is shown in Figure 2-12, where χ is the stiffness of the elastic foundation. The analysis is the same as in Model I, and equations (2.41), (2.42), (2.43), (2.44), and (2.45), are still valid. Then the displacement fields and the stresses are

Material (1) , $0 \leq x \leq h_1$, $0 \leq y < \infty$

$$\begin{aligned} \frac{1}{2\mu_1} \sigma_{1xx}(x,y) = & \frac{2}{\pi} \int_0^\infty [(C_1 \alpha + C_2 \{ \frac{\kappa_1 - 1}{2} + \alpha x \}) e^{x\alpha} \\ & + (-C_3 \alpha + C_4 \{ \frac{\kappa_1 - 1}{2} - \alpha x \}) e^{-x\alpha}] \cos y \alpha \, d\alpha \\ & + \frac{1}{2\pi} \int_{-\infty}^\infty A_1 (-1 + |\beta| y) e^{-y|\beta|} e^{i x \beta} d\beta, \end{aligned} \quad (a)$$

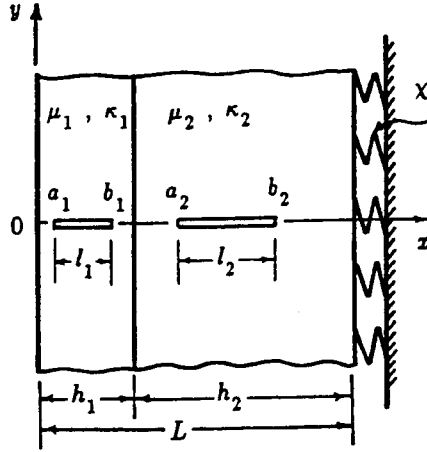


Figure 2-12: Crack geometry Model II

$$\begin{aligned} \frac{1}{2\mu_1}\sigma_{1yy}(x,y) = & \frac{2}{\pi}\int_0^\infty [(-C_1\alpha - C_2\{\frac{\kappa_1+3}{2} + \alpha x\})e^{x\alpha} \\ & + (C_3\alpha - C_4\{\frac{\kappa_1+3}{2} - \alpha x\})e^{-x\alpha}] \cos y\alpha d\alpha \\ & + \frac{1}{2\pi}\int_{-\infty}^\infty A_1(-1 - |\beta|y)e^{-y|\beta|}e^{ix\beta}d\beta, \end{aligned} \quad (b)$$

$$\begin{aligned} \frac{1}{2\mu_1}\sigma_{1xy}(x,y) = & \frac{2}{\pi}\int_0^\infty [(-C_1\alpha - C_2\{\frac{\kappa_1+1}{2} + \alpha x\})e^{x\alpha} \\ & + (-C_3\alpha + C_4\{\frac{\kappa_1+1}{2} - \alpha x\})e^{-x\alpha}] \sin y\alpha d\alpha \\ & + \frac{1}{2\pi}\int_{-\infty}^\infty iA_1\beta y e^{-y|\beta|}e^{ix\beta}d\beta, \end{aligned} \quad (c)$$

$$\begin{aligned} u_1(x,y) = & \frac{2}{\pi}\int_0^\infty [(C_1 + C_2x)e^{x\alpha} + (C_3 + C_4x)e^{-x\alpha}] \cos y\alpha d\alpha \\ & + \frac{1}{2\pi}\int_{-\infty}^\infty \frac{iA_1}{|\beta|}(\frac{|\beta|\kappa_1-1}{\beta} - \beta y)e^{-y|\beta|}e^{ix\beta}d\beta, \end{aligned} \quad (d)$$

$$\begin{aligned}
v_1(x,y) = & \frac{2}{\pi} \int_0^\infty [(-C_1 - C_2 \{\frac{\kappa_1}{\alpha} + x\}) e^{x\alpha} \\
& + (C_3 - C_4 \{\frac{\kappa_1}{\alpha} - x\}) e^{-x\alpha}] \sin y\alpha d\alpha \\
& + \frac{1}{2\pi} \int_{-\infty}^\infty \frac{A_1}{|\beta|} (\frac{\kappa_1 + 1}{2} + |\beta|y) e^{-y|\beta|} e^{ix\beta} d\beta.
\end{aligned} \tag{e}$$

Material (2) , $h_1 \leq x \leq h_1 + h_2$, $0 \leq y < \infty$

$$\begin{aligned}
\frac{1}{2\mu_2} \sigma_{2xx}(x,y) = & \frac{2}{\pi} \int_0^\infty [(C_7\alpha + C_8 \{\frac{\kappa_2 - 1}{2} + \alpha x\}) e^{x\alpha} \\
& + (-C_5\alpha + C_6 \{\frac{\kappa_2 - 1}{2} - \alpha x\}) e^{-x\alpha}] \cos y\alpha d\alpha \\
& + \frac{1}{2\pi} \int_{-\infty}^\infty A_2 (-1 + |\beta|y) e^{-y|\beta|} e^{ix\beta} d\beta,
\end{aligned} \tag{a}$$

$$\begin{aligned}
\frac{1}{2\mu_2} \sigma_{2yy}(x,y) = & \frac{2}{\pi} \int_0^\infty [(-C_7\alpha - C_8 \{\frac{\kappa_2 + 3}{2} + \alpha x\}) e^{x\alpha} \\
& + (C_5\alpha - C_6 \{\frac{\kappa_2 + 3}{2} - \alpha x\}) e^{-x\alpha}] \cos y\alpha d\alpha \\
& + \frac{1}{2\pi} \int_{-\infty}^\infty A_2 (-1 - |\beta|y) e^{-y|\beta|} e^{ix\beta} d\beta,
\end{aligned} \tag{b}$$

$$\begin{aligned}
\frac{1}{2\mu_2} \sigma_{2xy}(x,y) = & \frac{2}{\pi} \int_0^\infty [(-C_7\alpha - C_8 \{\frac{\kappa_2 + 1}{2} + \alpha x\}) e^{x\alpha} \\
& + (-C_5\alpha + C_6 \{\frac{\kappa_2 + 1}{2} - \alpha x\}) e^{-x\alpha}] \sin y\alpha d\alpha
\end{aligned} \tag{2.118}$$

$$+ \frac{1}{2\pi} \int_{-\infty}^\infty iA_2 \beta y e^{-y|\beta|} e^{ix\beta} d\beta, \tag{c}$$

$$\begin{aligned}
u_2(x,y) = & \frac{2}{\pi} \int_0^\infty [(C_7 + C_8 x) e^{x\alpha} + (C_5 + C_6 x) e^{-x\alpha}] \cos y\alpha d\alpha \\
& + \frac{1}{2\pi} \int_{-\infty}^\infty \frac{iA_2}{|\beta|} (\frac{|\beta|\kappa_2 - 1}{2} - \beta y) e^{-y|\beta|} e^{ix\beta} d\beta,
\end{aligned} \tag{d}$$

$$\begin{aligned}
v_2(x,y) = & \frac{2}{\pi} \int_0^\infty [(-C_7 - C_8 \{ \frac{\kappa_2}{\alpha} + x \}) e^{x\alpha} \\
& + (C_5 - C_6 \{ \frac{\kappa_2}{\alpha} - x \}) e^{-x\alpha}] \sin y\alpha d\alpha \\
& + \frac{1}{2\pi} \int_{-\infty}^\infty \frac{A_2}{|\beta|} \left(\frac{\kappa_2 + 1}{2} + |\beta|y \right) e^{-y|\beta|} e^{ix\beta} d\beta.
\end{aligned} \tag{e}$$

where C_j , ($j = 1, 2, \dots, 8$) are functions of α , and A_1, A_2 are functions of β , and are to be determined from the boundary and continuity conditions. Eight of these conditions are given by (2.48), (2.49) while the two remaining conditions at $x = h_1 + h_2$ are

$$\sigma_{2xx}(h_1 + h_2, y) = -p_x = -\chi u_2(h_1 + h_2, y), \tag{g}$$

$$\sigma_{2xy}(h_1 + h_2, y) = 0. \tag{h} \quad (2.119)$$

By using the same definition of the density functions $\phi_1(x)$, $\phi_2(x)$, as in equations (2.50), and by using the boundary conditions (2.48), (2.119) and the Fourier Inverse Transform, with the help of the integration formulas given in Appendix (B) we will have

$$-B_1 - e_1 C_2 - B_3 + e_1 C_4 = \frac{1}{\kappa_1 + 1} \int_{a_1}^{b_1} M_1 \phi_1(t_1) dt_1, \tag{a}$$

$$B_1 + e_2 C_2 - B_3 + e_2 C_4 = \frac{1}{\kappa_1 + 1} \int_{a_1}^{b_1} M_2 \phi_1(t_1) dt_1, \tag{b}$$

$$\begin{aligned}
& e_4 B_1 + e_3 C_2 - m B_3 + e_5 C_4 + B_5 + e_6 C_6 - e_{10} B_7 + e_{25} C_8 \\
& = \frac{1}{\kappa_1 + 1} \int_{a_1}^{b_1} M_3 \phi_1(t_1) dt_1 + \frac{1}{\kappa_2 + 1} \int_{a_2}^{b_2} M_4 \phi_2(t_2) dt_2,
\end{aligned} \tag{c}$$

$$\begin{aligned}
& -e_4 B_1 + e_7 C_2 - m B_3 + e_8 C_4 + B_5 + e_9 C_6 + e_{10} B_7 + e_{16} C_8 \\
& = \frac{1}{\kappa_1 + 1} \int_{a_1}^{b_1} M_5 \phi_1(t_1) dt_1 + \frac{1}{\kappa_2 + 1} \int_{a_2}^{b_2} M_6 \phi_2(t_2) dt_2,
\end{aligned} \tag{d}$$

(2.120)

$$\begin{aligned}
& e_{10}B_1 + e_{11}C_2 + B_3 + e_{12}C_4 - B_5 - e_{12}C_6 - e_{10}B_7 - e_{11}C_8 \\
& = \frac{1}{\kappa_1 + 1} \int_{a_1}^{b_1} M_7 \phi_1(t_1) dt_1 + \frac{1}{\kappa_2 + 1} \int_{a_2}^{b_2} M_8 \phi_2(t_2) dt_2,
\end{aligned} \tag{e}$$

$$\begin{aligned}
& -e_{10}B_1 + e_{13}C_2 + B_3 + e_{14}C_4 - B_5 + e_{15}C_6 + e_{10}B_7 + e_{17}C_8 \\
& = \frac{1}{\kappa_1 + 1} \int_{a_1}^{b_1} M_9 \phi_1(t_1) dt_1 + \frac{1}{\kappa_2 + 1} \int_{a_2}^{b_2} M_{10} \phi_2(t_2) dt_2,
\end{aligned} \tag{f}$$

$$-B_5 + e_{20}C_6 + e_{18}B_7 + e_{19}C_8 = \frac{1}{\kappa_2 + 1} \int_{a_2}^{b_2} M_{11} \phi_2(t_2) dt_2, \tag{g}$$

$$\begin{aligned}
& (\rho - 1)B_5 + (\rho e_{24} + e_{22})C_6 + (-\rho - 1)e_{18}B_7 + (\rho e_{23} + e_{21})C_8 \\
& = \frac{1}{\kappa_2 + 1} \int_{a_2}^{b_2} M_{12} \phi_2(t_2) dt_2.
\end{aligned} \tag{h}$$

where $B_1 = \alpha C_1$, $B_3 = \alpha C_3$, $B_5 = \alpha C_5$, $B_7 = \alpha C_7$, e's and M's are shown in Appendix (F), and $\rho = \chi/2\mu_2\alpha$.

Equations (2.120) give eight equations in ten unknowns. After long manipulations, we can obtain the unknowns C_j , ($j = 1, 2, \dots, 8$) in terms of the two other unknowns ϕ_1 , ϕ_2 . The results are shown in Appendix (F).

By using the mixed boundary conditions as in Model I, we obtain two singular integral equations of Cauchy-type in the same form as equations (2.62), (2.63), where G_{ij} , ($i, j = 1, 2, \dots$), in this case are

$$\begin{aligned}
G_{11}(x_1, t_1, \alpha) &= [-Q_1 - \left(\frac{\kappa_1 + 3}{2} + \alpha x_1\right)Q_3] e^{x_1 \alpha} \\
&+ [Q_5 - \left(\frac{\kappa_1 + 3}{2} - \alpha x_1\right)Q_7] e^{-x_1 \alpha},
\end{aligned} \tag{a}$$

$$\begin{aligned}
G_{12}(x_1, t_2, \alpha) &= \frac{\kappa_1 + 1}{\kappa_2 + 1} \left\{ \left[-Q_2 - \left(\frac{\kappa_1 + 3}{2} + \alpha x_1 \right) Q_4 \right] e^{x_1 \alpha} \right. \\
&\quad \left. + \left[Q_6 - \left(\frac{\kappa_1 + 3}{2} - \alpha x_1 \right) Q_8 \right] e^{-x_1 \alpha} \right\}, \tag{b}
\end{aligned}$$

$$\begin{aligned}
G_{21}(x_2, t_1, \alpha) &= \frac{\kappa_2 + 1}{\kappa_1 + 1} \left\{ \left[-\frac{Q_{13}}{D_0} - \left(\frac{\kappa_2 + 3}{2} + \alpha x_2 \right) \frac{Q_{15}}{D_0} \right] e^{x_2 \alpha} \right. \\
&\quad \left. + \left[Q_9 - \left(\frac{\kappa_2 + 3}{2} - \alpha x_2 \right) Q_{11} \right] e^{-x_2 \alpha} \right\}, \tag{c}
\end{aligned}$$

$$\begin{aligned}
G_{22}(x_2, t_2, \alpha) &= \left[-\frac{Q_{14}}{D_0} - \left(\frac{\kappa_2 + 3}{2} + \alpha x_2 \right) \frac{Q_{16}}{D_0} \right] e^{x_2 \alpha} \\
&\quad + \left[Q_{10} - \left(\frac{\kappa_2 + 3}{2} - \alpha x_2 \right) Q_{12} \right] e^{-x_2 \alpha}. \tag{d}
\end{aligned}$$

in which Q_j , ($j = 1, 2, \dots, 16$), D_0 , are found in Appendix (F),
 $a_i < x_i < b_i$, $a_i < t_i < b_i$, ($i=1, 2$).

Chapter 3

THE SINGULARITY AT THE CRACK TIP

It is well known that the stress fields around a crack tip is proportional to r^{-s} , where r is a small distance from the crack tip at which we measure the stress field, and s is called the power of singularity which should be between zero and one, i.e, $0 < s < 1$. If s is less than zero, the stress is bounded as $r \rightarrow 0$, and there is no singularity at the crack tip. If s is greater than one, the strain energy density is unbounded and goes to infinity as $r \rightarrow 0$, which also is impossible.

The value of singularity s is dependent on the crack configuration as well as the material properties. For each special crack configuration, some terms of the kernels in the singular integral equation (2.62), (2.63) become singular. By using Muskhelishvili's technique [37], the singular behavior of the stress state at the crack tip can then be examined for each case.

Since, the singularity at the crack tip will be the same for both Models I and II, the results would be valid for both models.

3.1 Embedded crack in both materials

The case of a crack embedded in both materials is shown in Figure 3-1. The only singular terms in the integral equations (2.62), (2.63) are the dominant terms $\frac{1}{t_1 - x_1}$ and $\frac{1}{t_2 - x_2}$, other kernels are bounded as $\alpha \rightarrow \infty$. The two singular integral equations can thus be written in the form

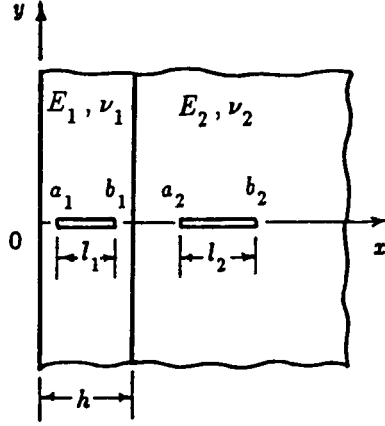


Figure 3-1: Geometry of embedded crack in both materials

$$\int_{a_1}^{b_1} \frac{\phi_1(t_1)}{t_1 - x_1} dt_1 + \text{B.T.} = -\frac{\pi(\kappa_1 + 1)}{4\mu_1} \sigma_1^I(x_1); a_1 < x_1 < b_1, \quad (\text{a})$$

(3.1)

$$\int_{a_2}^{b_2} \frac{\phi_2(t_2)}{t_2 - x_2} dt_2 + \text{B.T.} = -\frac{\pi(\kappa_2 + 1)}{4\mu_2} \sigma_2^I(x_2); a_2 < x_2 < b_2. \quad (\text{b})$$

where B.T. correspond to the bounded terms.

To examine the behavior of the unknown functions ϕ_1, ϕ_2 around the irregular points (end points), following Muskhelishvili [37], we assume that the unknown functions ϕ_1, ϕ_2 may be expressed as

$$\phi_j(t_j) = \frac{g_j(t_j)}{(t_j - a_j)^{\alpha_j} (b_j - t_j)^{\beta_j}} = g_j(t_j) w_j(t_j); j = 1, 2. \quad (3.2)$$

where $g_j(t_j)$ satisfies a Hölder condition in the closed interval $a_j \leq t_j \leq b_j$, ($j = 1, 2$) and $g_j(a_j) \neq 0$, $g_j(b_j) \neq 0$, ($j = 1, 2$). Also α_j, β_j , ($j = 1, 2$) are the singularity at the irregular points which should satisfy the condition $0 < \text{Re}(\alpha_j, \beta_j) < 1$, ($j = 1, 2$), and $w_j(t_j)$ is any definite branch which varies continuously on the interval $a_j < t_j < b_j$, ($j = 1, 2$).

Define the following sectionally holomorphic function

$$F_j(z) = \frac{1}{\pi} \int_{a_j}^{b_j} \frac{\phi_j(t_j)}{t_j - z} dt_j ; j=1, 2. \quad (3.3)$$

Substituting equation (3.2) into equation (3.3) we obtain

$$F_j(z) = \frac{1}{\pi} \int_{a_j}^{b_j} \frac{g_j(t_j) e^{\pi i \beta_j}}{(t_j - a_j)^{\alpha_j} (t_j - b_j)^{\beta_j} (t_j - z)} dt_j ; j=1, 2. \quad (3.4)$$

Following Muskhelishvili, equation (3.4) can be written as

$$F_j(z) = \frac{g_j(a_j) e^{\pi i \alpha_j}}{(b_j - a_j)^{\beta_j} (z - a_j)^{\alpha_j} \sin \pi \alpha_j} - \frac{g_j(b_j)}{(b_j - a_j)^{\alpha_j} (z - b_j)^{\beta_j} \sin \pi \beta_j} + F_{0j}(z) ; j=1, 2. \quad (3.5)$$

where $F_{0j}(z)$ is bounded everywhere except possibly at the end points $a_j, b_j, (j=1, 2)$, where it has the following behavior

$$|F_{0j}(z)| < \frac{C_{jk}}{|z - e_{jk}|^{p_{jk}}} ; j, k=1, 2. \quad (3.6)$$

where $e_{j1} = a_j, e_{j2} = b_j, p_{j1} < \operatorname{Re}(\alpha_j), p_{j2} < \operatorname{Re}(\beta_j)$, and C_{jk}, p_{jk} are real constants, i.e., $F_{0j}(z)$ has singularity less than $\alpha_j, \beta_j, (j=1, 2)$.

Using the Pelemelj formula [37]

$$\frac{1}{\pi} \int_{a_j}^{b_j} \frac{\phi_j(t_j)}{t_j - x_j} dt_j = \frac{1}{2} [F_j^+(x_j) + F_j^-(x_j)] ; a_j < x_j < b_j, j=1, 2. \quad (3.7)$$

which, by using equation (3.5), may be expressed as

$$\frac{1}{\pi} \int_{a_j}^{b_j} \frac{\phi_j(t_j)}{t_j - x_j} dt_j = \frac{g_j(a_j) \cot \pi \alpha_j}{(b_j - a_j)^{\beta_j} (x_j - a_j)^{\alpha_j}} - \frac{g_j(b_j) \cot \pi \beta_j}{(b_j - a_j)^{\alpha_j} (b_j - x_j)^{\beta_j}} + F_{0j}(x_j) ; j=1,2. \quad (3.8)$$

Substituting equation (3.8) into equation (3.1) we can find

$$\frac{g_j(a_j) \cot \pi \alpha_j}{(b_j - a_j)^{\beta_j} (x_j - a_j)^{\alpha_j}} - \frac{g_j(b_j) \cot \pi \beta_j}{(b_j - a_j)^{\alpha_j} (b_j - x_j)^{\beta_j}} = \psi_j(x_j) ; j=1,2. \quad (3.9)$$

where $\psi_j(x_j), (j=1,2)$ contain all the bounded functions.

By multiplying equation (3.9) first by $(x_j - a_j)^{\alpha_j}$, and letting $x_j \rightarrow a_j$, and then by $(b_j - x_j)^{\beta_j}$; and letting $x_j \rightarrow b_j, (j=1,2)$, we obtain the following characteristic equations for $\alpha_j, \beta_j, (j=1,2)$

$$\frac{g_j(a_j) \cot \pi \alpha_j}{(b_j - a_j)^{\beta_j}} = 0 ; j=1,2, \quad (a) \quad (3.10)$$

$$\frac{g_j(b_j) \cot \pi \beta_j}{(b_j - a_j)^{\alpha_j}} = 0 ; j=1,2, \quad (b) \quad (3.11)$$

Or

$$\cot \pi \alpha_j = 0 ; j=1,2, \quad (a) \quad (3.11)$$

$$\cot \pi \beta_j = 0 ; j=1,2. \quad (b)$$

The acceptable roots of this equation are $\alpha_j = \frac{1}{2}, \beta_j = \frac{1}{2}, (j=1,2)$, which are the known results in the crack problems. Hence, the fundamental functions of the singular integral equations are

$$w_j(x_j) = \frac{1}{(x_j - a_j)^{1/2} (b_j - x_j)^{1/2}}, \quad j=1, 2. \quad (3.12)$$

Therefore as long as we have internal cracks, the power of singularity will be $\frac{1}{2}$.

3.2 Edge crack

3.2.1 Edge crack for Model I

This case is shown in Figure 3-2, in which $a_1 = 0$, $b_1 < h$. If a_1 goes to

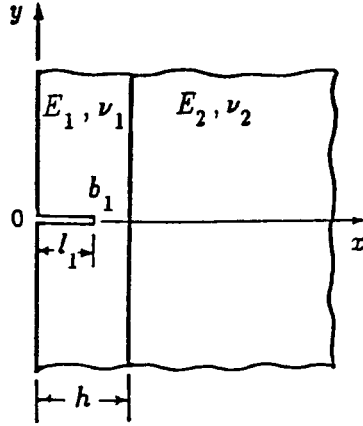


Figure 3-2: Geometry of edge crack (Model I)

zero, the singular terms in the singular integral equation (2.62) are the dominant term $\frac{1}{t_1 - x_1}$ and some terms in the kernel $k_{11}(x_1, t_1)$. Let

$$k_{11}(x_1, t_1) = k_{11e}^s(x_1, t_1) + k_{11}^b(x_1, t_1). \quad (3.13)$$

where k_{11e}^s is the singular term in edge crack case, and k_{11}^b is the bounded term. The singular part k_{11e}^s of the kernel is given by

$$k_{11e}^s(x_1, t_1) = \int_0^\infty G_{11e}^\infty(x_1, t_1, \alpha) d\alpha . \quad (3.14)$$

where G_{11e}^∞ is the asymptotic value of G_{11} for $\alpha \rightarrow \infty$, $t_1 \rightarrow 0$, $x_1 \rightarrow 0$. Then, from (2.65) and Appendix (C) it follows that

$$k_{11e}^s(x_1, t_1) = \int_0^\infty \left[\frac{1}{2} + \frac{\kappa_1}{2}(-1 + 2t_1\alpha) - \left(\frac{\kappa_1 + 3}{2} - \alpha x_1 \right)(-1 + 2t_1\alpha) \right] e^{-(t_1 + x_1)\alpha} d\alpha . \quad (3.15)$$

or

$$k_{11e}^s = -\frac{1}{t_1 + x_1} + \frac{6x_1}{(t_1 + x_1)^2} - \frac{4x_1^2}{(t_1 + x_1)^3} . \quad (3.16)$$

Equation (3.16) can also be written as

$$k_{11e}^s = \left[-2x_1^2 \frac{d^2}{dx_1^2} - 6x_1 \frac{d}{dx_1} - 1 \right] \frac{1}{(t_1 + x_1)} . \quad (3.17)$$

Then, singular integral equation (2.62) becomes

$$\begin{aligned} \int_{a_1}^{b_1} \left[\frac{1}{t_1 - x_1} + k_{11e}^s(x_1, t_1) \right] \phi_1(t_1) dt_1 + \text{bounded terms} \\ = -\frac{\pi(\kappa + 1)}{4\mu_1} \sigma_1 T(x_1) , \quad a_1 < x_1 < b_1 . \end{aligned} \quad (3.18)$$

Again, assume that

$$\phi_1(t_1) = \frac{g_1(t_1)}{(t_1)^{\alpha_1} (b_1 - t_1)^{\beta_1}} = g_1(t_1) w_1(t_1) . \quad (3.19)$$

where $g_1(t_1)$, $w_1(t_1)$ have the same properties as before.

Define sectionally holomorphic function

$$F_1(z) = \frac{1}{\pi} \int_0^{b_1} \frac{\phi_1(t_1)}{t_1 - z} dt_1. \quad (3.20)$$

Substituting equation (3.19) into equation (3.20) and following [37], we will have

$$F_1(z) = \frac{g_1(0) e^{\pi i \alpha_1}}{(b_1)^{\beta_1} (z)^{\alpha_1} \sin \pi \alpha_1} - \frac{g_1(b_1)}{(b_1)^{\alpha_1} (z - b_1)^{\beta_1} \sin \pi \beta_1} + F_{01}(z). \quad (3.21)$$

Then, as before by following [37], equation (3.21) becomes

$$F_1(x_1) = \frac{g_1(0) \cot \pi \alpha_1}{(b_1)^{\beta_1} (x_1)^{\alpha_1}} - \frac{g_1(b_1) \cot \pi \beta_1}{(b_1)^{\alpha_1} (b_1 - x_1)^{\beta_1}} + F_{01}(x_1). \quad (3.22)$$

and

$$F_1(-x_1) = \frac{g_1(0)}{(b_1)^{\beta_1} (x_1)^{\alpha_1} \sin \pi \alpha_1} + F_{01}^*(x_1). \quad (3.23)$$

where $F_{01}(x_1)$, $F_{01}^*(x_1)$ are similar to the $F_{0j}(x_j)$ in equation (3.8). Substituting equation (3.22) and equation (3.23) into equation (3.18), we obtain

$$\begin{aligned} & \frac{g_1(0) \cot \pi \alpha_1}{(b_1)^{\beta_1} (x_1)^{\alpha_1}} - \frac{g_1(b_1) \cot \pi \beta_1}{(b_1)^{\alpha_1} (b_1 - x_1)^{\beta_1}} \\ & + \left[-2x_1^2 \frac{d^2}{dx_1^2} - 6x_1 \frac{d}{dx_1} - 1 \right] \frac{g_1(0)}{(b_1)^{\beta_1} (x_1)^{\alpha_1} \sin \pi \alpha_1} = \psi_1(x_1). \end{aligned} \quad (3.24)$$

where $\psi_1(x_1)$ contains all the bounded functions. Equation (3.24) can be written as

$$\begin{aligned} & \frac{g_1(0) \cot \pi \alpha_1}{(b_1)^{\beta_1} (x_1)^{\alpha_1}} - \frac{g_1(b_1) \cot \pi \beta_1}{(b_1)^{\alpha_1} (b_1 - x_1)^{\beta_1}} \\ & + \frac{g_1(0)}{(b_1)^{\beta_1} (x_1)^{\alpha_1} \sin \pi \alpha_1} [-2\alpha_1(\alpha_1 + 1) + 6\alpha_1 - 1] = \psi_1(x_1). \end{aligned} \quad (3.25)$$

Multiply equation (3.25) by $(b_1 - x_1)^{\beta_1}$, and letting $x_1 \rightarrow b_1$, the characteristic equation for β_1 is found to be

$$\cot \pi \beta_1 = 0 \quad \rightarrow \quad \beta_1 = \frac{1}{2}. \quad (3.26)$$

Similarly, multiplying equation (3.25) by $(x_1)^{\alpha_1}$, and letting $x_1 \rightarrow 0$, the characteristic equation for α_1 is obtained as

$$\frac{g_1(0) \cot \pi \alpha_1}{(b_1)^{\beta_1}} + \frac{g_1(0)}{(b_1)^{\beta_1} \sin \pi \alpha_1} [-2\alpha_1(\alpha_1 + 1) + 6\alpha_1 - 1] = 0. \quad (3.27)$$

which can be written as

$$\cos \pi \alpha_1 - 2(\alpha_1 - 1)^2 + 1 = 0. \quad (3.28)$$

Since $\alpha_1 = 1$ is unacceptable, the only possible root of equation (3.28) is $\alpha_1 = 0$, giving the fundamental function as

$$w_1(x_1) = \frac{1}{(b_1 - x_1)^{1/2}}. \quad (3.29)$$

3.2.2 Edge crack for Model II

This case is shown in Figure 3-3, in which $a_2 > h_1$, $b_2 = h_1 + h_2$.

If b_2 goes to $h_1 + h_2$, the singular terms in the singular integral equation (2.63) are the dominant term $\frac{1}{t_2 - x_2}$ and some terms coming from the kernel $k_{22}(x_2, t_2)$. Let

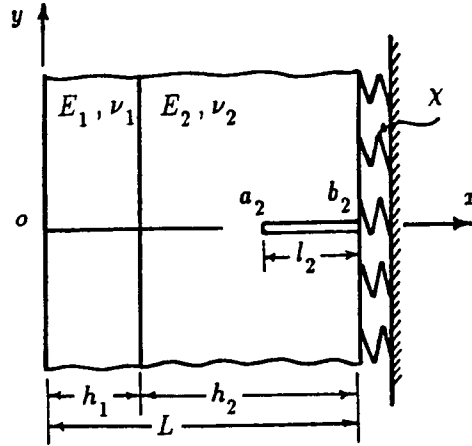


Figure 3-3: Geometry of edge crack (Model II)

$$k_{22}(x_2, t_2) = k_{22e}^s(x_2, t_2) + k_{22}^b(x_2, t_2) . \quad (3.30)$$

where $k_{22e}^s(x_2, t_2)$ is the singular term, $k_{22}^b(x_2, t_2)$ is bounded and

$$k_{22e}^s = \int_0^\infty G_{22e}^\infty(x_2, t_2, \alpha) d\alpha . \quad (3.31)$$

G_{22e}^∞ is the asymptotic value of G_{22} for $\alpha \rightarrow \infty, t_2 \rightarrow h_1 + h_2, x_2 \rightarrow h_1 + h_2$. From (2.121) and (3.31) it may be shown that

$$k_{22e}^s(x_2, t_2) = \int_0^\infty -\left[\frac{1}{2} + \{1 + 2(t_2 - L)\alpha\} \left\{\frac{3}{2} + (x_2 - L)\alpha\right\}\right] * e^{-(t_2 - x_2 + 2L)\alpha} d\alpha . \quad (3.32)$$

where $L = h_1 + h_2$. Evaluating the integrals equation (3.32) becomes

$$k_{22e}^s(x_2, t_2) = \frac{1}{(2L - x_2 - t_2)} - \frac{6(L - x_2)}{(2L - x_2 - t_2)^2} + \frac{4(L - x_2)^2}{(2L - x_2 - t_2)^3} . \quad (3.33)$$

which is similar to the equation (3.16). Thus, by doing the same analysis as in

section [3.2.1], we obtain the same singularities, i.e., $\alpha_2 = \frac{1}{2}, \beta_2 = 0$. The fundamental function would then be

$$w_2(x_2) = \frac{1}{(x_2 - a_2)^{1/2}}. \quad (3.34)$$

3.3 Crack tip terminating at the interface from material (1)

This case is shown in Figure 3-4, in which $a_1 > 0, b_1 = h$.

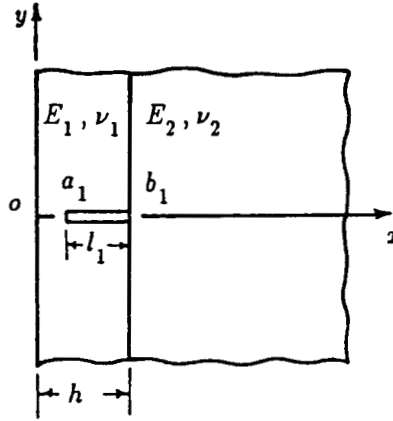


Figure 3-4: Geometry of the crack terminating at the interface from material (1)

If b_1 goes to h , the only singular terms in the singular integral equation (2.62) are the dominant term $\frac{1}{t_1 - x_1}$ and some terms coming from the kernel $k_{11}(x_1, t_1)$. Let

$$k_{11}(x_1, t_1) = k_{11i}^s(x_1, t_1) + k_{11}^b(x_1, t_1). \quad (3.35)$$

where $k_{11i}^s(x_1, t_1)$ is the singular term in the case of a crack terminating at the interface, and $k_{11}^b(x_1, t_1)$ is the bounded term. The singular term is found from

$$k_{11i}^s(x_1, t_1) = \int_0^\infty G_{11i}^\infty(x_1, t_1, \alpha) d\alpha. \quad (3.36)$$

where G_{11i}^{∞} is the asymptotic value of G_{11} for $\alpha \rightarrow \infty$, $t_1 \rightarrow h$, $x_1 \rightarrow h$. Thus, from (3.36) and (2.65) it may be shown that

$$k_{11i}^s(x_1, t_1) = \int_0^{\infty} \left[\frac{m-1}{m+\kappa_1} \{1+2(t_1-h)\alpha\} \left\{ -\frac{3}{2} - (x_1-h)\alpha \right\} - \frac{1}{2} \frac{m\kappa_2 - \kappa_1}{m\kappa_2 + 1} \right] e^{(t_1+x_1-2h)\alpha} d\alpha, \quad (3.37)$$

or

$$k_{11i}^s(x_1, t_1) = \frac{C_{11}}{(2h-x_1-t_1)} + \frac{C_{12}(h-x_1)}{(2h-x_1-t_1)^2} + \frac{C_{13}(h-x_1)^2}{(2h-x_1-t_1)^3}. \quad (3.38)$$

where

$$C_{11} = \frac{3}{2} \frac{m-1}{m+\kappa_1} - \frac{1}{2} \frac{m\kappa_2 - \kappa_1}{m\kappa_2 + 1}, \quad (a)$$

$$C_{12} = -6 \frac{m-1}{m+\kappa_1}, \quad (b)$$

$$C_{13} = 4 \frac{m-1}{m+\kappa_1}, \quad (c) \quad (3.39)$$

$$m = \frac{\mu_1}{\mu_2}. \quad (d)$$

Equation (3.38) can also be written in the form

$$k_{11i}^s(x_1, t_1) = \left[-\frac{1}{2} C_{13} (h-x_1)^2 \frac{d^2}{dx_1^2} - C_{12} (h-x_1) \frac{d}{dx_1} - C_{11} \right] * \left[\frac{1}{t_1 - (2h-x_1)} \right]. \quad (3.40)$$

Therefore, the singular integral equation (2.62) can be written as

$$\int_{a_1}^{b_1} \left[\frac{1}{t_1 - x_1} + k_{11i}^s(x_1, t_1) \right] \phi_1(t_1) dt_1 + \text{bounded terms} \\ = -\frac{\pi(\kappa_1 + 1)}{4\mu_1} \sigma_1^T(x_1) . \quad (3.41)$$

We again define

$$\phi_1(t_1) = \frac{g_1(t_1)}{(t_1 - a_1)^{\alpha_1} (h - t_1)^{\beta_1}} = g_1(t_1) w_1(t_1) . \quad (3.42)$$

Also, define the sectionally holomorphic function

$$F_1(z) = \frac{1}{\pi} \int_{a_1}^h \frac{\phi_1(t_1)}{t_1 - z} dt_1 . \quad (3.43)$$

Using equation (3.42) into equation (3.43) and following [37] we have

$$F_1(z) = \frac{g(a_1) e^{\pi i \alpha_1}}{(h - a_1)^{\beta_1} (z - a_1)^{\alpha_1} \sin \pi \alpha_1} - \frac{g_1(h)}{(h - a_1)^{\alpha_1} (z - h)^{\beta_1} \sin \pi \beta_1} \\ + F_{01}(z) . \quad (3.44)$$

From (3.44) it can be shown that for $a_1 < x_1 < h$

$$F_1(x_1) = \frac{g_1(a_1) \cot \pi \alpha_1}{(h - a_1)^{\beta_1} (x_1 - a_1)^{\alpha_1}} - \frac{g_1(h) \cot \pi \beta_1}{(h - a_1)^{\alpha_1} (h - x_1)^{\beta_1}} + F_{01}(x_1) . \quad (3.45)$$

$$F_1(2h - x_1) = -\frac{g_1(h)}{(h - a_1)^{\alpha_1} (h - x_1)^{\beta_1} \sin \pi \beta_1} + F_{01}^*(x_1) . \quad (3.46)$$

where $F_{01}(x_1)$, $F_{01}^*(x_1)$ are similar to $F_{0j}(x_j)$ in equation (3.8). Substituting from (3.45) and (3.46) into (3.41) we obtain

$$\begin{aligned}
& \frac{g_1(a_1) \cot \pi \alpha_1}{(h-a_1)^{\beta_1} (x_1-a_1)^{\alpha_1}} - \frac{g_1(h) \cot \pi \beta_1}{(h-a_1)^{\alpha_1} (h-x_1)^{\beta_1}} \\
& + \left[-\frac{1}{2} C_{13} (h-x_1)^2 \frac{d^2}{dx_1^2} - C_{12} (h-x_1) \frac{d}{dx_1} - C_{11} \right] * \\
& \left[\frac{-g_1(h)}{(h-a_1)^{\alpha_1} (h-x_1)^{\beta_1} \sin \pi \beta_1} \right] = \psi_1(x_1). \tag{3.47}
\end{aligned}$$

where $\psi_1(x_1)$ contains all the bounded terms. From (3.47) we have

$$\begin{aligned}
& \frac{g_1(a_1) \cot \pi \alpha_1}{(h-a_1)^{\beta_1} (x_1-a_1)^{\alpha_1}} - \frac{g_1(h) \cot \pi \beta_1}{(h-a_1)^{\alpha_1} (h-x_1)^{\beta_1}} \\
& - \frac{g_1(h)}{(h-a_1)^{\alpha_1} (h-x_1)^{\beta_1} \sin \pi \beta_1} * \\
& \left[-\frac{1}{2} C_{13} \beta_1 (\beta_1 + 1) - C_{12} \beta_1 - C_{11} \right] = \psi_1(x_1). \tag{3.48}
\end{aligned}$$

By multiplying equation (3.48) by $(x_1-a_1)^{\alpha_1}$ and letting $x_1 \rightarrow a_1$, the characteristic equation for α_1 is found to be

$$\cot \pi \alpha_1 = 0 \quad \rightarrow \quad \alpha_1 = \frac{1}{2}. \tag{3.49}$$

Also, by multiplying equation (3.48) by $(h-x_1)^{\beta_1}$ and letting $x_1 \rightarrow h$, the characteristic equation for β_1 becomes

$$\begin{aligned}
& -\frac{g_1(h) \cot \pi \beta_1}{(h-a_1)^{\alpha_1}} - \frac{g_1(h)}{(h-a_1)^{\alpha_1} \sin \pi \beta_1} * \\
& \left[-\frac{1}{2} C_{13} \beta_1 (\beta_1 + 1) - C_{12} \beta_1 - C_{11} \right] = 0. \tag{3.50}
\end{aligned}$$

which can be written as

$$\cos \pi \beta_1 - \frac{1}{2} C_{13} \beta_1 (\beta_1 + 1) - C_{12} \beta_1 - C_{11} = 0. \quad (3.51)$$

Equation (3.51) has a real root in the interval $(0, 1)$. The root is dependent on the material constants. If material 2 is stiffer than material 1, the root will be less than $\frac{1}{2}$. But if material 1 is stiffer than material 2, then the root will be larger than $\frac{1}{2}$. The fundamental function of this case is

$$w_1(x_1) = \frac{1}{(x_1 - a_1)^{1/2} (h - x_1)^{\beta_1}}. \quad (3.52)$$

3.4 Crack tip terminating at the interface from material (2)

This case is shown in Figure 3-5, in which $a_2 = h$, $b_2 > h$.

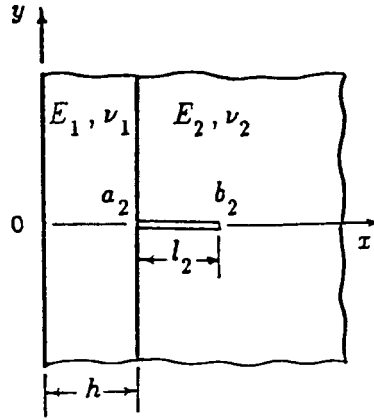


Figure 3-5: Geometry of the crack terminating at the interface from material (2)

If a_2 goes to h , the singular terms in the singular integral equation (2.63) are the dominant term $\frac{1}{t_2 - x_2}$ and some terms coming from the kernel $k_{22}(x_2, t_2)$.

Let

$$k_{22}(x_2, t_2) = k_{22i}^s(x_2, t_2) + k_{22}^b(x_2, t_2) . \quad (3.53)$$

where $k_{22i}^s(x_2, t_2)$ is the singular term for this case, and $k_{22}^b(x_2, t_2)$ is bounded.

$$k_{22i}^s(x_2, t_2) = \int_0^\infty G_{22i}^\infty(x_2, t_2, \alpha) d\alpha . \quad (3.54)$$

where G_{22i}^∞ is the asymptotic value of G_{22} for $\alpha \rightarrow \infty$, $t_2 \rightarrow h$, and $x_2 \rightarrow h$. From (2.65) and (3.54) it may then show that

$$k_{22i}^s(x_2, t_2) = \int_0^\infty \left[-\frac{1}{2} \frac{m\kappa_2 - \kappa_1}{m + \kappa_1} \frac{m-1}{m\kappa_2 + 1} \{-1 + 2(t_2 - h)\alpha\} \right. \\ \left. \left\{ -\frac{3}{2} + (x_2 - h)\alpha \right\} \right] e^{-(t_2 + x_2 - 2h)\alpha} d\alpha . \quad (3.55)$$

giving

$$k_{22i}^s(x_2, t_2) = \frac{C_{21}}{(t_2 + x_2 - 2h)} + \frac{C_{22}(x_2 - h)}{(t_2 + x_2 - 2h)^2} + \frac{C_{23}(x_2 - h)^2}{(t_2 + x_2 - 2h)^3} . \quad (3.56)$$

where

$$C_{21} = -\frac{1}{2} \frac{m\kappa_2 - \kappa_1}{m + \kappa_1} + \frac{3}{2} \frac{m-1}{m\kappa_2 + 1} , \quad (a)$$

$$C_{22} = -6 \frac{m-1}{m\kappa_2 + 1} , \quad (b)$$

$$C_{23} = 4 \frac{m-1}{m\kappa_2 + 1} , \quad (c) \quad (3.57)$$

$$m = \frac{\mu_1}{\mu_2} . \quad (d)$$

The kernel given by equation (3.56) is quite similar to the corresponding kernel given by equation (3.38). Thus, following the procedure leading to (3.49) and

(3.51) we obtain

$$k_{22i}^s(x_2, t_2) = \left[\frac{1}{2} C_{23}(x_2 - h)^2 \frac{d^2}{dx_2^2} - C_{22}(x_2 - h) \frac{d}{dx_2} + C_{21} \right] \left[\frac{1}{t_2 - (2h - x_2)} \right]. \quad (3.58)$$

$$\int_h^{b_2} \left[\frac{1}{t_2 - x_2} + k_{22i}^s(x_2, t_2) \right] \phi_2(t_2) dt_2 + \text{bounded terms} = -\frac{\pi(\kappa_2 + 1)}{4\mu_2} \sigma_2^T(x_2). \quad (3.59)$$

$$\frac{1}{\pi} \int_h^{b_2} \frac{\phi_2(t_2)}{t_2 - x_2} dt_2 = \frac{g_2(h) \cot \pi \alpha_2}{(b_2 - h)^{\beta_2} (x_2 - h)^{\alpha_2}} - \frac{g_2(b_2) \cot \pi \beta_2}{(b_2 - h)^{\alpha_2} (b_2 - x_2)^{\beta_2}} + F_{02}(x_2). \quad (3.60)$$

$$\frac{1}{\pi} \int_h^{b_2} \frac{\phi_2(t_2)}{t_2 - (2h - x_2)} dt_2 = \frac{g_2(h)}{(b_2 - h)^{\beta_2} (x_2 - h)^{\alpha_2} \sin \pi \alpha_2} + F_{02}^*(x_2). \quad (3.61)$$

$$\begin{aligned} & \frac{g_2(h) \cot \pi \alpha_2}{(b_2 - h)^{\beta_2} (x_2 - h)^{\alpha_2}} - \frac{g_2(b_2) \cot \pi \beta_2}{(b_2 - h)^{\alpha_2} (b_2 - x_2)^{\beta_2}} \\ & + \left[\frac{1}{2} C_{23}(x_2 - h)^2 \frac{d^2}{dx_2^2} - C_{22}(x_2 - h) \frac{d}{dx_2} + C_{21} \right] \\ & \frac{g_2(h)}{(b_2 - h)^{\beta_2} (x_2 - h)^{\alpha_2} \sin \pi \alpha_2} = \psi_2(x_2). \end{aligned} \quad (3.62)$$

$$\begin{aligned} & \frac{g_2(h) \cot \pi \alpha_2}{(b_2 - h)^{\beta_2} (x_2 - h)^{\alpha_2}} - \frac{g_2(b_2) \cot \pi \beta_2}{(b_2 - h)^{\alpha_2} (b_2 - x_2)^{\beta_2}} \\ & + \frac{g_2(h)}{(b_2 - h)^{\beta_2} (x_2 - h)^{\alpha_2} \sin \pi \alpha_2} \left[\frac{1}{2} C_{23} \alpha_2 (\alpha_2 + 1) + C_{22} \alpha_2 + C_{21} \right] = \psi_2(x_2). \end{aligned} \quad (3.63)$$

$$\cot \pi \beta_2 = 0 \quad \rightarrow \quad \beta_2 = \frac{1}{2} . \quad (3.64)$$

and

$$\cos \pi \alpha_2 + \frac{1}{2} C_{23} \alpha_2 (\alpha_2 + 1) + C_{22} \alpha_2 + C_{21} = 0 . \quad (3.65)$$

Equation (3.65) is identical to equation (3.51) if the material constants are changed. So, we have the same argument as before. If material 1 is stiffer than material 2, α_2 is less than $\frac{1}{2}$ and if material 2 is stiffer than material 1, α_2 is larger than $\frac{1}{2}$. The fundamental function in this case is

$$w_2(x_2) = \frac{1}{(x_2 - h)^{\alpha_2} (b_2 - x_2)^{1/2}} . \quad (3.66)$$

3.5 Crack going through the interface

This case is shown in Figure 3-6 in which $a_1 > 0$, $b_1 = h$ and $a_2 = h$, $b_2 > h$.

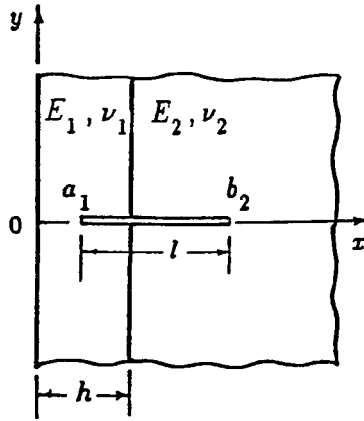


Figure 3-6: Geometry of crack going through the interface

In this case, the two singular integral equations (2.62) and (2.63) must be examined. If b_1 and a_2 go to the interface, we will have three irregular points $x = a_1$, h and b_2 .

The singular terms in the singular integral equation (2.62) are the dominant term $\frac{1}{t_1 - x_1}$ and some other terms coming from the kernels $k_{11}(x_1, t_1)$ and $k_{12}(x_1, t_2)$. Similarly, the singular terms in the singular integral equation (2.63) are the dominant term $\frac{1}{t_2 - x_2}$ and some other terms coming from the kernels $k_{21}(x_2, t_1)$ and $k_{22}(x_2, t_2)$. The singular terms in the kernels $k_{11}(x_1, t_1)$ and $k_{22}(x_2, t_2)$ are still the same as equations (3.40) and (3.58). By examining the singular terms in the kernels $k_{12}(x_1, t_2)$ and $k_{21}(x_2, t_1)$, let us define

$$k_{12}(x_1, t_2) = k_{12}^s(x_1, t_2) + k_{12}^b(x_1, t_2) , \quad (a) \quad (3.67)$$

$$k_{21}(x_2, t_1) = k_{21}^s(x_2, t_1) + k_{21}^b(x_2, t_1) . \quad (b)$$

where $k_{12}^s(x_1, t_2)$, $k_{21}^s(x_2, t_1)$ are the singular terms, and $k_{12}^b(x_1, t_2)$, $k_{21}^b(x_2, t_1)$ are the bounded terms. Since

$$k_{12}^s(x_1, t_2) = \int_0^\infty G_{12}^\infty(x_1, t_2, \alpha) d\alpha , \quad (a) \quad (3.68)$$

$$k_{21}^s(x_2, t_1) = \int_0^\infty G_{21}^\infty(x_2, t_1, \alpha) d\alpha . \quad (b)$$

where G_{12}^∞ , G_{21}^∞ are the asymptotic value of G_{12} , G_{21} for $\alpha \rightarrow \infty$, $t_2 \rightarrow h$, $x_1 \rightarrow h$ and $\alpha \rightarrow \infty$, $t_1 \rightarrow h$, $x_2 \rightarrow h$, respectively. From (3.68), (2.65) and Appendix (C) we then obtain

$$\begin{aligned}
k_{12}^s &= \int_0^\infty \left[\frac{\kappa_1+1}{m+\kappa_1} \left\{ \frac{3}{2} + (x_1-h)\alpha \right\} - \frac{1}{2} \frac{\kappa_1+1}{m\kappa_2+1} \{-1+2(t_2-h)\alpha\} \right] \\
&\quad e^{-(t_2-x_1)\alpha} d\alpha, \quad (a) \\
&\quad (3.69) \\
k_{21}^s &= \int_0^\infty \left[\frac{m(\kappa_2+1)}{m\kappa_2+1} \left\{ -\frac{3}{2} + (x_2-h)\alpha \right\} - \frac{1}{2} \frac{m(\kappa_2+1)}{m+\kappa_1} \{1+2(t_1-h)\alpha\} \right] \\
&\quad e^{-(x_2-t_1)\alpha} d\alpha. \quad (b)
\end{aligned}$$

or, evaluating the integrals we find

$$\begin{aligned}
k_{12}^s(x_1, t_2) &= \frac{d_{11}}{(t_2-x_1)} + \frac{d_{12}(x_1-h)}{(t_2-x_1)^2}, \quad (a) \\
&\quad (3.70) \\
k_{21}^s(x_2, t_1) &= \frac{d_{21}}{(x_2-t_1)} + \frac{d_{22}(x_2-h)}{(x_2-t_1)^2}. \quad (b)
\end{aligned}$$

where

$$\begin{aligned}
d_{11} &= \frac{3}{2} \frac{\kappa_1+1}{m+\kappa_1} - \frac{1}{2} \frac{\kappa_1+1}{m\kappa_2+1}, \quad (a) \\
d_{12} &= \frac{\kappa_1+1}{m+\kappa_1} - \frac{\kappa_1+1}{m\kappa_2+1}, \quad (b) \\
&\quad (3.71) \\
d_{21} &= -\frac{3}{2} \frac{m(\kappa_2+1)}{m\kappa_2+1} + \frac{1}{2} \frac{m(\kappa_2+1)}{m+\kappa_1}, \quad (c) \\
d_{22} &= \frac{m(\kappa_2+1)}{m\kappa_2+1} - \frac{m(\kappa_2+1)}{m+\kappa_1}, \quad (d) \\
m &= \frac{\mu_1}{\mu_2}. \quad (e)
\end{aligned}$$

Equations (3.70) can also be written as

$$k_{12}^s(x_1, t_2) = \left\{ d_{12}(x_1 - h) \frac{d}{dx_1} + d_{11} \right\} \frac{1}{t_2 - x_1}, \quad (a)$$

(3.72)

$$k_{21}^s(x_2, t_1) = \left\{ d_{22}(x_2 - h) \frac{d}{dx_2} - d_{21} \right\} \frac{1}{t_1 - x_2}. \quad (b)$$

The two singular integral equations (2.62) and (2.63) then become

$$\begin{aligned} \int_{a_1}^h \left\{ \frac{1}{t_1 - x_1} + k_{11i}^s(x_1, t_1) \right\} \phi_1(t_1) dt_1 + \int_h^{b_2} k_{12}^s(x_1, t_2) \phi_2(t_2) dt_2 \\ + \text{bounded terms} = - \frac{\pi(\kappa_1 + 1)}{4\mu_1} \sigma_1^T(x_1), \end{aligned} \quad (a)$$

(3.73)

$$\begin{aligned} \int_{a_1}^h k_{21}^s(x_2, t_1) \phi_1(t_1) dt_1 + \int_h^{b_2} \left\{ \frac{1}{t_2 - x_2} + k_{22i}^s(x_2, t_2) \right\} \phi_2(t_2) dt_2 \\ + \text{bounded terms} = - \frac{\pi(\kappa_2 + 1)}{4\mu_2} \sigma_2^T(x_2). \end{aligned} \quad (b)$$

Substituting equations (3.40), (3.58), and (3.72) into equations (3.73), and by using the same technique as before, we will end up with the same equations as (3.45), (3.46), (3.60) and (3.61). Also, from the two kernels $k_{12}^s(x_1, t_2)$ and $k_{21}^s(x_2, t_1)$, we obtain

$$\frac{1}{\pi} \int_h^{b_2} \frac{\phi_2(t_2)}{t_2 - x_1} dt_2 = \frac{g_2(h)}{(b_2 - h)^{\beta_2} (h - x_1)^{\alpha_2} \sin \pi \alpha_2} + F_{12}^*(x_1), \quad (a)$$

(3.74)

$$\frac{1}{\pi} \int_{a_1}^h \frac{\phi_1(t_1)}{t_1 - x_2} dt_1 = - \frac{g_1(h)}{(h - a_1)^{\alpha_1} (x_2 - h)^{\beta_1} \sin \pi \beta_1} + F_{21}^*(x_2). \quad (b)$$

where $F_{12}^*(x_1)$ and $F_{21}^*(x_2)$ are similar to $F_{0j}(x_j)$ in equation (3.8). Then the

singular integral equations (3.73) become

$$\begin{aligned}
& \frac{g_1(a_1) \cot \pi \alpha_1}{(h-a_1)^{\beta_1} (x_1-a_1)^{\alpha_1}} - \frac{g_1(h) \cot \pi \beta_1}{(h-a_1)^{\alpha_1} (h-x_1)^{\beta_1}} \\
& + \left[-\frac{1}{2} C_{13} (h-x_1)^2 \frac{d^2}{dx_1^2} - C_{12} (h-x_1) \frac{d}{dx_1} - C_{11} \right] \\
& \left[\frac{-g_1(h)}{(h-a_1)^{\alpha_1} (h-x_1)^{\beta_1} \sin \pi \beta_1} \right] \\
& + [d_{12}(x_1-h) \frac{d}{dx_1} + d_{11}] \left[\frac{g_2(h)}{(b_2-h)^{\beta_2} (h-x_1)^{\alpha_2} \sin \pi \alpha_2} \right] = \Psi_1(x_1) , \quad (a)
\end{aligned}$$

(3.75)

$$\begin{aligned}
& [d_{22}(x_2-h) \frac{d}{dx_2} - d_{21}] \left[\frac{-g_1(h)}{(h-a_1)^{\alpha_1} (x_2-h)^{\beta_1} \sin \pi \beta_1} \right] \\
& + \frac{g_2(h) \cot \pi \alpha_2}{(b_2-h)^{\beta_2} (x_2-h)^{\alpha_2}} - \frac{g_2(b_2) \cot \pi \beta_2}{(b_2-h)^{\alpha_2} (b_2-x_2)^{\beta_2}} \\
& + \left[\frac{1}{2} C_{23} (x_2-h)^2 \frac{d^2}{dx_2^2} - C_{22} (x_2-h) \frac{d}{dx_2} + C_{21} \right] \\
& \left[\frac{g_2(h)}{(b_2-h)^{\beta_2} (x_2-h)^{\alpha_2} \sin \pi \alpha_2} \right] = \Psi_2(x_2) . \quad (b)
\end{aligned}$$

where $\Psi_1(x_1)$, $\Psi_2(x_2)$ contain all the bounded functions. Then equations (3.75) can be written as

$$\begin{aligned}
& \frac{g_1(a_1) \cot \pi \alpha_1}{(h-a_1)^{\beta_1} (x_1-a_1)^{\alpha_1}} - \frac{g_1(h) \cot \pi \beta_1}{(h-a_1)^{\alpha_1} (h-x_1)^{\beta_1}} \\
& - \frac{g_1(h)}{(h-a_1)^{\alpha_1} (h-x_1)^{\beta_1} \sin \pi \beta_1} \left[-\frac{1}{2} C_{13} \beta_1 (\beta_1 + 1) - C_{12} \beta_1 - C_{11} \right] \\
& + \frac{g_2(h)}{(b_2-h)^{\beta_2} (h-x_1)^{\alpha_2} \sin \pi \alpha_2} [-d_{12} \alpha_2 + d_{11}] = \Psi_1(x_1) , \quad (a) \\
& \hspace{15em} (3.76) \\
& \frac{-g_1(h)}{(h-a_1)^{\alpha_1} (x_2-h)^{\beta_1} \sin \pi \beta_1} [-d_{22} \beta_1 - d_{21}] \\
& + \frac{g_2(h) \cot \pi \alpha_2}{(b_2-h)^{\beta_2} (x_2-h)^{\alpha_2}} - \frac{g_2(b_2) \cot \pi \beta_2}{(b_2-h)^{\alpha_2} (b_2-x_2)^{\beta_2}} \\
& + \frac{g_2(h)}{(b_2-h)^{\beta_2} (x_2-h)^{\alpha_2} \sin \pi \alpha_2} \left[\frac{1}{2} C_{23} \alpha_2 (\alpha_2 + 1) + C_{22} \alpha_2 + C_{21} \right] \\
& \hspace{15em} = \Psi_2(x_2) . \quad (b)
\end{aligned}$$

It is important to mention that, we just have one irregular point at the interface, therefore,

$$\beta_1 = \alpha_2 . \quad (3.77)$$

We now multiply equations (3.76)(a) and (3.76)(b) by $(x_1-a_1)^{\alpha_1}$ and $(b_2-x_2)^{\beta_2}$ respectively , and let $x_1 \rightarrow a_1$ and $x_2 \rightarrow b_2$. Then the characteristic equations for α_1 and β_2 are found to be

$$\cot \pi \alpha_1 = 0 \quad \rightarrow \quad \alpha_1 = \frac{1}{2} , \quad (a)$$

$$\cot \pi \beta_2 = 0 \quad \rightarrow \quad \beta_2 = \frac{1}{2} . \quad (b) \quad (3.78)$$

Also, multiply the same equations by $(h-x_1)^{\beta_1}$ and $(x_2-h)^{\beta_1}$ respectively, and let $x_1 \rightarrow h$ and $x_2 \rightarrow h$. Then we find

$$\begin{aligned} & \frac{g_1(h)}{(h-a_1)^{\alpha_1} \sin \pi \beta_1} \left[-\frac{1}{2} C_{13} \beta_1 (\beta_1 + 1) - C_{12} \beta_1 - C_{11} + \cos \pi \beta_1 \right] \\ & - \frac{g_2(h)}{(b_2-h)^{\beta_2} \sin \pi \beta_1} [-d_{12} \beta_1 + d_{11}] = 0, \quad (a) \end{aligned}$$

(3.79)

$$\begin{aligned} & \frac{g_1(h)}{(h-a_1)^{\alpha_1} \sin \pi \beta_1} [d_{22} \beta_1 + d_{21}] \\ & + \frac{g_2(h)}{(b_2-h)^{\beta_2} \sin \pi \beta_1} \left[\frac{1}{2} C_{23} \beta_1 (\beta_1 + 1) + C_{22} \beta_1 + C_{21} + \cos \pi \beta_1 \right] = 0. \quad (b) \end{aligned}$$

The solution of interest of (3.79) satisfies $0 < \operatorname{Re}(\beta_1) < 1$. Thus, since $g_1(h)$ and $g_2(h)$ are non-zero, the determinant of the coefficients in (3.79) must vanish, giving the characteristic equation for β_1 as follows

$$\begin{aligned} & \left[\cos \pi \beta_1 + \frac{1}{2} C_{23} \beta_1 (\beta_1 + 1) + C_{22} \beta_1 + C_{21} \right] \\ & \left[\cos \pi \beta_1 - \frac{1}{2} C_{13} \beta_1 (\beta_1 + 1) - C_{12} \beta_1 - C_{11} \right] \\ & + [d_{22} \beta_1 + d_{21}] [-d_{12} \beta_1 + d_{11}] = 0. \end{aligned} \quad (3.80)$$

It is clear from equation (3.79) that, $g_1(h)$ and $g_2(h)$ are not independent, and are related by

$$g_1(h) = -g_2(h) \frac{(h-a_1)^{\alpha_1}}{(b_2-h)^{\beta_2}} \frac{\cos \beta_1 + \frac{1}{2} C_{23} \beta_1 (\beta_1 + 1) + C_{22} \beta_1 + C_{21}}{d_{22} \beta_1 + d_{21}}. \quad (3.81)$$

Equation (3.81) will be necessary in order to obtain a unique solution for

the singular integral equations (2.62) , (2.63) . Equation (3.80) has always a real root in the interval $(0,1)$. The fundamental functions of the singular integral equations (2.62) , (2.63) are

$$w_1(x_1) = \frac{1}{(x_1 - a_1)^{1/2} (h - x_1)^{\beta_1}} , \quad (a)$$

$$w_2(x_2) = \frac{1}{(x_2 - h)^{\beta_1} (b_2 - x_2)^{1/2}} . \quad (b)$$

(3.82)

Chapter 4

Numerical Procedure

The solution of the problem depends on the two unknown density functions ϕ_1 , ϕ_2 which can be obtained by solving the two singular integral equations (2.62) , (2.63) numerically by using any one of the techniques available in [40] or [38 , 39]. In this work the expansion method described in [38 , 39] is used. In order to solve them let us rewrite these two equations (2.62) and (2.63) in the following form

$$\int_{a_1}^{b_1} \left[\frac{1}{t_1 - x_1} + k_{11}(x_1, t_1) \right] \phi_1(t_1) dt_1 + \int_{a_2}^{b_2} k_{12}(x_1, t_2) \phi_2(t_2) dt_2$$

$$= p_1(x_1) \quad ; \quad a_1 < x_1 < b_1, \quad (a)$$

(4.1)

$$\int_{a_1}^{b_1} k_{21}(x_2, t_1) \phi_1(t_1) dt_1 + \int_{a_2}^{b_2} \left[\frac{1}{t_2 - x_2} + k_{22}(x_2, t_2) \right] \phi_2(t_2) dt_2$$

$$= p_2(x_2) \quad ; \quad a_2 < x_2 < b_2. \quad (b)$$

where

$$p_1(x_1) = -\frac{\pi(\kappa_1 + 1)}{4\mu_1} \sigma_1^T(x_1),$$

$$p_2(x_2) = -\frac{\pi(\kappa_2 + 1)}{4\mu_2} \sigma_2^T(x_2).$$

(4.2)

Normalizing the two singular integral equations (4.1) by using the following transformations

$$t_i = \frac{b_i - a_i}{2} r_i + \frac{b_i + a_i}{2}, \quad (a_i \leq t_i \leq b_i, -1 \leq r_i \leq 1) \quad (\text{a})$$

$$x_i = \frac{b_i - a_i}{2} s_i + \frac{b_i + a_i}{2}, \quad (a_i \leq x_i \leq b_i, -1 \leq s_i \leq 1) \quad (\text{b}) \quad (4.3)$$

the two singular integral equations (4.1) may be expressed as

$$\int_{-1}^{+1} \left[\frac{1}{r_1 - s_1} + K_{11}(s_1, r_1) \right] \psi_1(r_1) dr_1 + \int_{-1}^{+1} K_{12}(s_1, r_2) \psi_2(r_2) dr_2 = P_1(s_1) \quad ; -1 < s_1 < 1, \quad (\text{a})$$

(4.4)

$$\int_{-1}^{+1} K_{21}(s_2, r_1) \psi_1(r_1) dr_1 + \int_{-1}^{+1} \left[\frac{1}{r_2 - s_2} + K_{22}(s_2, r_2) \right] \psi_2(r_2) dr_2 = P_2(s_2) \quad ; -1 < s_2 < 1. \quad (\text{b})$$

where

$$K_{ij}(s_i, r_j) = \frac{b_j - a_j}{2} k_{ij}(x_i, t_j) \quad ; (i, j = 1, 2). \quad (4.5)$$

and $\psi_i(r_i)$, $P_i(s_i)$ are respectively the transformation of $\phi_i(t_i)$, $p_i(x_i)$ ($i = 1, 2$). Since

$$\phi_1(t_1) = \frac{g_1(t_1)}{(t_1 - a_1)^{\alpha_1} (b_1 - t_1)^{\beta_1}} = g_1(t_1) w_1(t_1), \quad (\text{a})$$

(4.6)

$$\phi_2(t_2) = \frac{g_2(t_2)}{(t_2 - a_2)^{\alpha_2} (b_2 - t_2)^{\beta_2}} = g_2(t_2) w_2(t_2). \quad (\text{b})$$

Then, $\psi_1(r_1)$, $\psi_2(r_2)$ will be equal to

$$\psi_1(r_1) = \frac{F_1(r_1)}{(1+r_1)^{\alpha_1}(1-r_1)^{\beta_1}}, \quad (\text{a})$$

$$(4.7)$$

$$\psi_2(r_2) = \frac{F_2(r_2)}{(1+r_2)^{\alpha_2}(1-r_2)^{\beta_2}}. \quad (\text{b})$$

where

$$F_1(r_1) = \left(\frac{2}{b_1-a_1}\right)^{\alpha_1+\beta_1} A_1(r_1), \quad (\text{a})$$

$$(4.8)$$

$$F_2(r_2) = \left(\frac{2}{b_2-a_2}\right)^{\alpha_2+\beta_2} A_2(r_2). \quad (\text{b})$$

and $A_1(r_1)$ and $A_2(r_2)$ are the transformation of $g_1(t_1)$ and $g_2(t_2)$ respectively.

Then, the two singular integral equations (4.4) may be written as

$$\int_{-1}^{+1} \frac{F_1(r_1)}{(1+r_1)^{\alpha_1}(1-r_1)^{\beta_1}} \left[\frac{1}{r_1-s_1} + K_{11}(s_1, r_1) \right] dr_1$$

$$+ \int_{-1}^{+1} \frac{F_2(r_2)}{(1+r_2)^{\alpha_2}(1-r_2)^{\beta_2}} K_{12}(s_1, r_2) dr_2 = P_1(s_1); -1 < s_1 < 1, \quad (\text{a})$$

$$\int_{-1}^{+1} \frac{F_1(r_1)}{(1+r_1)^{\alpha_1}(1-r_1)^{\beta_1}} K_{21}(s_2, r_1) dr_1 + \int_{-1}^{+1} \frac{F_2(r_2)}{(1+r_2)^{\alpha_2}(1-r_2)^{\beta_2}} \quad (\text{b})$$

$$\left[\frac{1}{r_2-s_2} + K_{22}(s_2, r_2) \right] dr_2 = P_2(s_2); -1 < s_2 < 1. \quad (\text{b})$$

We may define

$$F_1(r_1) = \frac{\kappa_1 + 1}{4\mu_1} \sigma_0^T F_1^*(r_1), \quad (a)$$

(4.10)

$$F_2(r_2) = \frac{\kappa_2 + 1}{4\mu_2} \sigma_0^T F_2^*(r_2). \quad (b)$$

where

$$\sigma_0^T = -\frac{\alpha_1 \cdot E_1 \Theta_0}{1 - \nu_1}. \quad (4.11)$$

Then, the two singular integral equations (4.9) can be put in the form

$$\begin{aligned} & \int_{-1}^{+1} \frac{F_1^*(r_1)}{(1+r_1)^{\alpha_1} (1-r_1)^{\beta_1}} \left[\frac{1}{r_1 - s_1} + K_{11}(s_1, r_1) \right] dr_1 \\ & + \frac{\mu_1}{\mu_2} \frac{\kappa_2 + 1}{\kappa_1 + 1} \int_{-1}^{+1} \frac{F_2^*(r_2)}{(1+r_2)^{\alpha_2} (1-r_2)^{\beta_2}} K_{12}(s_1, r_2) dr_2 \\ & = -\pi \frac{\sigma_1^T(s_1)}{\sigma_0^T} ; -1 < s_1 < 1, \end{aligned} \quad (a)$$

$$\frac{\mu_2}{\mu_1} \frac{\kappa_1 + 1}{\kappa_2 + 1} \int_{-1}^{+1} \frac{F_1^*(r_1)}{(1+r_1)^{\alpha_1} (1-r_1)^{\beta_1}} K_{21}(s_2, r_1) dr_1 \quad (4.12)$$

$$\begin{aligned} & + \int_{-1}^{+1} \frac{F_2^*(r_2)}{(1+r_2)^{\alpha_2} (1-r_2)^{\beta_2}} \left[\frac{1}{r_2 - s_2} + K_{22}(s_2, r_2) \right] dr_2 \\ & = -\pi \frac{\sigma_2^T(s_2)}{\sigma_0^T} ; -1 < s_2 < 1. \end{aligned} \quad (b)$$

Let us assume that the two functions $F_1^*(r_1)$ and $F_2^*(r_2)$ are in the form of simple

power series such as

$$F_1^*(r_1) = \sum_{n=0}^N a_n r_1^n, \quad (\text{a})$$

(4.13)

$$F_2^*(r_2) = \sum_{m=0}^M b_m r_2^m. \quad (\text{b})$$

where a_n, b_m are the coefficients of these series to be determined, the numbers of which are $(N+1)$ and $(M+1)$, respectively. Substituting equation (4.13) into equation (4.12) we obtain

$$\sum_{n=0}^N a_n E_{11}^n(s_1) + \sum_{m=0}^M b_m E_{12}^m(s_1) = P_1(s_1) ; -1 < s_1 < 1, \quad (\text{a})$$

(4.14)

$$\sum_{n=0}^N a_n E_{21}^n(s_2) + \sum_{m=0}^M b_m E_{22}^m(s_2) = P_2(s_2) ; -1 < s_2 < 1. \quad (\text{b})$$

where

$$E_{11}^n(s_1) = \int_{-1}^{+1} \frac{r_1^n}{(1+r_1)^{\alpha_1}(1-r_1)^{\beta_1}} \left[\frac{1}{r_1-s_1} + K_{11}(s_1, r_1) \right] dr_1, \quad (\text{a})$$

$$E_{12}^m(s_1) = \frac{\mu_1 \kappa_2 + 1}{\mu_2 \kappa_1 + 1} \int_{-1}^{+1} \frac{r_2^m}{(1+r_2)^{\alpha_2}(1-r_2)^{\beta_2}} K_{12}(s_1, r_2) dr_2, \quad (\text{b})$$

$$E_{21}^n(s_2) = \frac{\mu_2 \kappa_1 + 1}{\mu_1 \kappa_2 + 1} \int_{-1}^{+1} \frac{r_1^n}{(1+r_1)^{\alpha_1}(1-r_1)^{\beta_1}} K_{21}(s_2, r_1) dr_1, \quad (\text{c})$$

(4.15)

$$E_{22}^m(s_2) = \int_{-1}^{+1} \frac{r_2^m}{(1+r_2)^{\alpha_2}(1-r_2)^{\beta_2}} \left[\frac{1}{r_2-s_2} + K_{22}(s_2, r_2) \right] dr_2, \quad (\text{d})$$

$$P_1(s_1) = -\pi \frac{\sigma_1^T(s_1)}{\sigma_0^T}, \quad (e)$$

$$P_2(s_2) = -\pi \frac{\sigma_2^T(s_2)}{\sigma_0^T}. \quad (f)$$

It is obvious that equation (4.14)(a) has $(N+1)$ coefficients a_n , and equation (4.14)(b) has $(M+1)$ coefficients b_m . By choosing the number of the collocation points for s_1, s_2 between $(-1, +1)$, which depend on the number of the unknown coefficients a_n, b_m , we can obtain a system of linear equations that can be solved to give these coefficients. It is clear that, the number of the coefficients a_n, b_m depend on the convergence of the series in equations (4.13).

Although there is no restriction on the choice of the collocation points, it was shown by Kaya [41] that a symmetric distribution with respect to the origin considering more points concentrated near the ends seems to help. So, the roots of the Chebeychev Polynomial will be used as collocation points.

To obtain a unique solution for the singular integral equations (2.62), (2.63) additional conditions are needed depending on the crack configuration. Each configuration will be investigated separately in the following subsection.

4.1 Embedded Crack

Figure 3-1 presents this case in which $a_1 > 0$, $b_1 < h$, $a_2 > h$ and $b_2 < \infty$. Also, the singularity at the end points are

$$\alpha_1 = \beta_1 = \alpha_2 = \beta_2 = \frac{1}{2}. \quad (4.16)$$

The collocation points for s_1 and s_2 are selected as

$$s_{1k} = \cos \frac{\pi(2k-1)}{2N} ; k = 1, 2, \dots, N, \quad (a)$$

(4.17)

$$s_{2l} = \cos \frac{\pi(2l-1)}{2M} ; l = 1, 2, \dots, M. \quad (b)$$

where s_{1k}, s_{2l} are the roots of the Chebeychev Polynomial. By substituting equations (4.17) into equations (4.14) we obtain the following system of $(N+M)$ equations for $(N+M+2)$ coefficients a_n, b_m

$$\sum_{n=0}^N a_n E_{11}^n(s_{1k}) + \sum_{m=0}^M b_m E_{12}^m(s_{1k}) = P_1(s_{1k}) \quad ; -1 < s_{1k} < +1$$

$$; k = 1, 2, \dots, N, \quad (a)$$

(4.18)

$$\sum_{n=0}^N a_n E_{21}^n(s_{2l}) + \sum_{m=0}^M b_m E_{22}^m(s_{2l}) = P_2(s_{2l}) \quad ; -1 < s_{2l} < +1$$

$$; l = 1, 2, \dots, M. \quad (b)$$

where

$$E_{11}^n(s_{1k}) = \int_{-1}^{+1} \frac{r_1^n}{\sqrt{1-r_1^2}} \left[\frac{1}{r_1-s_{1k}} + K_{11}(s_{1k}, r_1) \right] dr_1, \quad (a)$$

$$E_{12}^m(s_{1k}) = \frac{\mu_1 \kappa_2 + 1}{\mu_2 \kappa_1 + 1} \int_{-1}^{+1} \frac{r_2^m}{\sqrt{1-r_2^2}} K_{12}(s_{1k}, r_2) dr_2, \quad (b)$$

$$E_{21}^n(s_{2l}) = \frac{\mu_2 \kappa_1 + 1}{\mu_1 \kappa_2 + 1} \int_{-1}^{+1} \frac{r_1^n}{\sqrt{1-r_1^2}} K_{21}(s_{2l}, r_1) dr_1, \quad (c)$$

(4.19)

$$E_{22}^m(s_{2l}) = \int_{-1}^{+1} \frac{r_2^m}{\sqrt{1-r_2^2}} \left[\frac{1}{r_2-s_{2l}} + K_{22}(s_{2l}, r_2) \right] dr_2, \quad (d)$$

$$P_1(s_{1k}) = -\pi \frac{\sigma_1^T(s_{1k})}{\sigma_0^T}, \quad (e)$$

$$P_2(s_{2l}) = -\pi \frac{\sigma_2^T(s_{2l})}{\sigma_0^T}. \quad (f)$$

Two extra equations are needed. From the definition of the density functions ϕ_1, ϕ_2 , we have the following single valuedness conditions providing the $(N+1)^{th}$, and $(M+1)^{th}$ equations :

$$\int_{a_1}^{b_1} \phi_1(t_1) dt_1 = 0, \quad (a)$$

(4.20)

$$\int_{a_2}^{b_2} \phi_2(t_2) dt_2 = 0. \quad (b)$$

which can be written, after changing the variables t_1 and t_2 , and using equations (4.13), in the following form

$$\sum_{n=0}^N a_n G^n = 0, \quad (a)$$

(4.21)

$$\sum_{m=0}^M b_m G^m = 0. \quad (b)$$

where

$$G^n = \int_{-1}^{+1} \frac{r_1^n}{\sqrt{1-r_1^2}} dr_1, \quad (a)$$

(4.22)

$$G^m = \int_{-1}^{+1} \frac{r_2^m}{\sqrt{1-r_2^2}} dr_2. \quad (b)$$

The integrations in equations (4.19) and (4.22) can be found in appendix (G).

4.2 Edge Crack

Figure 3-2 shows this case in which $a_1 = 0$ and $b_1 < h$. Also, the singularity at the end points are

$$\alpha_1 = 0 \quad , \quad \beta_1 = \frac{1}{2}. \quad (4.23)$$

Since, we have one edge crack, then the collocation points for s_1 are

$$s_{1k} = \cos \frac{\pi(2k-1)}{2(N+1)} \quad ; \quad k = 1, 2, \dots, (N+1). \quad (4.24)$$

In this case, the number of the collocation points are $(N+1)$ which should be equal to the number of the unknown coefficient a_n , because the single valuedness condition (4.20)(a) is no longer valid. Thus, by substituting equation (4.24) into equation (4.14)(a), considering one crack in material (1), we obtain the following $(N+1)$ equations for $(N+1)$ coefficients a_n , which are

$$\sum_{n=0}^N a_n E_{11}^n(s_{1k}) = P_1(s_{1k}) \quad ; \quad -1 < s_1 < 1 \quad ; \quad k = 1, 2, \dots, (N+1). \quad (4.25)$$

where

$$E_{11}^n(s_{1k}) = \int_{-1}^{+1} \frac{r_1^n}{\sqrt{1-r_1}} \left[\frac{1}{r_1-s_{1k}} + K_{11}(s_{1k}, r_1) \right] dr_1, \quad (a)$$

(4.26)

$$P_1(s_{1k}) = -\pi \frac{\sigma_1^T(s_{1k})}{\sigma_0^T}. \quad (b)$$

The integration in equation (4.26) can be found in Appendix (G)

4.3 Crack Terminating at the Interface

Figure 3-4 shows the case in which $a_1 > 0$, $b_1 = h$, and the singularity at the end points are $\alpha_1 = \frac{1}{2}$ and β_1 , where β_1 can be obtained from equation (3.51).

Similarly Figure 3-5 shows the case in which $a_2 = h$, $b_2 < \infty$ and the singularity at the end points are $\beta_2 = \frac{1}{2}$ and α_2 , where α_2 can be obtained from equation (3.65).

For the case shown in Figure 3-4, the collocation points and equation (4.14)(a), (considering one internal crack in material 1), become

$$s_{1k} = \cos \frac{\pi(2k-1)}{2N} \quad ; \quad k = 1, 2, \dots, N, \quad (4.27)$$

$$\sum_{n=0}^N a_n E_{11}^n(s_{1k}) = P_1(s_{1k}) \quad ; \quad k = 1, 2, \dots, N. \quad (4.28)$$

where

$$E_{11}^n(s_{1k}) = \int_{-1}^{+1} \frac{r_1^n}{(1+r_1)^{1/2}(1-r_1)^{\beta_1}} \left[\frac{1}{r_1-s_{1k}} + K_{11}(s_{1k}, r_1) \right] dr_1. \quad (4.29)$$

Equation (4.28) has N-equations with (N+1) coefficients a_n . The (N+1)th equation necessary to obtain a unique solution can be obtained by using the following single valuedness condition;

$$\int_{a_1}^{b_1} \phi_1(t_1) dt_1 = 0, \quad (4.30)$$

which can be written in the form

$$\sum_{n=0}^N a_n G^n = 0. \quad (4.31)$$

where

$$G^n = \int_{-1}^{+1} \frac{r_1^n}{(1+r_1)^{1/2} (1-r_1)^{\beta_1}} dr_1. \quad (4.32)$$

Similarly, for the case shown in Figure 3-5, the collocation points and equation (4.14)(b) (considering one internal crack in material 2) will become

$$s_{2l} = \cos \frac{\pi(2l-1)}{2M} \quad ; \quad l = 1, 2, \dots, M, \quad (4.33)$$

$$\sum_{m=0}^M b_m E_{22}^m(s_{2l}) = P_2(s_{2l}) \quad ; \quad l = 1, 2, \dots, M. \quad (4.34)$$

where

$$E_{22}^m(s_{2l}) = \int_{-1}^{+1} \frac{r_2^m}{(1+r_2)^{\alpha_2} (1-r_2)^{1/2}} \left[\frac{1}{r_2 - s_{2l}} + K_{22}(s_{2l}, r_2) \right] dr_2. \quad (4.35)$$

Equation (4.34) has M-equations for (M+1) coefficients b_m . The (M+1)th equation can be obtained by using the following single valuedness condition;

$$\int_{a_2}^{b_2} \phi_2(t_2) dt_2 = 0. \quad (4.36)$$

which can be written as

$$\sum_{m=0}^M b_m G^m = 0. \quad (4.37)$$

where

$$G^m = \int_{-1}^{+1} \frac{r_2^m}{(1+r_2)^{\alpha_2}(1-r_2)^{1/2}} dr_2. \quad (4.38)$$

The integrations in equations (4.29), (4.32), (4.35), (4.38), can be found in Appendix (G).

4.4 Crack Going Through the Interface

Figure 3-4 presents this case in which $a_1 > 0$, $b_1 = h$, $a_2 = h$, $b_2 < \infty$, and the singularity at the end points are

$$\alpha_1 = \beta_2 = \frac{1}{2}, \quad \beta_1 = \alpha_2. \quad (4.39)$$

where β_1 or α_2 can be obtained from equation (3.80). In this case equations (4.17) and (4.18) will still be the same with

$$E_{11}^n(s_{1k}) = \int_{-1}^{+1} \frac{r_1^n}{(1+r_1)^{1/2}(1-r_1)^{\beta_1}} \left[\frac{1}{r_1-s_{1k}} + K_{11}(s_{1k}, r_1) \right] dr_1, \quad (a)$$

$$E_{12}^m(s_{1k}) = \frac{\mu_1}{\mu_2} \frac{\kappa_2 + 1}{\kappa_1 + 1} \int_{-1}^{+1} \frac{r_2^m}{(1+r_2)^{\beta_1}(1-r_2)^{1/2}} K_{12}(s_{1k}, r_2) dr_2. \quad (b)$$

(4.40)

$$E_{21}^n(s_{2l}) = \frac{\mu_2}{\mu_1} \frac{\kappa_1 + 1}{\kappa_2 + 1} \int_{-1}^{+1} \frac{r_1^n}{(1+r_1)^{1/2}(1-r_1)^{\beta_1}} K_{21}(s_{2l}, r_1) dr_1, \quad (c)$$

$$E_{22}^m(s_{2l}) = \int_{-1}^{+1} \frac{r_2^m}{(1+r_2)^{\beta_1}(1-r_2)^{1/2}} \left[\frac{1}{r_2-s_{2l}} + K_{22}(s_{2l}, r_2) \right] dr_2. \quad (d)$$

and $P_1(s_{1k}), P_2(s_{2l})$ can be found in equation (4.19)(e, f).

Equations (4.18) have $(N+M)$ equations for $(N+M+2)$ coefficients a_n, b_m .

So, the two extra conditions we need to obtain a unique solution are

$$\int_{a_1}^{b_1} \phi_1(t_1) dt_1 + \int_{a_2}^{b_2} \phi_2(t_2) dt_2 = 0. \quad (4.41)$$

and

$$g_1(h) = -g_2(h) \frac{(h-a_1)^{\alpha_1} \cos \pi \beta_1 + \frac{1}{2} C_{23} \beta_1 (\beta_1 + 1) + C_{22} \beta_1 + C_{22}}{(b_2-h)^{\beta_2} d_{22} \beta_1 + d_{21}}. \quad (4.42)$$

After changing the variable and substituting from equations (4.13), equations (4.41) and (4.42) become

$$\sum_{n=0}^N a_n G_1^n + R_1 \sum_{m=0}^M b_m G_2^m = 0. \quad (4.43)$$

$$R_2 \sum_{m=0}^M a_n (+1)^n + R_3 \sum_{m=0}^M b_m (-1)^m = 0. \quad (4.44)$$

where

$$R_1 = \frac{\mu_1 \kappa_2 + 1}{\mu_2 \kappa_1 + 1} \left(\frac{b_2 - h}{h - a_1} \right), \quad (a)$$

$$R_2 = (d_{22} \beta_1 + d_{21}), \quad (b)$$

$$R_3 = \frac{\mu_1 \kappa_2 + 1}{\mu_2 \kappa_1 + 1} \left(\frac{b_2 - h}{h - a_1} \right)^{\beta_1} \quad (4.45)$$

$$(2)^{\alpha_1 - \beta_2} [\cos \pi \beta_1 + \frac{1}{2} C_{23} \beta_1 (\beta_1 + 1) + C_{22} \beta_1 + C_{21}], \quad (c)$$

$$G_1^n = \int_{-1}^{+1} \frac{r_1^n}{(1+r_1)^{1/2} (1-r_1)^{\beta_1}} dr_1, \quad (d)$$

$$G_2^m = \int_{-1}^{+1} \frac{r_2^m}{(1+r_2)^{\beta_1} (1-r_2)^{1/2}} dr_2. \quad (e)$$

The integrations in equations (4.40), and (4.45) are found in Appendix (G).

4.5 Edge crack going through the interface

This case is shown in Figure 4-1, in which $a_1 = 0$, $b_1 = a_2 = h$, $b_2 > h$. Also, the singularity at the end points are

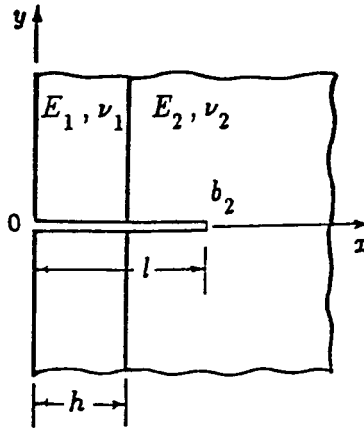


Figure 4-1: Geometry of edge crack going through the interface

$$\alpha_1 = 0, \quad \beta_2 = \frac{1}{2}, \quad \beta_1 = \alpha_2, \quad (4.46)$$

where β_1 or α_2 may be obtained from (3.80). The collocation points for s_1 and s_2 are

$$s_{1k} = \cos \frac{\pi(2k-1)}{2(N+1)} ; k = 1, 2, \dots, (N+1), \quad (a)$$

$$s_{2l} = \cos \frac{\pi(2l-1)}{2M} ; l = 1, 2, \dots, (M). \quad (b)$$
(4.47)

Equations (4.14) may then be expressed as

$$\sum_{n=0}^N a_n E_{11}^n(s_{1k}) + \sum_{m=0}^M b_m E_{12}^m(s_{1k}) = P_1(s_{1k}); k = 1, 2, \dots, (N+1), \quad (a)$$
(4.48)

$$\sum_{n=0}^N a_n E_{21}^n(s_{2l}) + \sum_{m=0}^M b_m E_{22}^m(s_{2l}) = P_2(s_{2l}); l = 1, 2, \dots, (M). \quad (b)$$

where

$$E_{11}^n(s_{1k}) = \int_{-1}^{+1} \frac{r_1^n}{(1-r_1)^{\beta_1}} \left[\frac{1}{r_1 - s_{1k}} + K_{11}(s_{1k}, r_1) \right] dr_1,$$
(4.49)

$$E_{21}^n(s_{2l}) = \frac{\mu_2 \kappa_1 + 1}{\mu_1 \kappa_2 + 1} \int_{-1}^{+1} \frac{r_1^n}{(1-r_1)^{\beta_1}} K_{21}(s_{2l}, r_1) dr_1.$$

and $E_{12}^m(s_{1k})$, $E_{22}^m(s_{2l})$ are the same as in equations (4.40)(b,d).

Now equations (4.48) have $(N+M+1)$ equations for $(N+M+2)$ coefficients a_n, b_m . Since, condition (4.41) is no longer valid, then the only extra condition that we need to obtain a unique solution is equation (4.41) or (4.44). Appendix (G) contains all the integrations needed.

Chapter 5

Stress Intensity Factors

5.1 Embedded Crack

The stress intensity factors at the irregular points a_1, b_1, a_2, b_2 may be defined by

$$k(a_1) = \lim_{x \rightarrow a_1} \sqrt{2(a_1 - x)} \sigma_{1yy}(x, 0), \quad (a)$$

$$k(b_1) = \lim_{x \rightarrow b_1} \sqrt{2(x - b_1)} \sigma_{1yy}(x, 0), \quad (b)$$

$$k(a_2) = \lim_{x \rightarrow a_2} \sqrt{2(a_2 - x)} \sigma_{2yy}(x, 0), \quad (c)$$

$$k(b_2) = \lim_{x \rightarrow b_2} \sqrt{2(b_2 - x)} \sigma_{2yy}(x, 0). \quad (d)$$

(5.1)

We note that the expression for the stresses $\sigma_{1yy}(x, 0)$ and $\sigma_{2yy}(x, 0)$ in equations (5.1) are for x outside the crack and can be obtained from the two singular integral equations (2.62) and (2.63), by observing that these equations give the stresses for $y=0$ outside as well as inside the cracks. Thus,

$$\begin{aligned} & \int_{a_1}^{b_1} \left[\frac{1}{t_1 - x} + K_{11}(x, t_1) \right] \phi_1(t_1) dt_1 + \int_{a_2}^{b_2} K_{12}(x, t_2) \phi_2(t_2) dt_2 \\ &= \frac{\pi(\kappa_1 + 1)}{4\mu_1} \sigma_{1yy}(x, 0); \quad 0 < x < a_1; \quad b_1 < x < h, \end{aligned} \quad (a)$$

(5.2)

$$\begin{aligned} & \int_{a_1}^{b_1} K_{21}(x, t_1) \phi_1(t_1) dt_1 + \int_{a_2}^{b_2} \left[\frac{1}{t_2 - x} + K_{22}(x, t_2) \right] \phi_2(t_2) dt_2 \\ &= \frac{\pi(\kappa_2 + 1)}{4\mu_2} \sigma_{2yy}(x, 0); \quad h < x < a_2; \quad b_2 < x < \infty. \end{aligned} \quad (b)$$

Substituting equation (5.2)(a) into equation (5.1)(a) we find

$$k(a_1) = \lim_{x \rightarrow a_1} \sqrt{2(a_1 - x)} \frac{4\mu_1}{\pi(\kappa_1 + 1)} \left\{ \int_{a_1}^{b_1} \left[\frac{1}{t_1 - x} + K_{11}(x, t_1) \right] \phi_1(t_1) dt_1 + \int_{a_2}^{b_2} K_{12}(x, t_2) \phi_2(t_2) dt_2 \right\}. \quad (5.3)$$

Since, for embedded cracks the kernels $K_{11}(x, t_1)$, $K_{12}(x, t_2)$ are bounded, equation (5.3) can be written as

$$k(a_1) = \frac{4\mu_1}{\pi(\kappa_1 + 1)} \lim_{x \rightarrow a_1} \sqrt{2} \sqrt{a_1 - x} \left\{ \int_{a_1}^{b_1} \frac{\phi_1(t_1)}{t_1 - x} dt_1 + \text{bounded terms} \right\}. \quad (5.4)$$

By defining the sectionally holomorphic function

$$F_1(z) = \frac{1}{\pi} \int_{a_1}^{b_1} \frac{\phi_1(t_1)}{t_1 - z} dt_1. \quad (5.5)$$

and observing that

$$\phi_1(t_1) = \frac{g_1(t_1)}{(t_1 - a_1)^{\alpha_1} (b_1 - t_1)^{\beta_1}} = \frac{g_1(t_1) e^{\pi i \beta_1}}{(t_1 - a_1)^{\alpha_1} (t_1 - b_1)^{\beta_1}}, \quad (5.6)$$

After separating the leading terms at the end points of the cut for $\alpha_1 = \beta_1 = \frac{1}{2}$, equation (5.5) can be expressed in the following form,

$$F_1(z) = \frac{g_1(a_1) e^{\frac{\pi i}{2}}}{(b_1 - a_1)^{1/2} (z - a_1)^{1/2}} - \frac{g_1(b_1)}{(b_1 - a_1)^{1/2} (z - b_1)^{1/2}} + F_{01}(z). \quad (5.7)$$

where $F_{01}(z)$ has the same properties as in equation (3.6). By using the Plemelj's formula, equation (5.7) can be written as follows

$$\frac{1}{\pi} \int_{a_1}^{b_1} \frac{\phi_1(t_1)}{t_1 - x} dt_1 = \frac{g_1(a_1)}{(b_1 - a_1)^{1/2} (a_1 - x)^{1/2}} - \frac{g_1(b_1)}{(b_1 - a_1)^{1/2} (x - b_1)^{1/2}} + F_{01}(x) ; x < a_1. \quad (5.8)$$

Substituting equation (5.8) into equation (5.4) we find

$$k(a_1) = \frac{4\mu_1}{(\kappa_1 + 1)} \lim_{x \rightarrow a_1} \sqrt{2} \sqrt{(a_1 - x)} \left[\frac{g_1(a_1)}{(b_1 - a_1)^{1/2} (a_1 - x)^{1/2}} - \frac{g_1(b_1)}{(b_1 - a_1)^{1/2} (x - b_1)^{1/2}} + \text{bounded terms} \right]. \quad (5.9)$$

giving

$$k(a_1) = \frac{4\mu_1}{\kappa_1 + 1} \sqrt{\frac{2}{b_1 - a_1}} g_1(a_1), \quad (a)$$

Similarly, the stress intensity factor at the other irregular points b_1, a_2, b_2 are found to be

$$k(b_1) = -\frac{4\mu_1}{\kappa_1 + 1} \sqrt{\frac{2}{b_1 - a_1}} g_1(b_1), \quad (b) \quad (5.10)$$

$$k(a_2) = \frac{4\mu_2}{\kappa_2 + 1} \sqrt{\frac{2}{b_2 - a_2}} g_2(a_2), \quad (c)$$

$$k(b_2) = -\frac{4\mu_2}{\kappa_2 + 1} \sqrt{\frac{2}{b_2 - a_2}} g_2(b_2). \quad (d)$$

Equations (5.10) may also be expressed as

$$k(a_1) = \sqrt{\frac{b_1 - a_1}{2}} \sigma_0^T F_1^*(-1), \quad (a)$$

$$k(b_1) = -\sqrt{\frac{b_1 - a_1}{2}} \sigma_0^T F_1^*(+1), \quad (b)$$

(5.11)

$$k(a_2) = \sqrt{\frac{b_2 - a_2}{2}} \sigma_0^T F_2^*(-1), \quad (c)$$

$$k(b_2) = -\sqrt{\frac{b_2 - a_2}{2}} \sigma_0^T F_2^*(+1). \quad (d)$$

5.2 Edge Crack

In this case, shown in Figure 3-2, the stresses are bounded at $a_1 = 0$, but have singular behavior at b_1 . So, the stress intensity factor at b_1 may be defined by

$$k(b_1) = \lim_{x \rightarrow b_1} \sqrt{2} \sqrt{(x - b_1)} \sigma_{1yy}(x, 0). \quad (5.12)$$

where $\sigma_{1yy}(x, 0)$ is the stress for x outside the crack, which can be obtained from equation (5.2)(a), by considering one crack, i.e

$$\int_0^{b_1} \left[\frac{1}{t_1 - x} + K_{11}(x, t_1) \right] \phi_1(t_1) dt_1 = \frac{\pi(\kappa_1 + 1)}{4\mu_1} \sigma_{1yy}(x, 0). \quad (5.13)$$

Substituting equation (5.13) into equation (5.12) and observing that the kernel $K_{11}(x, t_1)$ is bounded as $x \rightarrow b_1$ and $t_1 \rightarrow b_1$, equation (5.12) becomes

$$k(b_1) = \frac{4\mu_1}{\pi(\kappa_1+1)} \lim_{x \rightarrow b_1} \sqrt{2} \sqrt{x-b_1} \left\{ \int_0^{b_1} \frac{\phi_1(t)}{t_1-x} \phi_1(t_1) dt_1 + \text{bounded terms} \right\} . \quad (5.14)$$

The density function ϕ_1 for edge crack is given by

$$\phi_1(t_1) = \frac{g_1(t_1)}{(b_1-t_1)^{1/2}} . \quad (5.15)$$

Then, by following Muskhelishvili's technique, the singular term in equation (5.14) can be expressed as

$$\int_0^{b_1} \frac{\phi_1(t_1)}{(t_1-x)} dt_1 = \frac{g_1(0)}{(b_1)^{1/2}} - \frac{g_1(b_1)}{(x-b_1)^{1/2}} + F_{01}(x) . \quad (5.16)$$

So, the stress intensity factor at the irregular point b_1 , can be written as

$$k(b_1) = \frac{4\mu_1}{(\kappa_1+1)} \lim_{x \rightarrow b_1} \sqrt{2} \sqrt{x-b_1} \left\{ \frac{g_1(0)}{(b_1)^{1/2}} - \frac{g_1(b_1)}{(x-b_1)^{1/2}} + \text{bounded terms} \right\} . \quad (5.17)$$

Therefore

$$k(b_1) = -\frac{4\mu_2}{\kappa_1+1} \sqrt{2} g_1(b_1) . \quad (5.18)$$

which can be reduced to

$$k(b_1) = -\sqrt{b_1} \sigma_0^T F_1^* (+1) . \quad (5.19)$$

5.3 Crack Terminating at the Interface

The stresses have singular behavior, at the ends a_1 and $b_1 = h$ in Figure 3-4, and at the ends $a_2 = h$ and b_2 in Figure 3-5. First, consider Figure 3-4 in which the stress intensity factor at a_1 and $b_1 = h$ may be defined by

$$k(a_1) = \lim_{x \rightarrow a_1} \sqrt{2(a_1 - x)} \sigma_{1yy}(x, 0), \quad (a)$$

$$k(b_1 = h) = \lim_{x \rightarrow h+0} \sqrt{2} (x - h)^{\beta_1} \sigma_{2yy}(x, 0). \quad (b) \quad (5.20)$$

where the stresses $\sigma_{1yy}(x, 0)$ and $\sigma_{2yy}(x, 0)$ can be obtained from equations (5.2)(a) and (b) by considering one internal crack, i.e.

$$\int_{a_1}^h \left[\frac{1}{t_1 - x} + K_{11}(x, t_1) \right] \phi_1(t_1) dt_1 = \frac{\pi(\kappa_1 + 1)}{4\mu_1} \sigma_{1yy}(x, 0); 0 < x < a_1, \quad (a)$$

$$\int_{a_1}^h K_{21}(x, t_1) \phi_1(t_1) dt_1 = \frac{\pi(\kappa_2 + 1)}{4\mu_2} \sigma_{2yy}(x, 0); h < x. \quad (b) \quad (5.21)$$

Substituting from (5.21)(a) into (5.20)(a), and observing that the kernel $K_{11}(x, t_1)$ is bounded as $x \rightarrow a_1$, $t_1 \rightarrow a_1$, equation (5.20)(a) may be written as

$$k(a_1) = \frac{4\mu_1}{\pi(\kappa_1 + 1)} \lim_{x \rightarrow a_1} \sqrt{2} \sqrt{a_1 - x} * \left[\int_{a_1}^h \frac{\phi_1(t_1)}{t_1 - x} dt_1 + \text{bounded terms} \right]; a_1 < x < h. \quad (5.22)$$

Since, the density function ϕ_1 in this case is defined by

$$\phi_1(t_1) = \frac{g_1(t_1)}{(t_1 - a_1)^{1/2} (h - t_1)^{\beta_1}}, \quad (5.23)$$

by following Muskhelishvili's technique [37], the singular term may be

expressed as

$$\frac{1}{\pi} \int_{a_1}^{b_1} \frac{\phi_1(t_1)}{t_1 - x} dt_1 = \frac{g_1(a_1)}{(h-a_1)^{\beta_1} (a_1-x_1)^{1/2}} - \frac{g_1(h)}{(h-a_1)^{1/2} (x-h)^{\beta_1} \sin \pi \beta_1} + \text{bounded terms} . \quad (5.24)$$

Thus, equation (5.22) becomes

$$k(a_1) = \frac{4\mu_1}{(\kappa_1+1)} \lim_{x \rightarrow a_1} \sqrt{2} \sqrt{a_1 - x} \left[\frac{g_1(a_1)}{(h-a_1)^{\beta_1} (a_1-x_1)^{1/2}} - \frac{g_1(h)}{(h-a_1)^{1/2} (x-h)^{\beta_1}} + \text{bounded terms} \right] . \quad (5.25)$$

The stress intensity factor at the end a_1 may then be expressed as

$$k(a_1) = \frac{4\mu_1}{(\kappa_1+1)} \frac{\sqrt{2}}{(h-a_1)^{\beta_1}} g_1(a_1) . \quad (5.26)$$

Since, by definition

$$g_1(a_1) = \left(\frac{h-a_1}{2} \right)^{1/2 + \beta_1} \sigma_0^T \frac{\kappa_1+1}{4\mu_1} F_1^*(-1) . \quad (5.27)$$

Equation (5.26) would be reduced to

$$k(a_1) = \sqrt{\frac{h-a_1}{2}} \sigma_0^T (2)^{1/2 - \beta_1} F_1^*(-1) . \quad (5.28)$$

Similarly, the stress intensity factor at $b_1=h$ can be obtained by substituting equation (5.21)(b) into equation (5.20)(b), i.e.

$$k(b_1=h) = \frac{4\mu_2}{\pi(\kappa_2+1)} \lim_{x \rightarrow h} \sqrt{2} (x-h)^{\beta_1}$$

$$[\int_{a_1}^h K_{21}(x, t_1) \phi_1(t_1) dt_1] ; h < x . \quad (5.29)$$

The singular terms of the kernel $K_{21}(x, t_1)$, as $x \rightarrow h$, $t_1 \rightarrow h$ is

$$\begin{aligned} K_{21}^s(x, t_1) &= \frac{d_{21}}{(x-t_1)} + \frac{d_{22}(x-h)}{(x-t_1)^2} \\ &= [d_{22}(x-h) \frac{d}{dx} - d_{21}] \frac{1}{t_1-x} ; h < x. \end{aligned} \quad (5.30)$$

Thus, equation (5.29) may be expressed as

$$\begin{aligned} k(b_1=h) &= \frac{4\mu_2}{\pi(\kappa_2+1)} \lim_{x \rightarrow h} \sqrt{2} (x-h)^{\beta_1} * \\ &[\int_{a_1}^h \{ d_{22}(x-h) \frac{d}{dx} - d_{21} \} \frac{\phi_1(t_1)}{t_1-x} dt_1 + \text{bounded terms}] ; h < x. \end{aligned} \quad (5.31)$$

Since the density function is defined by

$$\phi_1(t_1) = \frac{g_1(t_1)}{(t_1-a_1)^{1/2} (h-t_1)^{\beta_1}} . \quad (5.32)$$

By following Muskhelishvili's technique, we have

$$\frac{1}{\pi} \int_{a_1}^h \frac{\phi_1(t_1)}{t_1-x} dt_1 = \frac{-g_1(h)}{(h-a_1)^{1/2} (x-h)^{\beta_1} \sin \pi \beta_1} + \text{bounded terms} . \quad (5.33)$$

From equation (5.31) it then follows that

$$k(b_1) = \frac{4\mu_2}{(\kappa_2+1)} \lim_{x \rightarrow h} \sqrt{2} (x-h)^{\beta_1} \left[\left\{ d_{22} (x-h) \frac{d}{dx} - d_{21} \right\} \frac{-g_1(h)}{(h-a_1)^{1/2} (x-h)^{\beta_1} \sin \pi \beta_1} + \text{bounded terms} \right]. \quad (5.34)$$

giving

$$k(b_1) = \frac{4\mu_2}{(\kappa_2+1)} \sqrt{2} \frac{d_{22} \beta_1 + d_{21}}{(h-a_1)^{1/2} \sin \pi \beta_1} g_1(h). \quad (5.35)$$

By using

$$g_1(h) = \left(\frac{h-a_1}{2} \right)^{1/2 + \beta_1} \sigma_0^T \frac{\kappa_1 + 1}{4\mu_1} F_1^*(+1). \quad (5.36)$$

Equation (5.35) may also be expressed as

$$k(b_1=h) = \frac{\mu_2}{\mu_1} \frac{\kappa_1 + 1}{\kappa_2 + 1} \frac{d_{22} \beta_1 + d_{21}}{\sin \pi \beta_1} \left(\frac{h-a_1}{2} \right)^{\beta_1} \sigma_0^T F_1^*(+1). \quad (5.37)$$

Similarly, in the case of Figure 3-5, it may easily be shown that the stress intensity factors at the end points $a_2=h$ and b_2 are given by

$$k(a_2=h) = \frac{\mu_1}{\mu_2} \frac{\kappa_2 + 1}{\kappa_1 + 1} \frac{-d_{12} \alpha_2 + d_{11}}{\sin \pi \alpha_2} \left(\frac{b_2-h}{2} \right)^{\alpha_2} \sigma_0^T F_2^*(-1), \quad (5.38)$$

$$k(b_2) = - \sqrt{\frac{b_2-h}{2}} \sigma_0^T (2)^{1/2 - \alpha_2} F_2^*(+1). \quad (5.39)$$

5.4 Crack going through the interface

As in the previous section [5.3] the stresses at the end point a_1 , b_2 have singular behavior, and the stress intensity factors at these points are still the same as equations (5.28) , (5.39) respectively, which can be put in the following form

$$k(a_1) = \sqrt{\frac{l}{2}} \sigma_0^T \sqrt{\frac{h-a_1}{l}} (2)^{1/2-\beta_1} F_1^*(-1). \quad (5.40)$$

$$k(b_2) = -\sqrt{\frac{l}{2}} \sigma_0^T \sqrt{\frac{b_2-h}{l}} (2)^{1/2-\beta_1} F_2^*(+1). \quad (5.41)$$

where l is the total crack length. At the irregular point $b_1=a_2=h$, the stresses $\sigma_{xx}(h,y)$, $\sigma_{xy}(h,y)$ become unbounded as $y \rightarrow 0$. Thus, the normal and shear components of the stress intensity factor may be defined as follows

$$k_x = \lim_{y \rightarrow 0} y^{\beta_1} \sigma_{xx}(h,y), \quad (a) \quad (5.42)$$

$$k_{xy} = \lim_{y \rightarrow 0} y^{\beta_1} \sigma_{xy}(h,y). \quad (b)$$

where $\sigma_{xx}(h,y)$ and $\sigma_{xy}(h,y)$ are the components of the stresses at the interface which after long manipulation, are found to be

$$\sigma_{xx}(h,y) = \frac{2\mu_2}{\pi(\kappa_2+1)} \left[\int_{a_1}^h k_{13}^s(h,t_1) \phi_1(t_1) dt_1 + \int_h^{b_2} k_{14}^s(h,t_2) \phi_2(t_2) dt_2 + \text{bounded terms} \right], \quad (a)$$

(5.43)

$$\sigma_{xy}(h,y) = \frac{2\mu_2}{\pi(\kappa_2+1)} \left[\int_{a_1}^h k_{23}^s(h,t_1) \phi_1(t_1) dt_1 + \int_h^{b_2} k_{24}^s(h,t_2) \phi_2(t_2) dt_2 + \text{bounded terms} \right]. \quad (b)$$

where $k_{13}^s, k_{14}^s, k_{23}^s, k_{24}^s$ are the singular kernels given by

$$k_{13}^s(h,t_1) = - \left[A \frac{(h-t_1)}{(h-t_1)^2+y^2} - B \frac{(h-t_1) \{3y^2-(h-t_1)^2\}}{\{(h-t_1)^2+y^2\}^2} \right], \quad (a)$$

$$k_{14}^s(h,t_2) = - \left[-B \frac{(t_2-h)}{(t_2-h)^2+y^2} + A \frac{(t_2-h) \{3y^2-(t_2-h)^2\}}{\{(t_2-h)^2+y^2\}^2} \right], \quad (b)$$

$$k_{23}^s(h,t_1) = A \frac{y}{(h-t_1)^2+y^2} + B \frac{y \{y^2-3(h-t_1)^2\}}{\{(h-t_1)^2+y^2\}^2}, \quad (c) \quad (5.44)$$

$$k_{24}^s(h,t_2) = B \frac{y}{(t_2-h)^2+y^2} + A \frac{y \{y^2-3(t_2-h)^2\}}{\{(t_2-h)^2+y^2\}^2}, \quad (d)$$

$$A = \frac{m(\kappa_2+1)}{m\kappa_2+1}, \quad B = \frac{m(\kappa_2+1)}{m+\kappa_1}. \quad (e)$$

$k_{13}^s, k_{14}^s, k_{23}^s, k_{24}^s$ can also be put in the following forms

$$k_{13}^s(h, t_1) = -\left[\left(\frac{A}{2} + \frac{B}{2}\right) \left\{ \frac{1}{(h-t_1)+iy} + \frac{1}{(h-t_1)-iy} \right\} \right. \\ \left. - Biy \left\{ \frac{1}{[(h-t_1)+iy]^2} - \frac{1}{[(h-t_1)-iy]^2} \right\} \right], \quad (\text{a})$$

$$k_{14}^s(h, t_2) = -\left[\left(-\frac{B}{2} - \frac{A}{2}\right) \left\{ \frac{1}{(t_2-h)+iy} + \frac{1}{(t_2-h)-iy} \right\} \right. \\ \left. + Aiy \left\{ \frac{1}{[(t_2-h)+iy]^2} - \frac{1}{[(t_2-h)-iy]^2} \right\} \right], \quad (\text{b})$$

$$k_{23}^s(h, t_1) = \left(\frac{A}{2} - \frac{B}{2}\right) i \left\{ \frac{1}{(h-t_1)+iy} - \frac{1}{(h-t_1)-iy} \right\} \quad (5.45)$$

$$-By \left\{ \frac{1}{[(h-t_1)+iy]^2} + \frac{1}{[(h-t_1)-iy]^2} \right\}, \quad (\text{c})$$

$$k_{24}^s(h, t_2) = \left(\frac{B}{2} - \frac{A}{2}\right) i \left\{ \frac{1}{(t_2-h)+iy} - \frac{1}{(t_2-h)-iy} \right\} \\ -Ay \left\{ \frac{1}{[(t_2-h)+iy]^2} + \frac{1}{[(t_2-h)-iy]^2} \right\}. \quad (\text{d})$$

Substituting from (5.43) into (5.42), we find

$$k_x = \lim_{y \rightarrow 0} y^{\beta_1} \frac{2\mu_2}{\pi(\kappa_2+1)} \left[\int_{a_1}^h k_{13}^s(h, t_1) \phi_1(t_1) dt_1 \right. \\ \left. + \int_h^{b_2} k_{14}^s(h, t_2) \phi_2(t_2) dt_2 + \text{bounded terms} \right], \quad (\text{a}) \quad (5.46)$$

$$k_{xy} = \lim_{y \rightarrow 0} y^{\beta_1} \frac{2\mu_2}{\pi(\kappa_2 + 1)} \left[\int_{a_1}^h k_{23}^s(h, t_1) \phi_1(t_1) dt_1 \right. \\ \left. + \int_h^{b_2} k_{24}^s(h, t_2) \phi_2(t_2) dt_2 + \text{bounded terms} \right]. \quad (b)$$

By observing that

$$\phi_1(t_1) = \frac{g_1(t_1)}{(t_1 - a_1)^{1/2} (h - t_1)^{\beta_1}}, \quad \phi_2(t_2) = \frac{g_2(t_2)}{(t_2 - h)^{\beta_1} (b_2 - t_2)^{1/2}}. \quad (5.47)$$

and following Muskhelishvili's technique, the singular terms can be written as

$$\frac{1}{\pi} \int_{a_1}^h \frac{\phi_1(t_1)}{(h - t_1) + iy} dt_1 = \frac{g_1(h) e^{-\frac{\pi}{2} i \beta_1}}{(h - a_1)^{\alpha_1} y^{\beta_1} \sin \pi \beta_1} + \text{bounded terms}. \quad (5.48)$$

$$\frac{1}{\pi} \int_{a_1}^h \frac{\phi_1(t_1)}{(h - t_1) - iy} dt_1 = \frac{g_1(h) e^{\frac{\pi}{2} i \beta_1}}{(h - a_1)^{\alpha_1} y^{\beta_1} \sin \pi \beta_1} + \text{bounded terms}. \quad (5.49)$$

$$\frac{1}{\pi} \int_h^{b_2} \frac{\phi_2(t_2)}{(t_2 - h) + iy} dt_2 = \frac{g_2(h) e^{-\frac{\pi}{2} i \beta_1}}{(b_2 - h)^{\beta_2} y^{\beta_1} \sin \pi \beta_1} + \text{bounded terms}. \quad (5.50)$$

$$\frac{1}{\pi} \int_h^{b_2} \frac{\phi_2(t_2)}{(t_2 - h) - iy} dt_2 = \frac{g_2(h) e^{\frac{\pi}{2} i \beta_1}}{(b_2 - h)^{\beta_2} y^{\beta_1} \sin \pi \beta_1} + \text{bounded terms}. \quad (5.51)$$

From (5.48)-(5.51) it follows that

$$\begin{aligned}
& \frac{1}{\pi} \int_{a_1}^h \left[\frac{1}{(h-t_1)+iy} + \frac{1}{(h-t_1)-iy} \right] \phi_1(t_1) dt_1 \\
&= \frac{g_1(h)}{(h-a_1)^{\alpha_1} y^{\beta_1} \sin \frac{\pi}{2} \beta_1} + \text{bounded terms} .
\end{aligned} \tag{5.52}$$

$$\begin{aligned}
& \frac{1}{\pi} \int_{a_1}^h iy \left\{ \frac{1}{[(h-t_1)+iy]^2} - \frac{1}{[(h-t_1)-iy]^2} \right\} \phi_1(t_1) dt_1 \\
&= -y \frac{d}{dy} \frac{1}{\pi} \int_{a_1}^h \left\{ \frac{1}{(h-t_1)+iy} + \frac{1}{(h-t_1)-iy} \right\} \phi_1(t_1) dt_1 \\
&= \frac{\beta_1 g_1(h)}{(h-a_1)^{\alpha_1} y^{\beta_1} \sin \frac{\pi}{2} \beta_1} + \text{bounded terms} .
\end{aligned} \tag{5.53}$$

$$\begin{aligned}
& \frac{1}{\pi} \int_h^{b_2} \left\{ \frac{1}{(t_2-h)+iy} + \frac{1}{(t_2-h)-iy} \right\} \phi_2(t_2) dt_2 \\
&= \frac{g_2(h)}{(b_2-h)^{\beta_2} y^{\beta_1} \sin \frac{\pi}{2} \beta_1} + \text{bounded terms} .
\end{aligned} \tag{5.54}$$

$$\begin{aligned}
& \frac{1}{\pi} \int_h^{b_2} iy \left\{ \frac{1}{[(t_2-h)+iy]^2} - \frac{1}{[(t_2-h)-iy]^2} \right\} \phi_2(t_2) dt_2 \\
&= -y \frac{d}{dy} \frac{1}{\pi} \int_h^{b_2} \left\{ \frac{1}{(t_2-h)+iy} + \frac{1}{(t_2-h)-iy} \right\} \phi_2(t_2) dt_2 \\
&= \frac{\beta_1 g_2(h)}{(b_2-h)^{\beta_2} y^{\beta_1} \sin \frac{\pi}{2} \beta_1} + \text{bounded terms} .
\end{aligned} \tag{5.55}$$

$$\begin{aligned}
& \frac{1}{\pi} \int_{a_1}^h \left[\frac{i}{(h-t_1)+iy} - \frac{i}{(h-t_1)-iy} \right] \phi_1(t_1) dt_1 \\
&= \frac{g_1(h)}{(h-a_1)^{\alpha_1} y^{\beta_1} \cos \frac{\pi}{2} \beta_1} + \text{bounded terms} .
\end{aligned} \tag{5.56}$$

$$\begin{aligned}
& \frac{1}{\pi} \int_{a_1}^h y \left\{ \frac{1}{[(h-t_1)+iy]^2} + \frac{1}{[(h-t_1)-iy]^2} \right\} \phi_1(t_1) dt_1 \\
&= y \frac{d}{dy} \frac{1}{\pi} \int_{a_1}^h \left[\frac{i}{(h-t_1)+iy} - \frac{i}{(h-t_1)-iy} \right] \phi_1(t_1) dt_1 \\
&= \frac{-\beta_1 g_1(h)}{(h-a_1)^{\alpha_1} y^{\beta_1} \cos \frac{\pi}{2} \beta_1} + \text{bounded terms} .
\end{aligned} \tag{5.57}$$

$$\begin{aligned}
& \frac{1}{\pi} \int_h^{b_2} \left[\frac{i}{(t_2-h)+iy} - \frac{i}{(t_2-h)-iy} \right] \phi_2(t_2) dt_2 \\
&= \frac{g_2(h)}{(b_2-h)^{\beta_2} y^{\beta_1} \cos \frac{\pi}{2} \beta_1} + \text{bounded terms} .
\end{aligned} \tag{5.58}$$

$$\begin{aligned}
& \frac{1}{\pi} \int_h^{b_2} y \left\{ \frac{1}{[(t_2-h)+iy]^2} + \frac{1}{[(t_2-h)-iy]^2} \right\} \phi_2(t_2) dt_2 \\
&= y \frac{d}{dy} \frac{1}{\pi} \int_h^{b_2} \left[\frac{i}{(t_2-h)+iy} - \frac{i}{(t_2-h)-iy} \right] \phi_2(t_2) dt_2 \\
&= \frac{-\beta_1 g_2(h)}{(b_2-h)^{\beta_2} y^{\beta_1} \cos \frac{\pi}{2} \beta_1} + \text{bounded terms} .
\end{aligned} \tag{5.59}$$

The two components of the stress intensity factor k_x, k_{xy} are then found to be

$$\begin{aligned}
k_x = \lim_{y \rightarrow 0} \frac{-2\mu_2}{\kappa_2 + 1} y^{\beta_1} \left[\left(\frac{A}{2} + \frac{B}{2} \right) \frac{g_1(h)}{(h-a_1)^{\alpha_1} y^{\beta_1} \sin \frac{\pi}{2} \beta_1} \right. \\
- B \frac{\beta_1 g_1(h)}{(h-a_1)^{\alpha_1} y^{\beta_1} \sin \frac{\pi}{2} \beta_1} + \left(-\frac{B}{2} - \frac{A}{2} \right) \frac{g_2(h)}{(b_2-h)^{\beta_2} y^{\beta_1} \sin \frac{\pi}{2} \beta_1} \\
\left. + A \frac{\beta_1 g_2(h)}{(b_2-h)^{\beta_2} y^{\beta_1} \sin \frac{\pi}{2} \beta_1} + \text{bounded terms} \right], \quad (a)
\end{aligned}$$

(5.60)

$$\begin{aligned}
k_{xy} = \lim_{y \rightarrow 0} \frac{2\mu_2}{\kappa_2 + 1} y^{\beta_1} \left[\left(\frac{A}{2} - \frac{B}{2} \right) \frac{g_1(h)}{(h-a_1)^{\alpha_1} y^{\beta_1} \cos \frac{\pi}{2} \beta_1} \right. \\
- B \frac{(-\beta_1) g_1(h)}{(h-a_1)^{\alpha_1} y^{\beta_1} \cos \frac{\pi}{2} \beta_1} + \left(\frac{B}{2} - \frac{A}{2} \right) \frac{g_2(h)}{(b_2-h)^{\beta_2} y^{\beta_1} \cos \frac{\pi}{2} \beta_1} \\
\left. - A \frac{(-\beta_1) g_2(h)}{(b_2-h)^{\beta_2} y^{\beta_1} \cos \frac{\pi}{2} \beta_1} + \text{bounded terms} \right]. \quad (b)
\end{aligned}$$

These can be written as

$$\begin{aligned}
k_x = \frac{-2\mu_2}{2(\kappa_2 + 1) \sin \frac{\pi}{2} \beta_1} \left[\{ A + (1 - 2\beta_1) B \} \frac{g_1(h)}{(h-a_1)^{\alpha_1}} \right. \\
\left. + \{ -B - (1 - 2\beta_1) A \} \frac{g_2(h)}{(b_2-h)^{\beta_2}} \right], \quad (a)
\end{aligned}$$

(5.61)

$$k_{xy} = \frac{2\mu_2}{2(\kappa_2+1)\cos\frac{\pi}{2}\beta_1} [\{A-(1-2\beta_1)B\} \frac{g_1(h)}{(h-a_1)^{\alpha_1}} + \{B-(1-2\beta_1)A\} \frac{g_2(h)}{(b_2-h)^{\beta_2}}]. \quad (b)$$

Since, by definition

$$g_1(h) = \left(\frac{h-a_1}{2}\right)^{\alpha_1+\beta_1} \sigma_0^T \frac{\kappa_1+1}{4\mu_1} F_1^*(+1), \quad (a)$$

(5.62)

$$g_2(h) = \left(\frac{b_2-h}{2}\right)^{\alpha_2+\beta_2} \sigma_0^T \frac{\kappa_2+1}{4\mu_2} F_2^*(-1). \quad (b)$$

where $\beta_1 = \alpha_2$ and $\alpha_1 = \beta_2 = 1/2$, equations (5.61) may also be expressed as

$$k_x = \left(\frac{l}{2}\right)^{\beta_1} \sigma_0^T \frac{-1}{\sin\frac{\pi}{2}\beta_1} \frac{1}{(2)^{1/2+2}} [\{A+(1-2\beta_1)B\} \left(\frac{h-a_1}{l}\right)^{\beta_1} \frac{\kappa_1+1}{\kappa_2+1} + \frac{\mu_2}{\mu_1} F_1^*(+1) + \{-B-(1-2\beta_1)A\} \left(\frac{b_2-h}{l}\right)^{\beta_1} F_2^*(-1)], \quad (a)$$

(5.63)

$$k_{xy} = \left(\frac{l}{2}\right)^{\beta_1} \sigma_0^T \frac{1}{\cos\frac{\pi}{2}\beta_1} \frac{1}{(2)^{1/2+2}} [\{A-(1-2\beta_1)B\} \left(\frac{h-a_1}{l}\right)^{\beta_1} \frac{\kappa_1+1}{\kappa_2+1} + \frac{\mu_2}{\mu_1} F_1^*(+1) + \{B-(1-2\beta_1)A\} \left(\frac{b_2-h}{l}\right)^{\beta_1} F_2^*(-1)]. \quad (b)$$

l being the total crack length ($l = b_2 - a_1$).

5.5 Edge crack going through the interface

In this case, as in section [5.4] the stresses at the end points b_2 and $b_1=a_2=h$ are unbounded (see Figure 4-1), but the stresses at $a_1=0$ is bounded. Equations (5.39), (5.61) (a,b) are still valid for stress intensity factor at the crack tip b_2 and at the interface $b_1=a_2=h$ respectively, provided we let $a_1=0$, $\alpha_1=0$, $\beta_1=\alpha_2$, and use the definition of $g_1(h)$ and $g_2(h)$ in equation (5.62). It may then be shown that

$$k(b_2) = -\sqrt{l} \sigma_0^T \sqrt{\left(\frac{b_2-h}{l}\right)} (2)^{-\beta_1} F_2^*(+1). \quad (5.64)$$

$$k_x = (l)^{\beta_1} \sigma_0^T \frac{-1}{\sin \frac{\pi}{2} \beta_1} \left[\frac{1}{(2)^{2+\beta_1}} \{ A + (1-2\beta_1)B \} \left(\frac{h}{l}\right)^{\beta_1} \frac{\kappa_1+1}{\kappa_2+1} \right. \\ \left. \frac{\mu_2}{\mu_1} F_1^*(+1) + \frac{1}{(2)^{1/2+2+\beta_1}} \{ -B - (1-2\beta_1)A \} \left(\frac{b_2-h}{l}\right)^{\beta_1} F_2^*(-1) \right]. \quad (5.65)$$

$$k_{xy} = (l)^{\beta_1} \sigma_0^T \frac{1}{\cos \frac{\pi}{2} \beta_1} \left[\frac{1}{(2)^{2+\beta_1}} \{ A - (1-2\beta_1)B \} \left(\frac{h}{l}\right)^{\beta_1} \frac{\kappa_1+1}{\kappa_2+1} \right. \\ \left. \frac{\mu_2}{\mu_1} F_1^*(+1) + \frac{1}{(2)^{1/2+2+\beta_1}} \{ B - (1-2\beta_1)A \} \left(\frac{b_2-h}{l}\right)^{\beta_1} F_2^*(-1) \right]. \quad (5.66)$$

where l is the total crack length.

Chapter 6

RESULTS AND DISCUSSION

As examples for the thermal shock crack problem two material combinations are considered. Material pair A corresponds to an austenitic stainless steel layer (material 1) and a ferritic steel base (material 2) which have the same elastic constants but different thermal properties [1]. Material pair B represents a ceramic coating (material 1) on a ferritic steel base (material 2) in which both the mechanical and the thermal properties are different. Since the problem is formulated in terms of dimensionless quantities, it is sufficient to consider only the ratios between the properties of the two material combinations shown in Table 6-1.

6.1 Model I

Figures 6-1 - 6-10 show the normalized transient temperature and thermal stresses distribution in material pair A given by equations (2.17) and (2.35) for $\tau_0 = 0$, and (2.26) and (2.35) for $\tau_0 > 0$. The temperature plots represent the ratio $\Theta(x^*, \tau)/\Theta_0$ ($\Theta = \Theta_1$ for $0 < x < h$, and $\Theta = \Theta_2$ for $h < x < \infty$) as a function of non-dimensional distance $x^* = x/h$ for various values of non-dimensional time (Fourier Number) τ and τ_0 defined by

$$\tau = \frac{tD_1}{h^2} \quad , \quad \tau_0 = \frac{t_0D_1}{h^2} \quad , \quad (6.1)$$

where t_0 is the actual duration time of the cooling ramp on the surface (see Figure 2-3(b)). The non-dimensional thermal stresses σ_{yy}/σ_0^T are plotted in the same way, where

$$\sigma_0^T = - \frac{\alpha_1' E_1 \Theta_0}{1 - \nu_1} \quad . \quad (6.2)$$

From Figures 6-1 - 6-10 it is clear that, the derivative of the temperature distribution, that is, the heat flux and the thermal stresses σ_{yy} ($\sigma_{yy}=\sigma_{1yy}$ for $0 < x < h$, $\sigma_{yy}=\sigma_{2yy}$ for $h < x < \infty$) are discontinuous at the interface. The discontinuity in the slope of the temperature, i.e., the heat flux, is due to the difference in the thermal conductivity of the two materials (see boundary condition (2.5)(c) or (2.19)(c)). Also, the discontinuity in the thermal stresses results from the difference in the coefficient of thermal expansion across the interface which is given by (see equations (2.33) or (2.35))

$$\frac{\sigma_{2yy}(h,t)}{\sigma_{1yy}(h,t)} = \frac{\alpha'_2 E_2 \Theta_2}{\alpha'_1 E_1 \Theta_1} \frac{1-\nu_1}{1-\nu_2} = \frac{\alpha'_2}{\alpha'_1} = 0.75 \quad (6.3)$$

since, there is no discontinuity in the temperature field itself $\Theta_1(h,t) = \Theta_2(h,t)$ and $E_1=E_2$, $\nu_1=\nu_2$ in material pair A. The influence of the ramp cooling τ_0 on the transient temperature and thermal stresses, particularly for small values of time, are also shown in Figures 6-1 - 6-10. As the rate of cooling surface temperature (τ_0) increases, the transient thermal stresses decrease.

The normalized stress intensity factors (SIF) for various crack geometries, subjected to thermal history shown in Figures 6-1 - 6-10, in material pair A are given in Figures 6-11 - 6-23. Figure 6-11 shows the variation of normalized SIF, $k(b_1)/\sigma_0^T \sqrt{l_1}$, for various edge crack lengths in material 1 ($a_1=0$, $b_1 < h$) and for $\tau_0=0$ as a function of Fourier Number τ . Note that, since the material pair A have the same mechanical properties, i.e. $E_1=E_2$, $\nu_1=\nu_2$, the normalized SIF would approach the uniformly loaded half plane solution of 1.1215 as $\tau \rightarrow \infty$. The influence of the cooling rate τ_0 on the surface $x=0$ for a fixed edge crack $b_1/h=0.5$ is shown in Figure 6-12. It is clear that, for small time τ , this influence could be quite considerable, and the normalized SIF decrease as τ_0 increases. Figure 6-13 shows the effect of τ_0 on the normalized SIF, $k(b_1)/\sigma_0^T \sqrt{l_1}$, for an edge crack

terminating at the interface ($a_1=0$, $b_1=h$). Since, $E_1=E_2$, $\nu_1=\nu_2$ in material pair A, the stress state at the crack tip $b_1=h$ has a square root singularity and the normalized SIF would again approach the uniformly loaded half plane solution of 1.1215 as $\tau \rightarrow \infty$.

Figures 6-14 - 6-15 show the normalized SIF for an under-clad crack at the crack tips a_2, b_2 ($a_2=h$, $h < b_2 < \infty$) , $k(a_2)/\sigma_0^T \sqrt{l_2/2}$, $k(b_2)/\sigma_0^T \sqrt{l_2/2}$, for various crack length and for $\tau_0=0$ as a function of time (Fourier Number). Since $E_1=E_2$, $\nu_1=\nu_2$, the singularity at the crack tip $a_2=h$ is the square root. The asymptotic values of the normalized SIF as $\tau \rightarrow \infty$ is depicted in the same Figures. The influence of τ_0 on the normalized SIF for an under-clad crack with fixed length $l_2/h=1.0$ is shown in Figures 6-16 - 6-17. It appears from the Figures that for small values of time, this influence could be quite significant.

The results of an edge crack crossing the interface are shown in Figures 6-18 - 6-19. In Figure 6-18 the normalized SIF at the crack tip b_2 , ($a_1=0$, $b_1=a_2=h$, $h < b_2 < \infty$), $k(b_2)/\sigma_0^T \sqrt{l}$, for various crack lengths and for $\tau_0=0$ are shown as a function of time. Note that, the tensile and shear stresses at the interface ($b_1=a_2=h$) are bounded, since the mechanical properties of the material pair A are the same, i.e. $E_1=E_2$, $\nu_1=\nu_2$. Figure 6-19 shows the effect of τ_0 on the normalized SIF for fixed crack length $l/h=4.0$. The limiting values of the normalized SIF as $\tau \rightarrow \infty$ are also shown in Figures 6-18 and 6-19.

Figures 6-20 - 6-23 show the results of an internal crack crossing the interface. The transient normalized SIFs at the crack tips a_1 and b_2 , ($a_1 > 0$, $b_1=h=a_2$, $b_2 < \infty$) , $k(a_1)/\sigma_0^T \sqrt{l/2}$, $k(b_2)/\sigma_0^T \sqrt{l/2}$, for various crack length are given in Figures 6-20 - 6-21. There is no stress singularity at the interface, since $E_1=E_2$, $\nu_1=\nu_2$. Figures 6-22 - 6-23 show the influence of the ramp cooling as measured by τ_0 on the normalized SIF at the crack tips a_1 and b_2 for a fixed crack length $a_1/h=0.2$, $b_2/h=2.0$.

The results for the material pair B are given in Figures 6-24 - 6-38. The normalized transient temperature and thermal stress distributions for various ramp durations (τ_0) are shown in Figures 6-24 - 6-29. Again, the discontinuity in the thermal stresses at the interface ($x=h$) is given by (see equations (2.33) or (2.35))

$$\frac{\sigma_{2yy}(h,t)}{\sigma_{1yy}(h,t)} = \frac{\alpha'_2 E_2 \Theta_2}{\alpha'_1 E_1 \Theta_1} \frac{1-\nu_1}{1-\nu_2} = \frac{\alpha'_2 E_2}{\alpha'_1 E_1} = 1.4019 \quad (6.4)$$

Note that in this case, $E_2 \neq E_1$, $\nu_2 = \nu_1$, and $\Theta_2 = \Theta_1$ at the interface.

Figure 6-30 shows the normalized SIF for an edge crack in material 1 ($a_1=0$, $b_1 < h$) for various crack lengths and for $\tau_0=0$. Since the materials in pair B have different mechanical properties and since $E_1 > E_2$, the normalized SIF would approach infinity as $b_1 \rightarrow h$, but for very small value of b_1 , it would approach to the half plane uniform load solution, 1.1215. Figure 6-31 shows the effect of τ_0 for a fixed edge crack $b_1/h=0.5$. The results for an edge crack terminating at the interface ($a_1=0$, $b_1=h$) are shown in Figure 6-32 for different values of τ_0 . In this case the singularity at the crack tip $b_1=h$ is $\beta_1=0.552538$.

Figures 6-33 - 6-38 show the results of an edge crack going through the interface ($a_1=0$, $b_1=a_2=h$, $h < b_2 < \infty$). Figures 6-33 - 6-35 give the normalized SIFs at the interface and at the crack tip b_2 , $k_x/\sigma_0^T l^{\beta_1}$, $k_{xy}/\sigma_0^T l^{\beta_1}$, $k(b_2)/\sigma_0^T \sqrt{l}$, for various crack lengths and for $\tau_0=0$. The values of k_x and k_{xy} control the tensile and shear cleavage stresses at the interface, ($x=h$, $y > 0$) (see equations (5.42) and (5.43)), where the singularity at the interface is $\beta_1=\alpha_2=0.01872238$. The influence of τ_0 on the normalized SIF is also shown in Figures 6-36 - 6-38 for a fixed crack length $b_2/h=2.0$.

If the transient thermal stresses are sufficient to cause yielding through the thickness of the clad, the stress intensity factors for an under-clad crack can

be analyzed by using a simple plastic strip model which assumes that the yielding in the clad is restricted to a very thin layer in the plane of the crack. Thus, the solution can be obtained by changing the boundary condition (2.49)(b) as

$$\sigma_{1yy}(x,0) = -\sigma_1^T(x) + \sigma_F ; 0 < x < h , \quad (6.5)$$

$$\sigma_{2yy}(x,0) = -\sigma_2^T(x) ; h < x < b_2 .$$

where σ_F is the average plastic flow stress. The normalized stress intensity factor at the crack tip b_2 is given by

$$\frac{k(b_2)}{\sigma_0^T \sqrt{l_2/2}} = k_1^*(b_2) + \frac{\sigma_F}{\sigma_0^T} k_2^*(b_2) . \quad (6.6)$$

where $k_1^*(b_2)$ is the stress intensity factor for an edge crack going through the interface subjected to $-\sigma_1^T(x)$ ($0 < x < h$) and $-\sigma_2^T(x)$ ($h < x < b_2$), and $k_2^*(b_2)$ is the stress intensity factor for an edge crack crossing the interface subjected to σ_F ($0 < x < h$). The values of $k_1^*(b_2)$ are given in Table 6-2, which shows the effect of clad yielding on the stress intensity factors. The SIFs decrease as the crack length increases. The comparison between the values of stress intensity factors as $\tau \rightarrow \infty$ for yielded clad and elastic clad for different values of crack length and σ_F/σ_0^T are shown in Table 6-3. It appears that, as σ_0^T becomes larger, yielding in the clad will result in a much higher stress intensity factor at b_2 .

6.2 Model II

To verify the computer program, the SIF for an edge crack in a homogeneous strip ($E_1=E_2$, $\nu_1=\nu_2$, $\chi=0$) under uniform load is calculated and compared with the results obtained by Kaya [41]. The results can be found in Table 6-4.

The problem of a crack terminating or going through the interface in two

bonded half planes can be obtained by letting the crack length very small compared to h_1 and h_2 . The normalized SIF for these two cases are calculated for material pair Aluminum and Epoxy and compared with the results obtained by Kaya [41] and Erdogan and Biricikogh [29], which can be found in Tables 6-5 and 6-6.

To see the effect of the elastic foundation on the SIF for a homogeneous strip, the normalized SIF for $\chi > 0$ (which is related to R_i/L through equations (2.106) and (2.116)) are calculated and compared with the results for $\chi=0$, (see Table 6-4). Also, the effect of the elastic foundation χ on the normalized SIF for a homogeneous strip with a fixed edge crack $b_1/L=0.5$ are shown in Table 6-7. In this Table, the limiting case $\chi=0$ means that the homogeneous strip has no elastic foundation. The case $\chi=\infty$ correspond to uniformly loaded strip of thickness $2L$ having symmetrically located coplanar edge cracks of depth b_1 on both surfaces. Note that in this case $u(L,y)=0$, $\sigma_{xy}(L,y)=0$, $-\infty < y < \infty$. As expected, the SIF is decreased for increasing χ .

To show the comparison between the homogeneous strip on an elastic foundation χ (which is related to R_i/L through the equation (2.106)) and a homogeneous cylinder the normalized SIFs for an edge crack under uniform tension are calculated and tabulated in Table 6-8 (see Nied [42] for cylinder results for $R_i/L=9.0$) . Also, the comparison between the transient temperature, thermal stress distribution and normalized SIF for the homogeneous strip on an elastic foundation and a hollow cylinder obtained from Nied [43] for $R_i/L=9.0$, are shown in Tables 6-9, 6-10, and 6-11, respectively.

Figures 6-39 - 6-62 show the normalized transient temperature and the thermal stress distribution in material pair A given by equations (2.80) and (2.100) for $\tau_0=0$, and equations (2.86) and (2.100) for $\tau_0 > 0$. The normalization of the temperature and the stress is similar to in Model I, varying with the

nondimensional distance $x^*=x/h_1$ and nondimensional time (Fourier Number) $\tau=tD_1/h_1^2$. The results are given for different values of $h_2/h_1=3.0, 9.0, 24.0$, and different values of cooling rate as measured by $\tau_0=t_0D_1/h_1^2$, where t_0 is the actual duration of the ramp cooling. The discontinuity in the slope of the temperature as well as the thermal stress have already been discussed in the previous section [6.1] for Model I. It is clear from the Figures that, at any instant in time and for fixed h_2/h_1 , the transient thermal stresses decrease as τ_0 increases.

The normalized SIFs for various crack geometries and different values of τ_0 and $h_2/h_1=3.0, 9.0, 24.0$ in material pair A are shown in Figures 6-63 - 6-107. These results correspond to the thermal history shown in Figures 6-39 - 6-62. The stiffness of the elastic foundation χ are taken to be function of R_i/L through the equation (2.106), where R_i is the inner radius of the cylinder and L is the total thickness (h_1+h_2). All the results are calculated based on $R_i/L=9.0$, which means that the thickness $L=h_1+h_2$ is fixed, but the ratio h_2/h_1 is varied.

The results of the normalized SIF for an edge crack in material 1 ($a_1=0$, $b_1 < h_1$), $k(b_1)/\sigma_0^T\sqrt{l_1}$, are shown in Figures 6-63 - 6-74. The variation of normalized SIF with time τ , for various edge crack lengths for $h_2/h_1=3.0$, $\tau_0=0.0, 6.0$, $h_2/h_1=9.0$, $\tau_0=0.0, 10.0$, and $h_2/h_1=24.0$, $\tau_0=0.0, 20.0$ are shown in Figures 6-63 - 6-64, Figures 6-67 - 6-68, and Figures 6-71 - 6-72, respectively. Also, Figures 6-65 - 6-66, Figures 6-69 - 6-70, and Figures 6-73 - 6-74 show the influence of the cooling rate τ_0 for a fixed edge crack and $h_2/h_1=3.0$, $b_1/h_1=0.2, 0.9$, $h_2/h_1=9.0$, $b_1/h_1=0.2, 0.9$, and $h_2/h_1=24.0$, $b_1/h_1=0.2, 0.9$, respectively. It is clear that, as the cooling rate or τ_0 increases, the maximum normalized SIF decrease. Noting that, the total thickness L of the clad and base material is fixed, and as h_2/h_1 increases the clad thickness h_1 decreases with respect to h_2 . So, by comparing Figures 6-63, 6-67 and 6-71 in which $\tau_0=0.0$ and

$h_2/h_1 = 3.0, 9.0, 24.0$ respectively, and by normalizing the crack length by L , i.e. l_1/L instead of l_1/h_1 , it can be seen that the maximum SIF for fixed edge crack length (l_1/L) would decrease as h_2/h_1 is increased, (see [1]). In the case of broken clad the influence of τ_0 for $h_2/h_1 = 3.0, 9.0, 24.0$ are shown in Figures 6-75 - 6-77.

The normalized SIF for under-clad crack at the crack tips a_2, b_2 ($a_2 = h_1$, $b_2 > h_1$), $k(a_2)/\sigma_0^T \sqrt{l_2/2}$, $k(b_2)/\sigma_0^T \sqrt{l_2/2}$ are shown in Figures 6-78 - 6-95. The normalized SIF at the crack tips, for various crack length for $h_2/h_1 = 9.0$ and $\tau_0 = 0.0, 10.0$ are shown in Figures 6-80 - 6-83. It is apparent that, initially the two crack tips have negative SIF, and then reach maximum values at different times. Also, it is clear that, the maximum normalized SIF at the crack tip b_2 is dropping faster than that at the crack tip just touching the interface ($a_2 = h_1$). The slope discontinuity in Figure 6-83 is due to the ramp function and takes place $\tau = \tau_0 = 10.0$. Figures 6-88 - 6-91 show the normalized SIF at the crack tips for $h_2/h_1 = 24.0$, $\tau_0 = 0.0, 20.0$. The transient behavior of the normalized SIFs at the crack tips $a_2 = h_1$ and b_2 for $l_2/h_1 = 9.0$ and $\tau_0 = 0.0, 20.0$ is shown in Figure 6-88 and Figure 6-90. The results of the normalized SIF at the crack tip b_2 for various crack length for $h_2/h_1 = 24.0$ and $\tau_0 = 0.0, 20.0$ are also shown in Figure 6-89 and Figure 6-91. Again the slope discontinuity which appears in Figure 6-91 is due to the ramp cooling and takes place at $\tau = \tau_0 = 20.0$. The influence of the cooling rate or τ_0 on the behavior of the normalized SIF for fixed length of under-clad crack and for $h_2/h_1 = 3.0$, $l_2/h_1 = 0.004$, $h_2/h_1 = 9.0$, $l_2/h_1 = 1.0, 3.0$, and $h_2/h_1 = 24.0$, $l_2/h_1 = 0.5, 4.0$, at the crack tips a_2, b_2 are shown in Figures 6-78 - 6-79, Figures 6-84 - 6-87, and Figures 6-92 - 6-95, respectively.

The transient normalized SIFs for an edge crack going through the interface ($a_1 = 0$, $b_1 = a_2 = h_1$, $b_2 > h_1$) are plotted in Figures 6-96 - 6-107. Figures 6-96 - 6-97, Figures 6-100 - 6-101, and Figures 6-104 - 6-105 show the variation as a function of time τ for various crack length and for $h_2/h_1 = 3.0$, $\tau_0 = 0.0, 6.0$,

$h_2/h_1=9.0$, $\tau_0=0.0, 10.0$, and $h_2/h_1=24.0$, $\tau_0=0.0, 20.0$, respectively. The influence of τ_0 on the normalized SIF for fixed crack length for $h_2/h_1=3.0$, $b_2/h_1=1.2, 2.0$, $h_2/h_1=9.0$, $b_2/h_1=1.5, 4.0$, and $h_2/h_1=24.0$, $b_2/h_1=1.5, 5.0$, are shown in Figures 6-98 - 6-99, Figures 6-102 - 6-103, and 6-106 - 6-107, respectively. It is seen that for any given crack length the normalized SIF increases until it reaches a maximum value and then decreases as τ increases. Also, as the cooling rate or τ_0 increases the maximum value of the normalized SIF decreases for any fixed crack length.

Tables 6-12 - 6-14 give the maximum of normalized SIFs for an under-clad crack ($a_2=h_1$, $b_2 > h_1$), and their comparison with the results obtained by Nied [1]. Similarly Tables 6-15 - 6-17 give the maximum of normalized SIFs for an edge crack crossing the interface ($a_1=0$, $b_1=a_2=h_1$, $b_2 > h_1$, $\tau_0=0.0$) and their comparison with the results of Nied [1]. Note that, in this study the analytical solution of the temperature, thermal stresses and the crack problem is based on R_i/L being very large. In Nied's work [1], $R_i/L=9.0$ which still corresponds to a relatively thick cylinder.

The normalized transient temperature and thermal stress distributions in material pair B for $h_2/h_1=9.0$ as given by equations (2.80) and (2.100) for $\tau_0=0.0$, and equations (2.86) and (2.100) for $\tau_0 > 0$, are shown in Figures 6-108 - 6-115. The stress discontinuity at the interface is due to the difference in Young's modulus and coefficient of thermal expansion ($E_1 \neq E_2$, $\alpha'_1 \neq \alpha'_2$).

Figures 6-116 - 6-117 represent the transient normalized SIF for various lengths of an edge crack ($a_1=0$, $b_1 < h_1$) for $\tau_0=0.0, 10.0$. It is clear that, since $E_1 > E_2$, the maximum normalized SIF would increase to ∞ as b_1 approaches the interface. The effect of τ_0 on the normalized SIF for an edge crack having a fixed length $b_1/h_1=0.2$ is shown in Figure 6-118. The influence of τ_0 on the normalized SIF for broken clad ($a_1=0$, $b_1=h_1$) is shown in Figure 6-119, in this case the

singularity at the crack tip $b_1=h_1$ is equal to $\beta_1=0.552538$. As expected, the singularity is greater than $1/2$ because $E_1 > E_2$.

In case of under-clad crack for material pair B ($a_2=h_1$, $b_2 > h_1$) , the normalized SIF $k(a_2)/\sigma_0^T(l_2/2)^{\alpha_2}$, $k(b_2)/\sigma_0^T\sqrt{l_2/2}$, at the crack tips a_2, b_2 for $\tau_0=0.0, 10.0$ are shown in Figures 6-120 - 6-121, and Figures 6-122 - 6-123, respectively. Since the crack touches the interface from material (2) and since $E_1 > E_2$, the singularity is less than $1/2$, and is equal to $\alpha_2=0.4512416$. The effect of the cooling rate or τ_0 on the normalized SIFs at the crack tips $a_2=h_1$ and b_2 for a fixed crack length $l_2/h_1=1.0$ is shown in Figures 6-124 - 6-125.

The normalized SIFs for an edge crack crossing the interface ($a_1=0$, $b_1=a_2=h_1$, $b_2 > h_1$) in material pair B, for $\tau_0=0.0$ and 10.0 are shown in Figures 6-126 - 6-128, and Figures 6-129 - 6-131, respectively. The normalized SIFs $k_x/\sigma_0^T\beta_1$, $k_{xy}/\sigma_0^T\beta_1$ control the tensile and shear cleavage stresses at the interface. The singularity at the interface is equal to $\beta_1=\alpha_2=0.01872238$. The influence of τ_0 on the normalized SIFs at the interface $x=h_1$, $y > 0$, and the crack tip b_2 for a fixed crack length $b_2/h_1=1.5$, is shown in Figures 6-132 - 6-134.

6.3 Conclusions

Very often in transient thermal stress analysis it is assumed that the relevant thermal boundary condition is a step change in temperature which is used as a model to describe the sudden cooling or heating at the boundary. In the case of clad pressure vessels, the temperature of the inner wall of the cylinder is suddenly brought down to the temperature of the cooling liquid (from 288° c to 20° c). A simple calculation would show that under this idealized thermal boundary condition the maximum thermal stress in the clad would exceed the corresponding yield strength of the material (which, for austenitic

steel, is 390 MN/m^2). It is therefore, clear that in this case the unit step function in temperature is not a realistic representation of the actual boundary condition. By using a more realistic thermal boundary condition such as ramp function with cooling rate measured by the ramp duration τ_0 , the peak values of the thermal stresses as well as the maximum stress intensity factors are shown to reduce below the corresponding values given by the step function temperature boundary condition.

In Model I it is seen that the stress intensity factors are monotonically increasing functions of time. This implies that in this case the fracture process would be unstable. On the other hand in the composite plate represented by Model II, invariably the stress intensity factors increase, going through a maximum and then tend to their steady state values asymptotically. In some cases the under-clad crack may have initially negative stress intensity factors. In such cases it should be understood that the negative stress intensity factors may have a meaning only when they are used in a superposition with other loading conditions in such a way that the resulting stress intensity factor is positive.

The transient thermal stresses are strongly dependent on the material properties. Thus, the steady state thermal stresses and consequently the corresponding stress intensity factors for material pairs A and B are found to be opposite in sign.

The results show that the initial flaw (the edge or the internal crack) in a coated medium subjected to transient thermal loading generally tend to propagate towards the interface. Since the power of singularity for a crack terminating at the interface is not $1/2$, the propagating crack would slow down and possibly be arrested if it is located in the less stiff side of the interface and would grow faster if it is in the stiffer material. The process of the propagating

crack to cross the interface would be controlled by the relative magnitudes of material toughness and energy release rate.

The effect of the clad yielding on the stress intensity factors for an under-clad crack in Model I was investigated and it was shown in Table 6-3 that for a fixed crack length the stress intensity factor is higher in the yielded clad case than that for the elastic clad. Also, as the thermal stresses increase yielding in the clad would cause an increase in the stress intensity factor.

As expected, it was found that an increase in the stiffness (χ) of the elastic foundation would cause a decrease in the stress intensity factors as it increased.

The results for the beam on an elastic foundation showed very good agreement with that obtained from the axisymmetric elasticity solution for a thick-walled cylinder, indicating that the model can be used quite satisfactory to study the highly complicated problem of a composite cylinder containing a circumferential crack.

6.4 Suggestions for Future Research

The way by which the crack problem in a composite beam on an elastic foundation was formulated in this study would benefit the future research as an extension of our work in the following areas :

- i. The cracking of layered materials perpendicular to the interface with a stress free boundary ($\chi=0$) under residual and transient thermal stresses.
- ii. The cracking of fully constrained layered materials perpendicular to the interface under residual and transient thermal stresses.

Other interesting problems can also be done in the future such as :

- iii. The cracking of layered materials along the interface with free and fully constrained boundaries under residual and transient thermal stresses.

- iv. The cracking of layered materials perpendicular to and along the interface under residual and transient thermal stresses.
- v. The "free-end" problem in bonded layers under thermal cycling.

Table 6-1: Properties of materials pairs used in this work

	k'_2 / k'_1	D_2 / D_1	α'_2 / α'_1	E_2 / E_1	ν_2 / ν_1
material pair A	3	3	0.75	1	1
material pair B	3.385	4.070	2.2939	0.6111	1

Table 6-2: Normalized stress intensity factor for an embedded crack (equation (6.6)), obtained from the plastic strip model, $\tau_0=0.0$, $\sigma_0^T = -\alpha'_1 E_1 \Theta_0 / (1 - \nu_1)$, for Model I. (Material pair A)

l_2 / h	$k_1^*(b_2)$ as $\tau \rightarrow \infty$	$k_2^*(b_2)$
0.025	9.8776	- 8.9580
1.0	1.9008	- 0.8354
4.0	1.4048	- 0.2598
6.5	1.3450	- 0.1882

Table 6-3: Comparison of the normalized stress intensity factors obtained from a yielded clad and an elastic clad for various values of the crack length, $\tau_0=0.0$, $\sigma_0^T = -\alpha'_1 E_1 \Theta_0 / (1 - \nu_1)$, for Model I. (Material pair A)

$k(b_2) / \sigma_0^T \sqrt{l_2/2}$ as $\tau \rightarrow \infty$ (yield clad)					$k(b_2) / \sigma_0^T \sqrt{l_2/2}$ as $\tau \rightarrow \infty$ (elastic clad)
l_2 / h	$\sigma_F / \sigma_0^T = 1$	1 / 2	1 / 5	1 / 10	
0.025	0.92157	5.39959	8.08640	8.98201	0.7554
1.0	1.06539	1.48309	1.73372	1.81726	0.7740
4.0	1.14489	1.27478	1.35272	1.37870	0.8285
6.5	1.17684	1.26092	1.31138	1.32820	0.8532

Table 6-4: Normalized stress intensity factors for an edge crack in a homogeneous strip of thickness L under uniform load σ_0 (without elastic foundation, $\chi=0.0$ and with elastic foundation $R_i/L=9.0$ and $\chi L/E=0.01108$)

	Kaya	present work	
b_1 / L	$k(b_1) / \sigma_0 \sqrt{b_1}, \chi=0$	$k(b_1) / \sigma_0 \sqrt{b_1}, \chi=0$	$k(b_1) / \sigma_0 \sqrt{b_1}, R_i / L = 9.0$
0.001	1.1215	1.1215	1.1215
0.1	1.1892	1.1892	1.1574
0.2	1.3673	1.3673	1.2725
0.3	1.6599	1.6599	1.4267
0.4	2.1114	2.1114	1.5983
0.5	2.8246	2.8246	1.8135
0.6	4.0332	4.0332	2.0775
0.7	6.3549	6.3553	2.3801
0.8	11.955	11.958	2.7399
0.85	18.628	18.635	2.9835
0.9	34.632	34.641	3.3660

Table 6-5: Normalized stress intensity factors for a crack terminating at the interface under uniform load σ_0 , ($l_2/h_1=0.1$ in the present work).

		$k(a_2) / \sigma_0 \sqrt{l_2/2}$	$k(b_2) / \sigma_0 \sqrt{l_2/2}$
Aluminum-Epoxy $\nu_1=0.3$, $\nu_2=0.35$ $\mu_1/\mu_2=23.077$ $\alpha_2=0.3381$	Kaya present work	2.7997 2.7948	0.8826 0.8842
Epoxy-Aluminum $\nu_1=0.35$, $\nu_2=0.3$ $\mu_1/\mu_2=0.0433$ $\alpha_2=0.8248$	Kaya present work	0.0955 0.0983	1.3398 1.3403

Table 6-6: Normalized stress intensity factors for an embedded crack going through the interface under loading $P_1/P_2=(E_1/E_2)(1-\nu_2^2/1-\nu_1^2)$, $\nu_1=0.3$, $\nu_2=0.35$, $\mu_1/\mu_2=23.077$, $\beta=\beta_1=\alpha_2=0.273692$, $l_1/h_1=0.1$, $l_2/h_1=0.05, 0.025$.

l_2/l_1		$\frac{k(a_1)}{P_1 \sqrt{l/2}}$	$\frac{k_z}{P_1 (l/2)^\beta}$	$\frac{k_{zy}}{P_1 (l/2)^\beta}$	$\frac{k(b_2)}{P_2 \sqrt{l/2}}$
0.5	present work	1.2408	- 0.08127	- 0.02034	1.5528
	Erd. & Biri.	1.2378	- 0.05900	- 0.02158	1.5561
0.25	present work	1.3409	- 0.08458	- 0.03088	2.1320
	Erd. & Biri.	1.3324	- 0.08113	- 0.03184	2.1391

Table 6-7: Normalized stress intensity factors for an edge crack in a homogeneous strip of thickness L under uniform stress σ_0 and for fixed crack length $b_1/L=0.5$, various values of χ (stiffness of the elastic foundation)

$\chi L, N/m^2$	$k(b_1) / \sigma_0 \sqrt{b_1}$
0.0	2.8248
10^3	2.8238
10^6	2.5282
10^9	1.8940
10^{12}	1.2000
10^{15}	1.1693
10^{20}	1.1601
∞	1.1546

Table 6-8: Comparison between normalized stress intensity factors for an edge crack under uniform loading σ_0 in a homogeneous strip on an elastic foundation χ , and a homogeneous cylinder $R_i/L=9.0$.

b_1 / L	$k(b_1) / \sigma_0 \sqrt{b_1}$	$k(b_1) / \sigma_0 \sqrt{b_1}$
	cylinder	strip
0.1	1.158	1.1574
0.2	1.253	1.2725
0.3	1.392	1.4267
0.4	1.568	1.5983
0.5	1.779	1.8135
0.6	2.025	2.0775

Table 6-9: Comparison between transient temperature distribution Θ/Θ_0 for a hollow cylinder and a homogeneous strip on an elastic foundation χ due to a unit step temperature change on the inner wall, $R_i/L=9.0$ and $\chi L/E=0.01108$, $\tau=tD/L^2$.

x/L	$\Theta/\Theta_0, \tau=0.01$		$\Theta/\Theta_0, \tau=0.05$	
	Nied	present work	Nied	present work
0.00	1.000	1.000	1.000	1.000
0.05	0.723	0.724	0.872	0.874
0.10	0.477	0.480	0.748	0.752
0.15	0.288	0.289	0.630	0.635
0.20	0.158	0.157	0.521	0.527
0.25	0.076	0.077	0.423	0.429
0.30	0.033	0.034	0.337	0.343
0.35	0.013	0.013	0.263	0.268
0.40	0.005	0.005	0.201	0.206
0.45	0.001	0.001	0.151	0.155
0.50	0.000	0.000	0.111	0.114
0.55	0.000	0.000	0.080	0.082
0.60	0.000	0.000	0.058	0.058
0.65	0.000	0.000	0.038	0.040
0.70	0.000	0.000	0.026	0.027
0.75	0.000	0.000	0.017	0.018
0.80	0.000	0.000	0.011	0.012
0.85	0.000	0.000	0.007	0.007
0.90	0.000	0.000	0.005	0.005
0.95	0.000	0.000	0.003	0.003
1.00	0.000	0.000	0.003	0.003

table 6-9, continued

x/L	$\theta/\theta_0, \tau=0.1$		$\theta/\theta_0, \tau=0.5$	
	Nied	present work	Nied	present work
0.00	1.000	1.000	0.999	1.000
0.05	0.908	0.911	0.987	0.971
0.10	0.818	0.823	0.937	0.942
0.15	0.731	0.737	0.906	0.913
0.20	0.648	0.655	0.877	0.885
0.25	0.568	0.576	0.848	0.858
0.30	0.494	0.502	0.820	0.832
0.35	0.426	0.434	0.794	0.806
0.40	0.363	0.371	0.769	0.782
0.45	0.307	0.315	0.745	0.759
0.50	0.257	0.264	0.723	0.738
0.55	0.213	0.220	0.703	0.718
0.60	0.176	0.181	0.685	0.700
0.65	0.144	0.149	0.668	0.684
0.70	0.117	0.121	0.654	0.670
0.75	0.095	0.099	0.641	0.657
0.80	0.078	0.081	0.631	0.647
0.85	0.065	0.067	0.623	0.639
0.90	0.056	0.058	0.617	0.634
0.95	0.050	0.053	0.614	0.630
1.00	0.048	0.051	0.613	0.629

Table 6-10: Comparison between Stress distribution σ_{yy}/σ_0 for a hollow cylinder and a homogeneous strip on an elastic foundation χ due to a unit step temperature change on the inner wall, $R_i/L=9.0$ and $\chi L/E=0.01108$, $\tau=tD/L^2$.

x/L	$\sigma_{yy}/\sigma_0^T, \tau=0.01$		$\sigma_{yy}/\sigma_0^T, \tau=0.05$	
	Nied	present work	Nied	present work
0.00	0.892	0.8872	0.758	0.7477
0.05	0.814	0.8108	0.630	0.6221
0.10	0.369	0.3666	0.508	0.4995
0.15	0.179	0.1760	0.388	0.3829
0.20	0.048	0.0445	0.280	0.2748
0.25	- 0.031	- 0.0357	0.182	0.1769
0.30	- 0.074	- 0.0789	0.096	0.0905
0.35	- 0.094	- 0.0995	0.022	0.0161
0.40	- 0.103	- 0.1082	- 0.040	- 0.0464
0.45	- 0.106	- 0.1114	- 0.091	- 0.0976
0.50	- 0.107	- 0.1124	- 0.131	- 0.1385
0.55	- 0.107	- 0.1127	- 0.162	- 0.1703
0.60	- 0.107	- 0.1128	- 0.186	- 0.1945
0.65	- 0.107	- 0.1128	- 0.203	- 0.2125
0.70	- 0.107	- 0.1128	- 0.216	- 0.2254
0.75	- 0.107	- 0.1128	- 0.224	- 0.2345
0.80	- 0.107	- 0.1128	- 0.230	- 0.2308
0.85	- 0.107	- 0.1128	- 0.234	- 0.2449
0.90	- 0.107	- 0.1128	- 0.237	- 0.2474
0.95	- 0.107	- 0.1128	- 0.238	- 0.2488
1.00	- 0.107	- 0.1128	- 0.239	- 0.2492

table 6-10, continued

x / L	$\sigma_{yy} / \sigma_0^T, \tau = 0.1$		$\sigma_{yy} / \sigma_0^T, \tau = 0.5$	
	Nied	present work	Nied	present work
0.00	0.658	0.6432	0.251	0.2361
0.05	0.585	0.5542	0.220	0.2089
0.10	0.475	0.4683	0.189	0.1780
0.15	0.388	0.3805	0.159	0.1495
0.20	0.304	0.2979	0.129	0.1215
0.25	0.225	0.2194	0.100	0.0942
0.30	0.151	0.1457	0.073	0.0677
0.35	0.083	0.0772	0.046	0.0423
0.40	0.020	0.0146	0.021	0.0181
0.45	- 0.038	- 0.0420	- 0.002	- 0.0047
0.50	- 0.088	- 0.0925	- 0.025	- 0.0261
0.55	- 0.130	- 0.1369	- 0.045	- 0.0459
0.60	- 0.167	- 0.1754	- 0.063	- 0.0639
0.65	- 0.200	- 0.2082	- 0.080	- 0.0801
0.70	- 0.226	- 0.2356	- 0.094	- 0.0943
0.75	- 0.248	- 0.2581	- 0.106	- 0.1065
0.80	- 0.265	- 0.2759	- 0.117	- 0.1168
0.85	- 0.279	- 0.2894	- 0.125	- 0.1245
0.90	- 0.288	- 0.2988	- 0.130	- 0.1302
0.95	- 0.293	- 0.3043	- 0.134	- 0.1336
1.00	- 0.295	- 0.3061	- 0.135	- 0.1347

Table 6-11: Comparison between normalized stress intensity factors for an edge crack subjected to transient thermal stresses in a hollow cylinder and a homogeneous strip on an elastic foundation χ , $R_i/L=9.0$ and $\chi L/E=0.01108$, $\tau=tD/L^2$, $\sigma_0^T=-\alpha E \Theta_0/(1-\nu)$.

b_1 / L	$k(b_1) / \sigma_0^T \sqrt{b_1}, \tau = 0.01$		$k(b_1) / \sigma_0^T \sqrt{b_1}, \tau = 0.05$	
	Nied	present work	Nied	present work
0.01	0.962	0.9588	0.833	0.8214
0.1	0.657	0.6532	0.701	0.6913
0.2	0.426	0.4316	0.589	0.5916
0.3	0.300	0.3072	0.501	0.5094
0.4	0.238	0.2402	0.432	0.4353
0.5	0.205	0.2066	0.378	0.3793
0.6	0.185	0.1868	0.334	0.3369

b_1 / L	$k(b_1) / \sigma_0^T \sqrt{b_1}, \tau = 0.1$		$k(b_1) / \sigma_0^T \sqrt{b_1}, \tau = 0.5$	
	Nied	present work	Nied	present work
0.01	0.724	0.7093	0.277	0.2608
0.1	0.633	0.6207	0.247	0.2327
0.2	0.560	0.5589	0.224	0.2147
0.3	0.502	0.5069	0.206	0.1997
0.4	0.453	0.4536	0.190	0.1829
0.5	0.408	0.4085	0.174	0.1677
0.6	0.367	0.3687	0.158	0.1529

Table 6-12: The maximum of normalized stress intensity factors for an under-clad crack subjected to transient thermal stresses, $h_2/h_1=3.0$, $R_i/L=9.0$ and $\chi L/E_2=0.01108$. (material pair A).

	Nied		present work			
l_2/h_1	$\tau = 0.0$		$\tau = 0.0$		$\tau = 1.0$	
	$\frac{k(a_2)}{\sigma_0 T \sqrt{l_2/2}}$	$\frac{k(b_2)}{\sigma_0 T \sqrt{l_2/2}}$	$\frac{k(a_2)}{\sigma_0 T \sqrt{l_2/2}}$	$\frac{k(b_2)}{\sigma_0 T \sqrt{l_2/2}}$	$\frac{k(a_2)}{\sigma_0 T \sqrt{l_2/2}}$	$\frac{k(b_2)}{\sigma_0 T \sqrt{l_2/2}}$
0.004	0.0114	0.0111	0.0068	0.0065	0.0051	0.0048
0.040	0.0101	0.0073	0.0056	0.0027		
0.200	0.0046	- 0.0088	0.0000	- 0.0138		
0.400	- 0.0022	- 0.0277	- 0.0071	- 0.0333		
0.600	- 0.0090	- 0.0453	- 0.0142	- 0.0514		

Table 6-13: The maximum of normalized stress intensity factors for an under-clad crack subjected to transient thermal stresses, $h_2/h_1=9.0$, $R_i/L=9.0$ and $\chi L/E_2=0.01108$. (material pair A).

	Nied		present work			
l_2/h_1	$\tau = 0.0$		$\tau = 0.0$		$\tau = 10.0$	
	$\frac{k(a_2)}{\sigma_0 T \sqrt{l_2/2}}$	$\frac{k(b_2)}{\sigma_0 T \sqrt{l_2/2}}$	$\frac{k(a_2)}{\sigma_0 T \sqrt{l_2/2}}$	$\frac{k(b_2)}{\sigma_0 T \sqrt{l_2/2}}$	$\frac{k(a_2)}{\sigma_0 T \sqrt{l_2/2}}$	$\frac{k(b_2)}{\sigma_0 T \sqrt{l_2/2}}$
0.01	0.2245	0.2240	0.2270	0.2264	0.2032	0.2027
0.5	0.2150	0.1897	0.2171	0.1915	0.1945	0.1717
1.0	0.2080	0.1589	0.2101	0.1603	0.1883	0.1437
2.0	0.1951	0.1030	0.1950	0.1018	0.1749	0.0908
3.0	0.1800	0.0523	0.1790	0.0498	0.1604	0.0429
4.0	0.1618	0.0066	0.1604	0.0026	0.1434	- 0.0002

Table 6-14: The maximum of normalized stress intensity factors for an under-clad crack subjected to transient thermal stresses, $h_2/h_1=24.0$, $R_i/L=9.0$ and $\chi L/E_2=0.01108$. (material pair A).

	<div>Nied</div> <div>present work</div>					
l_2/h_1	$\tau = 0.0$		$\tau = 0.0$		$\tau = 20.0$	
	$\frac{k(a_2)}{\sigma_0 T \sqrt{l_2/2}}$	$\frac{k(b_2)}{\sigma_0 T \sqrt{l_2/2}}$	$\frac{k(a_2)}{\sigma_0 T \sqrt{l_2/2}}$	$\frac{k(b_2)}{\sigma_0 T \sqrt{l_2/2}}$	$\frac{k(a_2)}{\sigma_0 T \sqrt{l_2/2}}$	$\frac{k(b_2)}{\sigma_0 T \sqrt{l_2/2}}$
0.025	0.3908	0.3899	0.3980	0.3971	0.3877	0.3869
0.5	0.3873	0.3701	0.3941	0.3766	0.3842	0.3677
1.5	0.3904	0.3369	0.3980	0.3436	0.3886	0.3365
4.0	0.4006	0.2622	0.4057	0.2657	0.3974	0.2612
9.0	0.3919	0.1309	0.3942	0.1306	0.3874	0.1285
14.0	0.3494	0.0200	0.3520	0.0166	0.3463	0.0161

Table 6-15: The maximum of normalized stress intensity factors for an edge crack subjected to transient thermal stresses, $h_2/h_1=3.0$, $R_i/L=9.0$ and $\chi L/E_2=0.01108$. (material pair A).

	Nied	present work	
l/h_1	$\tau = 0.0$	$\tau = 0.0$	$\tau = 6.0$
	$\frac{k(b_2)}{\sigma_0 T \sqrt{l}}$	$\frac{k(b_2)}{\sigma_0 T \sqrt{l}}$	$\frac{k(b_2)}{\sigma_0 T \sqrt{l}}$
1.004	0.4760	0.4629	0.3793
1.2	0.4097	0.4000	0.3143
1.4	0.3726	0.3574	0.2779
1.6	0.3449	0.3252	0.2515
2.0	0.3062	0.2759	0.2127

Table 6-16: The maximum of normalized stress intensity factors for an edge crack subjected to transient thermal stresses, $h_2/h_1=9.0$, $R_i/L=9.0$ and $\chi L/E_2=0.01108$. (material pair A).

	Nied	present work	
l/h_1	$\tau = 0.0$	$\tau = 0.0$	$\tau = 10.0$
	$\frac{k(b_2)}{\sigma_0 T \sqrt{l}}$	$\frac{k(b_2)}{\sigma_0 T \sqrt{l}}$	$\frac{k(b_2)}{\sigma_0 T \sqrt{l}}$
1.01	0.6090	0.6298	0.5898
1.5	0.4740	0.5050	0.4683
2.0	0.4151	0.4529	0.4196
3.0	0.3461	0.4044	0.3751
4.0	0.3034	0.3867	0.3589
5.0	0.2722	0.3839	0.3567

Table 6-17: The maximum of normalized stress intensity factors for an edge crack subjected to transient thermal stresses, $h_2/h_1=24.0$, $R_i/L=9.0$ and $\chi L/E_2=0.01108$. (material pair A).

	Nied	present work	
l/h_1	$\tau = 0.0$	$\tau = 0.0$	$\tau = 20.0$
	$\frac{k(b_2)}{\sigma_0 T \sqrt{l}}$	$\frac{k(b_2)}{\sigma_0 T \sqrt{l}}$	$\frac{k(b_2)}{\sigma_0 T \sqrt{l}}$
1.025	0.7383	0.7531	0.7372
1.5	0.6136	0.6307	0.6168
2.0	0.5554	0.5708	0.5589
5.0	0.4071	0.4353	0.4282
7.5	0.3531	0.4172	0.4110

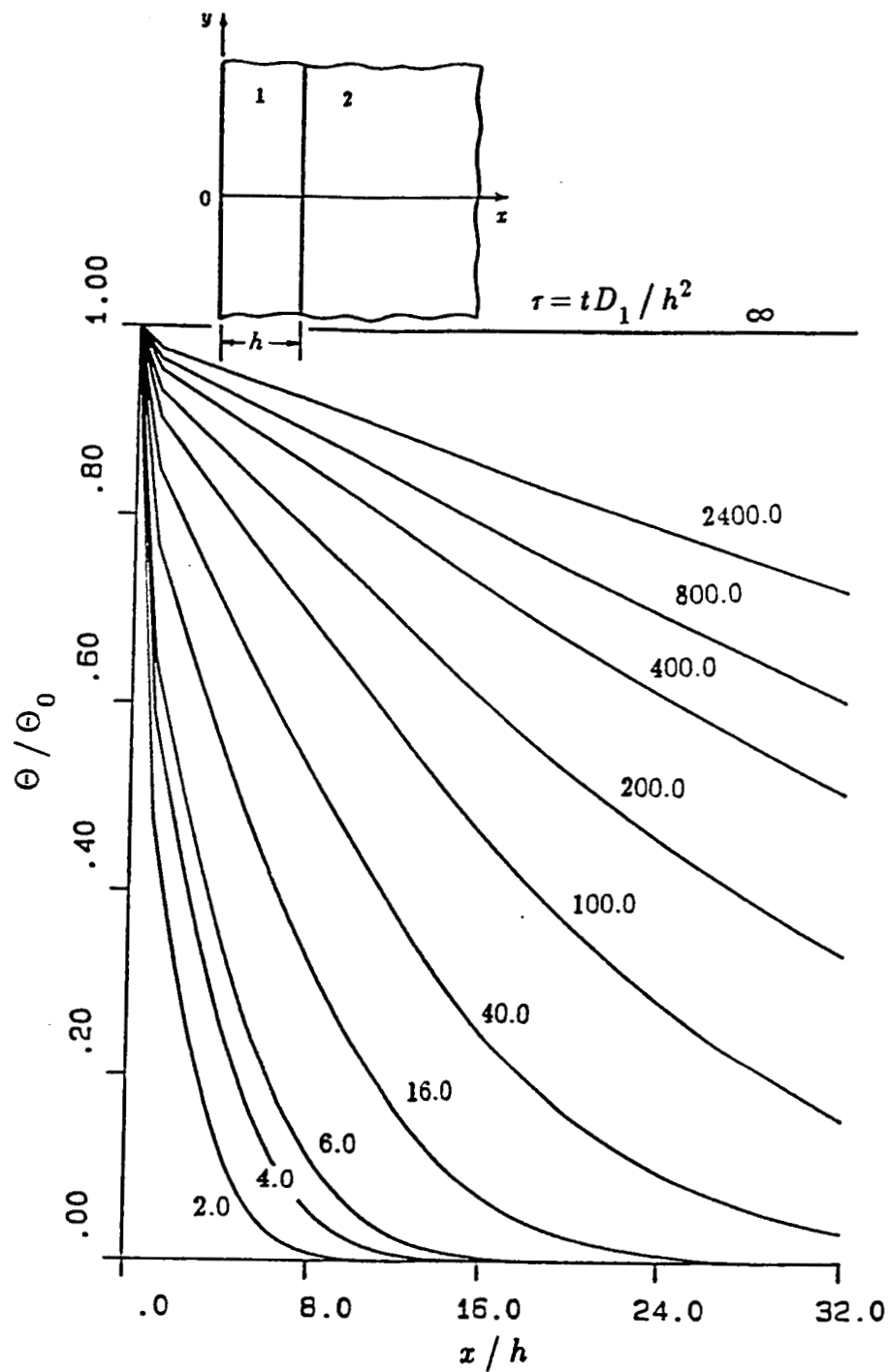


Figure 6-1: The normalized transient temperature distribution in Model I for $\tau_0=0.0$, $\tau_0=t_0D_1/h^2$, (Material pair A)

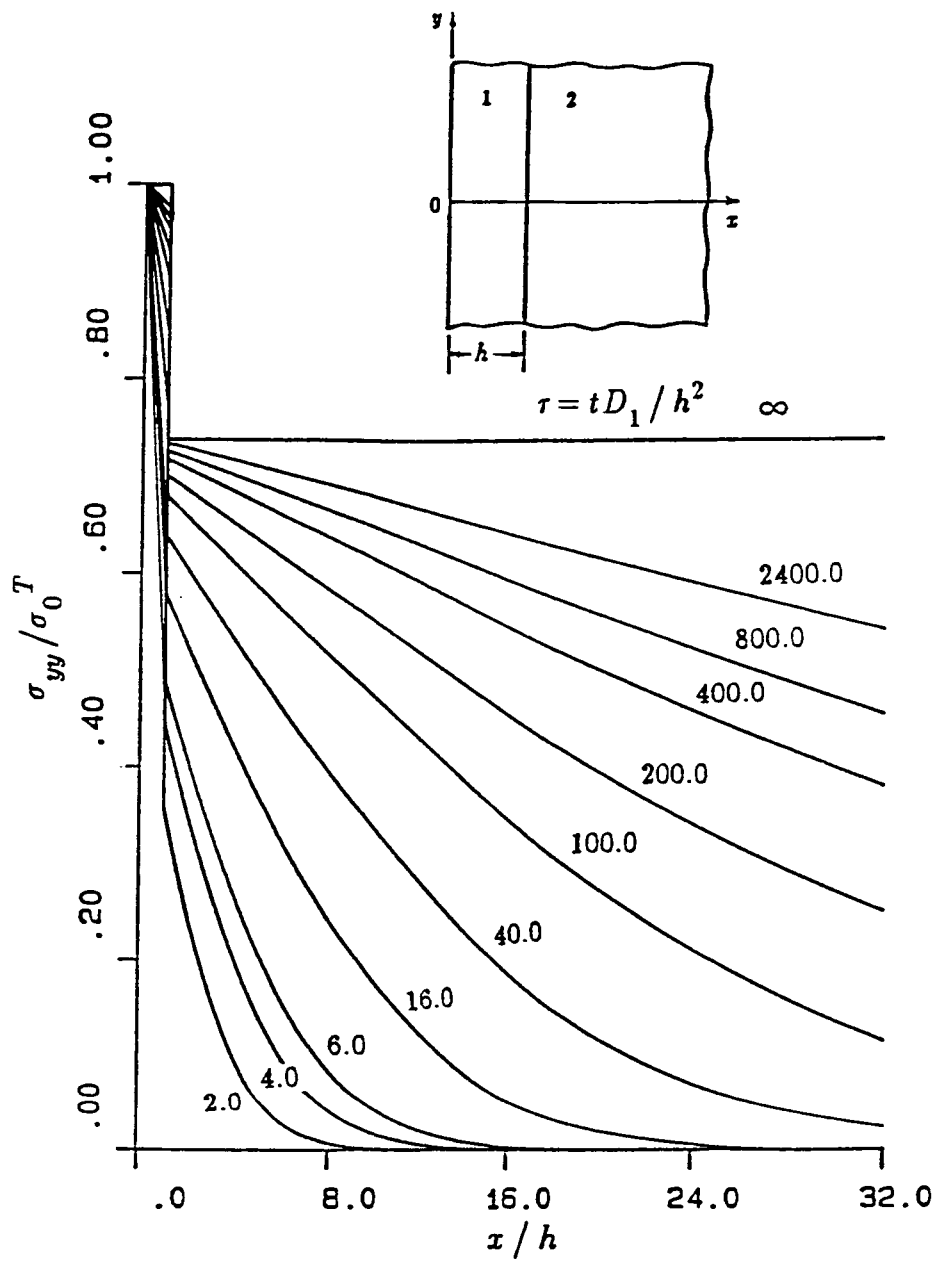


Figure 6-2: The normalized transient stress distribution σ_{yy}/σ_0^T in Model I for $\tau_0=0.0, \tau_0=t_0D_1/h^2, \sigma_0^T=-\alpha_1'E_1\Theta_0/(1-\nu_1)$. (Material pair A)

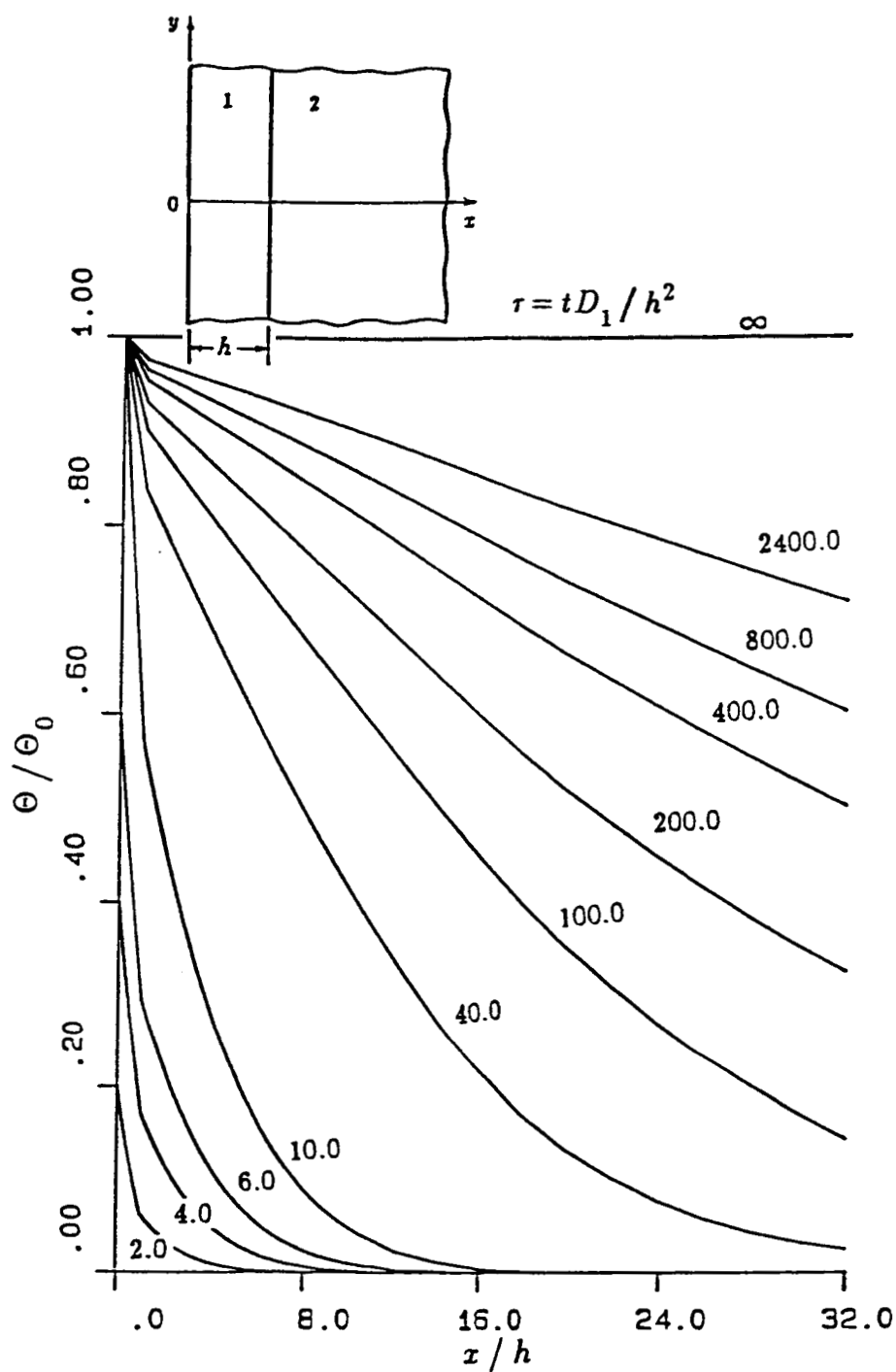


Figure 6-3: The normalized transient temperature distribution in Model I for $\tau_0 = 10.0$, $\tau_0 = t_0 D_1 / h^2$, (Material pair A)

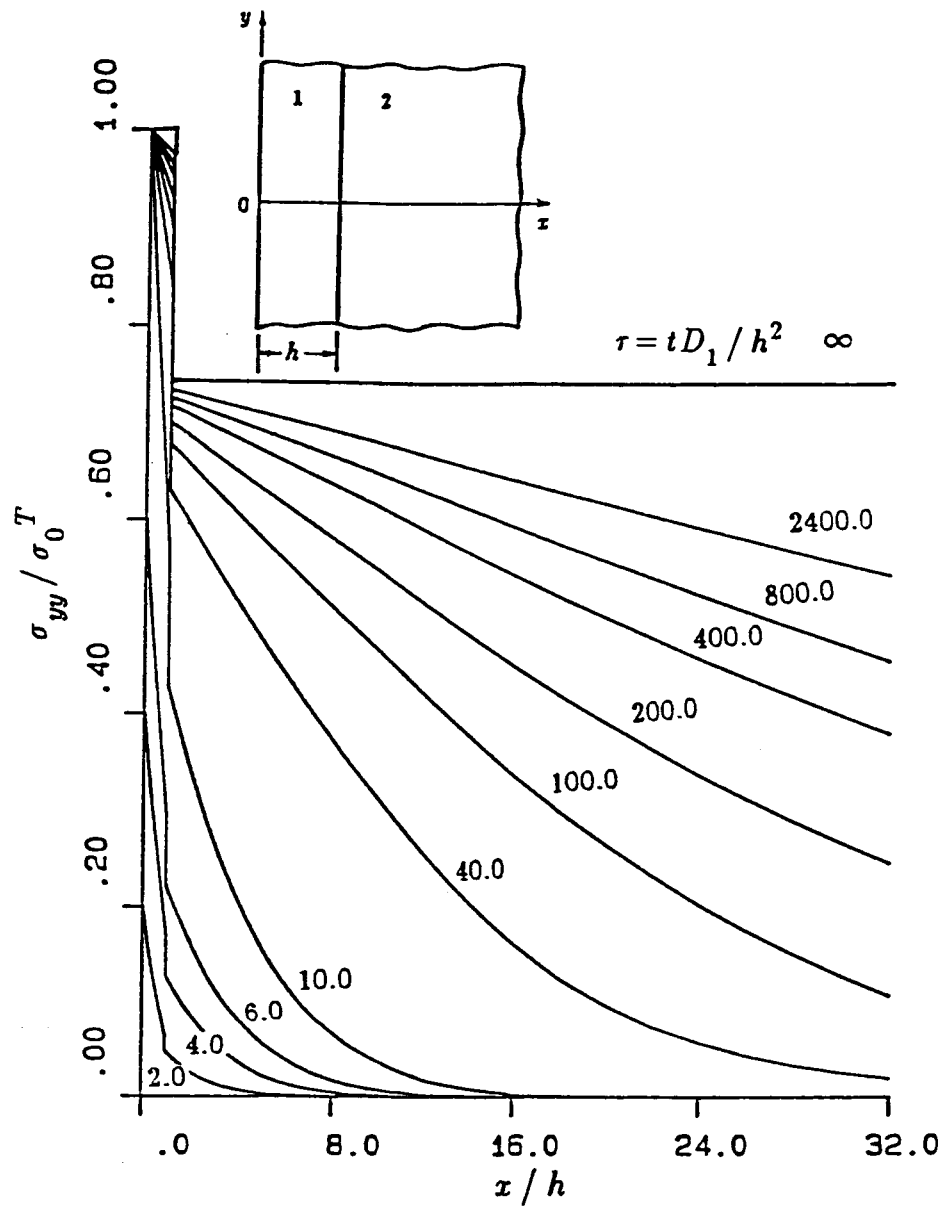


Figure 6-4: The normalized transient stress distribution σ_{yy}/σ_0^T in Model I for $\tau_0=10.0$, $\tau_0=t_0D_1/h^2$, $\sigma_0^T=-\alpha_1' E_1 \Theta_0/(1-\nu_1)$ (Material pair A)

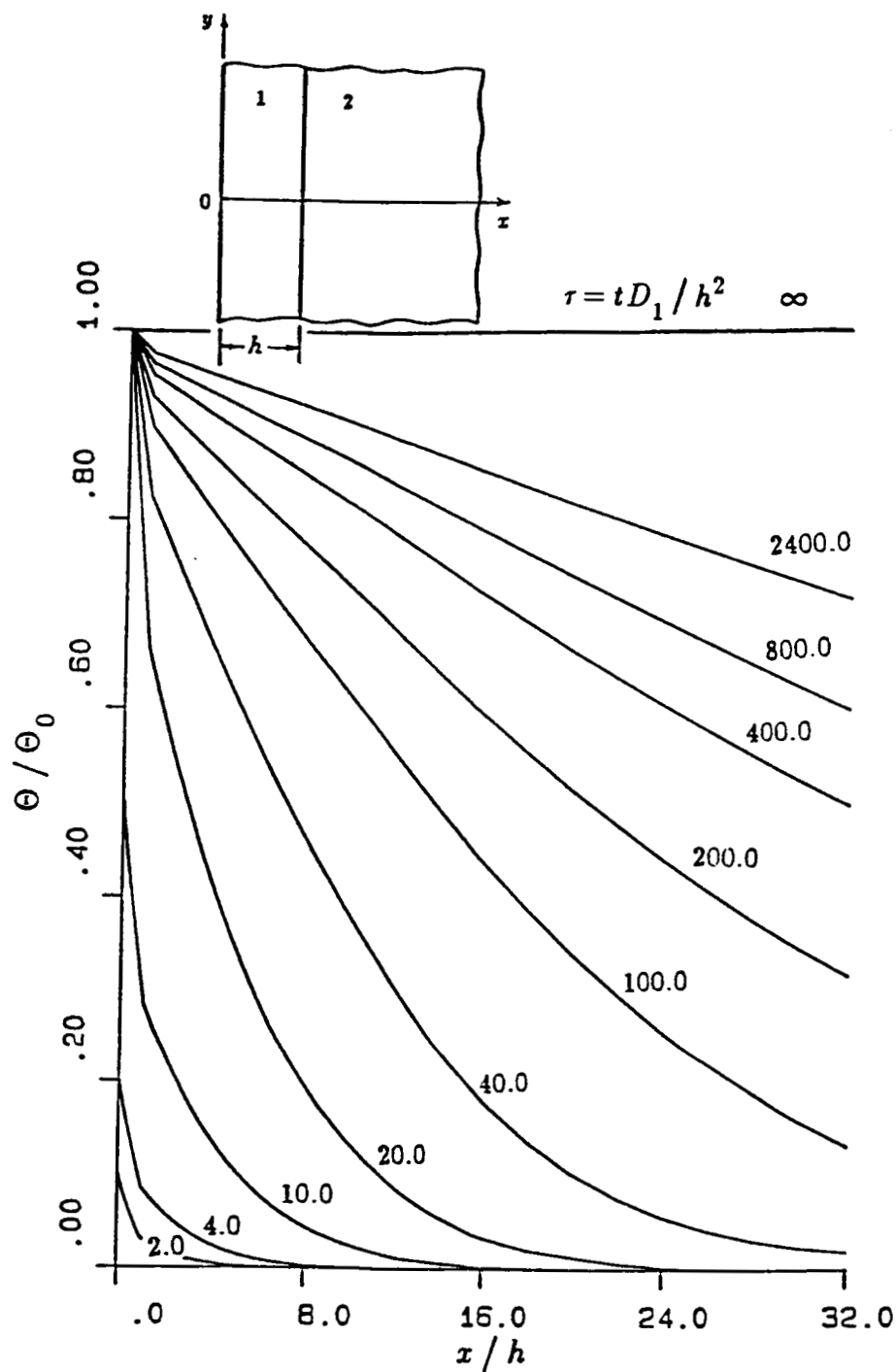


Figure 6-5: The normalized transient temperature distribution in Model I for $\tau_0 = 20.0$, $\tau_0 = t_0 D_1 / h^2$, (Material pair A)

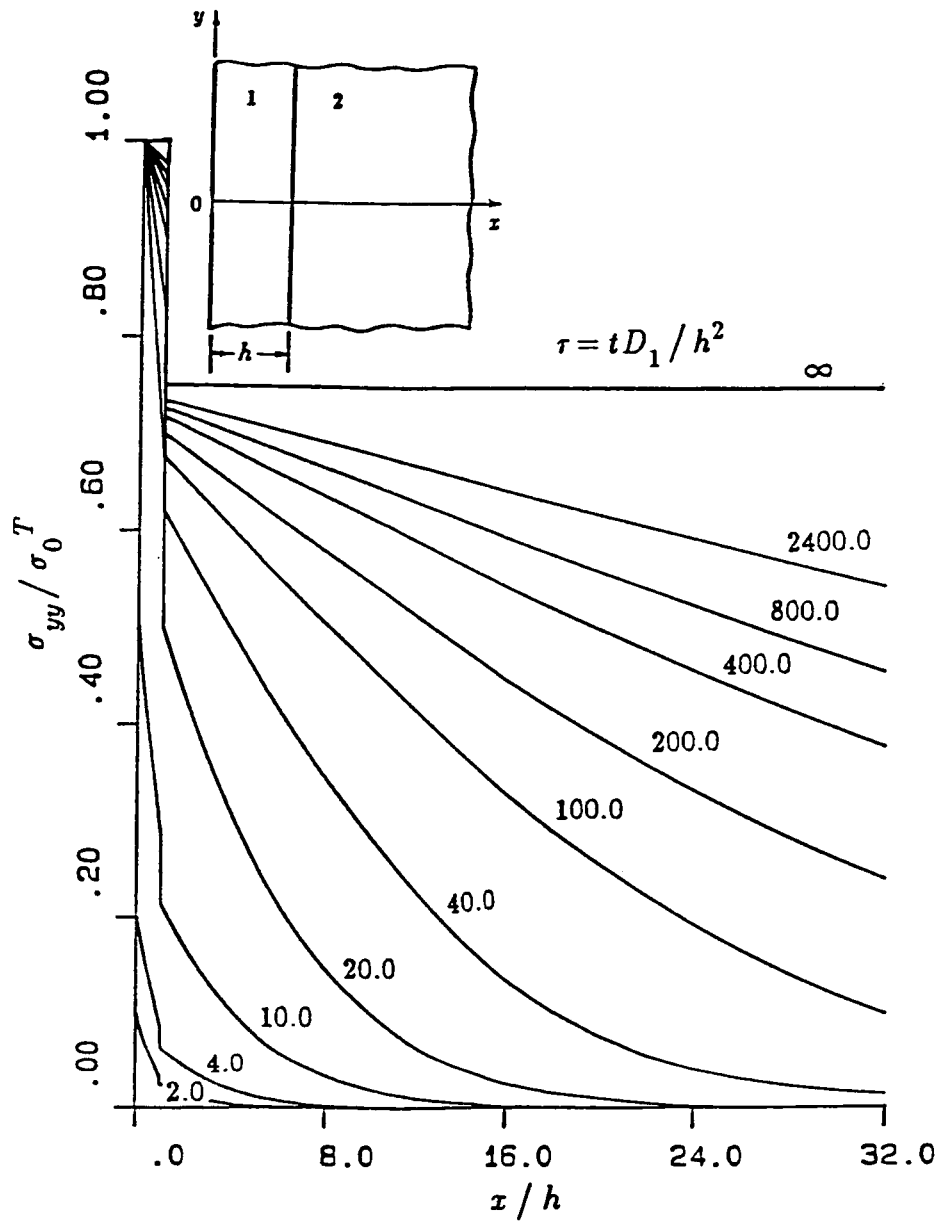


Figure 6-6: The normalized transient stress distribution σ_{yy}/σ_0^T in Model I for $\tau_0=20.0$, $\tau_0=t_0D_1/h^2$, $\sigma_0^T=-\alpha_1'E_1\Theta_0/(1-\nu_1)$ (Material pair A)

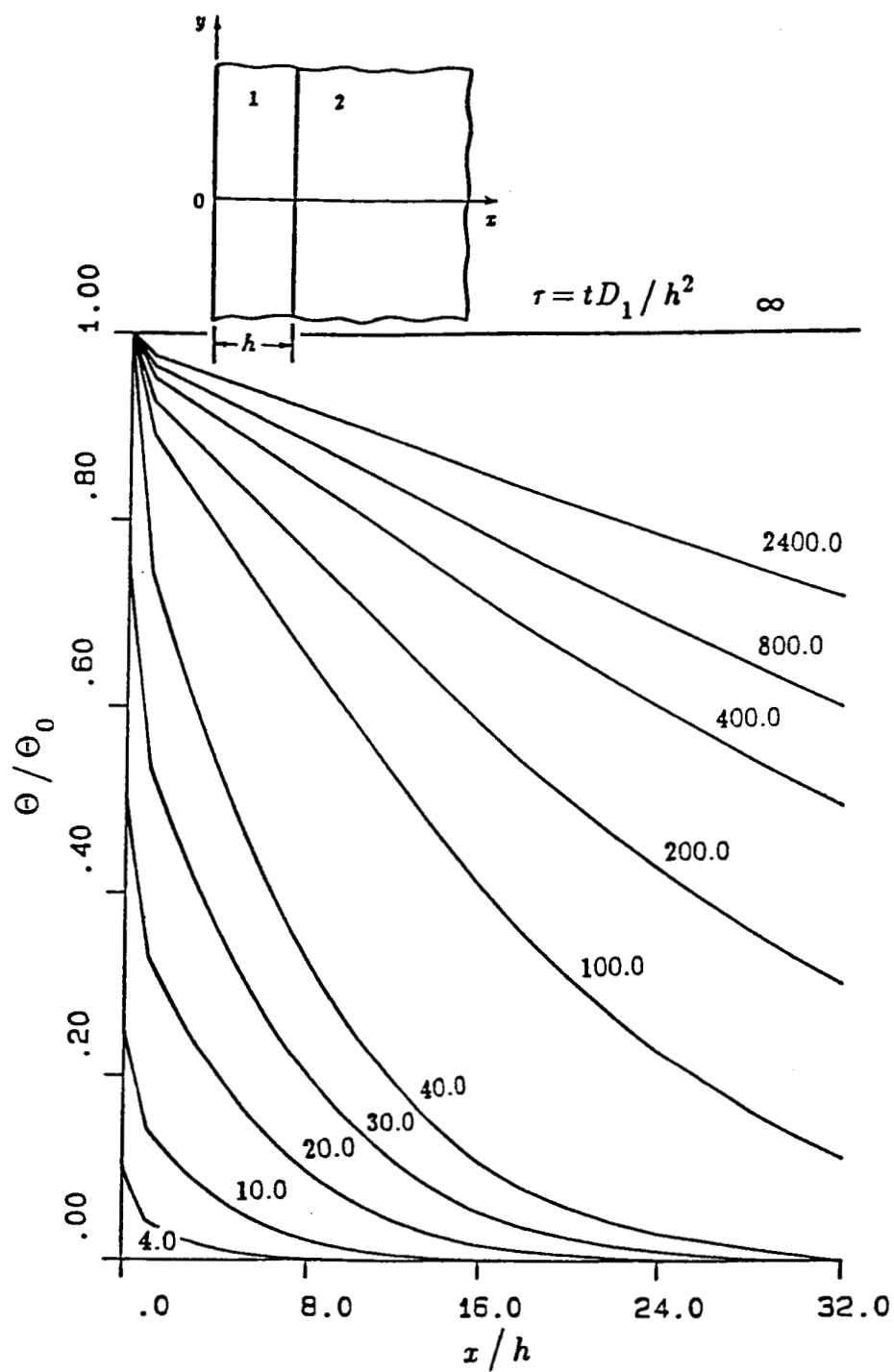


Figure 6-7: The normalized transient temperature distribution in Model I for $\tau_0 = 40.0$, $\tau_0 = t_0 D_1 / h^2$, (Material pair A)

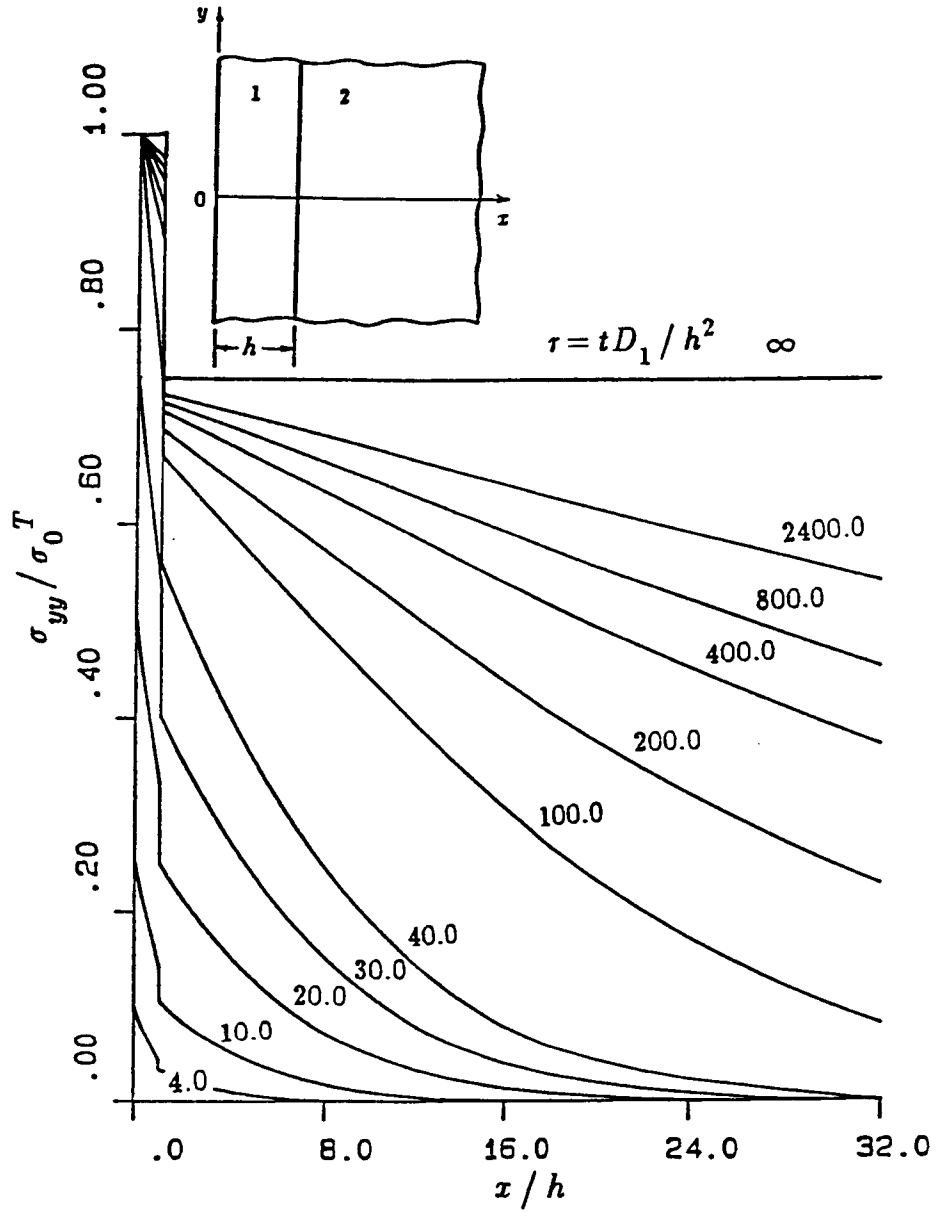


Figure 6-8: The normalized transient stress distribution σ_{yy}/σ_0^T in Model I for $\tau_0=40.0$, $\tau_0=t_0D_1/h^2$, $\sigma_0^T=-\alpha'_1 E_1 \Theta_0/(1-\nu_1)$ (Material pair A)

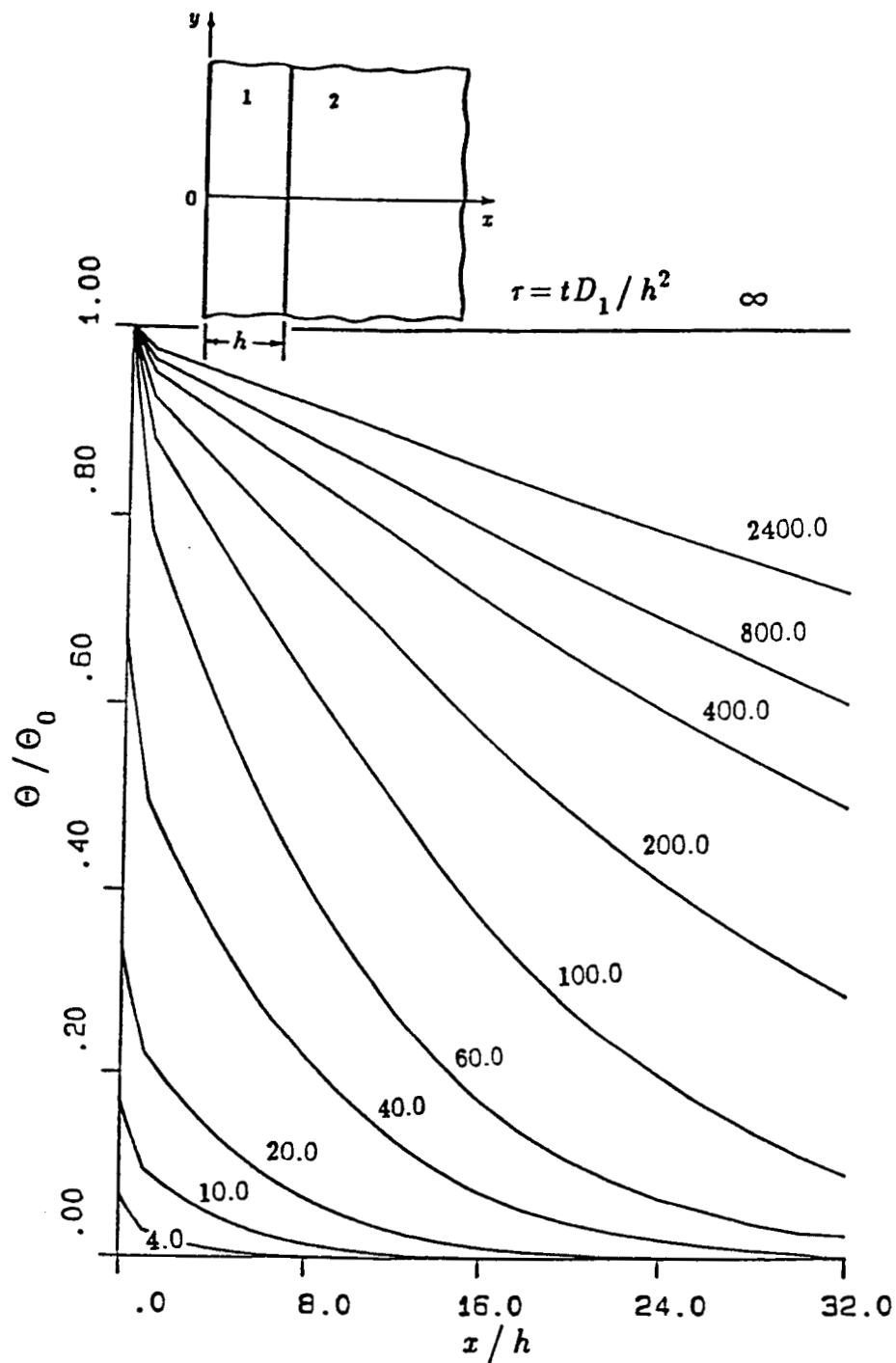


Figure 6-9: The normalized transient temperature distribution in Model I for $\tau_0 = 60.0$, $\tau_0 = t_0 D_1 / h^2$, (Material pair A)

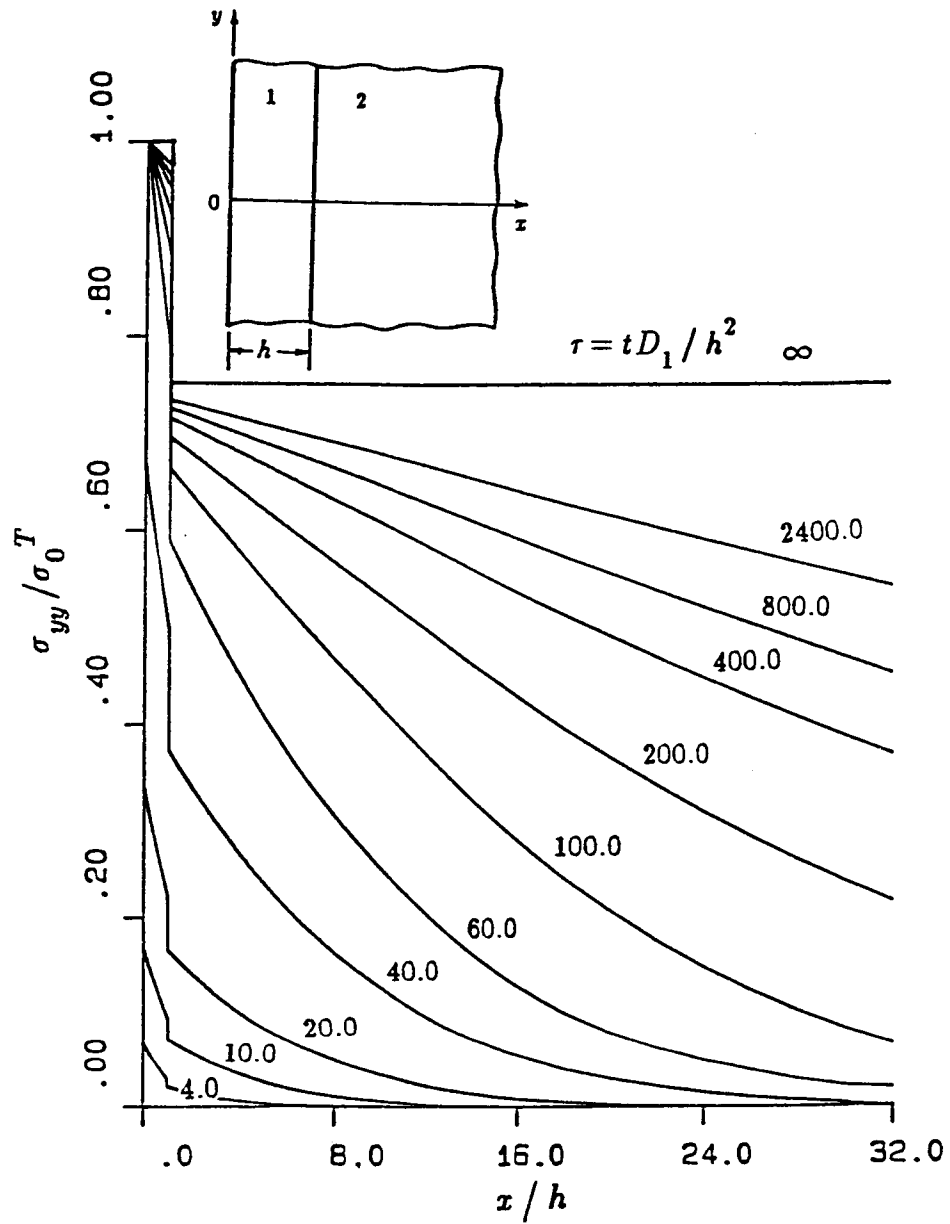


Figure 6-10: The normalized transient stress distribution σ_{yy}/σ_0^T in Model I for $\tau_0=60.0$, $\tau_0=t_0D_1/h^2$, $\sigma_0^T=-\alpha_1' E_1 \Theta_0/(1-\nu_1)$ (Material pair A)

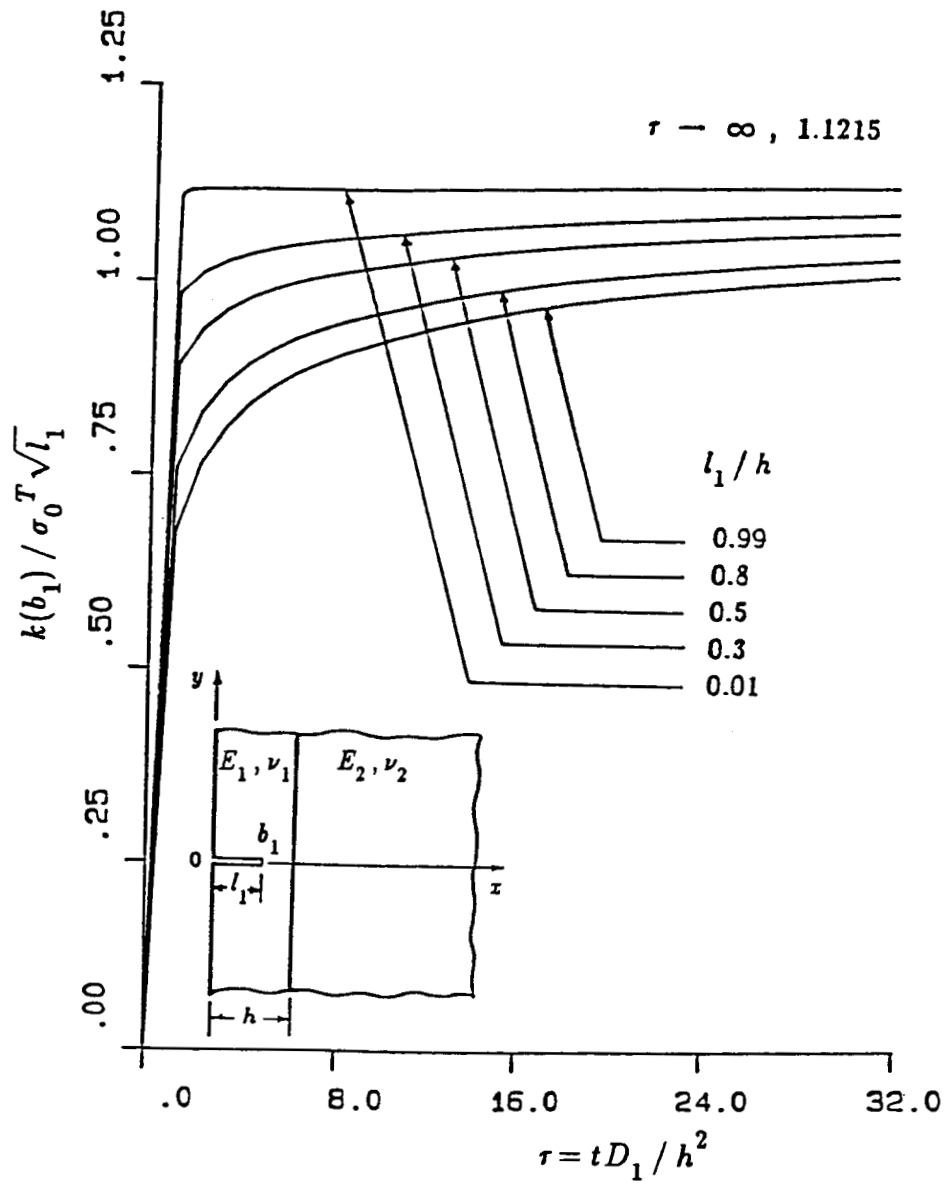


Figure 6-11: The normalized stress intensity factor $k(b_1)$ as a function of nondimensional time τ for an edge crack of various lengths in Model I for $\tau_0 = 0.0$, $\tau_0 = t_0 D_1 / h^2$, $\sigma_0^T = -\alpha_1' E_1 \Theta_0 / (1 - \nu_1)$ (Material pair A)

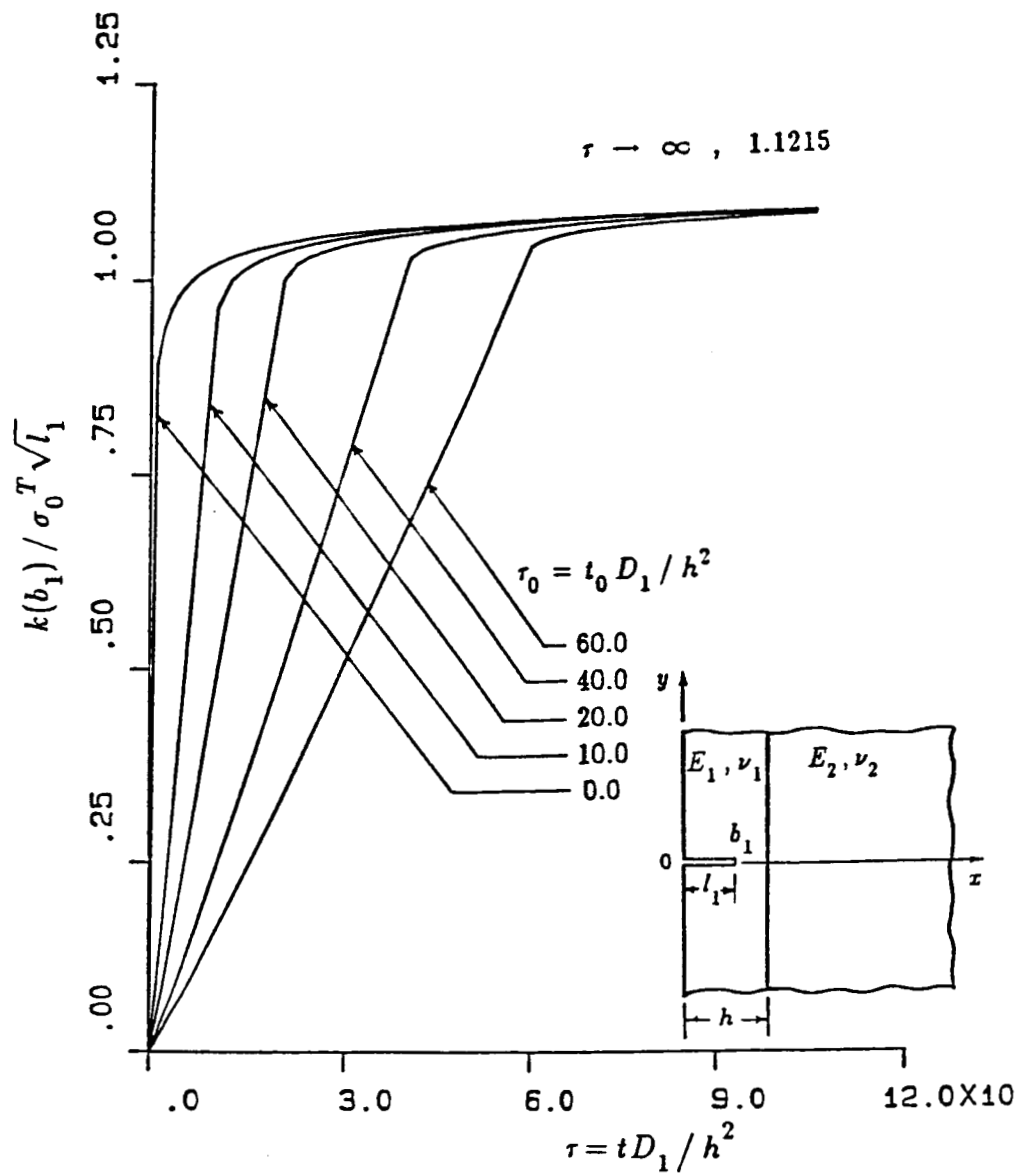


Figure 6-12: The influence of τ_0 on the normalized stress intensity factor $k(b_1)$ as a function of nondimensional time τ for an edge crack of length $l_1/h=0.5$ in Model I, $\tau_0=t_0 D_1/h^2$, $\sigma_0^T = -\alpha'_1 E_1 \Theta_0/(1-\nu_1)$ (Material pair A)

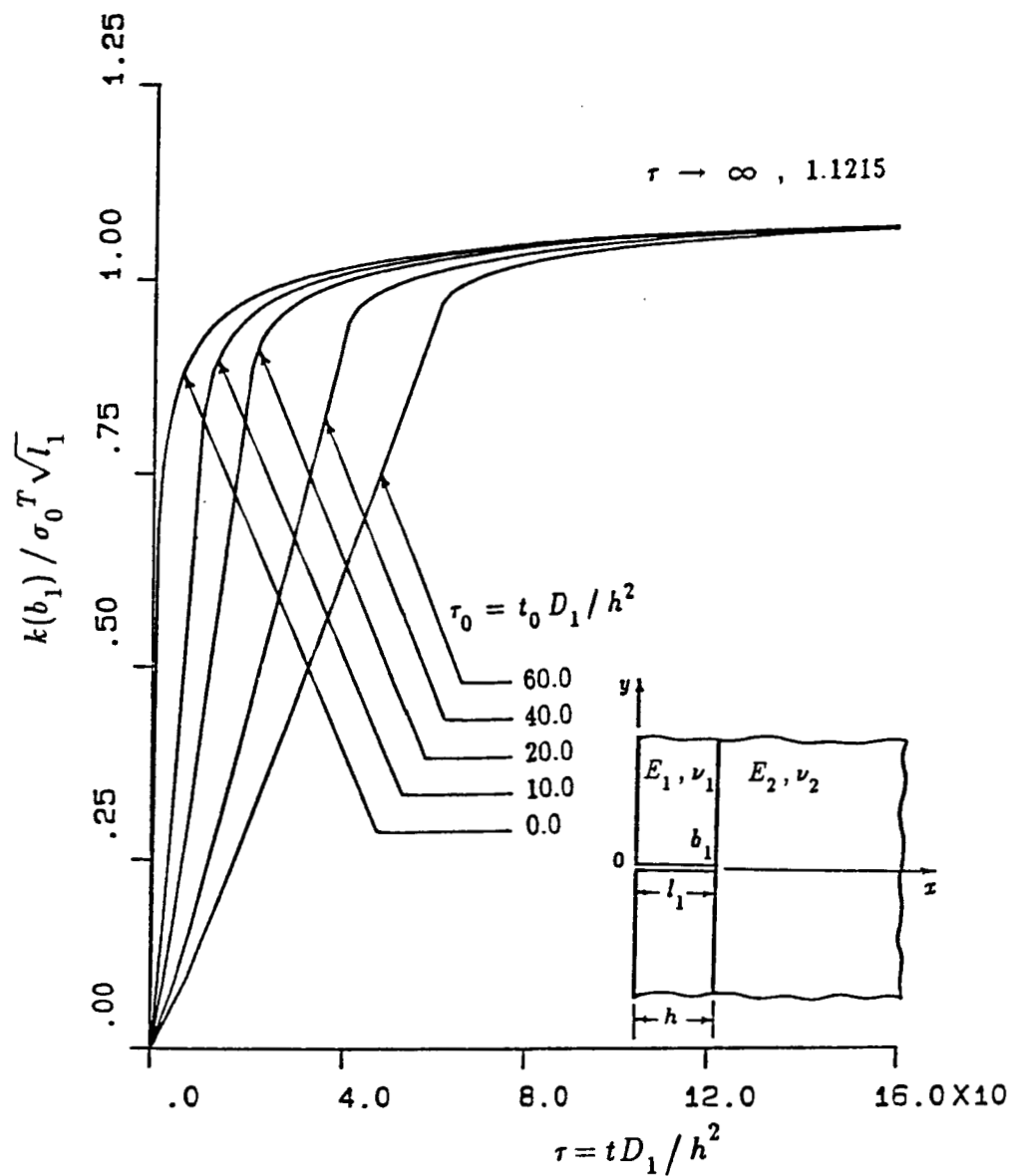


Figure 6-13: The influence of τ_0 on the normalized stress intensity factor $k(b_1)$ as a function of nondimensional time τ for a broken clad in Model I, $\tau_0 = t_0 D_1 / h^2$, $\sigma_0^T = -\alpha_1' E_1 \Theta_0 / (1 - \nu_1)$ (Material pair A)

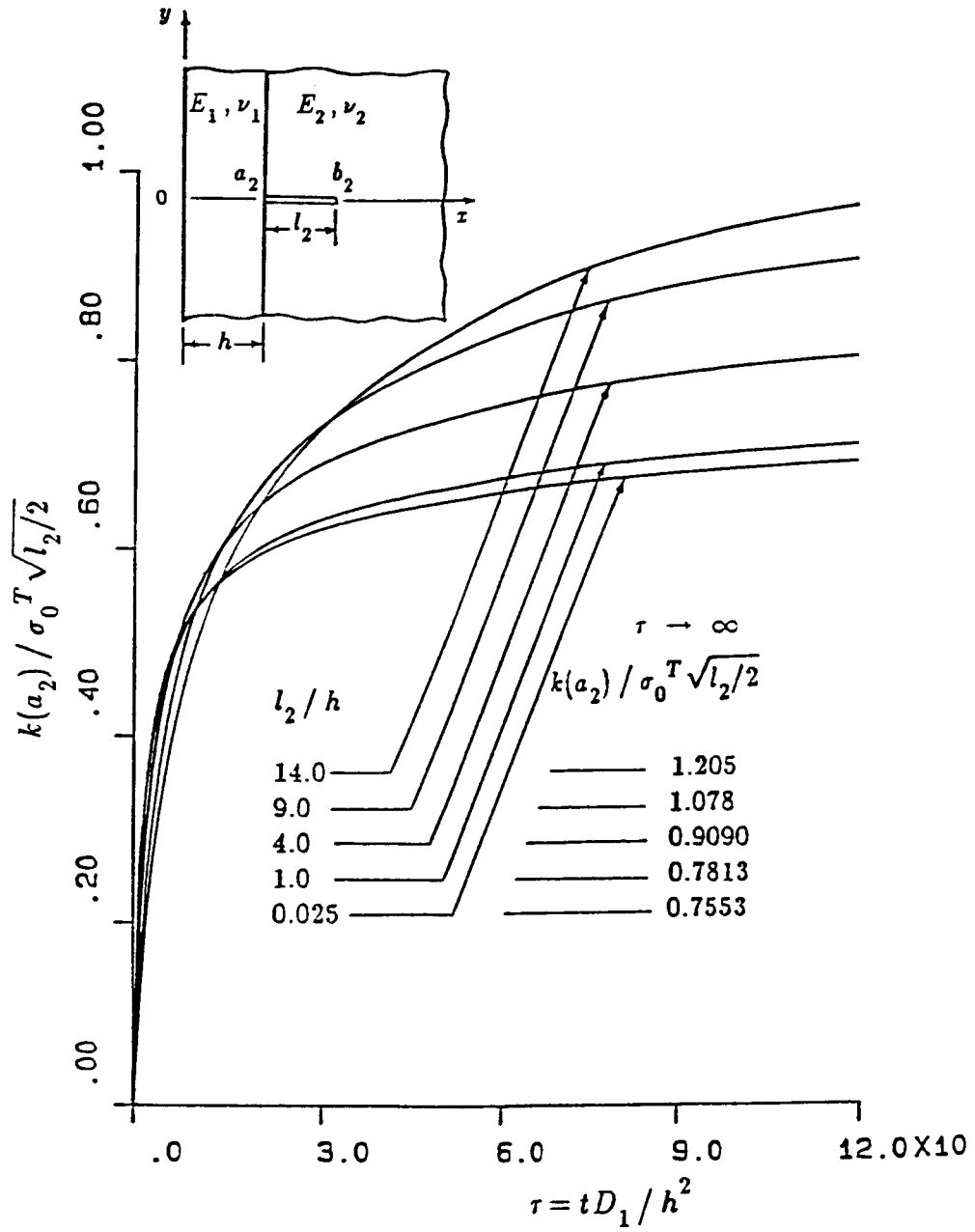


Figure 6-14: The normalized stress intensity factor $k(a_2)$ as a function of nondimensional time τ for an under-clad crack of various lengths in Model I for $\tau_0=0.0$, $\tau_0=t_0D_1/h^2$, $\sigma_0^T=-\alpha_1 E_1 \Theta_0/(1-\nu_1)$.(Material pair A)

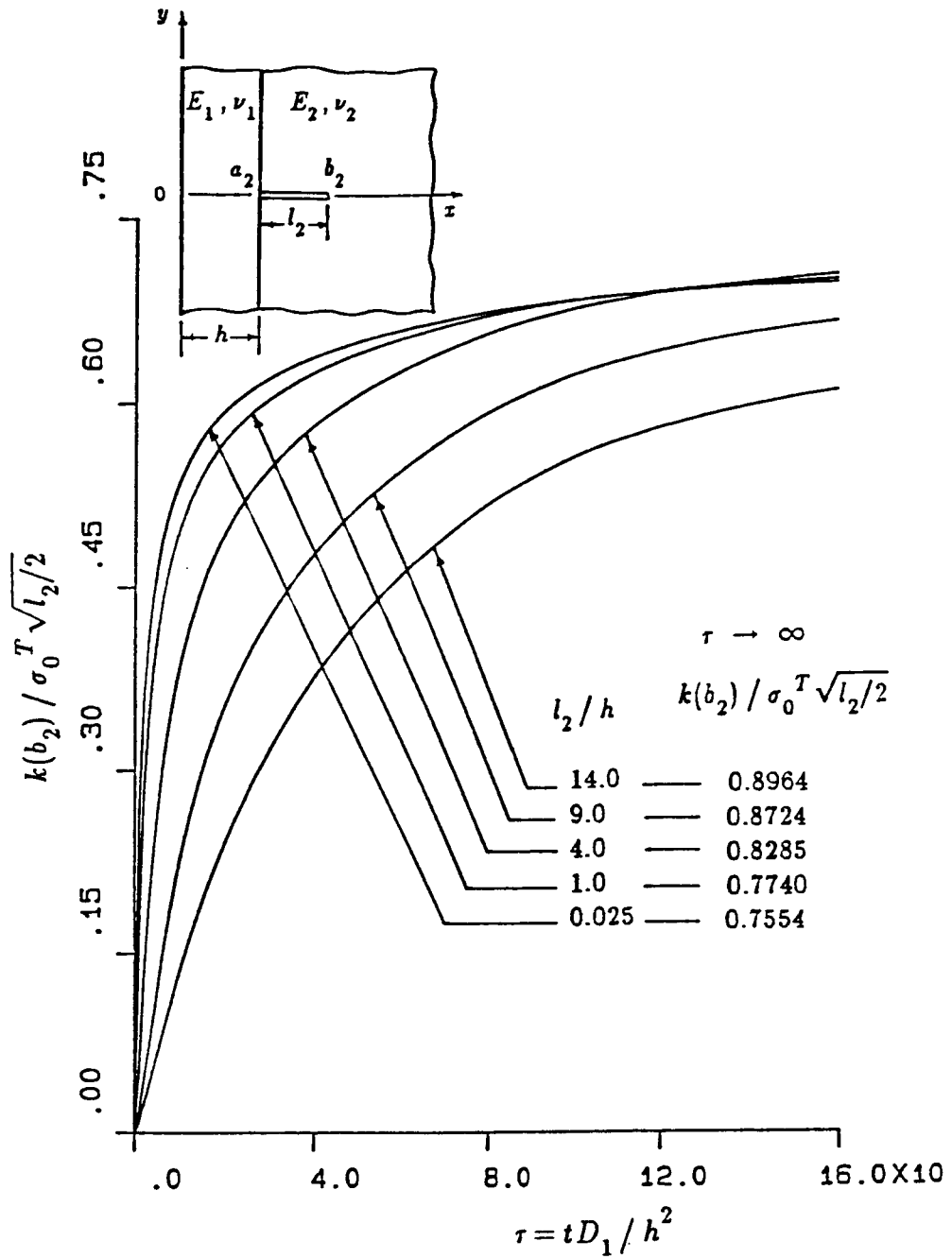


Figure 6-15: The normalized stress intensity factor $k(b_2)$ as a function of nondimensional time τ for an under-clad crack of various lengths in Model I for $\tau_0=0.0$, $\tau_0=t_0D_1/h^2$, $\sigma_0^T=-\alpha'_1 E_1 \Theta_0/(1-\nu_1)$.(Material pair A)

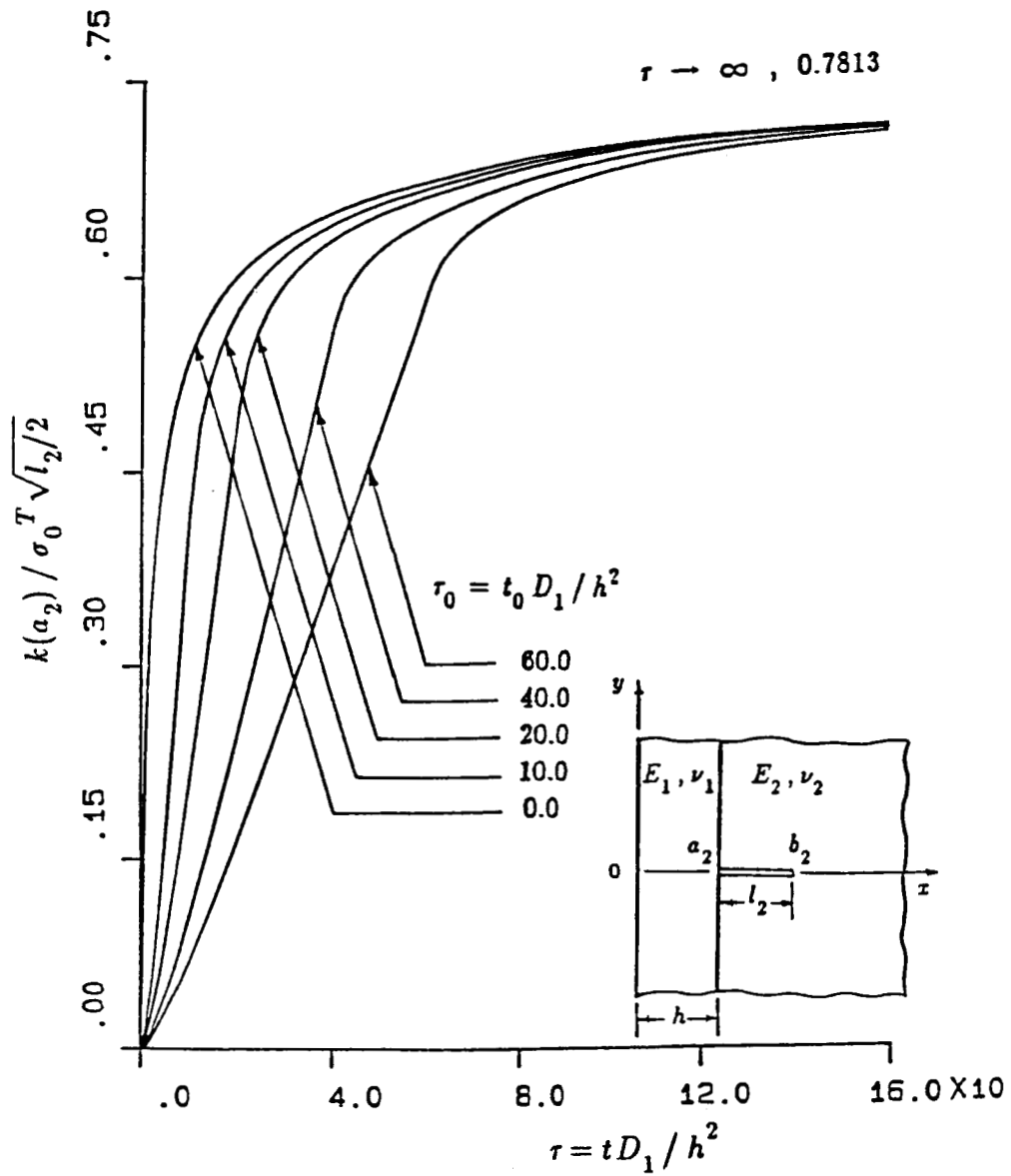


Figure 6-16: The influence of τ_0 on the normalized stress intensity factor $k(a_2)$ as a function of nondimensional time τ for an under-clad crack of length $l_2/h=1.0$ in Model I, $\tau_0=t_0 D_1/h^2$, $\sigma_0^T = -\alpha_1 E_1 \Theta_0/(1-\nu_1)$ (Material pair A)

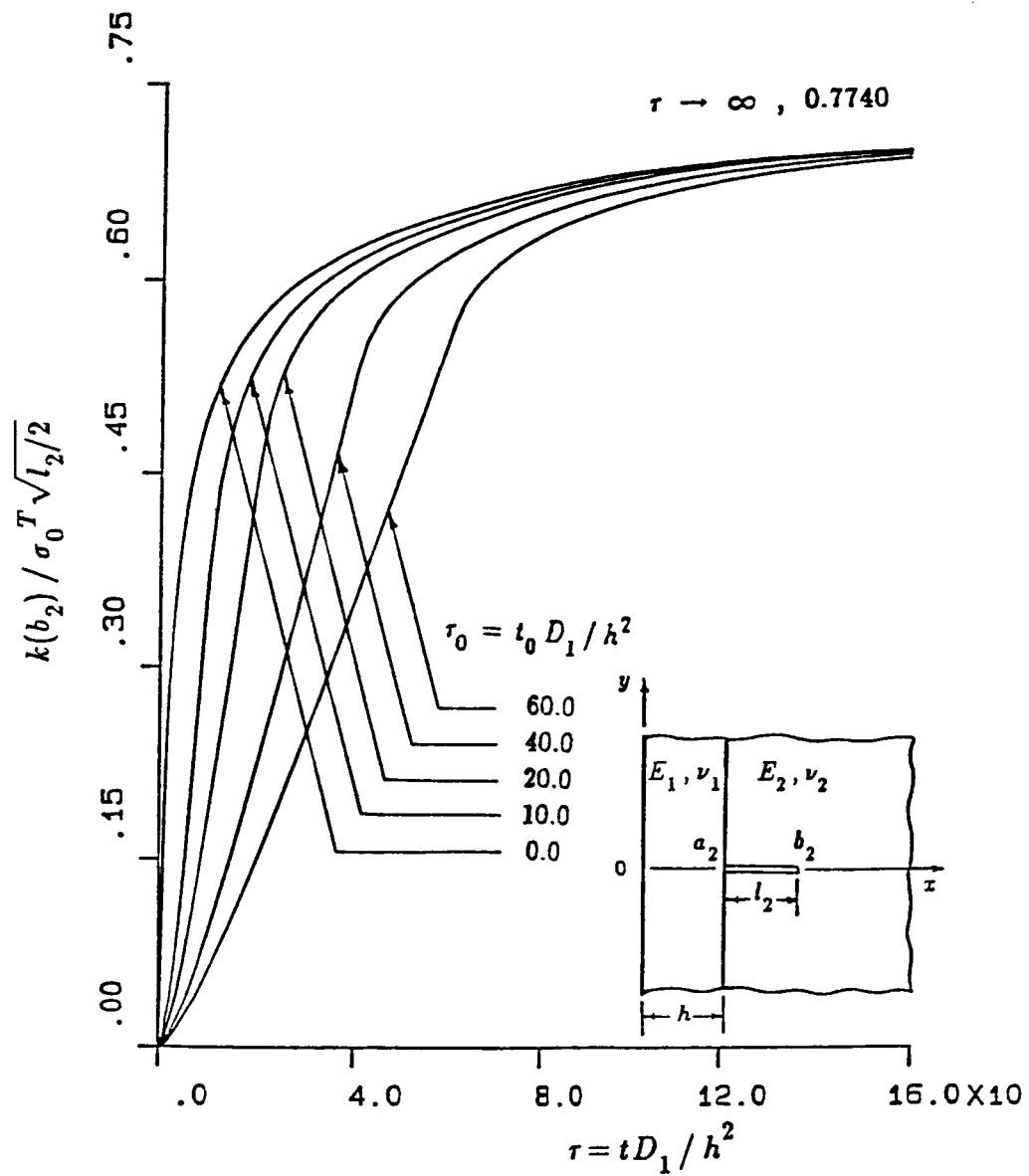


Figure 6-17: The influence of τ_0 on the normalized stress intensity factor $k(b_2)$ as a function of nondimensional time τ for an under-clad crack of length $l_2/h=1.0$ in Model I, $\tau_0=t_0 D_1/h^2$, $\sigma_0^T = -\alpha_1 E_1 \Theta_0/(1-\nu_1)$ (Material pair A)

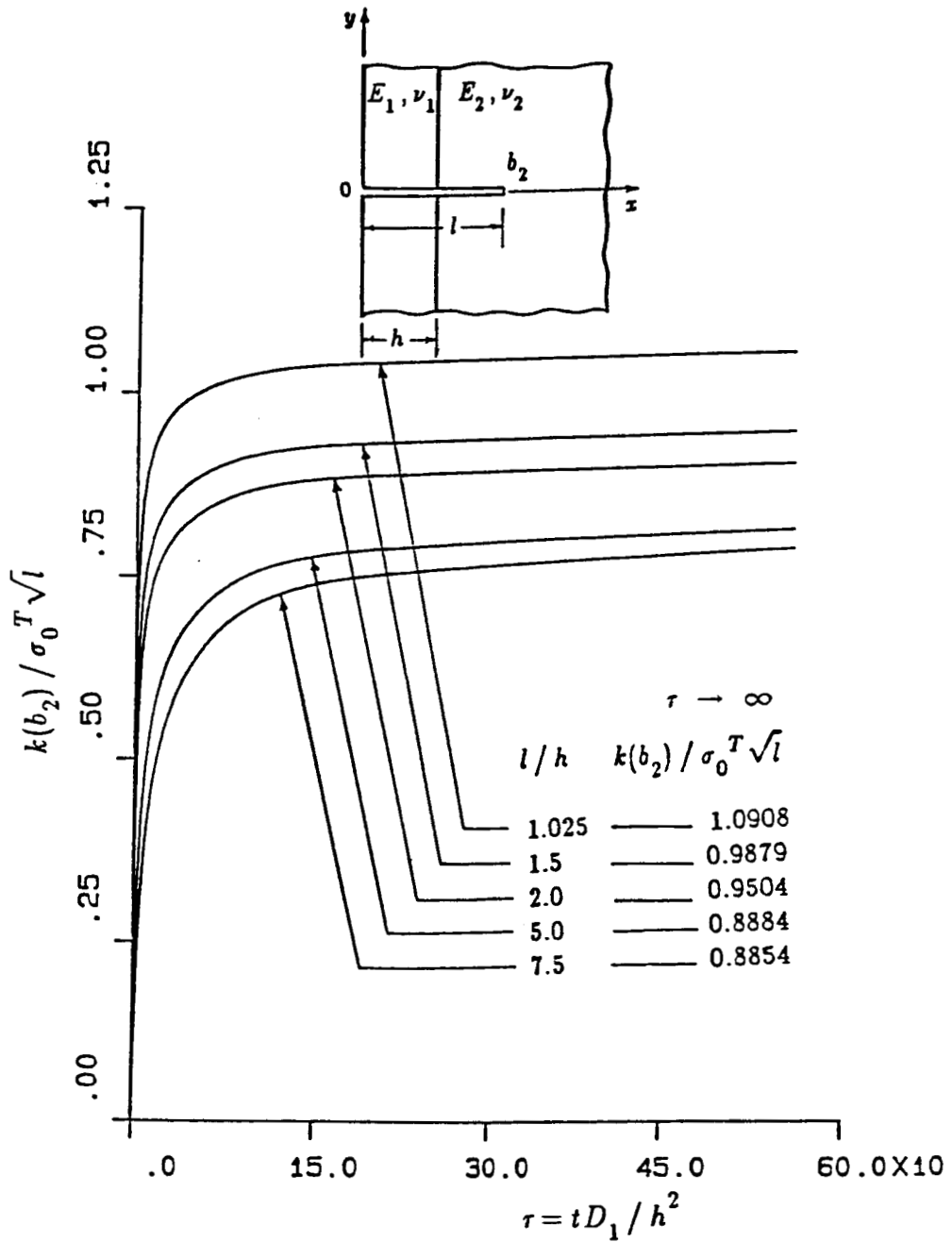


Figure 6-18: The normalized stress intensity factor $k(b_2)$ as a function of nondimensional time τ for an edge crack of various lengths crossing the interface of in Model I for $\tau_0=0.0$, $\tau_0=t_0 D_1/h^2$, $\sigma_0^T = -\alpha_1' E_1 \Theta_0 / (1-\nu_1)$ (Material pair A)

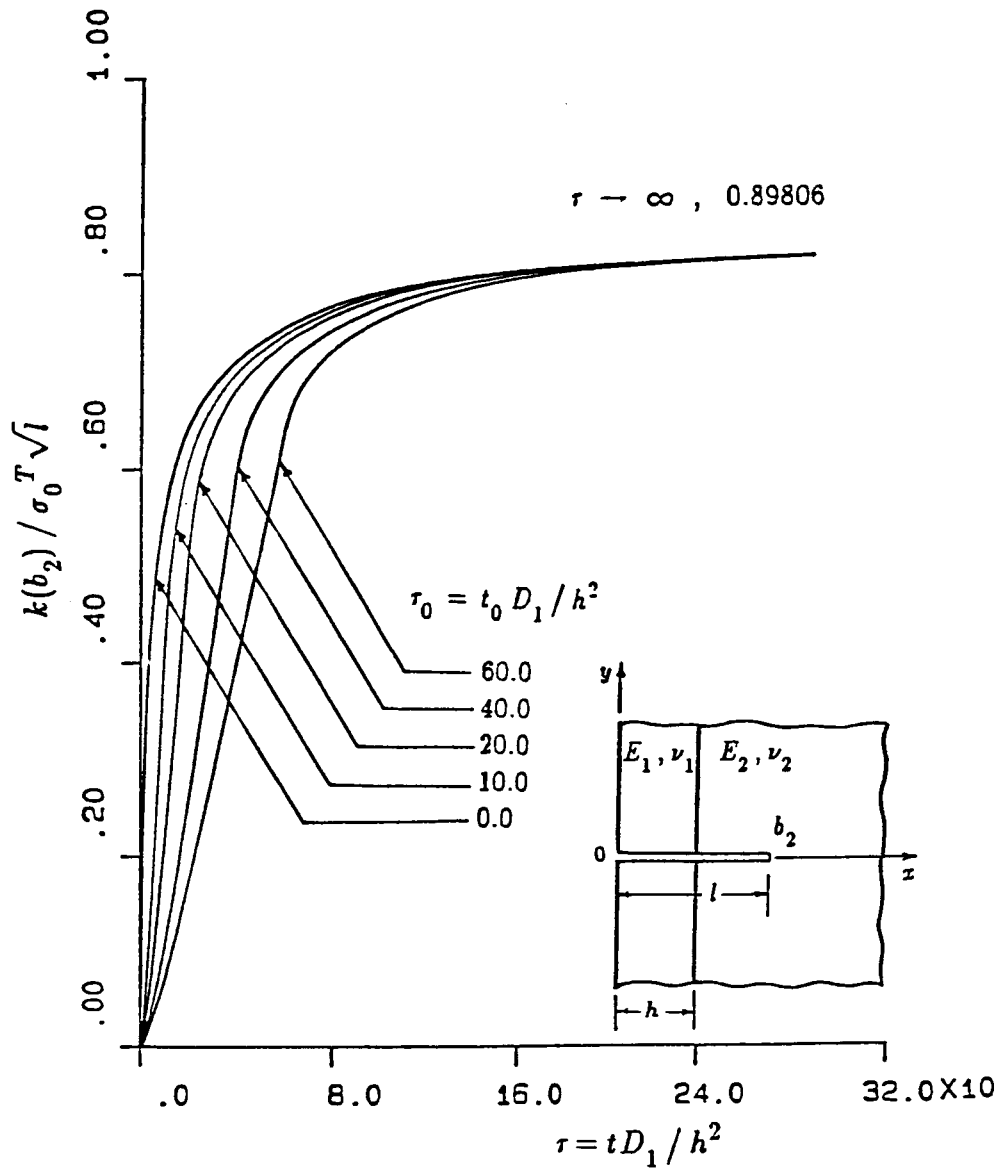


Figure 6-19: The influence of τ_0 on the normalized stress intensity factor $k(b_2)$ as a function of nondimensional time τ for an edge crack crossing the interface in Model I for $l/h=4.0$, $\tau_0=t_0 D_1/h^2$, $\sigma_0^T = -\alpha'_1 E_1 \Theta_0 / (1-\nu_1)$ (Material pair A)

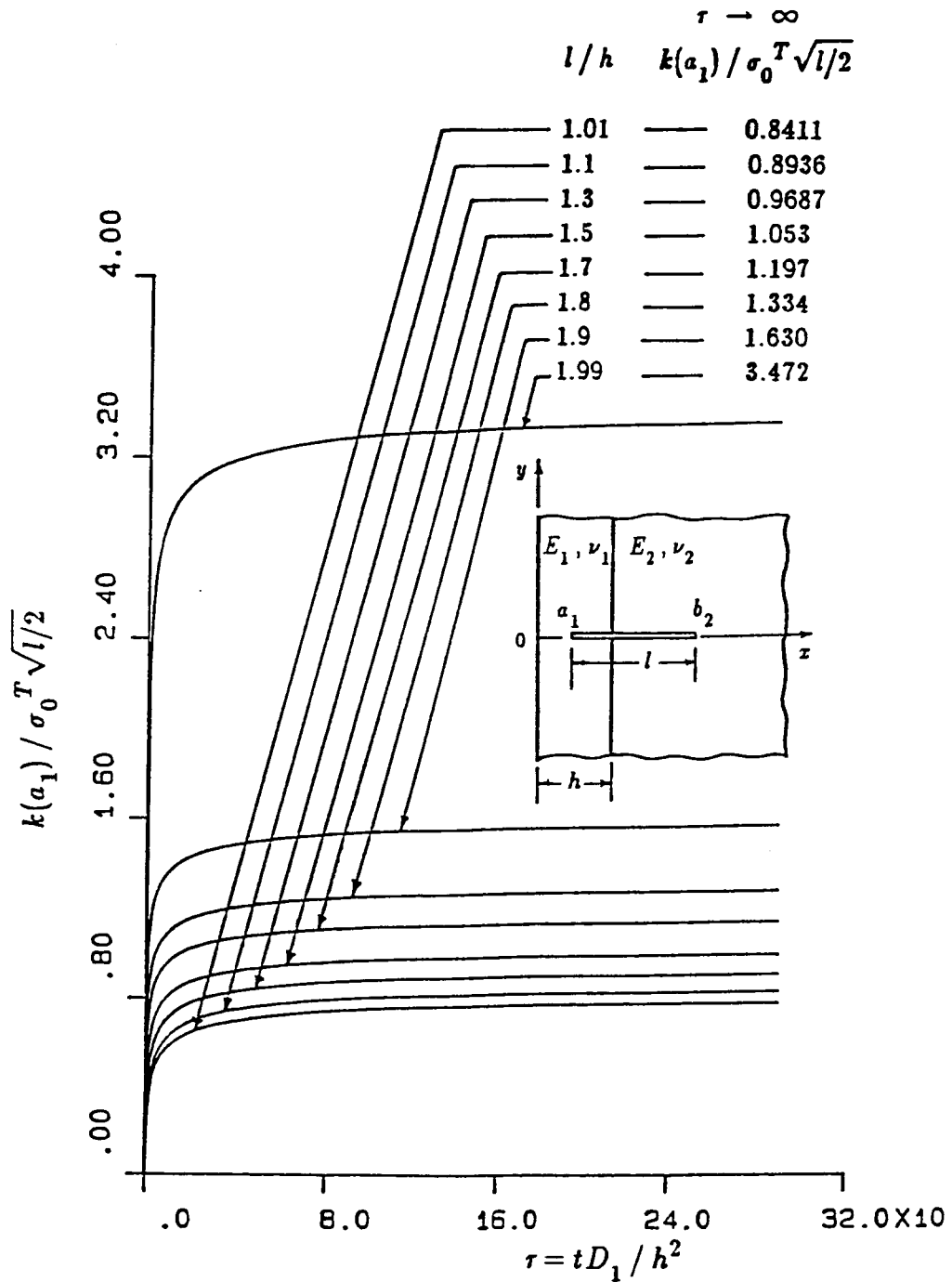


Figure 6-20: The normalized stress intensity factor $k(a_1)$ as a function of nondimensional time τ for an embedded crack of various lengths crossing the interface in Model I for $b_2/h=2.0$, $\tau_0=0.0$, $\tau_0=t_0 D_1/h^2$, $\sigma_0^T = -\alpha'_1 E_1 \Theta_0/(1-\nu_1)$ (Material pair A)

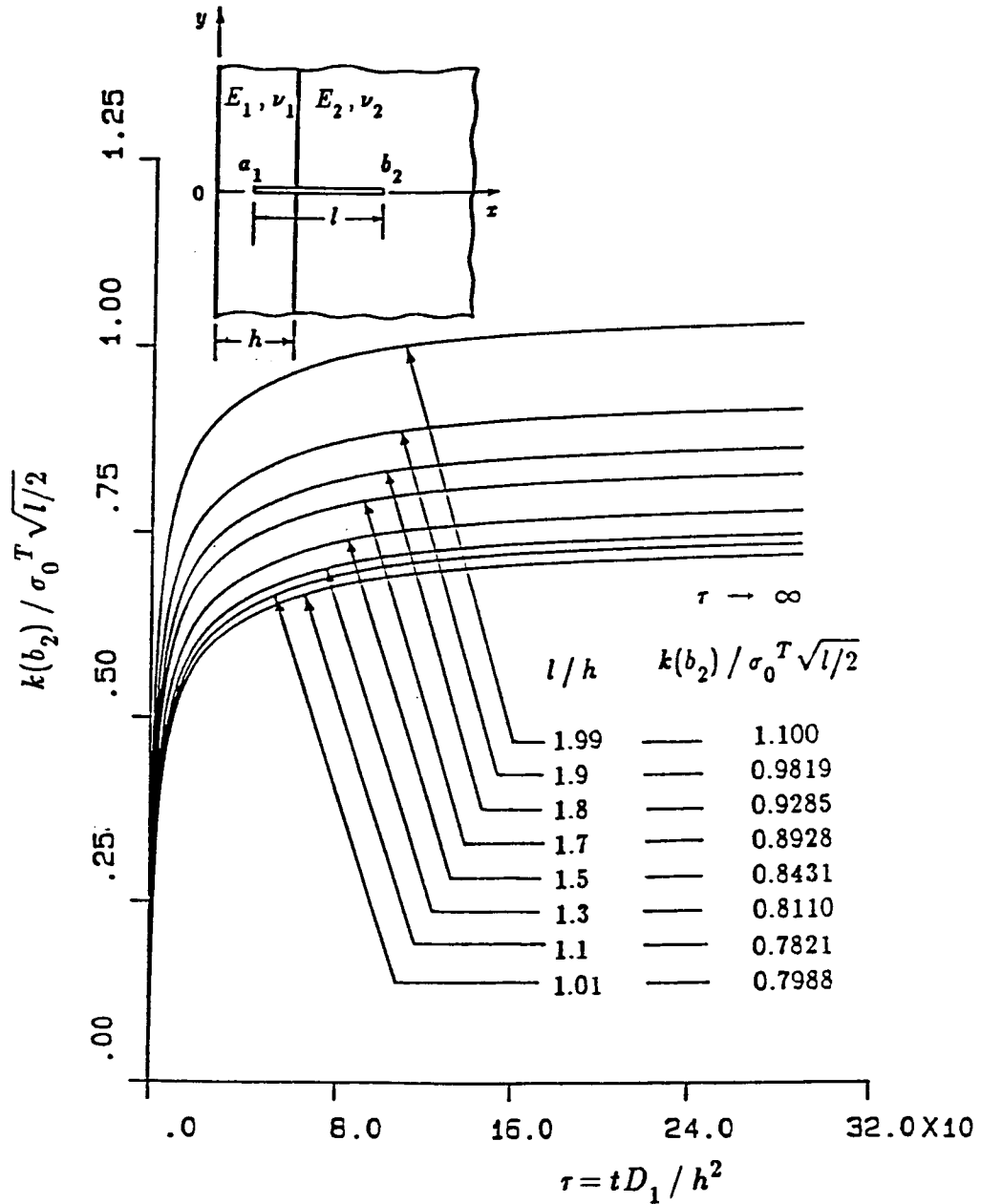


Figure 6-21: The normalized stress intensity factor $k(b_2)$ as a function of nondimensional time τ for an embedded crack of various lengths crossing the interface in Model I for $b_2/h=2.0$, $\tau_0=0.0$, $\tau_0=t_0D_1/h^2$, $\sigma_0^T = -\alpha_1' E_1 \Theta_0 / (1-\nu_1)$ (Material pair A)

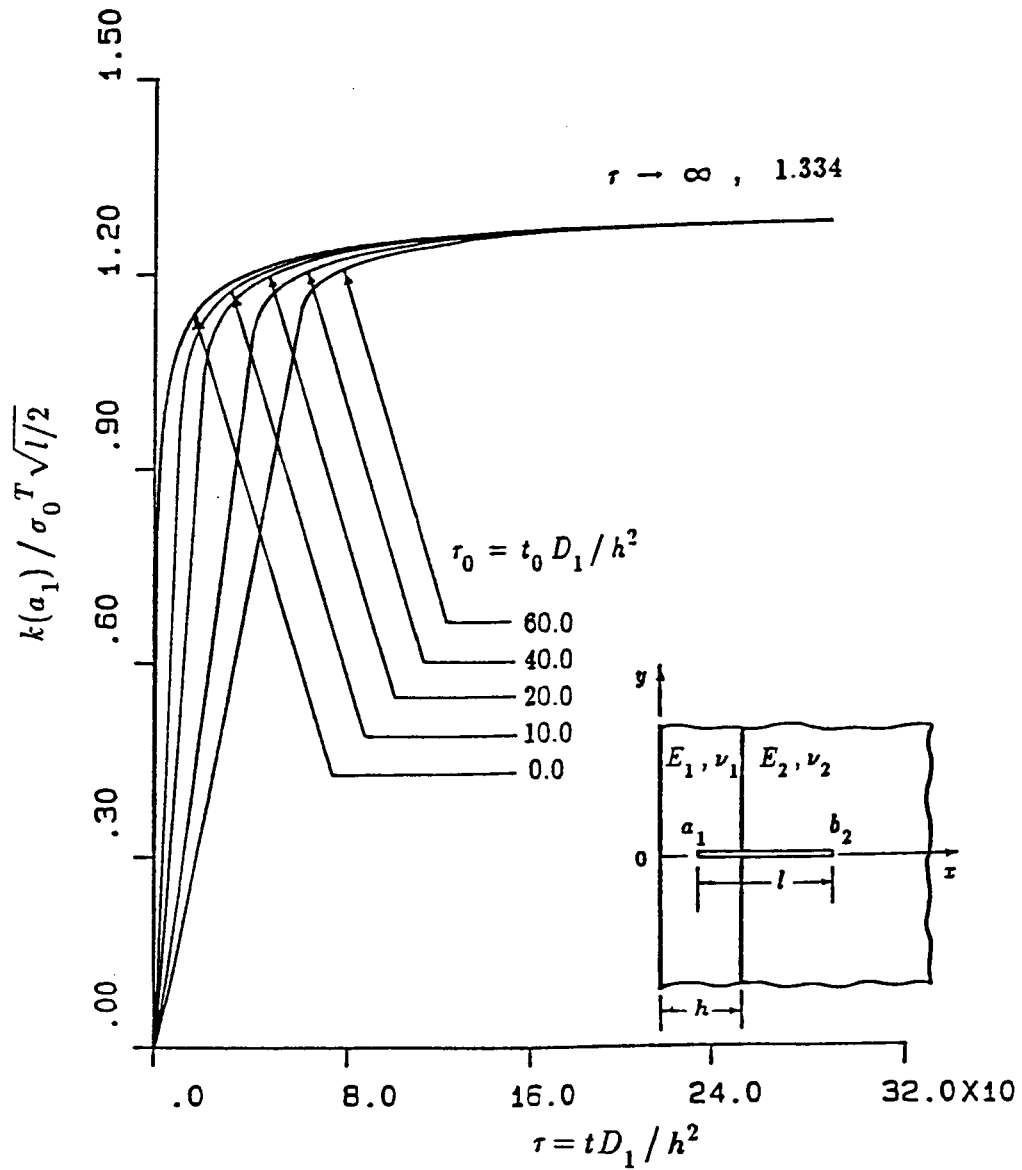


Figure 6-22: The influence of τ_0 on the normalized stress intensity factor $k(a_1)$ as a function of nondimensional time τ for an embedded crack crossing the interface, $a_1/h=0.2$, $b_1/h=2.0$ in Model I, $\tau_0=t_0 D_1/h^2$, $\sigma_0^T = -\alpha_1' E_1 \Theta_0 / (1-\nu_1)$ (Material pair A)

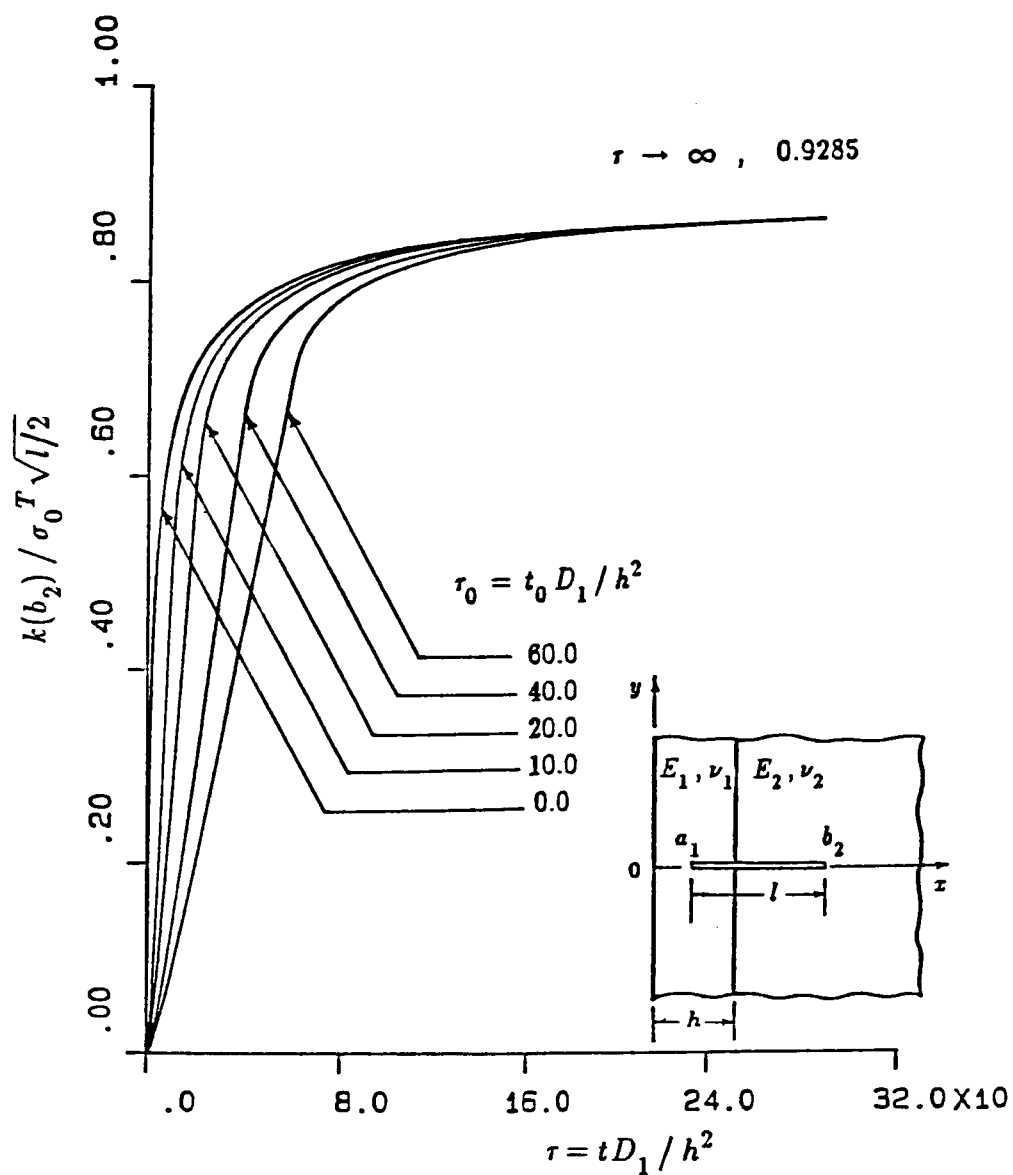


Figure 6-23: The influence of τ_0 on the normalized stress intensity factor $k(b_2)$ as a function of nondimensional time τ for an embedded crack crossing the interface in Model I for $a_1/h=0.2$, $b_1/h=2.0$, $\tau_0=t_0 D_1/h^2$, $\sigma_0^T = -\alpha_1 E_1 \Theta_0/(1-\nu_1)$ (Material pair A)

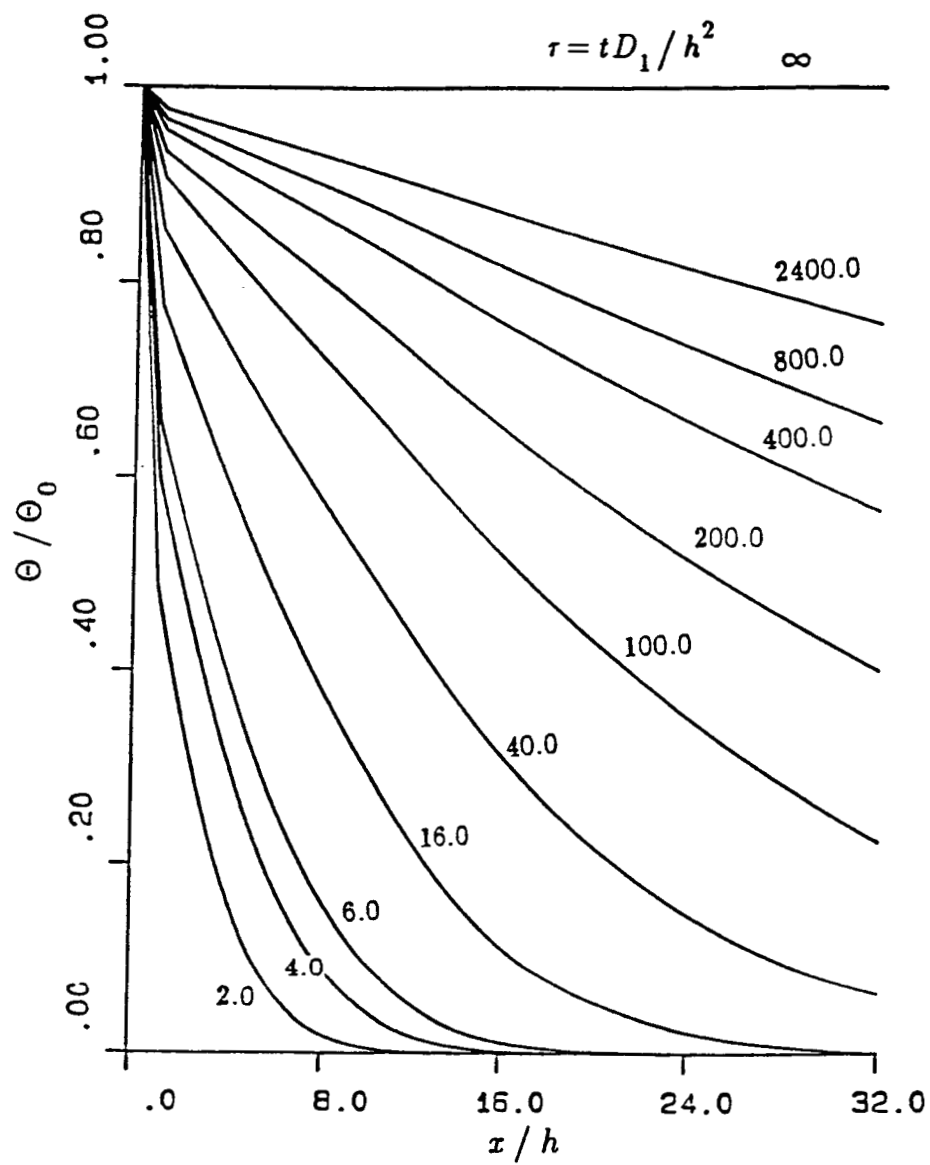


Figure 6-24: The normalized transient temperature distribution in Model I for $\tau_0 = 0.0$, $\tau_0 = t_0 D_1 / h^2$, (Material pair B)

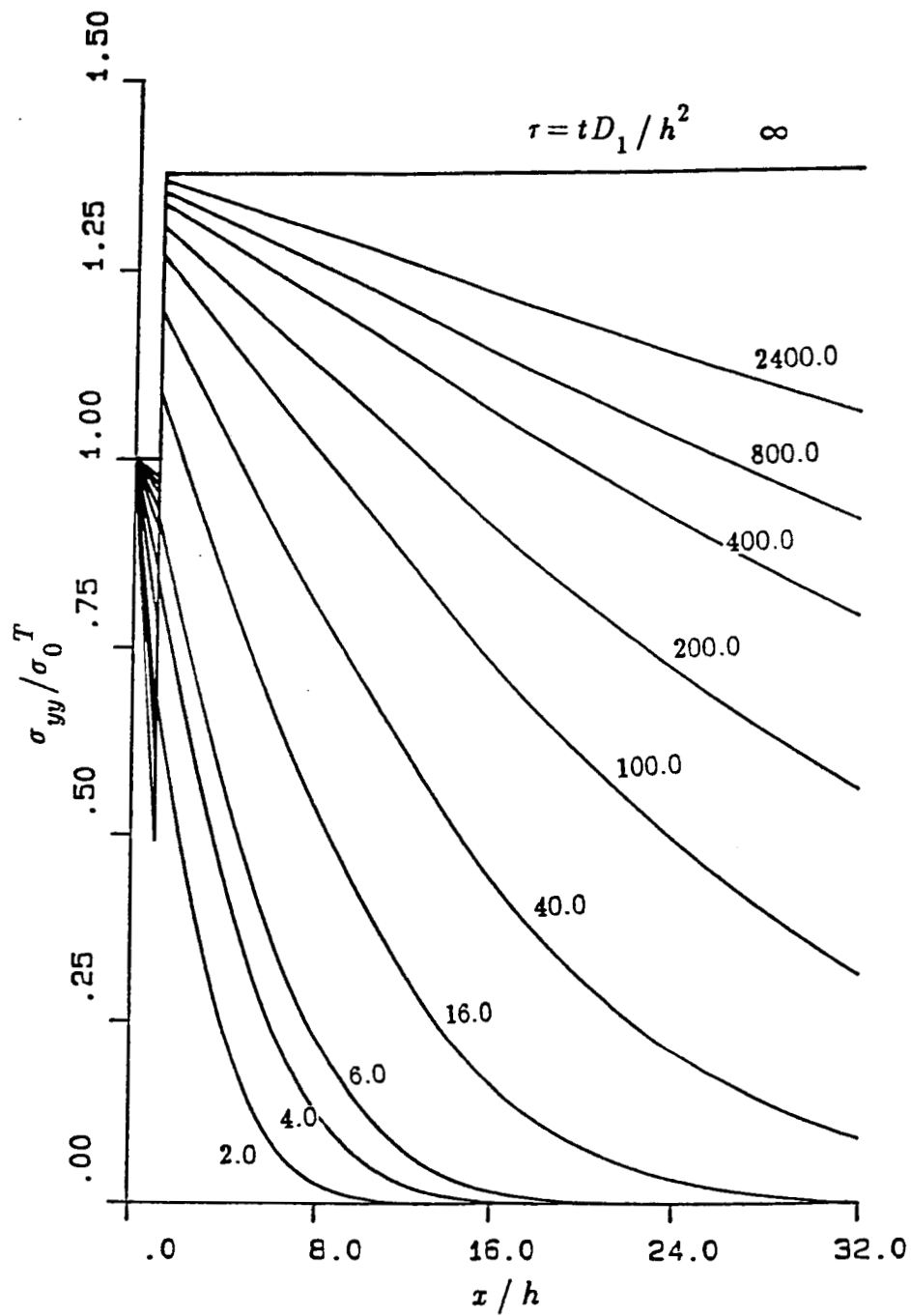


Figure 6-25: The normalized transient stress distribution σ_{yy}/σ_0^T in Model I for $\tau_0=0.0$, $\tau_0=t_0D_1/h^2$, $\sigma_0^T=-\alpha_1 E_1 \Theta_0/(1-\nu_1)$ (Material pair B)

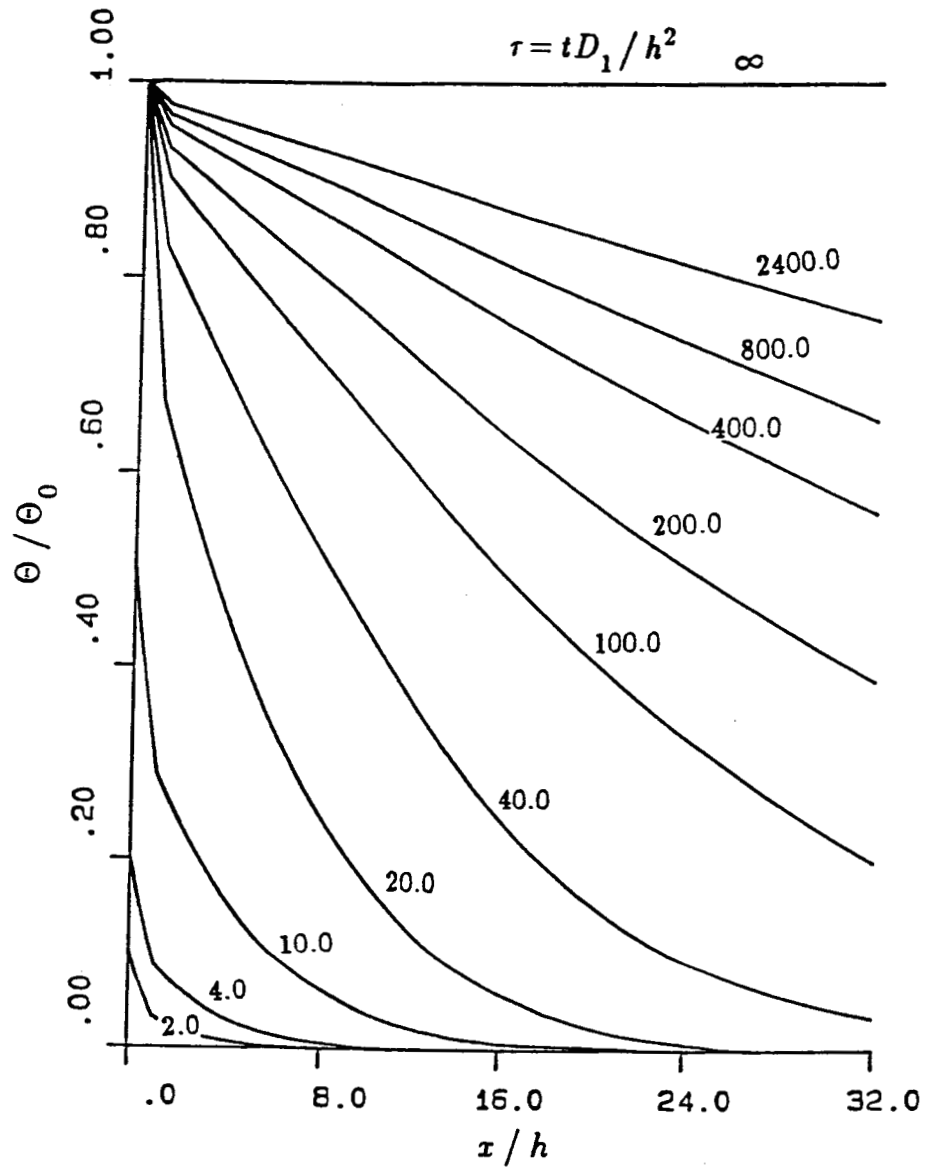


Figure 6-26: The normalized transient temperature distribution in Model I for $\tau_0=20.0$, $\tau_0=t_0D_1/h^2$, (Material pair B)

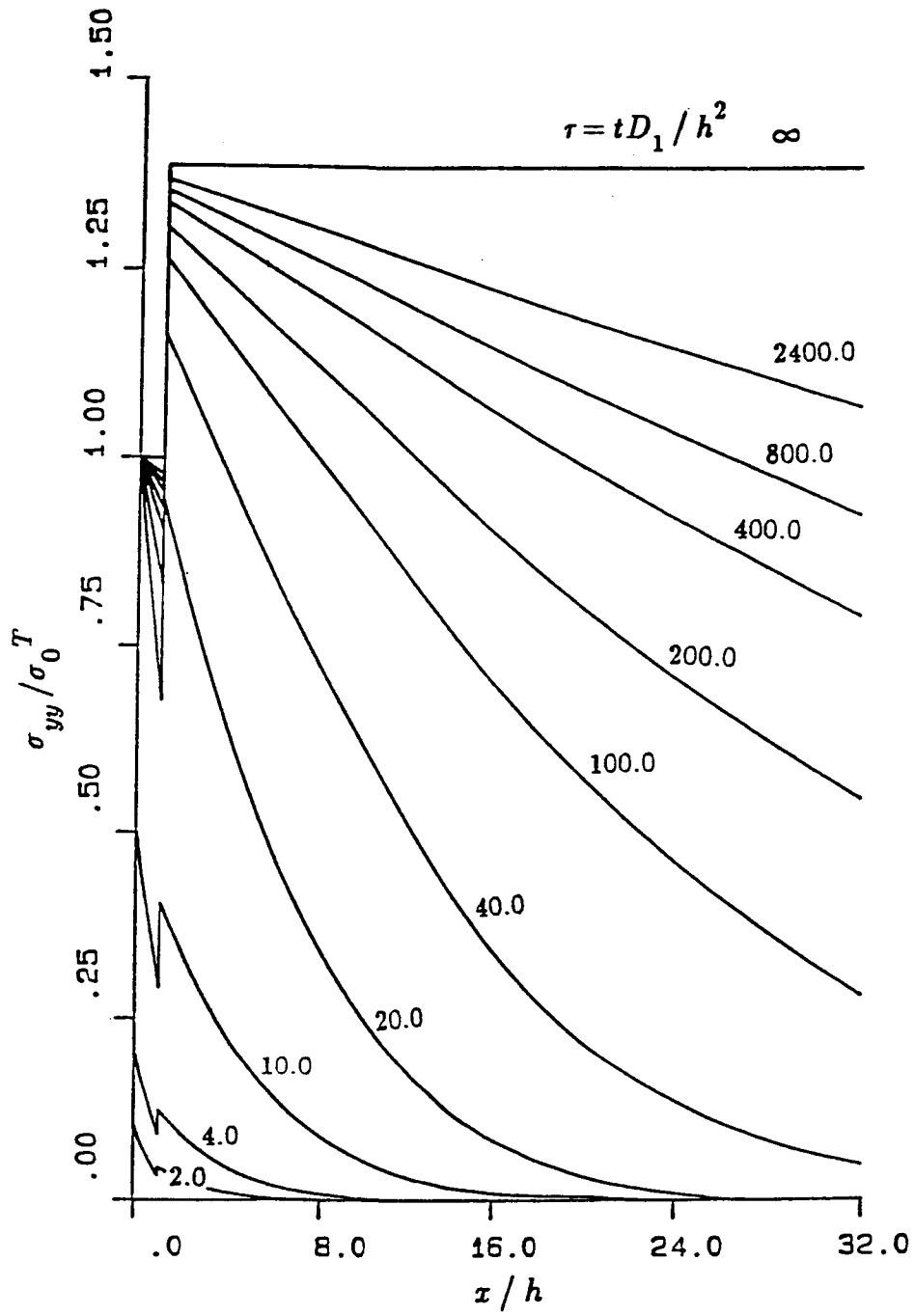


Figure 6-27: The normalized transient stress distribution σ_{yy}/σ_0^T in Model I for $\tau_0=20.0$, $\tau_0=t_0D_1/h^2$, $\sigma_0^T=-\alpha'_1 E_1 \Theta_0/(1-\nu_1)$ (Material pair B)

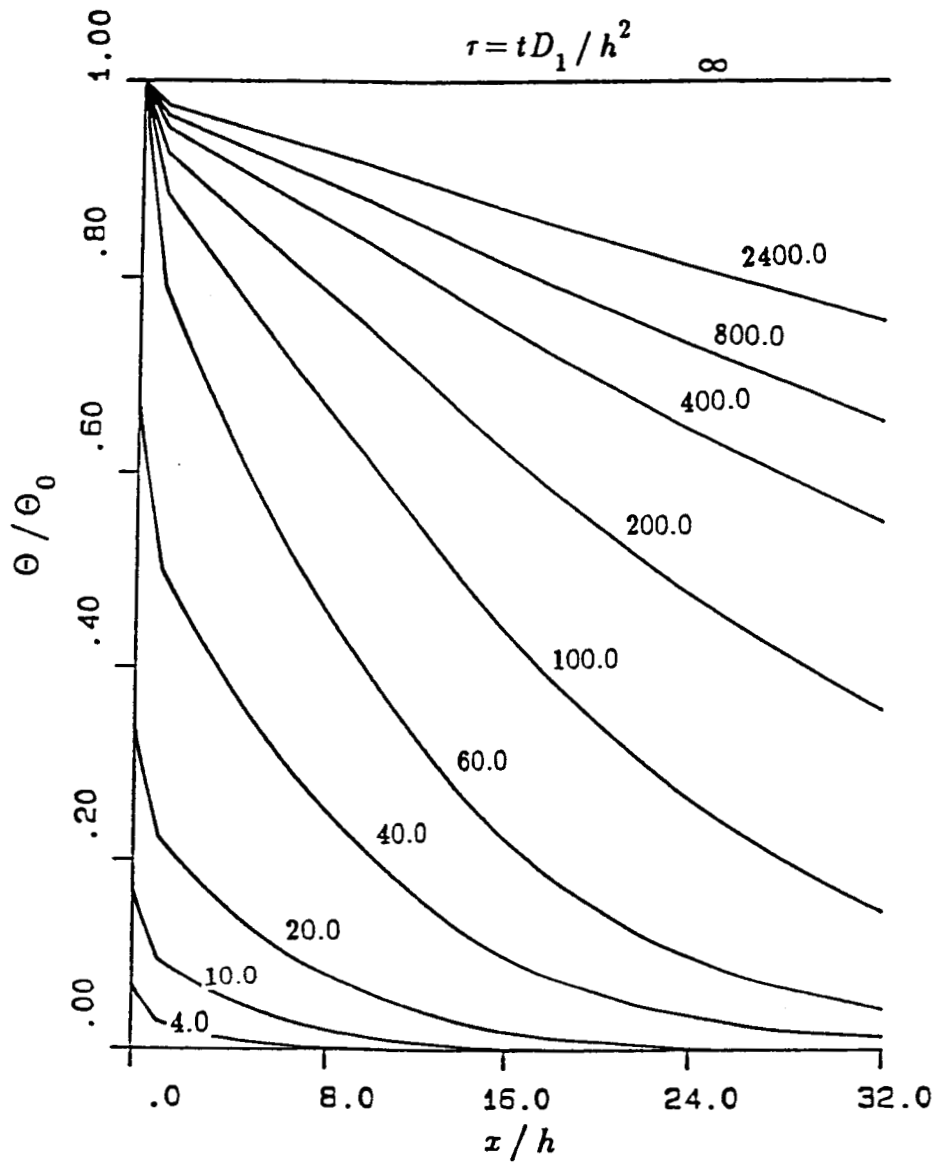


Figure 6-28: The normalized transient temperature distribution in Model I for $\tau_0 = 60.0$, $\tau_0 = t_0 D_1 / h^2$, (Material pair B)

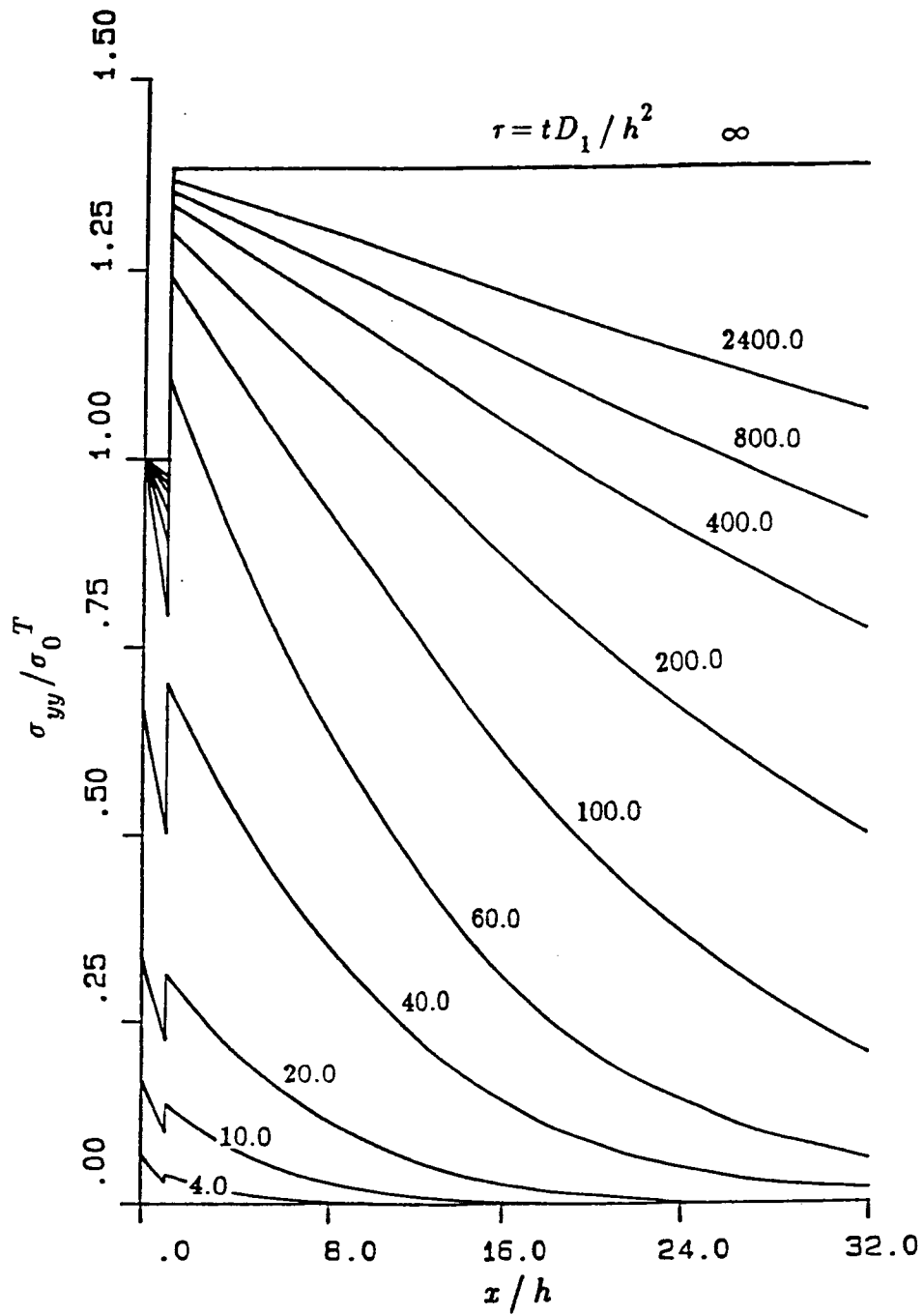


Figure 6-29: The normalized transient stress distribution σ_{yy}/σ_0^T in Model I for $\tau_0 = 60.0$, $\tau_0 = t_0 D_1 / h^2$, $\sigma_0^T = -\alpha_1 E_1 \Theta_0 / (1 - \nu_1)$ (Material pair B)

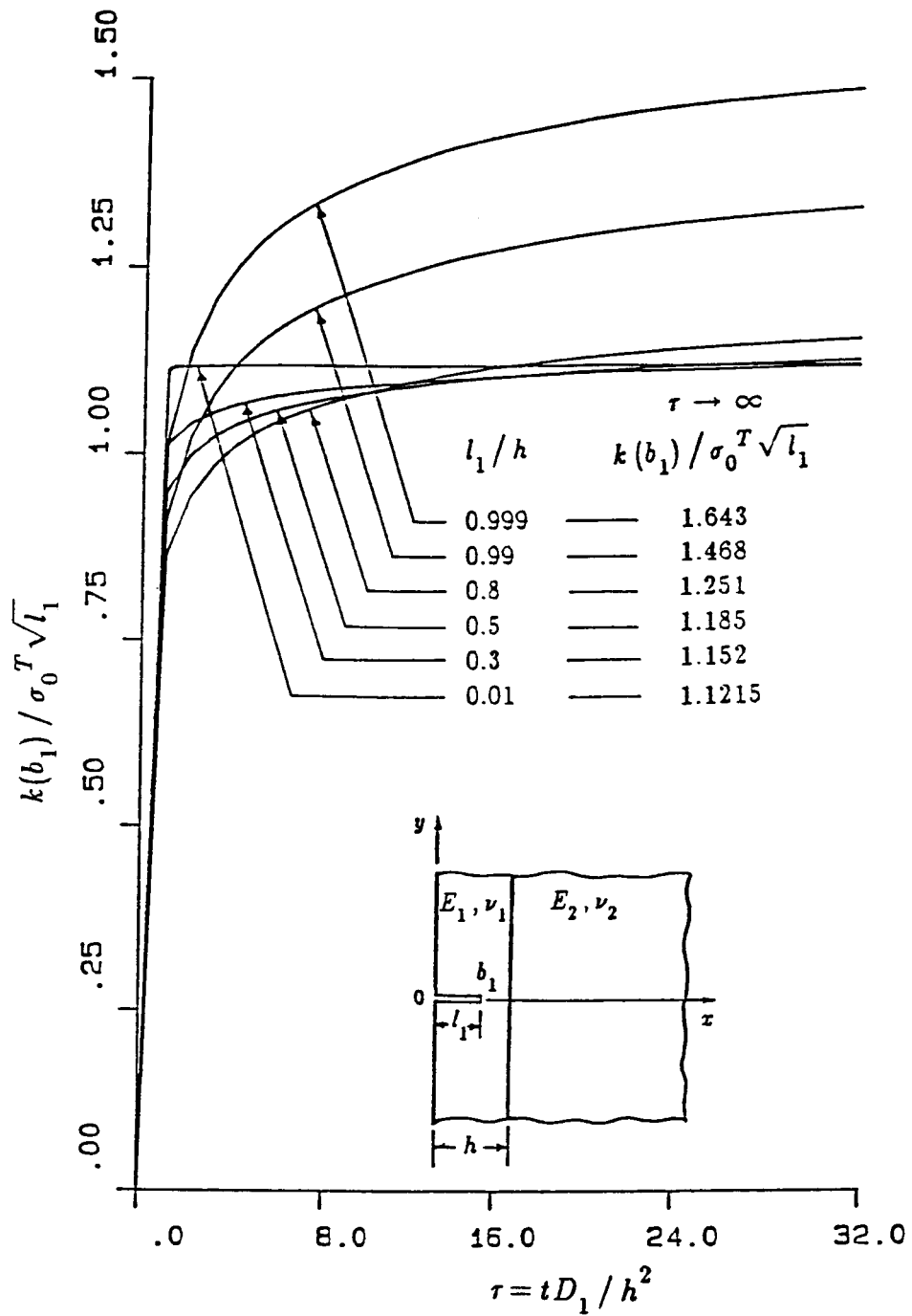


Figure 6-30: The normalized stress intensity factor $k(b_1)$ as a function of nondimensional time τ for an edge crack of various lengths in Model I for $\tau_0=0.0$, $\tau_0=t_0 D_1/h^2$, $\sigma_0^T=-\alpha_1 E_1 \Theta_0/(1-\nu_1)$ (Material pair B)

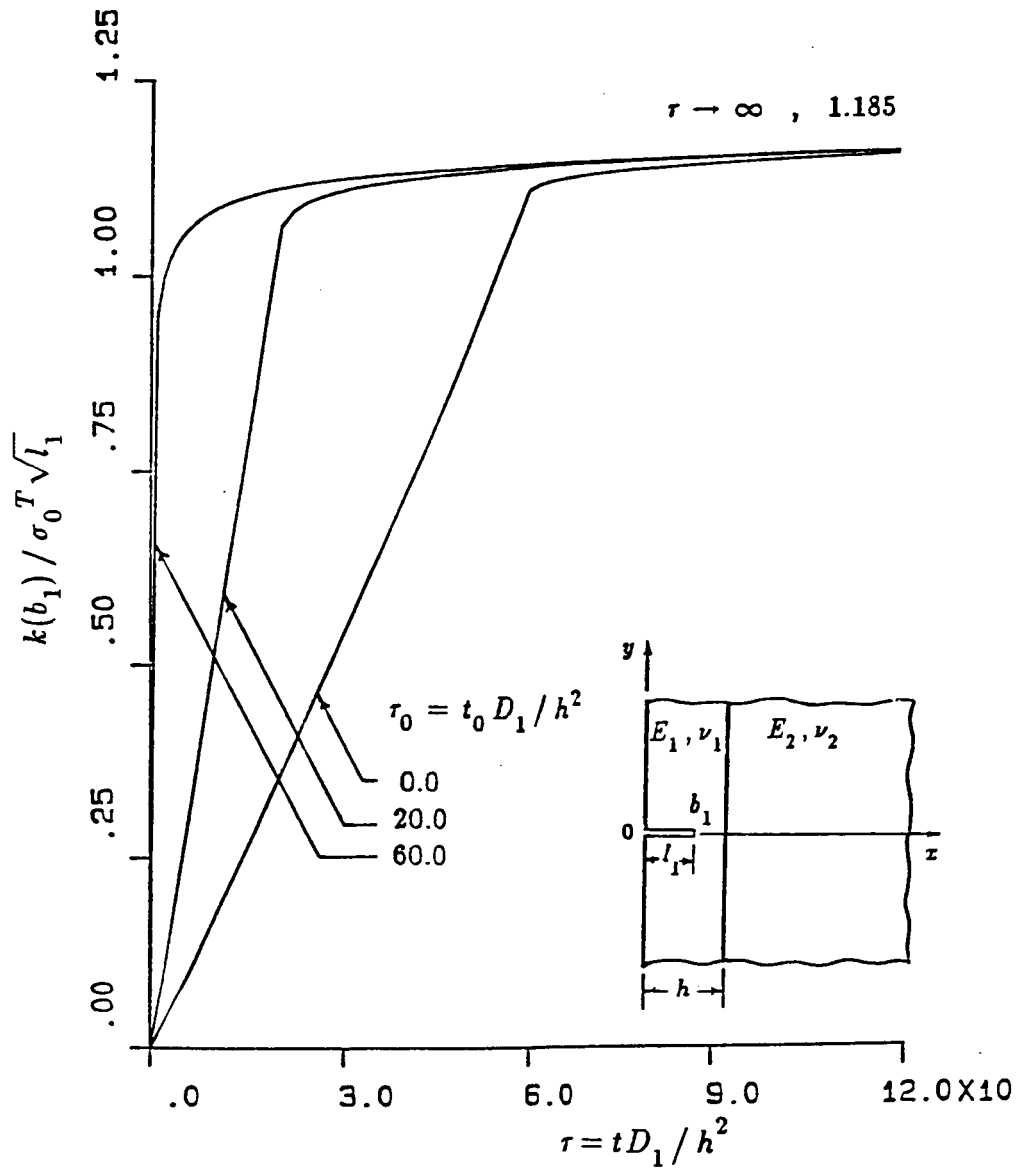


Figure 6-31: The influence of τ_0 on the normalized stress intensity factor $k(b_1)$ as a function of nondimensional time τ for an edge crack of length $l_1/h=0.5$ in Model I, $\tau_0=t_0 D_1/h^2$, $\sigma_0^T = -\alpha'_1 E_1 \Theta_0/(1-\nu_1)$ (Material pair B)

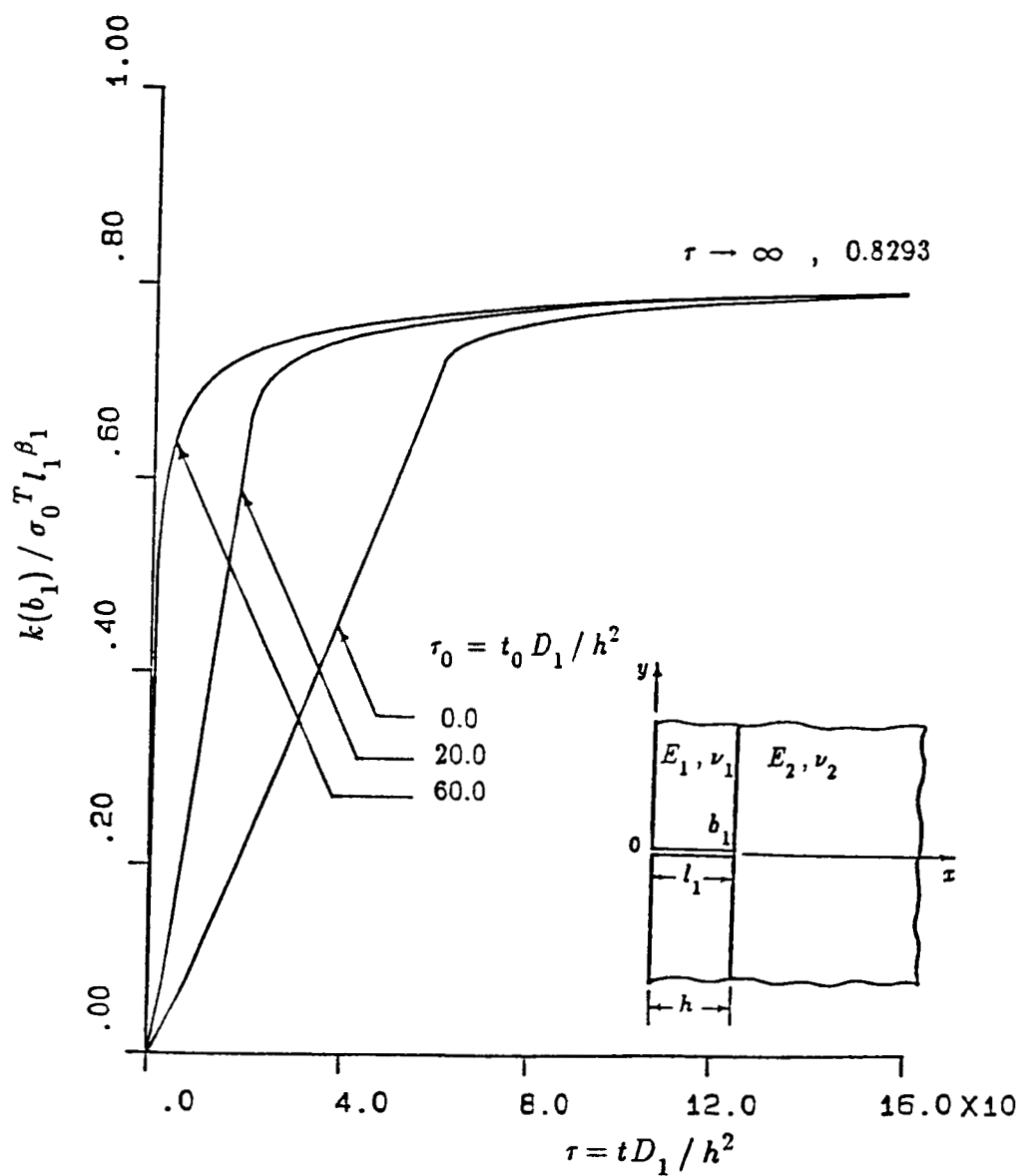


Figure 6-32: The influence of τ_0 on the normalized stress intensity factor $k(b_1)$ as a function of nondimensional time τ for a broken clad in Model I, $\tau_0 = t_0 D_1 / h^2$, $\sigma_0^T = -\alpha_1 E_1 \Theta_0 / (1 - \nu_1)$, $\beta_1 = 0.552538$. (Material pair B)

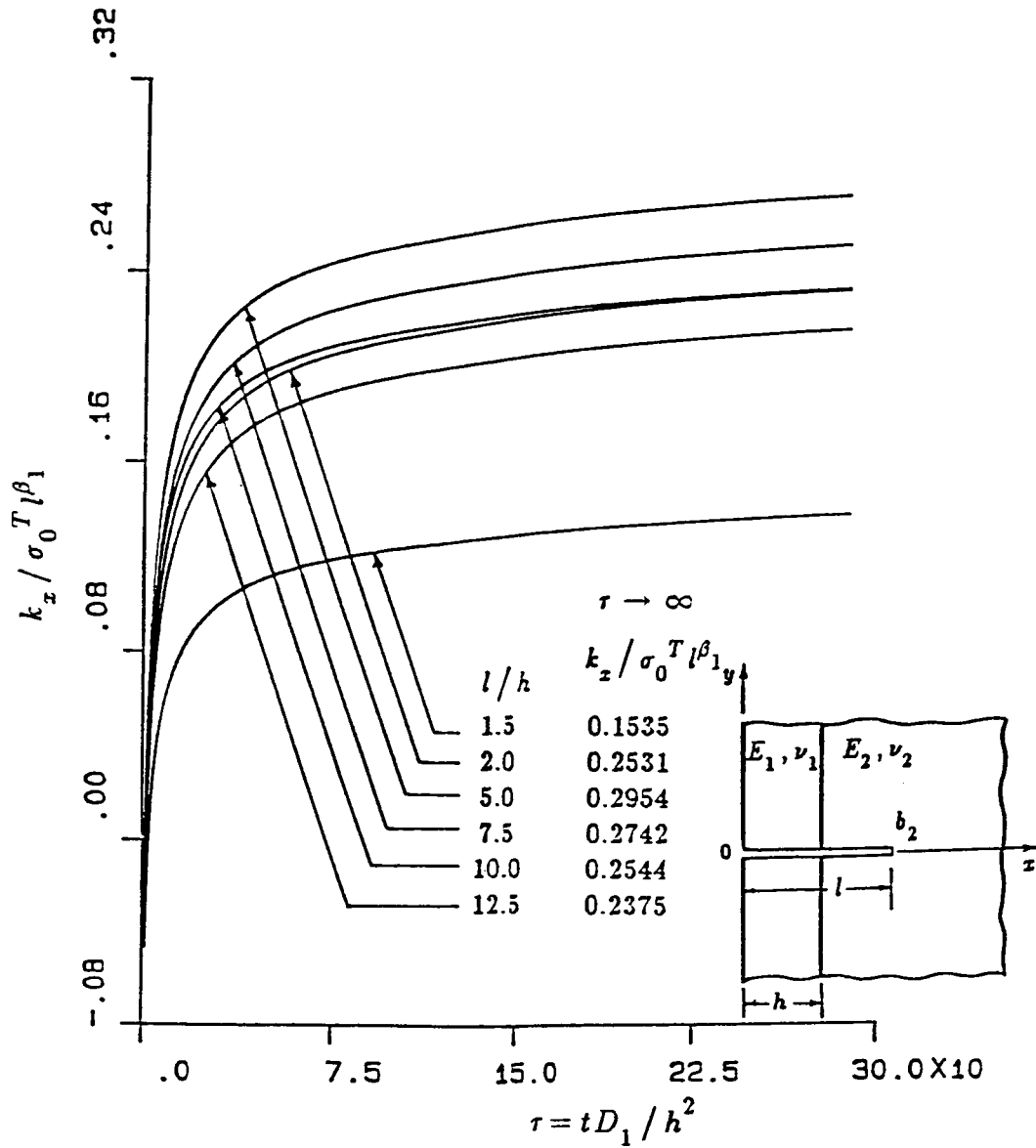


Figure 6-33: The normalized stress intensity factor k_x as a function of nondimensional time τ for an edge crack of various lengths crossing the interface in Model I for $\tau_0=0.0$, $\tau_0=t_0 D_1/h^2$, $\sigma_0^T = -\alpha'_1 E_1 \Theta_0/(1-\nu_1)$, $\beta_1=\alpha_2=0.01872238$. (Material pair B)

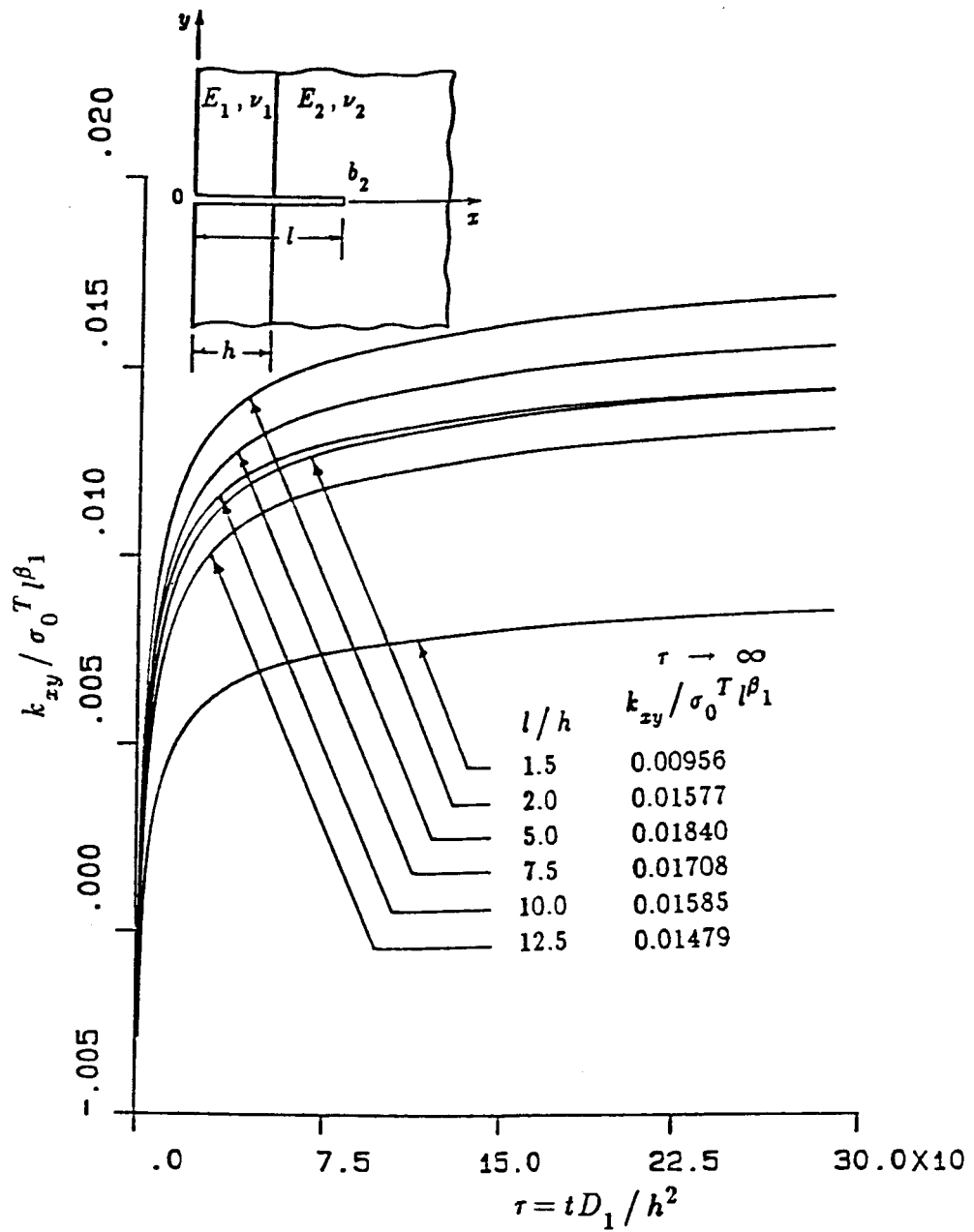


Figure 6-34: The normalized stress intensity factor k_{xy} as a function of nondimensional time τ for an edge crack for various lengths crossing the interface in Model I for $\tau_0=0.0$, $\tau_0=t_0 D_1/h^2$, $\sigma_0^T = -\alpha_1' E_1 \Theta_0/(1-\nu_1)$, $\beta_1 = \alpha_2 = 0.01872238$. (Material pair B)

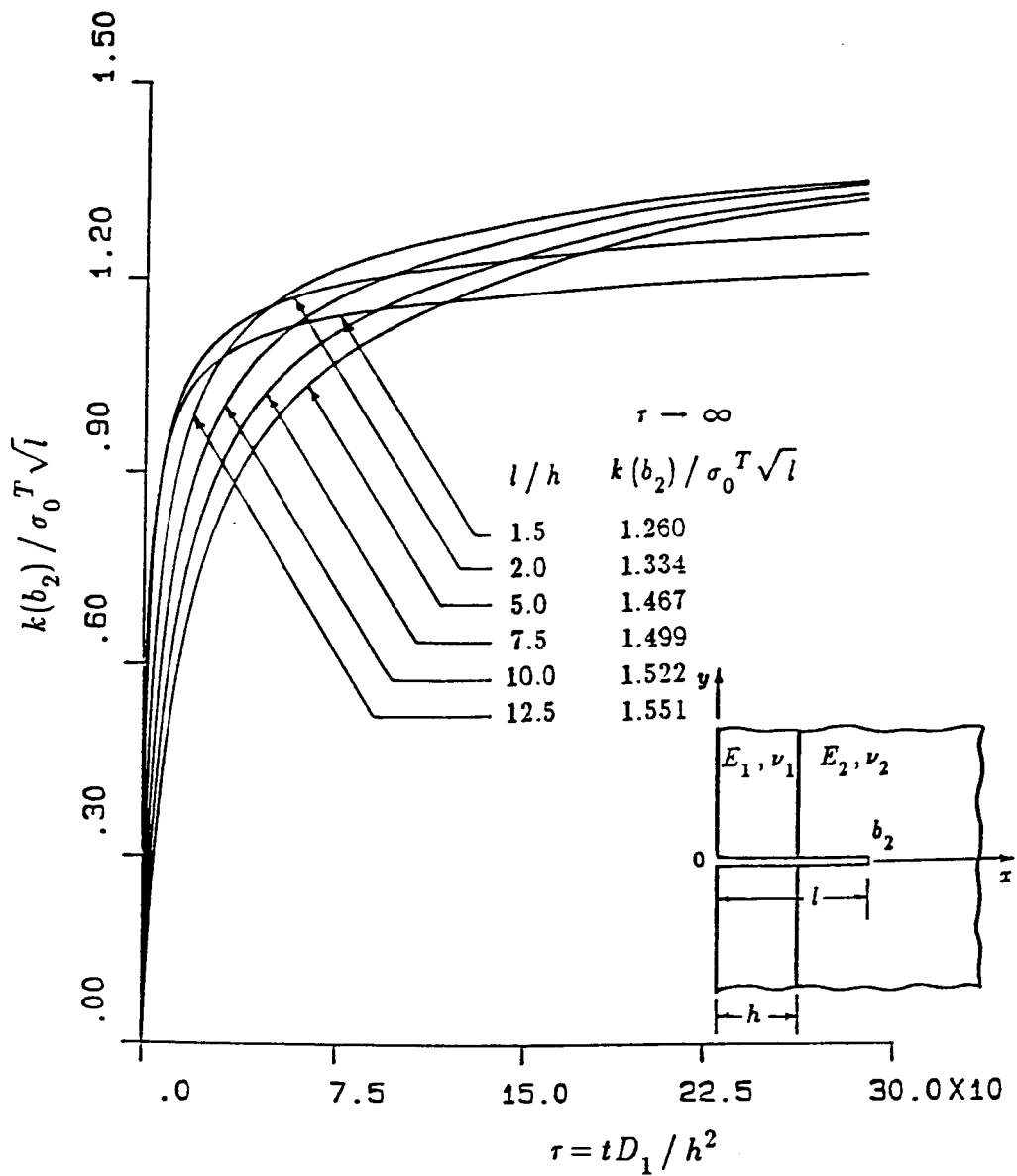


Figure 6-35: The normalized stress intensity factor $k(b_2)$ as a function of nondimensional time τ for an edge crack of various lengths crossing the interface in Model I for $\tau_0=0.0$, $\tau_0=t_0 D_1/h^2$, $\sigma_0^T = -\alpha_1' E_1 \Theta_0 / (1-\nu_1)$, $\beta_1 = \alpha_2 = 0.01872238$. (Material pair B)

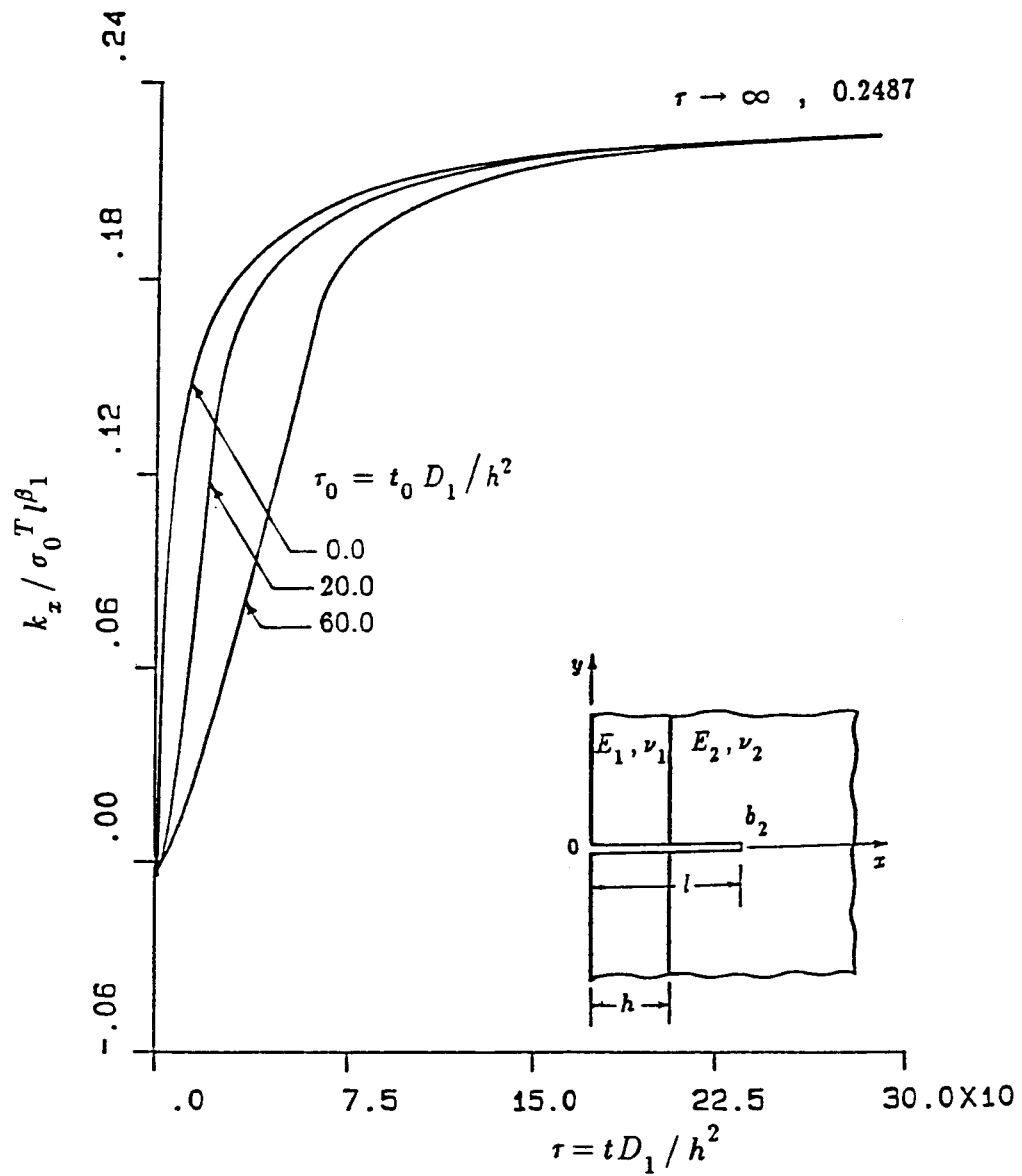


Figure 6-36: The influence of τ_0 on the normalized stress intensity factor k_x as a function of nondimensional time τ for an edge crack crossing the interface $l/h=2.0$ in Model I, $\tau_0=t_0 D_1/h^2$, $\sigma_0^T = -\alpha_1' E_1 \Theta_0/(1-\nu_1)$, $\beta_1=\alpha_2=0.01872238$. (Material pair B)

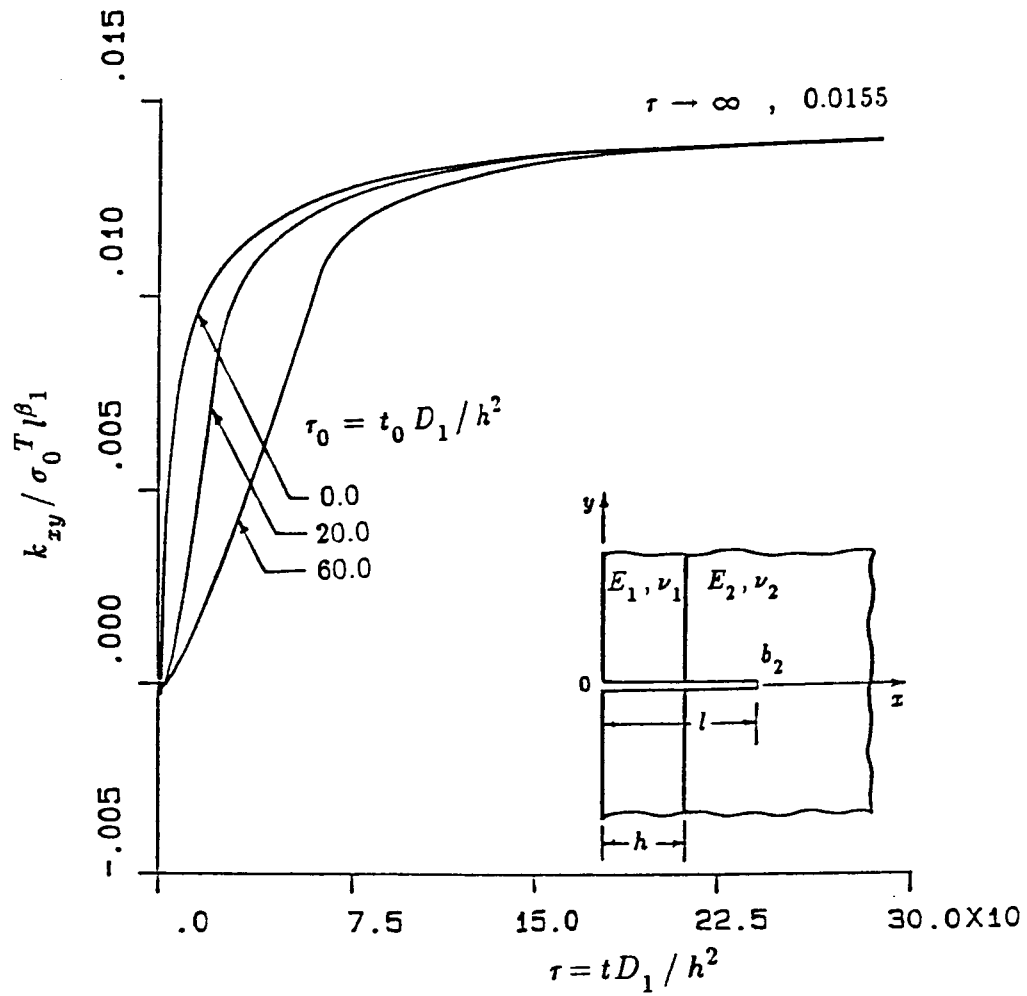


Figure 6-37: The influence of τ_0 on the normalized stress intensity factor k_{xy} as a function of nondimensional time τ for an edge crack crossing the interface $l/h=2.0$ in Model I, $\tau_0=t_0 D_1/h^2$, $\sigma_0^T = -\alpha_1' E_1 \Theta_0/(1-\nu_1)$, $\beta_1=\alpha_2=0.01872238$. (Material pair B)

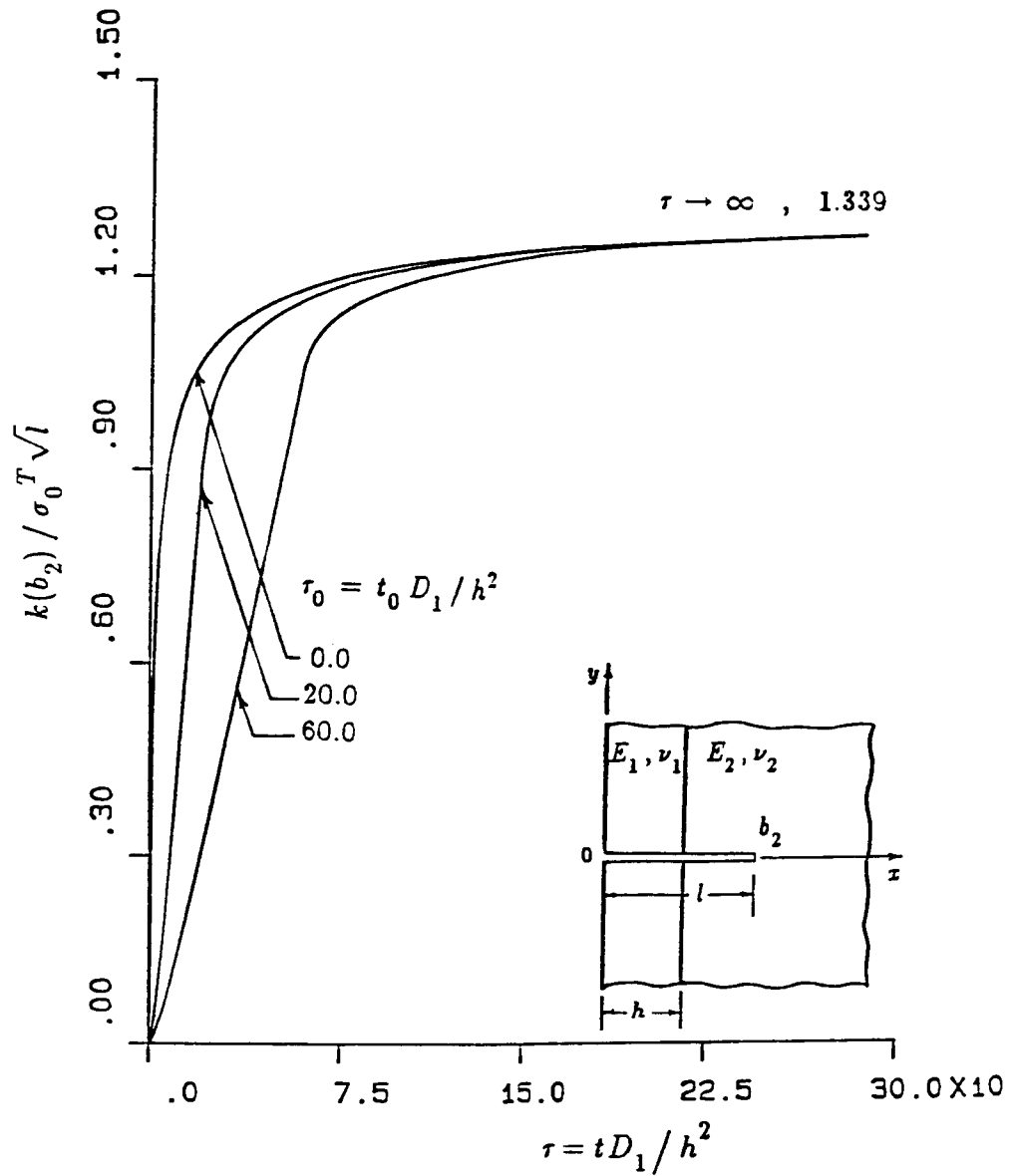


Figure 6-38: The influence of τ_0 on the normalized stress intensity factor $k(b_2)$ as a function of nondimensional time τ for an edge crack crossing the interface $l/h=2.0$ in Model I , $\tau_0 = t_0 D_1 / h^2$, $\sigma_0^T = -\alpha_1' E_1 \Theta_0 / (1-\nu_1)$, $\beta_1 = \alpha_2 = 0.01872238$. (Material pair B)

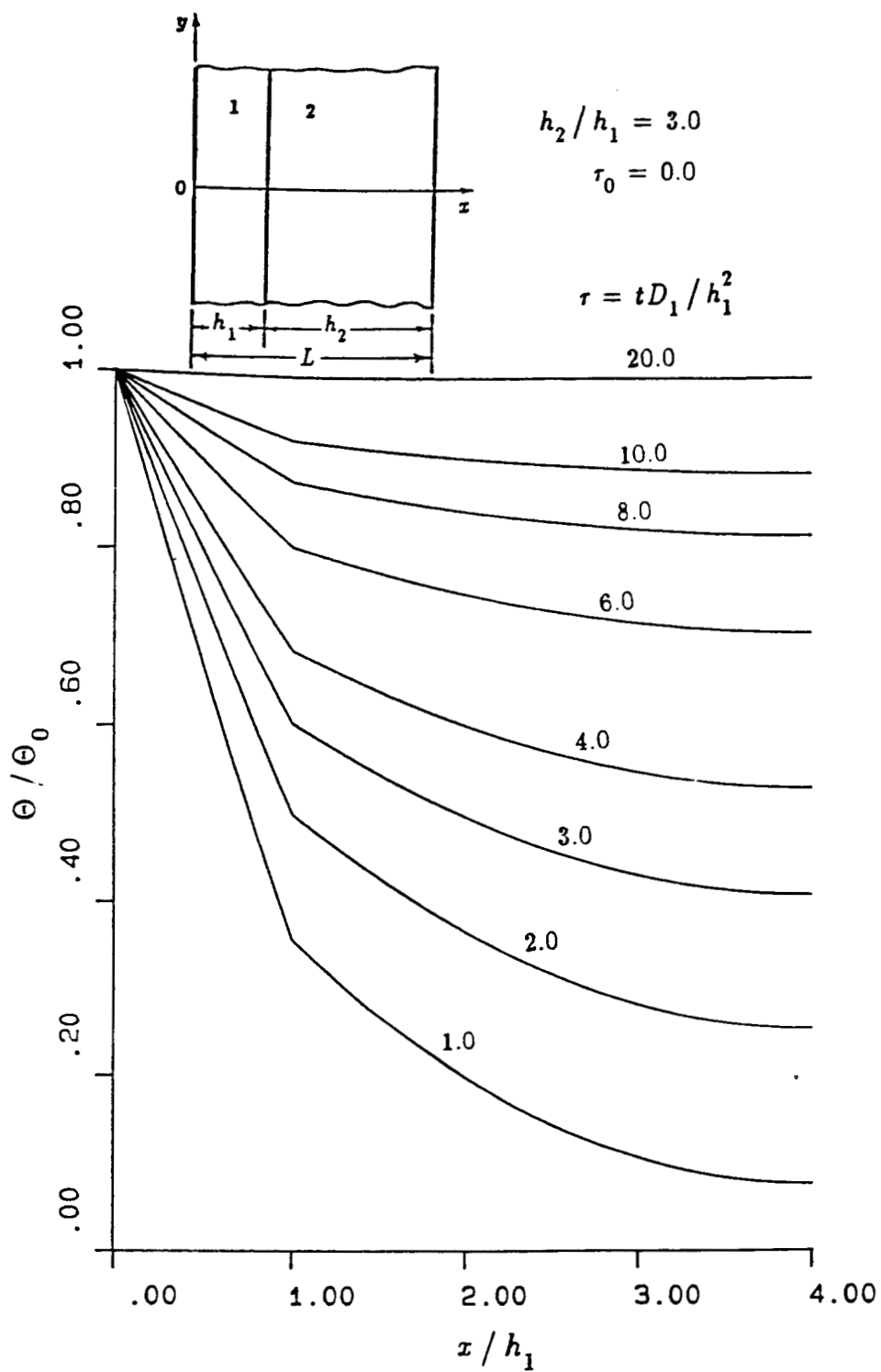


Figure 6-39: The normalized transient temperature distribution in Model II for $\tau_0=0.0$, $h_2/h_1=3.0$, $\tau_0=t_0D_1/h_1^2$, (Material pair A)

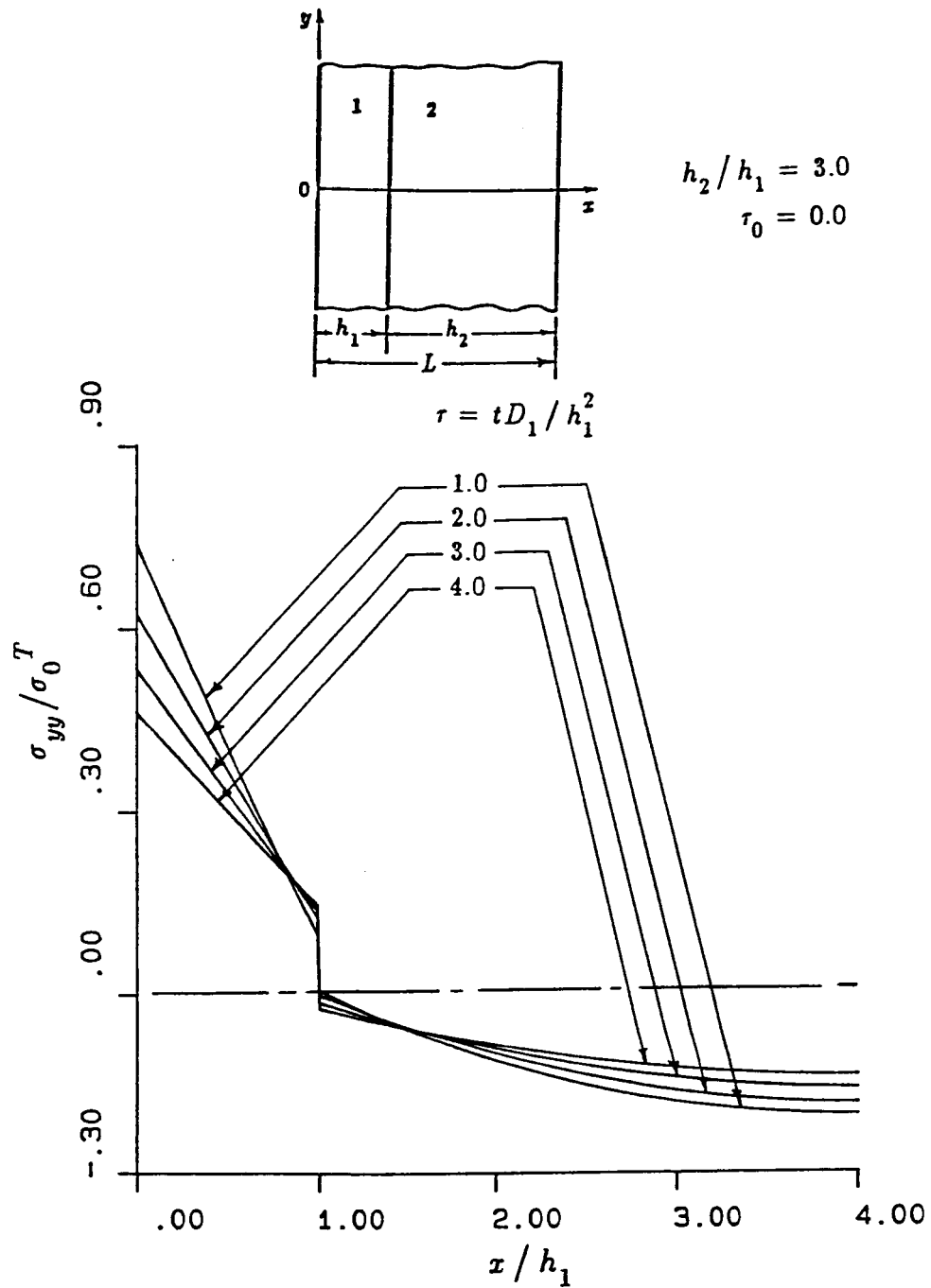


Figure 6-40: The normalized transient stress distribution σ_{yy}/σ_0^T in Model II for $\tau_0=0.0$, $h_2/h_1=3.0$, $\tau_0=t_0D_1/h_1^2$, $\sigma_0^T=-\alpha_1' E_1 \Theta_0/(1-\nu_1)$. (Material pair A)

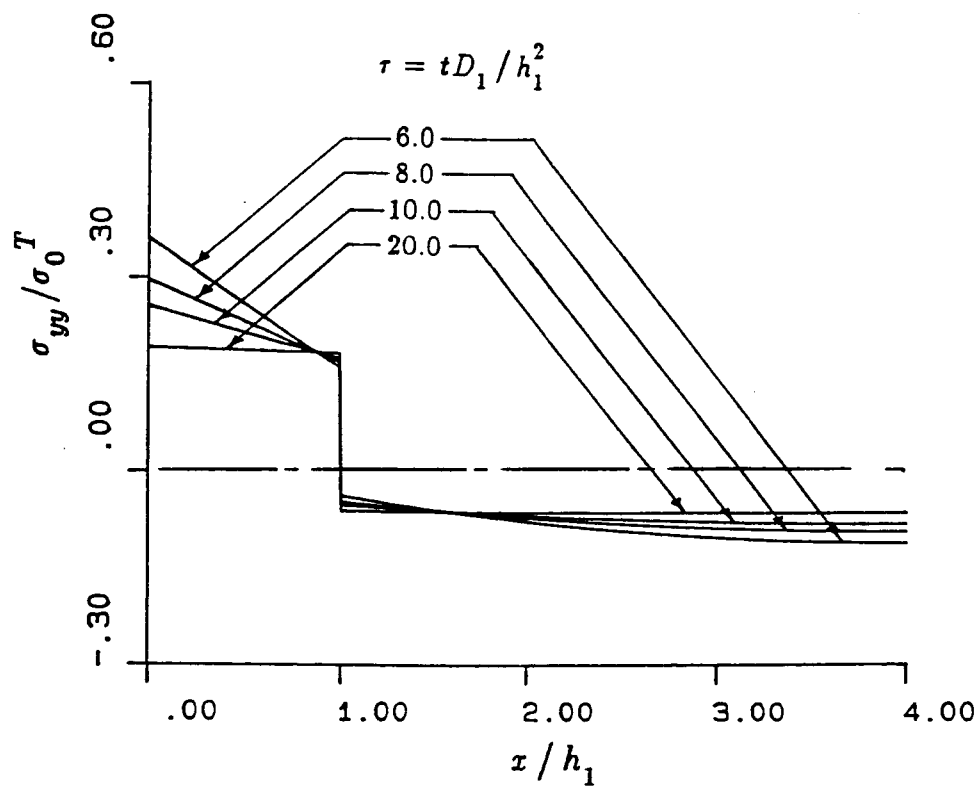


Figure 6-40, continued

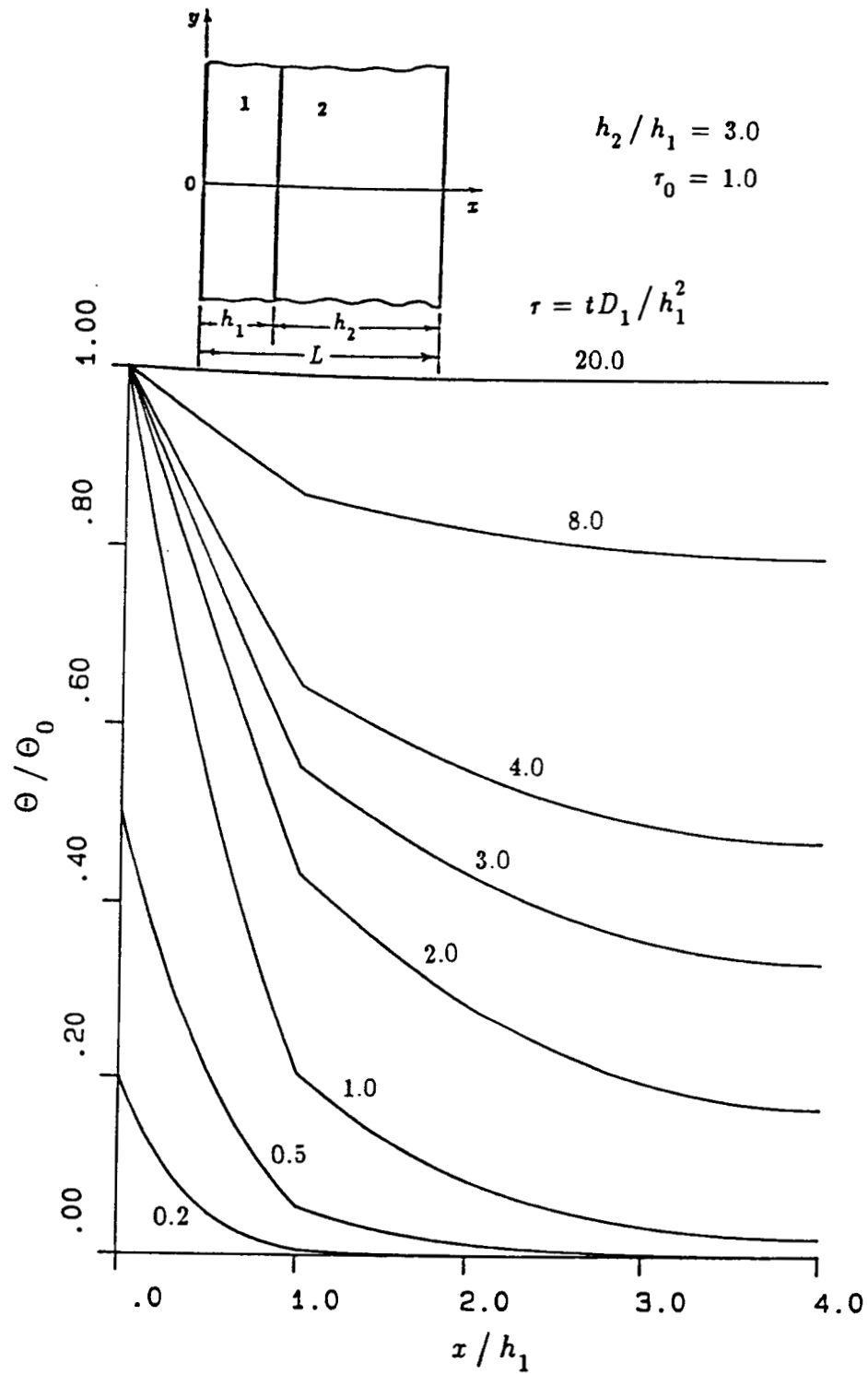


Figure 6-41: The normalized transient temperature distribution in Model II for $\tau_0 = 1.0$, $h_2/h_1 = 3.0$, $\tau_0 = t_0 D_1 / h_1^2$, (Material pair A)

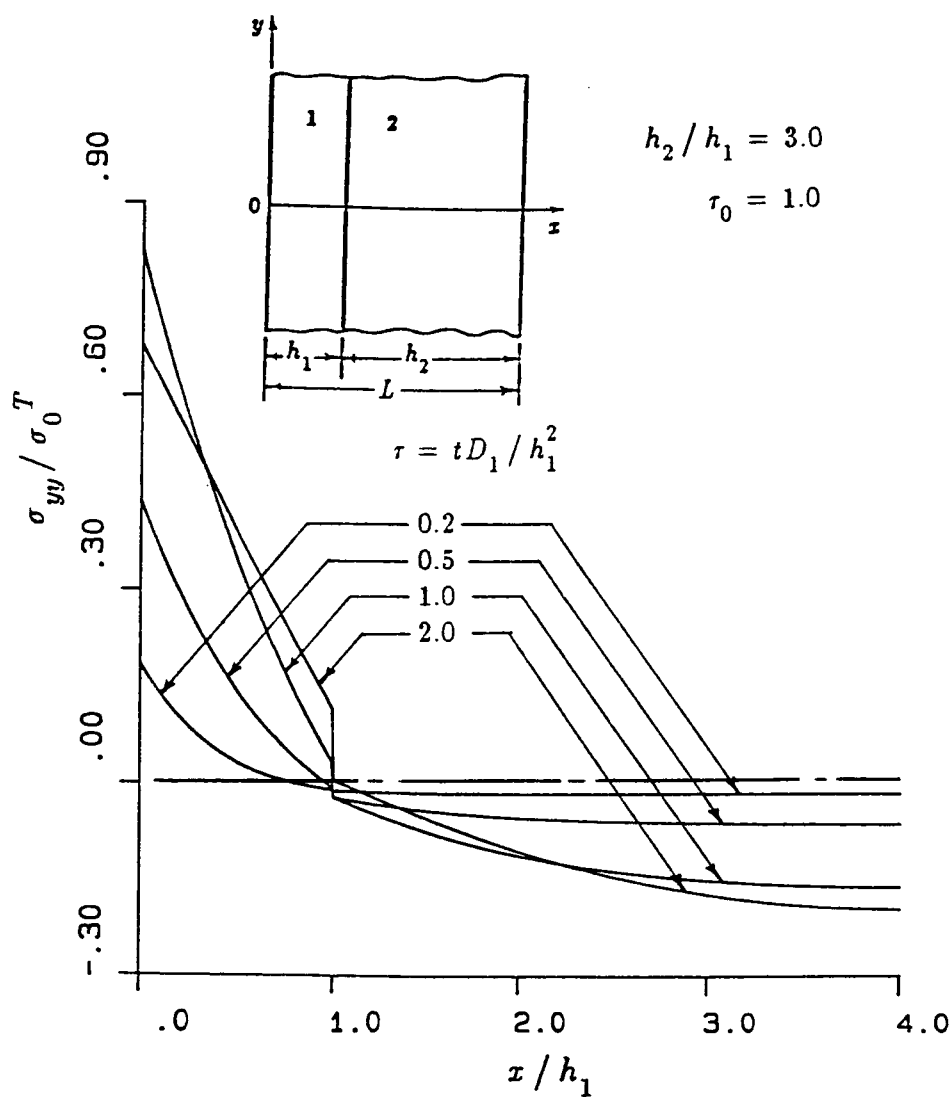


Figure 6-42: The normalized transient stress distribution σ_{yy}/σ_0^T in Model II for $\tau_0=1.0$, $h_2/h_1=3.0$, $\tau_0=t_0D_1/h_1^2$, $\sigma_0^T=-\alpha_1 E_1 \Theta_0/(1-\nu_1)$. (Material pair A)

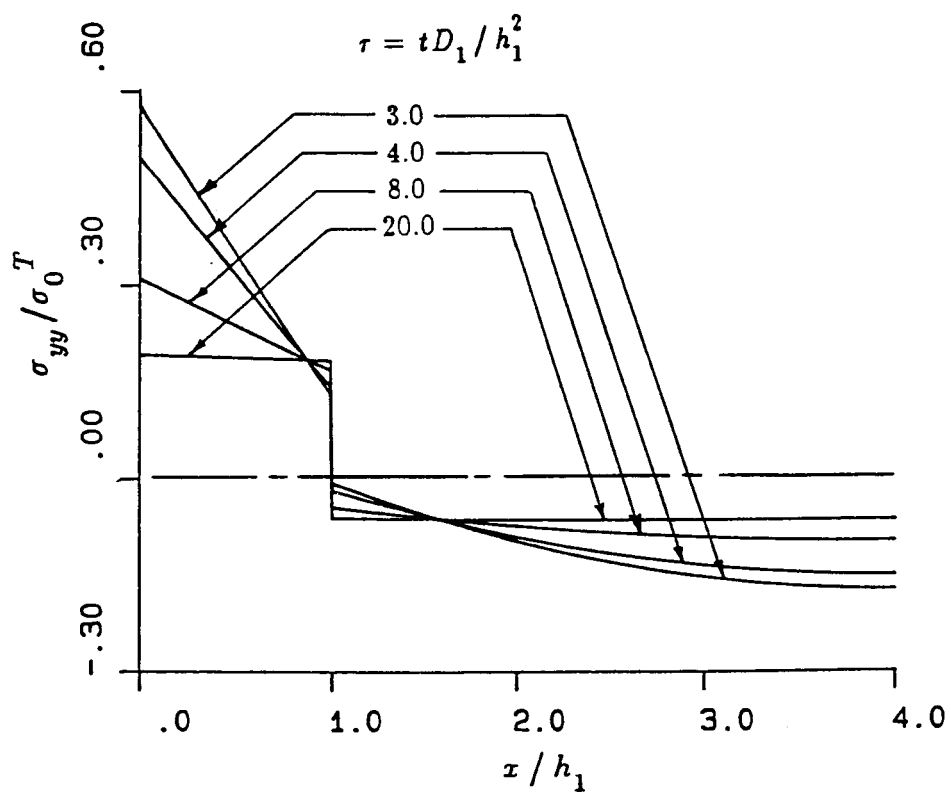


Figure 6-42, continued

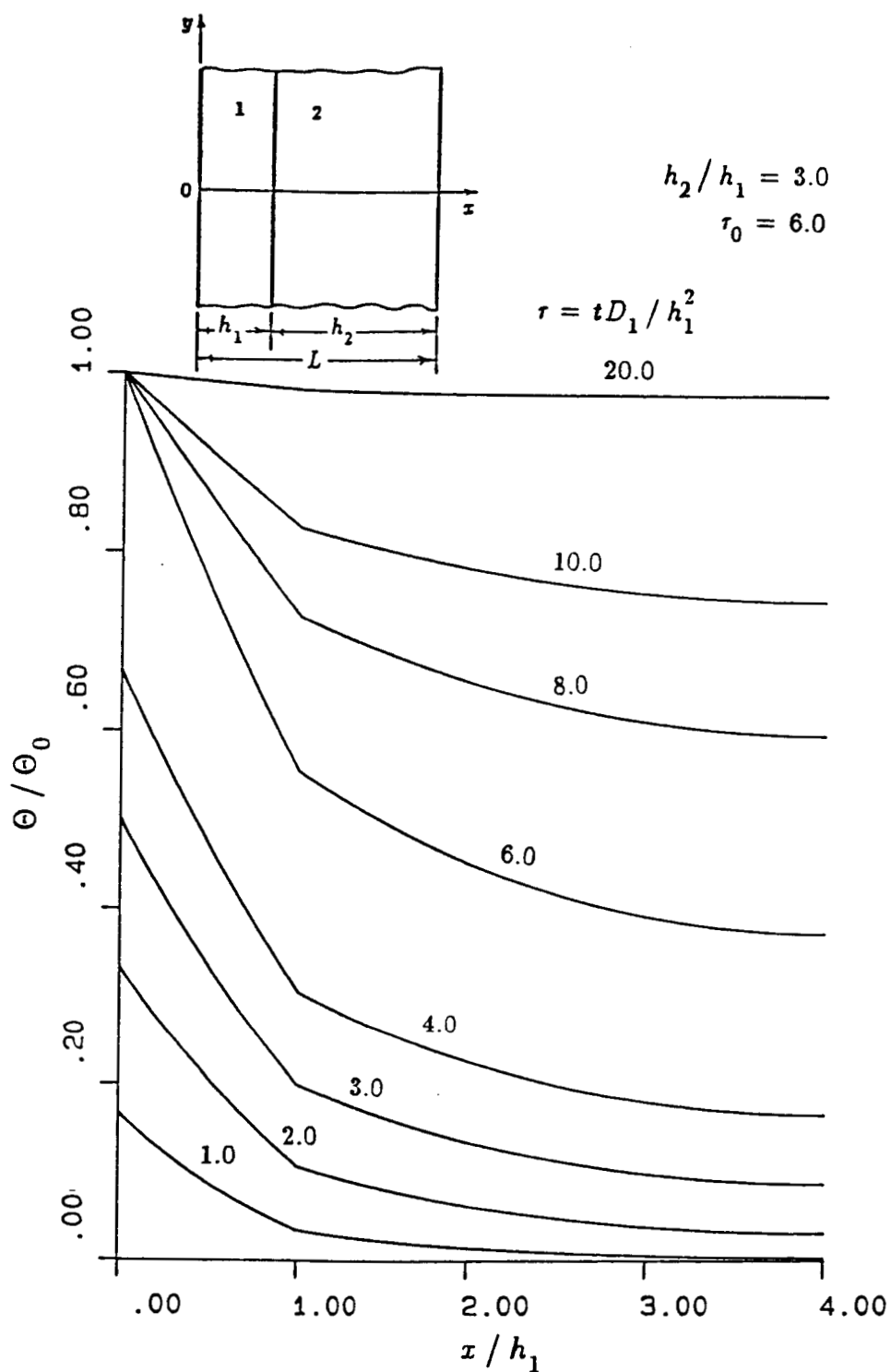


Figure 6-43: The normalized transient temperature distribution in Model II for $\tau_0=6.0$, $h_2/h_1=3.0$, $\tau_0=t_0D_1/h_1^2$, (Material pair A)

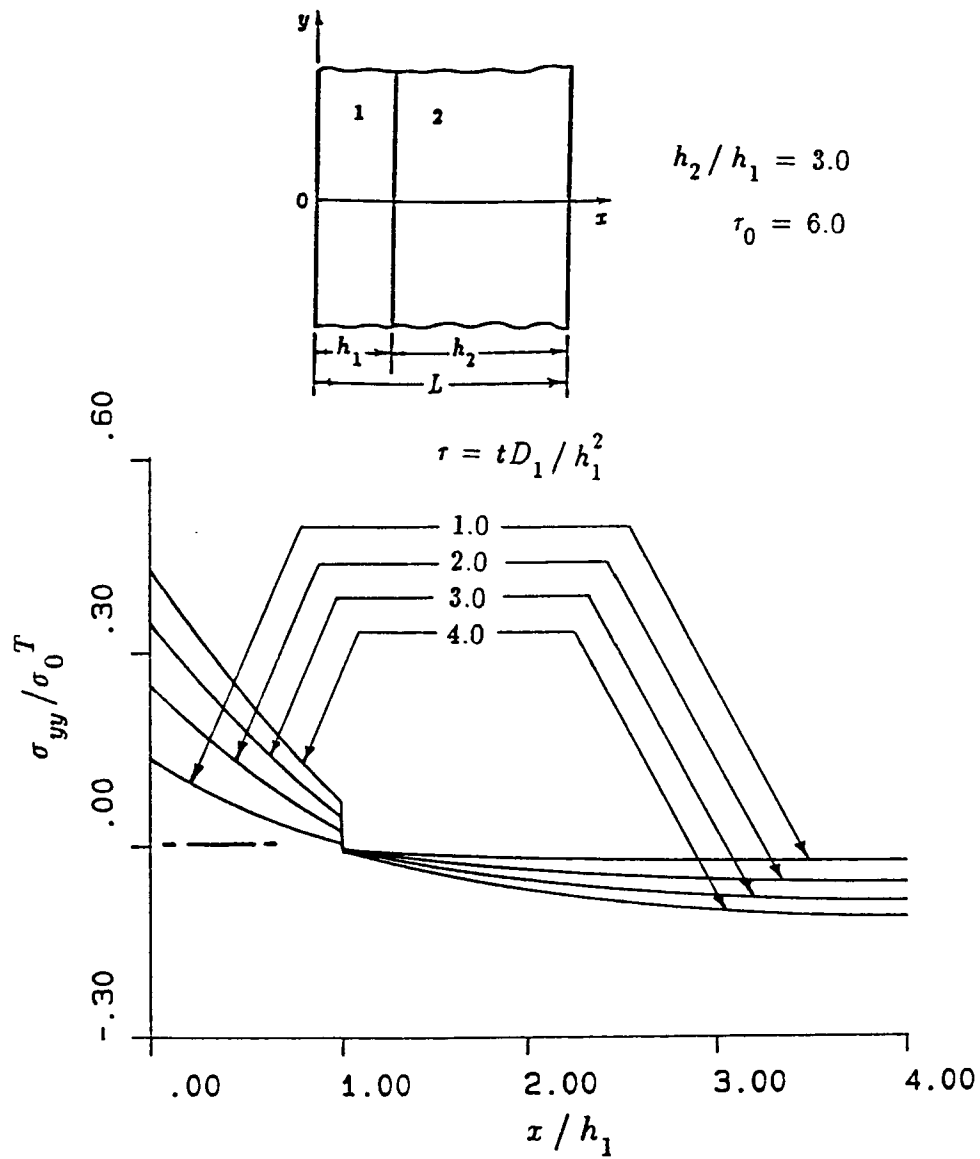


Figure 6-44: The normalized transient stress distribution σ_{yy} / σ_0^T in Model II for $\tau_0 = 6.0$, $h_2 / h_1 = 3.0$, $\tau_0 = t_0 D_1 / h_1^2$, $\sigma_0^T = -\alpha_1' E_1 \Theta_0 / (1 - \nu_1)$. (Material pair A)

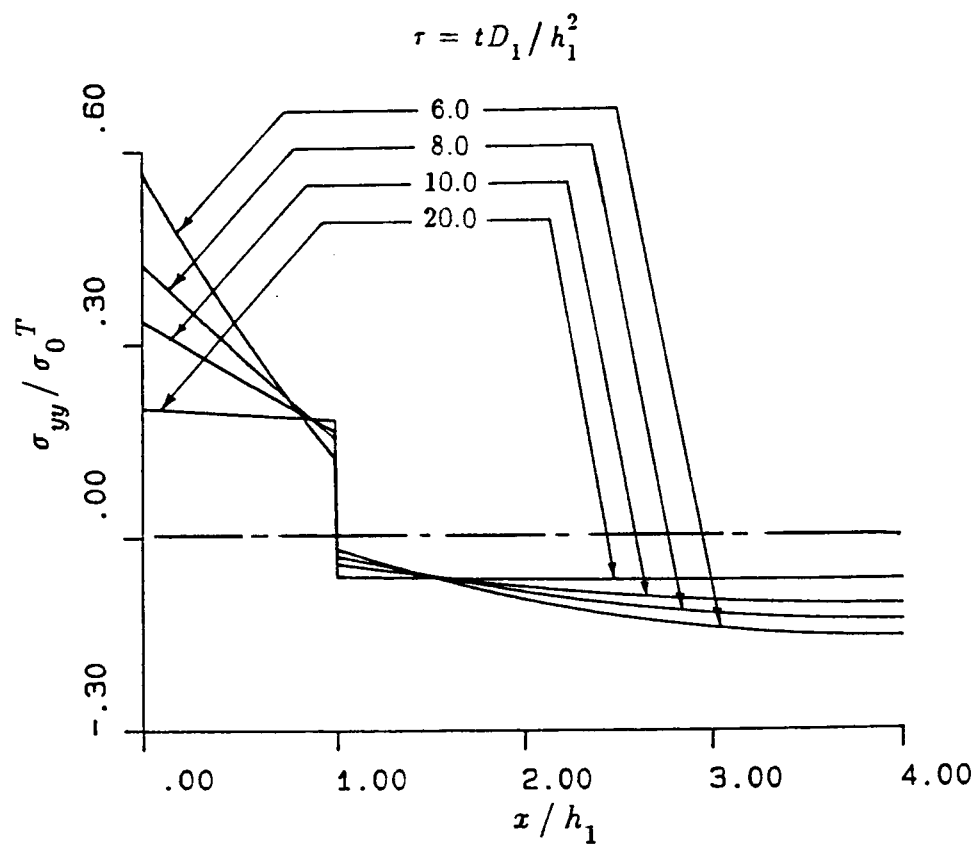


Figure 6-44, continued

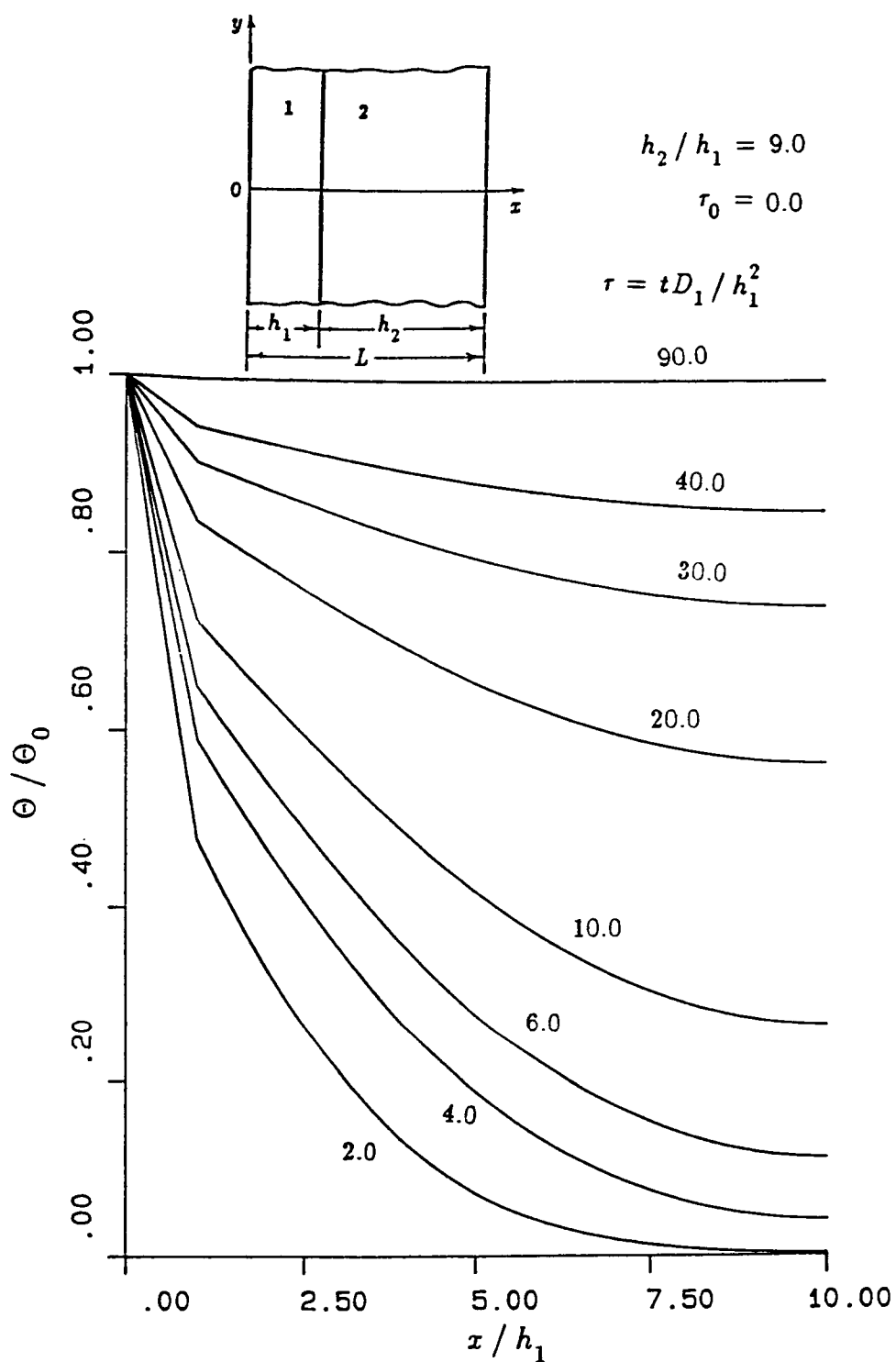


Figure 6-45: The normalized transient temperature distribution in Model II for $\tau_0=0.0$, $h_2/h_1=9.0$, $\tau_0=t_0 D_1/h_1^2$, (Material pair A)

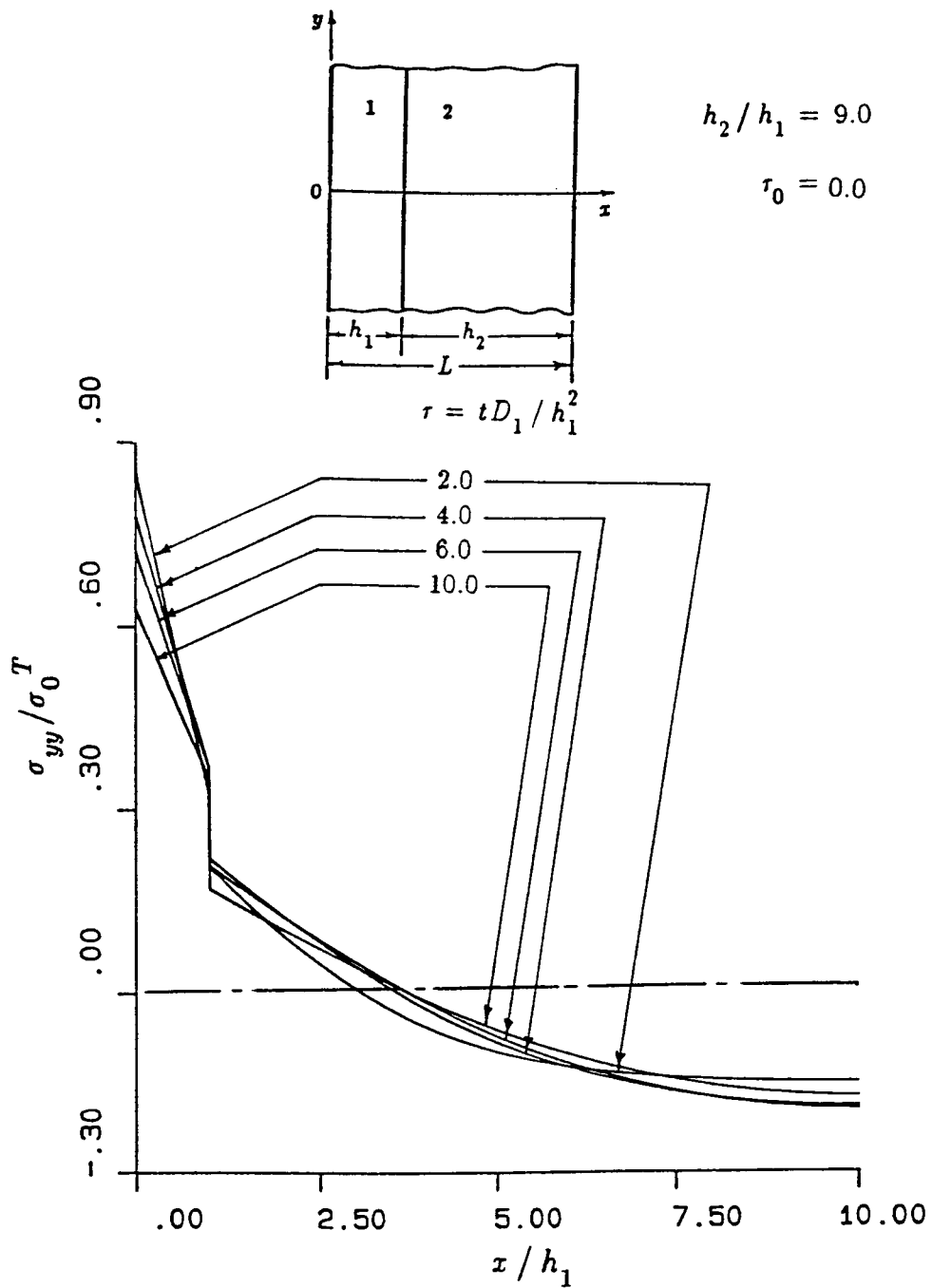


Figure 6-46: The normalized transient stress distribution σ_{yy}/σ_0^T in Model II for $\tau_0=0.0$, $h_2/h_1=9.0$, $\tau_0=t_0 D_1/h_1^2$, $\sigma_0^T=-\alpha_1' E_1 \Theta_0/(1-\nu_1)$. (Material pair A)

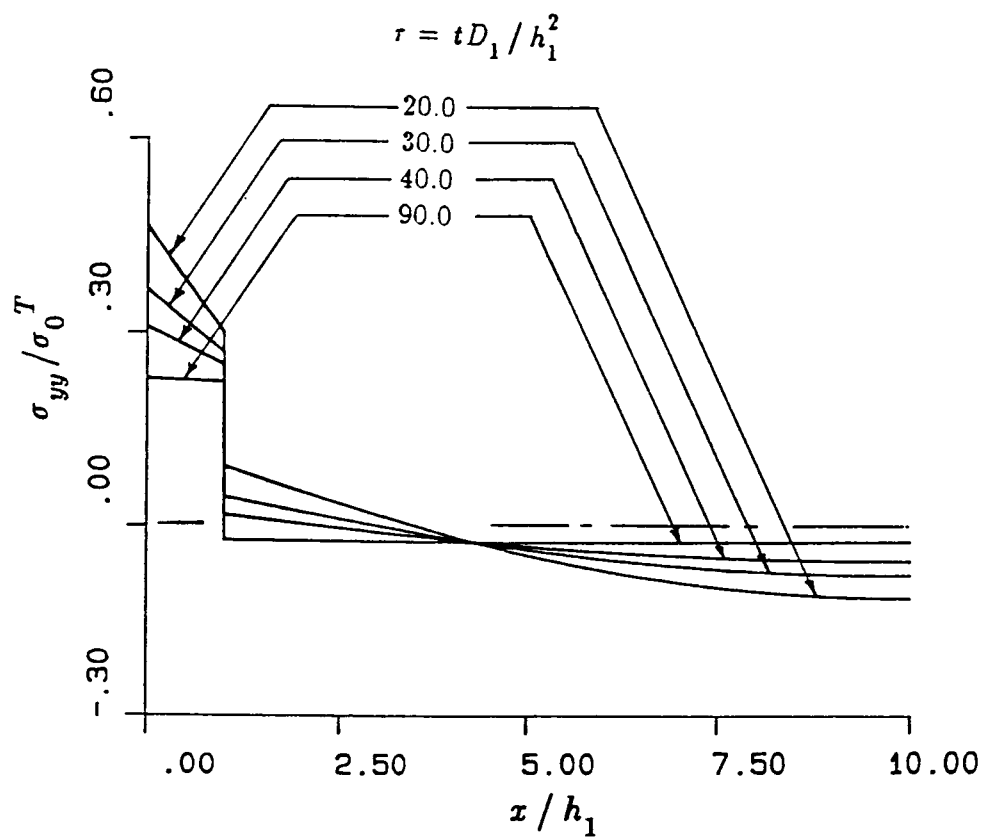


Figure 6-46, continued

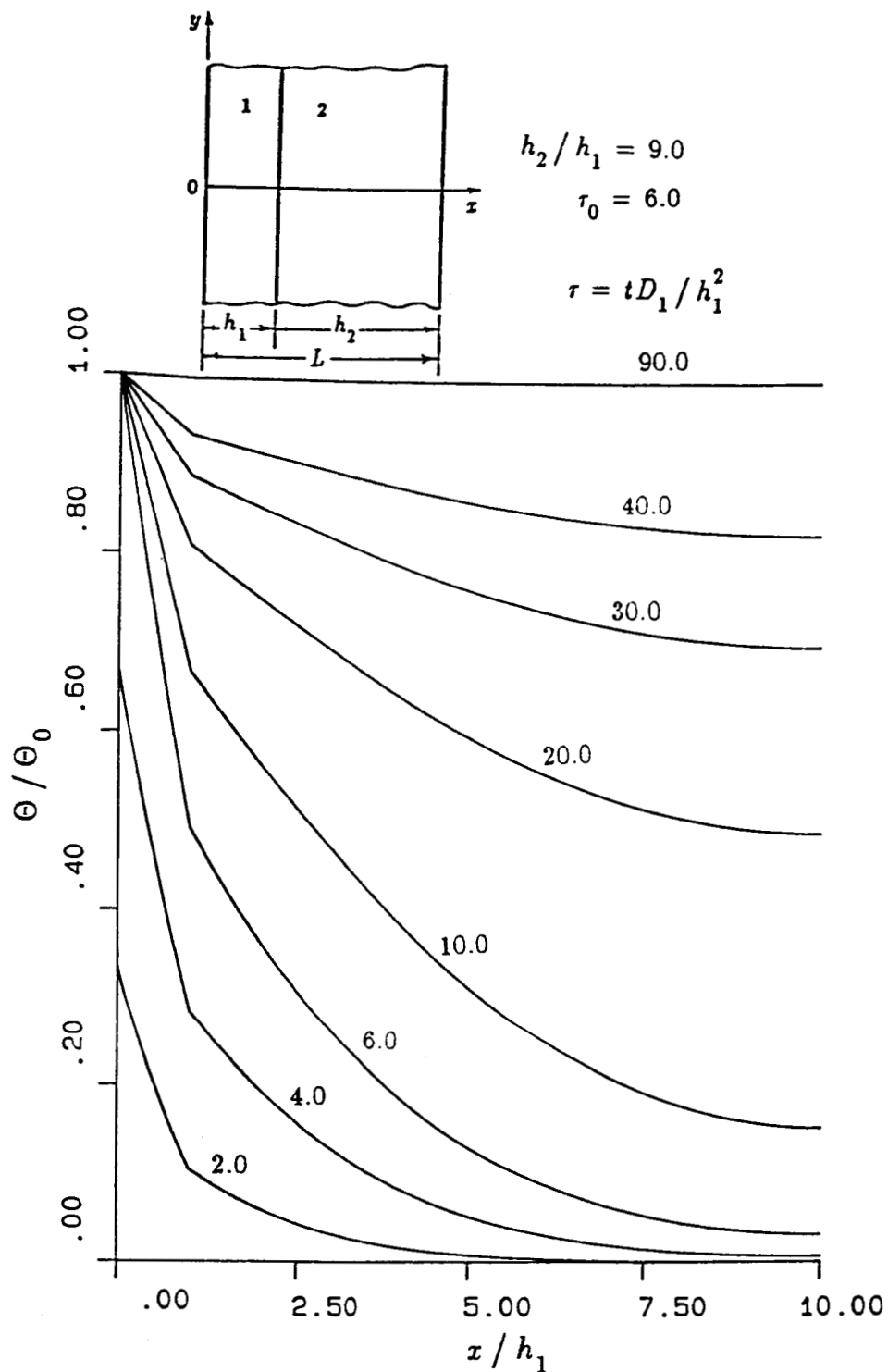


Figure 6-47: The normalized transient temperature distribution in Model II for $\tau_0=6.0$, $h_2/h_1=9.0$, $\tau_0=t_0D_1/h_1^2$, (Material pair A)

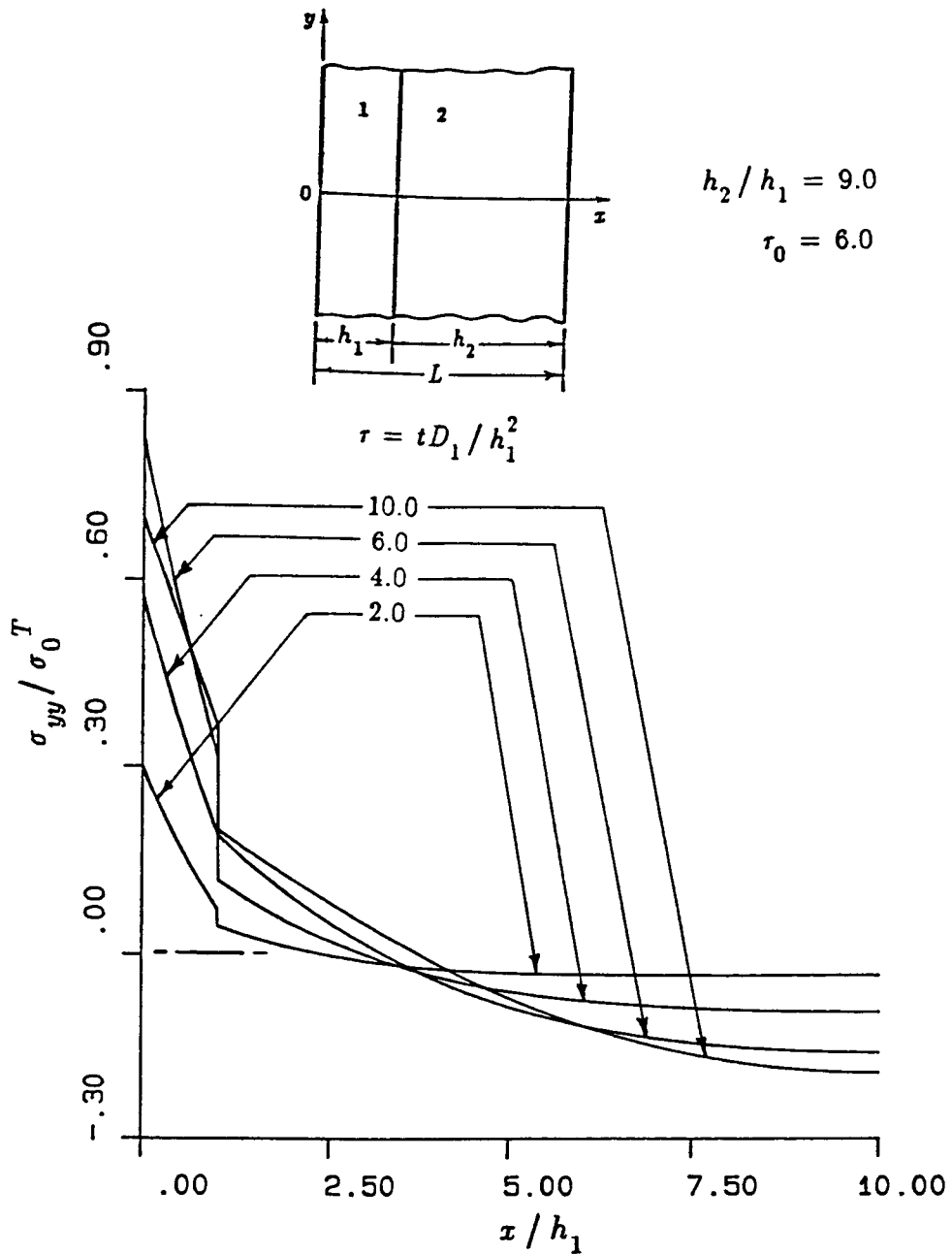


Figure 6-48: The normalized transient stress distribution σ_{yy}/σ_0^T in Model II for $\tau_0=6.0$, $h_2/h_1=9.0$, $\tau_0=t_0D_1/h_1^2$, $\sigma_0^T=-\alpha_1'E_1\Theta_0/(1-\nu_1)$. (Material pair A)

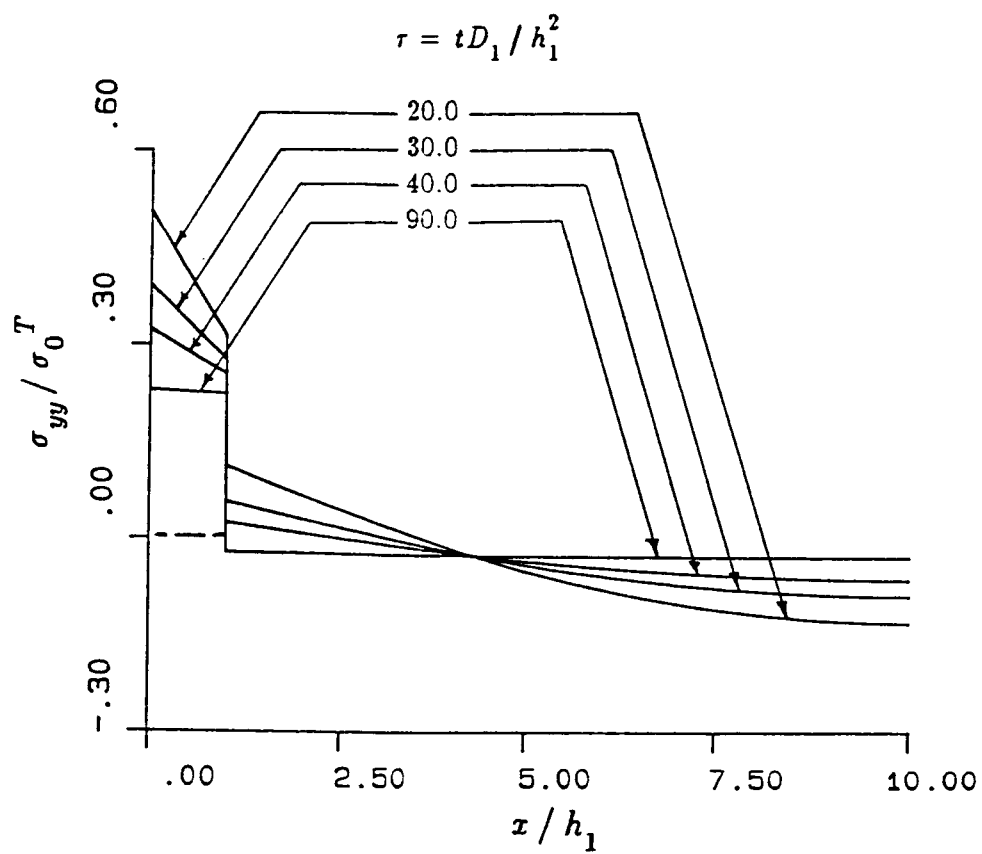


Figure 6-48, continued

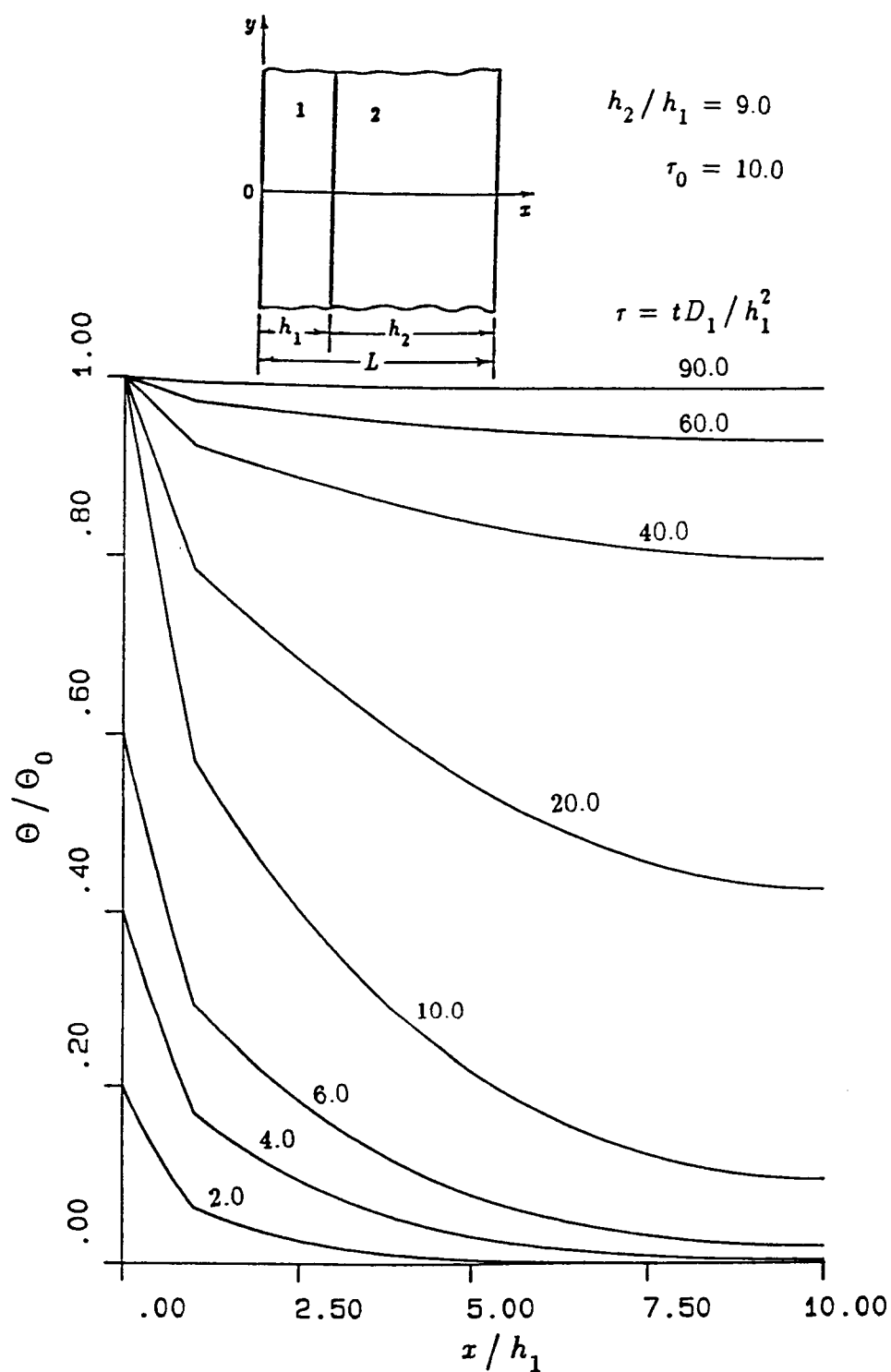


Figure 6-49: The normalized transient temperature distribution in Model II for $\tau_0=10.0$, $h_2/h_1=9.0$, $\tau_0=t_0D_1/h_1^2$, (Material pair A)

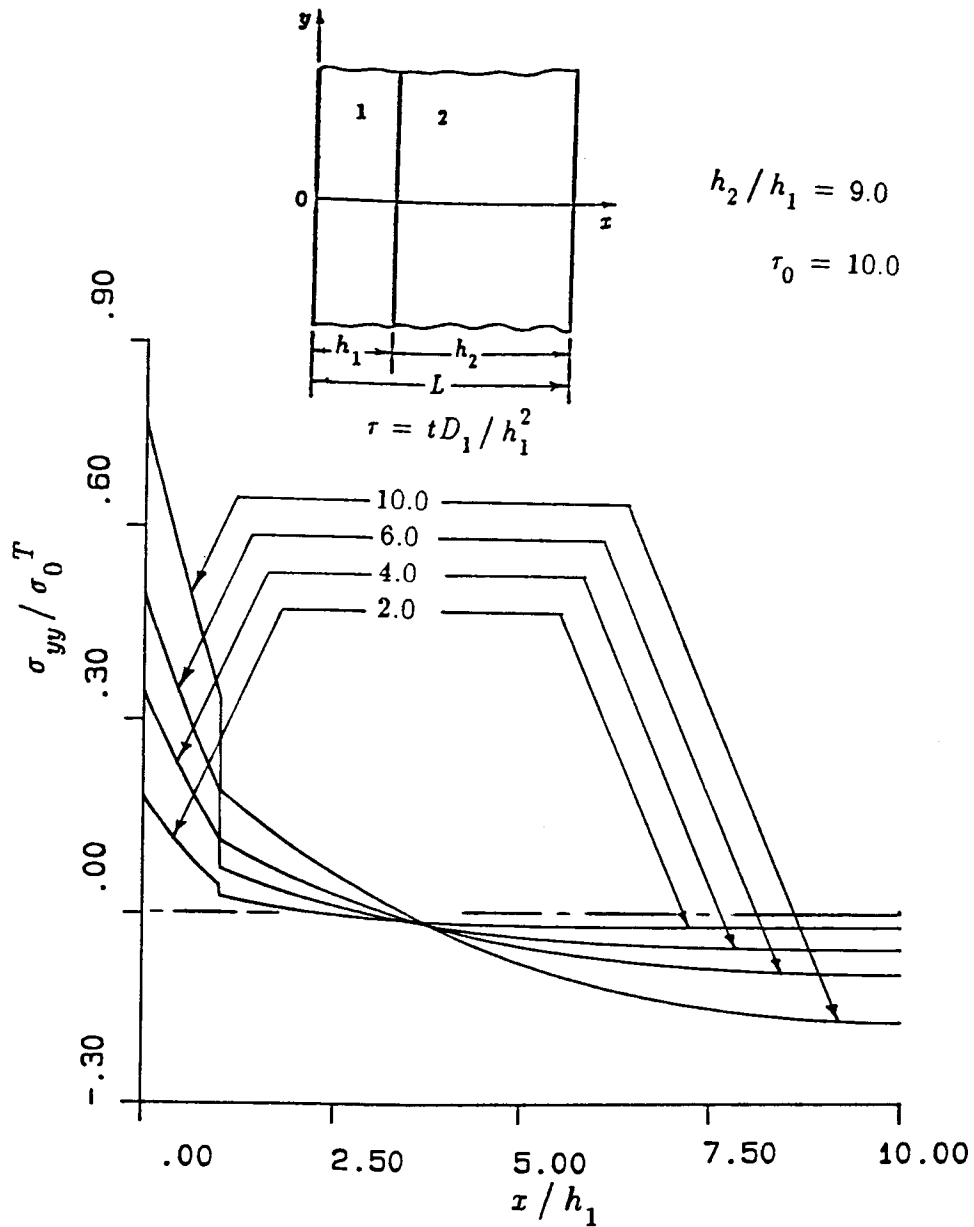


Figure 6-50: The normalized transient stress distribution σ_{yy}/σ_0^T in Model II for $\tau_0=10.0$, $h_2/h_1=9.0$, $\tau_0=t_0D_1/h_1^2$, $\sigma_0^T=-\alpha'_1 E_1 \Theta_0/(1-\nu_1)$. (Material pair A)

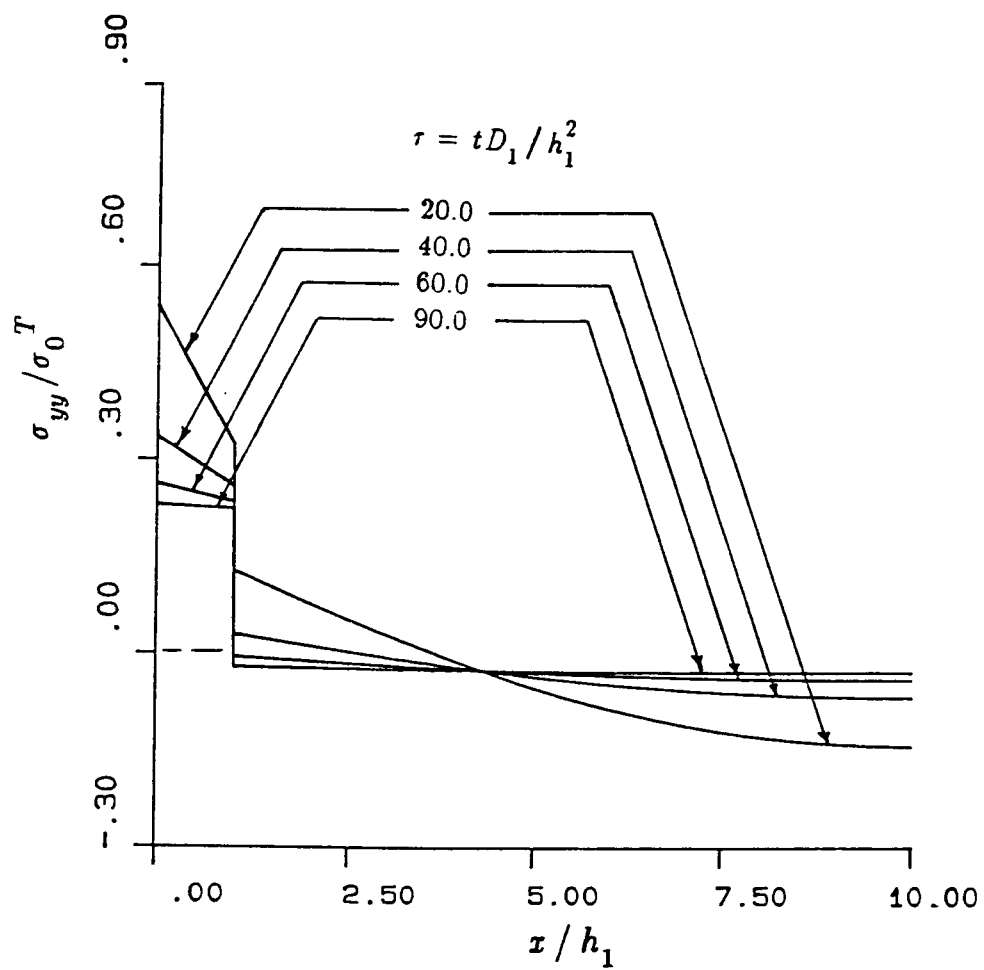


Figure 6-50, continued

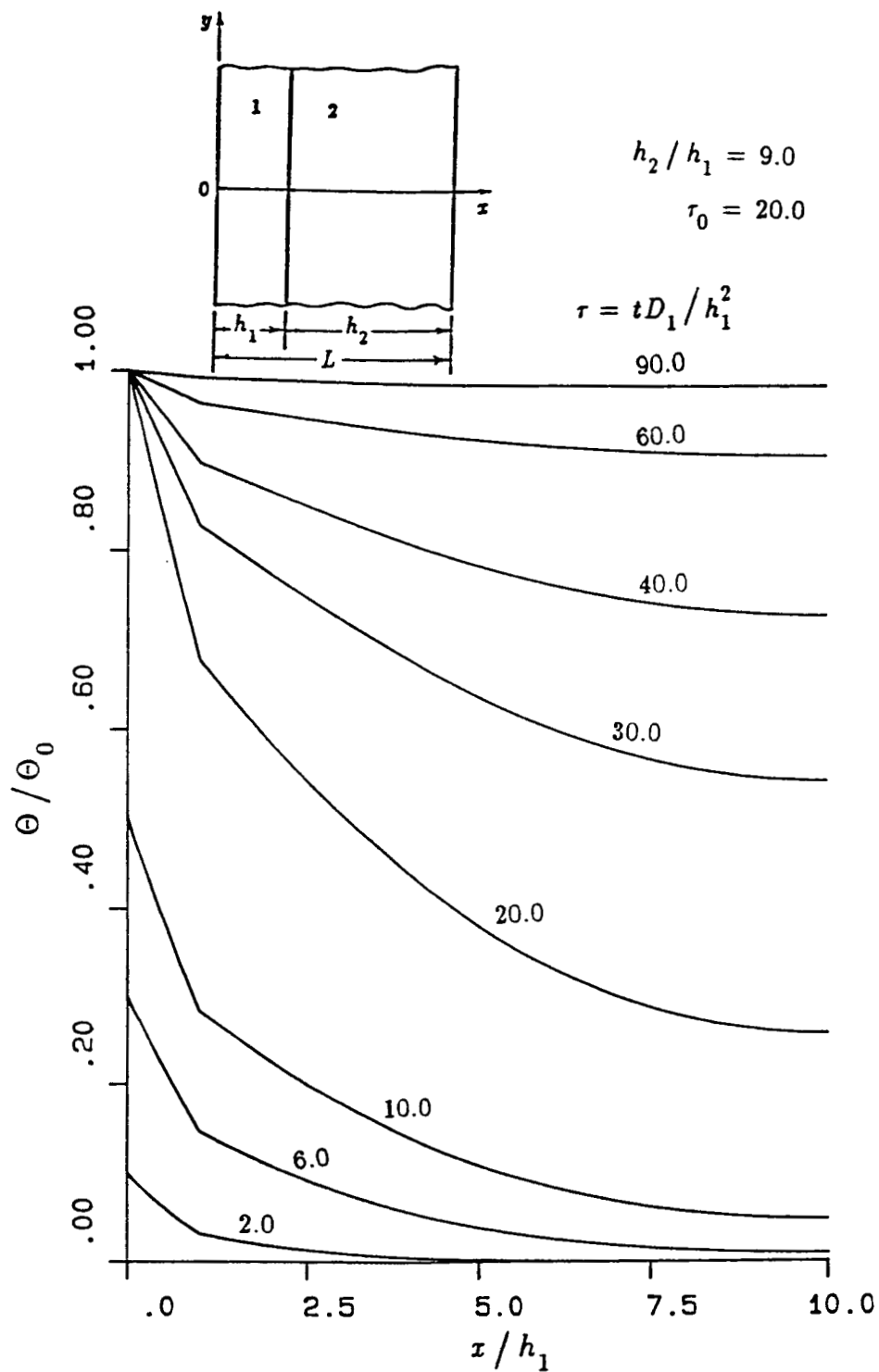


Figure 6-51: The normalized transient temperature distribution in Model II for $\tau_0=20.0$, $h_2/h_1=9.0$, $\tau_0=t_0D_1/h_1^2$, (Material pair A)

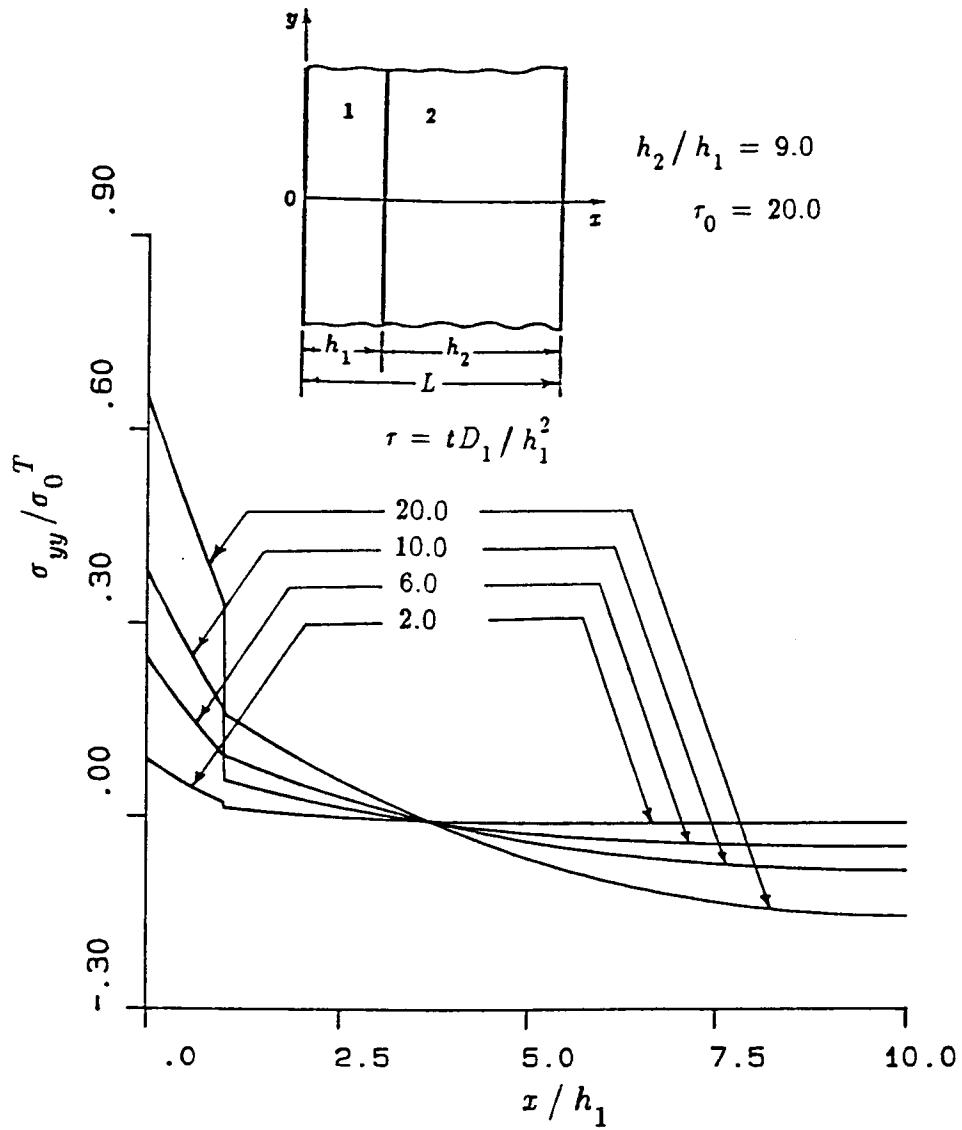


Figure 6-52: The normalized transient stress distribution σ_{yy}/σ_0^T in Model II for $\tau_0=20.0$, $h_2/h_1=9.0$, $\tau_0=t_0D_1/h_1^2$, $\sigma_0^T=-\alpha_1' E_1 \Theta_0/(1-\nu_1)$. (Material pair A)

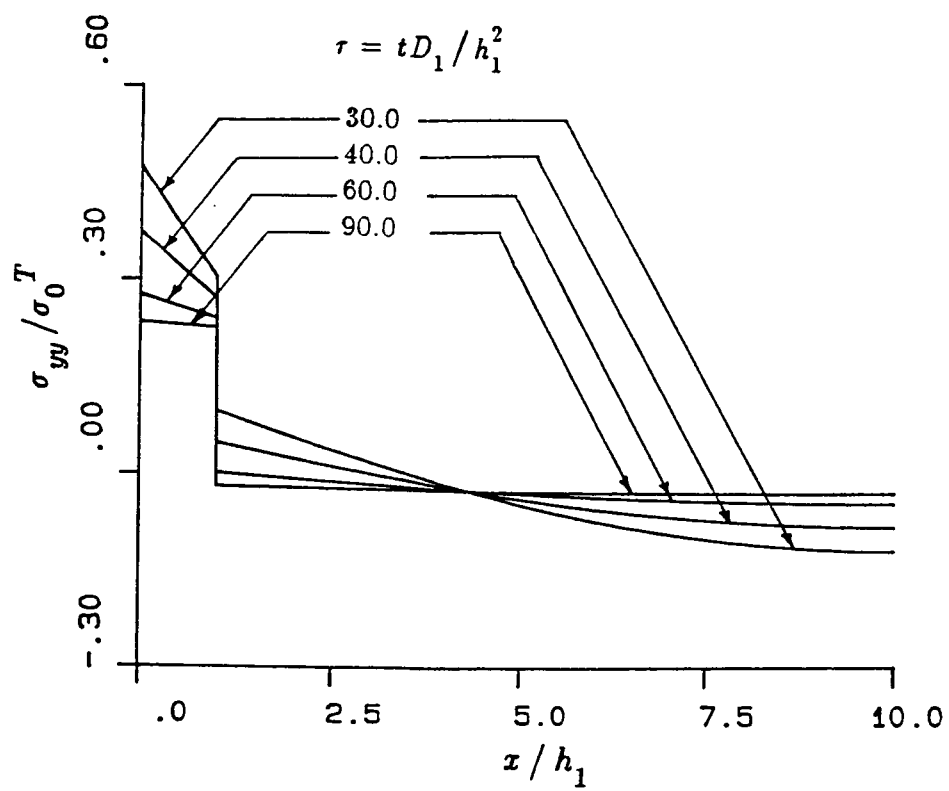


Figure 6-52, continued

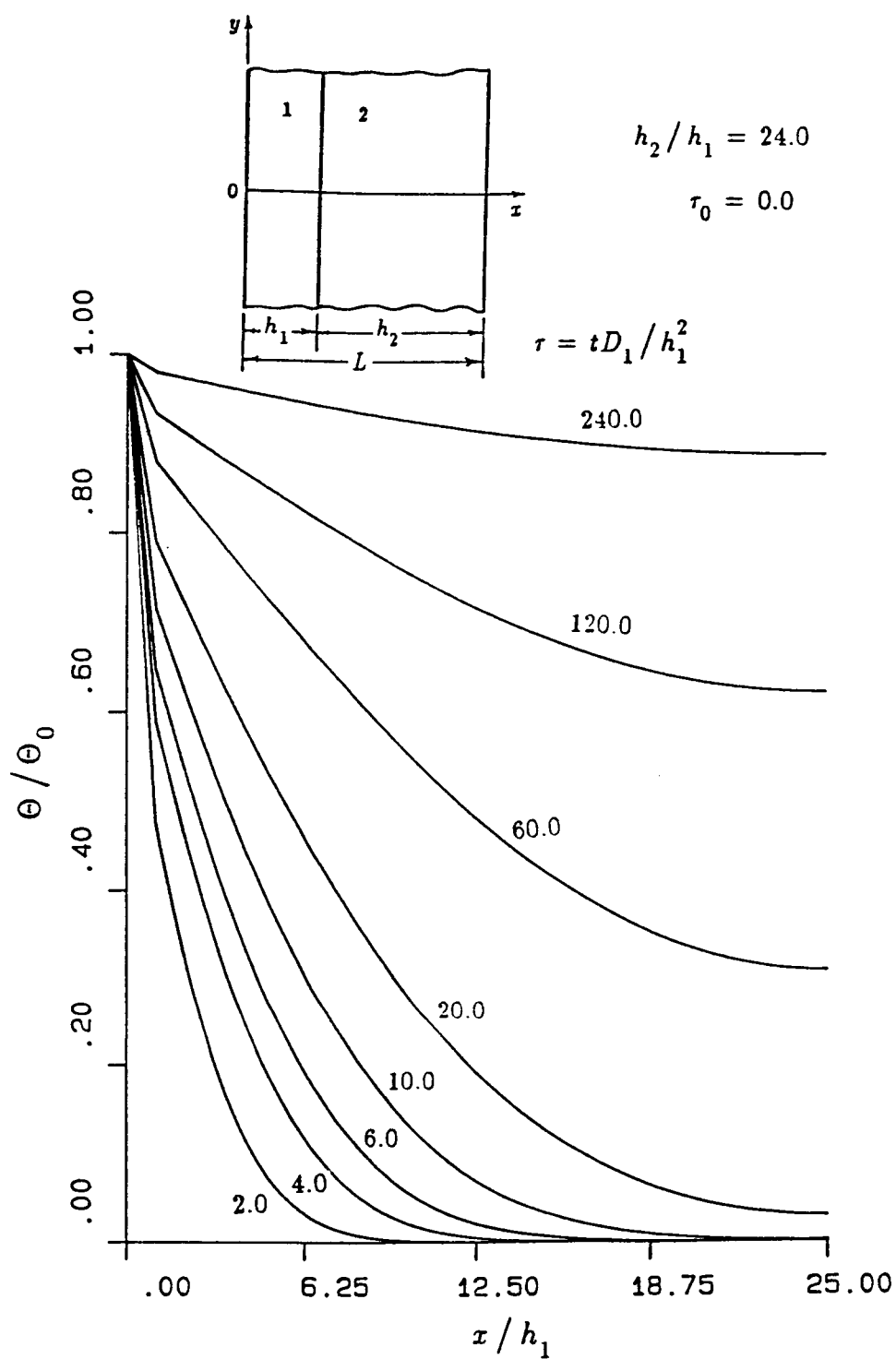


Figure 6-53: The normalized transient temperature distribution in Model II for $\tau_0=0.0$, $h_2/h_1=24.0$, $\tau_0=t_0D_1/h_1^2$, (Material pair A)

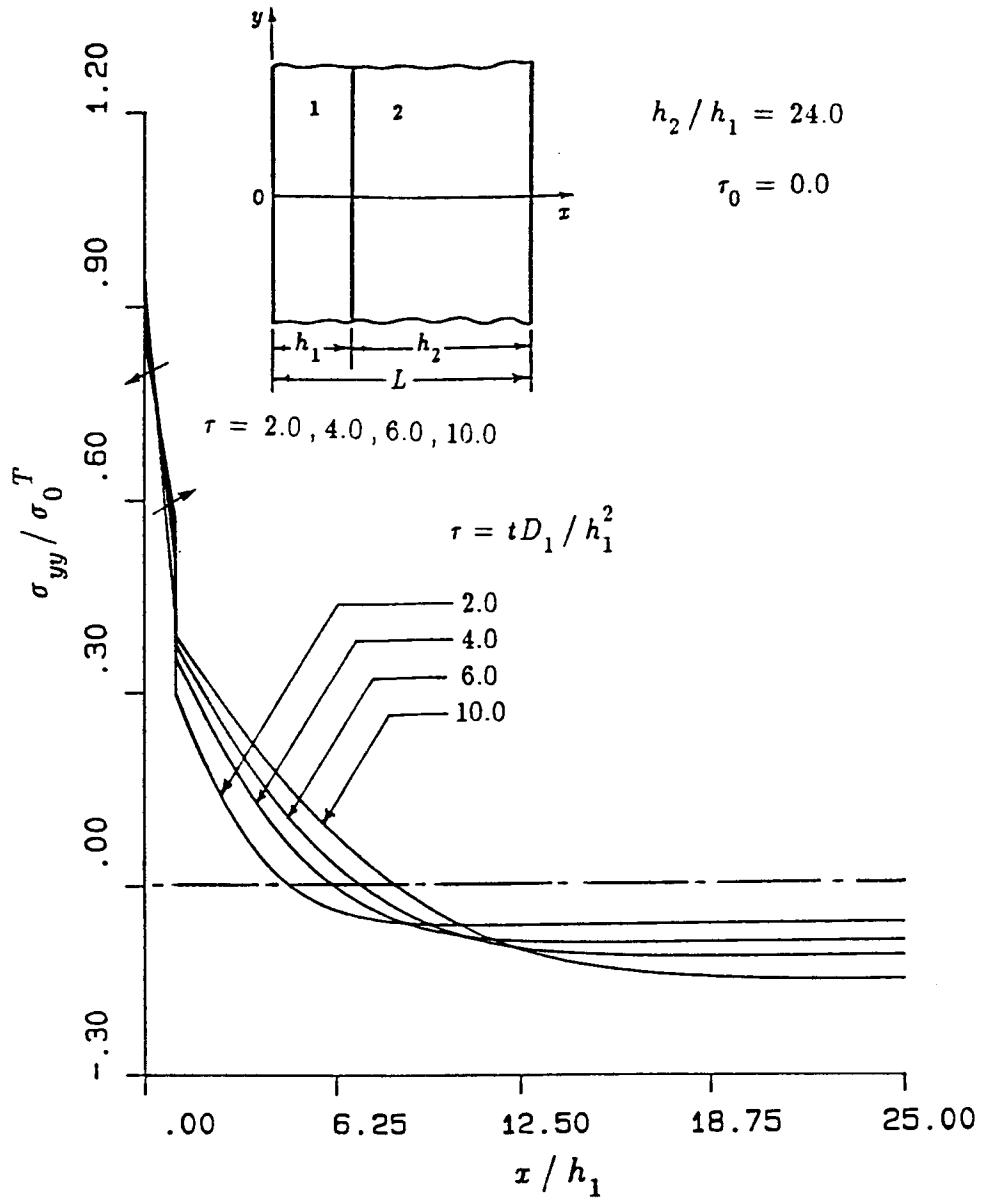


Figure 6-54: The normalized transient stress distribution σ_{yy}/σ_0^T in Model II for $\tau_0=0.0$, $h_2/h_1=24.0$, $\tau_0=t_0D_1/h_1^2$, $\sigma_0^T=-\alpha'_1 E_1 \Theta_0/(1-\nu_1)$. (Material pair A)

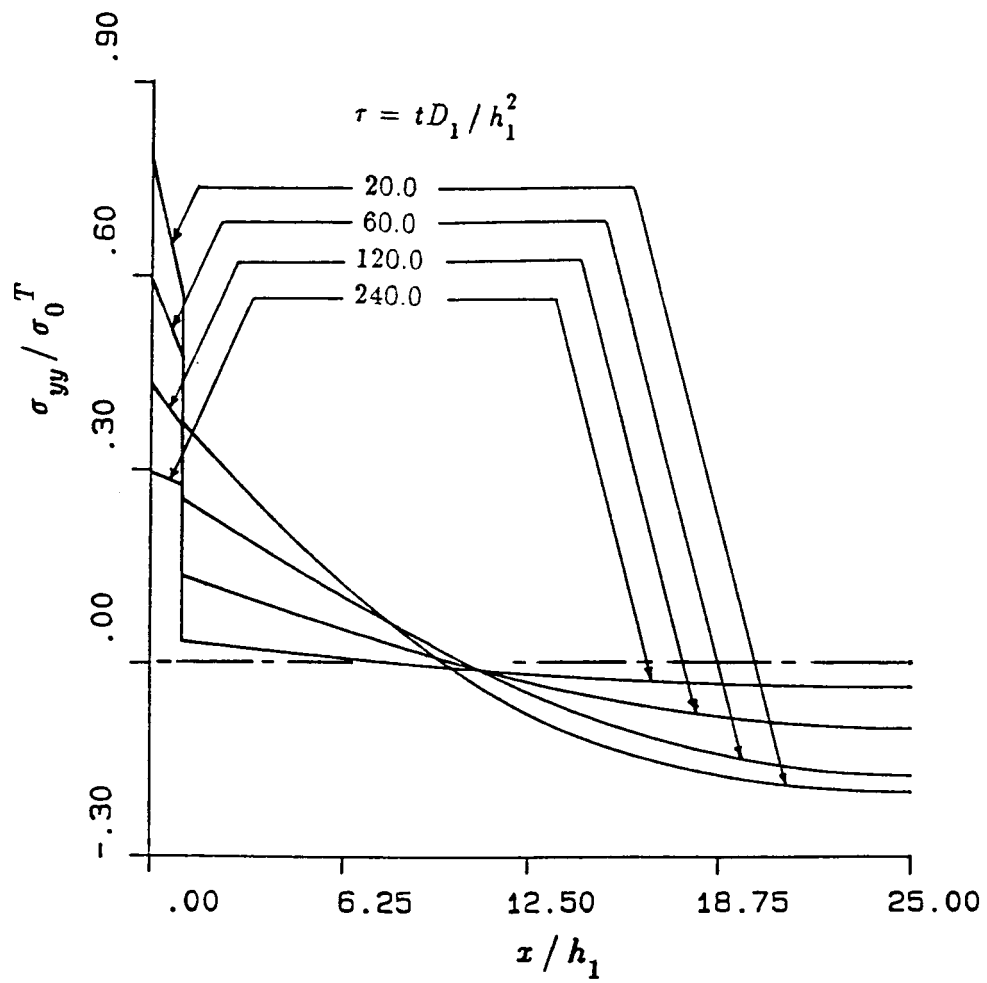


Figure 6-54, continued

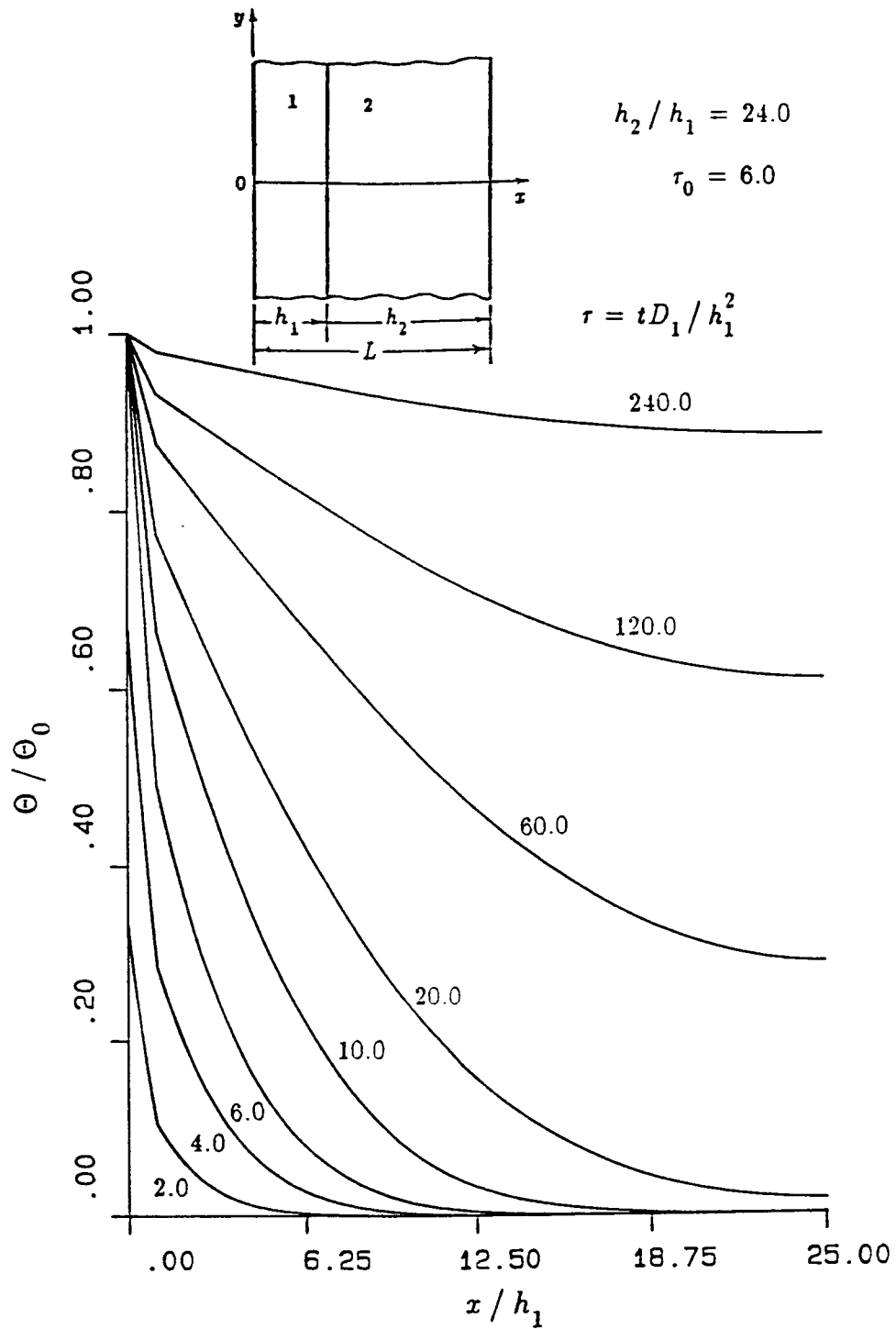


Figure 6-55: The normalized transient temperature distribution in Model II for $\tau_0=6.0$, $h_2/h_1=24.0$, $\tau_0=t_0D_1/h_1^2$, (Material pair A)

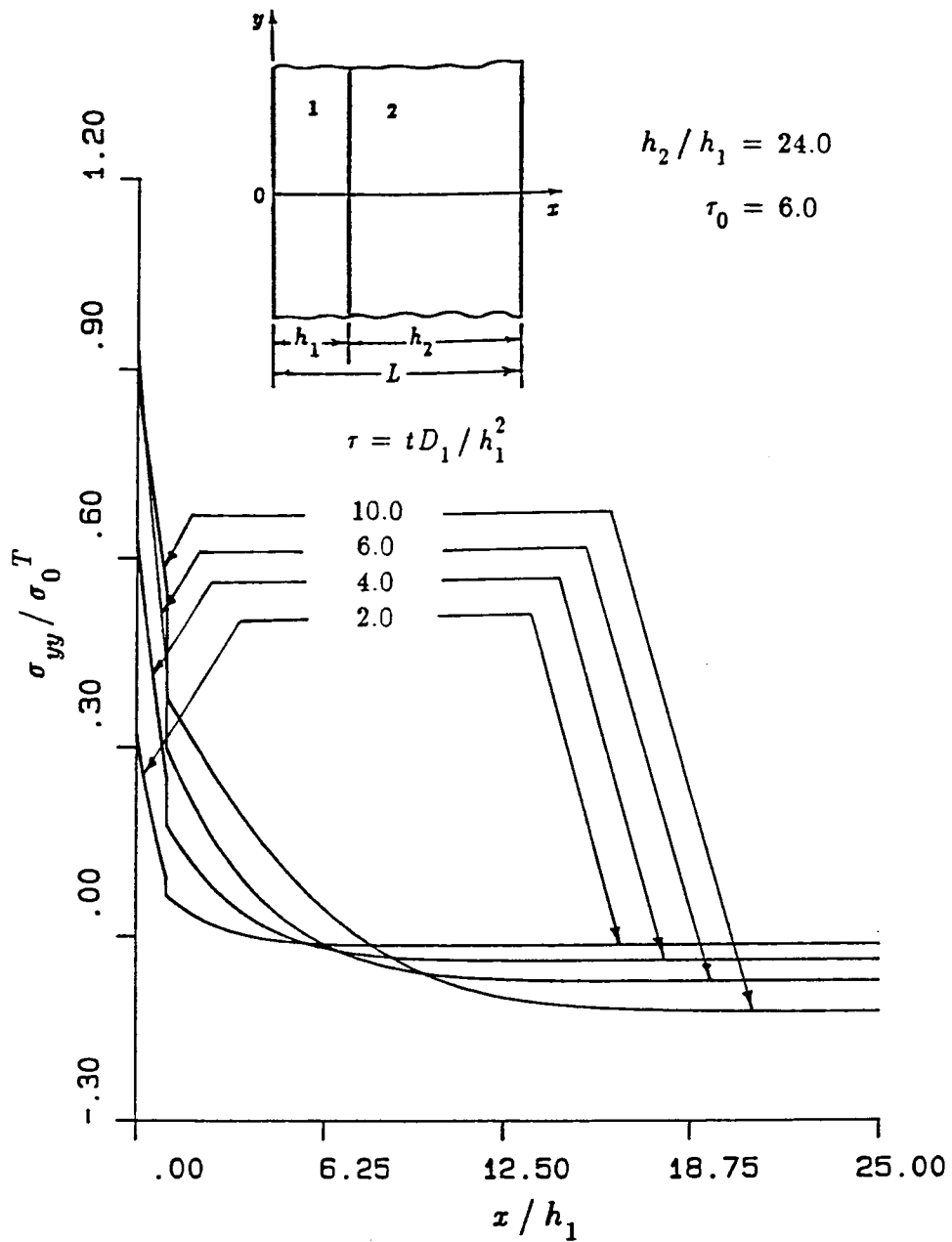


Figure 6-56: The normalized transient stress distribution σ_{yy}/σ_0^T in Model II
 for $\tau_0=6.0$, $h_2/h_1=24.0$, $\tau_0=t_0 D_1/h_1^2$, $\sigma_0^T=-\alpha_1' E_1 \Theta_0/(1-\nu_1)$.
 (Material pair A)

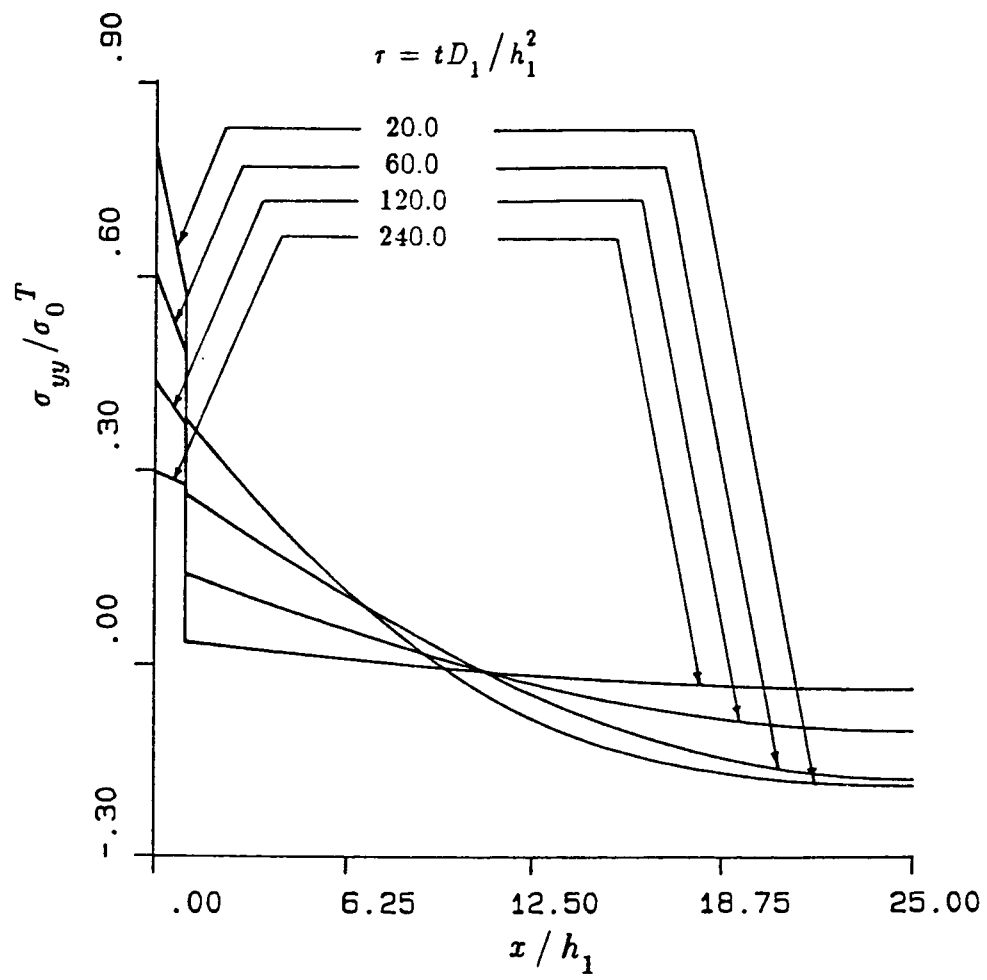


Figure 6-56, continued

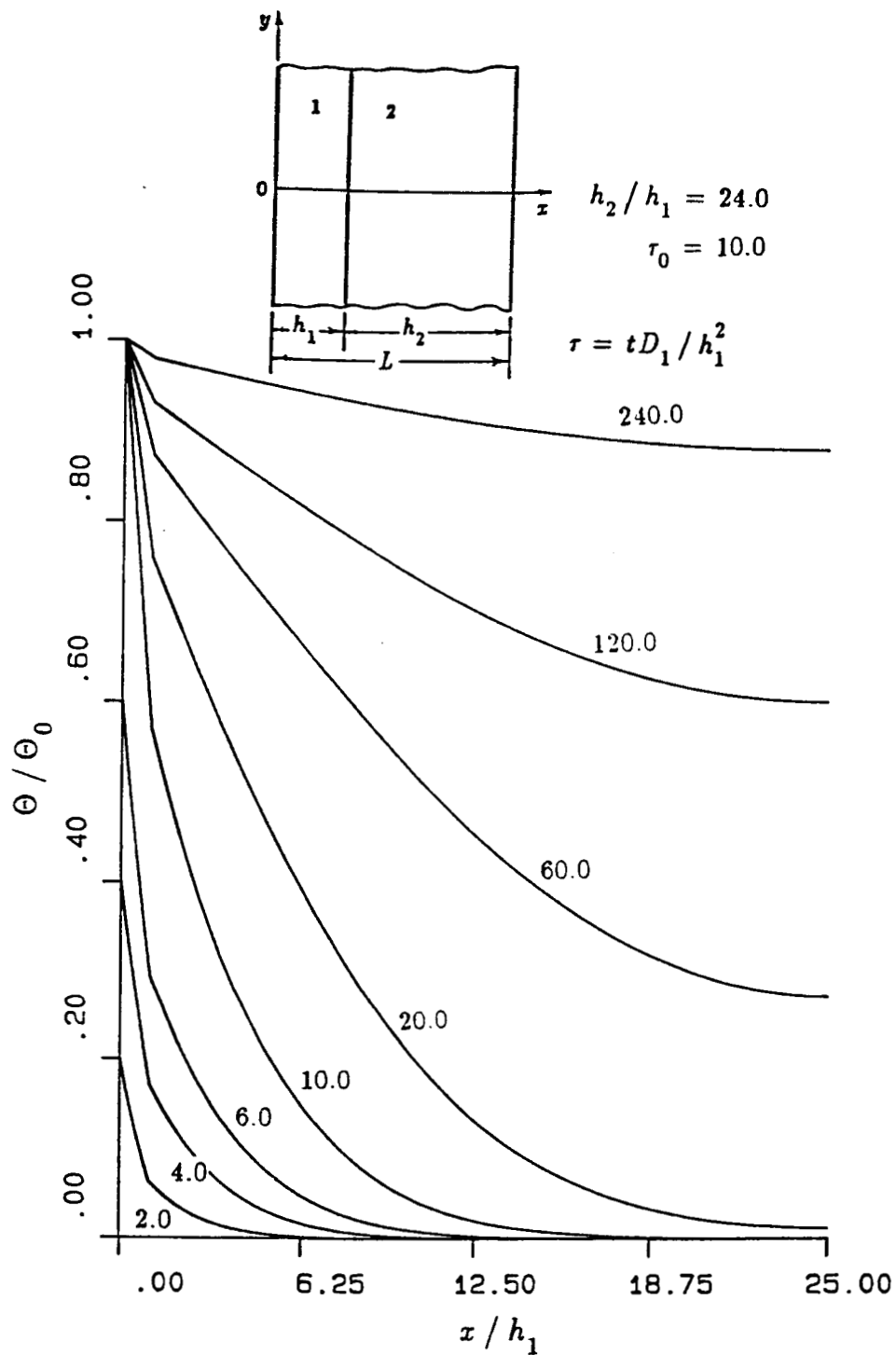


Figure 6-57: The normalized transient temperature distribution in Model II for $\tau_0=10.0$, $h_2/h_1=24.0$, $\tau_0=t_0D_1/h_1^2$, (Material pair A)

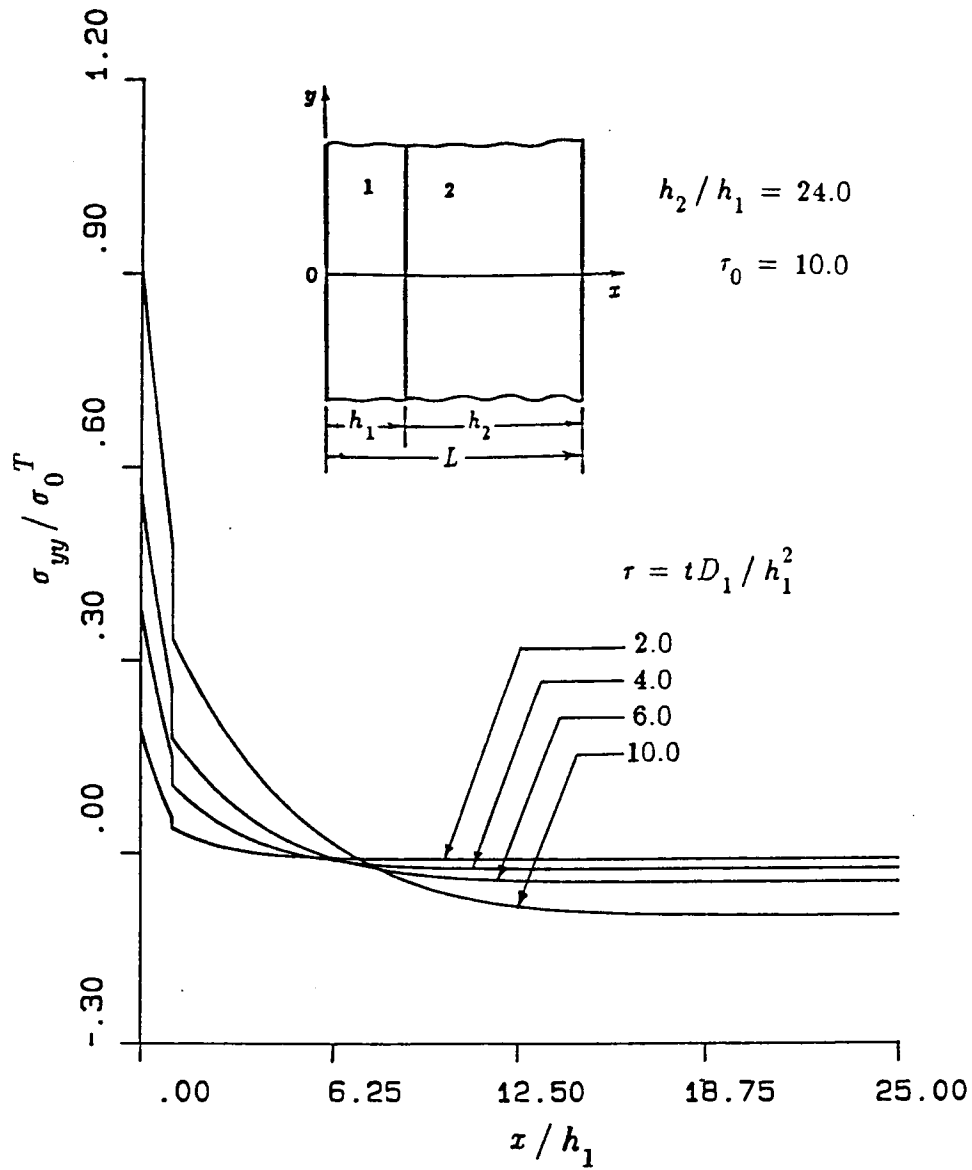


Figure 6-58: The normalized transient stress distribution σ_{yy}/σ_0^T in Model II for $\tau_0=10.0$, $h_2/h_1=24.0$, $\tau_0=t_0D_1/h_1^2$, $\sigma_0^T=-\alpha_1 E_1 \Theta_0/(1-\nu_1)$. (Material pair A)

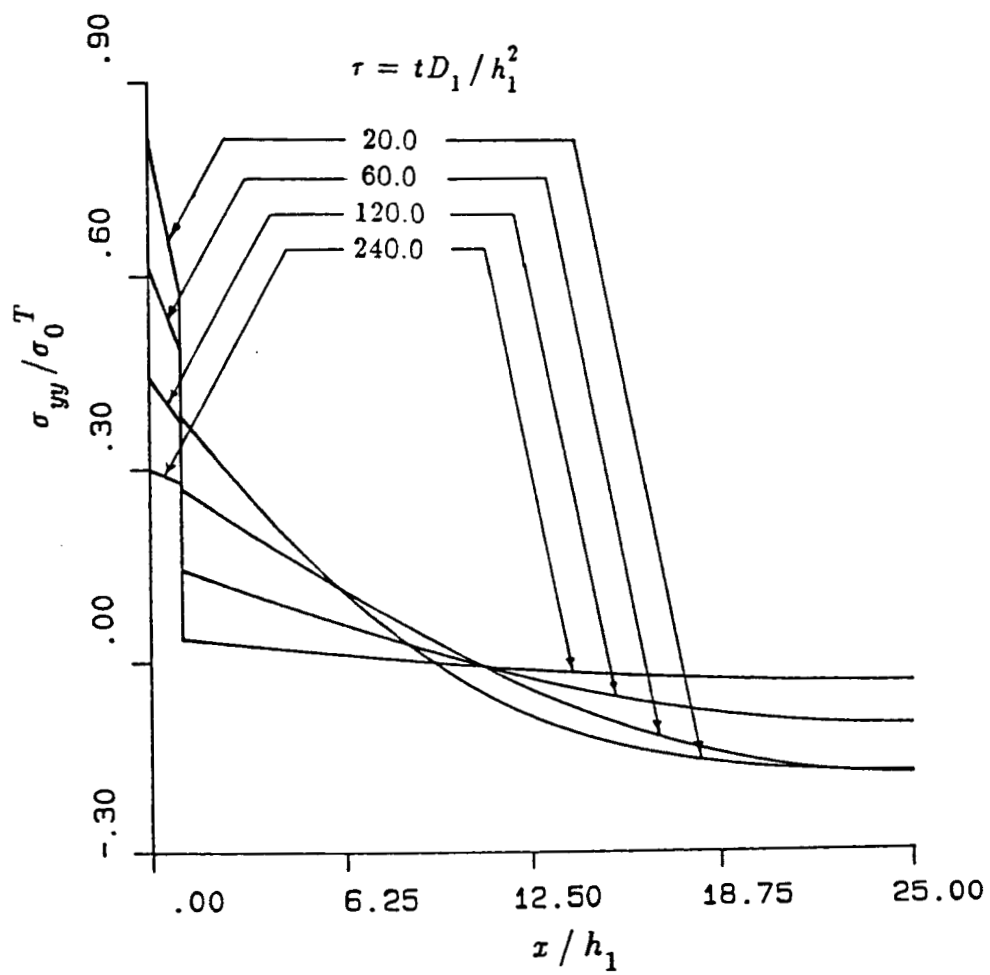


Figure 6-58, continued

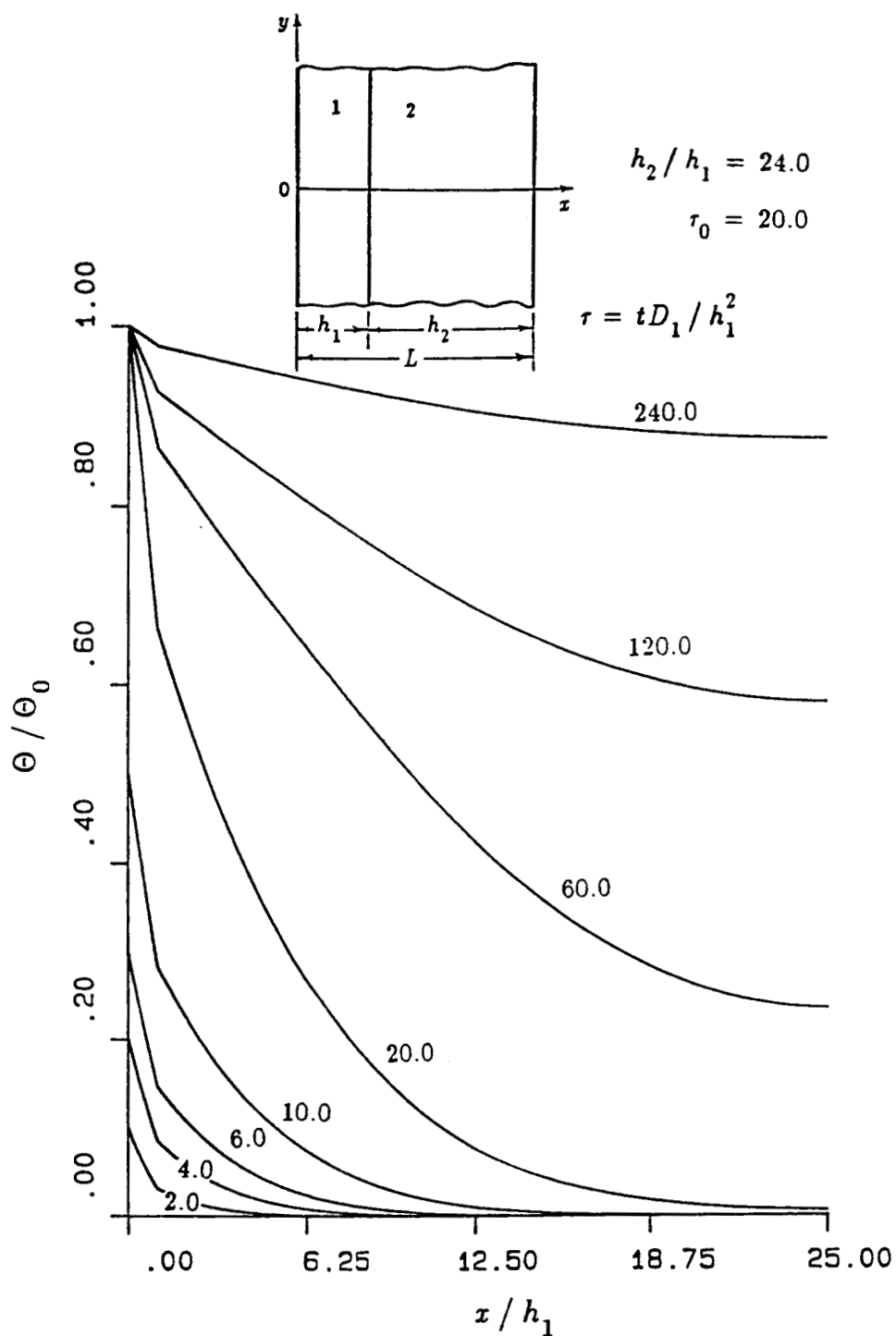


Figure 6-59: The normalized transient temperature distribution in Model II for $\tau_0=20.0$, $h_2/h_1=24.0$, $\tau_0=t_0D_1/h_1^2$, (Material pair A)

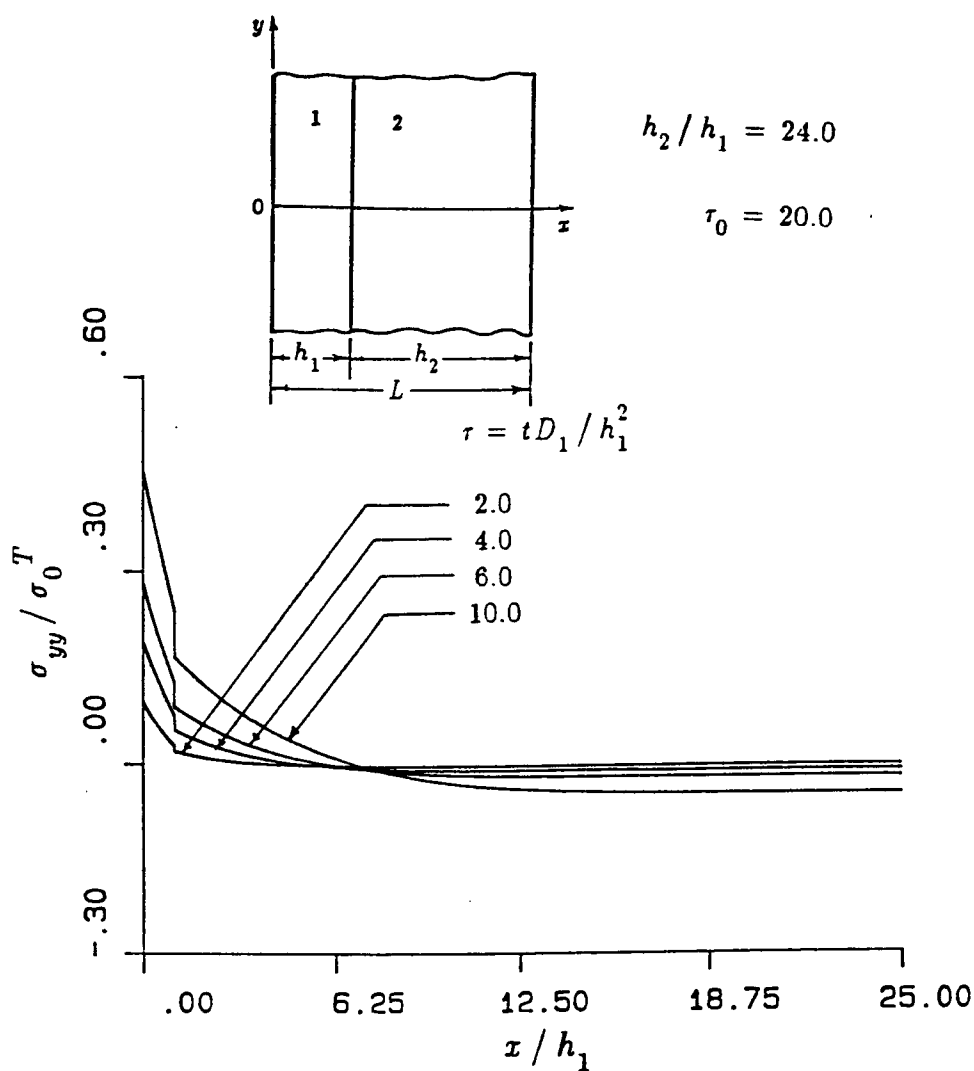


Figure 6-60: The normalized transient stress distribution σ_{yy}/σ_0^T in Model II for $\tau_0=20.0$, $h_2/h_1=24.0$, $\tau_0=t_0D_1/h_1^2$, $\sigma_0^T=-\alpha_1' E_1 \Theta_0/(1-\nu_1)$. (Material pair A)

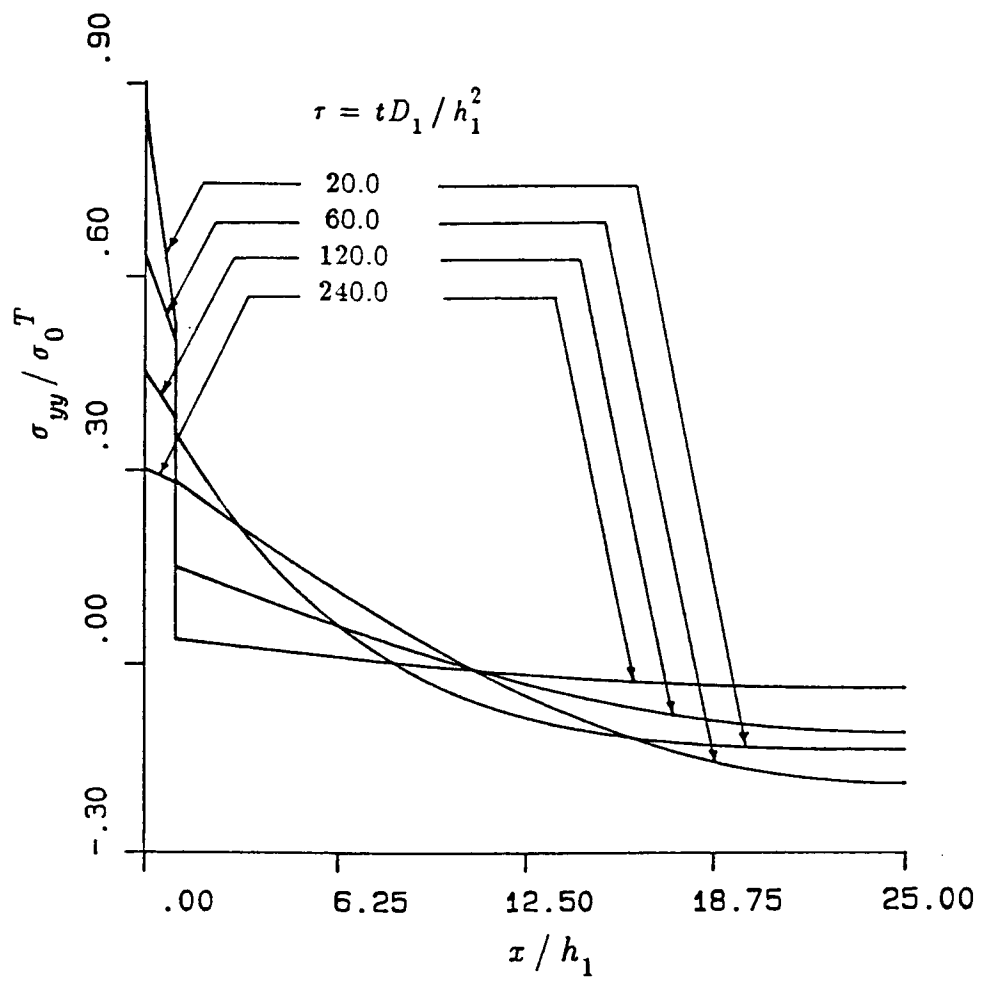


Figure 6-60, continued

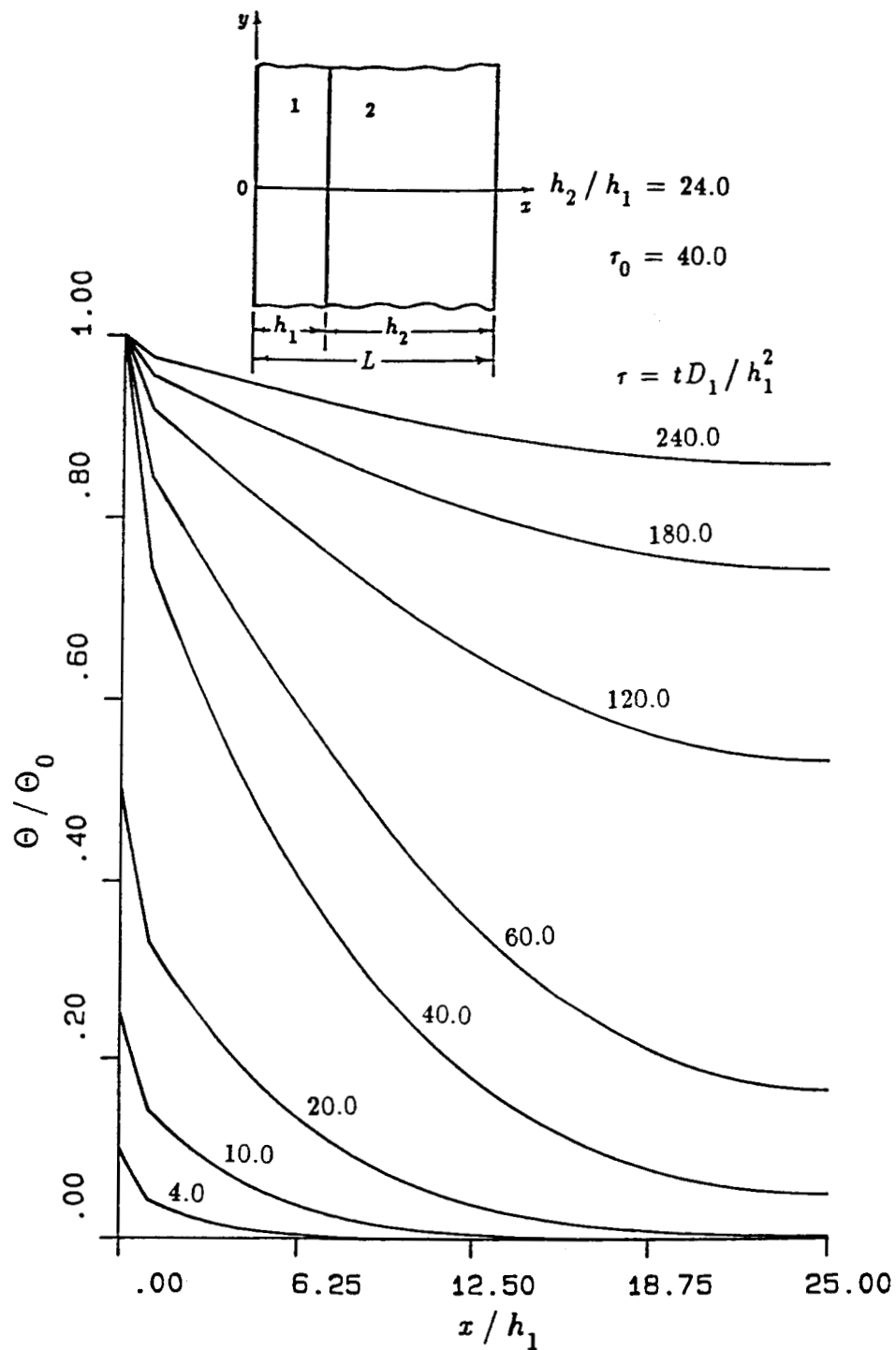


Figure 6-61: The normalized transient temperature distribution in Model II for $\tau_0 = 40.0$, $h_2/h_1 = 24.0$, $\tau_0 = t_0 D_1 / h_1^2$, (Material pair A)

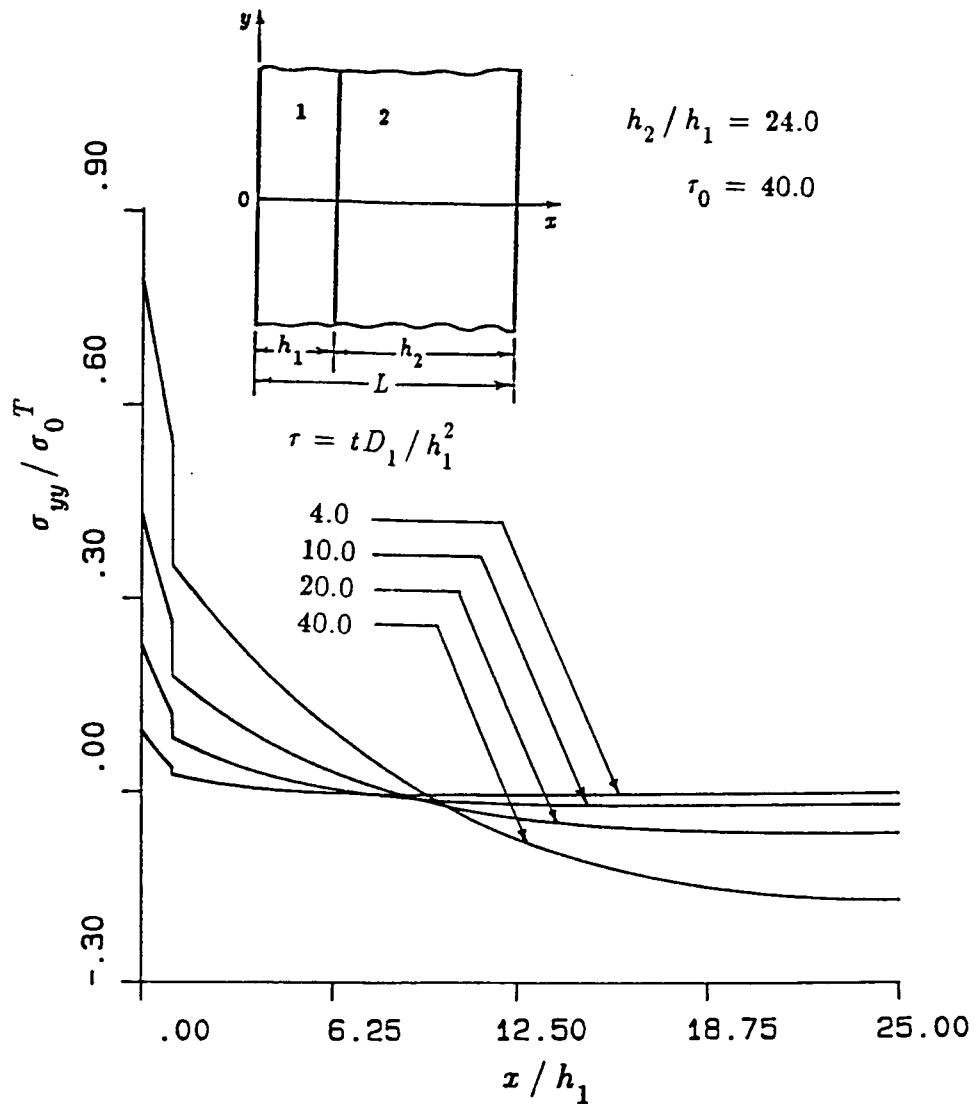


Figure 6-62: The normalized transient stress distribution σ_{yy}/σ_0^T in Model II for $\tau_0=40.0$, $h_2/h_1=24.0$, $\tau_0=t_0D_1/h_1^2$, $\sigma_0^T=-\alpha'_1 E_1 \Theta_0/(1-\nu_1)$. (Material pair A)

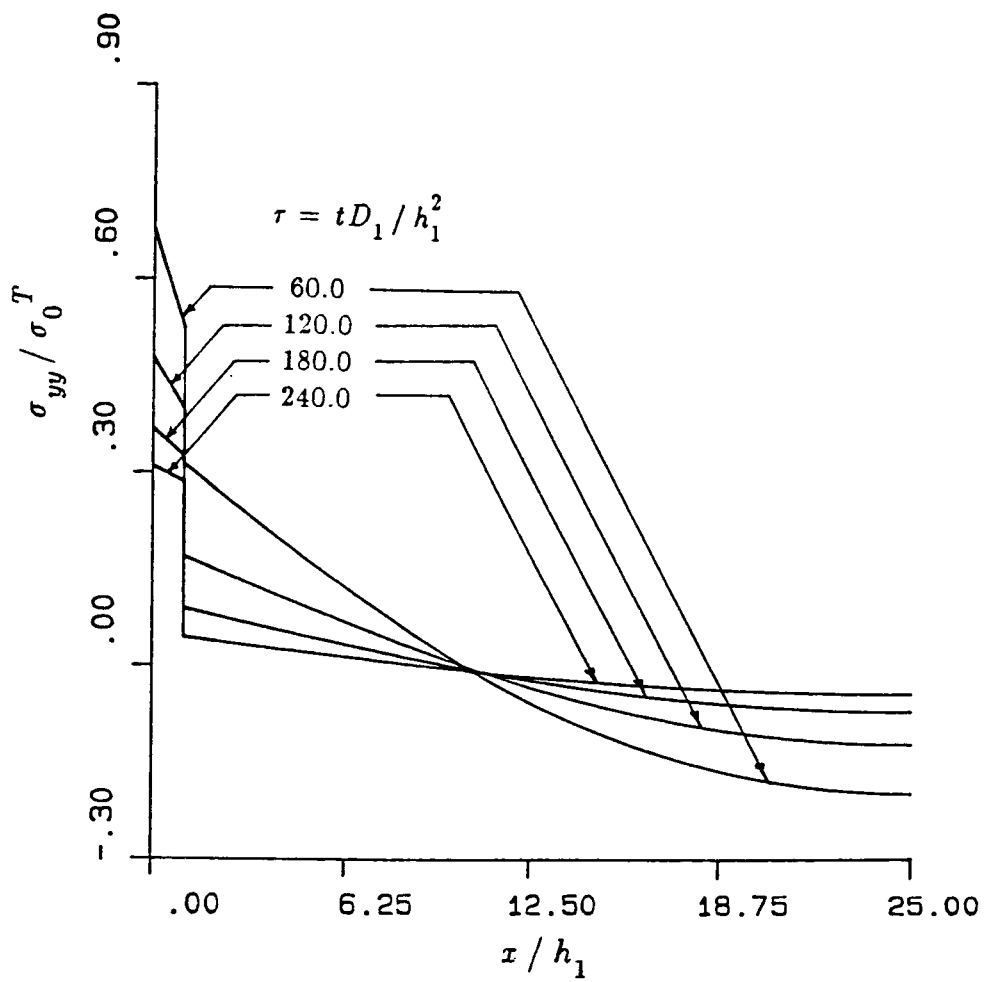


Figure 6-62, continued

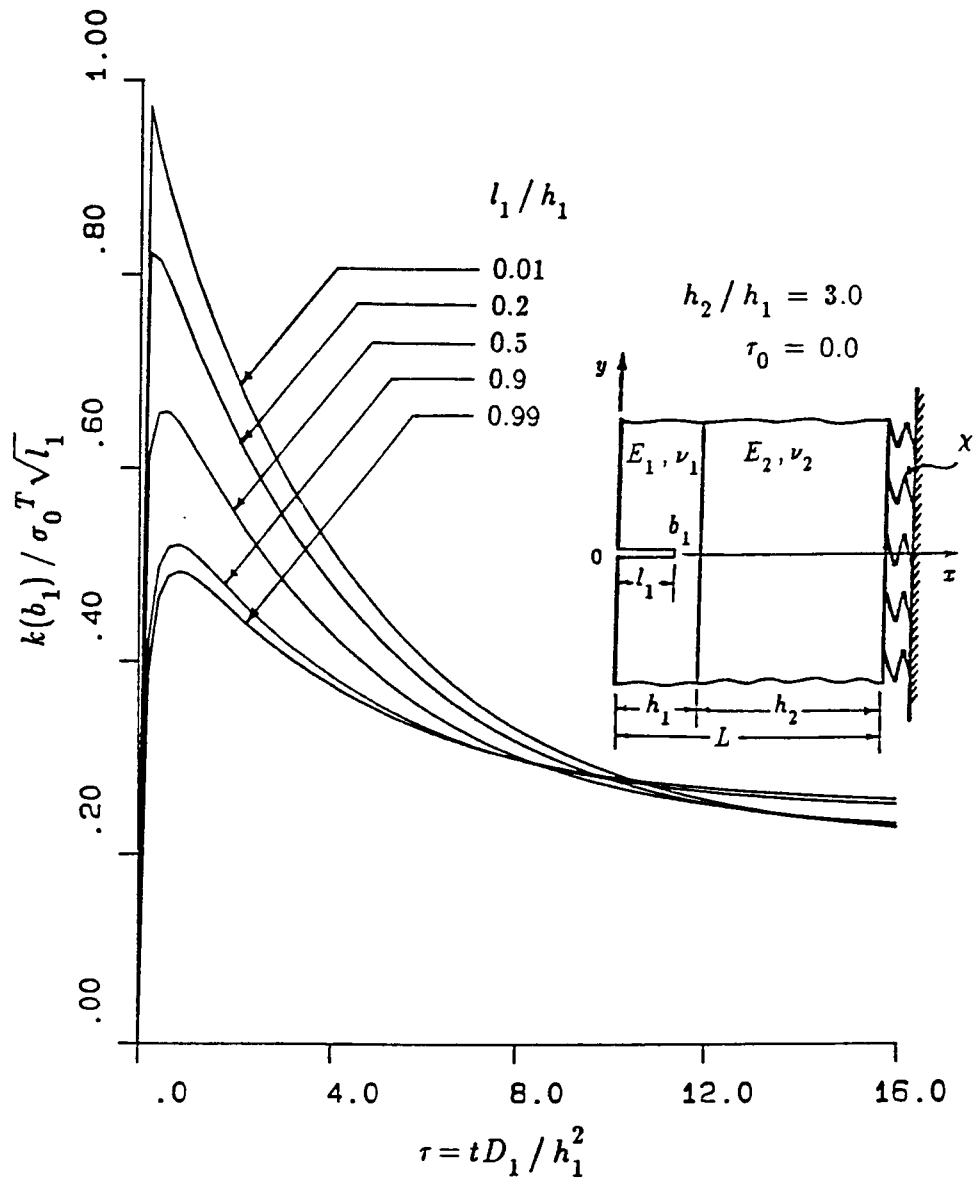


Figure 6-63: The normalized stress intensity factor $k(b_1)$ as a function of nondimensional time τ for an edge crack in Model II for $\tau_0=0.0$, $h_2/h_1=3.0$, $R_i/L=9.0$ and $\chi L/E_2=0.01108$, $\tau_0=t_0 D_1/h_1^2$, $\sigma_0^T = -\alpha'_1 E_1 \Theta_0 / (1-\nu_1)$ (material pair A)

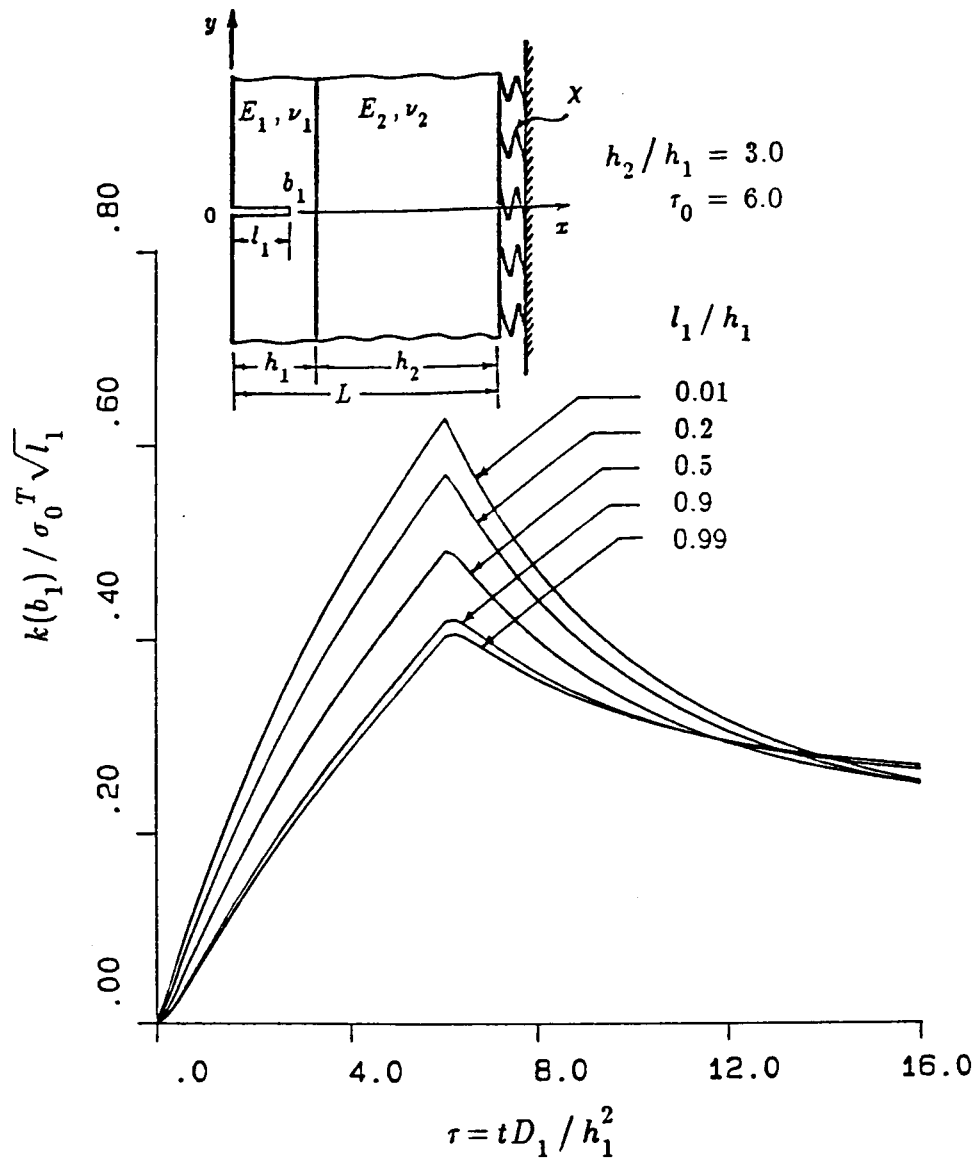


Figure 6-64: The normalized stress intensity factor $k(b_1)$ as a function of nondimensional time τ for an edge crack in Model II for $\tau_0=6.0$, $h_2/h_1=3.0$, $R_i/L=9.0$ and $\chi L/E_2=0.01108$, $\tau_0=t_0 D_1/h_1^2$, $\sigma_0^T = -\alpha_1 E_1 \Theta_0 / (1-\nu_1)$ (material pair A)

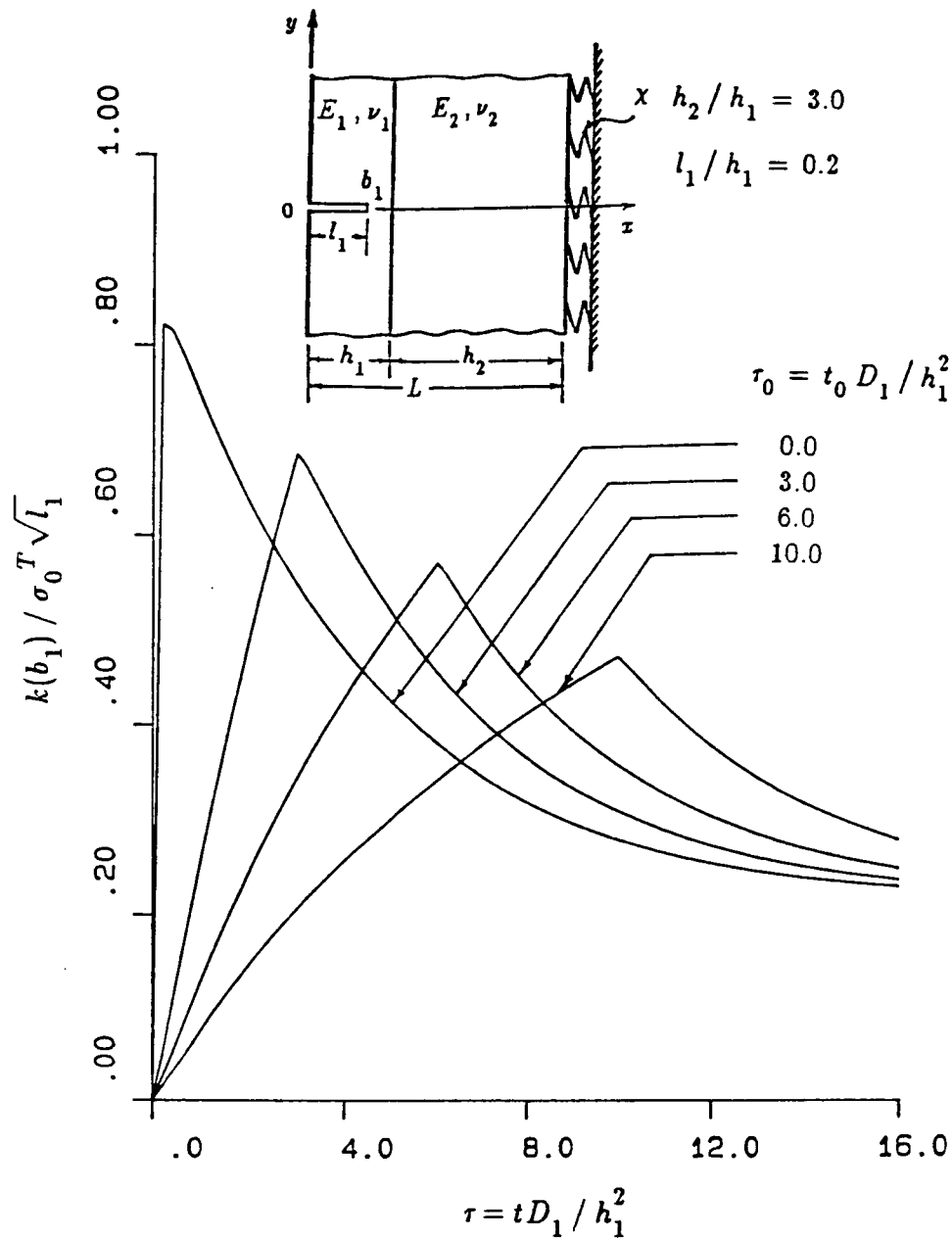


Figure 6-65: The influence of τ_0 on the normalized stress intensity factor $k(b_1)$ as a function of nondimensional time τ for an edge crack of length $l_1/h_1=0.2$ in Model II, $h_2/h_1=3.0$, $R_i/L=9.0$ and $\chi L/E_2=0.01108$, $\tau_0=t_0 D_1/h_1^2$, $\sigma_0^T = -\alpha_1' E_1 \Theta_0 / (1-\nu_1)$ (material pair A)

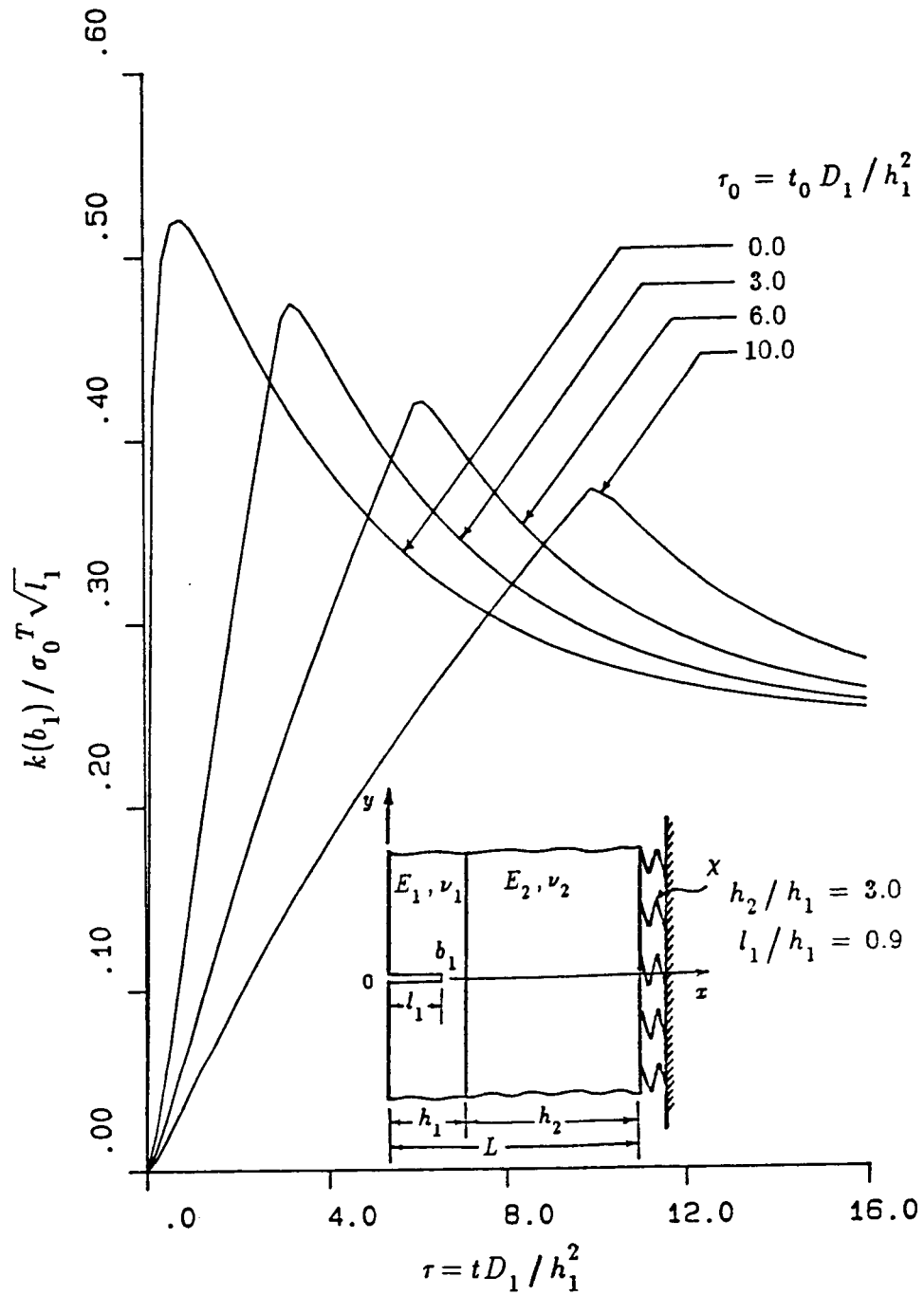


Figure 6-66: The influence of τ_0 on the normalized stress intensity factor $k(b_1)$ as a function of nondimensional time τ for an edge crack of length $l_1/h_1=0.9$ in Model II, $h_2/h_1=3.0$, $R_i/L=9.0$ and $\chi L/E_2=0.01108$, $\tau_0=t_0 D_1/h_1^2$, $\sigma_0^T = -\alpha'_1 E_1 \Theta_0/(1-\nu_1)$ (material pair A)

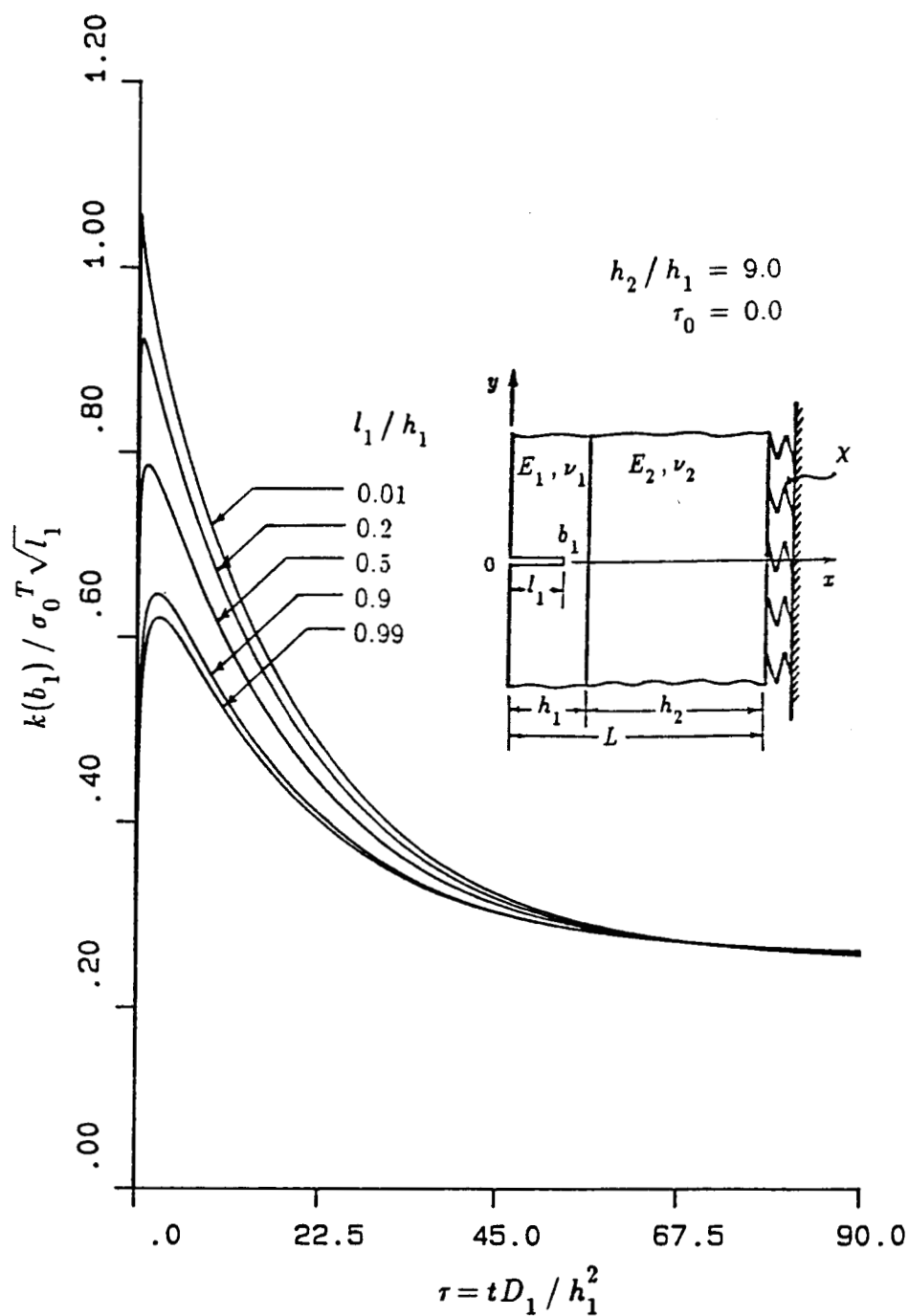


Figure 6-67: The normalized stress intensity factor $k(b_1)$ as a function of nondimensional time τ for an edge crack in Model II for $\tau_0=0.0$, $h_2/h_1=9.0$, $R_i/L=9.0$ and $\chi L/E_2=0.01108$, $\tau_0=t_0 D_1/h_1^2$, $\sigma_0^T = -\alpha_1' E_1 \Theta_0 / (1-\nu_1)$ (material pair A)

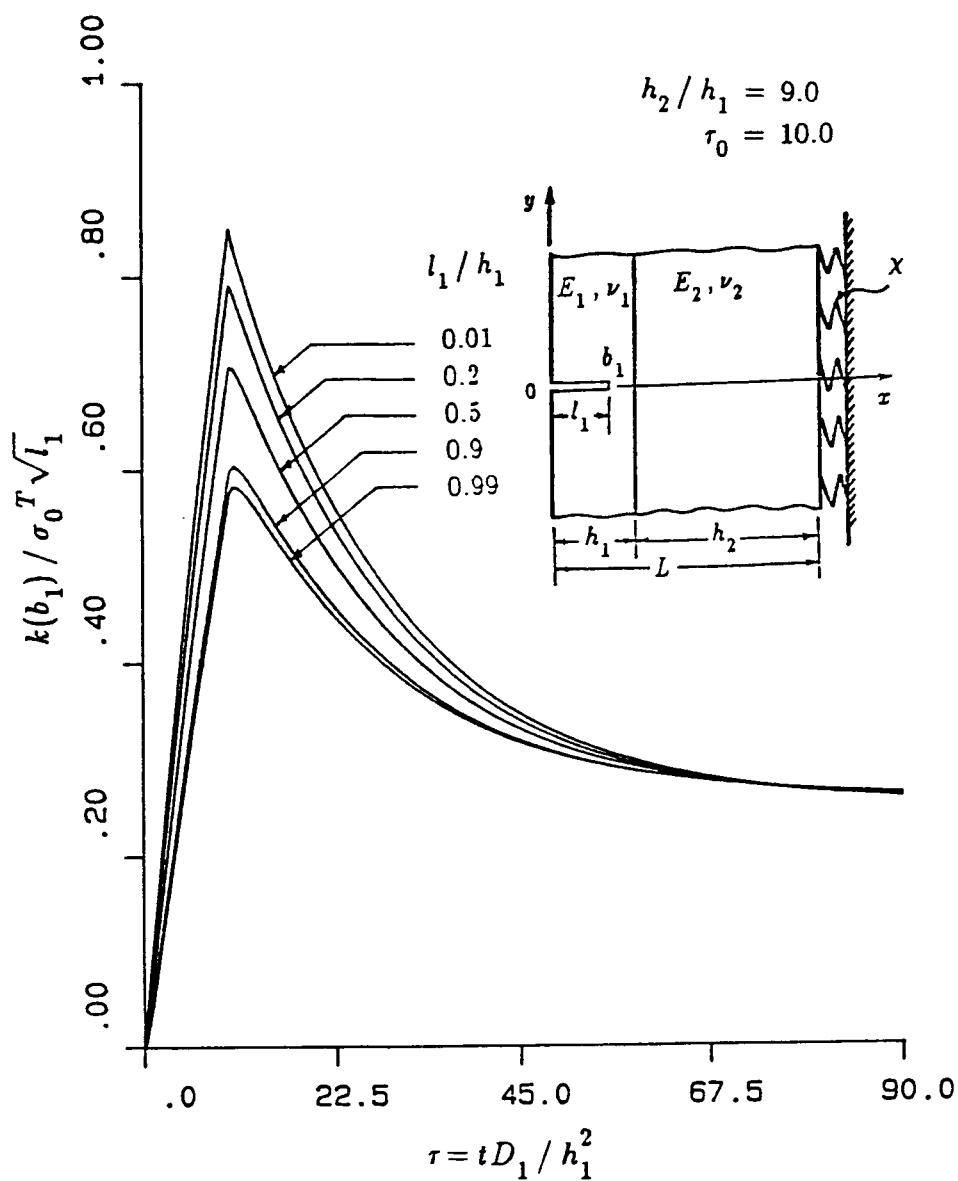


Figure 6-68: The normalized stress intensity factor $k(b_1)$ as a function of nondimensional time τ for an edge crack in Model II for $\tau_0 = 10.0$, $h_2/h_1 = 9.0$, $R_i/L = 9.0$ and $\chi L/E_2 = 0.01108$, $\tau_0 = t_0 D_1 / h_1^2$, $\sigma_0^T = -\alpha'_1 E_1 \Theta_0 / (1 - \nu_1)$ (material pair A)

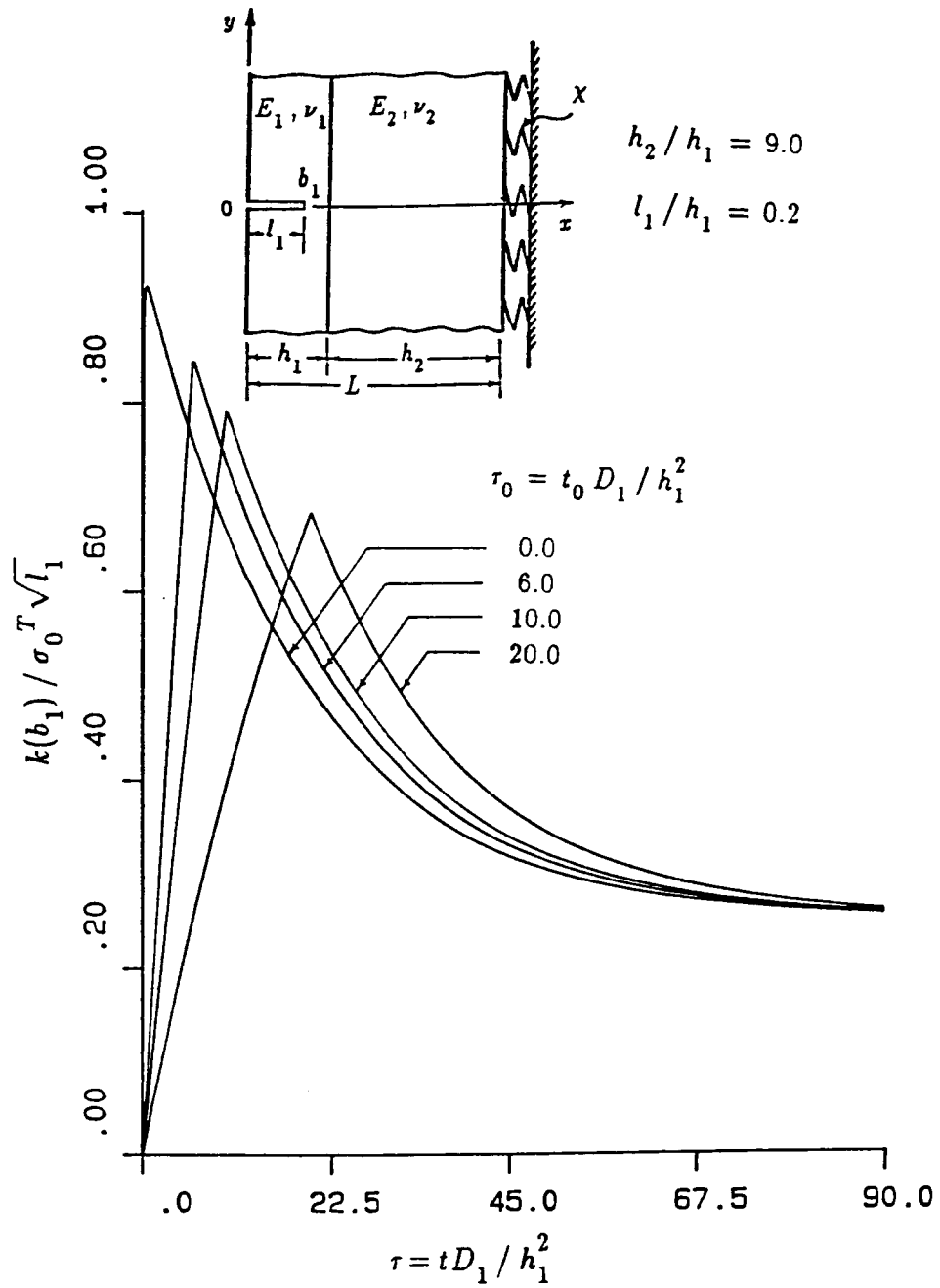


Figure 6-69: The influence of τ_0 on the normalized stress intensity factor $k(b_1)$ as a function of nondimensional time τ for an edge crack of length $l_1/h_1=0.2$ in Model II, $h_2/h_1=9.0$, $R_i/L=9.0$ and $\chi L/E_2=0.01108$, $\tau_0=t_0 D_1/h_1^2$, $\sigma_0^T = -\alpha_1' E_1 \Theta_0 / (1-\nu_1)$ (material pair A)

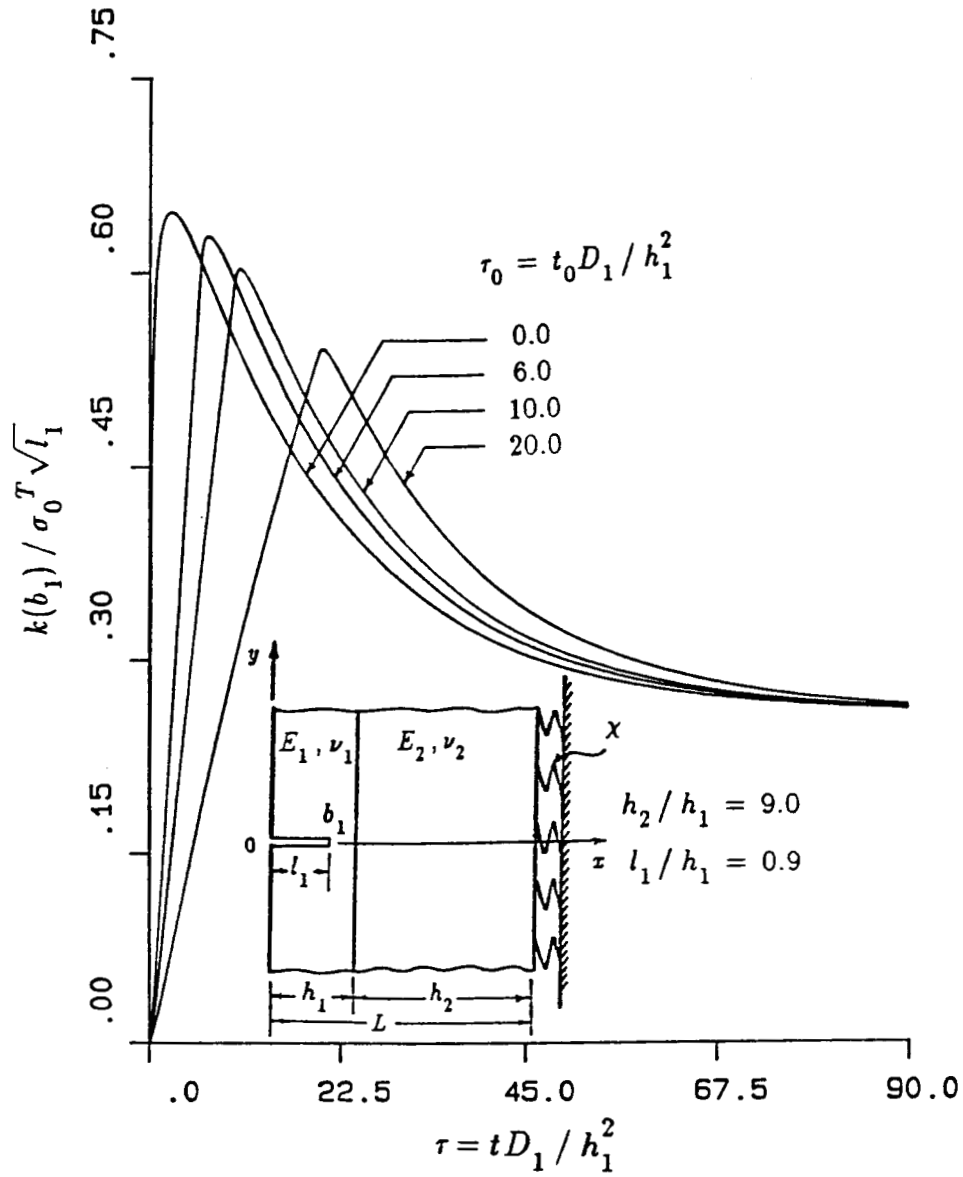


Figure 6-70: The influence of τ_0 on the normalized stress intensity factor $k(b_1)$ as a function of nondimensional time τ for an edge crack of length $l_1/h_1=0.9$ in Model II, $h_2/h_1=9.0$, $R_i/L=9.0$ and $\chi L/E_2=0.01108$, $\tau_0=t_0 D_1/h_1^2$, $\sigma_0^T = -\alpha_1 E_1 \Theta_0/(1-\nu_1)$ (material pair A)

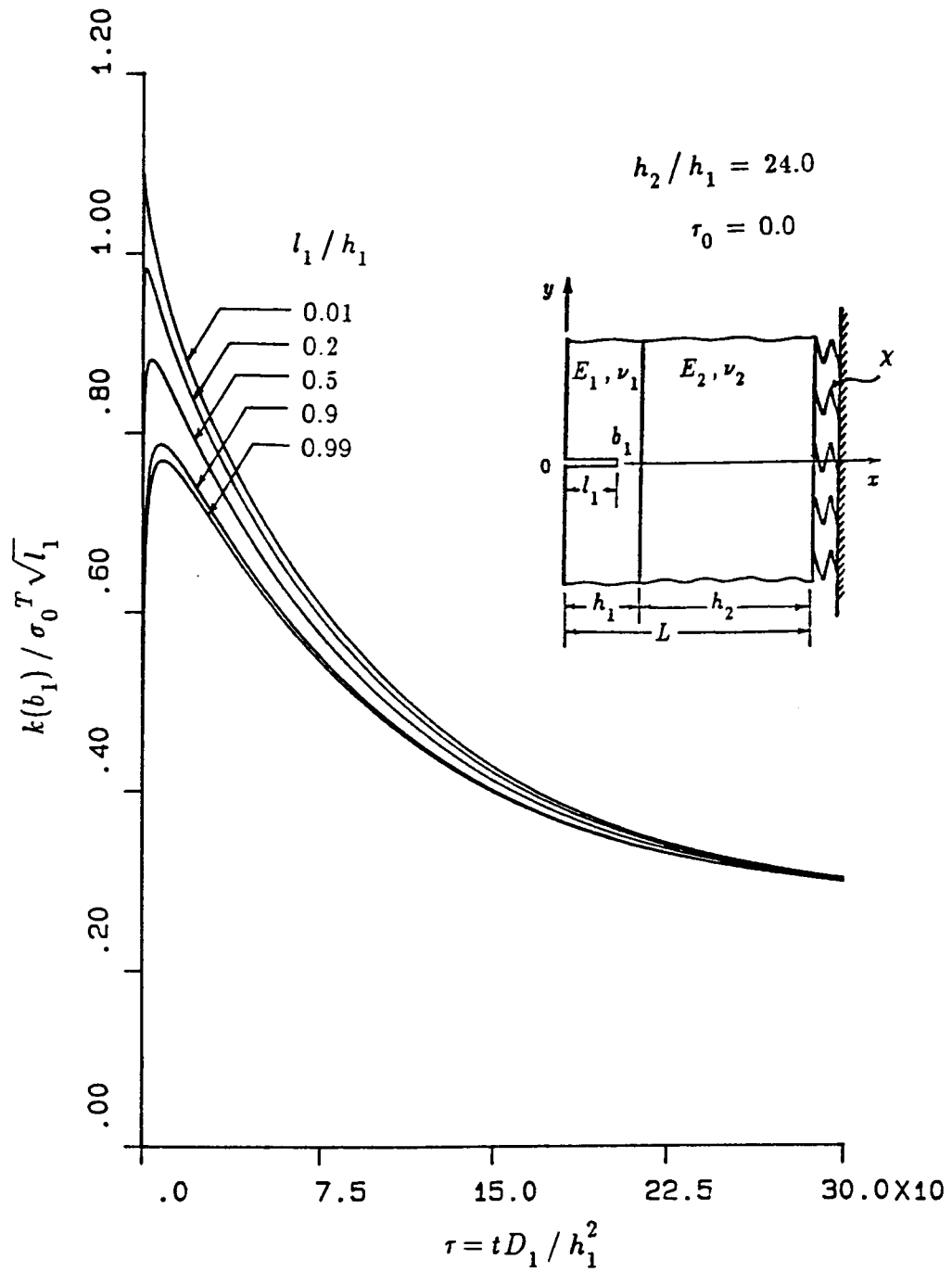


Figure 6-71: The normalized stress intensity factor $k(b_1)$ as a function of nondimensional time τ for an edge crack in Model II for $\tau_0=0.0$, $h_2/h_1=24.0$, $R_i/L=9.0$ and $\chi L/E_2=0.01108$, $\tau_0=t_0 D_1/h_1^2$, $\sigma_0^T = -\alpha_1' E_1 \Theta_0 / (1-\nu_1)$ (material pair A)

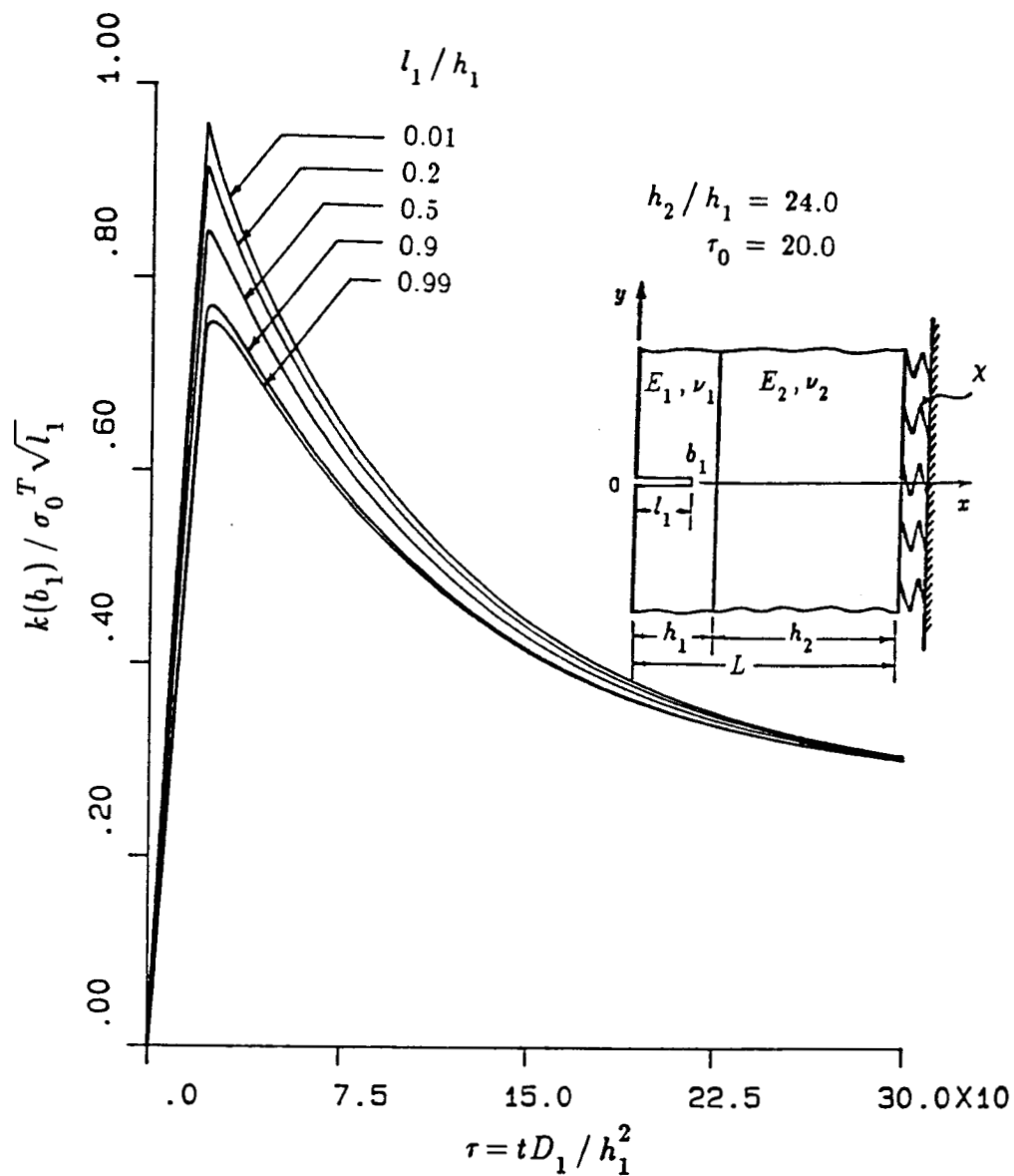


Figure 6-72: The normalized stress intensity factor $k(b_1)$ as a function of nondimensional time τ for an edge crack in Model II for $\tau_0=20.0$, $h_2/h_1=24.0$, $R_i/L=9.0$ and $\chi L/E_2=0.01108$, $\tau_0=t_0 D_1/h_1^2$, $\sigma_0^T = -\alpha'_1 E_1 \Theta_0 / (1-\nu_1)$ (material pair A)

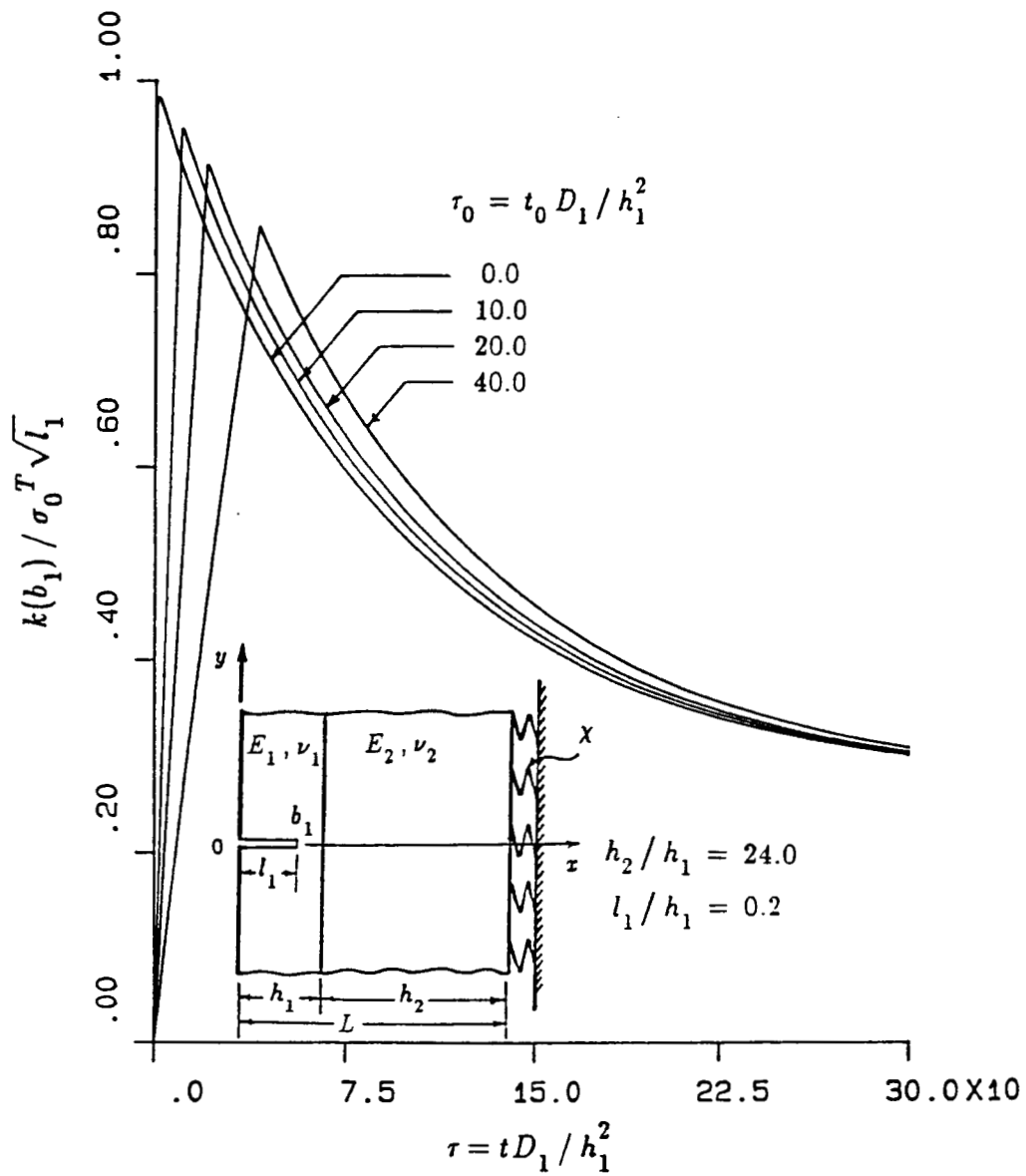


Figure 6-73: The influence of τ_0 on the normalized stress intensity factor $k(b_1)$ as a function of nondimensional time τ for an edge crack of length $l_1/h_1=0.2$ in Model II, $h_2/h_1=24.0$, $R_i/L=9.0$ and $\chi L/E_2=0.01108$, $\tau_0=t_0 D_1/h_1^2$, $\sigma_0^T=-\alpha_1 E_1 \Theta_0/(1-\nu_1)$ (material pair A)

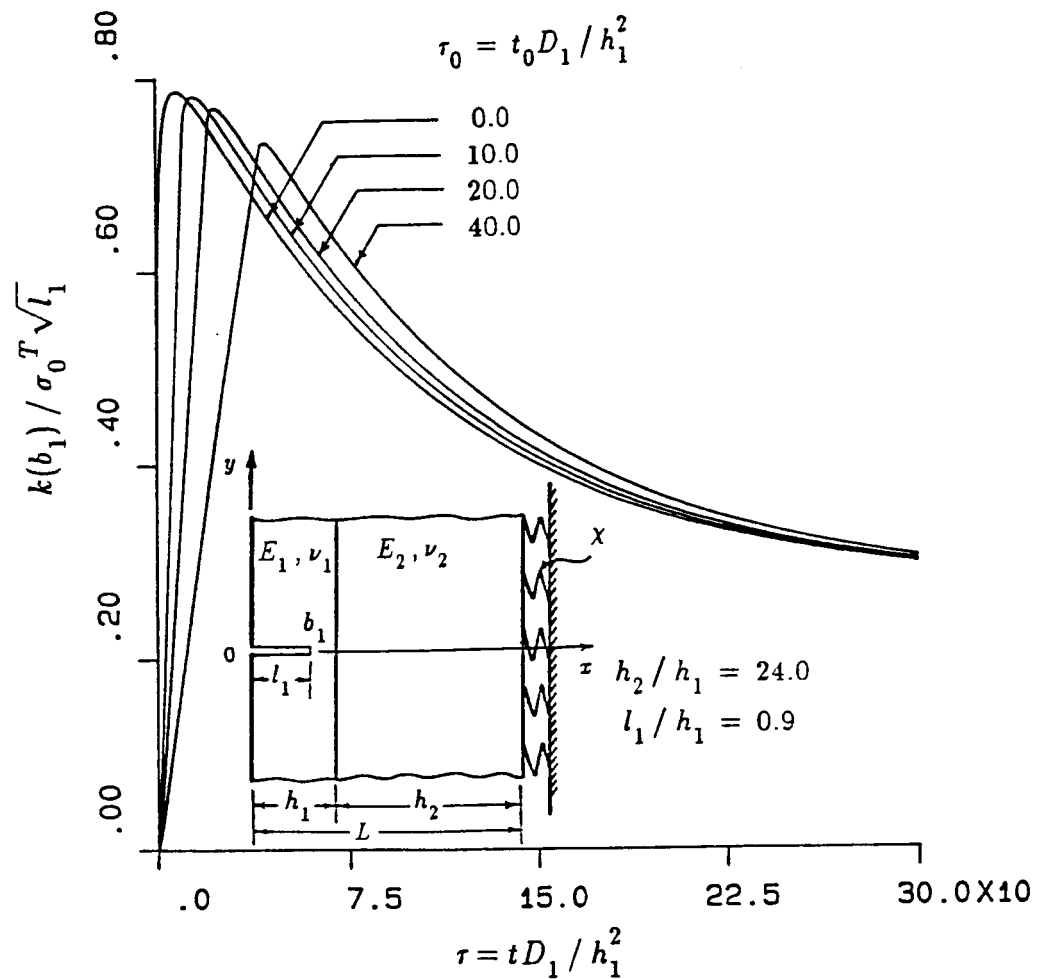


Figure 6-74: The influence of τ_0 on the normalized stress intensity factor $k(b_1)$ as a function of nondimensional time τ for an edge crack of length $l_1/h_1=0.9$ in Model II, $h_2/h_1=24.0$, $R_i/L=9.0$ and $\chi L/E_2=0.01108$, $\tau_0=t_0 D_1/h_1^2$, $\sigma_0^T=-\alpha_1' E_1 \Theta_0/(1-\nu_1)$ (material pair A)

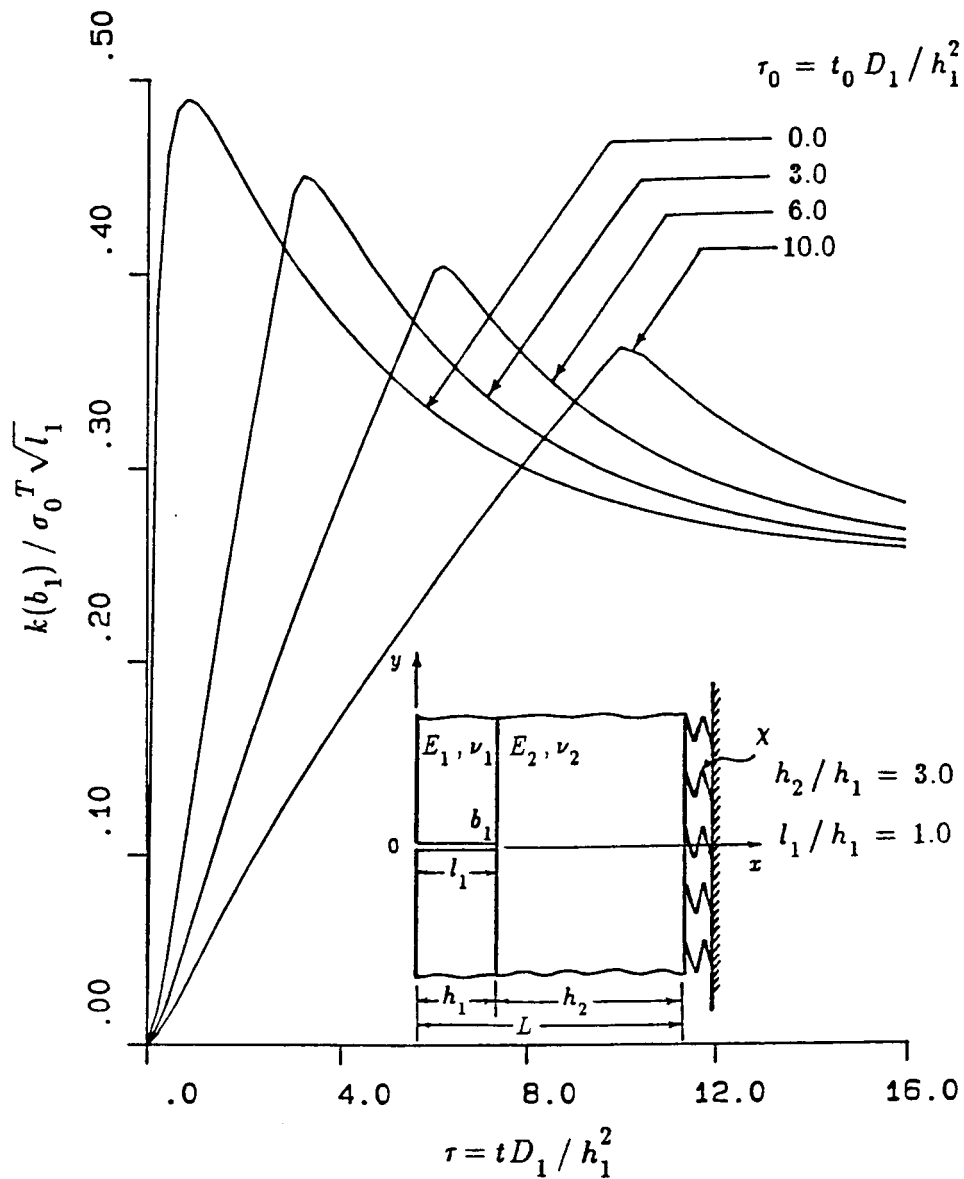


Figure 6-75: The influence of τ_0 on the normalized stress intensity factor $k(b_1)$ as a function of nondimensional time τ for a broken clad in Model II $h_2/h_1=3.0$, $R_i/L=9.0$ and $\chi L/E_2=0.01108$, $\tau_0=t_0 D_1/h_1^2$, $\sigma_0^T = -\alpha_1' E_1 \Theta_0 / (1-\nu_1)$ (material pair A)

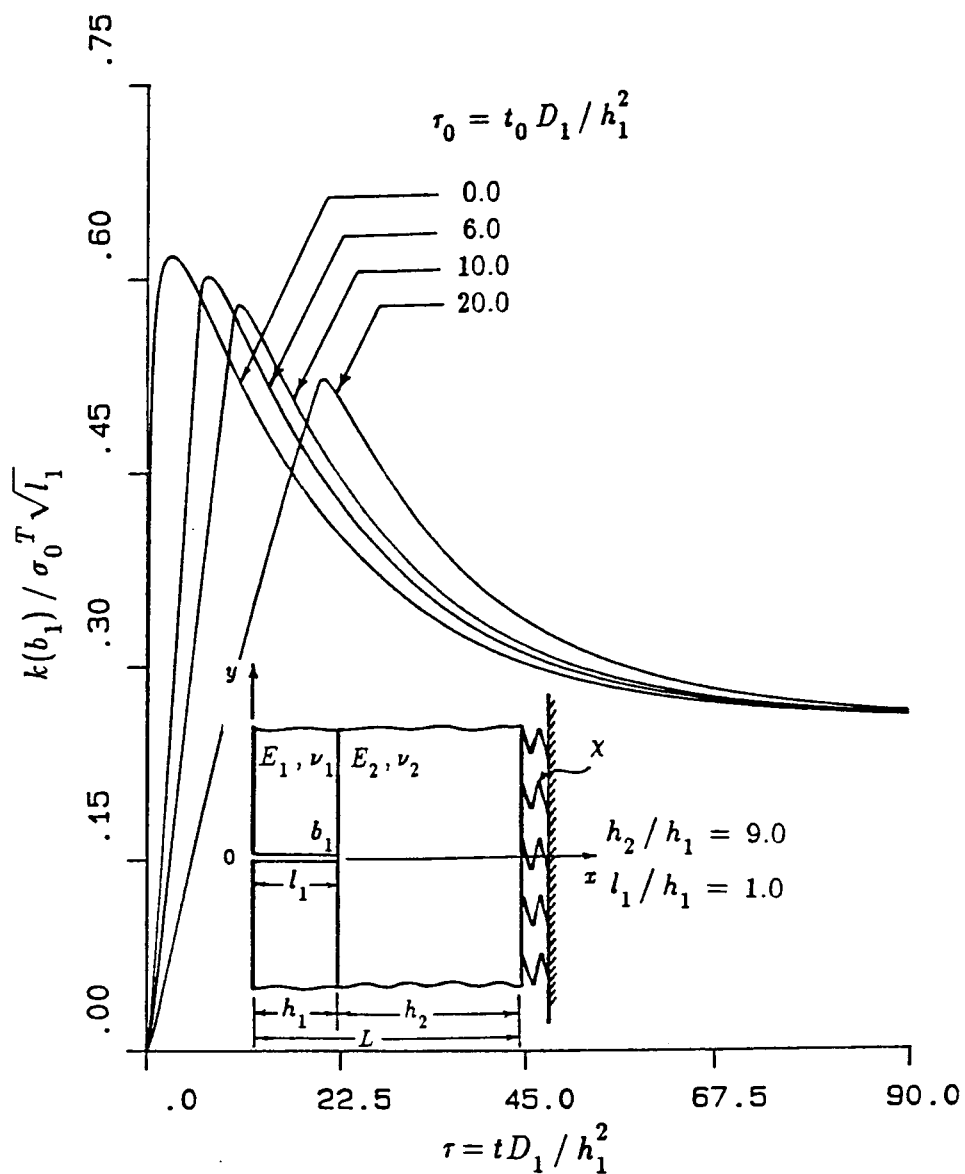


Figure 6-76: The influence of τ_0 on the normalized stress intensity factor $k(b_1)$ as a function of nondimensional time τ for a broken clad in Model II $h_2/h_1=9.0$, $R_i/L=9.0$ and $\chi L/E_2=0.01108$, $\tau_0=t_0 D_1/h_1^2$, $\sigma_0^T = -\alpha_1' E_1 \Theta_0 / (1-\nu_1)$ (material pair A)

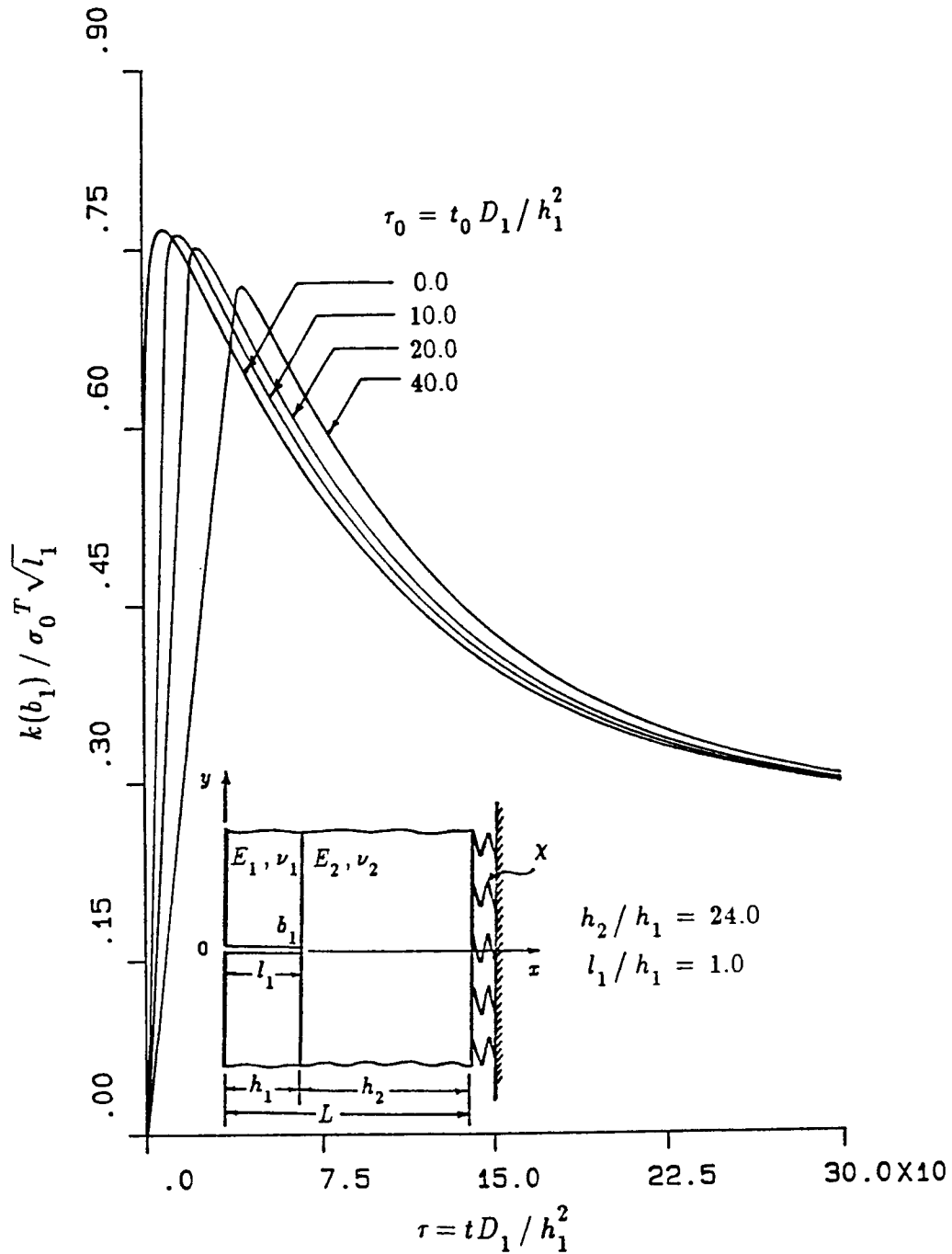


Figure 6-77: The influence of τ_0 on the normalized stress intensity factor $k(b_1)$ as a function of nondimensional time τ for a broken clad in Model II $h_2/h_1=24.0$, $R_i/L=9.0$ and $\chi L/E_2=0.01108$, $\tau_0=t_0 D_1/h_1^2$, $\sigma_0^T = -\alpha'_1 E_1 \Theta_0 / (1-\nu_1)$ (material pair A)

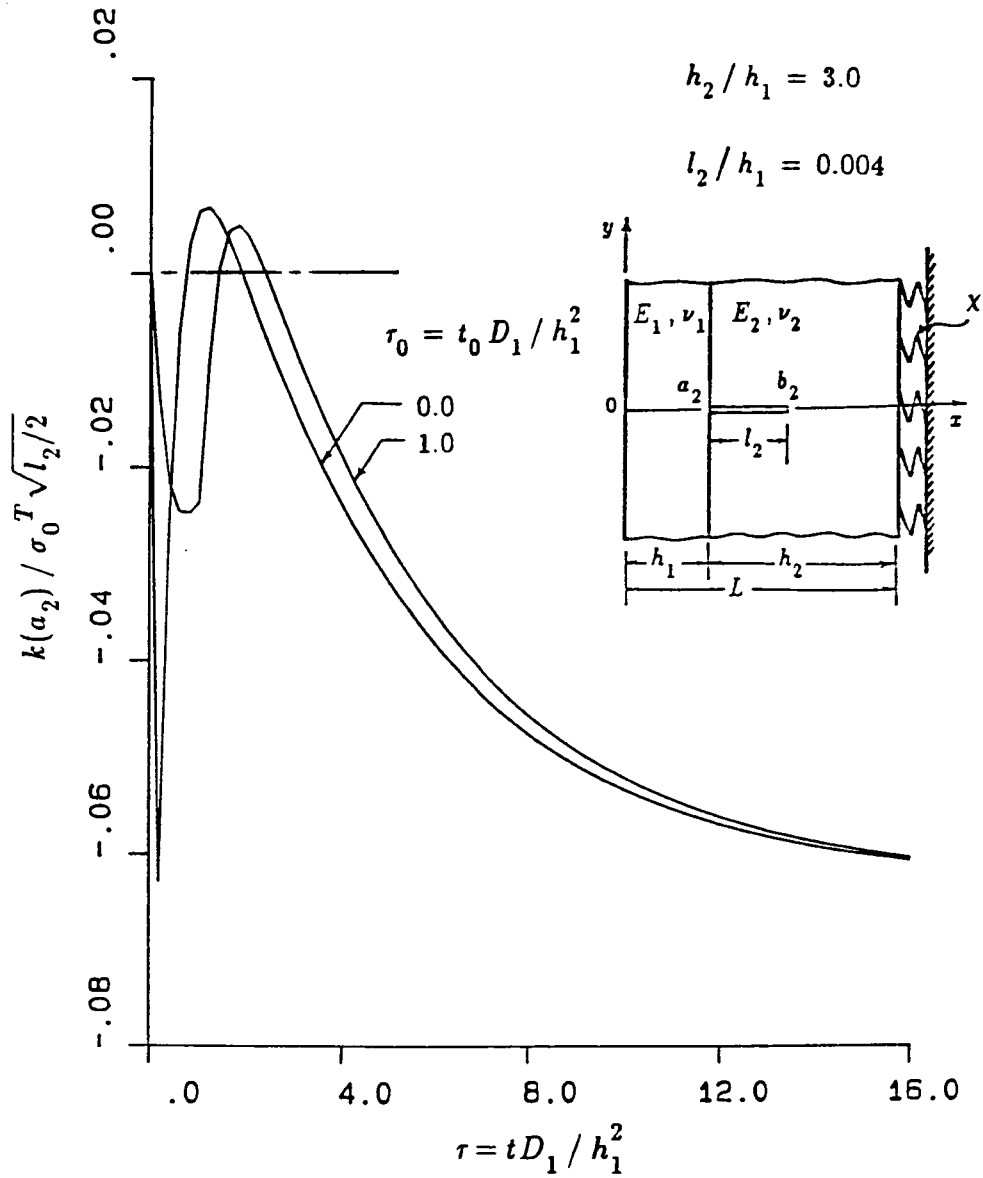


Figure 6-78: The influence of τ_0 on the normalized stress intensity factor $k(a_2)$ as a function of nondimensional time τ for an under-clad crack of length $l_2/h_1=0.004$ in Model II $h_2/h_1=3.0$, $R_i/L=9.0$ and $\chi L/E_2=0.01108$, $\tau_0=t_0 D_1/h_1^2$, $\sigma_0^T = -\alpha'_1 E_1 \Theta_0/(1-\nu_1)$ (material pair A)

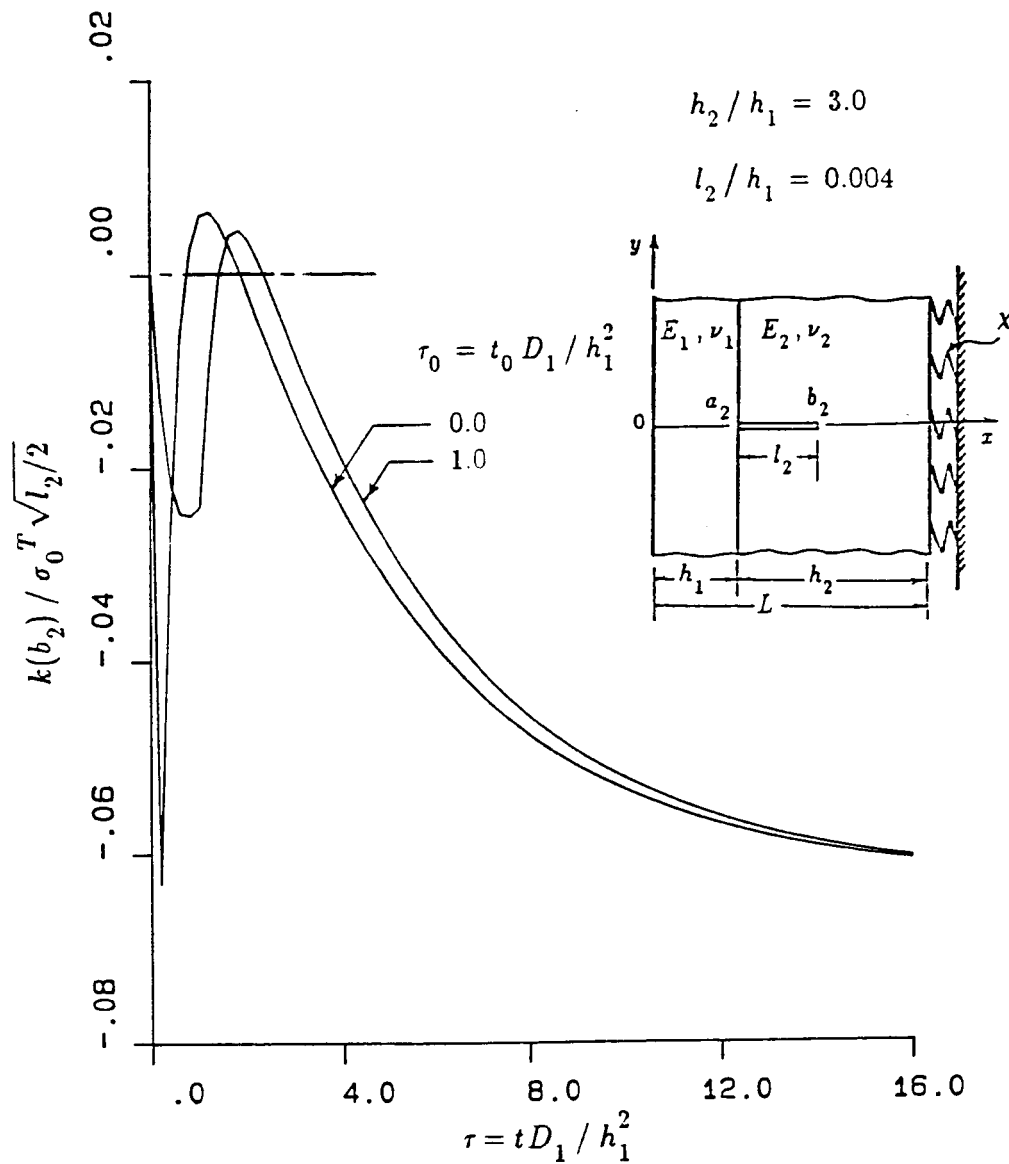


Figure 6-79: The influence of τ_0 on the normalized stress intensity factor $k(b_2)$ as a function of nondimensional time τ for a fixed under-clad crack length $l_2/h_1=0.004$ in Model II $h_2/h_1=3.0$, $R_i/L=9.0$ and $\chi L/E_2=0.01108$, $\tau_0=t_0 D_1/h_1^2$, $\sigma_0^T=-\alpha_1' E_1 \Theta_0/(1-\nu_1)$ (material pair A)

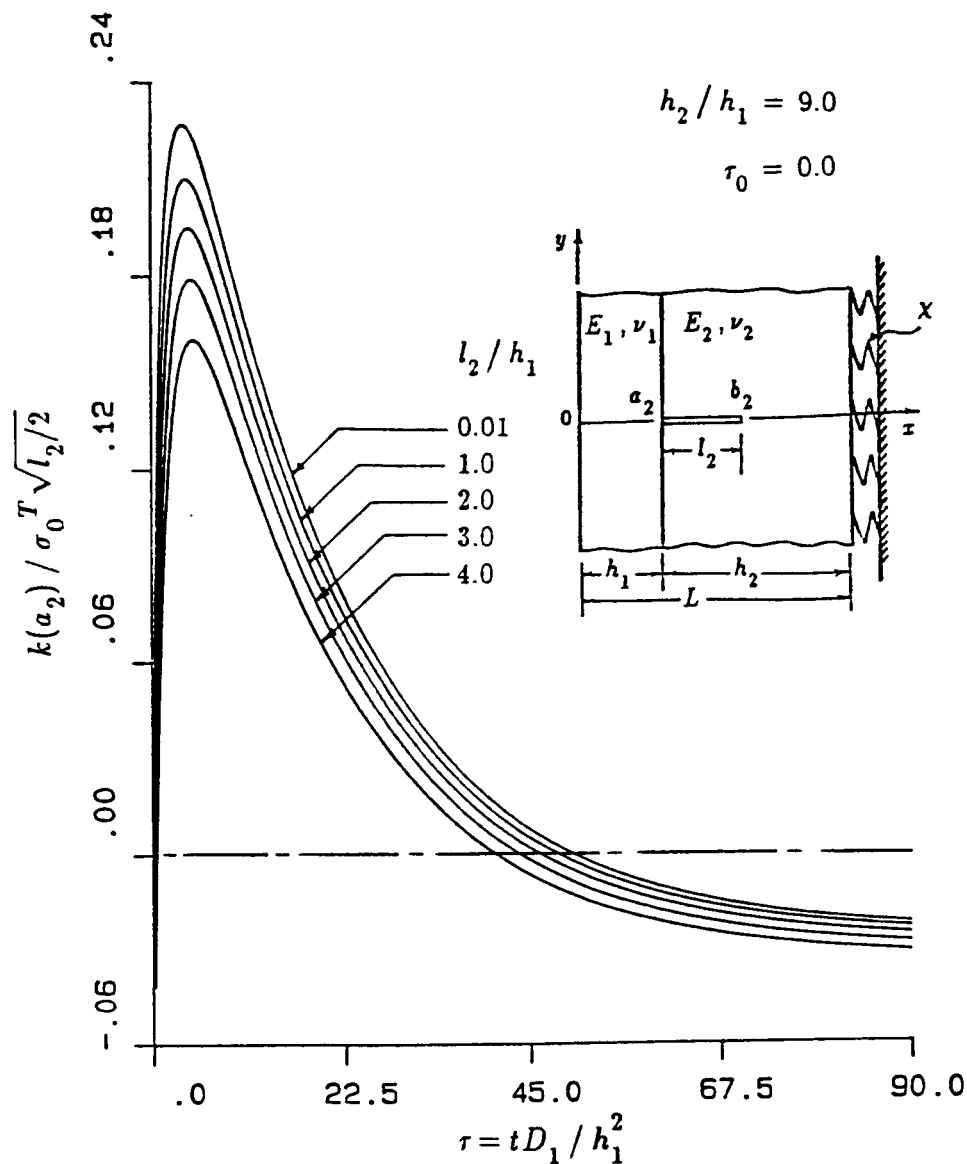


Figure 6-80: The normalized stress intensity factor $k(a_2)$ as a function of nondimensional time τ for an under-clad crack in Model II for $\tau_0=0.0$, $h_2/h_1=9.0$, $R_i/L=9.0$ and $\chi L/E_2=0.01108$, $\tau_0=t_0 D_1/h_1^2$, $\sigma_0^T = -\alpha_1' E_1 \Theta_0 / (1-\nu_1)$.(material pair A)

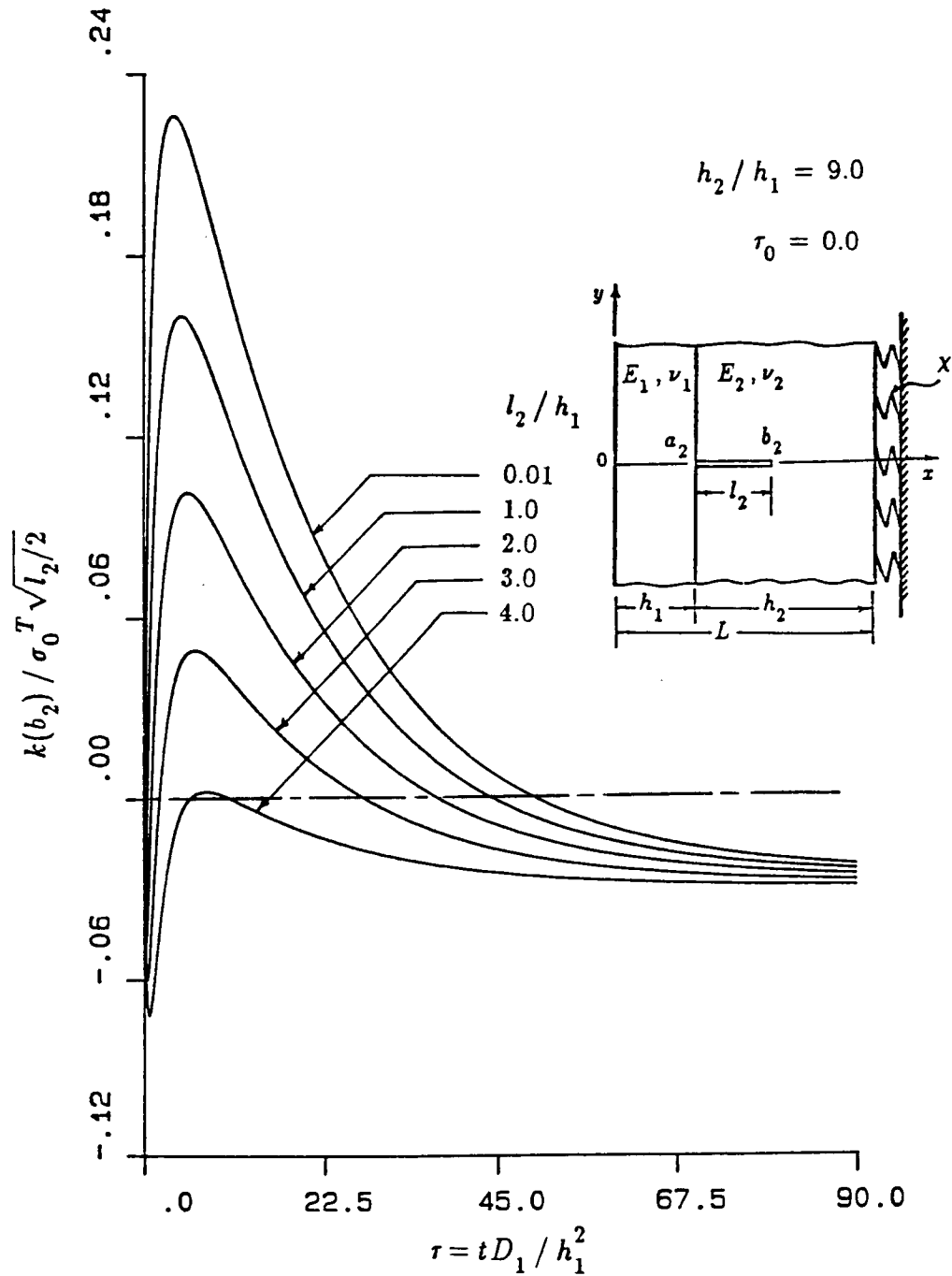


Figure 6-81: The normalized stress intensity factor $k(b_2)$ as a function of nondimensional time τ for an under-clad crack in Model II for $\tau_0=0.0$, $h_2/h_1=9.0$, $R_i/L=9.0$ and $\chi L/E_2=0.01108$, $\tau_0=t_0 D_1/h_1^2$, $\sigma_0^T = -\alpha_1' E_1 \Theta_0 / (1-\nu_1)$. (material pair A)

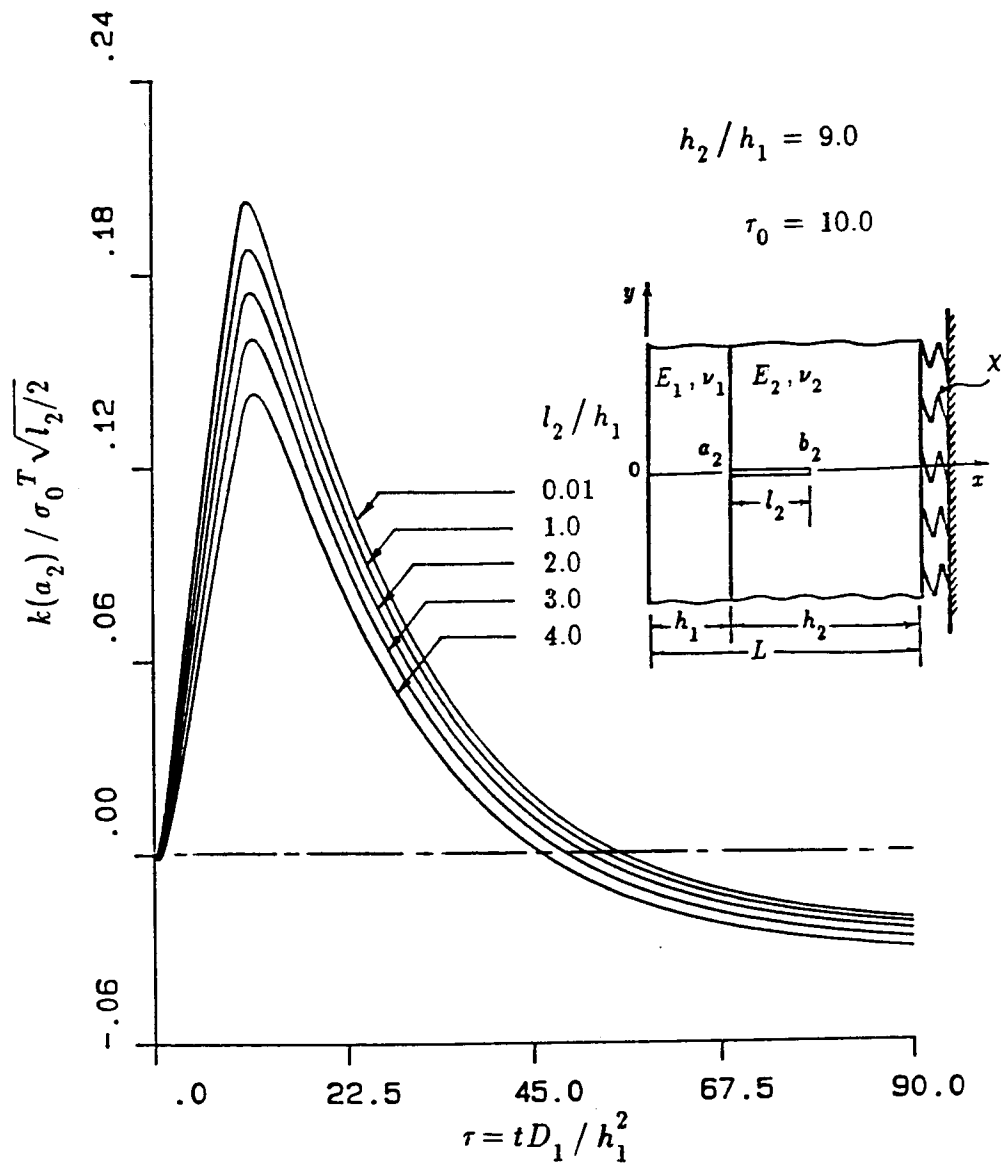


Figure 6-82: The normalized stress intensity factor $k(a_2)$ as a function of nondimensional time τ for an under-clad crack in Model II for $\tau_0=10.0$, $h_2/h_1=9.0$, $R_i/L=9.0$ and $\chi L/E_2=0.01108$, $\tau_0=t_0 D_1/h_1^2$, $\sigma_0^T = -\alpha'_1 E_1 \Theta_0 / (1-\nu_1)$. (material pair A)

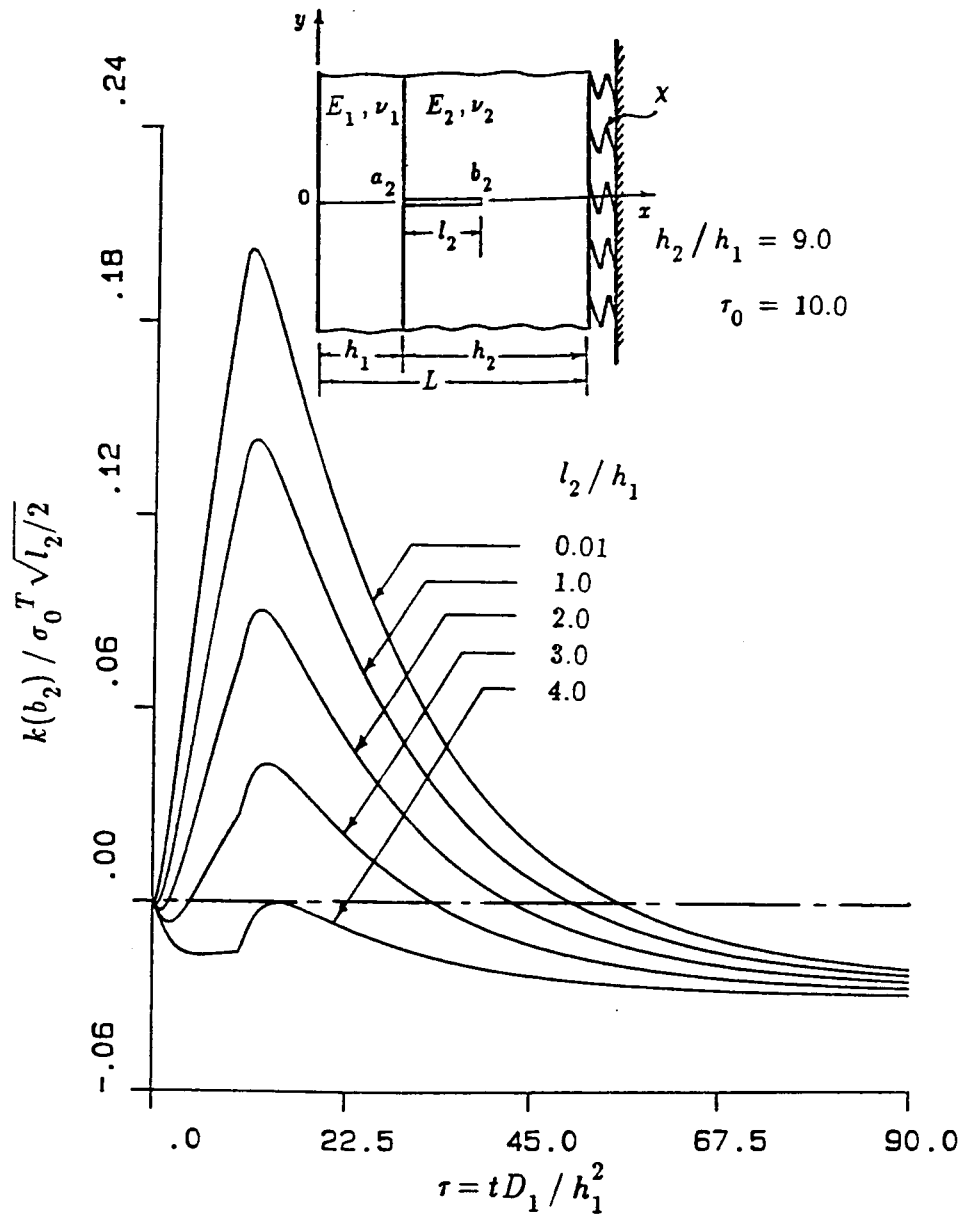


Figure 6-83: The normalized stress intensity factor $k(b_2)$ as a function of nondimensional time τ for an under-clad crack in Model II for $\tau_0=10.0$, $h_2/h_1=9.0$, $R_i/L=9.0$ and $\chi L/E_2=0.01108$, $\tau_0=t_0D_1/h_1^2$, $\sigma_0^T = -\alpha'_1 E_1 \Theta_0 / (1-\nu_1)$.(material pair A)

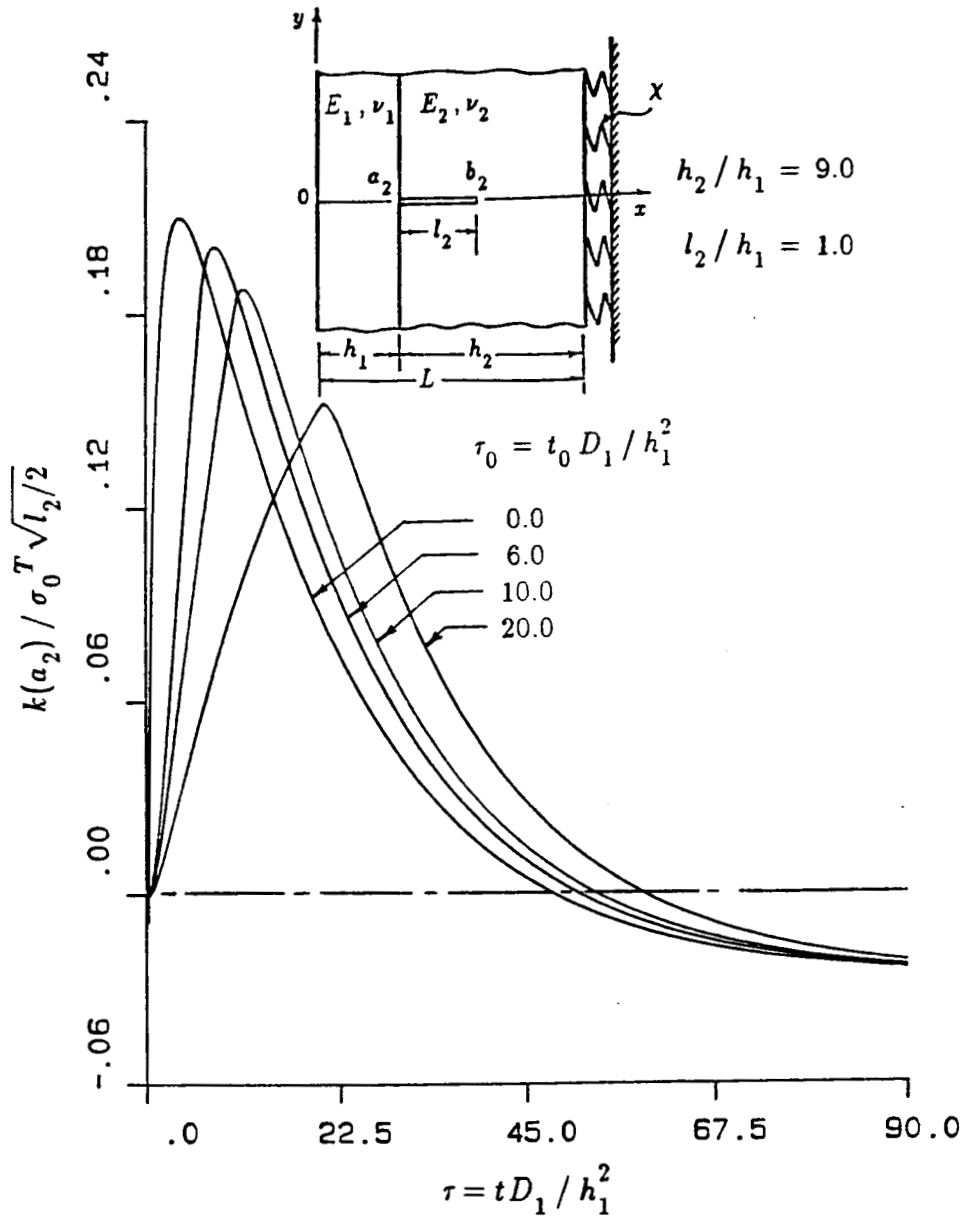


Figure 6-84: The influence of τ_0 on the normalized stress intensity factor $k(a_2)$ as a function of nondimensional time τ for an under-clad crack of length $l_2/h_1=1.0$ in Model II $h_2/h_1=9.0$, $R_i/L=9.0$ and $\chi L/E_2=0.01108$, $\tau_0=t_0 D_1/h_1^2$, $\sigma_0^T = -\alpha_1 E_1 \Theta_0/(1-\nu_1)$ (material pair A)

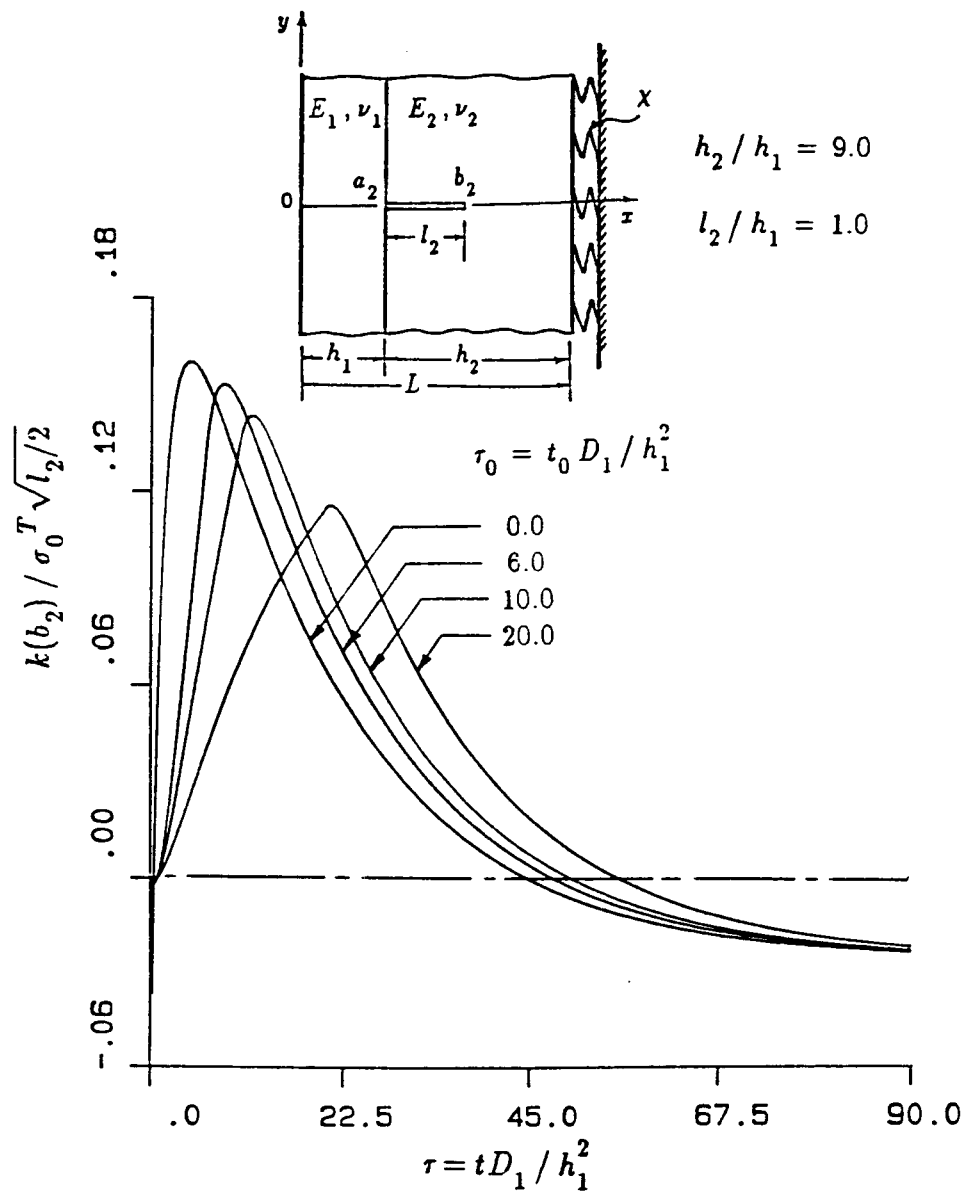


Figure 6-85: The influence of τ_0 on the normalized stress intensity factor $k(b_2)$ as a function of nondimensional time τ for an under-clad crack of length $l_2/h_1=1.0$ in Model II $h_2/h_1=9.0$, $R_i/L=9.0$ and $\chi L/E_2=0.01108$, $\tau_0=t_0 D_1/h_1^2$, $\sigma_0^T = -\alpha_1' E_1 \Theta_0 / (1-\nu_1)$ (material pair A)

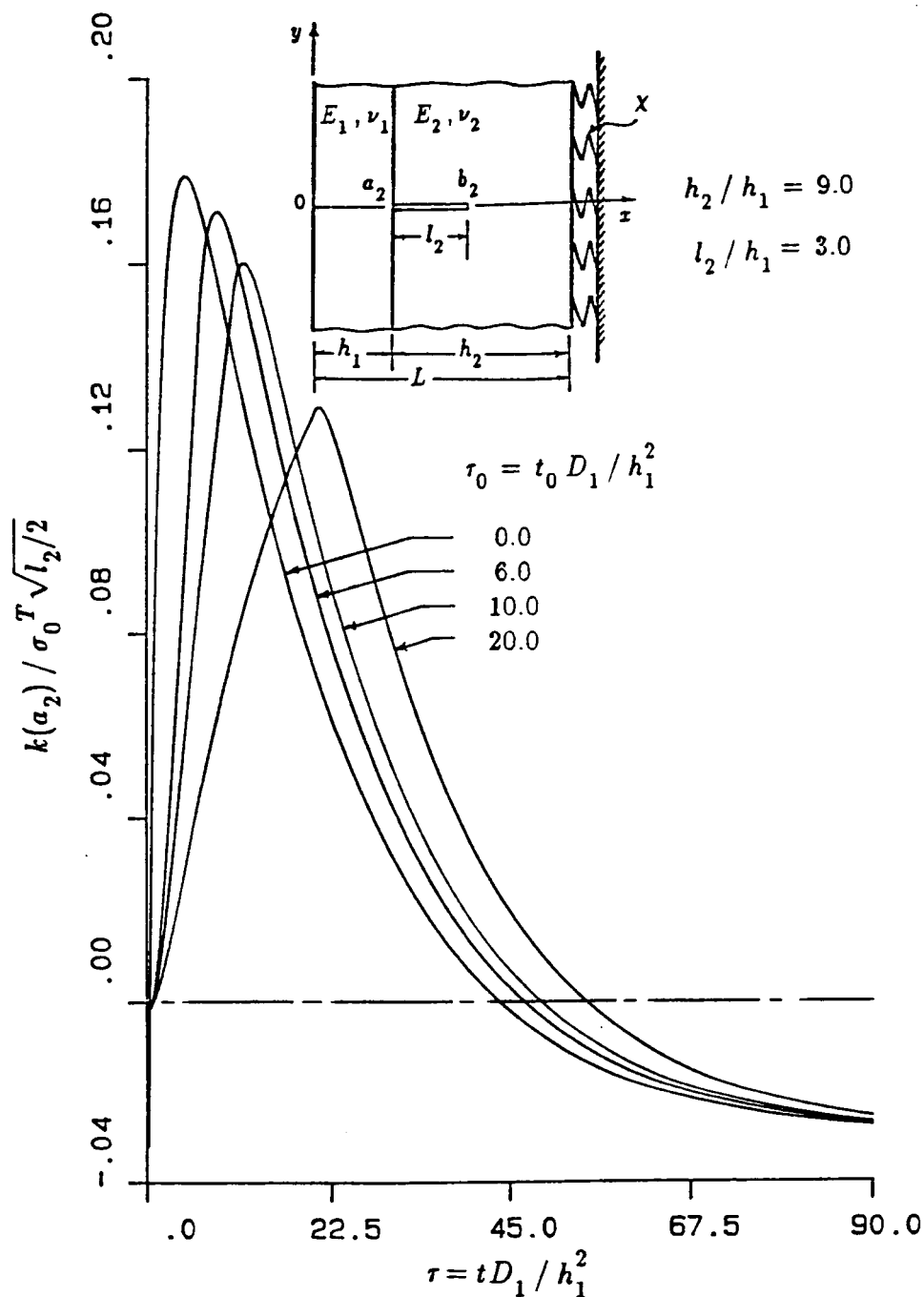


Figure 6-86: The influence of τ_0 on the normalized stress intensity factor $k(a_2)$ as a function of nondimensional time τ for an under-clad crack of length $l_2/h_1=3.0$ in Model II $h_2/h_1=9.0$, $R_i/L=9.0$ and $\chi L/E_2=0.01108$, $\tau_0=t_0 D_1/h_1^2$, $\sigma_0^T=-\alpha'_1 E_1 \Theta_0/(1-\nu_1)$ (material pair A)

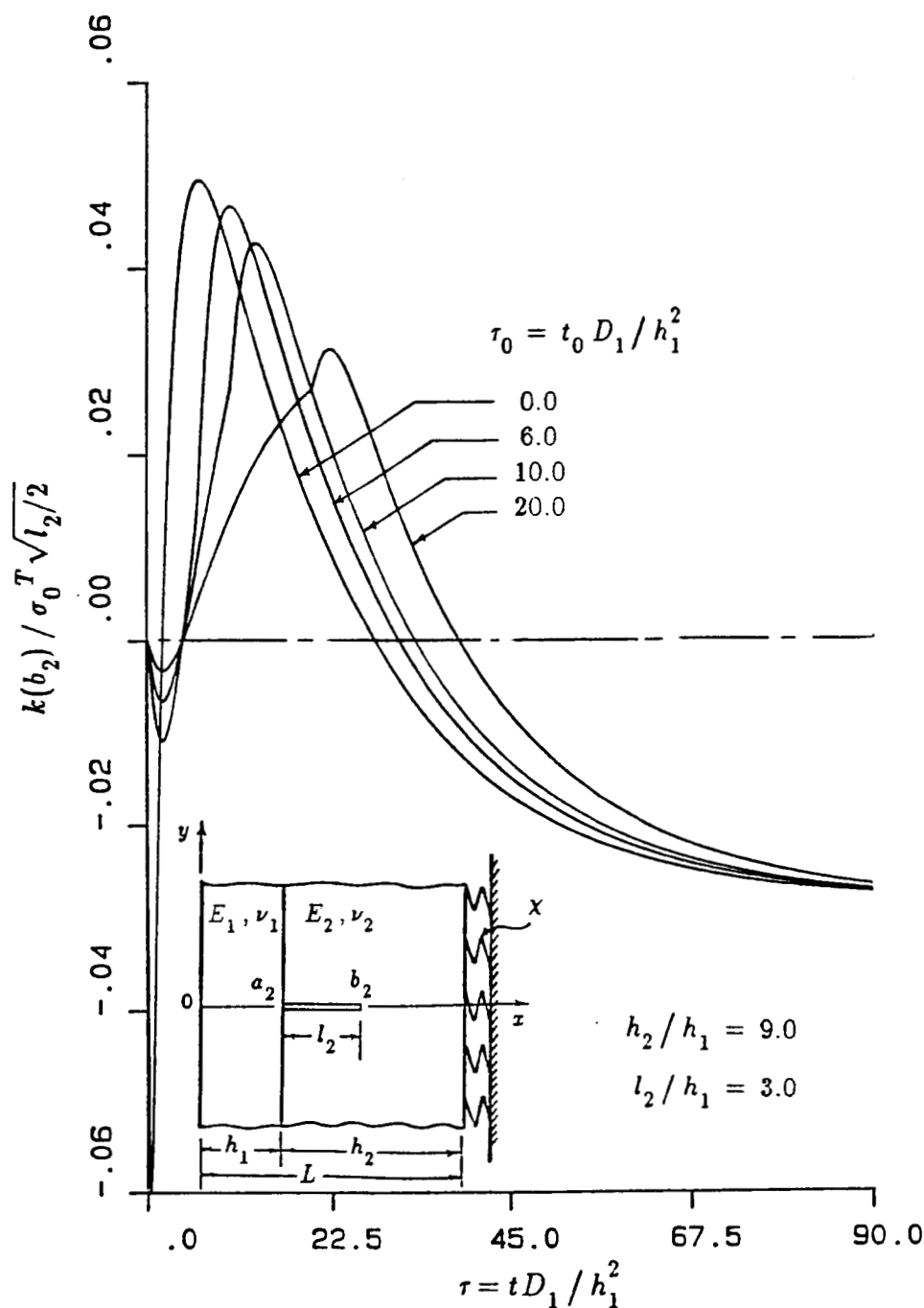


Figure 6-87: The influence of τ_0 on the normalized stress intensity factor $k(b_2)$ as a function of nondimensional time τ for an under-clad crack of length $l_2/h_1=3.0$ in Model II $h_2/h_1=9.0$, $R_i/L=9.0$ and $\chi L/E_2=0.01108$, $\tau_0=t_0 D_1/h_1^2$, $\sigma_0^T=-\alpha'_1 E_1 \Theta_0/(1-\nu_1)$ (material pair A)

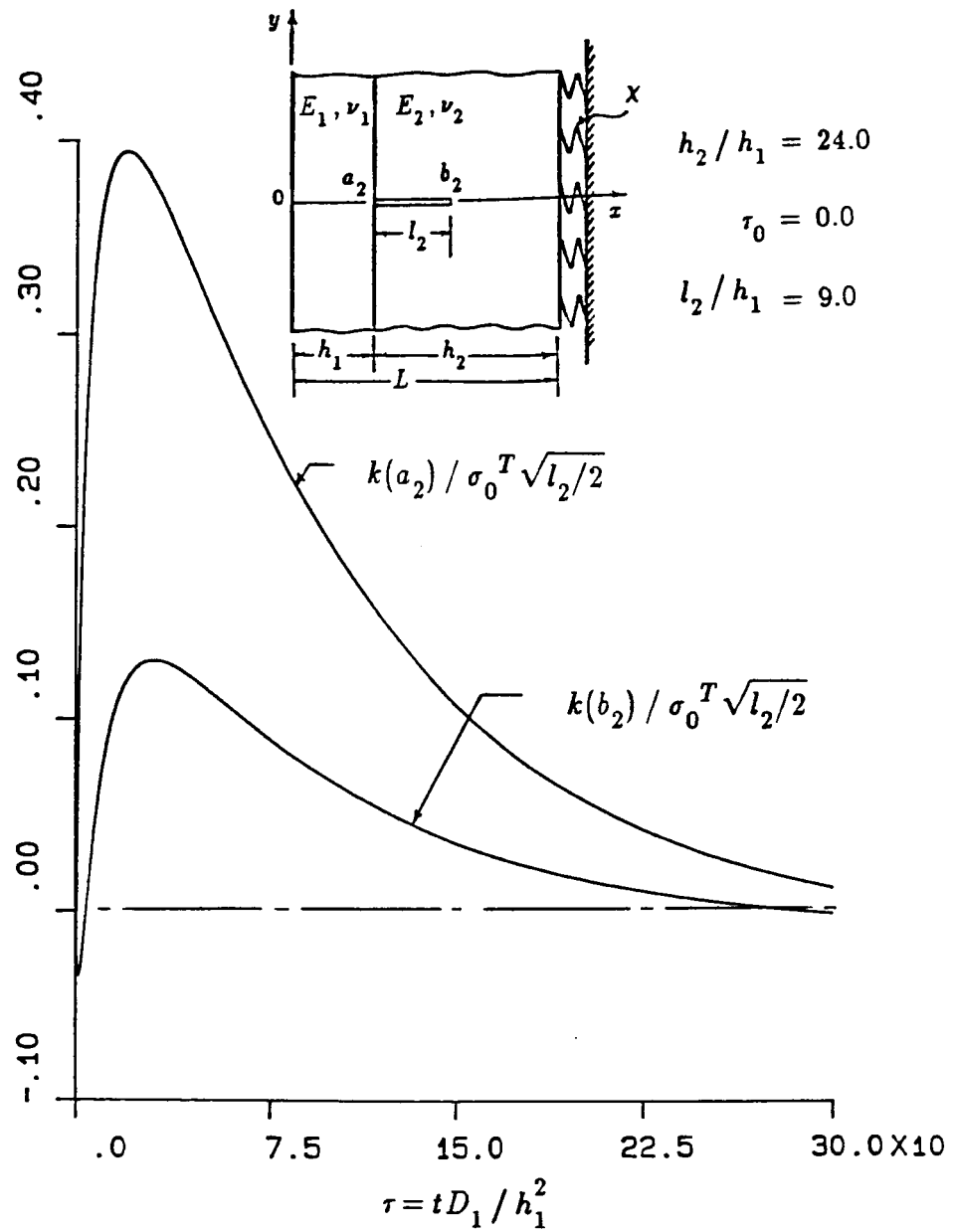


Figure 6-88: The normalized stress intensity factor $k(a_2)$, $k(b_2)$ as a function of nondimensional time τ for under-clad crack in Model II for $l_2/h_1=9.0$, $\tau_0=0.0$, $h_2/h_1=24.0$, $R_i/L=9.0$ and $\chi L/E_2=0.01108$, $\tau_0=t_0 D_1/h_1^2$, $\sigma_0^T = -\alpha_1' E_1 \Theta_0/(1-\nu_1)$ (material pair A)

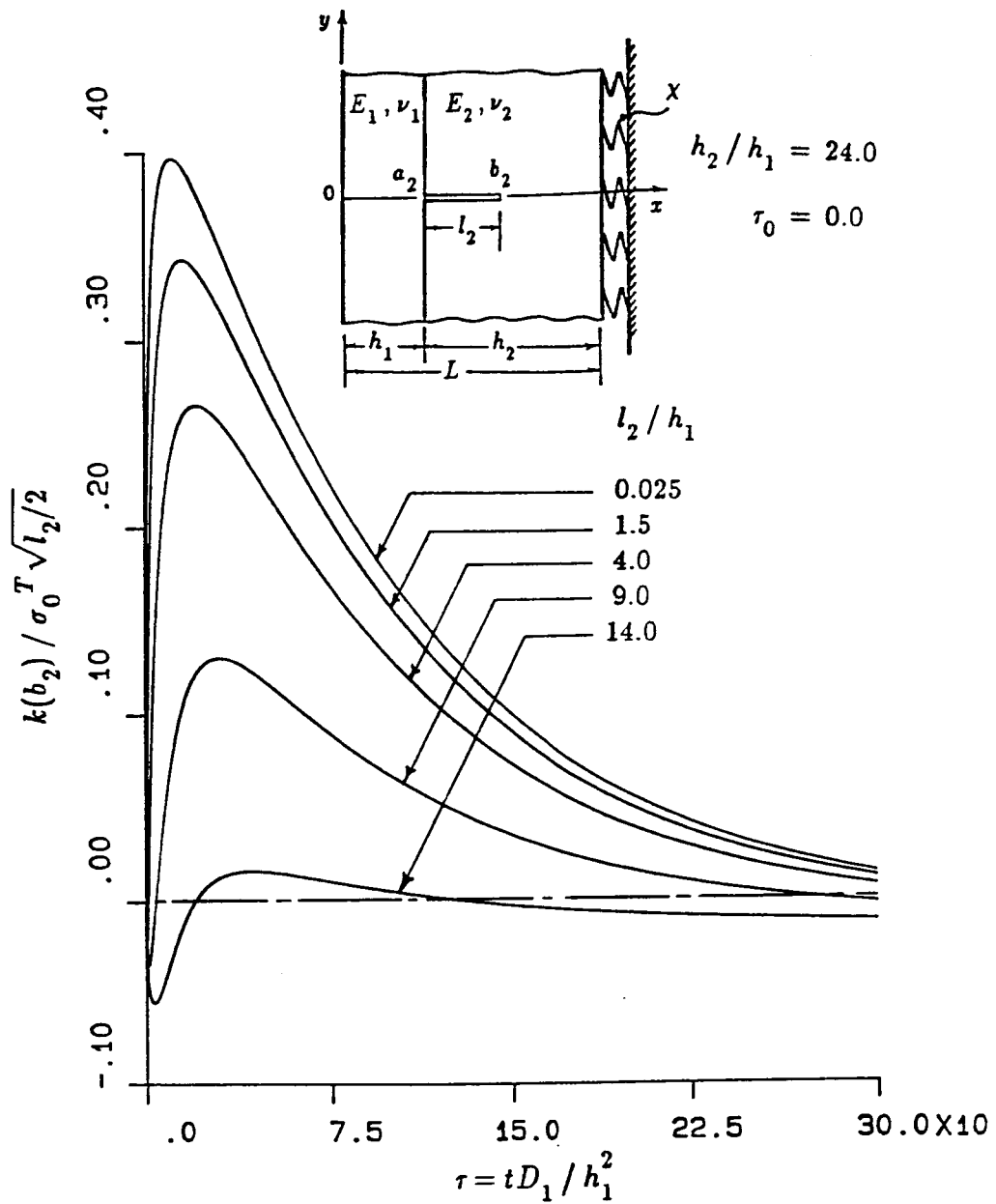


Figure 6-89: The normalized stress intensity factor $k(b_2)$ as a function of nondimensional time τ for an under-clad crack in Model II for $\tau_0=0.0$, $h_2/h_1=24.0$, $R_i/L=9.0$ and $\chi L/E_2=0.01108$, $\tau_0=t_0 D_1/h_1^2$, $\sigma_0^T = -\alpha_1' E_1 \Theta_0 / (1-\nu_1)$ (material pair A)

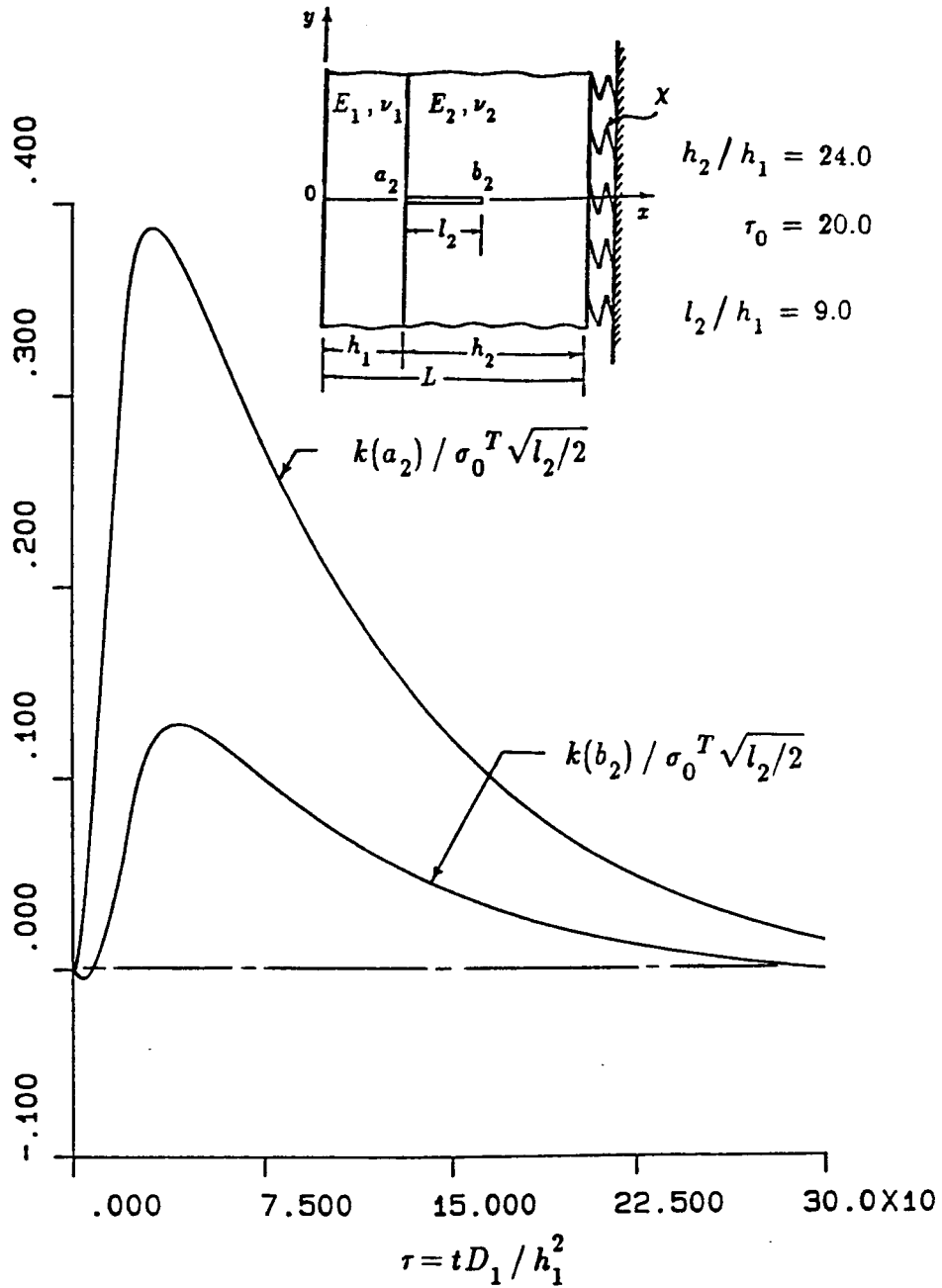


Figure 6-90: The normalized stress intensity factor $k(a_2)$, $k(b_2)$ as a function of nondimensional time τ for an under-clad crack in Model II for $l_2/h_1=9.0$, $\tau_0=20.0$, $h_2/h_1=24.0$, $R_i/L=9.0$ and $\chi L/E_2=0.01108$, $\tau_0=t_0D_1/h_1^2$, $\sigma_0^T=-\alpha_1 E_1 \Theta_0/(1-\nu_1)$ (material pair A)

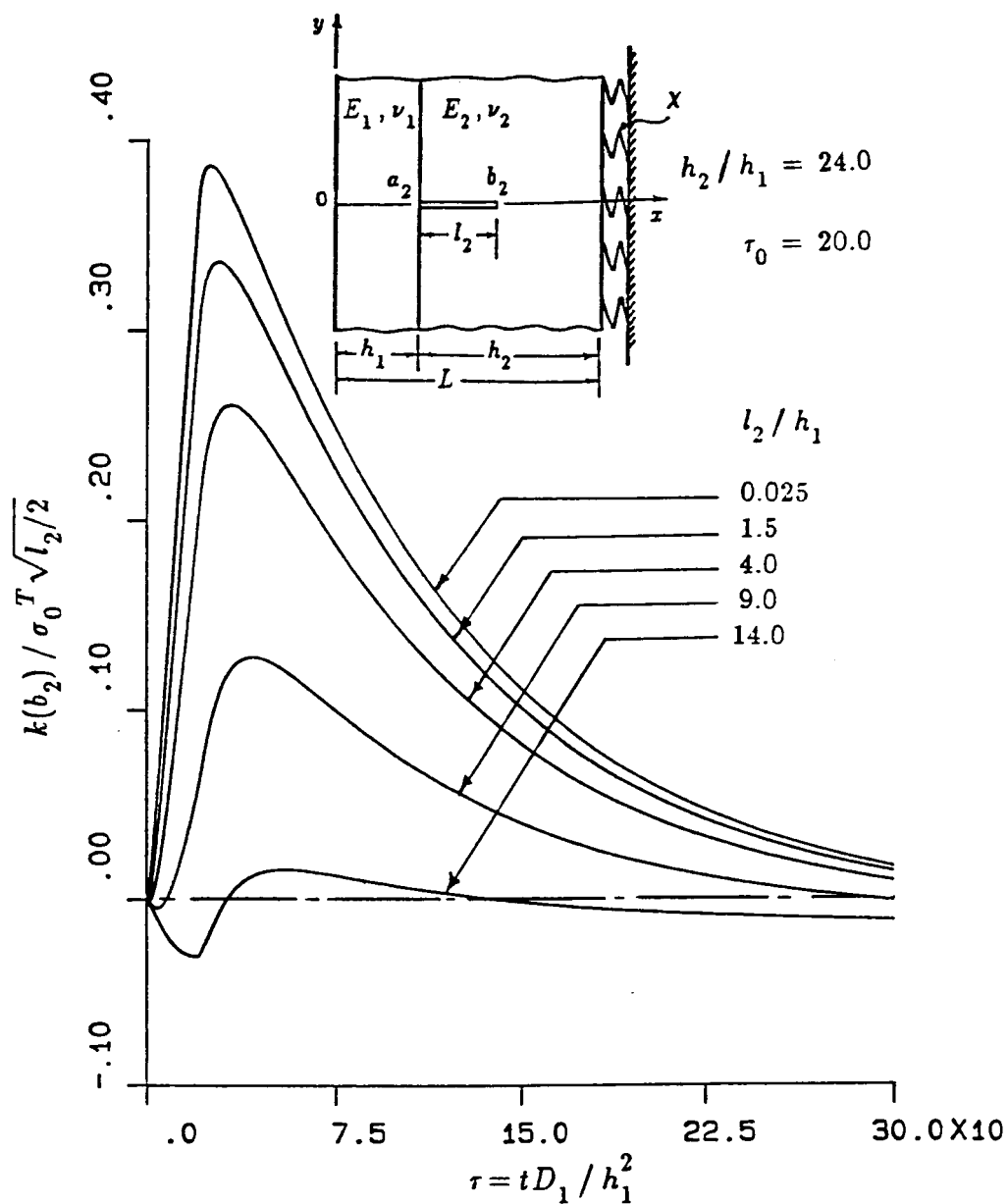


Figure 6-91: The normalized stress intensity factor $k(b_2)$ as a function of nondimensional time τ for an under-clad crack in Model II for $\tau_0=20.0$, $h_2/h_1=24.0$, $R_i/L=9.0$ and $\chi L/E_2=0.01108$, $\tau_0=t_0 D_1/h_1^2$, $\sigma_0^T = -\alpha'_1 E_1 \Theta_0 / (1-\nu_1)$ (material pair A)

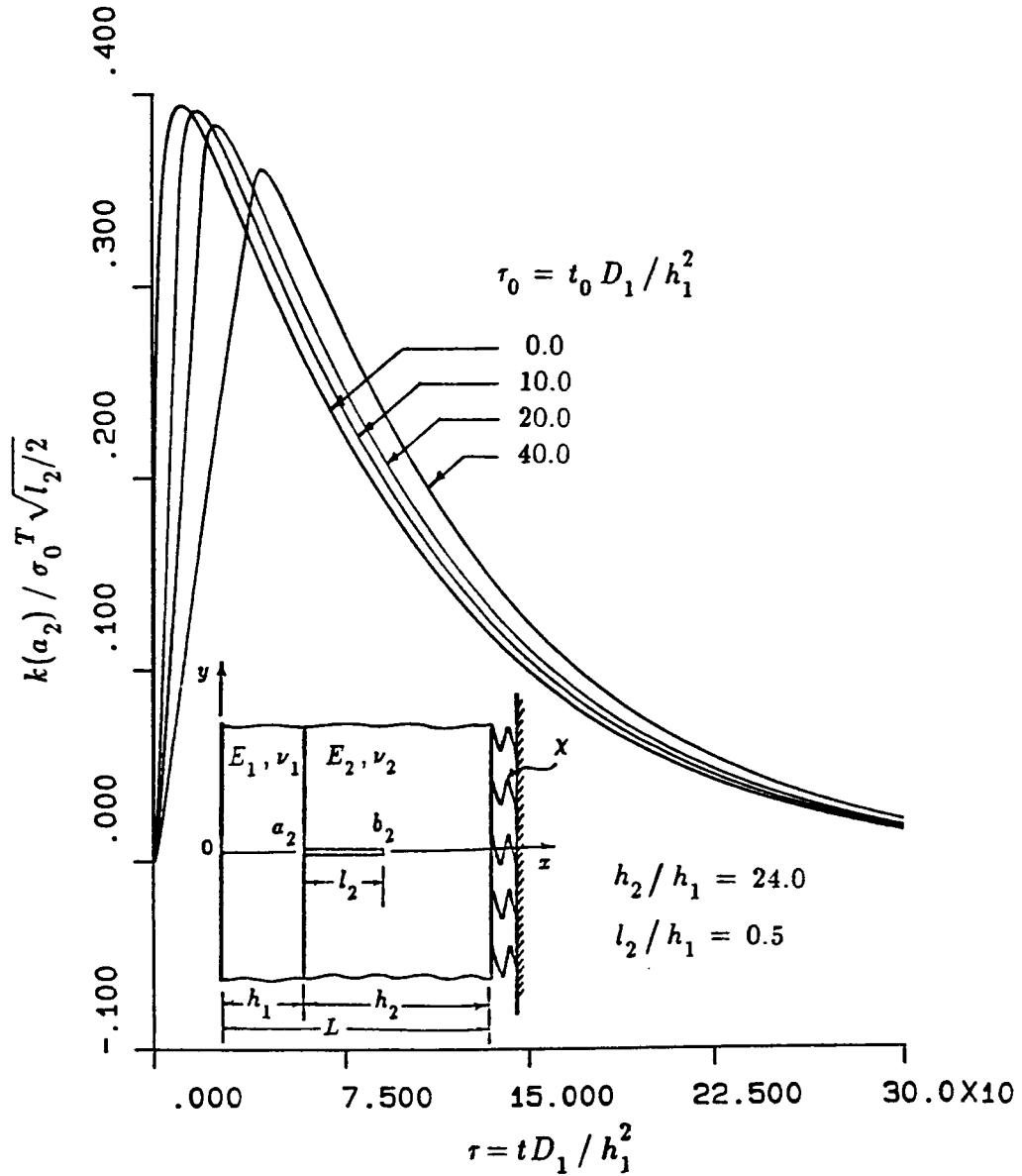


Figure 6-92: The influence of τ_0 on the normalized stress intensity factor $k(a_2)$ as a function of nondimensional time τ for an under-clad crack of length $l_2/h_1=0.5$ in Model II, $h_2/h_1=24.0$, $R_i/L=9.0$ and $\chi L/E_2=0.01108$, $\tau_0=t_0 D_1/h_1^2$, $\sigma_0^T = -\alpha_1' E_1 \Theta_0/(1-\nu_1)$ (material pair A)

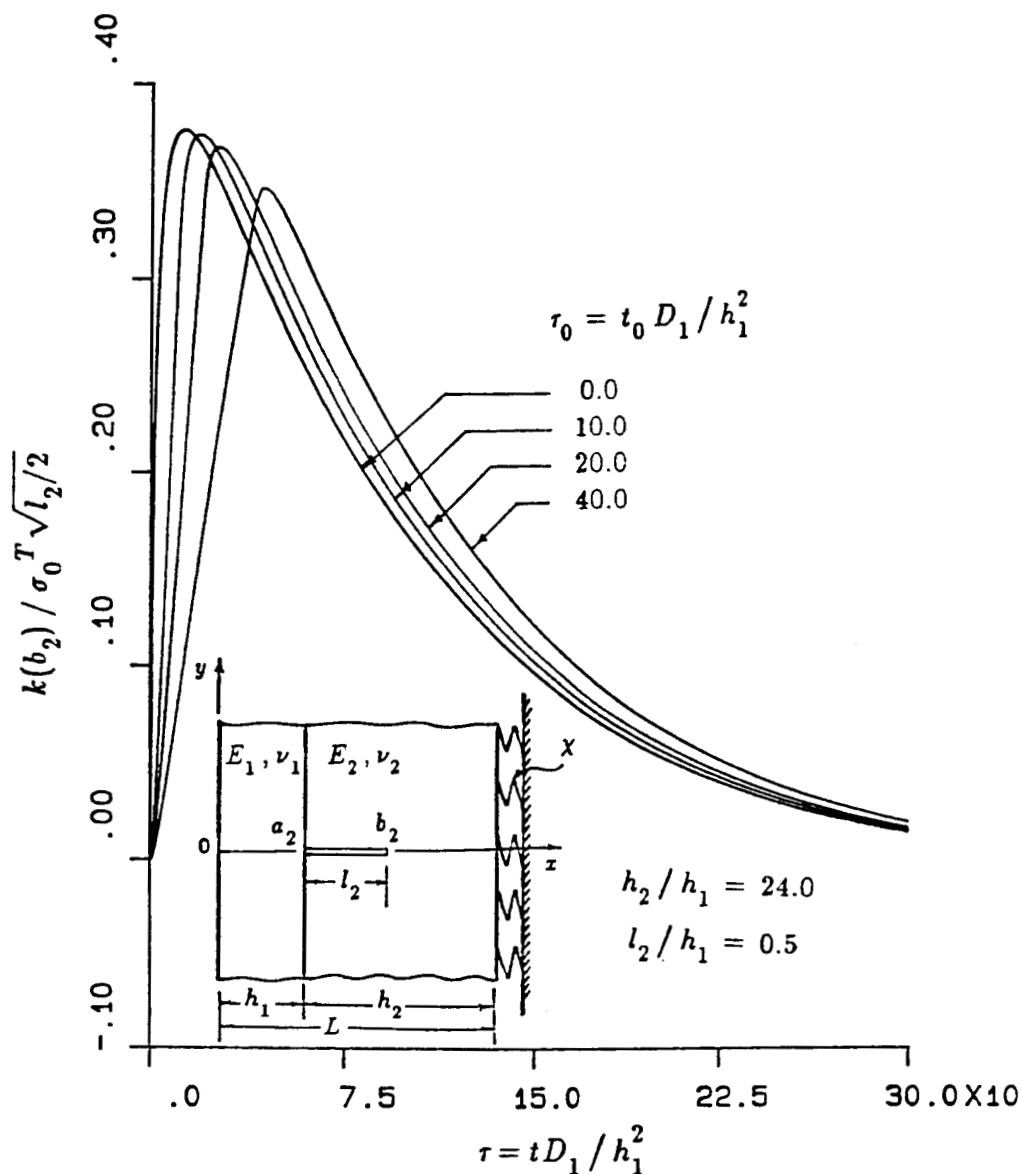


Figure 6-93: The influence of τ_0 on the normalized stress intensity factor $k(b_2)$ as a function of nondimensional time τ for an under-clad crack of length $l_2/h_1=0.5$ in Model II, $h_2/h_1=24.0$, $R_i/L=9.0$ and $\chi L/E_2=0.01108$, $\tau_0=t_0 D_1/h_1^2$, $\sigma_0^T = -\alpha'_1 E_1 \Theta_0/(1-\nu_1)$ (material pair A)

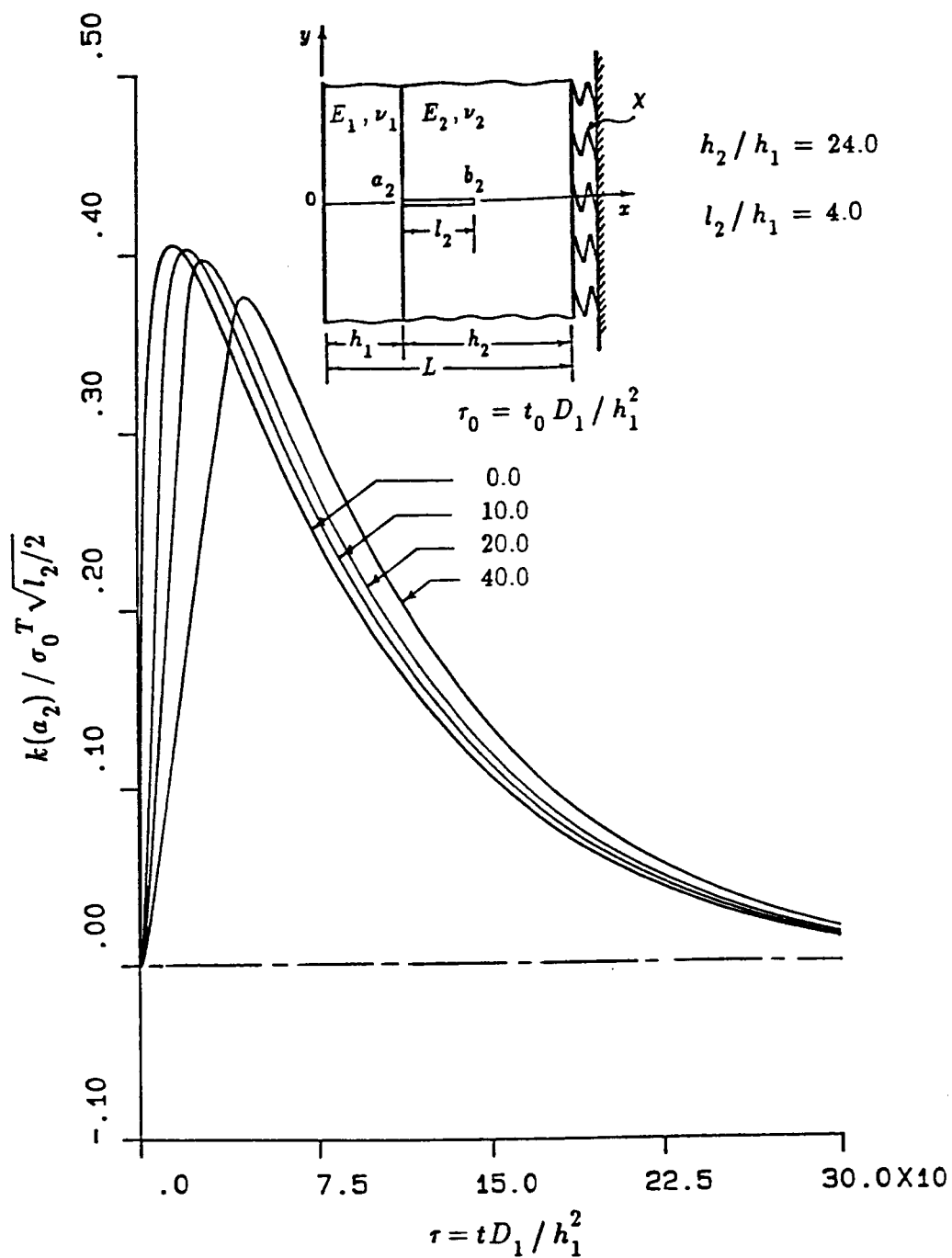


Figure 6-94: The influence of τ_0 on the normalized stress intensity factor $k(a_2)$ as a function of nondimensional time τ for an under-clad crack of length $l_2/h_1=4.0$ in Model II, $h_2/h_1=24.0$, $R_i/L=9.0$ and $\chi L/E_2=0.01108$, $\tau_0=t_0 D_1/h_1^2$, $\sigma_0^T = -\alpha_1' E_1 \Theta_0/(1-\nu_1)$ (material pair A)

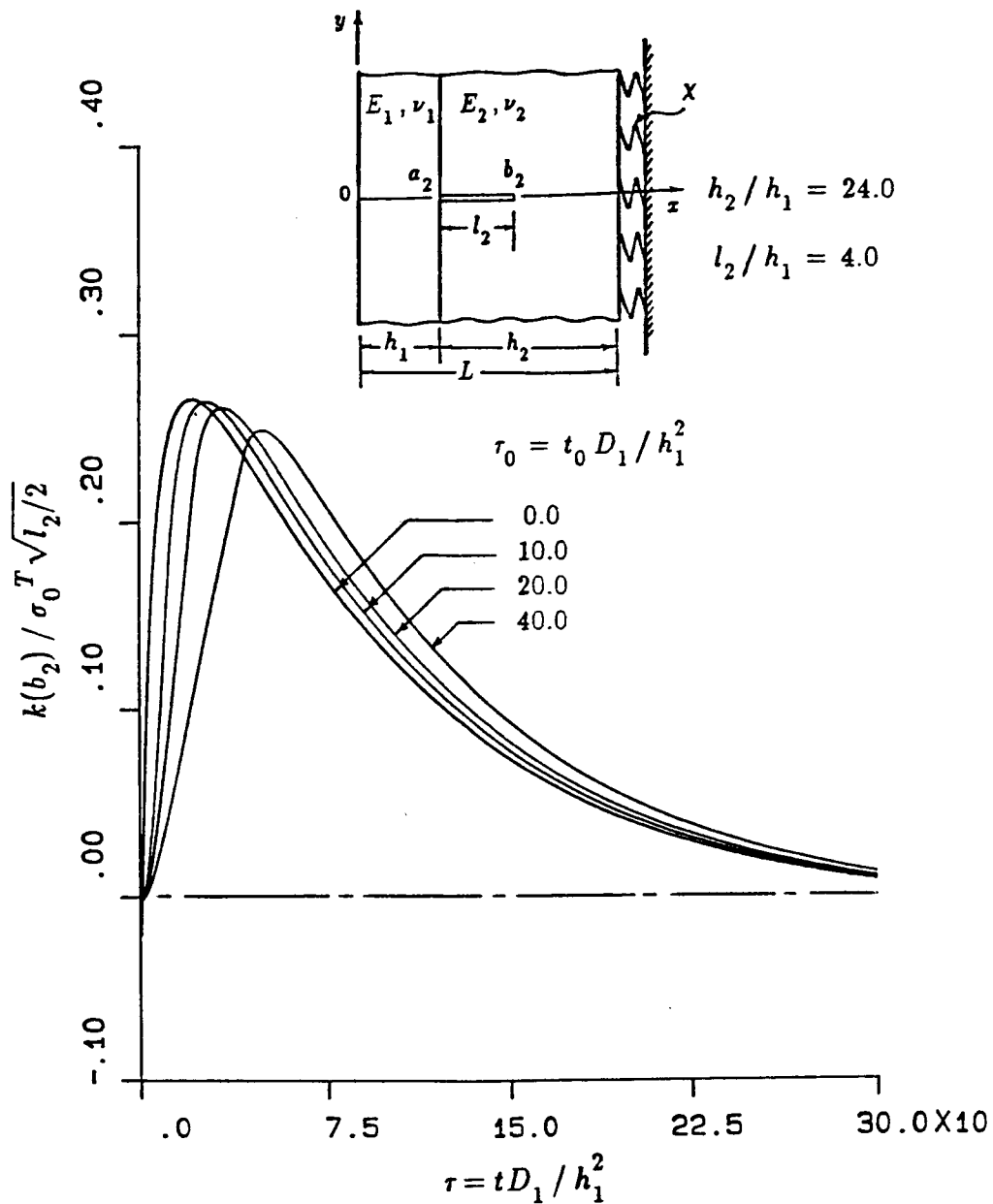


Figure 6-95: The influence of τ_0 on the normalized stress intensity factor $k(b_2)$ as a function of nondimensional time τ for an under-clad crack of length $l_2/h_1=4.0$ in Model II, $h_2/h_1=24.0$, $R_i/L=9.0$ and $\chi L/E_2=0.01108$, $\tau_0=t_0 D_1/h_1^2$, $\sigma_0^T = -\alpha_1 E_1 \Theta_0 / (1-\nu_1)$ (material pair A)

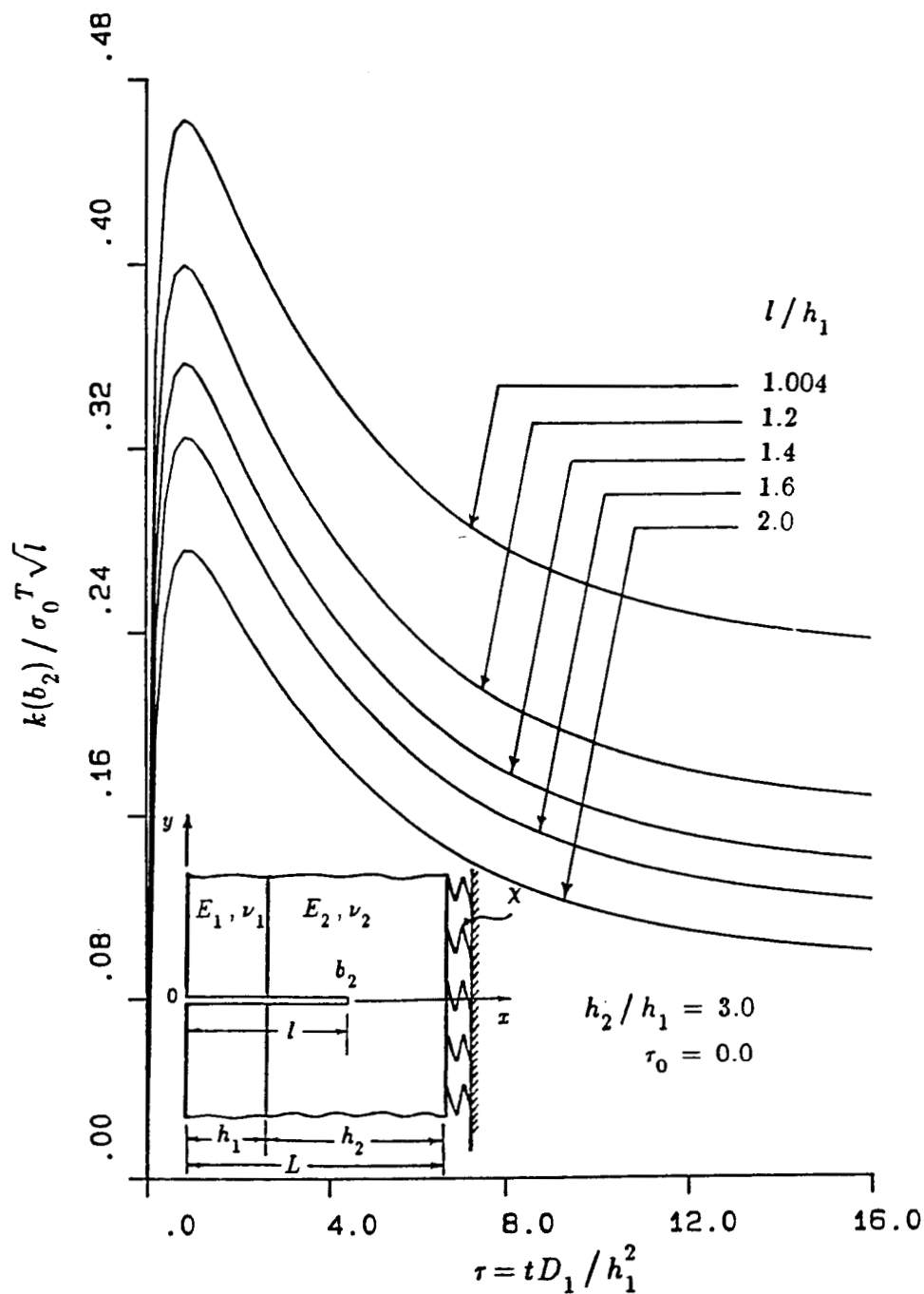


Figure 6-96: The normalized stress intensity factor $k(b_2)$ as a function of nondimensional time τ for an edge crack crossing the interface in Model II for $\tau_0=0.0$, $h_2/h_1=3.0$, $R_i/L=9.0$ and $\chi L/E_2=0.01108$, $\tau_0=t_0 D_1/h_1^2$, $\sigma_0^T = -\alpha_1^T E_1 \Theta_0/(1-\nu_1)$ (material pair A)

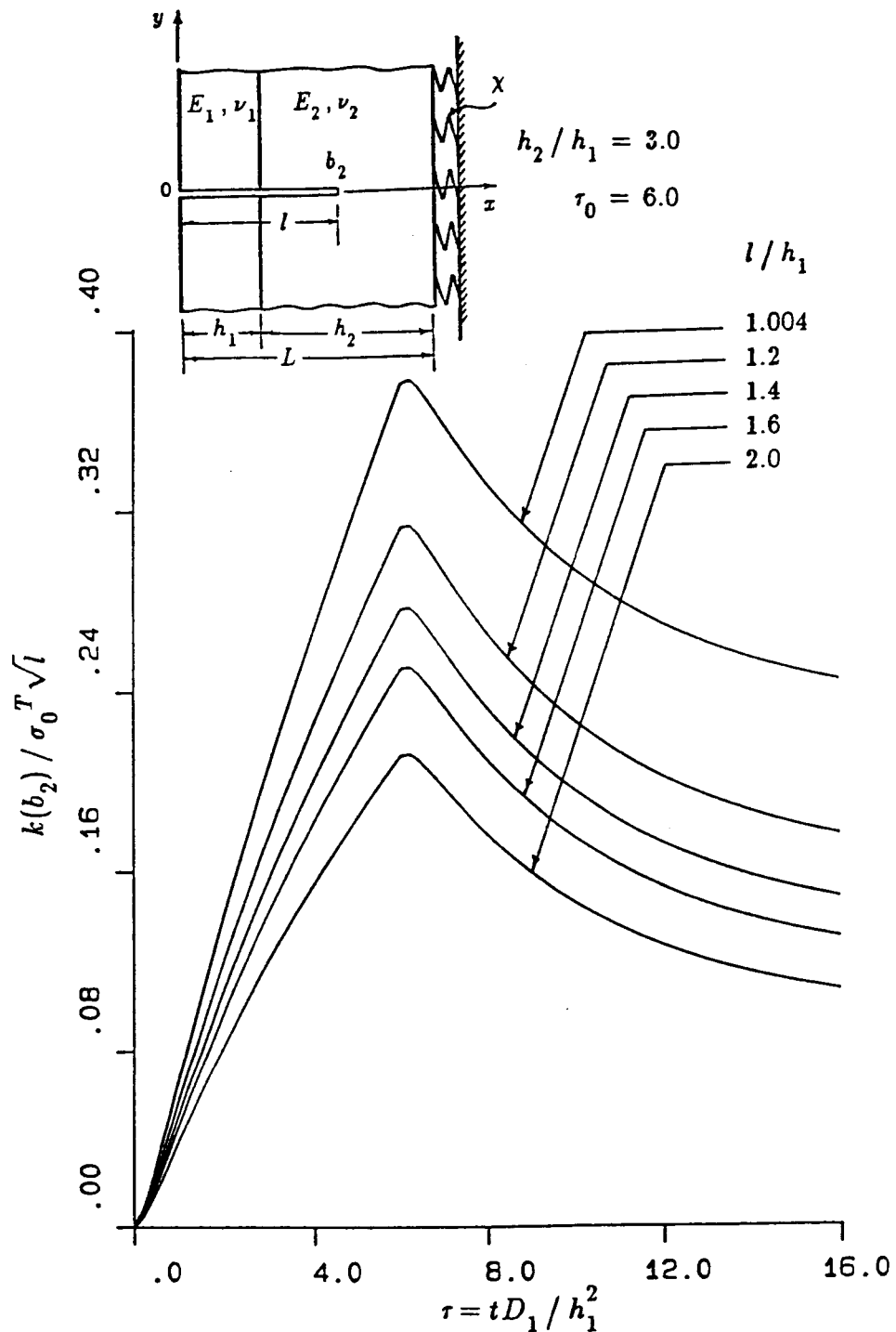


Figure 6-97: The normalized stress intensity factor $k(b_2)$ as a function of nondimensional time τ for an edge crack crossing the interface in Model II for $\tau_0=6.0$, $h_2/h_1=3.0$, $R_i/L=9.0$ and $\chi L/E_2=0.01108$, $\tau_0=t_0 D_1/h_1^2$, $\sigma_0^T = -\alpha_1' E_1 \Theta_0/(1-\nu_1)$ (material pair A)

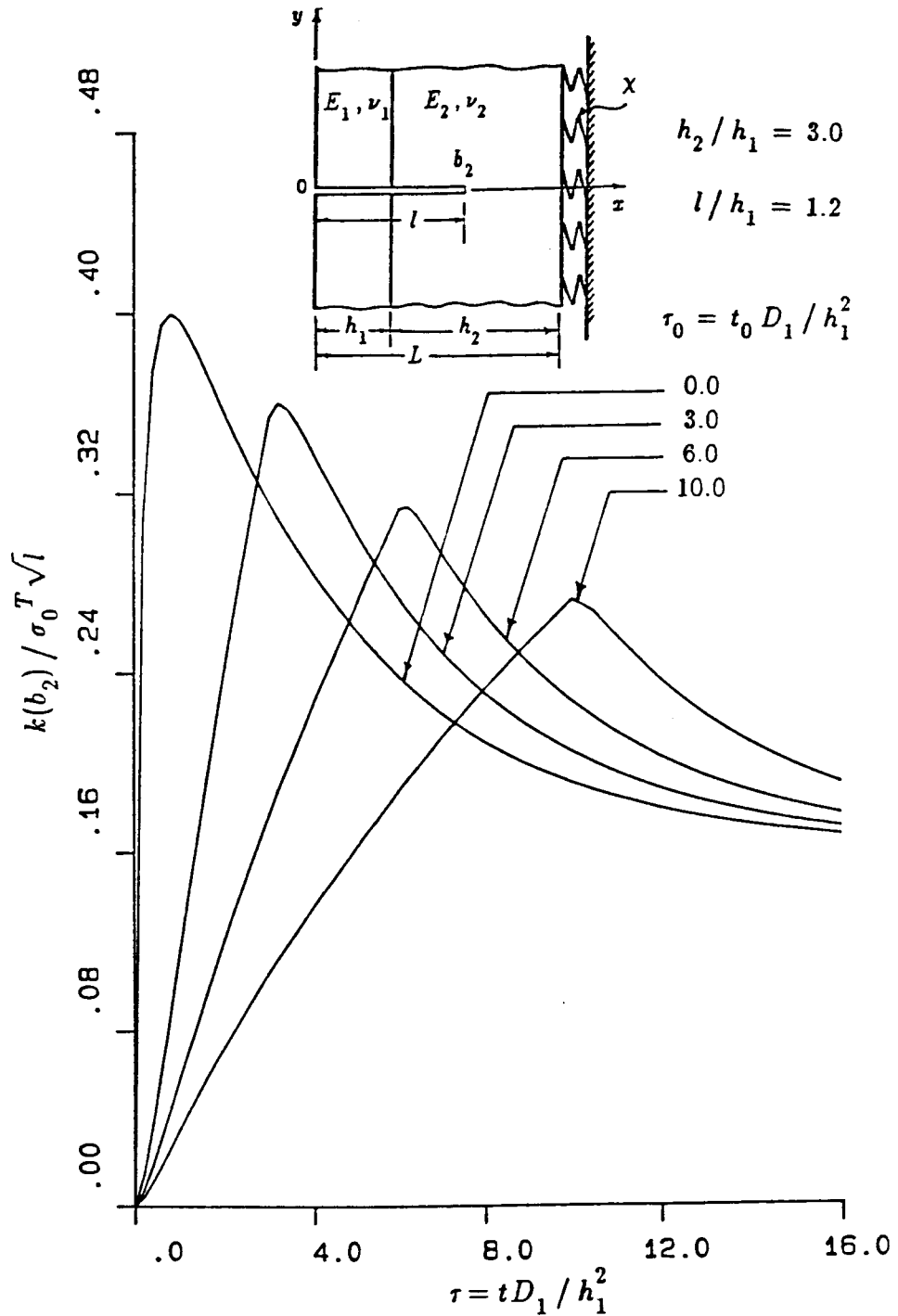


Figure 6-98: The influence of τ_0 on the normalized stress intensity factor $k(b_2)$ as a function of nondimensional time τ for an edge crack of length $l/h_1=1.2$ crossing the interface in Model II, $h_2/h_1=3.0$, $R_i/L=9.0$ and $\chi L/E_2=0.01108$, $\tau_0=t_0 D_1/h_1^2$, $\sigma_0^T = -\alpha_1 E_1 \Theta_0/(1-\nu_1)$ (material pair A)

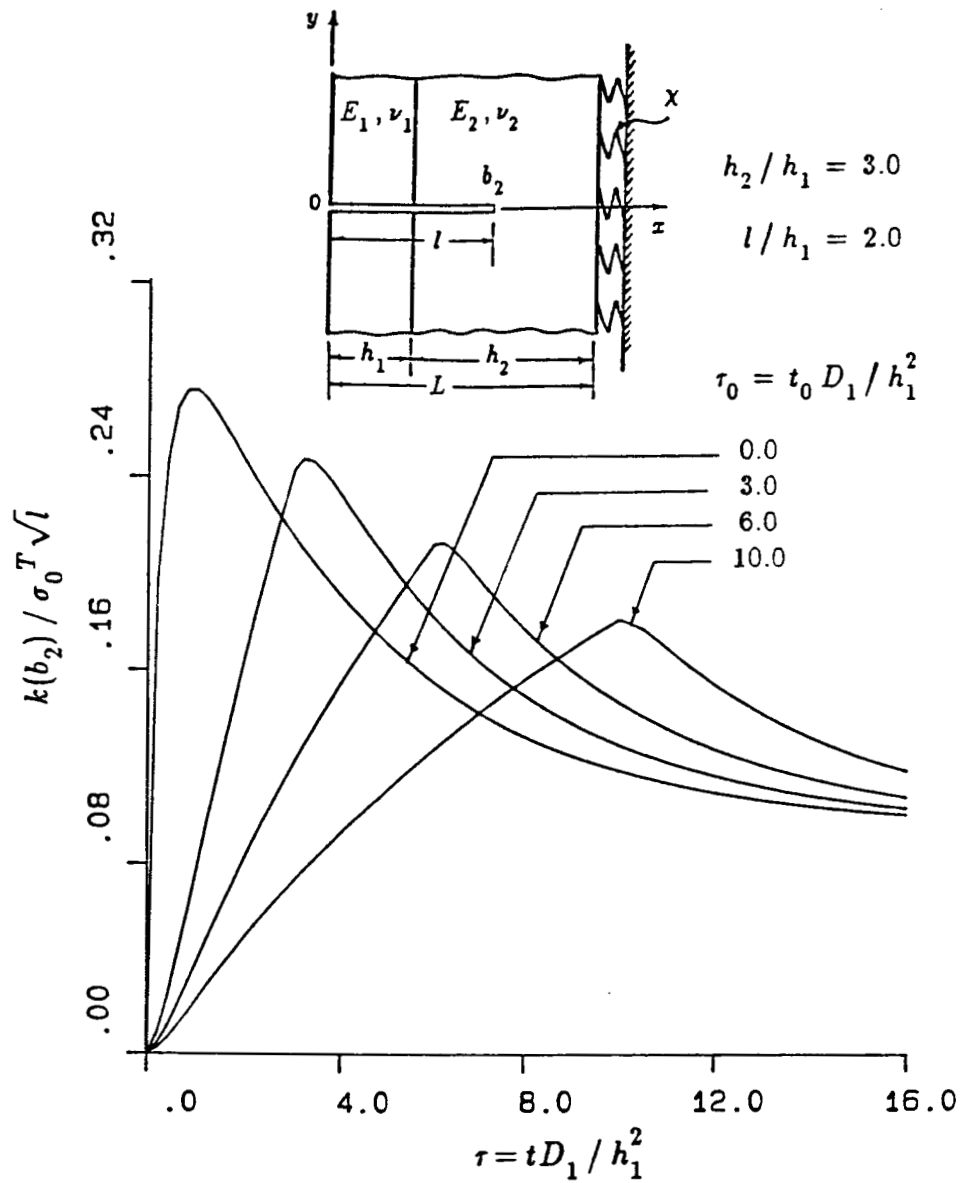


Figure 6-99: The influence of τ_0 on the normalized stress intensity factor $k(b_2)$ as a function of nondimensional time τ for an edge crack of length $l/h_1=2.0$ crossing the interface in Model II, $h_2/h_1=3.0$, $R_i/L=9.0$ and $\chi L/E_2=0.01108$, $\tau_0=t_0 D_1/h_1^2$, $\sigma_0^T = -\alpha'_1 E_1 \Theta_0/(1-\nu_1)$ (material pair A)

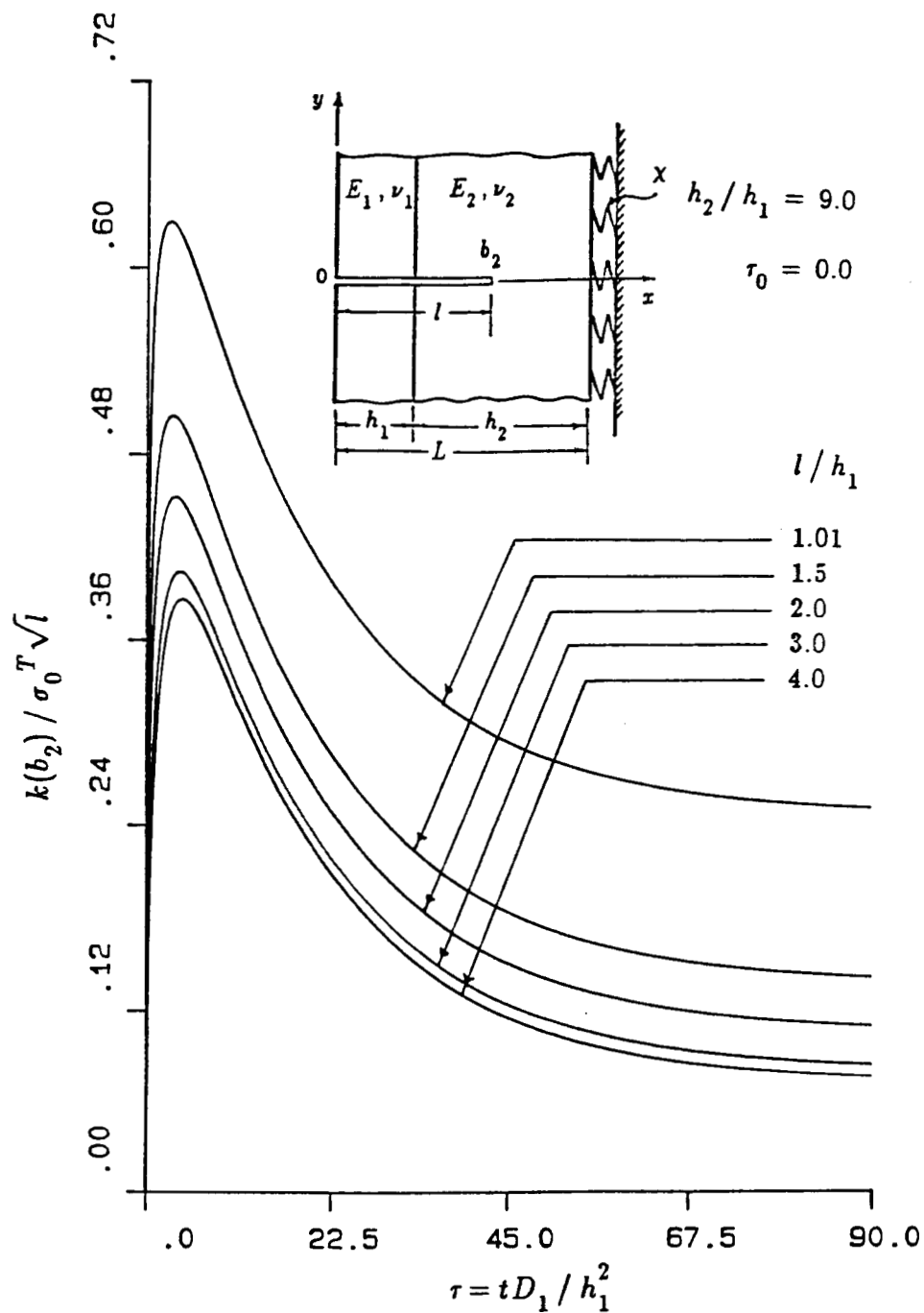


Figure 6-100: The normalized stress intensity factor $k(b_2)$ as a function of nondimensional time τ for an edge crack crossing the interface in Model II for $\tau_0=0.0$, $h_2/h_1=9.0$, $R_i/L=9.0$ and $\chi L/E_2=0.01108$, $\tau_0=t_0 D_1/h_1^2$, $\sigma_0^T = -\alpha_1' E_1 \Theta_0/(1-\nu_1)$ (material pair A)

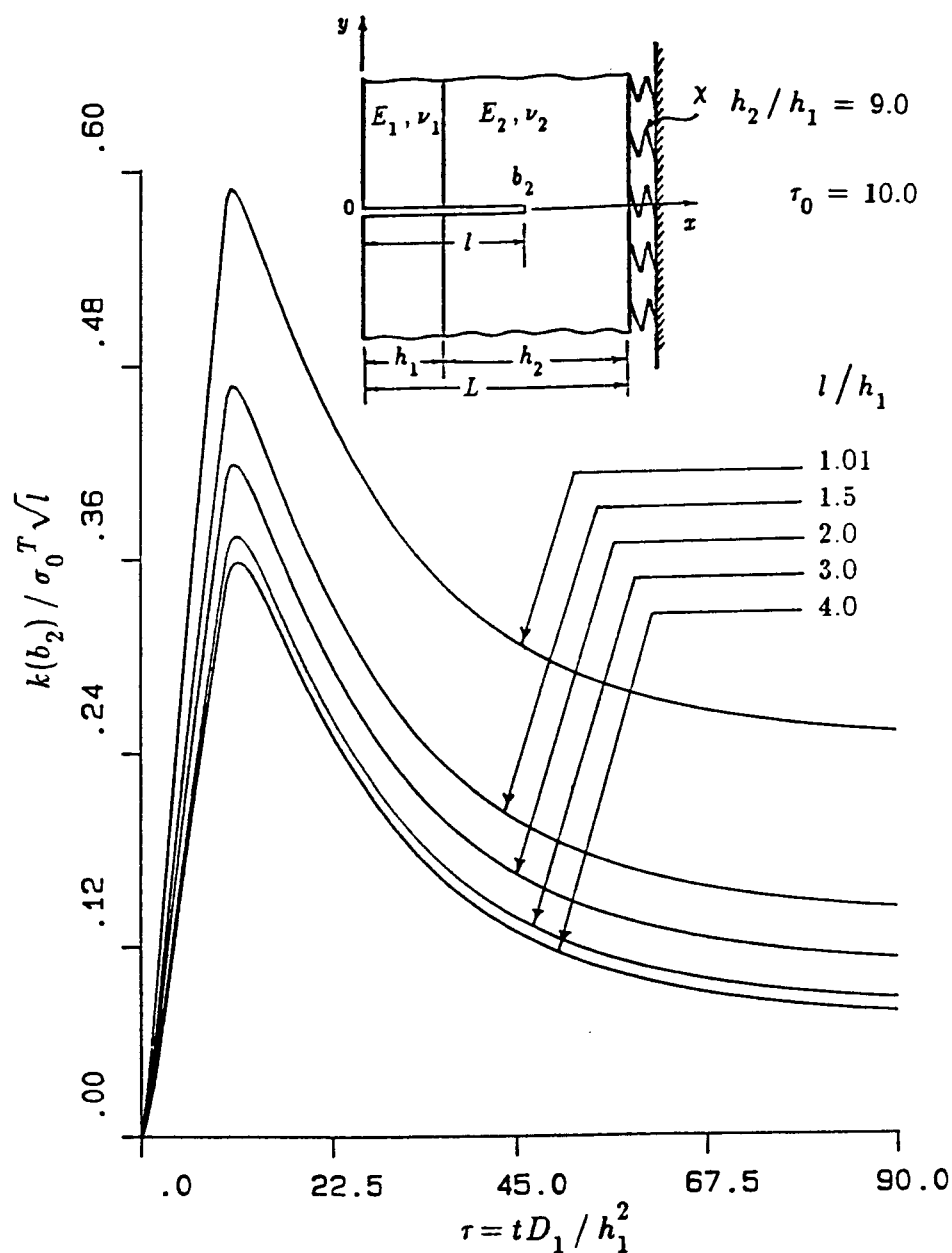


Figure 6-101: The normalized stress intensity factor $k(b_2)$ as a function of nondimensional time τ for an edge crack crossing the interface in Model II for $\tau_0=10.0$, $h_2/h_1=9.0$, $R_i/L=9.0$ and $\chi L/E_2=0.01108$, $\tau_0=t_0 D_1/h_1^2$, $\sigma_0^T = -\alpha'_1 E_1 \Theta_0/(1-\nu_1)$ (material pair A)

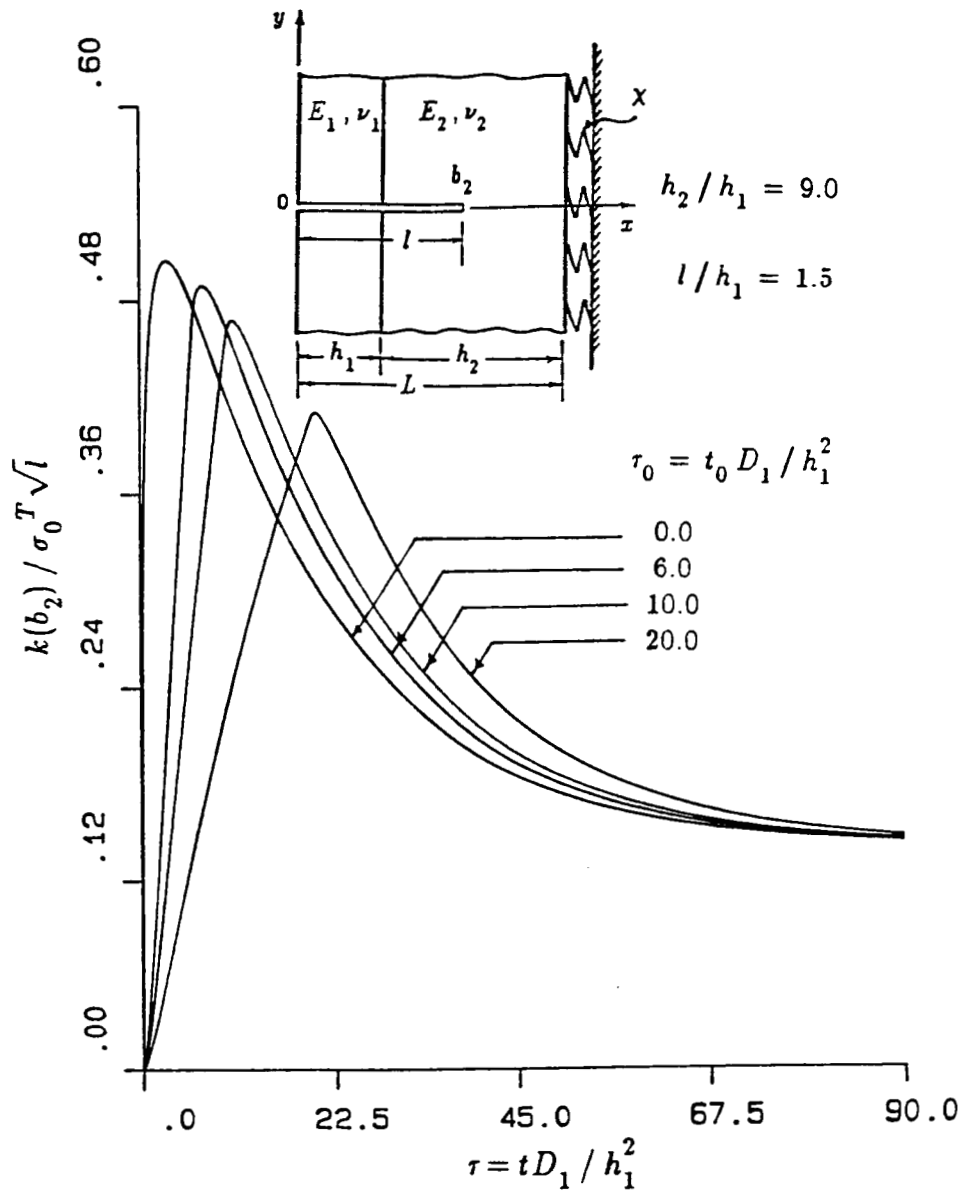


Figure 6-102: The influence of τ_0 on the normalized stress intensity factor $k(b_2)$ as a function of nondimensional time τ for an edge crack of length $l/h_1=1.5$ crossing the interface in Model II, $h_2/h_1=9.0$, $R_i/L=9.0$ and $\chi L/E_2=0.01108$, $\tau_0=t_0 D_1/h_1^2$, $\sigma_0^T = -\alpha'_1 E_1 \Theta_0/(1-\nu_1)$ (material pair A)

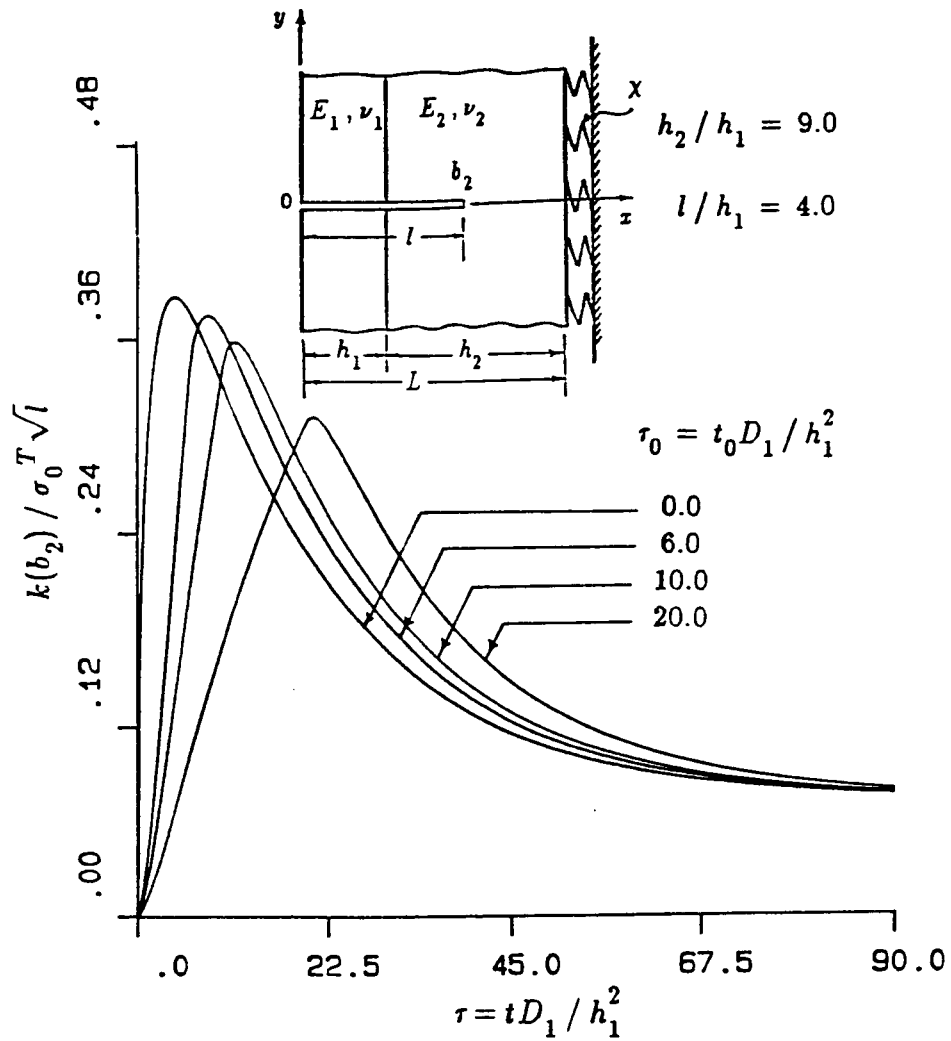


Figure 6-103: The influence of τ_0 on the normalized stress intensity factor $k(b_2)$ as a function of nondimensional time τ for an edge crack of length $l/h_1=4.0$ crossing the interface in Model II, $h_2/h_1=9.0$, $R_i/L=9.0$ and $\chi L/E_2=0.01108$, $\tau_0=t_0 D_1/h_1^2$, $\sigma_0^T=-\alpha_1' E_1 \Theta_0/(1-\nu_1)$ (material pair A)

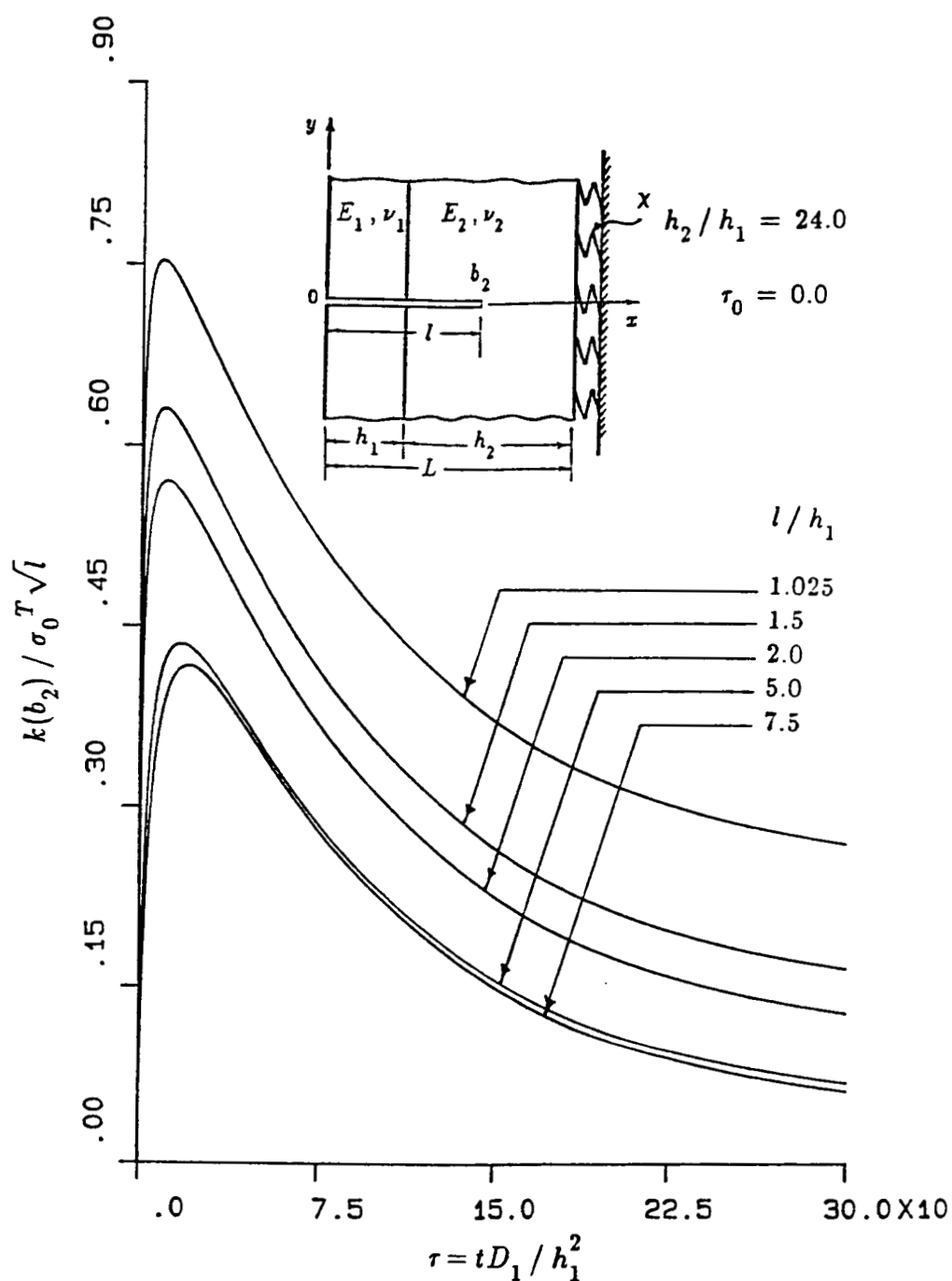


Figure 6-104: The normalized stress intensity factor $k(b_2)$ as a function of nondimensional time τ for an edge crack crossing the interface in Model II for $\tau_0=0.0$, $h_2/h_1=24.0$, $R_i/L=9.0$ and $\chi L/E_2=0.01108$, $\tau_0=t_0 D_1/h_1^2$, $\sigma_0^T=-\alpha_1 E_1 \Theta_0/(1-\nu_1)$ (material pair A)

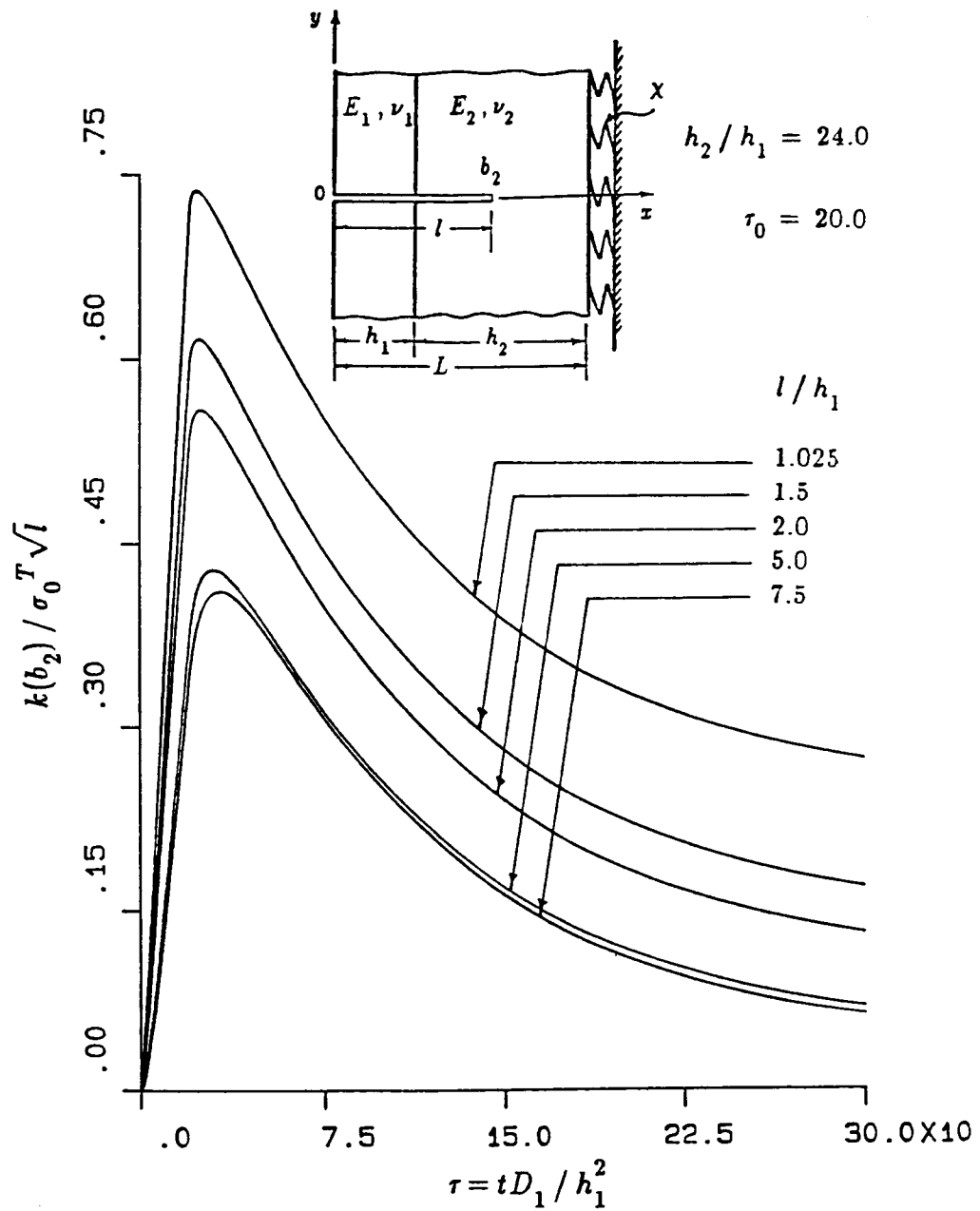


Figure 6-105: The normalized stress intensity factor $k(b_2)$ as a function of nondimensional time τ for an edge crack crossing the interface in Model II for $\tau_0=20.0$, $h_2/h_1=24.0$, $R_i/L=9.0$ and $\chi L/E_2=0.01108$, $\tau_0=t_0 D_1/h_1^2$, $\sigma_0^T=-\alpha_1^* E_1 \Theta_0/(1-\nu_1)$ (material pair A)

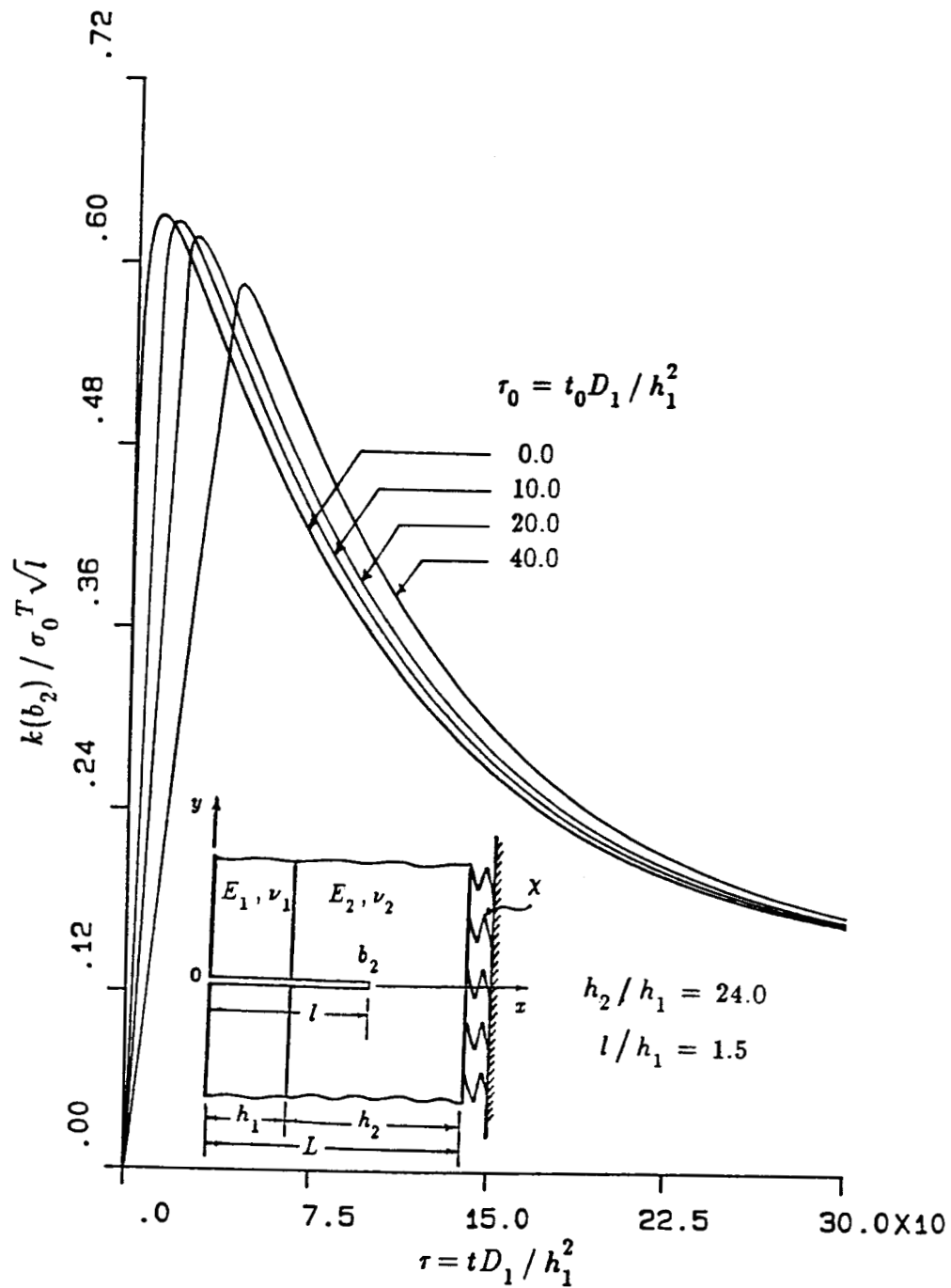


Figure 6-106: The influence of τ_0 on the normalized stress intensity factor $k(b_2)$ as a function of nondimensional time τ for an edge crack of length $l/h_1=1.5$ crossing the interface in Model II, $h_2/h_1=24.0$, $R_i/L=9.0$ and $\chi L/E_2=0.01108$, $\tau_0=t_0 D_1/h_1^2$, $\sigma_0^T=-\alpha_1' E_1 \Theta_0/(1-\nu_1)$ (material pair A)

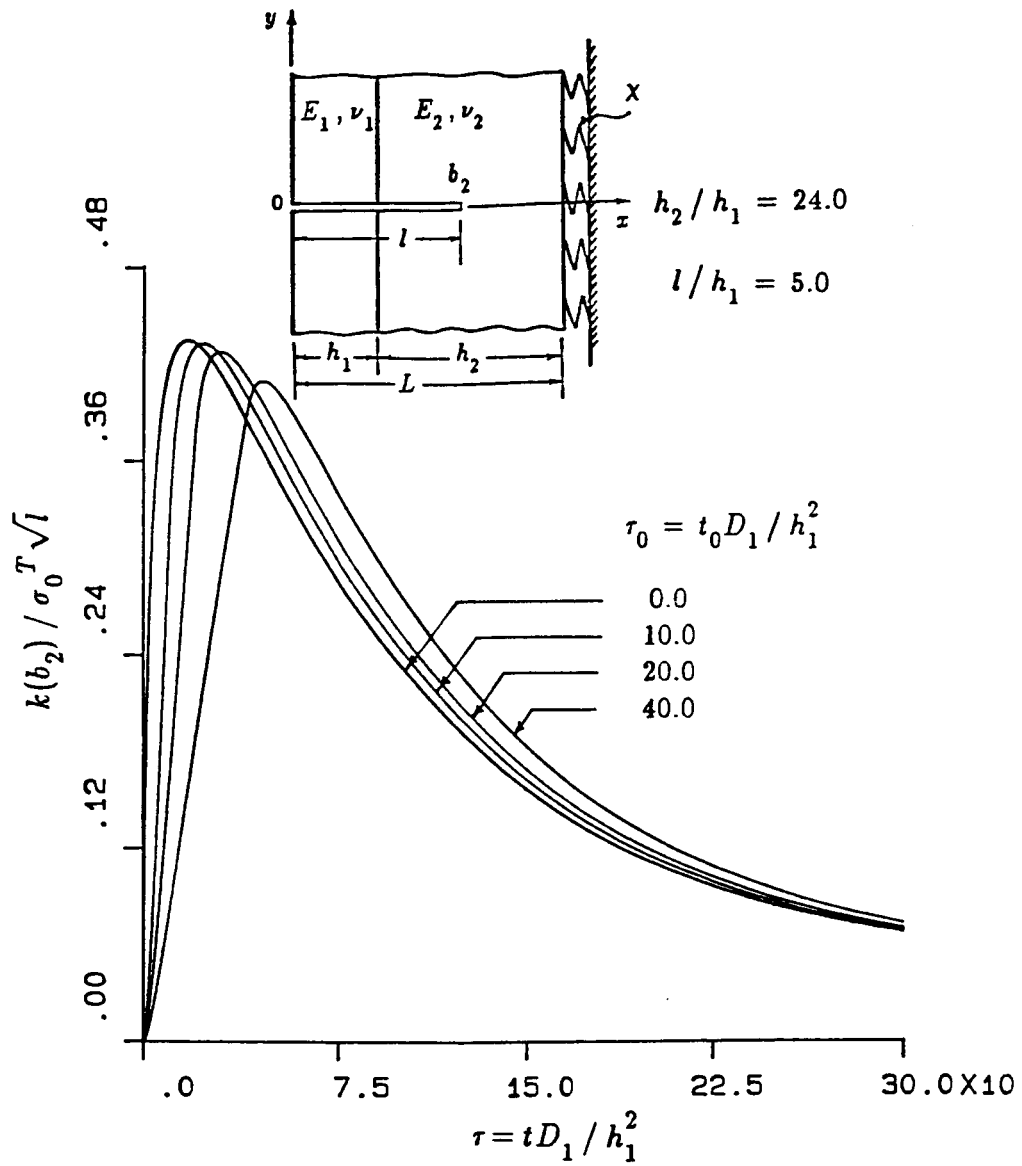


Figure 6-107: The influence of τ_0 on the normalized stress intensity factor $k(b_2)$ as a function of nondimensional time τ for an edge crack of length $l/h_1=5.0$ crossing the interface in Model II, $h_2/h_1=24.0$, $R_i/L=9.0$ and $\chi L/E_2=0.01108$, $\tau_0=t_0 D_1/h_1^2$, $\sigma_0^T=-\alpha_1 E_1 \Theta_0/(1-\nu_1)$ (material pair A)

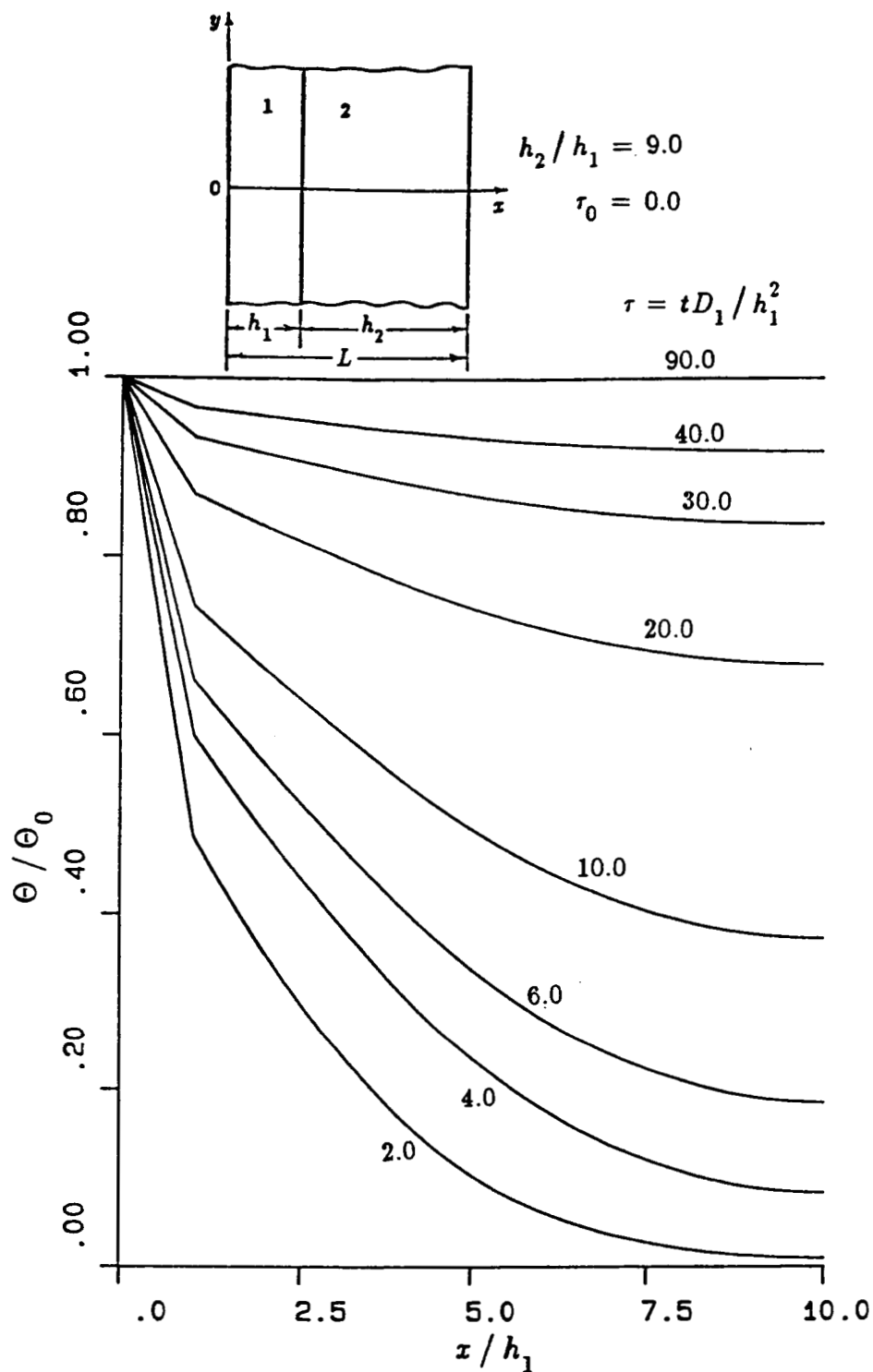


Figure 6-108: The normalized transient temperature distribution in Model II for $\tau_0=0.0$, $h_2/h_1=9.0$, $\tau_0=t_0D_1/h_1^2$, (material pair B)

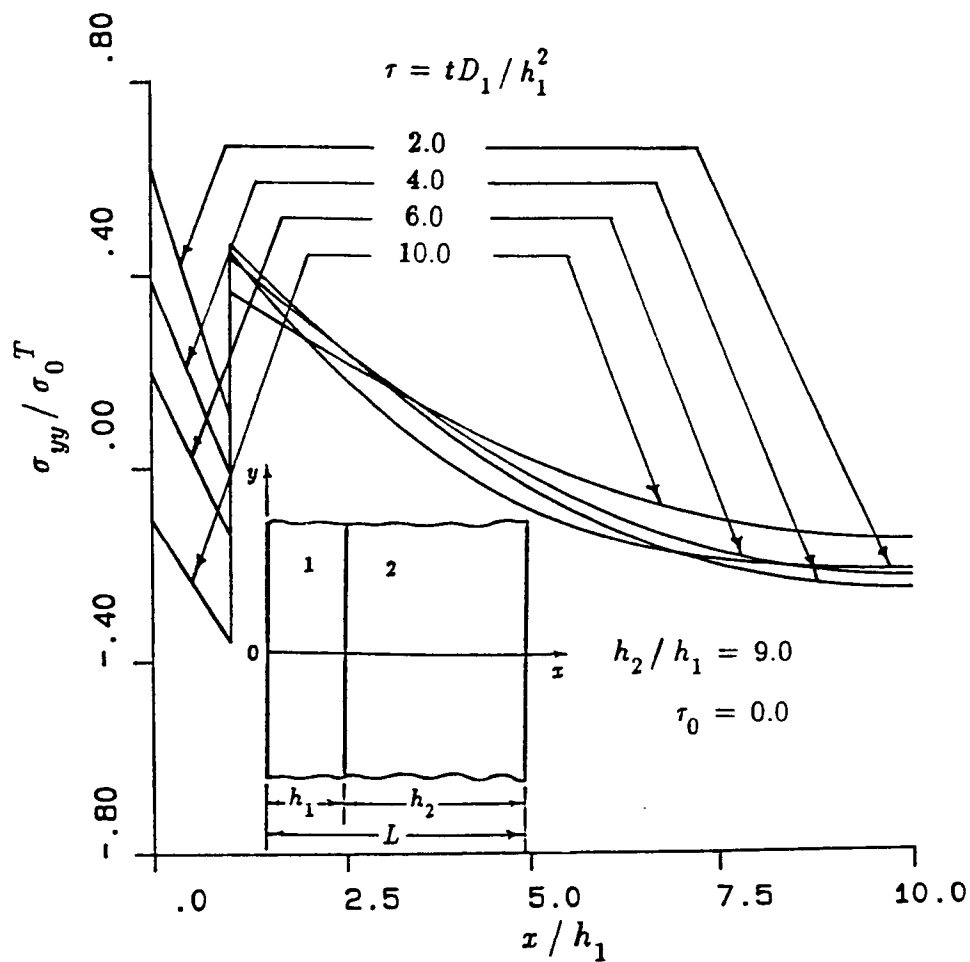


Figure 6-109: The normalized transient stress distribution σ_{yy}/σ_0^T in Model II for $\tau_0=0.0$, $h_2/h_1=9.0$, $\tau_0=t_0D_1/h_1^2$, $\sigma_0^T=-\alpha_1' E_1 \Theta_0/(1-\nu_1)$. (material pair B)

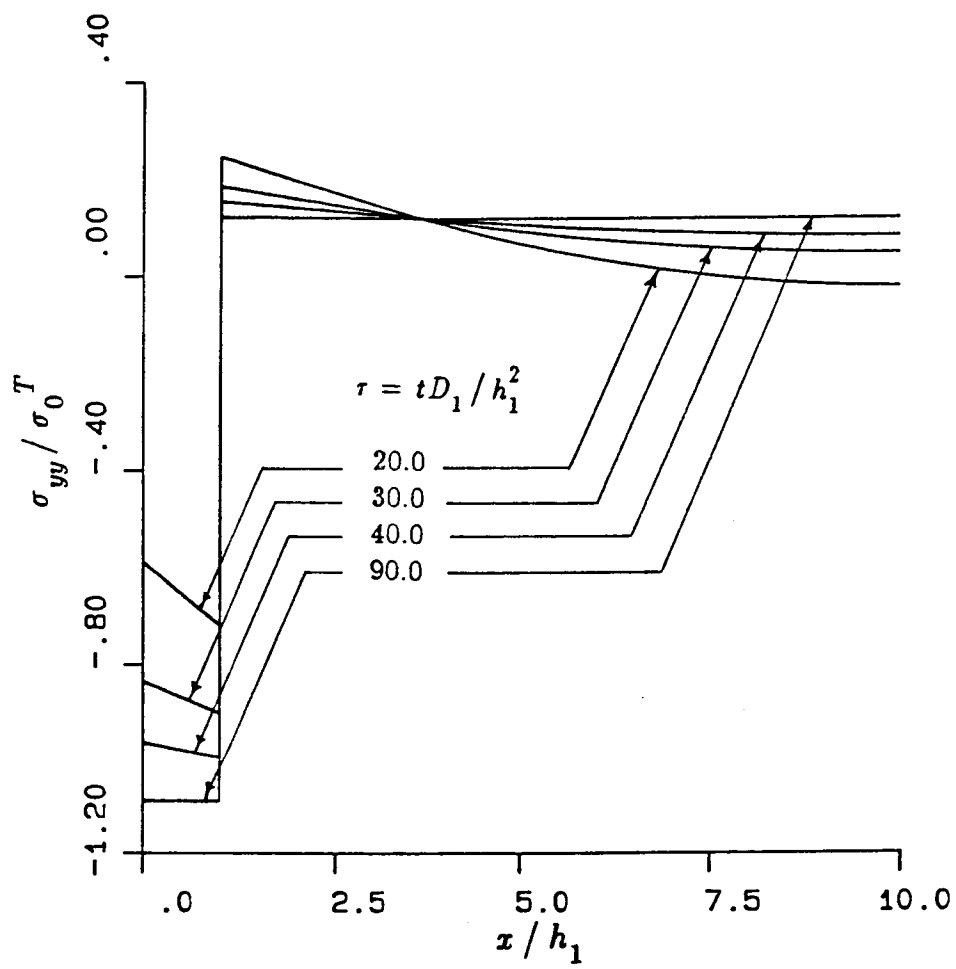


Figure 6-109, continued

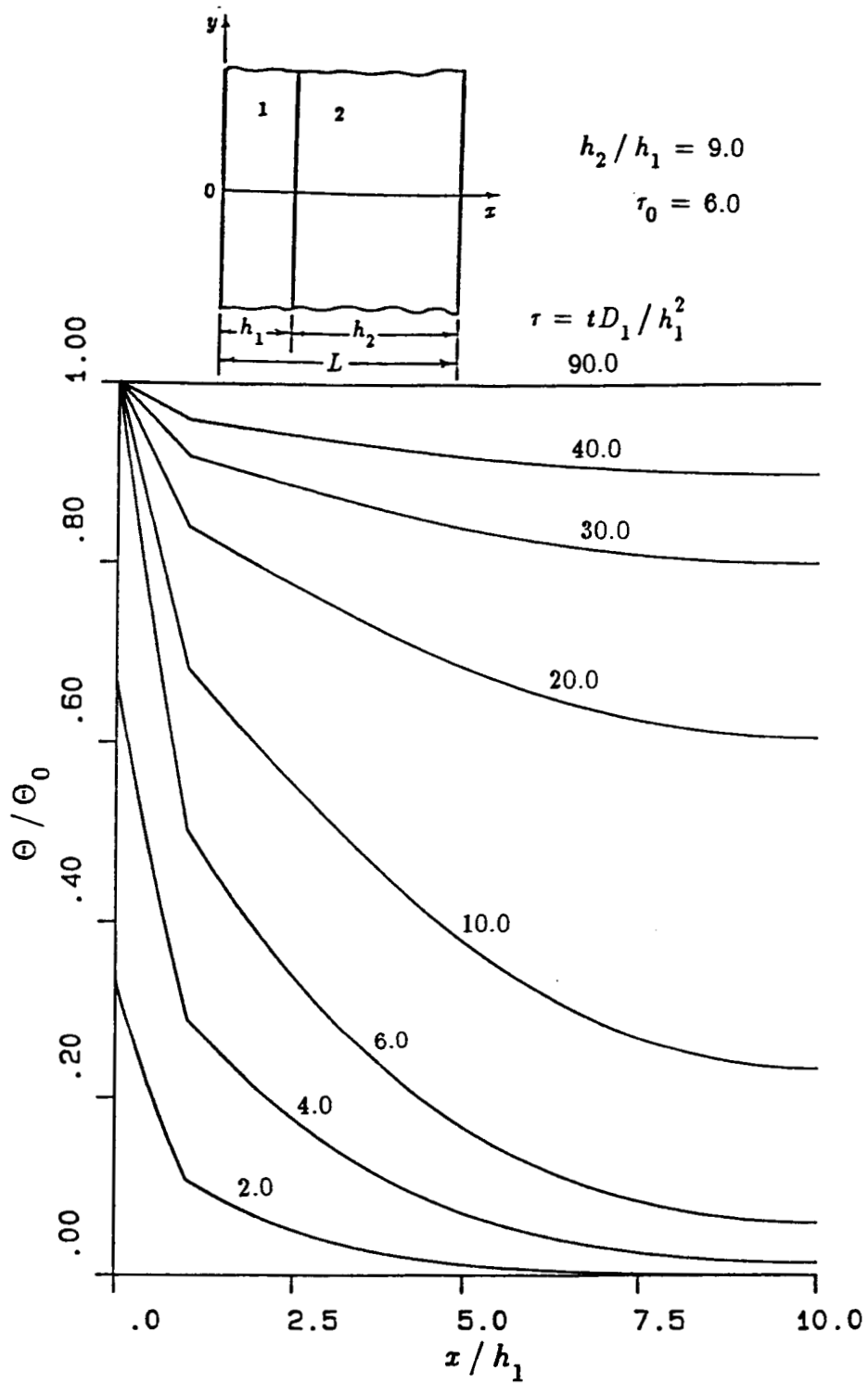


Figure 6-110: The normalized transient temperature distribution in Model II for $\tau_0=6.0$, $h_2/h_1=9.0$, $\tau_0=t_0D_1/h_1^2$, (material pair B)

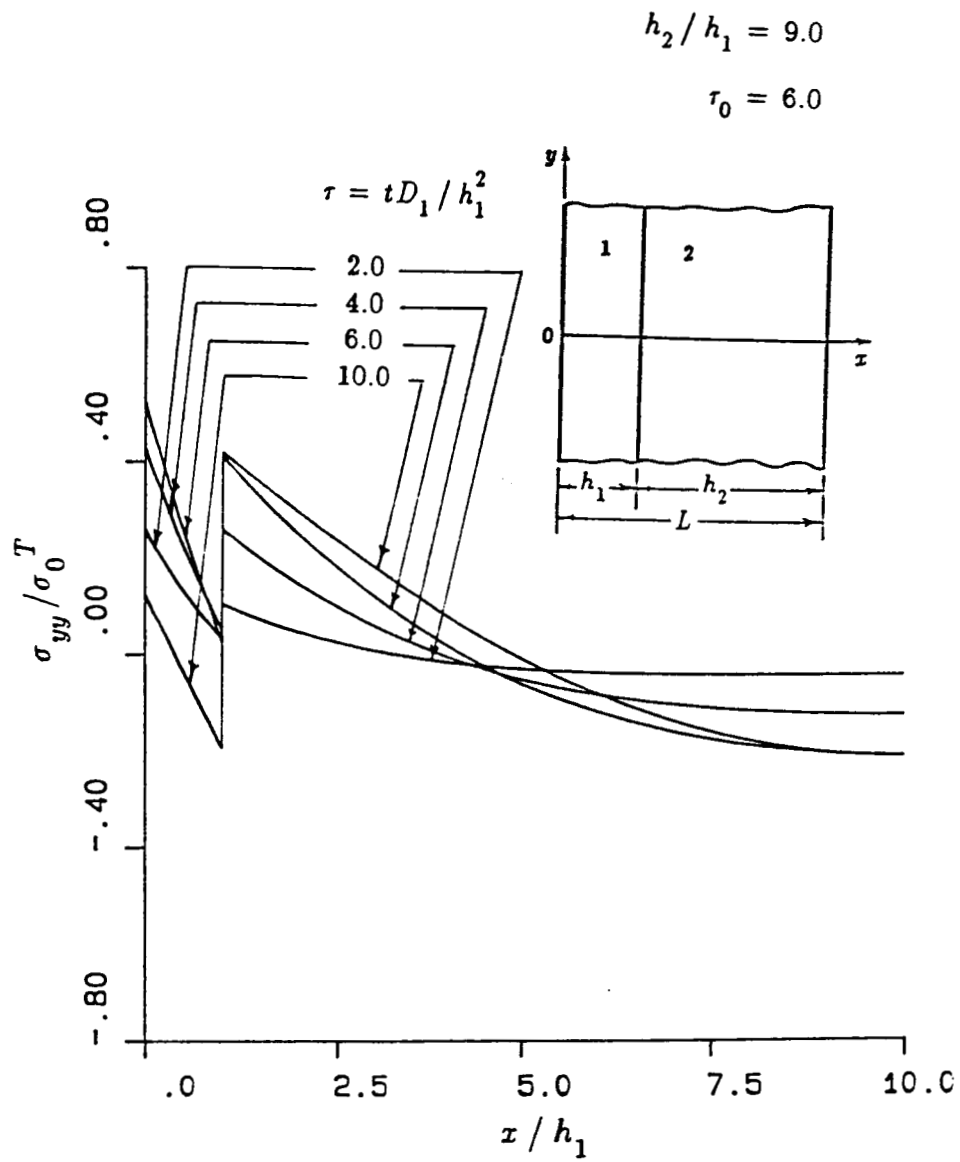


Figure 6-111: The normalized transient stress distribution σ_{yy}/σ_0^T in Model II for $\tau_0=6.0$, $h_2/h_1=9.0$, $\tau_0=t_0D_1/h_1^2$, $\sigma_0^T=-\alpha_1 E_1 \Theta_0/(1-\nu_1)$. (material pair B)

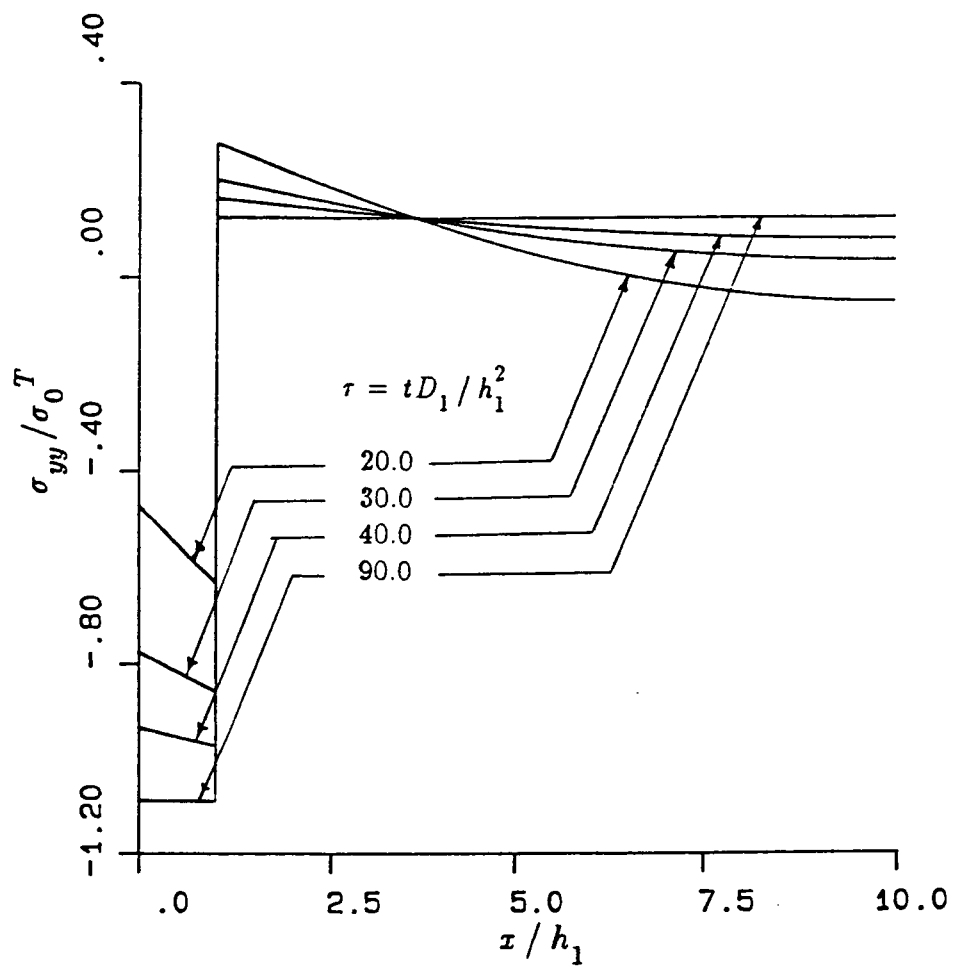


Figure 6-111, continued

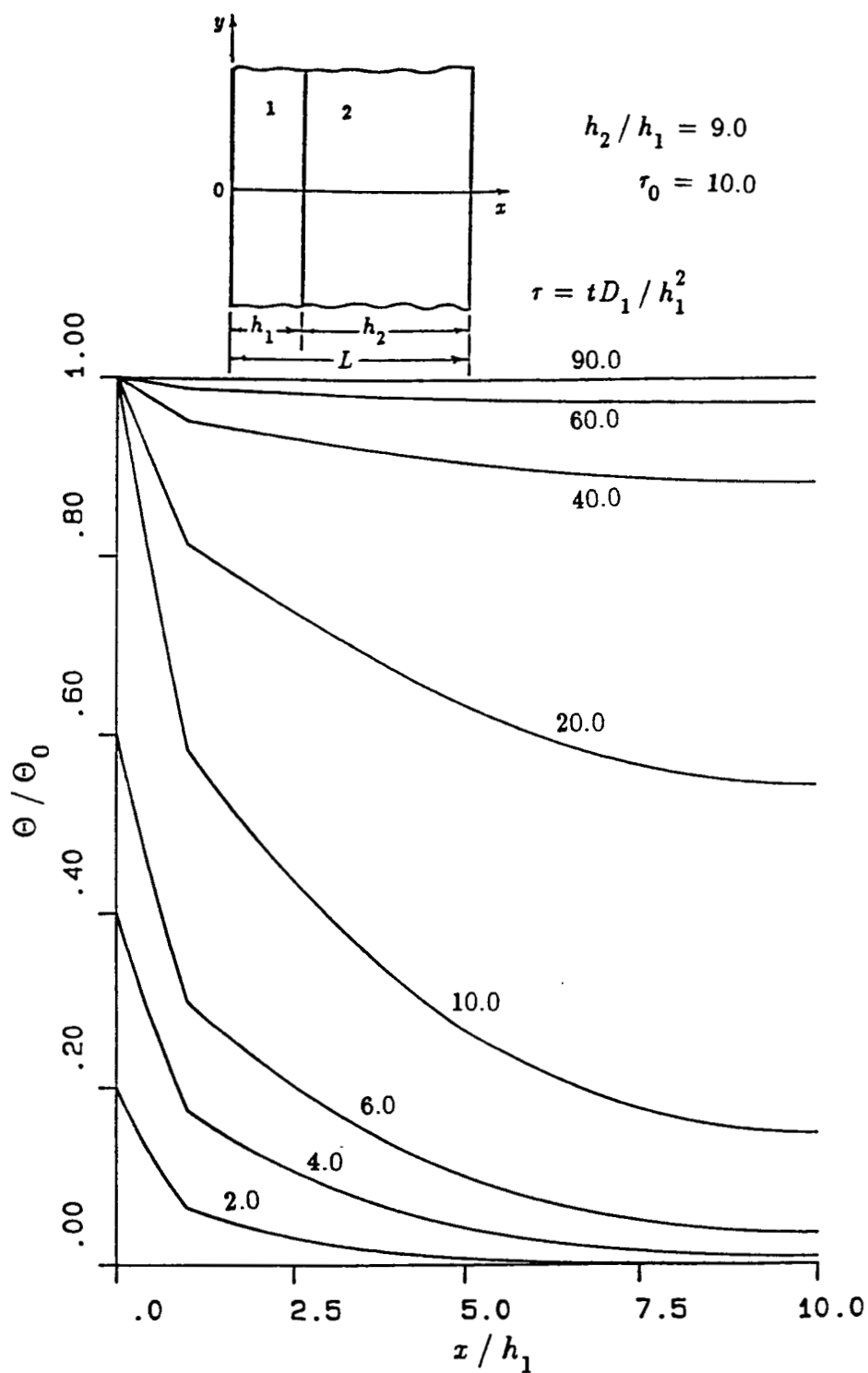


Figure 6-112: The normalized transient temperature distribution in Model II
for $\tau_0 = 10.0$, $h_2 / h_1 = 9.0$, $\tau_0 = t_0 D_1 / h_1^2$, (material pair B)

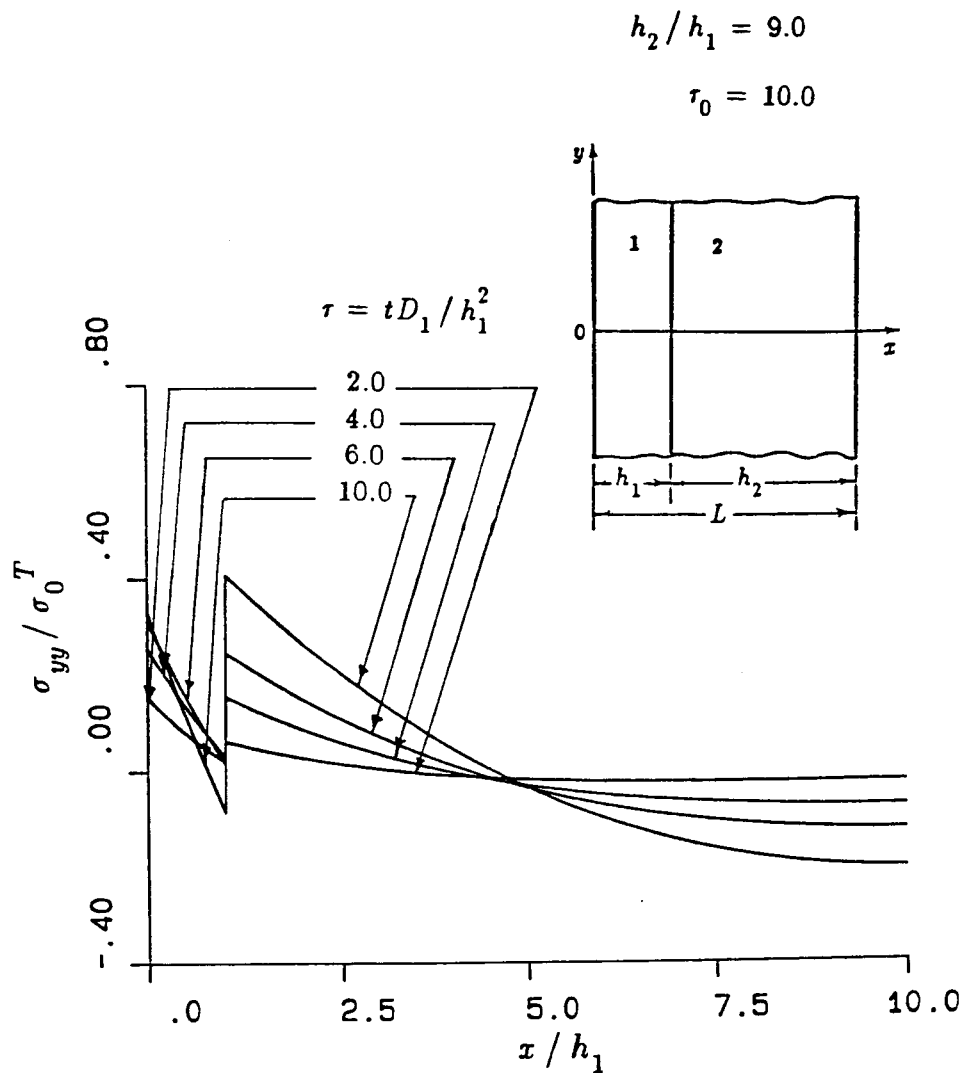


Figure 6-113: The normalized transient stress distribution σ_{yy}/σ_0^T in Model II for $\tau_0=10.0$, $h_2/h_1=9.0$, $\tau_0=t_0D_1/h_1^2$, $\sigma_0^T=-\alpha_1' E_1 \Theta_0/(1-\nu_1)$. (material pair B)

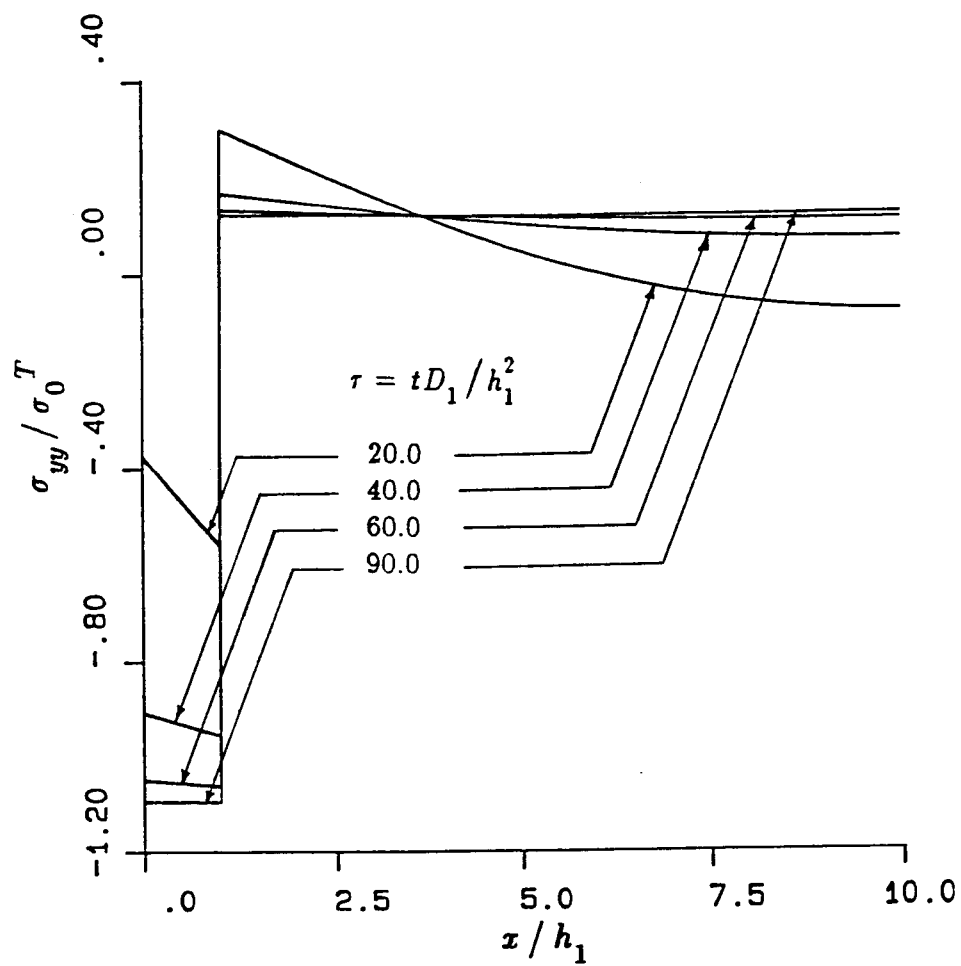


Figure 6-113, continued

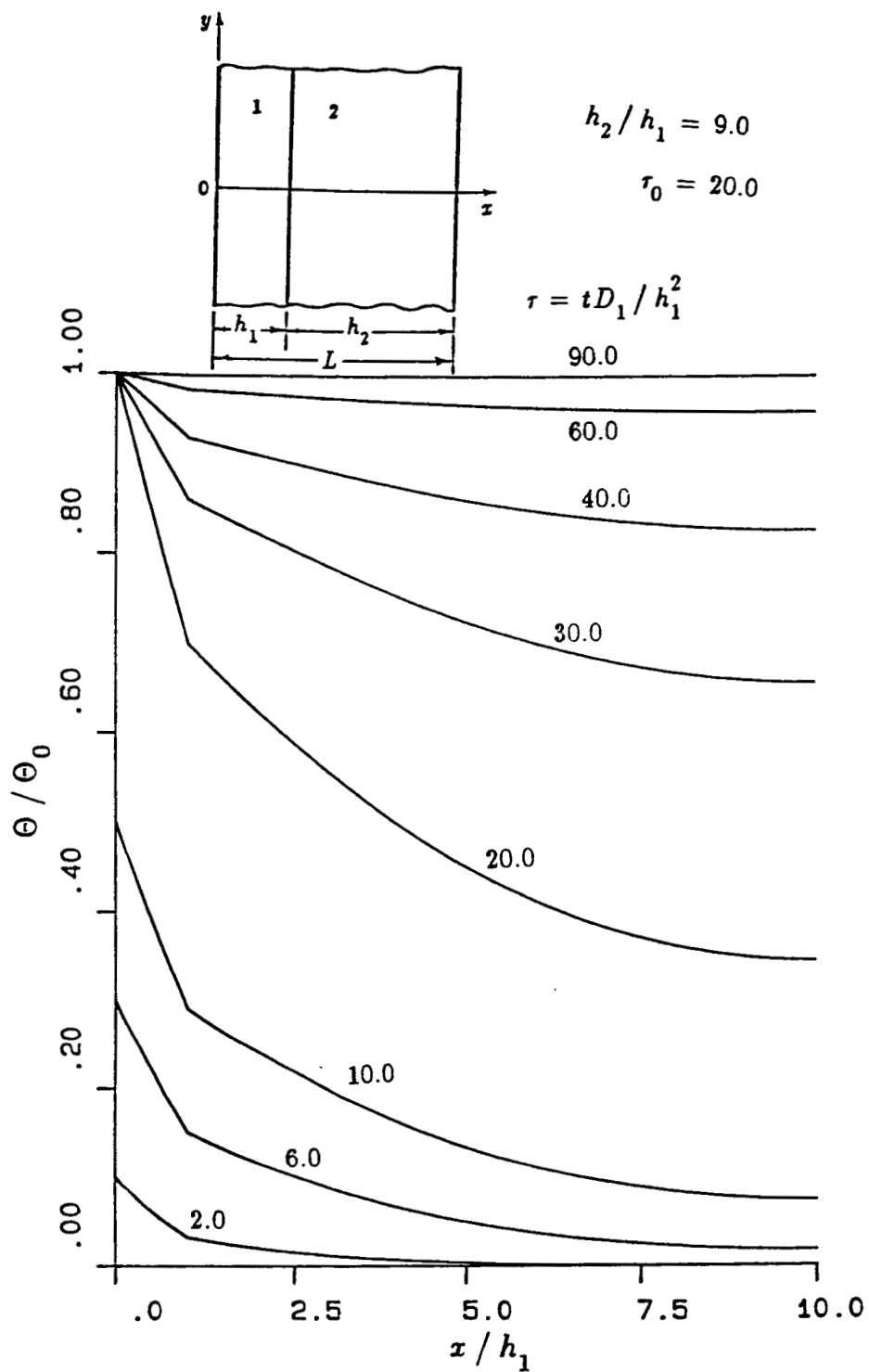


Figure 6-114: The normalized transient temperature distribution in Model II for $\tau_0=20.0$, $h_2/h_1=9.0$, $\tau_0=t_0D_1/h_1^2$, (material pair B)

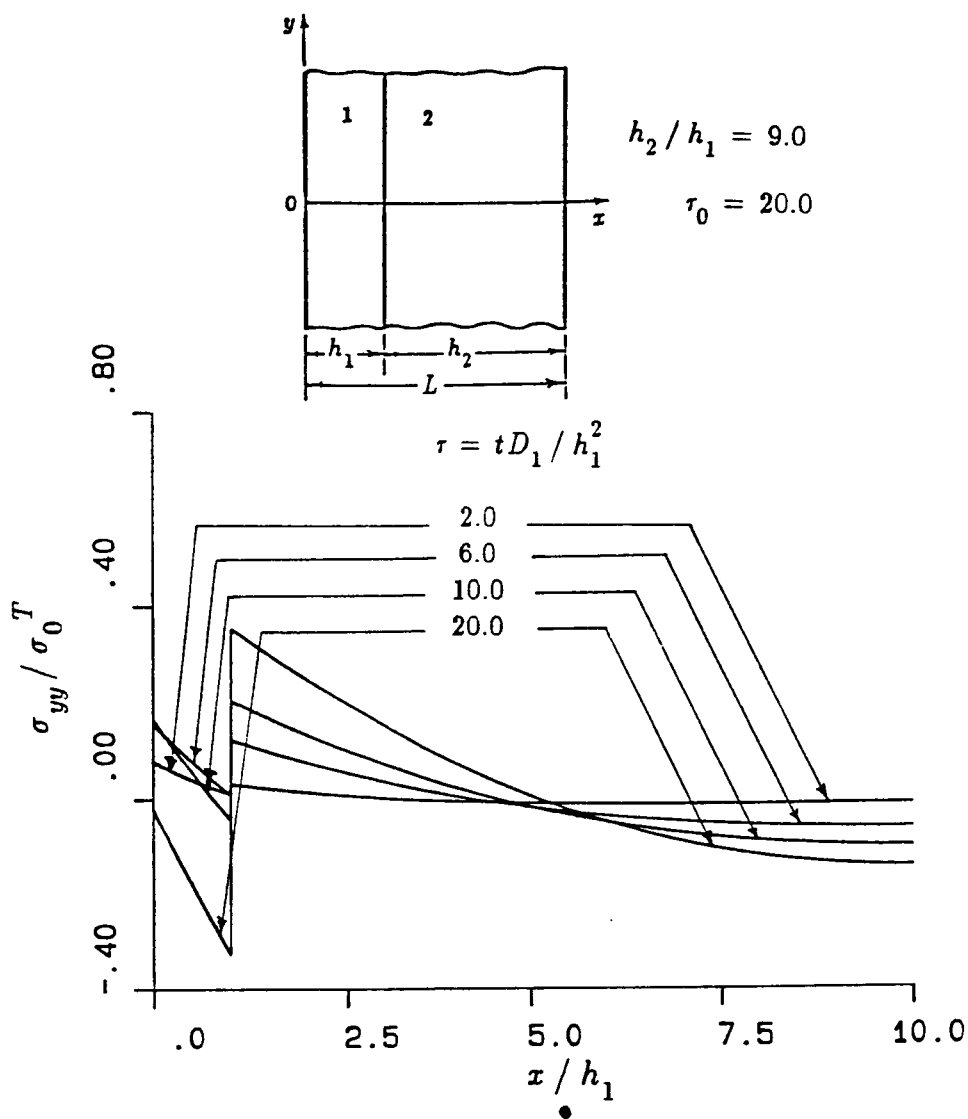


Figure 6-115: The normalized transient stress distribution σ_{yy}/σ_0^T in Model II for $\tau_0=20.0$, $h_2/h_1=9.0$, $\tau_0=t_0D_1/h_1^2$, $\sigma_0^T=-\alpha_1' E_1 \Theta_0/(1-\nu_1)$. (material pair B)

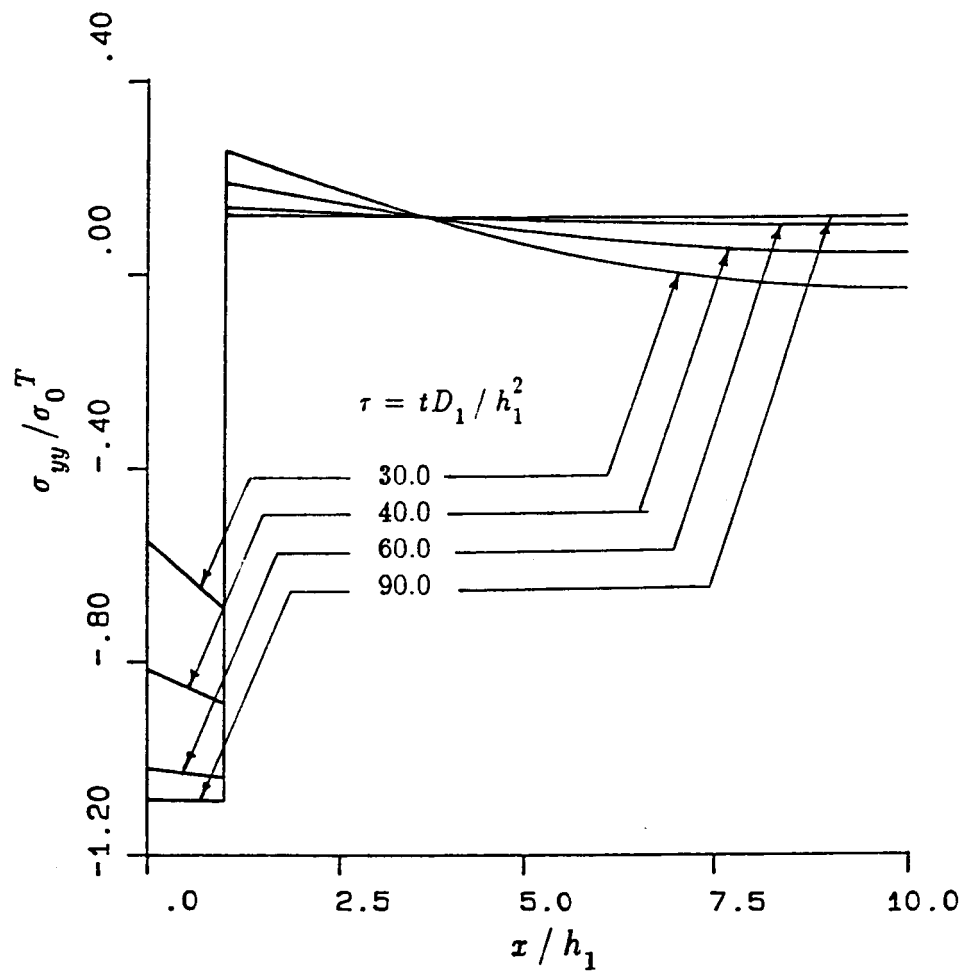


Figure 6-115, continued

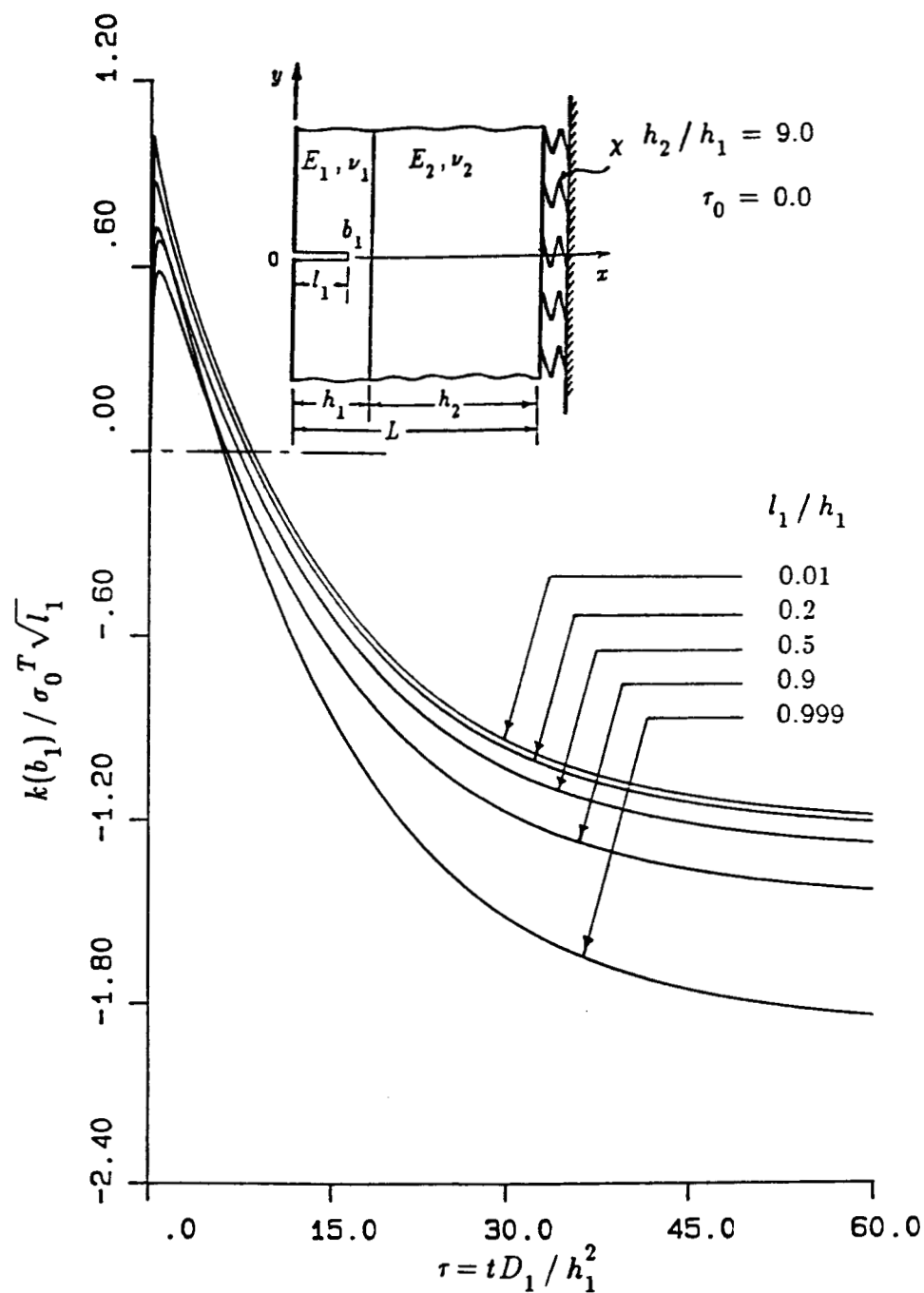


Figure 6-116: The normalized stress intensity factor $k(b_1)$ as a function of nondimensional time τ for an edge crack in Model II for $\tau_0=0.0$, $h_2/h_1=9.0$, $R_i/L=9.0$ and $\chi L/E_2=0.01185$, $\tau_0=t_0 D_1/h_1^2$, $\sigma_0^T = -\alpha_1' E_1 \Theta_0 / (1-\nu_1)$ (material pair B)

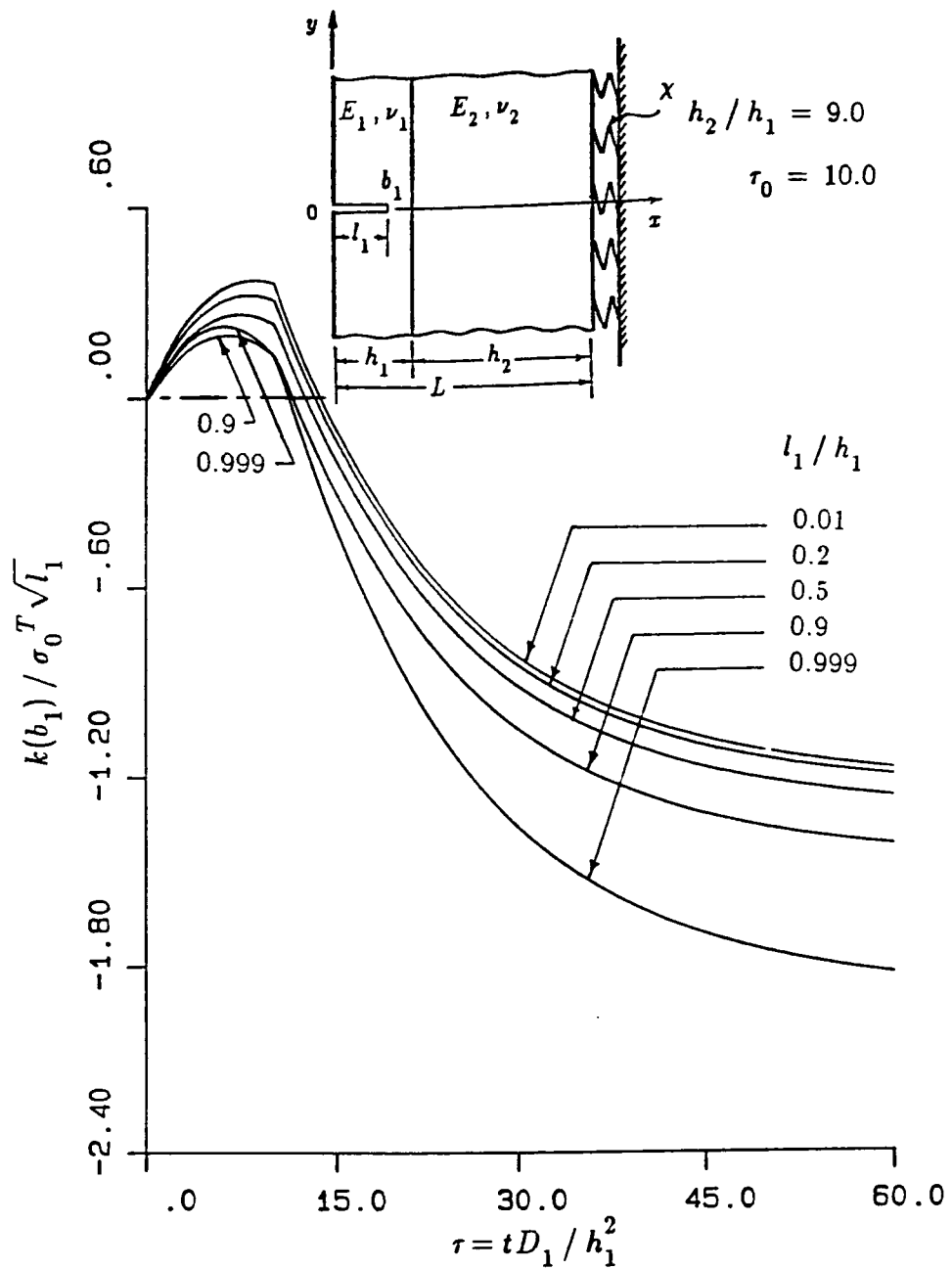


Figure 6-117: The normalized stress intensity factor $k(b_1)$ as a function of nondimensional time τ for an edge crack in Model II for $\tau_0=10.0$, $h_2/h_1=9.0$, $R_i/L=9.0$ and $\chi L/E_2=0.01185$, $\tau_0=t_0 D_1/h_1^2$, $\sigma_0^T = -\alpha'_1 E_1 \Theta_0/(1-\nu_1)$ (material pair B)

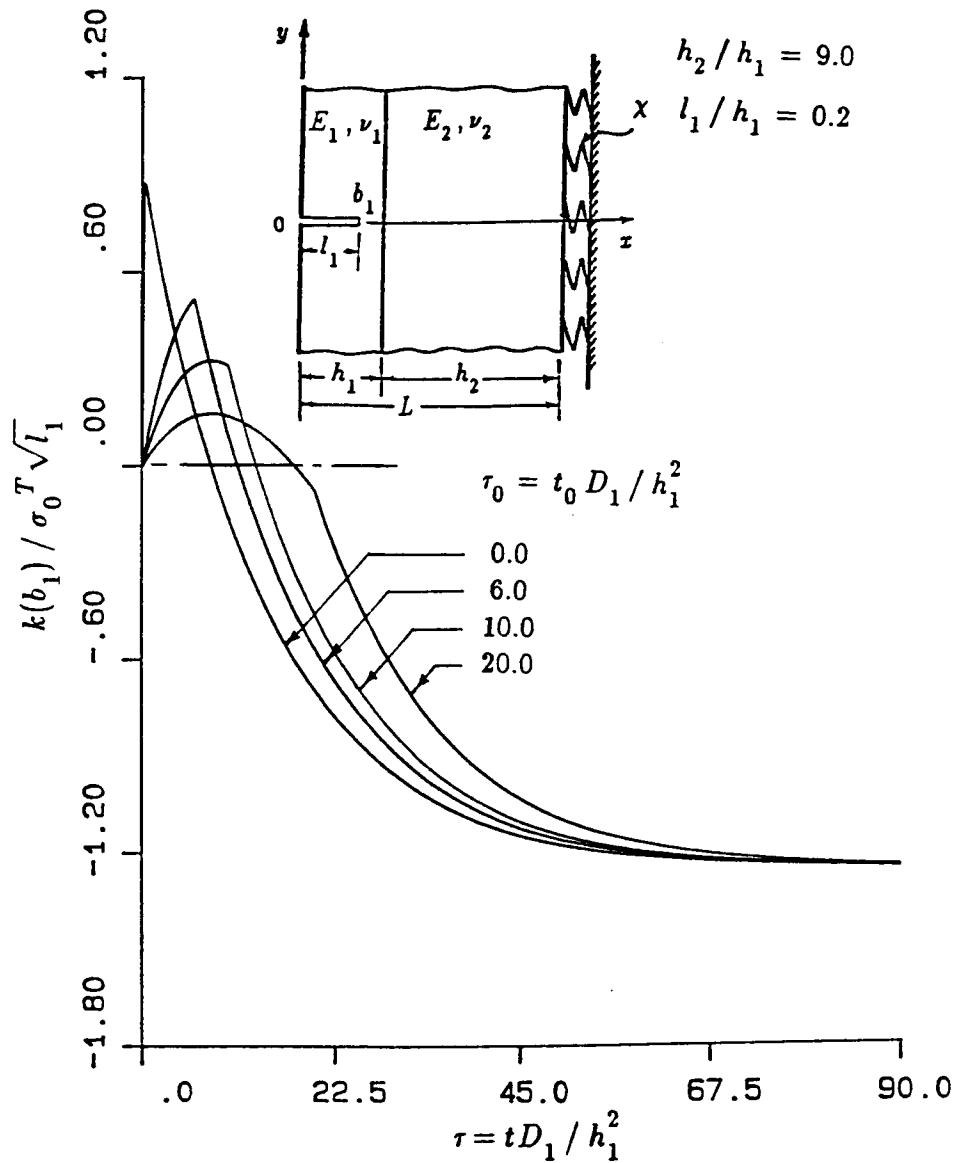


Figure 6-118: The influence of τ_0 on the normalized stress intensity factor $k(b_1)$ as a function of nondimensional time τ for an edge crack of length $l_1/h_1=0.2$ in Model II, $h_2/h_1=9.0$, $R_i/L=9.0$ and $\chi L/E_2=0.01185$, $\tau_0=t_0 D_1/h_1^2$, $\sigma_0^T=-\alpha_1' E_1 \Theta_0/(1-\nu_1)$ (material pair B)

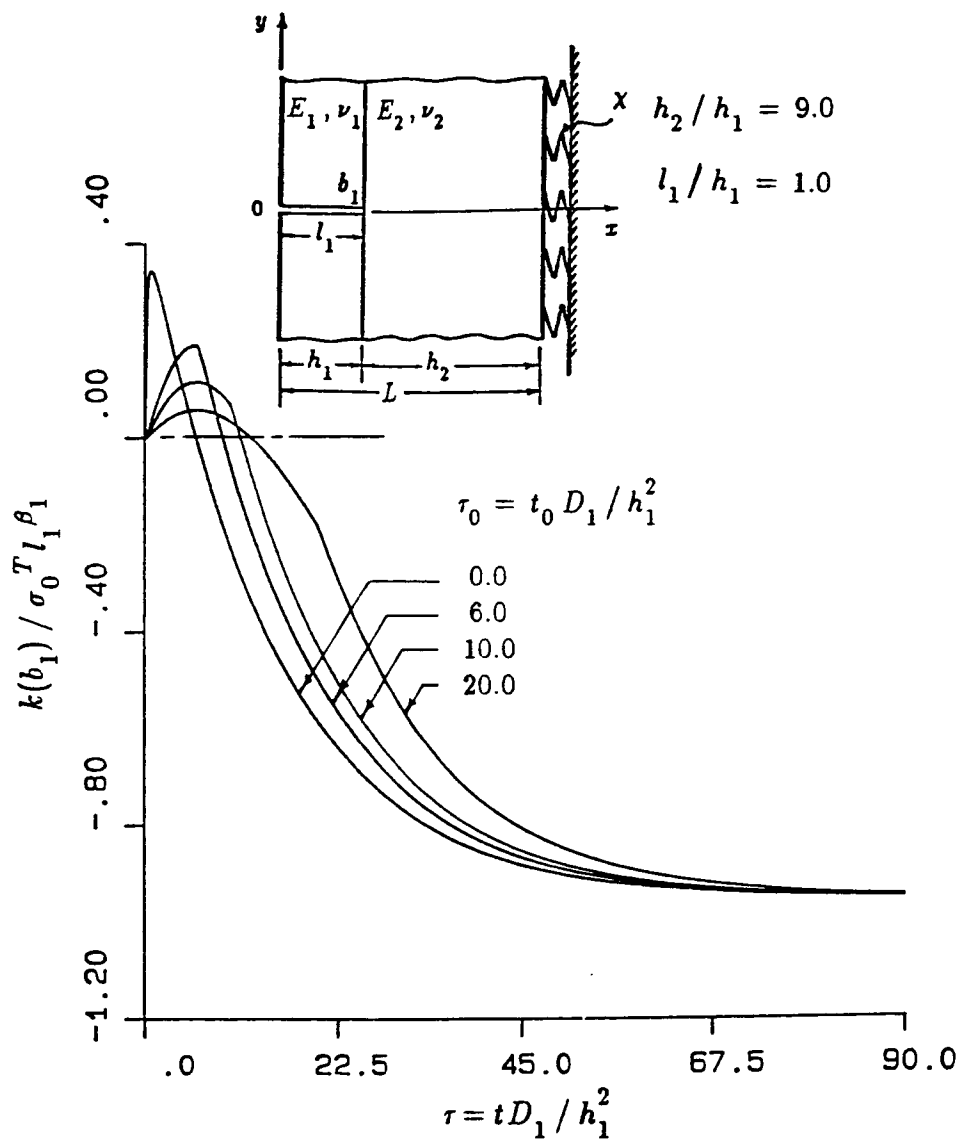


Figure 6-119: The influence of τ_0 on the normalized stress intensity factor $k(b_1)$ as a function of nondimensional time τ for a broken clad in Model II for $\beta_1=0.552538$, $h_2/h_1=9.0$, $R_i/L=9.0$ and $\chi L/E_2=0.01185$, $\tau_0=t_0 D_1/h_1^2$, $\sigma_0^T=-\alpha_1' E_1 \Theta_0/(1-\nu_1)$ (material pair B)

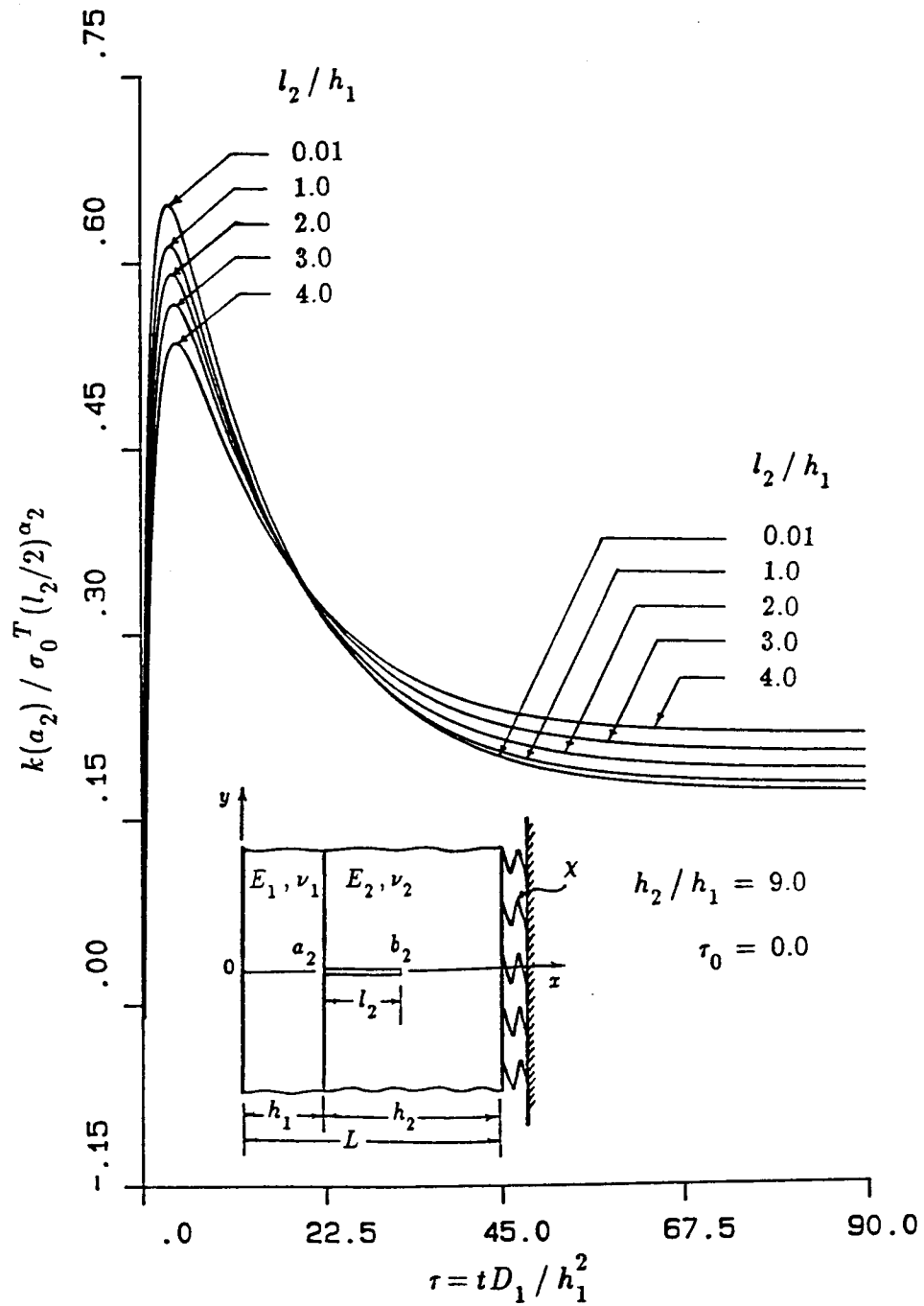


Figure 6-120: The normalized stress intensity factor $k(a_2)$ as a function of nondimensional time τ for an under-clad crack in Model II for $\alpha_2=0.4512416$, $\tau_0=0.0$, $h_2/h_1=9.0$, $R_i/L=9.0$ and $\chi L/E_2=0.01185$, $\tau_0=t_0 D_1/h_1^2$, $\sigma_0^T=-\alpha_1 E_1 \Theta_0/(1-\nu_1)$. (material pair B)

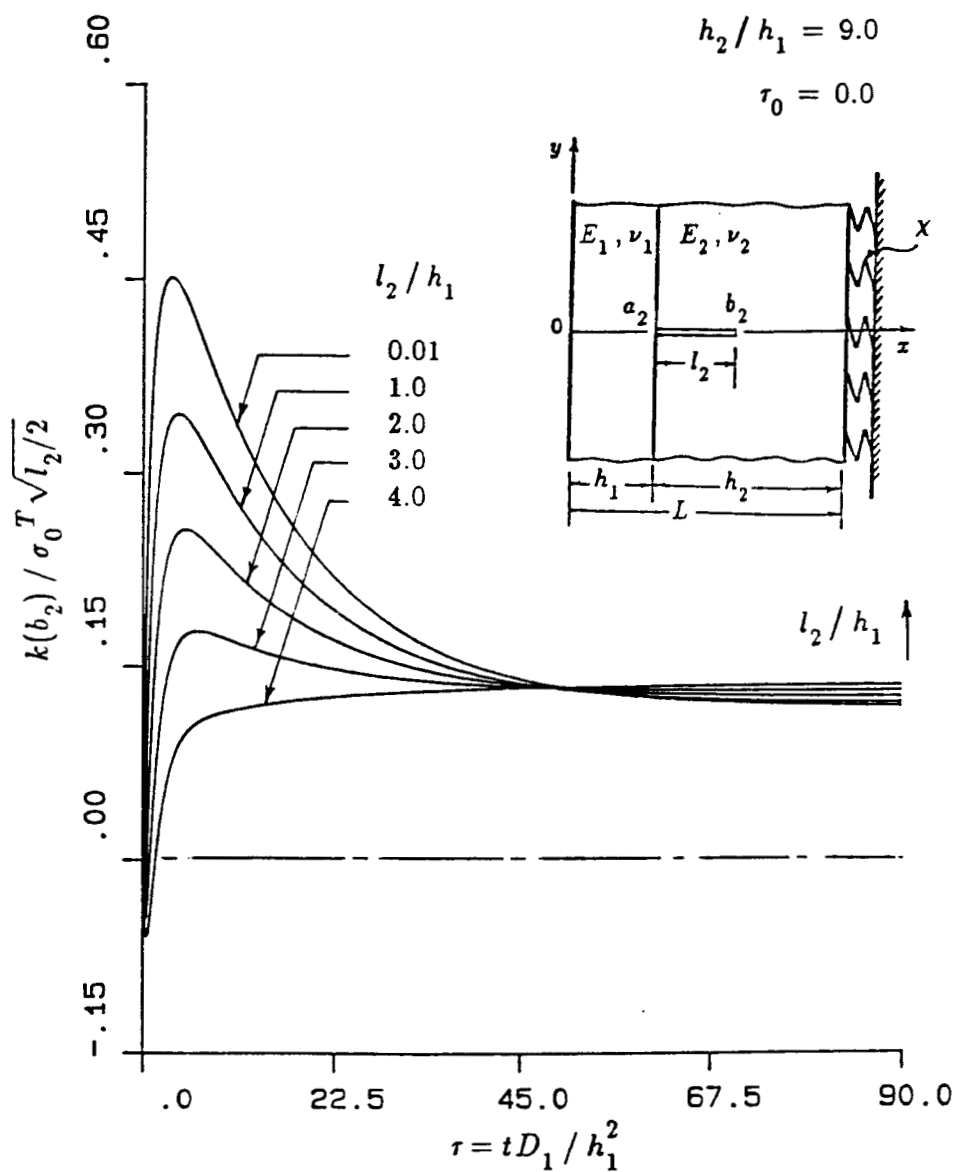


Figure 6-121: The normalized stress intensity factor $k(b_2)$ as a function of nondimensional time τ for an under-clad crack in Model II for $\alpha_2=0.4512416$, $\tau_0=0.0$, $h_2/h_1=9.0$, $R_i/L=9.0$ and $\chi L/E_2=0.01185$, $\tau_0=t_0D_1/h_1^2$, $\sigma_0^T=-\alpha_1'E_1\Theta_0/(1-\nu_1)$. (material pair B)

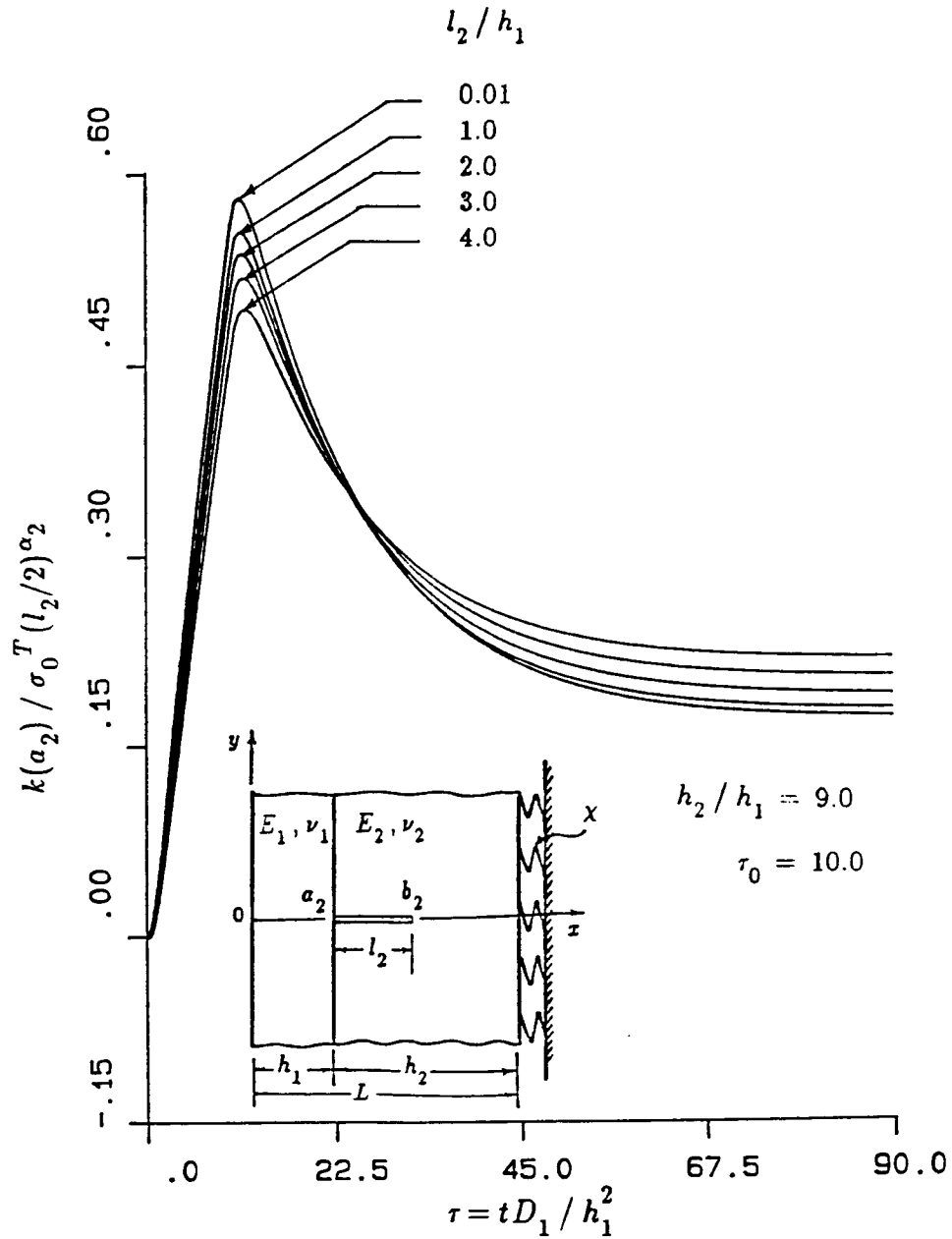


Figure 6-122: The normalized stress intensity factor $k(a_2)$ as a function of nondimensional time τ for an under-clad crack in Model II for $\alpha_2=0.4512416$, $\tau_0=10.0$, $h_2/h_1=9.0$, $R_i/L=9.0$ and $\chi L/E_2=0.01185$, $\tau_0=t_0 D_1/h_1^2$, $\sigma_0^T=-\alpha_1' E_1 \Theta_0/(1-\nu_1)$ (material pair B)

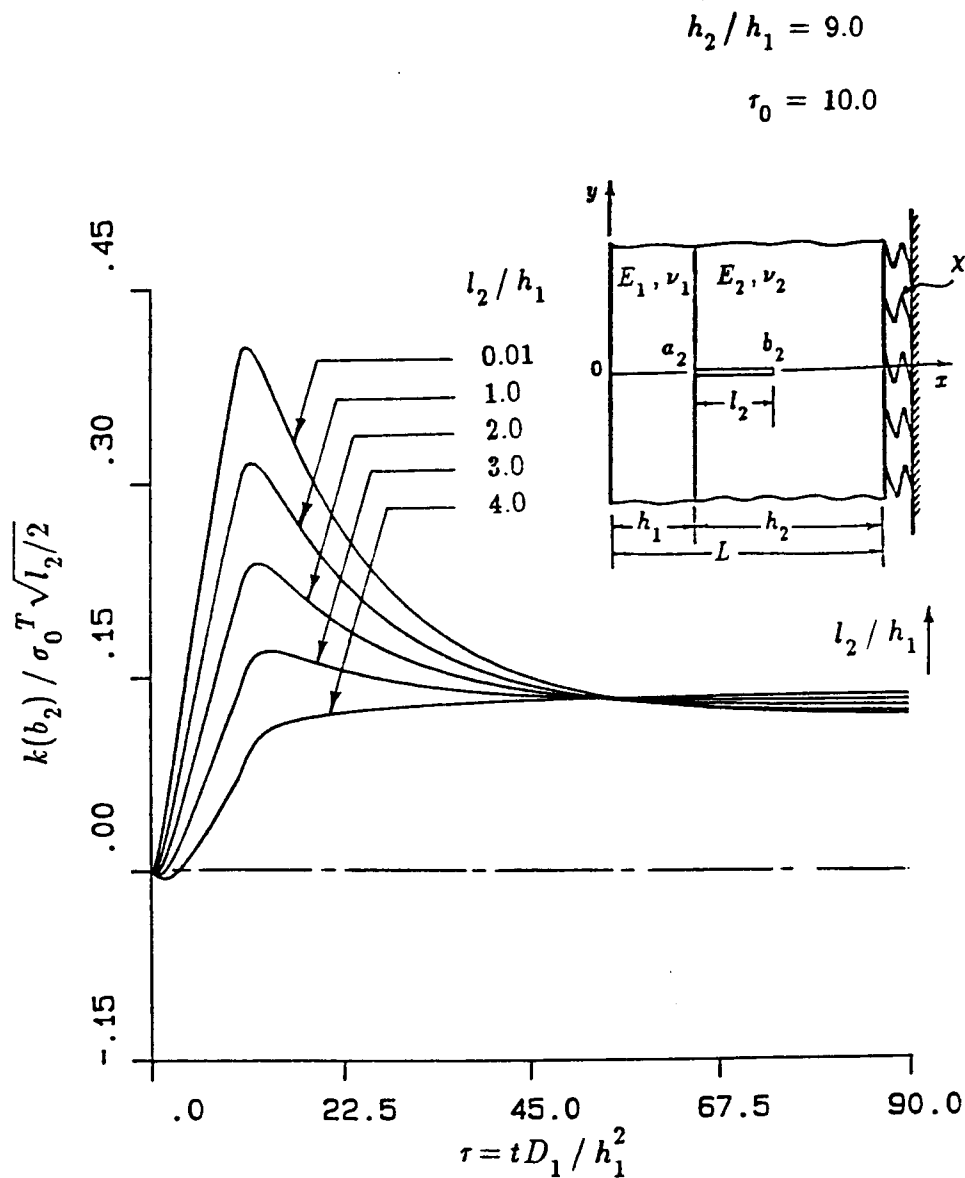


Figure 6-123: The normalized stress intensity factor $k(b_2)$ as a function of nondimensional time τ for an under-clad crack in Model II for $\alpha_2=0.4512416$, $\tau_0=10.0$, $h_2/h_1=9.0$, $R_i/L=9.0$ and $\chi L/E_2=0.01185$, $\tau_0=t_0 D_1/h_1^2$, $\sigma_0^T=-\alpha_1' E_1 \Theta_0/(1-\nu_1)$ (material pair B)

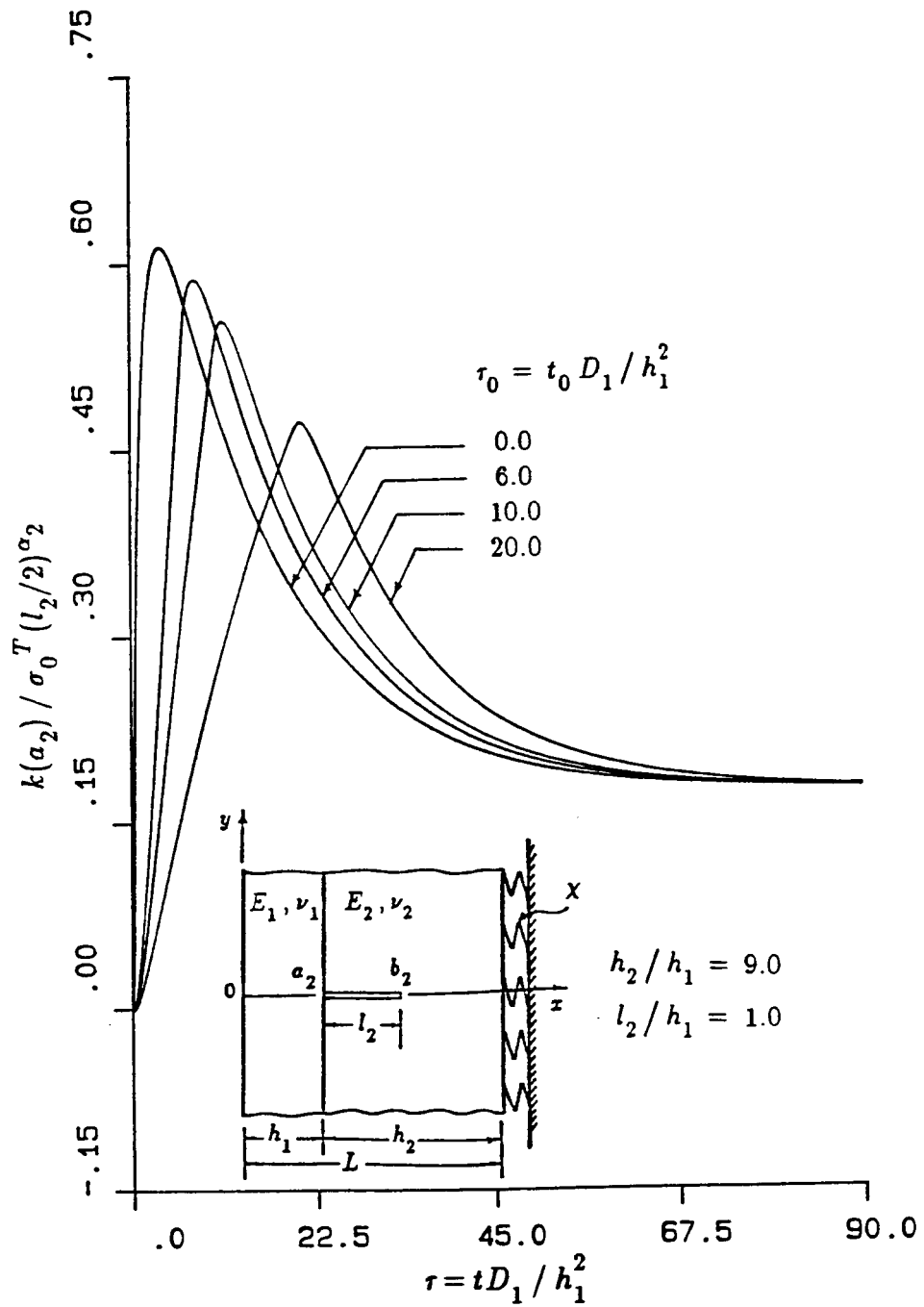


Figure 6-124: The influence of τ_0 on the normalized stress intensity factor $k(a_2)$ as a function of nondimensional time τ for an under-clad crack of length $l_2/h_1=1.0$ in Model II, $\alpha_2=0.4512416$ $h_2/h_1=9.0$, $R_i/L=9.0$ and $\chi L/E_2=0.01185$, $\tau_0=t_0 D_1/h_1^2$, $\sigma_0^T=-\alpha_1' E_1 \Theta_0/(1-\nu_1)$ (material pair B)

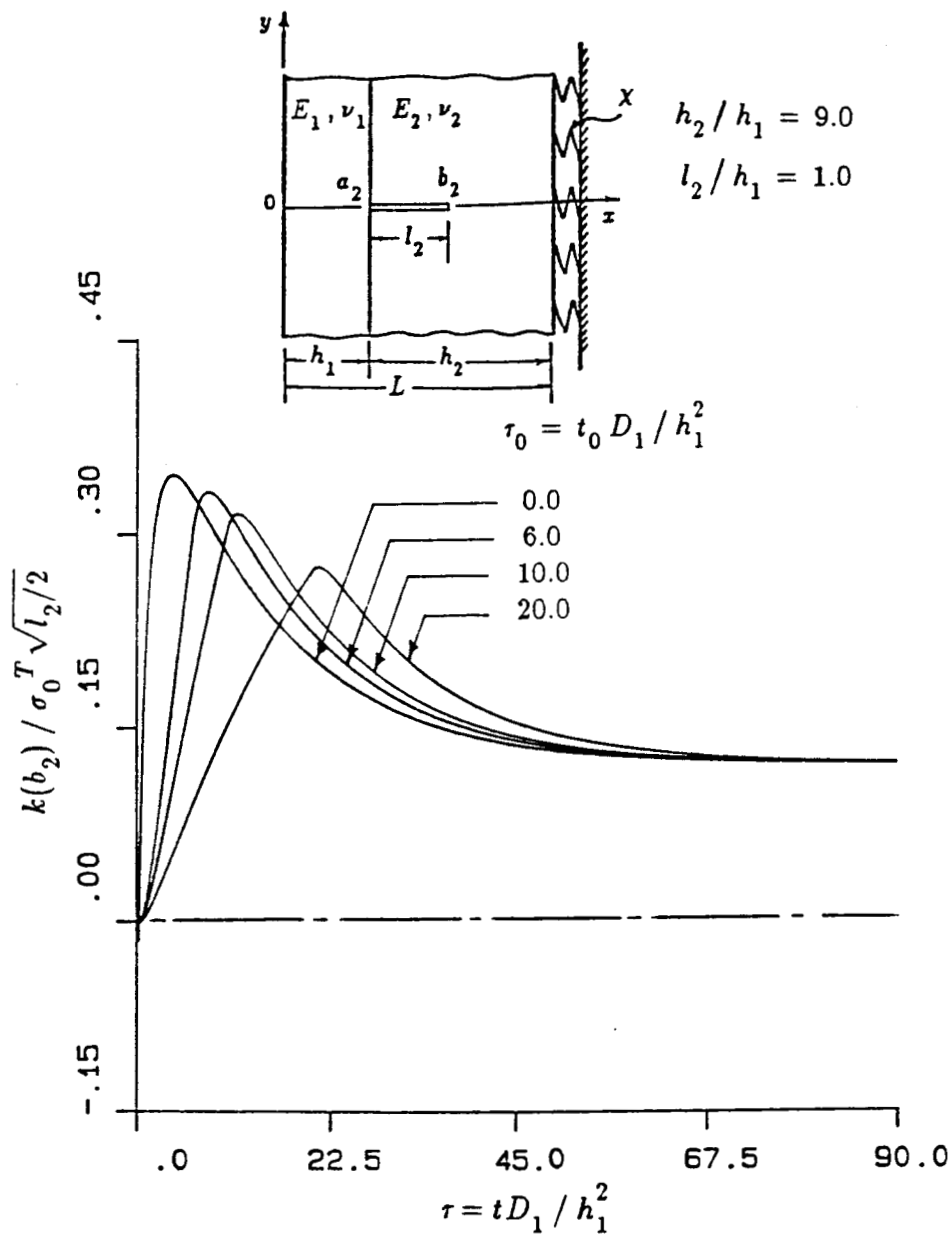


Figure 6-125: The influence of τ_0 on the normalized stress intensity factor $k(b_2)$ as a function of nondimensional time τ for an under-clad crack of length $l_2/h_1=1.0$ in Model II, $\alpha_2=0.4512416$, $h_2/h_1=9.0$, $R_i/L=9.0$ and $\chi L/E_2=0.01185$, $\tau_0=t_0 D_1/h_1^2$, $\sigma_0^T=-\alpha_1 E_1 \Theta_0/(1-\nu_1)$ (material pair B)

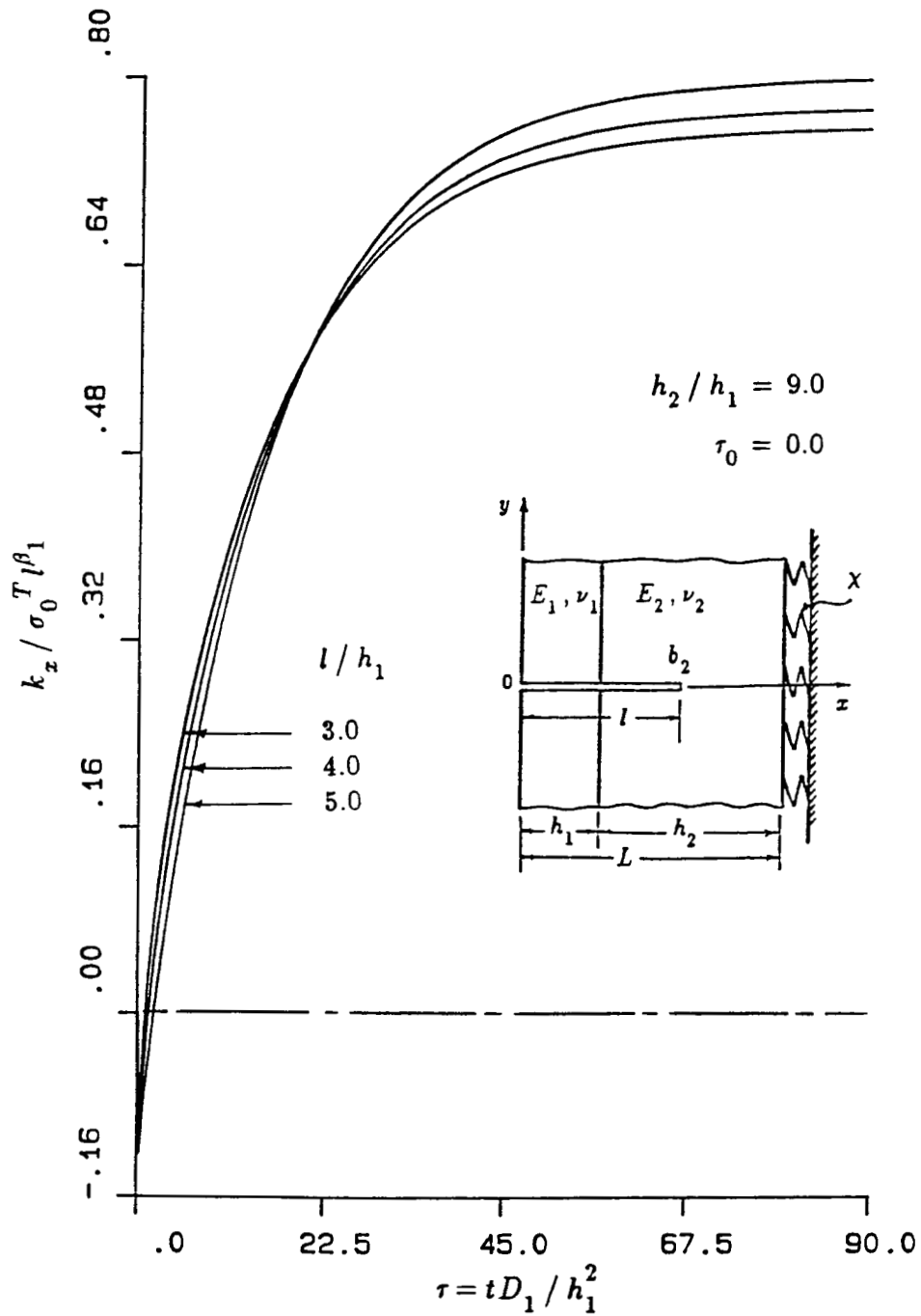


Figure 6-126: The normalized stress intensity factor k_x as a function of nondimensional time τ for an edge crack crossing the interface in Model II for $\beta_1 = \alpha_2 = 0.0187223$, $\tau_0 = 0.0$, $h_2/h_1 = 9.0$, $R_i/L = 9.0$ and $\chi L/E_2 = 0.01185$, $\tau_0 = t_0 D_1/h_1^2$, $\sigma_0^T = -\alpha_1^* E_1 \Theta_0/(1-\nu_1)$. (material pair B)

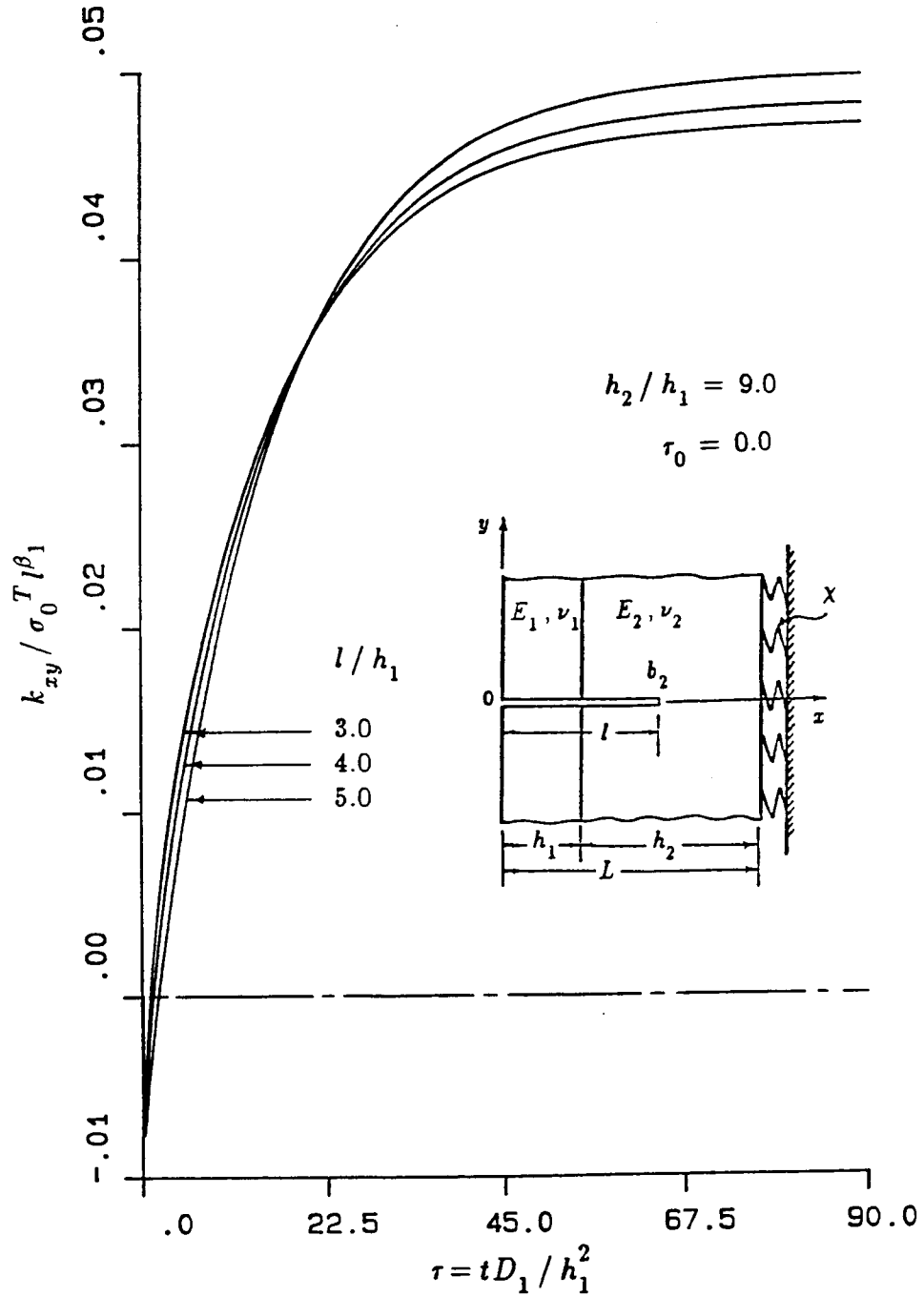


Figure 6-127: The normalized stress intensity factor k_{xy} as a function of nondimensional time τ for an edge crack crossing the interface in Model II for $\beta_1 = \alpha_2 = 0.0187223$, $\tau_0 = 0.0$, $h_2/h_1 = 9.0$, $R_i/L = 9.0$ and $\chi L/E_2 = 0.01185$, $\tau_0 = t_0 D_1/h_1^2$, $\sigma_0^T = -\alpha_1^i E_1 \Theta_0/(1-\nu_1)$. (material pair B)

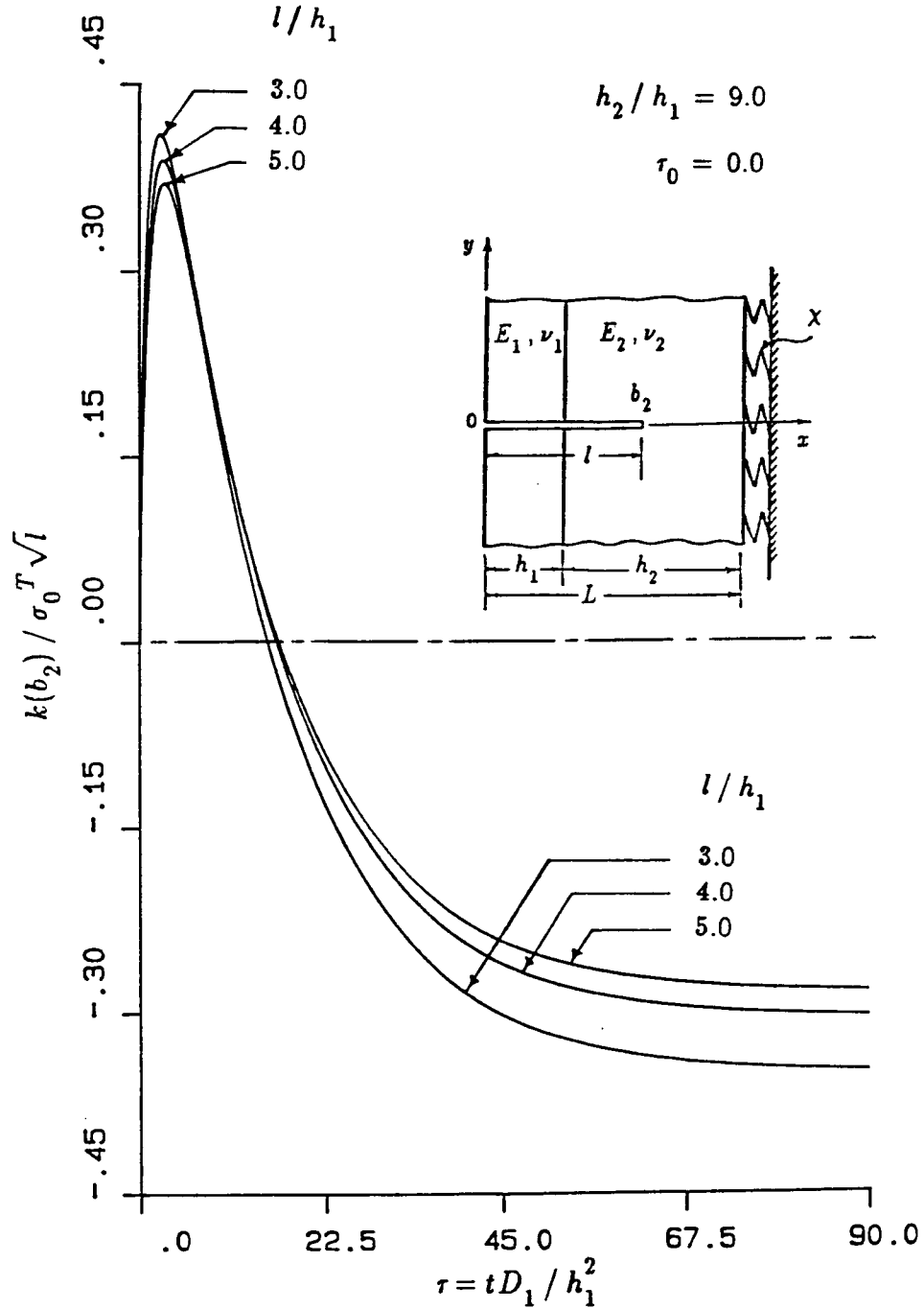


Figure 6-128: The normalized stress intensity factor $k(b_2)$ as a function of nondimensional time τ for an edge crack crossing the interface in Model II for $\beta_1 = \alpha_2 = 0.0187223$, $\tau_0 = 0.0$, $h_2/h_1 = 9.0$, $R_i/L = 9.0$ and $\chi L/E_2 = 0.01185$, $\tau_0 = t_0 D_1/h_1^2$, $\sigma_0^T = -\alpha_1 E_1 \Theta_0 / (1 - \nu_1)$. (material pair B)

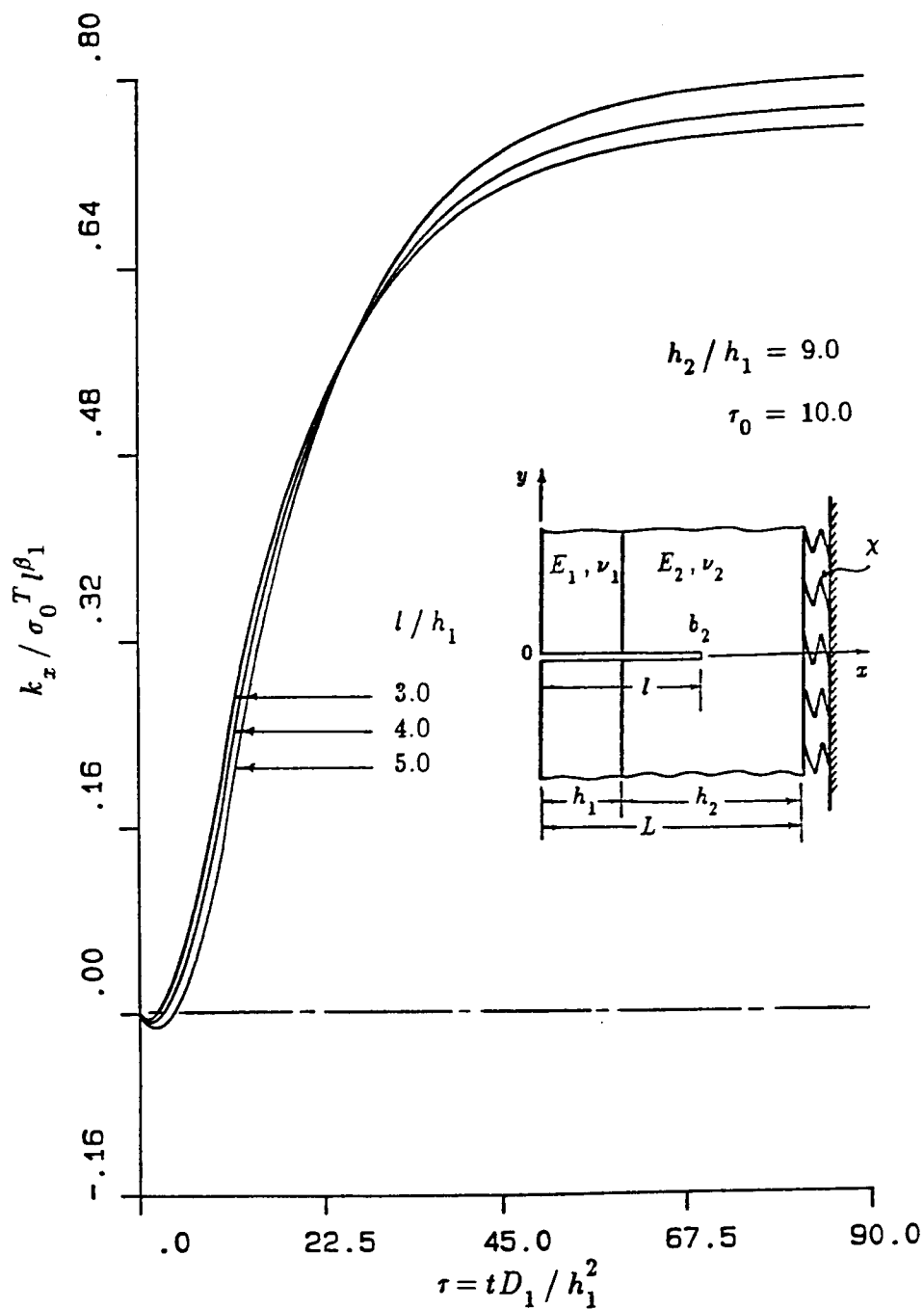


Figure 6-129: The normalized stress intensity factor k_x as a function of nondimensional time τ for an edge crack crossing the interface in Model II for $\beta_1 = \alpha_2 = 0.0187223$, $\tau_0 = 10.0$, $h_2/h_1 = 9.0$, $R_i/L = 9.0$ and $\chi L/E_2 = 0.01185$, $\tau_0 = t_0 D_1/h_1^2$, $\sigma_0^T = -\alpha_1' E_1 \Theta_0/(1-\nu_1)$. (material pair B)

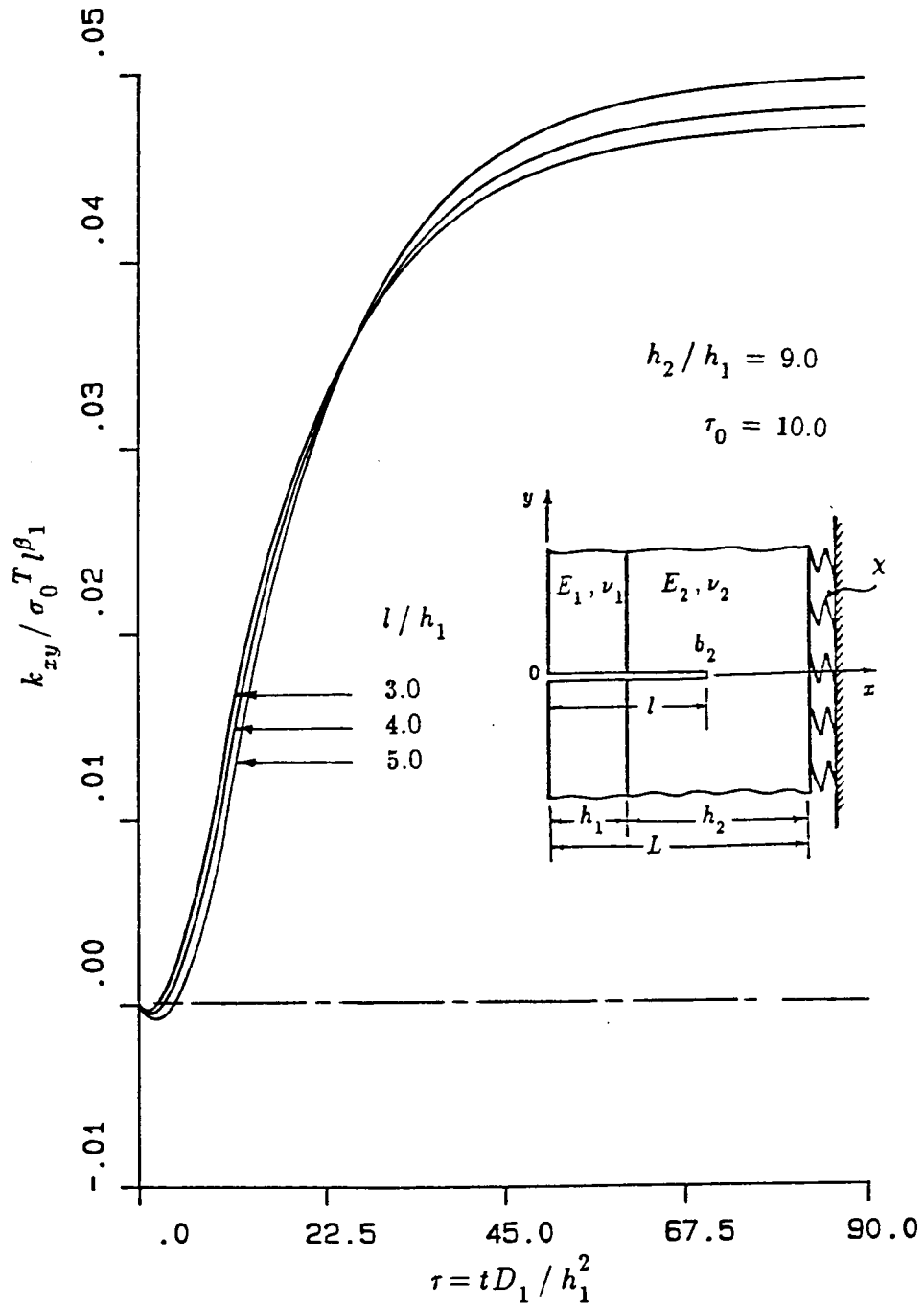


Figure 6-130: The normalized stress intensity factor k_{xy} as a function of nondimensional time τ for an edge crack crossing the interface in Model II for $\beta_1 = \alpha_2 = 0.0187223$, $\tau_0 = 10.0$, $h_2/h_1 = 9.0$, $R_i/L = 9.0$ and $\chi L/E_2 = 0.01185$, $\tau_0 = t_0 D_1/h_1^2$, $\sigma_0^T = -\alpha_1^* E_1 \Theta_0 / (1 - \nu_1)$. (material pair B)

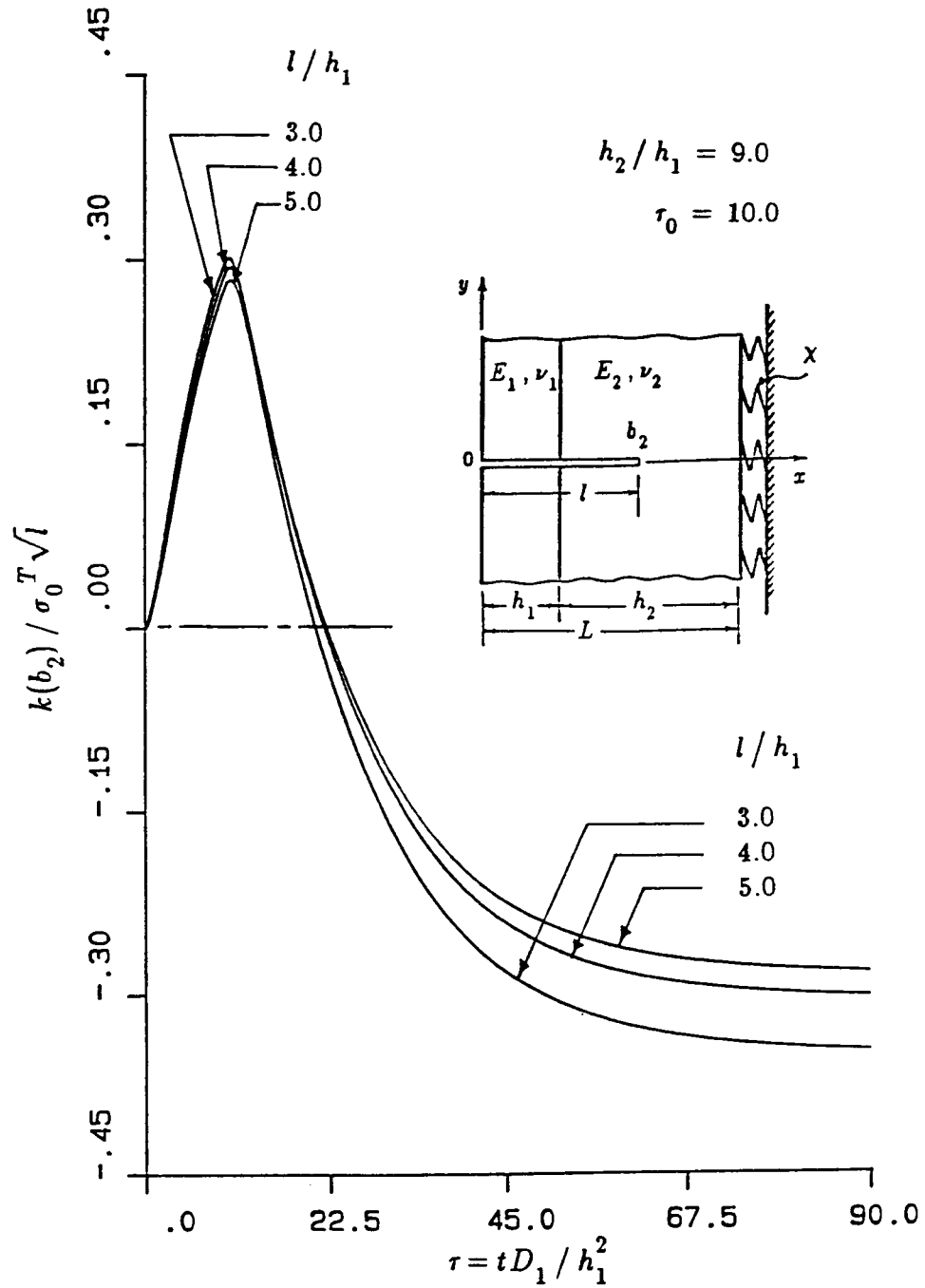


Figure 6-131: The normalized stress intensity factor $k(b_2)$ as a function of nondimensional time τ for an edge crack crossing the interface in Model II for $\beta_1 = \alpha_2 = 0.0187223$, $\tau_0 = 10.0$, $h_2/h_1 = 9.0$, $R_i/L = 9.0$ and $\chi L/E_2 = 0.01185$, $\tau_0 = t_0 D_1/h_1^2$, $\sigma_0^T = -\alpha_1' E_1 \Theta_0/(1-\nu_1)$. (material pair B)

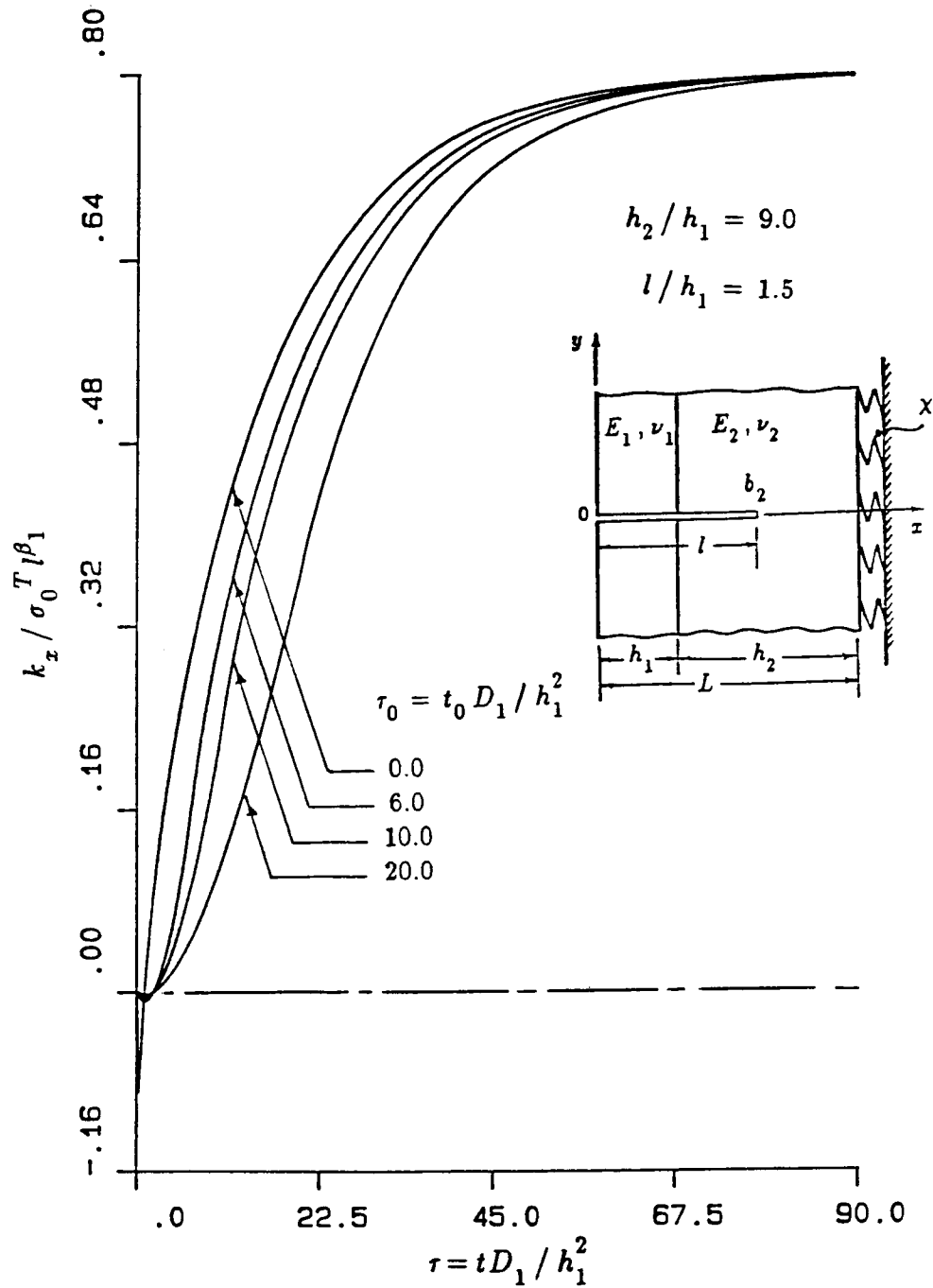


Figure 6-132: The influence of τ_0 on the normalized stress intensity factor k_x as a function of nondimensional time τ for an edge crack of length $l/h_1=1.5$ crossing the interface, in Model II for $\beta_1=\alpha_2=0.01872238$, $h_2/h_1=9.0$, $R_i/L=9.0$ and $\chi L/E_2=0.01185$, $\tau_0=t_0 D_1/h_1^2$, $\sigma_0^T = -\alpha_1' E_1 \Theta_0 / (1-\nu_1)$. (material pair B)

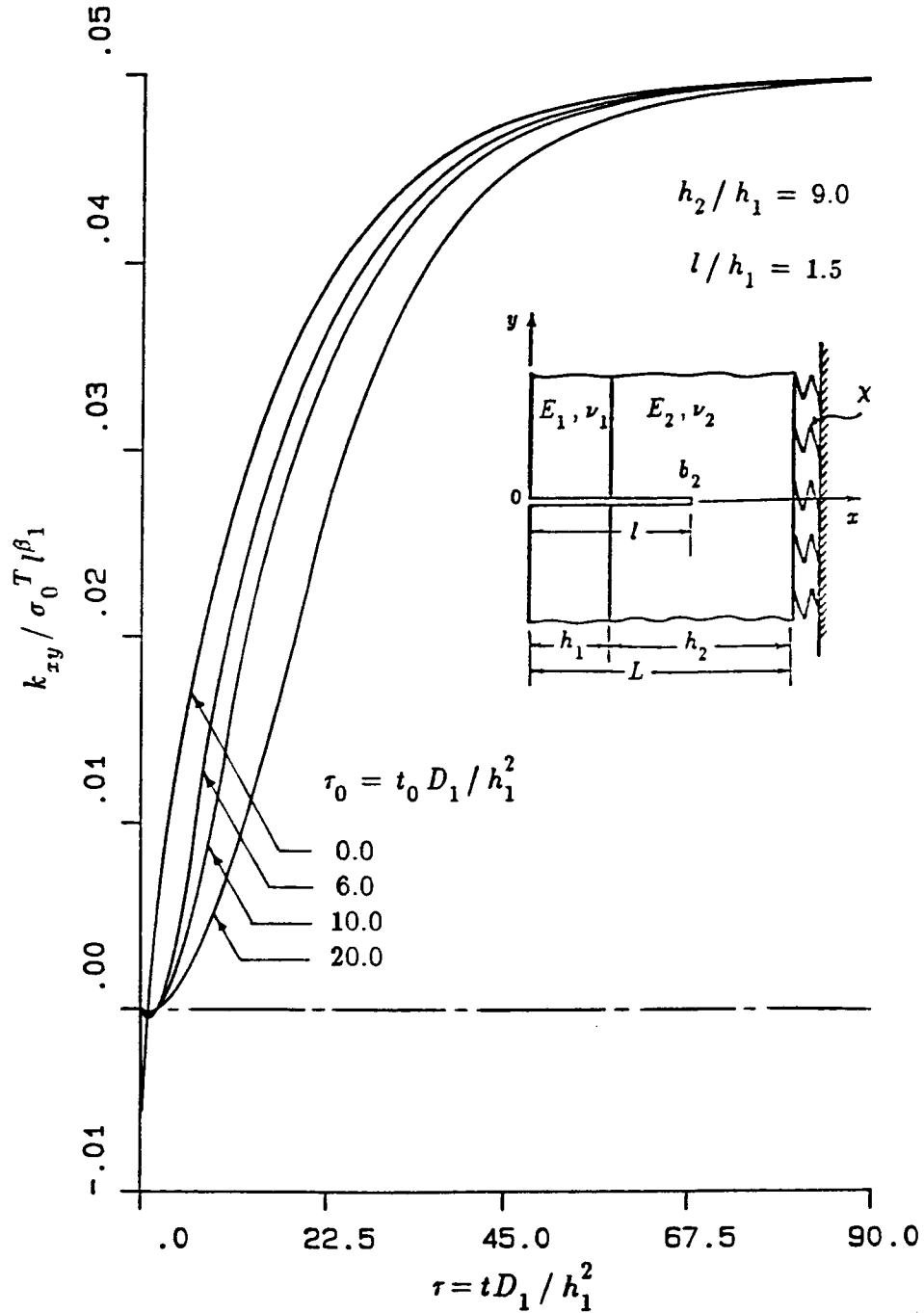


Figure 6-133: The influence of τ_0 on the normalized stress intensity factor k_{xy} as a function of nondimensional time τ for an edge crack of length $l/h_1=1.5$ crossing the interface, in Model II for $\beta_1=\alpha_2=0.01872238$, $h_2/h_1=9.0$, $R_i/L=9.0$ and $\chi L/E_2=0.01185$, $\tau_0=t_0 D_1/h_1^2$, $\sigma_0^T = -\alpha_1' E_1 \Theta_0 / (1-\nu_1)$. (material pair B)

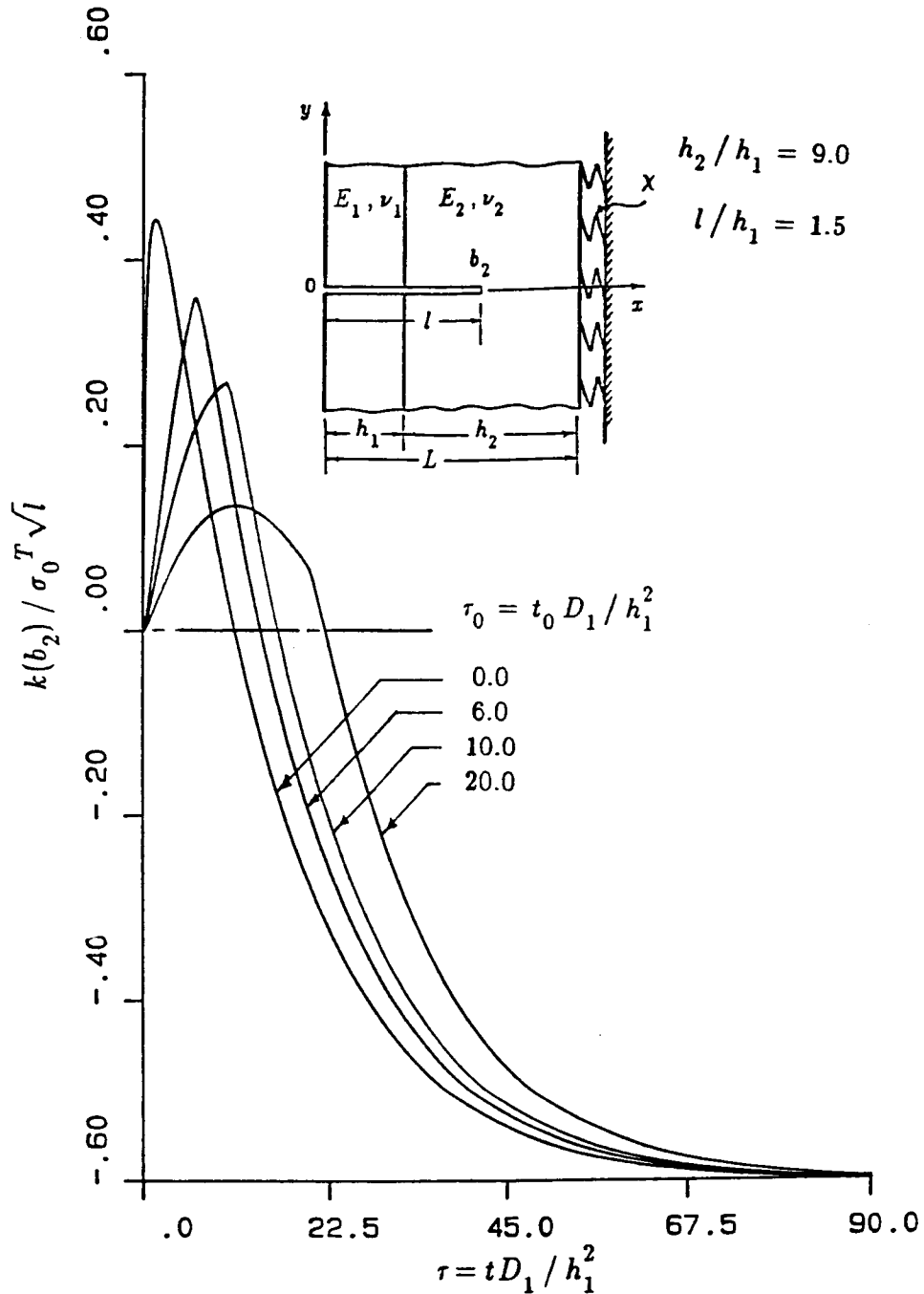


Figure 6-134: The influence of τ_0 on the normalized stress intensity factor $k(b_2)$ as a function of nondimensional time τ for an edge crack of length $l/h_1=1.5$ crossing the interface, in Model II for $\beta_1=\alpha_2=0.01872238$, $h_2/h_1=9.0$, $R_i/L=9.0$ and $\chi L/E_2=0.01185$, $\tau_0=t_0 D_1/h_1^2$, $\sigma_0^T = -\alpha_1' E_1 \Theta_0/(1-\nu_1)$. (material pair B)

References

1. Nied, H.F., "Thermal Shock in a Circumferentially Cracked Hollow Cylinder With Cladding". Eng. Fracture Mechanics, vol. 20, pp. 113-137, 1984.
2. Erdogan, F., "The Study of The Effect of Cladding on The stress Intensity Factors in a Circumferentially Cracked Pressure Vessel Subjected to Thermal Shock". Fraunhofer - Institut for Werkstoffmechanik Wohlerstr. 11, D-7800 Freiburg, v13/84, 1984.
3. Nied, H.F., Erdogan, F., "Transient Thermal Stress Problem for a Circumferentially Cracked Hollow Cylinder". J. of Thermal Stresses, vol. 6, pp. 1-14, 1983.
4. Blauel, J.G., "Sicherheitsanalyse RDB-KKS Bericht des Frannhofer". Institute fur Werkstoffmechanik v31/83, 1983.
5. Hetenyi, M. "Beams on Elastic foundation". The University of Michigan, By The Waverly press, Baltimore, 1952.
6. Williams, M.L., "The Stresses Around a Fault or Crack in Dissimilar Media". Bull. Seismological Society of America, pp.199-204, 1959.
7. Rice, J.R., and Sih, G.C., "Plane Problems of Cracks in Dissimilar Media". Journal of Applied Mechanics, 32, pp. 418-423, 1965.
8. Sih, G.C., and Rice, J.R., "The Bending of Plates of Dissimilar Materials With Cracks". Journal of Applied Mechanics, 31, pp. 477-482, 1964.
9. England, A.H., "A crack Between Dissimilar Media". Journal of Applied Mechanics, 32, pp. 400-402, 1965.
10. Erdogan, F., "Stress Distribution in Bonded Dissimilar Materials with Cracks". Journal of Applied Mechanics, 32, pp. 403-410, 1965.
11. Erdogan, F., and Gupta, G.D., "Layered Composites with an Interface Flow". Int. J. Solids Structures, vol 7, pp. 1089-1107, 1971.
12. Lowengrub, M., and Sneddon, I.N., "The Effect of Shear on a Penny-shaped Crack at The Interface of an Elastic Half-Space and Rigid Foundation". Int. J. Engin. Sci., vol 10, pp. 899-913, 1972.
13. Lowengrub, M., "Stress Distribution Due to a Griffith Crack at The Interface of an Elastic Half Plane and Rigid Foundation". Int. J. Engin. Sci., vol 11, pp. 477-488, 1973.
14. Willes, J.R., "The Penny-shaped Crack on an Interface". The Quarterly Journal of Mechanics and Applied Mathematics, vol 25, pp. 367-385, 1972.

15. Perlman, A.B., and Sih, G.C., "Elastostatic Problems of Curvilinear Cracks in Bonded Dissimilar Materials". *Int. J. of Engin. Sci.*, vol 5, pp. 845-867, 1967.
16. Perlman, A.B., and Sih, G.C., "Circular Arc Cracks in Bimaterial Plates Under Bending". *Int. J. of Fracture Mechanics*, vol 3, pp. 193-206, 1967.
17. Khrapkov, A.A., "First Fundamental Problem for a Piecewise-Homogenous Plane with a Slit Perpendicular to The Line of Separation". *J. of Applied Mathematics and Mechanics*, vol 32, pp. 666-678, 1968.
18. Cook, T.S., and Erdogan, F., "Stresses in Bonded Materials with a Crack Perpendicular to The Interface". *Int. J. of Engin. Sci.*, vol 10, pp. 677-697, 1972.
19. Ashbaugh, N.E., "Stresses in Laminated Composite Containing a Broken Layer". ASME Paper No. 72-WA/AIM-14, 1972.
20. Gupta, G.D., "A Layered Composite with Broken Laminate". *Int. J. of Solids and Structures*, vol 9, pp. 1141-1154, 1973.
21. Erdogan, F., "The Crack Problem for Bonded Nonhomogenous Materials Under Antiplane Shear Loading". Contributed by The Applied Mechanics Division for Presentation at The Winter Annual Meeting Miami, Fla, Nov. 17-21, 1985, of ASME.
22. Hilton, P.D., and Sih, G.C., "A Laminate Composite with a Crack Normal to The Interface". *Int. J. of Solids and Structures*, vol 7, pp. 913-930, 1971.
23. Bogy, D.B., "The Plane Elastostatic Solution for a Symmetrically Loaded Crack in a Strip Composites". *Int. J. Eng. Sci.*, vol 11, pp. 985-996, 1973.
24. Arin, K., "A Note on The Fracture of Laminated Composites". *Letters in Applied and Eng. Sci.*, vol 3, pp. 81-85, 1975.
25. Hilton, P.D., and Sih, G.C., "A Sandwiched Layer of Dissimilar Material Weakened by Crack-Like Imperfections". *Proceedings of Fifth South Eastern Conference on Theoretical and Applied Mechanics*, Edited by G. Rogers, S.C. Krance and E.G. Henneke.
26. Chen, E.P., and Sih, G.C., "Interfacial Delamination of a Layered Composite Under Anti-Plane Shear". *J. of Composite Materials*, vol 5, pp. 12-23, 1971.
27. Arin, K., and Erdogan, F., "Penny-Shaped Crack in an Elastic Layer Bonded to Dissimilar Half Spaces". *Int. J. Engng Sci.*, vol 9, pp. 213-232, 1971.
28. Sih, G.C., and Chen, E.P., "Torsion of a Laminar Composite Debonded Over a Penny-Shaped Area". *J. of The Franklin*

Institute, vol 293, pp. 251-261, 1972.

29. Erdogan, F., and Biricikoglu, V., "Two Bonded Half-Planes with a Crack Going Through The Interface". *Int. J. Eng. Sci.*, vol 11, pp. 745-766, 1973.
30. Erdogan, F., and Cook, T.S., "Antiplane Shear Cracks Terminating at and Going Through a Bimaterial Interface". *Int. J. of Fracture*, vol 10, pp. 227-240, 1974.
31. Erdogan, F., and Bakioglu, M., "Fracture of Plates which Consist of Periodic Dissimilar Strips". *Int. J. of Fracture*, vol 12, pp. 71-84, 1976.
32. Erdogan, F., and Bakioglu, M., "Stress Free End Problem in Layered Materials". *Int. J. of Fracture*, vol 13, pp. 739-749, 1977.
33. Delale, F., and Erdogan, F., "Bonded Orthotropic Strips with Cracks". *Int. J. of Fracture*, vol 15, pp. 343-364, 1979.
34. Goree, J.C., and Venezia, W.A., "Bonded Elastic Half-Planes with an Interface Crack and a Perpendicular Intersecting Crack that Extends into The Adjacent Material - I and II". *Int. J. Eng. Sci.*, vol 15, pp. 1-27, 1977.
35. Erdogan, F., "Bonded Dissimilar Materials Containing Cracks Parallel to The Interface". *Eng. Fracture Mechanics*, vol 3, pp. 231-240, 1971.
36. Erdogan, F., "Fracture Problems in Composite Materials". *Eng. Fracture Mechanics*, vol 4, pp. 811-840, 1972.
37. Muskhelishvili, N.I., "Singular Integral Equations". Noordhoff, Groningen, The Netherlands, 1953.
38. Kaya, A.C., and Erdogan, F., "On The Solution of Integral Equations with Strongly Singular Kernels". *Quarterly of Applied Mathematics*, vol xlv, pp. 105-122, 1987.
39. Kaya, A.C., and Erdogan, F., "On The Solution of Integral Equations with a Generalized Cauchy Kernel". *Quarterly of Applied Mathematics*, vol xlv, pp. 455-469, 1987.
40. Erdogan, F., "Mixed Boundary Value Problems in Mechanics". *Mechanics Today*, S. Nemat Nasser, ed., vol 4, pp. 1-86, 1978.
41. Kaya, A.C., "Applications of Integral Equations with Strong Singularities in Fracture Mechanics". Ph.D. Thesis, Lehigh University, 1984.
42. Nied, H.F., "Circumferentially Cracked Cylinders Under Extension and Bending". Ph.D. Thesis, Lehigh University, 1981.
43. Nied, H.F., and Erdogan, F., "Transient Thermal Stress Problem for a Circumferentially Cracked Hollow Cylinder". *J. Thermal*

Stresses, vol 6, pp. 1-14, 1983.

44. Stroud, A., and Secrest, D., "Guassian Quadrature Formulas".
Prentice-Hall, New York, 1966.

Appendix (A)

The Governing Equations for the Displacements

For a two dimensional, isotropic, elastic material in the absence of the body forces, we have the equilibrium equations

$$\begin{aligned}\frac{\partial \sigma_{xx}}{\partial x} + \frac{\partial \sigma_{xy}}{\partial y} &= 0, & (a) \\ \frac{\partial \sigma_{xy}}{\partial x} + \frac{\partial \sigma_{yy}}{\partial y} &= 0, & (b)\end{aligned}\tag{1}$$

the strain displacement relations

$$\begin{aligned}\epsilon_{xx} &= \frac{\partial u}{\partial x}, & (a) \\ \epsilon_{yy} &= \frac{\partial v}{\partial y}, & (b) \\ \gamma_{xy} &= \frac{\partial u}{\partial y} + \frac{\partial v}{\partial x}, & (c)\end{aligned}\tag{2}$$

and the strain-stress relations (Hooke's law)

for plane stress

$$\begin{aligned}\sigma_{zz} = \tau_{xz} = \tau_{yz} &= 0, \\ \epsilon_{xx} &= \frac{1}{E}(\sigma_{xx} - \nu \sigma_{yy}), & (a) \\ \epsilon_{yy} &= \frac{1}{E}(\sigma_{yy} - \nu \sigma_{xx}), & (b)\end{aligned}\tag{3}$$

and for plane strain

$$\epsilon_y = \gamma_{xz} = \gamma_{yz} = 0 ,$$

$$\epsilon_{xx} = \frac{1-\nu^2}{E} \left(\sigma_{xx} - \frac{\nu}{1-\nu} \sigma_{yy} \right) , \quad (a)$$

$$\epsilon_{yy} = \frac{1-\nu^2}{E} \left(\sigma_{yy} - \frac{\nu}{1-\nu} \sigma_{xx} \right) . \quad (b)$$

(4)

By solving equations (1), (2), and (3) for the plane stress, and equations (1), (2), and (4) for the plane strain, we end up with the governing equations as follows

$$(\kappa-1)\nabla^2 u + 2\left(\frac{\partial^2 u}{\partial x^2} + \frac{\partial^2 v}{\partial x \partial y}\right) = 0 , \quad (a)$$

$$(\kappa-1)\nabla^2 v + 2\left(\frac{\partial^2 u}{\partial x \partial y} + \frac{\partial^2 v}{\partial y^2}\right) = 0 , \quad (b)$$

(5)

where

$$\kappa = (3-4\nu) \quad \text{for plane strain.}$$

$$\kappa = \frac{3-\nu}{1+\nu} \quad \text{for generalized plane stress}$$

$$\nu = \quad \text{Poisson's ratio}$$

Appendix (B)

Some useful integrals

$$\int_0^{\infty} e^{-px} \sin qx \, dx = \frac{q}{p^2 + q^2}$$

$$\int_0^{\infty} x e^{-px} \sin qx \, dx = \frac{2pq}{(p^2 + q^2)^2}$$

$$\int_0^{\infty} e^{-px} \cos qx \, dx = \frac{p}{p^2 + q^2}$$

$$\int_0^{\infty} x e^{-px} \cos qx \, dx = \frac{p^2 - q^2}{(p^2 + q^2)^2}$$

$$\int_{-\infty}^{\infty} \frac{p}{(p^2 + t^2)^2} e^{-ip(s-x)} \, dp = -\frac{\pi}{2} \left[\frac{i(s-x)}{t} \right] e^{-t(s-x)} \quad ; s > x$$

$$\int_{-\infty}^{\infty} \frac{p^2}{(p^2 + t^2)^2} e^{-ip(s-x)} \, dp = \frac{\pi}{2} \left[\frac{1}{t} - (s-x) \right] e^{-t(s-x)} \quad ; s > x$$

$$\int_{-\infty}^{\infty} \frac{1}{(p^2 + t^2)} e^{-ip(s-x)} \, dp = \frac{\pi}{t} e^{-t(s-x)} \quad ; s > x$$

$$\int_{-\infty}^{\infty} \frac{1}{(p^2 + t^2)^2} e^{-ip(s-x)} \, dp = \frac{\pi}{2} \frac{1}{t^3} [1 + (s-x)t] e^{-t(s-x)} \quad ; s > x$$

$$\int_{-\infty}^{\infty} \frac{1}{p(p^2 + t^2)} e^{-ip(s-x)} \, dp = \frac{\pi i}{t^2} [e^{-t(s-x)} - 1] \quad ; s > x$$

$$\int_{-\infty}^{\infty} \frac{p}{(p^2 + t^2)^2} e^{-ip(s-x)} \, dp = -\frac{\pi}{2} \left[\frac{i(s-x)}{t} \right] e^{(s-x)t} \quad ; s < x$$

$$\int_{-\infty}^{\infty} \frac{p^2}{(p^2 + t^2)^2} e^{-ip(s-x)} \, dp = \frac{\pi}{2} \left[\frac{1}{t} + (s-x) \right] e^{(s-x)t} \quad ; s < x$$

$$\int_{-\infty}^{\infty} \frac{1}{(p^2 + t^2)} e^{-ip(s-x)} dp = \frac{\pi}{2} e^{(s-x)t} \quad ; s < x$$

$$\int_{-\infty}^{\infty} \frac{1}{(p^2 + t^2)^2} e^{-ip(s-x)} dp = \frac{\pi}{2} \frac{1}{t^3} [1 - (s-x)t] e^{(s-x)t} \quad ; s < x$$

$$\int_{-\infty}^{\infty} \frac{1}{p(p^2 + t^2)} e^{-ip(s-x)} dp = \frac{\pi i}{t^2} [1 - e^{(s-x)t}] \quad ; s < x$$

Appendix (C)

The functions that appear in the solution of crack problems given in Chapter 2.

$$e_1 = \frac{\kappa_1 + 1}{2}$$

$$e_2 = \frac{\kappa_1 - 1}{2}$$

$$e_3 = m \left(\frac{\kappa_1 - 1}{2} + h\alpha \right) e^{2h\alpha}$$

$$e_4 = m e^{2h\alpha}$$

$$e_5 = m \left(\frac{\kappa_1 - 1}{2} - h\alpha \right)$$

$$e_6 = - \left(\frac{\kappa_2 - 1}{2} - h\alpha \right)$$

$$e_7 = -m \left(\frac{\kappa_1 + 1}{2} + h\alpha \right) e^{2h\alpha}$$

$$e_8 = m \left(\frac{\kappa_1 + 1}{2} - h\alpha \right)$$

$$e_9 = - \left(\frac{\kappa_2 + 1}{2} - h\alpha \right)$$

$$e_{10} = e^{2h\alpha}$$

$$e_{11} = h\alpha e^{2h\alpha}$$

$$e_{12} = h\alpha$$

$$e_{13} = -(\kappa_1 + h\alpha) e^{2h\alpha}$$

$$e_{14} = -(\kappa_1 - h\alpha)$$

$$e_{15} = (\kappa_2 - h\alpha)$$

$$M_1 = -(1 - t_1 \alpha) e^{-t_1 \alpha}$$

$$M_2 = (-t_1 \alpha) e^{-t_1 \alpha}$$

$$M_3 = -m(t_1 - h) \alpha e^{t_1 \alpha}$$

$$M_4 = (t_2 - h) \alpha e^{-(t_2 - 2h) \alpha}$$

$$M_5 = -m[1 + (t_1 - h) \alpha] e^{t_1 \alpha}$$

$$M_6 = [1 - (t_2 - h) \alpha] e^{-(t_2 - 2h) \alpha}$$

$$M_7 = -\left[\frac{\kappa_1 - 1}{2} - (t_1 - h) \alpha\right] e^{t_1 \alpha}$$

$$M_8 = \left[\frac{\kappa_2 - 1}{2} + (t_2 - h) \alpha\right] e^{-(t_2 - 2h) \alpha}$$

$$M_9 = \left[\frac{\kappa_1 + 1}{2} + (t_1 - h) \alpha\right] e^{t_1 \alpha}$$

$$M_{10} = \left[\frac{\kappa_2 + 1}{2} - (t_2 - h) \alpha\right] e^{-(t_2 - 2h) \alpha}$$

$$m = \frac{\mu_1}{\mu_2}$$

$$B_1 = \frac{1}{\kappa_1 + 1} \int_{a_1}^{b_1} H_1 \phi_1(t_1) dt_1 + \frac{1}{\kappa_2 + 1} \int_{a_2}^{b_2} H_2 \phi_2(t_2) dt_2$$

$$C_2 = \frac{1}{\kappa_1 + 1} \int_{a_1}^{b_1} \frac{1}{D} H_3 \phi_1(t_1) dt_1 + \frac{1}{\kappa_2 + 1} \int_{a_2}^{b_2} \frac{1}{D} H_4 \phi_2(t_2) dt_2$$

$$B_3 = \frac{1}{\kappa_1 + 1} \int_{a_1}^{b_1} H_5 \phi_1(t_1) dt_1 + \frac{1}{\kappa_2 + 1} \int_{a_2}^{b_2} H_6 \phi_2(t_2) dt_2$$

$$C_4 = \frac{1}{\kappa_1 + 1} \int_{a_1}^{b_1} \frac{1}{D} H_7 \phi_1(t_1) dt_1 + \frac{1}{\kappa_2 + 1} \int_{a_2}^{b_2} \frac{1}{D} H_8 \phi_2(t_2) dt_2$$

$$B_5 = \frac{1}{\kappa_1 + 1} \int_{a_1}^{b_1} H_9 \phi_1(t_1) dt_1 + \frac{1}{\kappa_2 + 1} \int_{a_2}^{b_2} H_{10} \phi_2(t_2) dt_2$$

$$C_6 = \frac{1}{\kappa_1 + 1} \int_{a_1}^{b_1} H_{11} \phi_1(t_1) dt_1 + \frac{1}{\kappa_2 + 1} \int_{a_2}^{b_2} H_{12} \phi_2(t_2) dt_2$$

where

$$H_1 = \frac{1}{2} (1 - 2t_1 \alpha) e^{-t_1 \alpha} - \frac{\kappa_1}{2} \frac{1}{D} H_3 + \frac{1}{2} \frac{1}{D} H_7$$

$$H_2 = -\frac{\kappa_1}{2} \frac{1}{D} H_4 + \frac{1}{2} \frac{1}{D} H_8$$

$$\begin{aligned} H_3 = & \{ d_2 d_3 [1 + 2h\alpha(2t_1\alpha - 1)] \} e^{-(t_1 + 2h)\alpha} \\ & + \{ -d_2 d_3 [1 + 2(t_1 - h)\alpha] \} e^{(t_1 - 2h)\alpha} \\ & + \{ d_1 d_3 [1 + 2t_1\alpha] \} e^{(t_1 - 4h)\alpha} \\ & + \{ -d_1 d_3 \} e^{-(t_1 + 4h)\alpha} \end{aligned}$$

$$\begin{aligned} H_4 = & \{ -d_3 d_5 (2h\alpha) [1 - 2(t_2 - h)\alpha] - d_1 d_5 \} e^{-(t_2 + 2h)\alpha} \\ & + \{ d_2 d_5 \} e^{-t_2 \alpha} \end{aligned}$$

$$H_5 = \frac{1}{2} e^{-t_1 \alpha} - \frac{1}{2} \frac{1}{D} H_3 + \frac{\kappa_1}{2} \frac{1}{D} H_7$$

$$H_6 = -\frac{1}{2} \frac{1}{D} H_4 + \frac{\kappa_1}{2} \frac{1}{D} H_8$$

$$\begin{aligned}
H_7 = & \{ d_2 d_4 (1 - 2t_1 \alpha) \} e^{-t_1 \alpha} \\
& + \{ -d_2 d_3 [1 - 2(t_1 - h) \alpha] \} e^{-(t_1 + 2h) \alpha} \\
& + \{ d_2 d_3 (2h \alpha) [1 + 2(t_1 - h) \alpha] - d_1 d_4 \} e^{(t_1 - 2h) \alpha} \\
& + \{ d_1 d_3 \} e^{(t_1 - 4h) \alpha}
\end{aligned}$$

$$\begin{aligned}
H_8 = & \{ -d_2 d_5 (2h \alpha) + d_4 d_5 [1 - 2(t_2 - h) \alpha] \} e^{-t_2 \alpha} \\
& + \{ -d_3 d_5 [1 - 2(t_2 - h) \alpha] \} e^{-(t_2 + 2h) \alpha}
\end{aligned}$$

$$H_9 = -\frac{d_6}{2d_3} \frac{1}{D} H_3 e^{2h\alpha} + \frac{1}{2} (\kappa_2 - 2h\alpha) H_{11}$$

$$H_{10} = -\frac{d_2}{2d_3} e^{-(t_2 - 2h)\alpha} - \frac{d_6}{2d_3} \frac{1}{D} H_4 e^{2h\alpha} + \frac{1}{2} (\kappa_2 - 2h\alpha) H_{12}$$

$$H_{11} = \frac{d_6}{d_2} e^{t_1 \alpha} + \frac{d_6}{d_2} \frac{1}{D} H_7$$

$$H_{12} = \frac{d_3}{d_2} [1 - 2(t_2 - h) \alpha] e^{-(t_2 - 2h) \alpha} + \frac{d_6}{d_2} \frac{1}{D} H_8$$

and

$$D = -d_2 d_4 + [d_1 d_4 + d_2 d_3 + d_2 d_3 (2h\alpha)^2] e^{-2h\alpha} - d_1 d_3 e^{-4h\alpha}$$

$$d_1 = m\kappa_2 - \kappa_1$$

$$d_2 = m\kappa_2 + 1$$

$$d_3 = m - 1$$

$$d_4 = m + \kappa_1$$

$$d_5 = \kappa_2 + 1$$

$$d_6 = m(\kappa_1 + 1)$$

Appendix (D)

If the function $f(z)$ has a pole of order m at $z = a$, then the residue of $f(z)$ at $z = a$, is given by

$$Res(z = a) = \lim_{z \rightarrow a} \frac{1}{(m-1)!} \left[\frac{d^{m-1}}{dz^{m-1}} \{ (z-a)^m f(z) \} \right]. \quad (1)$$

In the case of a simple pole ($m = 1$), equation (1) gives

$$Res(z = a) = \lim_{z \rightarrow a} [(z-a)f(z)]. \quad (2)$$

If, $f(z)$ is expressed as the ratio

$$f(z) = \frac{N(z)}{D(z)}. \quad (3)$$

where $N(a)$ is finite and nonzero and $D(z)$ vanishes at $z = a$ in such a way that $\frac{D(z)}{(z-a)}$ approaches a finite limit as $z \rightarrow a$, then equation (2) can be written as

$$Res(z = a) = \lim_{z \rightarrow a} [(z-a) \frac{N(z)}{D(z)}]. \quad (4)$$

By using L'Hopital rule to evaluate the limits we have

$$Res(z = a) = \left[\frac{\frac{N(z)}{dz}}{\frac{D(z)}{dz}} \right]_{z=a}. \quad (5)$$

Now, let equations (2.72) be written in the form

$$\Theta_j(x, t) = \frac{1}{2\pi i} \int_{\gamma-i\infty}^{\gamma+i\infty} f_j(z) dz, \quad (j = 1, 2). \quad (6)$$

where

$$f_1(z) = \frac{\Theta_0 e^{tz} [\cosh \zeta_2 h_2 \cosh \zeta_1 x' - \eta \sinh \zeta_2 h_2 \sinh \zeta_1 x']}{z [\cosh \zeta_1 h_1 \cosh \zeta_2 h_2 + \eta \sinh \zeta_1 h_1 \sinh \zeta_2 h_2]}, \quad (a)$$

(7)

$$f_2(z) = \frac{\Theta_0 e^{tz} \cosh \zeta_2 (x' - h_2)}{z [\cosh \zeta_1 h_1 \cosh \zeta_2 h_2 + \eta \sinh \zeta_1 h_1 \sinh \zeta_2 h_2]}. \quad (b)$$

and

$$\zeta_1 = \sqrt{\frac{z}{D_1}}, \quad \zeta_2 = \sqrt{\frac{z}{D_2}}. \quad (8)$$

$f_1(z)$, $f_2(z)$ have simple poles at $z = 0$, and at $z_m = -D_1 w_m^2$, where $\pm w_m$ are the roots of the equation

$$\cos w_m h_1 \cos \delta w_m h_2 - \eta \sin w_m h_1 \sin \delta w_m h_2 = 0 \quad (9)$$

and

$$\eta = \frac{k_2}{k_1} \sqrt{\frac{D_1}{D_2}}, \quad \delta = \sqrt{\frac{D_1}{D_2}}. \quad (10)$$

By applying equation (5) the residue at $z = 0$ and $z = -D_1 w_m^2$ for both $f_1(z)$ and $f_2(z)$ are

$$\text{Res}[z = 0; f_1(z)] = \Theta_0. \quad (11)$$

$$\text{Res}[z = 0; f_2(z)] = \Theta_0. \quad (12)$$

$$\begin{aligned}
\text{Res}[z = -D_1 w_m^2 ; f_1(z)] &= -\frac{\Theta_0 e^{-iD_1 w_m^2}}{\frac{w_m}{2}} * \\
&\frac{[\cos w_m x \cos w_m \delta h_2 + \eta \sin w_m x \sin w_m \delta h_2]}{[(h_1 + \eta \delta h_2) \sin w_m h_1 \cos w_m \delta h_2 + (\delta h_2 + \eta h_1) \cos w_m h_1 \sin w_m \delta h_2]}.
\end{aligned} \tag{13}$$

$$\begin{aligned}
\text{Res}[z = -D_1 w_m^2 ; f_2(z)] &= -\frac{\Theta_0 e^{iD_1 w_m^2}}{\frac{w_m}{2}} * \\
&\frac{\cos w_m \delta (x - h_2)}{[(h_1 + \eta \delta h_2) \sin w_m h_1 \cos w_m \delta h_2 + (\delta h_2 + \eta h_1) \cos w_m h_1 \sin w_m \delta h_2]}.
\end{aligned} \tag{14}$$

Appendix (E)

For $\tau_0 = 0$

$$\int_0^1 \frac{\Theta_1(x^*, \tau)}{\Theta_0} dx^* = 1 - 2 \sum_{m=1}^{\infty} \frac{e^{-\tau \lambda_m^2}}{\lambda_m^2} * \frac{[\sin \lambda_m \cos \lambda_m \delta R + \eta (\cos \lambda_m - 1) \sin \lambda_m \delta R]}{[(1 + \eta \delta R) \sin \lambda_m \cos \lambda_m \delta R + (\delta R + \eta) \cos \lambda_m \sin \lambda_m \delta R]} \quad (1)$$

$$\int_1^{1+R} \frac{\Theta_2(x^*, \tau)}{\Theta_0} dx^* = R - 2 \sum_{m=1}^{\infty} \frac{e^{-\tau \lambda_m^2}}{\lambda_m^2 \delta} * \frac{\sin \lambda_m \delta R}{[(1 + \eta \delta R) \sin \lambda_m \cos \lambda_m \delta R + (\delta R + \eta) \cos \lambda_m \sin \lambda_m \delta R]} \quad (2)$$

For $\tau \leq \tau_0$

$$\int_0^1 \frac{\Theta_1(x^*, \tau)}{\Theta_0} dx^* = \frac{\tau}{\tau_0} + 2 \sum_{m=1}^{\infty} \frac{(e^{-\tau \lambda_m^2} - 1)}{\tau_0 \lambda_m^4} * \frac{[\sin \lambda_m \cos \lambda_m \delta R + \eta (\cos \lambda_m - 1) \sin \lambda_m \delta R]}{[(1 + \eta \delta R) \sin \lambda_m \cos \lambda_m \delta R + (\delta R + \eta) \cos \lambda_m \sin \lambda_m \delta R]} \quad (3)$$

$$\int_1^{1+R} \frac{\Theta_2(x^*, \tau)}{\Theta_0} dx^* = \frac{\tau}{\tau_0} R + 2 \sum_{m=1}^{\infty} \frac{(e^{-\tau \lambda_m^2} - 1)}{\tau_0 \lambda_m^4 \delta} * \frac{\sin \lambda_m \delta R}{[(1 + \eta \delta R) \sin \lambda_m \cos \lambda_m \delta R + (\delta R + \eta) \cos \lambda_m \sin \lambda_m \delta R]} \quad (4)$$

For $\tau > \tau_0$

$$\int_0^1 \frac{\Theta_1(x^*, \tau)}{\Theta_0} dx^* = 1 - 2 \sum_{m=1}^{\infty} \frac{e^{-\tau \lambda_m^2} (e^{\tau_0 \lambda_m^2} - 1)}{\tau_0 \lambda_m^4} * \\ \frac{[\sin \lambda_m \cos \lambda_m \delta R + \eta (\cos \lambda_m - 1) \sin \lambda_m \delta R]}{[(1 + \eta \delta R) \sin \lambda_m \cos \lambda_m \delta R + (\delta R + \eta) \cos \lambda_m \sin \lambda_m \delta R]} \quad (5)$$

$$\int_1^{1+R} \frac{\Theta_2(x^*, \tau)}{\Theta_0} dx^* = R - 2 \sum_{m=1}^{\infty} \frac{e^{-\tau \lambda_m^2} (e^{\tau_0 \lambda_m^2} - 1)}{\tau_0 \lambda_m^4 \delta} * \\ \frac{\sin \lambda_m \delta R}{[(1 + \eta \delta R) \sin \lambda_m \cos \lambda_m \delta R + (\delta R + \eta) \cos \lambda_m \sin \lambda_m \delta R]} \quad (6)$$

where

$$R = \frac{h_2}{h_1} \quad \delta = \sqrt{\frac{D_1}{D_2}} \quad \eta = \frac{k_2}{k_1} \sqrt{\frac{D_1}{D_2}} \quad (7)$$

and λ_m are the roots of the following equation

$$\cos \lambda_m \cos \lambda_m \delta R - \eta \sin \lambda_m \sin \lambda_m \delta R = 0 \quad (8)$$

Appendix (F)

Further definitions to support the solution of the crack problems given in Chapter 2. $e_i, (i=1, 15)$, $M_j, (j=1, 10)$ are found in Appendix (C).

$$e_{16} = \left(\frac{\kappa_2 + 1}{2} + h_1 \alpha \right) e^{2h_1 \alpha}$$

$$e_{17} = (\kappa_2 + h_1 \alpha) e^{2h_1 \alpha}$$

$$e_{18} = -e^{2L\alpha}$$

$$e_{19} = -\left(\frac{\kappa_2 + 1}{2} + \alpha L \right) e^{2L\alpha}$$

$$e_{20} = \left(\frac{\kappa_2 + 1}{2} - \alpha L \right)$$

$$e_{21} = \left(\frac{\kappa_2 - 1}{2} + \alpha L \right) e^{2L\alpha}$$

$$e_{22} = \left(\frac{\kappa_2 - 1}{2} - \alpha L \right)$$

$$e_{23} = \alpha L e^{2L\alpha}$$

$$e_{24} = \alpha L$$

$$e_{25} = -\left(\frac{\kappa_2 - 1}{2} + h_1 \alpha \right) e^{2h_1 \alpha}$$

$$M_{11} = -[1 + (t_2 - L)\alpha] e^{t_2 \alpha}$$

$$M_{12} = -[(t_2 - L)\alpha + \rho \left\{ \frac{\kappa_2 - 1}{2} - (t_2 - L)\alpha \right\}] e^{t_2 \alpha}$$

$$B_1 = \frac{1}{\kappa_1 + 1} \int_{a_1}^{b_1} Q_1 \phi_1(t_1) dt_1 + \frac{1}{\kappa_2 + 1} \int_{a_2}^{b_2} Q_2 \phi_2(t_2) dt_2$$

$$C_2 = \frac{1}{\kappa_1 + 1} \int_{a_1}^{b_1} Q_3 \phi_1(t_1) dt_1 + \frac{1}{\kappa_2 + 1} \int_{a_2}^{b_2} Q_4 \phi_2(t_2) dt_2$$

$$B_3 = \frac{1}{\kappa_1 + 1} \int_{a_1}^{b_1} Q_5 \phi_1(t_1) dt_1 + \frac{1}{\kappa_2 + 1} \int_{a_2}^{b_2} Q_6 \phi_2(t_2) dt_2$$

$$C_4 = \frac{1}{\kappa_1 + 1} \int_{a_1}^{b_1} Q_7 \phi_1(t_1) dt_1 + \frac{1}{\kappa_2 + 1} \int_{a_2}^{b_2} Q_8 \phi_2(t_2) dt_2$$

$$B_5 = \frac{1}{\kappa_1 + 1} \int_{a_1}^{b_1} Q_9 \phi_1(t_1) dt_1 + \frac{1}{\kappa_2 + 1} \int_{a_2}^{b_2} Q_{10} \phi_2(t_2) dt_2$$

$$C_6 = \frac{1}{\kappa_1 + 1} \int_{a_1}^{b_1} Q_{11} \phi_1(t_1) dt_1 + \frac{1}{\kappa_2 + 1} \int_{a_2}^{b_2} Q_{12} \phi_2(t_2) dt_2$$

$$B_7 = \frac{1}{\kappa_1 + 1} \int_{a_1}^{b_1} \frac{Q_{13}}{D_0} \phi_1(t_1) dt_1 + \frac{1}{\kappa_2 + 1} \int_{a_2}^{b_2} \frac{Q_{14}}{D_0} \phi_2(t_2) dt_2$$

$$C_8 = \frac{1}{\kappa_1 + 1} \int_{a_1}^{b_1} \frac{Q_{15}}{D_0} \phi_1(t_1) dt_1 + \frac{1}{\kappa_2 + 1} \int_{a_2}^{b_2} \frac{Q_{16}}{D_0} \phi_2(t_2) dt_2$$

where

$$Q_1 = \frac{1}{2}(1 - 2t_1\alpha)e^{-t_1\alpha} - \frac{\kappa_1}{2}Q_3 + \frac{1}{2}Q_7$$

$$Q_2 = -\frac{\kappa_1}{2}Q_4 + \frac{1}{2}Q_8$$

$$Q_3 = \frac{H_3}{D} + \frac{1}{D} \frac{1}{D_0} \{ (2d_3 d_5) (2h_1 \alpha) Q'_{13} + (-d_5 d_2) Q_{15}$$

$$+ [(d_1 d_5) + (d_3 d_5) (2h_1 \alpha) (\kappa_2 + 2h_1 \alpha)] Q'_{15} \}$$

$$Q_4 = \frac{H_4}{D} + \frac{1}{D} \frac{1}{D_0} \{ (2d_3 d_5) (2h_1 \alpha) Q'_{14} + (-d_5 d_2) Q_{16}$$

$$+ [(d_1 d_5) + (d_3 d_5) (2h_1 \alpha) (\kappa_2 + 2h_1 \alpha)] Q'_{16} \}$$

$$Q_5 = \frac{1}{2} e^{-t_1 \alpha} - \frac{1}{2} Q_3 + \frac{\kappa_1}{2} Q_7$$

$$Q_6 = -\frac{1}{2} Q_4 + \frac{\kappa_1}{2} Q_8$$

$$Q_7 = \frac{H_7}{D} + \frac{1}{D} \frac{1}{D_0} \{ (-2d_5 d_4) Q_{13} + (2d_5 d_3) Q'_{13}$$

$$+ [(d_2 d_5) (2h_1 \alpha) + (-d_4 d_5) (\kappa_2 + 2h_1 \alpha)] Q_{15}$$

$$+ [(d_3 d_5) (\kappa_2 + 2h_1 \alpha)] Q'_{15} \}$$

$$Q_8 = \frac{H_8}{D} + \frac{1}{D} \frac{1}{D_0} \{ (-2d_5 d_4) Q_{14} + (2d_5 d_3) Q'_{14} \\ + [(d_2 d_5)(2h_1 \alpha) + (-d_4 d_5)(\kappa_2 + 2h_1 \alpha)] Q_{16} \\ + [(d_3 d_5)(\kappa_2 + 2h_1 \alpha)] Q'_{16} \}$$

$$Q_9 = \left(-\frac{d_6}{2d_3}\right) Q_3 e^{2h_1 \alpha} + \frac{1}{2} (\kappa_2 - 2h_1 \alpha) Q_{11} \\ + \left(\frac{d_2}{2d_3}\right) \frac{1}{D_0} Q_{15} e^{2h_1 \alpha}$$

$$Q_{10} = \left(-\frac{d_2}{2d_3}\right) e^{-(t_2 - 2h_1 \alpha)} + \frac{d_6}{2d_3} Q_4 e^{2h_1 \alpha} \\ + \frac{1}{2} (\kappa_2 - 2h_1 \alpha) Q_{12} \\ + \left(\frac{d_2}{2d_3}\right) \frac{1}{D_0} Q_{16} e^{2h_1 \alpha}$$

$$Q_{11} = \left(\frac{d_6}{d_2}\right) e^{t_1 \alpha} + \left(\frac{d_6}{d_2}\right) Q_7 + \left(-\frac{2d_3}{d_2}\right) \frac{1}{D_0} Q_{13} e^{2h_1 \alpha} \\ + \left(-\frac{d_3}{d_2}\right) (\kappa_2 + 2h_1 \alpha) \frac{1}{D_0} Q_{15} e^{2h_1 \alpha}$$

$$Q_{12} = \left(\frac{d_3}{d_2}\right) [1 - 2(t_2 - h_1) \alpha] e^{-(t_2 - 2h_1 \alpha)} + \left(\frac{d_6}{d_2}\right) Q_8 \\ + \left(-\frac{2d_3}{d_2}\right) \frac{1}{D_0} Q_{14} e^{2h_1 \alpha} + \left(-\frac{d_3}{d_2}\right) (\kappa_2 + 2h_1 \alpha) \frac{1}{D_0} Q_{16} e^{2h_1 \alpha}$$

$$\begin{aligned}
Q_{13} = & (q_7 s_1 + q_9 s_4 - p_4 r_2 - p_5 r_4) e^{-(4L+t_1)\alpha} \\
& + (q_7 s_2 + q_9 s_3 - p_4 r_1 - p_5 r_3) e^{-(4L-t_1)\alpha} \\
& + (q_7 s_3 + q_8 s_2 - p_4 r_3 - p_6 r_1) e^{-(4L+2h_1-t_1)\alpha} \\
& + (q_7 s_4 + q_8 s_1 - p_4 r_4 - p_6 r_2) e^{-(4L+2h_1+t_1)\alpha} \\
& + (q_9 s_1 - p_5 r_2) e^{-(4L-2h_1+t_1)\alpha} \\
& + (q_9 s_2 - p_5 r_1) e^{-(4L-2h_1-t_1)\alpha} \\
& + (q_8 s_4 - p_6 r_4) e^{-(4L+4h_1+t_1)\alpha} \\
& + (q_8 s_3 - p_6 r_3) e^{-(4L+4h_1-t_1)\alpha} \\
& + (q_{10} s_1 - p_7 r_2) e^{-(2L+t_1)\alpha} \\
& + (q_{10} s_2 - p_7 r_1) e^{-(2L-t_1)\alpha} \\
& + (q_{10} s_3 + q_{11} s_2 - p_7 r_3 - p_8 r_1) e^{-(2L+2h_1-t_1)\alpha} \\
& + (q_{10} s_4 + q_{11} s_1 - p_7 r_4 - p_8 r_2) e^{-(2L+2h_1+t_1)\alpha} \\
& + (q_{11} s_3 + q_{12} s_2 - p_8 r_3 - p_9 r_1) e^{-(2L+4h_1-t_1)\alpha} \\
& + (q_{11} s_4 + q_{12} s_1 - p_8 r_4 - p_9 r_2) e^{-(2L+4h_1+t_1)\alpha} \\
& + (q_{12} s_3 - p_9 r_3) e^{-(2L+6h_1-t_1)\alpha} \\
& + (q_{12} s_4 - p_9 r_4) e^{-(2L+6h_1+t_1)\alpha}
\end{aligned}$$

$$\begin{aligned}
Q_{14} = & (q_7 s_5 + q_9 s_6 - p_4 r_5 - p_5 r_6) e^{-(4L-t_2)\alpha} \\
& + (q_7 s_9 + q_8 s_8 + q_9 s_{10} - p_4 r_9 - p_5 r_{10} - p_6 r_8) e^{-(4L+t_2)\alpha} \\
& + (q_7 s_6 + q_8 s_5 + q_9 s_7 - p_4 r_6 - p_5 r_7 - p_6 r_5) e^{-(4L+2h_1-t_2)\alpha} \\
& + (q_7 s_8 + q_9 s_9 - p_4 r_8 - p_5 r_9) e^{-(4L-2h_1+t_2)\alpha} \\
& + (q_7 s_{10} + q_8 s_9 - p_4 r_{10} - p_6 r_9) e^{-(4L+2h_1+t_2)\alpha} \\
& + (q_9 s_5 - p_5 r_5) e^{-(4L-2h_1-t_2)\alpha} \\
& + (q_7 s_7 + q_8 s_6 - p_4 r_7 - p_6 r_6) e^{-(4L+4h_1-t_2)\alpha} \\
& + (q_8 s_{10} - p_6 r_{10}) e^{-(4L+4h_1+t_2)\alpha} \\
& + (q_9 s_8 - p_5 r_8) e^{-(4L-4h_1+t_2)\alpha} \\
& + (q_8 s_7 - p_6 r_7) e^{-(4L+6h_1-t_2)\alpha} \\
& + (q_{10} s_5 - p_7 r_5) e^{-(2L-t_2)\alpha} \\
& + (q_{10} s_9 + q_{11} s_8 - p_7 r_9 - p_8 r_8) e^{-(2L+t_2)\alpha} \\
& + (q_{10} s_8 - p_7 r_8) e^{-(2L-2h_1+t_2)\alpha} \\
& + (q_{10} s_{10} + q_{11} s_9 + q_{12} s_8 - p_7 r_{10} - p_8 r_9 - p_9 r_8) e^{-(2L+2h_1+t_2)\alpha} \\
& + (q_{10} s_6 + q_{11} s_5 - p_7 r_6 - p_8 r_5) e^{-(2L+2h_1-t_2)\alpha} \\
& + (q_{10} s_7 + q_{11} s_6 + q_{12} s_5 - p_7 r_7 - p_8 r_6 - p_9 r_5) e^{-(2L+4h_1-t_2)\alpha} \\
& + (q_{11} s_{10} + q_{12} s_9 - p_8 r_{10} - p_9 r_9) e^{-(2L+4h_1+t_2)\alpha} \\
& + (q_{11} s_7 + q_{12} s_6 - p_8 r_7 - p_9 r_6) e^{-(2L+6h_1-t_2)\alpha} \\
& + (q_{12} s_{10} - p_9 r_{10}) e^{-(2L+6h_1+t_2)\alpha} \\
& + (q_{12} s_7 - p_9 r_7) e^{-(2L+8h_1-t_2)\alpha}
\end{aligned}$$

$$\begin{aligned}
Q_{15} = & (p_1 r_1 + p_3 r_3 - q_1 s_2 - q_3 s_3) e^{-(4L-t_1)\alpha} \\
& + (p_1 r_2 + p_3 r_4 - q_1 s_1 - q_3 s_4) e^{-(4L+t_1)\alpha} \\
& + (p_1 r_3 + p_2 r_1 - q_1 s_3 - q_2 s_2) e^{-(4L+2h_1-t_1)\alpha} \\
& + (p_1 r_4 + p_2 r_2 - q_1 s_4 - q_2 s_1) e^{-(4L+2h_1+t_1)\alpha} \\
& + (p_2 r_3 - q_2 s_3) e^{-(4L+4h_1-t_1)\alpha} \\
& + (p_2 r_4 - q_2 s_4) e^{-(4L+4h_1+t_1)\alpha} \\
& + (p_3 r_1 - q_3 s_2) e^{-(4L-2h_1-t_1)\alpha} \\
& + (p_3 r_2 - q_3 s_1) e^{-(4L-2h_1+t_1)\alpha} \\
& + (-q_4 s_1) e^{-(2L+t_1)\alpha} \\
& + (-q_4 s_2) e^{-(2L-t_1)\alpha} \\
& + (-q_4 s_3 - q_5 s_2) e^{-(2L+2h_1-t_1)\alpha} \\
& + (-q_4 s_4 - q_5 s_1) e^{-(2L+2h_1+t_1)\alpha} \\
& + (-q_5 s_3 - q_6 s_2) e^{-(2L+4h_1-t_1)\alpha} \\
& + (-q_5 s_4 - q_6 s_1) e^{-(2L+4h_1+t_1)\alpha} \\
& + (-q_6 s_3) e^{-(2L+6h_1-t_1)\alpha} \\
& + (-q_6 s_4) e^{-(2L+6h_1+t_1)\alpha}
\end{aligned}$$

$$\begin{aligned}
Q_{16} = & (p_1 r_5 + p_3 r_6 - q_1 s_5 - q_3 s_6) e^{-(4L-t_2)\alpha} \\
& + (p_1 r_9 + p_2 r_8 + p_3 r_{10} - q_1 s_9 - q_2 s_8 - q_3 s_{10}) e^{-(4L+t_2)\alpha} \\
& + (p_1 r_6 + p_2 r_5 + p_3 r_7 - q_1 s_6 - q_2 s_5 - q_3 s_7) e^{-(4L+2h_1-t_2)\alpha} \\
& + (p_1 r_7 + p_2 r_6 - q_1 s_7 - q_2 s_6) e^{-(4L+4h_1-t_2)\alpha} \\
& + (p_1 r_8 + p_3 r_9 - q_1 s_8 - q_3 s_9) e^{-(4L-2h_1+t_2)\alpha} \\
& + (p_1 r_{10} + p_2 r_9 - q_1 s_{10} - q_2 s_9) e^{-(4L+2h_1+t_2)\alpha} \\
& + (p_2 r_7 - q_2 s_7) e^{-(4L+6h_1-t_2)\alpha} \\
& + (p_2 r_{10} - q_2 s_{10}) e^{-(4L+4h_1+t_2)\alpha} \\
& + (p_3 r_5 - q_3 s_5) e^{-(4L-2h_1-t_2)\alpha} \\
& + (p_3 r_8 - q_3 s_8) e^{-(4L-4h_1+t_2)\alpha} \\
& + (-q_4 s_5) e^{-(2L-t_2)\alpha} \\
& + (-q_4 s_9 - q_5 s_8) e^{-(2L+t_2)\alpha} \\
& + (-q_4 s_6 - q_5 s_5) e^{-(2L+2h_1-t_2)\alpha} \\
& + (-q_4 s_8) e^{-(2L-2h_1+t_2)\alpha} \\
& + (-q_4 s_7 - q_5 s_6 - q_6 s_5) e^{-(2L+4h_1-t_2)\alpha} \\
& + (-q_4 s_{10} - q_5 s_9 - q_6 s_8) e^{-(2L+2h_1+t_2)\alpha} \\
& + (-q_5 s_7 - q_6 s_6) e^{-(2L+6h_1-t_2)\alpha} \\
& + (-q_5 s_{10} - q_6 s_9) e^{-(2L+4h_1+t_2)\alpha} \\
& + (-q_6 s_{10}) e^{-(2L+6h_1+t_2)\alpha} \\
& + (-q_6 s_7) e^{-(2L+8h_1-t_2)\alpha}
\end{aligned}$$

$$\begin{aligned}
D_0 = & (p_1 q_7 + p_2 q_9 + p_3 q_8 - q_1 p_4 - q_2 p_5 - q_3 p_6) e^{-4L\alpha} \\
& + (p_1 q_8 + p_2 q_7 - q_1 p_6 - q_2 p_4) e^{-2(2L+h_1)\alpha} \\
& + (p_1 q_9 + p_3 q_7 - q_1 p_5 - q_3 p_4) e^{-2(2L-h_1)\alpha} \\
& + (p_1 q_{10} + p_3 q_{11} - q_1 p_7 - q_3 p_8 - q_4 p_4 - q_5 p_5) e^{-2L\alpha} \\
& + (p_1 q_{11} + p_2 q_{10} + p_3 q_{12} - q_1 p_8 - q_2 p_7 \\
& \quad - q_3 p_9 - q_4 p_6 - q_5 p_4 - q_6 p_5) e^{-2(L+h_1)\alpha} \\
& + (p_1 q_{12} + p_2 q_{11} - q_1 p_9 - q_2 p_8 - q_5 p_6 - q_6 p_4) e^{-2(L+2h_1)\alpha} \\
& + (p_2 q_8 - q_2 p_6) e^{-4(L+h_1)\alpha} \\
& + (p_3 q_9 - q_3 p_5) e^{-4(L-h_1)\alpha} \\
& + (p_2 q_{12} - q_2 p_9 - q_6 p_6) e^{-2(L+3h_1)\alpha} \\
& + (p_3 q_{10} - q_3 p_7 - q_4 p_5) e^{-2(L-h_1)\alpha} \\
& + (-q_4 p_7) \\
& + (-q_4 p_8 - q_5 p_7) e^{-2h_1\alpha} \\
& + (-q_4 p_9 - q_5 p_8 - q_6 p_7) e^{-4h_1\alpha} \\
& + (-q_5 p_9 - q_6 p_8) e^{-6h_1\alpha} \\
& + (-q_6 p_9) e^{-8h_1\alpha}
\end{aligned}$$

$$Q'_{13} = Q_{13} e^{-2h_1\alpha}$$

$$Q'_{14} = Q_{14} e^{-2h_1\alpha}$$

$$Q'_{15} = Q_{15} e^{-2h_1\alpha}$$

$$Q'_{16} = Q_{16} e^{-2h_1\alpha}$$

$$\begin{aligned}
q_1 = & (d_7 - 1) \{ (-2d_6 d_5 d_4) + (-2d_3 d_1 d_4) + (-2d_3 d_2 d_3) \\
& + (-2d_3 d_2 d_3)(2h_1\alpha)^2 \}
\end{aligned}$$

$$q_2 = (d_7 - 1) \{ (2d_6 d_5 d_3) + (2d_3 d_1 d_3) \}$$

$$q_3 = (d_7 - 1) \{ 2d_3 d_2 d_4 \}$$

$$q_4 = \{ -2d_2 d_2 d_4 \}$$

$$q_5 = \{ (2d_2 d_2 d_3)(2h_1 \alpha)^2 + (2d_2 d_1 d_4) + (2d_2 d_2 d_3) \}$$

$$q_6 = \{ -2d_2 d_1 d_3 \}$$

$$q_7 = (d_7 - 1) \{ (d_6 d_2 d_5)(2h_1 \alpha) + (\kappa_2 + 2h_1 \alpha) [(-d_6 d_4 d_5) \\ + (-d_3 d_1 d_4) + (-d_3 d_2 d_3) + (-d_3 d_2 d_3)(2h_1 \alpha)^2] \}$$

$$q_8 = (d_7 - 1)(\kappa_2 + 2h_1 \alpha) \{ (d_6 d_3 d_5) + (d_3 d_1 d_3) \}$$

$$q_9 = (d_7 - 1)(\kappa_2 + 2h_1 \alpha) \{ d_3 d_2 d_4 \}$$

$$q_{10} = \{ d_7 - (\kappa_2 + 2\alpha L) \} \{ d_2 d_2 d_4 \}$$

$$q_{11} = \{ d_7 - (\kappa_2 + 2\alpha L) \} \{ (-d_2 d_2 d_3)(2h_1 \alpha)^2 + (-d_2 d_1 d_4) \\ + (-d_2 d_2 d_3) \}$$

$$q_{12} = \{ d_7 - (\kappa_2 + 2\alpha L) \} \{ d_2 d_1 d_3 \}$$

$$r_1 = (d_7 - 1) \{ d_6 d_2 d_4 \}$$

$$r_2 = (d_7 - 1) \{ d_6 d_2 d_4 \} (-1 + 2i_1 \alpha)$$

$$r_3 = (d_7 - 1) \{-d_6 d_2 d_3\} \{1 + (2h_1 \alpha)(1 + 2t_1 \alpha)\}$$

$$r_4 = (d_7 - 1) \{d_6 d_2 d_3\} \{1 + 2(h_1 - t_1) \alpha\}$$

$$r_5 = (d_7 - 1) \{d_2 d_2 d_4\}$$

$$r_6 = (d_7 - 1) (-d_2) \{(d_2 d_3)(2h_1 \alpha)^2 + d_1 d_4 + d_2 d_3\}$$

$$r_7 = (d_7 - 1) \{d_2 d_1 d_3\}$$

$$r_8 = (d_7 - 1) \{-d_3 d_2 d_4\} \{-1 + 2(t_2 - h_1) \alpha\}$$

$$r_9 = (d_7 - 1) \{[-1 + 2(t_2 - h_1) \alpha] [(d_2 d_3 d_3)(2h_1 \alpha)^2 + (d_1 d_4 d_3) \\ + (d_2 d_3 d_3) + (d_4 d_5 d_6)] + (d_2 d_5 d_6)(2h_1 \alpha)\}$$

$$r_{10} = (d_7 - 1) \{[-1 + 2(t_2 - h_1) \alpha] [(-d_3 d_1 d_3) + (-d_3 d_6 d_5)]\}$$

$$p_1 = \{(d_6 d_2)(-2d_3 d_5)(2h_1 \alpha) + (-d_3)[-d_7 + 2(L - h_1) \alpha] \\ [(2d_5 d_4 d_6) + (2d_2 d_3 d_3)(2h_1 \alpha)^2 + (2d_1 d_4 d_3) + (2d_2 d_3 d_3)]\}$$

$$p_2 = \{(2d_3 d_3)[-d_7 + 2(L - h_1) \alpha] [(d_6 d_5) + (d_1 d_3)]\}$$

$$p_3 = \{(2d_3 d_3 d_2 d_4)[-d_7 + 2(L - h_1) \alpha]\}$$

$$\begin{aligned}
p_4 = & \{(-d_6 d_2 d_3 d_5)(2h_1 \alpha)(\kappa_2 + 2h_1 \alpha) - (d_6 d_2 d_1 d_5) \\
& + (d_2 d_2)[(d_2 d_3)(2h_1 \alpha)^2 + d_1 d_4 + d_2 d_3] \\
& + [-d_7 + 2(L - h_1) \alpha][(d_6 d_3 d_2 d_5)(2h_1 \alpha) + (-d_6 d_3 d_4 d_5)(\kappa_2 + 2h_1 \alpha) \\
& + (-d_3 d_3 d_2 d_3)(2h_1 \alpha)^2(\kappa_2 + 2h_1 \alpha) \\
& + (-d_3 d_3)(\kappa_2 + 2h_1 \alpha)(d_1 d_4 + d_2 d_3)]\}
\end{aligned}$$

$$\begin{aligned}
p_5 = & \{(d_6 d_2 d_2 d_5) - (d_2 d_2 d_2 d_4) \\
& + (d_3 d_3 d_2 d_4)(\kappa_2 + 2h_1 \alpha)[-d_7 + 2(L - h_1) \alpha]\}
\end{aligned}$$

$$\begin{aligned}
p_6 = & \{(-d_2 d_2 d_1 d_3) + (\kappa_2 + 2h_1 \alpha)[-d_7 + 2(L - h_1) \alpha] \\
& [(d_6 d_3 d_3 d_5) + (d_3 d_3 d_1 d_3)]\}
\end{aligned}$$

$$p_7 = \{(-d_2 d_3 d_2 d_4)(d_7 + 1)\}$$

$$p_8 = \{(d_2 d_3)(d_7 + 1)[(d_2 d_3)(2h_1 \alpha)^2 + d_1 d_4 + d_2 d_3]\}$$

$$p_9 = \{(-d_2 d_3 d_1 d_3)(d_7 + 1)\}$$

$$\begin{aligned}
s_1 = & \{(d_2 d_6 d_2 d_3)(2h_1 \alpha)(-1 + 2t_1 \alpha) + (d_2 d_6 d_2 d_3) \\
& + [-d_7 + 2(L - h_1) \alpha](d_3 d_6 d_2 d_4)(-1 + 2t_1 \alpha)\}
\end{aligned}$$

$$\begin{aligned}
s_2 = & \{(-d_2 d_6 d_2 d_3)[1 + 2(t_1 - h_1) \alpha] \\
& + [-d_7 + 2(L - h_1) \alpha](d_3 d_6 d_2 d_4)\}
\end{aligned}$$

$$\begin{aligned}
s_3 = & \{(d_2 d_6 d_1 d_3)(1 + 2t_1 \alpha) \\
& + [-d_7 + 2(L - h_1) \alpha](-d_3 d_6 d_2 d_3)[1 + (2h_1 \alpha)(1 + 2t_1 \alpha)]\}
\end{aligned}$$

$$s_4 = \{(-d_2 d_6 d_1 d_3) + [-d_7 + 2(L - h_1)\alpha] \\ (d_3 d_6 d_2 d_3)[1 - 2(t_1 - h_1)\alpha]\}$$

$$s_5 = \{[d_7 + 1 + 2(t_2 - L)\alpha](-d_2 d_3 d_2 d_4)\}$$

$$s_6 = \{[d_7 + 1 + 2(t_2 - L)\alpha](d_2 d_3)[(d_2 d_3)(2h_1\alpha)^2 + d_1 d_4 + d_2 d_3]\}$$

$$s_7 = \{[d_7 + 1 + 2(t_2 - L)\alpha](-d_2 d_3 d_1 d_3)\}$$

$$s_8 = \{(-d_2 d_2 d_2 d_4) + (d_2 d_6 d_2 d_5) \\ + [-d_7 + 2(L - h_1)\alpha](-d_3 d_3 d_2 d_4)[-1 + 2(t_2 - h_1)\alpha]\}$$

$$s_9 = \{(d_2 d_2)[d_2 d_3(2h_1\alpha)^2 + d_1 d_4 + d_2 d_3] \\ + (d_2 d_6)[(d_3 d_5)(2h_1\alpha)(-1 + 2(t_2 - h_1)\alpha) - d_1 d_5] \\ + [-d_7 + 2(L - h_1)\alpha](d_3 d_3)[-1 + 2(t_2 - h_1)\alpha] \\ [d_2 d_3(2h_1\alpha)^2 + d_1 d_4 + d_2 d_3] \\ + [-d_7 + 2(L - h_1)\alpha](-d_3 d_6) \\ [(-d_2 d_5)(2h_1\alpha) - d_4 d_5(-1 + 2(t_2 - h_1)\alpha)]\}$$

$$s_{10} = \{(-d_2 d_2 d_1 d_3) \\ + [-d_7 + 2(L - h_1)\alpha][-1 + 2(t_2 - h_1)\alpha] \\ [(-d_3 d_3 d_1 d_3) + (-d_3 d_6 d_3 d_5)]\}$$

where $H_3, H_4, H_7, H_8, D, d_1, d_2, d_3, d_4, d_5, d_6$ can be found in Appendix (C), and

$$d_7 = \rho \frac{\kappa_2 + 1}{2}$$

$$\rho = \frac{\chi}{2\mu_2\alpha}$$

Appendix (G)

In general, the singular integral of the form

$$\int_{-1}^{+1} \frac{w(r)f(r)}{r-s} dr. \quad (1)$$

with

$$w(r) = (1+r)^{-\alpha} (1-r)^{-\beta}. \quad (2)$$

$$f(r) = r^n. \quad (3)$$

can be obtained by using a Gaussian Quadrature formula. Let us rewrite equation (1) in the following form.

$$\int_{-1}^{+1} \frac{w(r)f(r)}{r-s} dr = \int_{-1}^{+1} w(r) \left[\frac{f(r)-f(s)}{r-s} \frac{w(s)}{w(r)} \right] dr + w(s)f(s) \int_{-1}^{+1} \frac{dr}{r-s} \quad (4)$$

The first integral in the right hand side of (4) is bounded as $r \rightarrow s$, i.e.

$$\begin{aligned} \lim_{r \rightarrow s} \int_{-1}^{+1} w(r) \left[\frac{f(r)-f(s)}{r-s} \frac{w(s)}{w(r)} \right] dr \\ = \int_{-1}^{+1} w(r) \left[f'(s) - f(s)w(s) \left\{ \frac{1}{w(s)} \right\}' \right] dr \end{aligned} \quad (5)$$

where $(\cdot)'$, is $\frac{d}{dr}$.

Equation (4) may now be written as

$$\int_{-1}^{+1} \frac{w(r)f(r)}{r-s} dr = \int_{-1}^{+1} w(r) \left[\frac{f(r)-f(s)}{r-s} \frac{w(s)}{w(r)} \right] dr + w(s)f(s) \log \frac{1-s}{1+s} \quad (6)$$

Since the weight function $w(r)$ is in the form of equation (2), then by using Jacobi-Gauss Quadrature formula (see, Erdogan [40] or Stroud [44]), we may have

$$\int_{-1}^{+1} w(r) g(r) dr \approx \sum_{l=1}^n A_l g(r_l). \quad (7)$$

where r_l is the l^{th} zero of the Jacobi polynomial

$$P_n^{(-\beta, -\alpha)}(r_l) = 0; \quad l = 1, 2, \dots, n. \quad (8)$$

and the weighting functions A_l are

$$A_l = -\frac{(2n - \alpha - \beta + 2) \Gamma(n - \alpha + 1) \Gamma(n - \beta + 1)}{(n - 1)! (n - \alpha - \beta + 1) \Gamma(n - \alpha - \beta + 1)} * \frac{2^{-\alpha - \beta}}{\frac{d}{dr} P_n^{(-\beta, -\alpha)}(r_l) P_{n+1}^{(-\beta, -\alpha)}(r_l)}. \quad (9)$$

In our case $g(r)$ is in the form

$$g(r) = \frac{f(r) - f(s) \frac{w(s)}{w(r)}}{r - s}. \quad (10)$$

or as $r \rightarrow s$, $g(r)$ will be equal to

$$g(r) = f'(s) - f(s) w(s) \left\{ \frac{1}{w(s)} \right\}'. \quad (11)$$

In the special case, if $\alpha = \beta = -\frac{1}{2}$, the closed form solution of the integral (1) can be put in the following form

$$\int_{-1}^{+1} \frac{r^n}{\sqrt{1 - r^2} (r - s)} dr = \sum_{i=0}^{n-1} d_i s^i. \quad (12)$$

where

$$d_i = \sqrt{\pi} \frac{\Gamma(\frac{n-i}{2})}{\Gamma(\frac{n-i+1}{2})}, n-i = \text{odd},$$

$$d_i = 0, n-i = \text{even}.$$
(13)

Also, the function $g(r)$ in equation (7) may be in the form

$$g(r) = f(r).$$
(14)

or

$$g(r) = f(r) K_{ij}(s, r), i, j = 1, 2.$$
(15)

where $f(r)$ is given in equation (3), and $K_{ij}(s, r)$, $(i, j = 1, 2)$ are the kernels of the singular integral equations (4.4).

The integral as in equations (2.64), i.e.

$$\int_0^\infty G_{ij}(x, t, \alpha) d\alpha, i, j = 1, 2.$$
(16)

may be evaluated by using Laguerre-Gauss Quadrature formula, by changing the integral (16) into

$$\int_0^\infty G_{ij}(x, t, \alpha) d\alpha = \int_0^\infty [G_{ij}(x, t, \alpha) e^\alpha] e^{-\alpha} d\alpha, i, j = 1, 2.$$
(17)

then, the integral becomes (see, Stroud [44]),

$$\int_0^\infty [G_{ij}(x, t, \alpha) e^\alpha] e^{-\alpha} d\alpha \approx \sum_{l=1}^n A_l [G_{ij}(x, t, \alpha_l) e^{\alpha_l}]$$
(18)

$(i, j = 1, 2).$

where α_l is the l^{th} zero of Laguerre polynomial

$$L_n(\alpha_l) = 0, l = 1, 2, \dots, n.$$
(19)

and the weighting function A_l given by

$$A_l = \frac{(n!)^2}{\alpha_l \left[\frac{d}{d\alpha} L_n(\alpha_l) \right]^2}, \quad l=1, 2, \dots, n. \quad (20)$$